THE UNIVERSITY OF HULL

SURFACTANT PROPERTIES OF CORROSION INHIBITORS

being a Thesis submitted for the Degree of Doctor of Philosophy
in the University of Hull

by

Ibrahim S. EL Moaty, M.Sc.
(Helwan University, Egypt)

January 2011

SUMMARY OF THESIS

Surfactant addition is one of many ways to inhibit the corrosion of metals, especially on hard to reach surfaces such as the inside of a pipe through which crude oil is transported. Despite the popularity of surfactants as corrosion inhibitors, their actual behaviour inside a pipeline is not well understood. The homologous alkylbenzyldimethylammonium chlorides (CnBDMAC) series is one of the most common corrosion inhibitors used in the oil industry. This thesis addresses some of the surfactant properties of these corrosion inhibitors.

Firstly, the adsorption behaviour of these surfactants has been investigated at the air-water interface. The surfactant chain length and brine addition were found to have a great influence on the adsorption behaviour and hence on the critical micelle concentration (cmc).

Secondly, the ability of CnBDMAC corrosion inhibitors to stabilize both oil-in-water and water-in-oil emulsions and the phase inversion of the emulsions as the inhibitor structure, temperature, electrolyte concentration and oil type change have been studied.

The partitioning behaviour of hexadecylbenzyldimethylammonium chloride (C16BDMAC) between an aqueous brine phase and an oil phase has been investigated as well as a function of electrolyte concentration.

In addition, the adsorption behaviour of CnBDMAC molecules has been studied as a function of the surfactant chain length, temperature and electrolyte concentration using the Quartz Crystal Microbalance (QCM) technique.

Moreover, the effects of surfactant structure, temperature and electrolyte concentration on the adsorption behaviour of CnBDMAC onto mild steel and sand particles using the depletion method have been investigated.

The adsorption studies performed revealed that these inhibitors have a strong affinity for sand particles, particularly at low temperatures and diluted inhibitor concentrations.

Finally, a model has been proposed and applied successfully to determine the percentage depletion in the corrosion inhibition efficiency of C16BDMAC with changes in the amount of sand added.

ACKNOWLEDGMENTS

I would like to express my sincere gratitude to my supervisors Prof. Bernard P. Binks and Prof. Paul D.I. Fletcher for their continuous and excellent guidance, support, constant availability throughout this study and for reviewing this thesis with constructive comments.

I am also grateful to Nalco for the provision of a studentship. In particular, I would like to thank Dr. David I. Horsup and Dr. Jennifer A. Moore from Nalco, Sugar Land, USA for their support during this project.

I would like to express my gratitude to all members of the Surfactant and Colloid Group for their help and friendship. I also thankful for all the technical staff in the chemistry department for their help and support.

I would like to express my gratitude for Prof. Stephen M Kelly for the time, effort and the careful examination he provided to examine this thesis.

Special thanks are to all the staff in the Brynmor Jones Library, Hull University for their understanding and endless support.

I am also grateful to Prof. Kamal Rabie, NMA, Egypt for his help and support. Thanks are extended to reach all my friends and colleagues in NMA for their support.

I am indebted to my parents for their support and encouragement throughout my life as well as my friends. Finally, I thank my wife, Shaza and Hala for their patience and constant support and encouragement during the time I spent in researching and writing this thesis.

PUBLICATIONS AND PRESENTATIONS

This thesis has contributed to the following publication:

1. B. P. Binks, P. D. I. Fletcher, I. E. Salama, D. I. Horsup and J. A. Moore, ***Quantitative Prediction of the Reduction of Corrosion Inhibitor Effectiveness Due to Parasitic Adsorption onto a Competitor Surface***, Langmuir, **27**, 469 (2010).

This work has also been presented by the author at the following events:

1. Oral presentation entitled: "**Corrosion inhibitors behaviour in multiphase systems**", at Nalco, Aberdeen, UK (8th October 2009).

2. Oral presentation entitled: "**Surfactant properties of corrosion inhibitors**", at the University of Hull, Departmental Research Colloquium, UK (10th June 2009).

3. Poster presentation entitled: "**Competitive adsorption of cationic surfactant onto different solids**", at the 14th UKPCF Annual Meeting, The University of Hull, UK (14th -16th September 2009).

4. Poster presentation entitled: "**Adsorption of cationic surfactants at oil-water and steel-water interfaces**", at the 17th International Conference "Surfactants in Solution", Max Planck Institute for Colloids and Interfaces, Berlin, Germany (17th -22nd August 2008).

5. Oral presentation entitled: "**Adsorption of alkylbenzyldimethylammonium chloride corrosion inhibitors onto stainless steel using the qnartz crystal microbalance technique**" Surfactants and Colloids Group Seminar, University of Hull, UK (25th February 2008).

ABSTRACT

ABSTRACT

Corrosion is one of the most common, costly and widespread industrial problems in the oil and gas production industry. Surfactant addition is one of many ways to inhibit the corrosion of metals, especially on hard-to-reach surfaces such as the inside of a pipe through which fluid is flowing. The application of small quantities of an inhibitor to production fluids is the most cost-effective method for imparting corrosion protection to a system. Despite the popularity of surfactants as corrosion inhibitors, their actual behaviour inside a pipeline is not well understood. The homologous alkylbenzyldimethylammonium chlorides CnBDMAC series is one of the most common corrosion inhibitors used in the oil industry. This thesis addresses some of the surfactant properties of these corrosion inhibitors which are not studied in detail (or often ignored) through electrochemical studies.

Firstly, the adsorption behaviour of these corrosion inhibitors at the air-water interface was investigated as a function of the alkyl chain length, temperature and the concentration of the added electrolyte. The surfactant chain length and brine addition were found to have a great influence on the adsorption behaviour and hence on the critical micelle concentration (cmc).

Secondly, the ability of CnBDMAC corrosion inhibitors to stabilize both oil-in-water and water-in-oil emulsions and the phase inversion of the emulsions as the inhibitor structure, temperature, electrolyte concentration and oil type change has been studied. The partitioning behaviour of C16BDMAC between an aqueous brine phase and an oil phase has been investigated as well as a function of electrolyte concentration.

Studying the adsorption behaviour of surfactant corrosion inhibitors at solid-liquid interfaces provides important information about their action mechanism,

which in turn helps in improving their efficiency. The adsorption behaviour of CnBDMAC molecules has been studied as a function of the surfactant chain length, temperature and electrolyte concentration using the Quartz Crystal Microbalance (QCM) technique. The QCM technique provides an effective, easy to setup and quick *in-situ* monitoring method for studying qualitatively the adsorption of surfactants at the solid-liquid interface. However, the determined adsorption isotherms were found to overestimate the amount of surfactant adsorbed. Therefore, the depletion method has been used to study the adsorption characteristics of CnBDMAC onto a stainless steel powder.

Pipes used in oilfields for crude oil transportation are mainly made of mild steel. Accordingly, it is crucial to understand the adsorption behaviour of these corrosion inhibitors onto the mild steel surface. The effect of surfactant structure, temperature and electrolyte concentration on the adsorption behaviour of CnBDMAC onto mild steel particles using the depletion method has been investigated.

In addition, the depletion method has been used to study the adsorption of CnBDMAC onto sand which is one of the main corrosion inhibitor consuming-solids encountered naturally in the oilfield. The adsorption studies performed revealed that these inhibitors have a strong affinity for sand particles, particularly at low temperatures and diluted inhibitor concentrations.

Finally, the corrosion inhibition performance of hexadecylbenzyldimethylammonium chloride (C16BDMAC) corrosion inhibitor has been investigated through the linear polarisation resistance technique as a function of the added sand amount. A model has been proposed and applied successfully to determine the percentage decrease in the corrosion inhibition efficiency of C16BDMAC with changes in the amount of sand added.

CONTENTS

TABLE OF CONTENTS

Page

CHAPTER 1 INTRODUCTION

CHAPTER 2 EXPERIMENTAL

CHAPTER 3 ADSORPTION OF ALKYLBENZYLDIMETHYLAMMONIUM CHLORIDES AT THE AIR-WATER INTERFACE

CHAPTER 4 PHASE BEHAVIOUR OF ALKYLBENZYLDIMETHYLAMMONIUM CHLORIDES IN OIL-WATER SYSTEMS

CHAPTER 5 OPTIMIZATION AND APPLICATION OF THE QUARTZ CRYSTAL MICROBALANCE FOR STUDYING THE ADSORPTION OF ALKYLBENZYLDIMETHYLAMMONIUM CHLORIDES AT THE STEEL-WATER INTERFACE

CHAPTER 6 ADSORPTION OF ALKYLBENZYLDIMETHYLAMMONIUM CHLORIDES AT THE STEEL-WATER INTERFACE USING THE DEPLETION METHOD

CHAPTER 7 ADSORPTION OF ALKYLBENZYLDIMETHYLAMMONIUM CHLORIDES AT THE SAND-WATER INTERFACE USING THE DEPLETION METHOD

CHAPTER 8 CORROSION INHIBITION BY ALKYLBENZYLDIMETHYLAMMONIUM CHLORIDES AND THE EFFECT OF PARASITIC ADSORPTION

CHAPTER 9 SUMMARY OF CONCLUSIONS AND FUTURE WORK

List of Tables

LIST OF TABLES

Table **Page**

List of Figures

LIST OF FIGURES

CHAPTER 1

Chapter 1

INTRODUCTION

1.1. CORROSION IN THE OIL INDUSTRY

1.1.1. General background

Corrosion is one of the most common, costly and widespread industrial problems in today's modern world. Corrosion comes from the Latin word *"corrodere"* which means *"to gnaw away"* [1]. It is defined as the degradation or breaking of bonds between the atoms in a metal and the formation of thermodynamically more stable compounds. The processes of corrosion impair the mechanical properties and compromise the structural integrity of a metal. In the field of oil and gas exploration and refining, there is a constant battle against corrosion due to the severe environments encountered in this field. Table 1-1 shows the estimated annual cost of corrosion per industrial segment in the petroleum industry in 2001 [2]. Improvement in corrosion monitoring, control and prevention can lead to a significant reduction in the production cost.

Table 1-1. Annual estimated corrosion costs in oil and gas exploration, production and refining sectors in 2001 [2].

Industrial sector	**Annual estimated cost / US dollars**	
OIL AND GAS EXPLORATION AND PRODUCTION	Piping and facilities	589 M
	Down-hole tubing	463 M
	Capital expenditures	320 M
	Total cost	\$1.4 Bn
PETROLEUM REFINING	Maintenance	1.8 Bn
	Vessel turnaround	1.4 Bn
	Fouling cost	0.5 Bn
	Total cost	\$3.7 Bn

Oilfield corrosion manifests itself in several forms amongst which carbon dioxide corrosion (*sweet corrosion*) and hydrogen sulphide corrosion (*sour corrosion*) in the produced fluids and oxygen corrosion in water injection systems are by far the most predominant forms of attack encountered in oil and gas production.

Corrosion occurs when a metal in contact with water forms a corrosion cell. The corrosion cell has four components: the aqueous phase which acts as an electrolyte (through which ions migrate), an anode on the metal surface (where the metal is oxidized and goes into the solution as metal ions), a cathode (where excess electrons are consumed) and a metallic path connecting the cathode to the anode. Anodes and cathodes can form on the steel surface of a pipe (due to the slight differences in composition) when it is exposed to brine (Figure 1-2). The electrolyte in this case is the brine. Under these conditions, iron atoms in the steel will dissolve into the solution as Fe^{2+} ions. As each Fe^{2+} ion is formed, two electrons are left behind, giving that area of the metal a small negative charge. If nothing happens to remove Fe^{2+} ions around the anodic site, the tendency of iron metal to dissolve will diminish. In oilfield systems, Fe^{2+} ions are commonly removed by reacting with oxygen and/or hydrogen sulphide and/or carbon dioxide. The corrosion products are precipitates or scales of rust (Fe_2O_3) or iron sulphides (FeS_x) or iron carbonate ($FeCO_3$) or as a mixture of all these compounds. Excess electrons flow away from the anodic site to a site where they form a cathode and where reduction occurs. Reduction of oxygenated water forms hydroxyl ions. If oxygen is not present, but CO_2 or H_2S, then the dominant cathodic reaction is the reduction of hydrogen ions to produce hydrogen gas. If the electrolyte is salty water, chlorine gas is produced [3].

Figure 1-1. Internal corrosion of a crude oil pipeline made of a mild steel. Reproduced from [3].

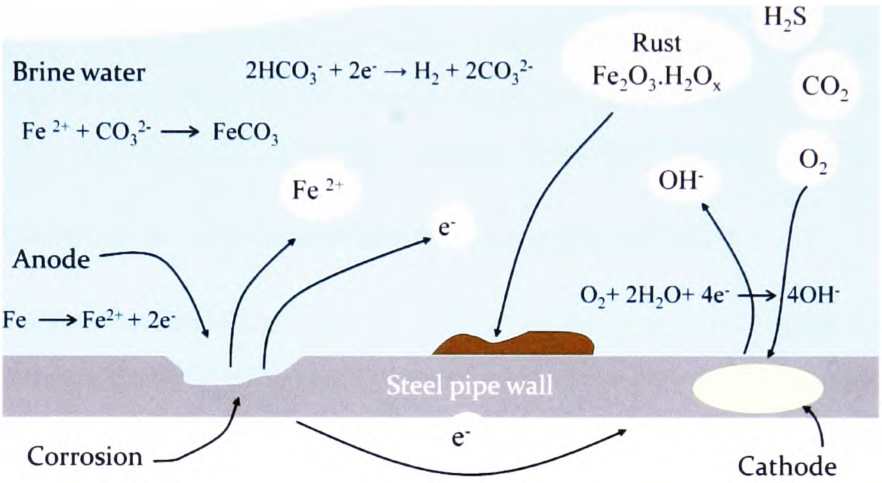

1.1.2. Corrosion control by organic corrosion inhibitors

The corrosion of metals cannot be stopped completely, but it can be controlled by decreasing the rate of corrosion. Corrosion control functions by eliminating or reducing the effectiveness of one or more of the corrosion cell components. Corrosion control methods in oilfield systems include cathodic protection, protective coatings, chemical inhibitors, plastic or cement liners, use of special alloys, solids removal and removal of corrosive gases.

In general, cathodic protection is an approach where the metal surface to be protected is made into the cathode of a corrosion cell. Since corrosion and material loss occurs at the anode, this approach protects the metal. Protective coatings can be used to protect tubing, downhole equipment, wellhead components and pressure vessels. Coatings work by reducing the cathodic area available for the corrosion reaction. The use of organic corrosion inhibitors is the most effective way of protecting internal corrosion of carbon steel pipelines for oil product transportation [4].

An inhibitor is a chemical compound which, when added to a system in a small quantity, serves to retard or reduce the corrosion rate of a metal exposed to a corrosive medium. There are many types of corrosion inhibitors with different modes of actions. Inhibition is used internally with carbon steel pipes and vessels as an economic corrosion control alternative to stainless steels, coatings and non-metallic composites. A particular advantage of the corrosion inhibitor is that it can be introduced *in-situ* without disrupting the transportation process and it adsorbs into the hard-to-reach surfaces inside the pipes. The major industries using corrosion inhibitors are oil and gas exploration and production, petroleum refining, chemical manufacturing, heavy manufacturing, water treatment and the product additive industries. The total consumption of corrosion inhibitors in the United States doubled from approximately 600 million in 1982 to nearly 1.1 billion US dollars in 1998 [2].

1.1.3. Mechanism of the corrosion inhibition by organic inhibitors

The corrosion inhibitors used in oilfield applications are organic or ioni compounds that are employed in small concentrations (less than 0.1 wt.%). They are often categorised as mixed inhibitors as they adsorb on the steel surface and inhibit both anodic and cathodic reactions. Almost all organic molecules used in oilfield corrosion inhibitor packages are strongly polar, with many being based on nitrogen, such as the amines [5], amides [6], imidazolines [7] or quaternary ammonium salts [8, 9] and compounds containing P, S and O elements [10]. Molecular structures for some of the most commonly used organic corrosion inhibitors in the oilfield system are given in Table 1-2. The organic corrosion inhibitors are typical surface-active agents due to the presence of hydrophilic and hydrophobic moieties within the same molecule.

Typically, the molecules have a hydrocarbon chain attached to the polar group, the length of which varies (e.g. carbon numbers between 12 and 18). The mechanism by which the organic corrosion inhibitor used to reduce the corrosion is not fully understood so far. The polar group of the molecule provides the functionality that displaces the water molecules from the surface (Figure 1-2). The adsorption of the corrosion inhibitor from aqueous solution onto the metal surface is driven by both of the polar head group and the hydrocarbon tail group. The concentration of inhibitor has a profound effect upon corrosion inhibition.

Table 1-2. Basic molecular structures of oil field corrosion inhibitors [10].

Chemical Name	Structure
Amide	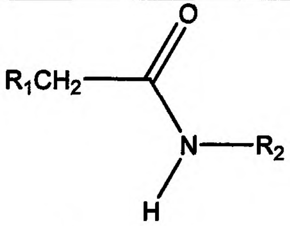
Primary amine	RCH_2NH_2
Imidazoline	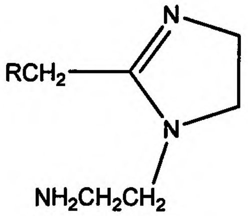
Quaternary ammonium ion	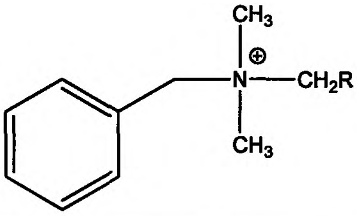

-R and R_1 represent different alkyl groups.

Figure 1-2. Schematic of action of oilfield corrosion inhibitor [10].

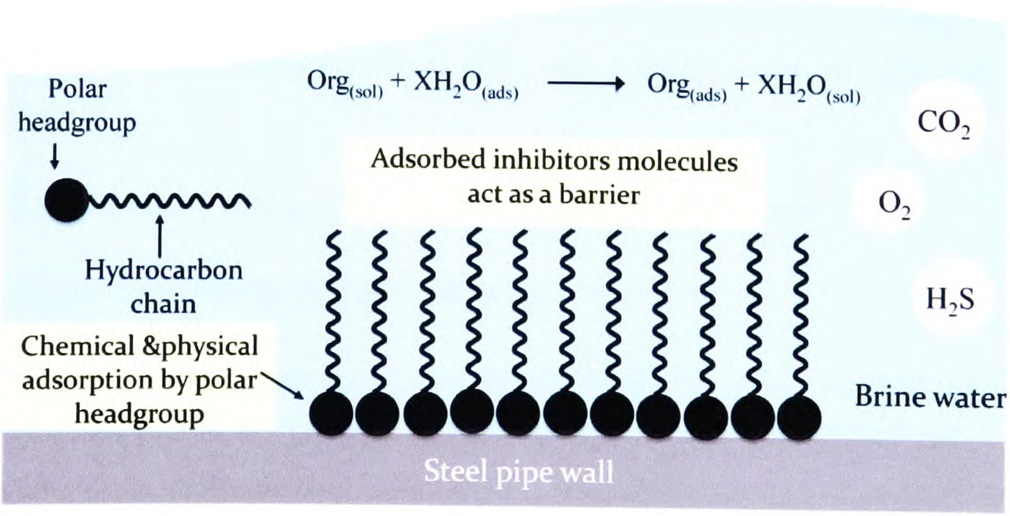

At low concentrations, the inhibitor adsorbs parallel or tilted onto the steel surface [11]. As the bulk concentration increases, the hydrophobic tail groups begin to protrude into the aqueous phase to accommodate more surfactant molecules, which increases the surface coverage. At the critical micelle concentration (cmc), a monolayer coverage is achieved and the tailgroups are parallel to each other and perpendicular to the metal surface [11] which becomes hydrophobic. McMahon has shown that the adsorption of oleic imidazoline onto steel surfaces produces a completely hydrophobic surface that has no affinity for water [12]. Therefore, the adsorbed corrosion inhibitor molecules are believed to act as a waterproof barrier between the corrosive aqueous phase and the steel pipe.

An investigation into the inhibition of iron corrosion by a series of imidazoline derivatives by Ramachandran *et al.* [13, 14] suggests a self-assembled monolayer mechanism for corrosion inhibition. The model suggests the following criteria for an efficient corrosion inhibitor:

I. Adequate solubility and rate of transport of the inhibitor from solution to the surface.
II. Strong binding of the surfactant headgroups to the metal surface.
III. Self-assembly of headgroups to form a dense and ordered layer.
IV. Self-assembly of hydrocarbon tails to form a hydrophobic barrier.

Commercially available oilfield corrosion inhibitors usually contain up to six surface active organic compounds dissolved in a carrier solvent. The carrier solvent can be water or an alcohol or a hydrocarbon. A low freezing point solvent (e.g. ethylene glycol) is required for products used in very cold conditions. Demulsifier species may also be included in order to reduce any impact on water-oil separation in the field [10].

1.2. SURFACTANT ASPECTS OF CORROSION INHIBITORS

1.2.1. General structure of corrosion inhibitors

As stated earlier, the organic corrosion inhibitors, by nature of their structure, are surfactants due to the presence of both hydrophilic and hydrophobic moieties within the same molecule. An example of a frequently used corrosion inhibitor molecule is shown in Figure 1-3. The amphiphilic nature of corrosion inhibitors has not been fully used in interpreting their corrosion inhibition performance until very recently [15, 16]. Surfactants are amphiphilic molecules, comprising a hydrophilic part (usually referred to as the head group) and a hydrophobic part (often referred to as the tail group). A surfactant molecule may consist of one, two or three tail groups. Surfactants are classified according to the nature of their headgroup and examples of anionic head groups include sulphonates, sulphates and carboxylates. Cationic headgroups are usually quaternary ammonium or alkyl pyridinium compounds. The zwitterionic surfactants, which are surfactants with both positive and negative groups present in the headgroup, include betaines and sulphobetaines. The fourth class is non-ionic surfactants. The vast majority of non-ionic surfactants contain a polyoxyethylene headgroup.

Figure 1-3. Schematic diagram of an alkylbenzyldimethylammonium chloride corrosion inhibitor (CnBDMAC).

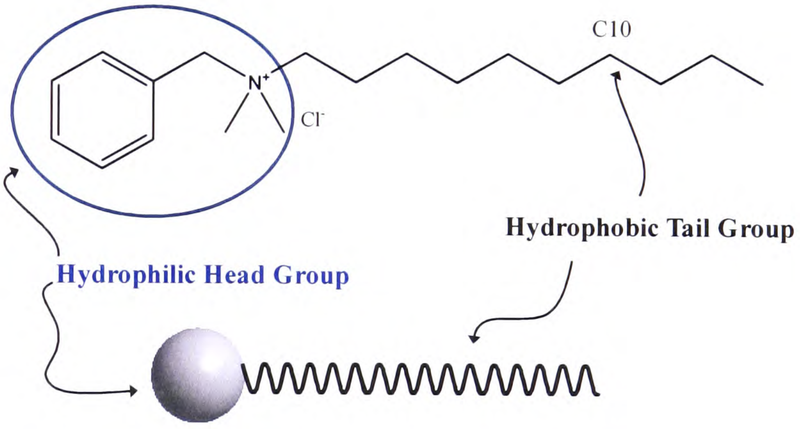

1.2.2. Adsorption of surfactants at the air-water interface

When a surfactant molecule is added to water, the hydrophilic head group is in a medium of similar polarity to itself but the hydrophobic tail group is not. For this reason, it tends to distribute itself between the bulk solution and the interface between water and air. At the interface, the tail group projects into the air, while the head group remains in the water. The adsorption of surfactant molecules at the air-water interface lowers the polarity difference between air and water, and therefore, lowers the surface tension as well. The surface tension decreases with increasing surfactant concentration as the amount of adsorbed surfactant increases and reaches a saturation value at the cmc (Figure 1-4).

For an uncharged solute, the surface tension changes as a function of the solute activity according to the Gibbs' adsorption equation [17]:

$$\Gamma = -(\frac{1}{RT} \cdot \frac{d\gamma}{d\ln a}) \tag{1-1}$$

where γ is the surface tension, Γ is the surface excess concentration at the air-water interface, R is the gas constant, T is absolute temperature and a is the activity of surfactant. The Gibbs' adsorption equation shows that Γ is positive when the surface tension is lowered by the addition of surfactant. Positive values of Γ indicate that the concentration of surfactant at the surface is higher than that in the bulk solution. The surface tension of pure water (72 mN m^{-1} at 293 K) can be reduced to about 30-35 mN m^{-1} by adding a surfactant with a sufficiently long hydrocarbon chain [18]. The above equation is applicable to non-ionic surfactants, neutral molecules or ionic surfactants in the presence of excess inorganic electrolytes (with respect to the surfactant concentration). For monovalent ionic surfactants with monovalent counterions (1:1 ionic surfactants) and zero added electrolyte, both the anions and cations adsorb at the surface to maintain local electrical neutrality, therefore a factor of two is needed for this in the Gibbs' equation. The modified equation for ionic surfactants is:

$$\Gamma = -(\frac{1}{2RT} \cdot \frac{d\gamma}{d\ln a}) \tag{1-2}$$

If a non-adsorbed electrolyte is present in large excess then the Gibbs adsorption equation for 1:1 ionic surfactants reduces to equation (1-1).

1.2.3. Aggregation of surfactant in aqueous solution

As more and more surfactant molecules are added to the solution, it eventually becomes energetically more favourable for them to form aggregates in the bulk solution rather than adsorb further at the interface. The concentration at which this happens is called the critical micelle concentration (cmc). A surfactant micelle is schematically represented in Figure 1-5.

Figure 1-4. The effect of surfactant adsorption at the air-water interface on the solution surface tension [19].

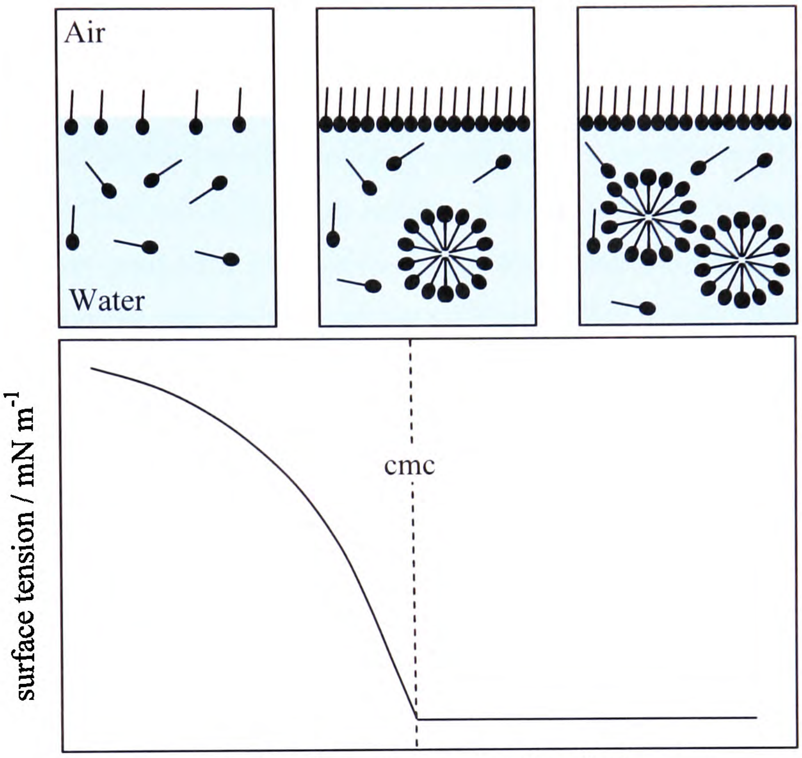

ln (surfactant concentration / M)

A micelle is an aggregate of surfactant molecules with hydrophilic headgroups directed into the bulk solution and hydrophobic tails towards the inner space of the micelle. Inside the micelle, practically no water molecules are present, and thus no energetically unfavourable hydrocarbon-water interactions occur.

Figure 1-5. Schematic diagram of a surfactant micelle.

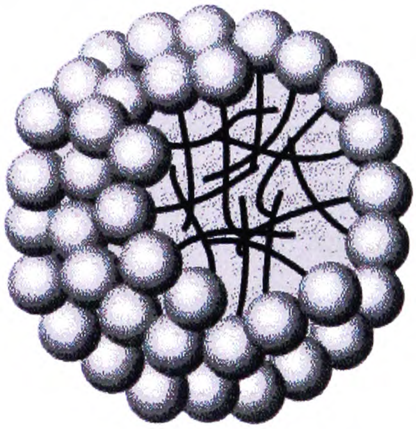

Generally, micelles can exist in a spherical, rod-like and disc shaped structures depending on the length of the hydrocarbon chain, the size of the hydrophilic head group and the aggregation number (the number of surfactant molecules comprising the micelle) [20].

Micellisation is a reversible chemical process. There is an equilibrium condition for micellisation between surfactant molecules in micelles and those at the saturated surface. The cmc in aqueous solution is a characteristic property for the surfactant at a given temperature and an inorganic electrolyte concentration. Micelles can only form when the temperature is above the Krafft point. The Krafft point is the temperature (more precisely, narrow temperature range) above which the solubility of a surfactant in the aqueous solution rises sharply [21].

1.3. MICROEMULSIONS AND EMULSIONS

1.3.1. Equilibrium microemulsion phase behaviour and its relation to the preferred monolayer curvature

As for the air-water interface, surfactants adsorb at the oil-water interface. Water and hydrocarbon oils when placed together will commonly separate into two phases. When surfactant is added to such a system, its state of lowest energy occurs when it is adsorbed at the interface with the head group in the water phase and the tail group in the oil phase. Again, adsorption continues until a critical concentration, known as the critical microemulsion concentration (cμc), is reached [20]. At this concentration, aggregates form either in the water phase, the oil phase or in a third phase depending on a number of factors to be discussed in the following sections.

Microemulsions are thermodynamically stable dispersions of oil and water stabilised by a surfactant. Microemulsions generally appear transparent because the dispersed droplet size is typically 5-50 nm and are similar in structure to the micelles in that they arrange themselves so that the part of the surfactant with a polarity most like the solvent is on the outside of the aggregate and the other is held in the core. Thus for equal volumes of oil and water, if the aggregates form in the water phase, the head groups are on the outside and if the aggregates are formed in the hydrocarbon oil, the tail groups are on the outside.

The microemulsion type formed in a surfactant + water + oil system, where the surfactant concentration is above the cμc, is dependent on the preferred curvature of the surfactant molecule. The preferred curvature of the surfactant monolayer is controlled by geometrical packing considerations of the adsorbed molecules. The packing factor, P, can be defined as [22]:

$$P = \frac{A_h}{A_t} \tag{1-3}$$

where A_h is the effective area of the surfactant tail group and A_t is the effective area of the surfactant tail group.

A Winsor I microemulsion system contains oil-in-water (o/w) aggregates in the water phase plus an excess oil phase (Figure 1-6). The preferred monolayer curvature for this system is positive (i.e. the effective area of the head group is larger than the effective area of the chain region, P > 1). Alternatively, a Winsor II microemulsion system contains water-in-oil (w/o) aggregates in the oil phase plus an excess water phase and the preferred monolayer curvature is negative. In between these two cases the net curvature is approximately zero and a three phase system is commonly formed. The third phase can either be a bicontinuous microemulsion, which consists of regions of positive and negative curvature (with zero net curvature), or a lamellar phase with planar arrays of surfactant and alternate layers of oil and water. The other two phases are excess oil and water. This is called a Winsor III system [20].

Figure 1-6. Schematic representation of the transition from a two-phase system with an oil-in-water droplet microemulsion (Winsor I) to a three phase system with a bicontinuous microemulsion (Winsor III) to a two-phase system with a water-in-oil droplet microemulsion (Winsor II). The shaded areas represent microemulsions.

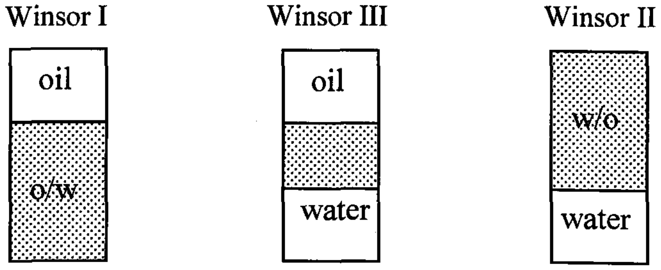

In Winsor I, II and III systems, the system is free to adopt a spontaneous curvature since the droplets are free to swell or shrink by more or less solubilisation of the excess dispersed phase until the preferred droplet size (and hence preferred monolayer curvature) is attained at equilibrium. It is possible to produce a change in curvature by affecting the relative sizes of the surfactant head group and tail group, hence yielding a Winsor progression (Winsor I → Winsor III → Winsor II). If a surfactant + water + oil system is initially a Winsor I microemulsion with aggregates of positive curvature, changing certain parameters of the system can either reduce the effective area of the head group or increase the effective area of the tail group. This in turn reduces P, reduces curvature and causes the system to move through a progression Winsor I → Winsor III → Winsor II that is known as microemulsion phase inversion [23].

Several factors may cause this progression and they are surfactant dependent [24-26]. Changing the surfactant molecular structure changes the effective area of the headgroup and tailgroup and thus affects the preferred curvature. For non-ionic surfactants, temperature effects are large [23]. At low temperatures, the aggregates form in the water phase (Winsor I). As the temperature is increased it has the effect of dehydrating the head group of the surfactant, reducing A_h and P, and thus causing a phase inversion from o/w into w/o microemulsion. Changing the curvature of ionic surfactants can be achieved by adding an electrolyte to the system. This has the effect of screening the repulsions that exist between the charged headgroups, thus reducing the monolayer curvature [25].

1.3.2. Relation between emulsion type and Winsor behaviour

Emulsions are defined as thermodynamically-unstable mixtures of two or more immiscible liquids (usually oil and water) where one phase is dispersed in the other as drops [27]. Simple emulsions can be either oil-in-water (o/w) or water-in-oil (w/o). For o/w emulsions, oil drops are dispersed in an aqueous continuous phase and in w/o emulsions water drops are dispersed in an oil continuous phase. Preparation of an emulsion requires the formation of a large interfacial area between the two liquids. The work required to disperse one liquid within another remains in the system as a potential energy. This means that the system is thermodynamically-unstable and must reduce this energy by decreasing the interfacial area. Therefore, an emulsion will eventually separate into the two bulk phases, if is not stabilised by an appropriate emulsifier. Emulsifiers are surfactants, which facilitate emulsion formation by reducing the interfacial tension between the two immiscible liquids through adsorption at the oil-water interface. The reduction in the interfacial tension reduces the amount of work required to produce the emulsion but the system will only be thermodynamically stable if the interfacial tension can be reduced to near zero. However, emulsions can be considered to be kinetically stable, if the rate of separation of the two phases is sufficiently slow.

It is always observed that in mixtures of equal volumes of water and oil, the type of emulsion formed by the homogenisation of Winsor I or II systems is the same as the equilibrium microemulsion type [27]. For a ternary mixture of oil, water, and surfactant, which phase separates into a surfactant-rich aqueous phase containing an o/w microemulsion and almost pure oil (Winsor I), the surfactant is said to have a positive spontaneous curvature. Under stirring, an o/w emulsion is obtained from a Winsor I system. For a ternary mixture of oil, water, and surfactant, which phase separates into an oil phase containing a w/o microemulsion, and almost pure water (Winsor II), on stirring, a w/o emulsion is obtained. In other words, emulsification of a Winsor I system generally produces an o/w emulsion, the continuous phase of which is an o/w microemulsion. On the other hand, emulsification of a Winsor II system generally produces a w/o emulsion, the continuous phase of which is a w/o microemulsion.

1.3.3. Emulsion stability

Emulsions are thermodynamically unstable. Hence, their stability is a kinetic rather than a thermodynamic effect. Emulsion stability can be favoured by the formation of a mechanically strong and elastic interfacial film and electrostatic repulsion between the dispersed droplets, depending upon the nature of the emulsifier [27]. In emulsion studies, an emulsion is considered stable, if it is resistant to physical changes over a practical length of time. Several physical processes can indicate instability in an emulsion. The different methods by which an emulsion can become unstable or breakdown are outlined in Figure 1-7 [28].

During destabilization by the flocculation of an emulsion Figure 1-7 (a), droplets come together and form aggregates without losing their original size as illustrated in Figure 1-7 (b). Flocculation depends on the forces between the droplets, which include van der Waals interactions, electrostatic forces and a variety of short-range forces. Creaming and sedimentation processes shown by Figure 1-7 (c) can take place where the size and size-distribution of emulsion droplets do not change. Creaming and sedimentation are caused by gravity, creating a concentration gradient due to density differences of the two immiscible liquids. For example, oil droplets from an o/w emulsion may be subject to creaming when the oil has a lower density than the aqueous phase. Ostwald ripening shown in Figure 1-7 (d) occurs in emulsions where the dispersed phase has a limited solubility in the continuous phase so that large drops grow as smaller drops decrease in size due to transport of the soluble liquid from the small droplet to the large droplet through the continuous phase. Coalescence shown in Figure 1-7 (e) is a phenomenon where many droplets merge to create fewer larger droplets, thereby reducing the total interfacial area of the system. Clearly, the emulsion droplet size-distribution is not conserved and ultimately complete coalescence can occur to yield the two bulk liquids. Another process by which an emulsion is transformed is phase inversion. During this process, the dispersed phase becomes the continuous phase and vice versa. These breaking mechanisms can take place simultaneously or consecutively, depending on several factors.

Figure 1-7. The different processes involved in the breakdown of an unstable emulsion [28].

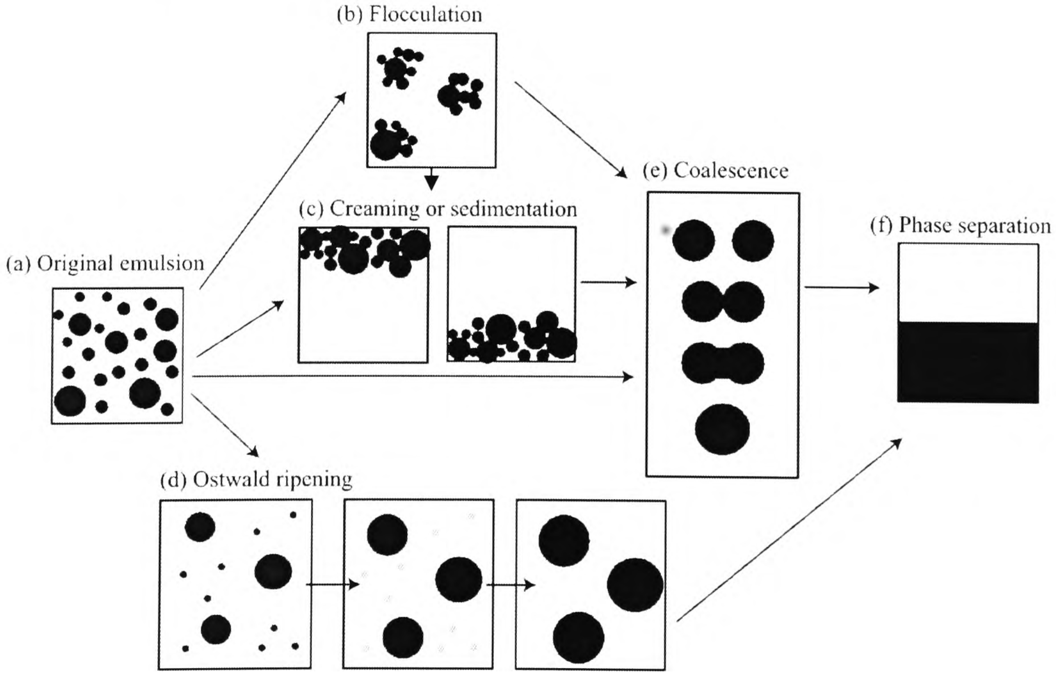

1.4. SURFACTANT ADSORPTION AT THE SOLID-LIQUID INTERFACE

Corrosion inhibitors protect metals against corrosion by adsorbing onto the surface where it acts as a barrier between the metal surface and the corrosive media. Accordingly, the inhibitor efficiency is directly related to the amount of surface-active inhibitor adsorbed as well as the structure of the adsorbed surfactant layer. In this section, we are going to discuss some of the basic concepts about the adsorption of surfactants (mainly ionic surfactants) at the solid-liquid interface (polar surfaces). These include the electrical properties of surfactant ions near the metal surface, the mechanism of ionic surfactant adsorption, the adsorption isotherms and finally recent models for ionic surfactant adsorption at the solid-liquid interface.

1.4.1. The nature of metal-aqueous solution interface and the Electrical Double Layer (EDL)

Most solid surfaces become charged when placed into aqueous solution. Different processes can lead to charging such as ions adsorbing to a surface or dissociating from it. Most metal oxides are often negatively charged when in contact with aqueous neutral solution due to the dissociation of protons from the surface hydroxyl groups ($MOH \rightarrow MO^- + H^+$). These surface charges cause an electric field, which attracts counterions to maintain electrical neutrality. The layer of surface charges and counter ions is called "The Electric Double Layer" [29].

The concept of the existence of the double layer at a flat surface of a metal in contact with an aqueous solution appeared in 1879 by Helmholtz [30]. This first theoretical model assumed the presence of a *compact layer* of ions in contact with the charged metal surface. The next model of Gouy [31] and Chapman [32], involves *a diffuse double layer* in which the accumulated ions, due to the Boltzmann distribution, extend to some distance from the solid surface. In further developments, Stern [33] suggested that the solid-liquid interface includes both the rigid Helmholtz layer and the diffuse one of Gouy and Chapman. Specific adsorption of ions at the metal surface was pointed out by Graham in 1947 [34]. In 1963, Bockris *et. al.* [35] pointed out the role of the solvent at the interface. They suggested that orientation of solvent molecules would occur depending on the excess charges at the electrode and the presence or absence of specifically adsorbed ions at the surface.

In the Gouy-Chapman-Stern model (Figure 1-8), the double layer is divided into two parts: an inner part, the Stern layer, and an outer part, the Gouy or diffuse layer. Essentially, the Stern layer is a layer of ions that is directly adsorbed to the surface and that is immobile. In contrast, the Gouy-Chapman layer consists of mobile ions. The Stern layer is then subdivided into an *inner Helmholtz layer* (IHL) and an *outer Helmholtz layer* (OHL). The IHL contains ions that are specifically adsorbed and bind tightly at a short distance. Due to the size of the counter ions, which in water might include their hydration shell, the adsorbed solvated cations cannot get infinitely close to the surface, but always remain at a certain distance and will be located in the OHL. Two planes are usually associated with the double layer. The first one, the inner *Helmholtz plane* (IHP), passes through the centre of specifically adsorbed ions. The second plane is called the outer *Helmholtz plane* (OHP) and passes through the centres of the hydrated ions that are in contact with the metal surface [37].

A good model for the structure of many metallic surfaces in an aqueous medium is shown in Figure 1-8 [36]. The metal oxide itself is negatively charged. This can be due to an applied potential or due to the dissolution of metal cations. Certain anions can bind specifically to metal. Water molecules show a distinct preferential orientation and they determine the inner Helmholtz plane. Next, comes a layer of non-specifically adsorbed counter ions with their hydration shell. This layer specifies the outer Helmholtz plane. Finally, there is the diffuse layer.

The change in the electric potential within the double layer is illustrated in Figure 1-9. It is assumed that the solid surface is negatively charged. The figure shows the variation of electrical potential from the metal surface, where its value is ψ^o, to a distance far into the solution, where the potential is taken as zero. The potential at the OHP, at distance *d* from the surface, is called the *diffuse-layer potential*, ψ^d (also known as the *Stern potential*, ψ^s): it is the potential at the beginning of the diffuse part of the double layer. The potential at the IHP, located at distance β ($0 \leq \beta \leq d$) from the surface, the IHP potential, is given the symbol ψ^i. All potentials are defined with respect to the potential in bulk solution. Generally there will be various dissolved salts in the aqueous phase and hence a range of cations and anions. In fact, because of electrostatic repulsion, there will also be a deficit of co-ions (anions in this case) close to the charged surface.

Figure 1-8. Schematic model of the electrical double layer (EDL) at the metal oxide-aqueous solution interface, showing elements of the Gouy-Chapman-Stern model, including specifically adsorbed anions (Graham model). Reproduced with modifications from [36].

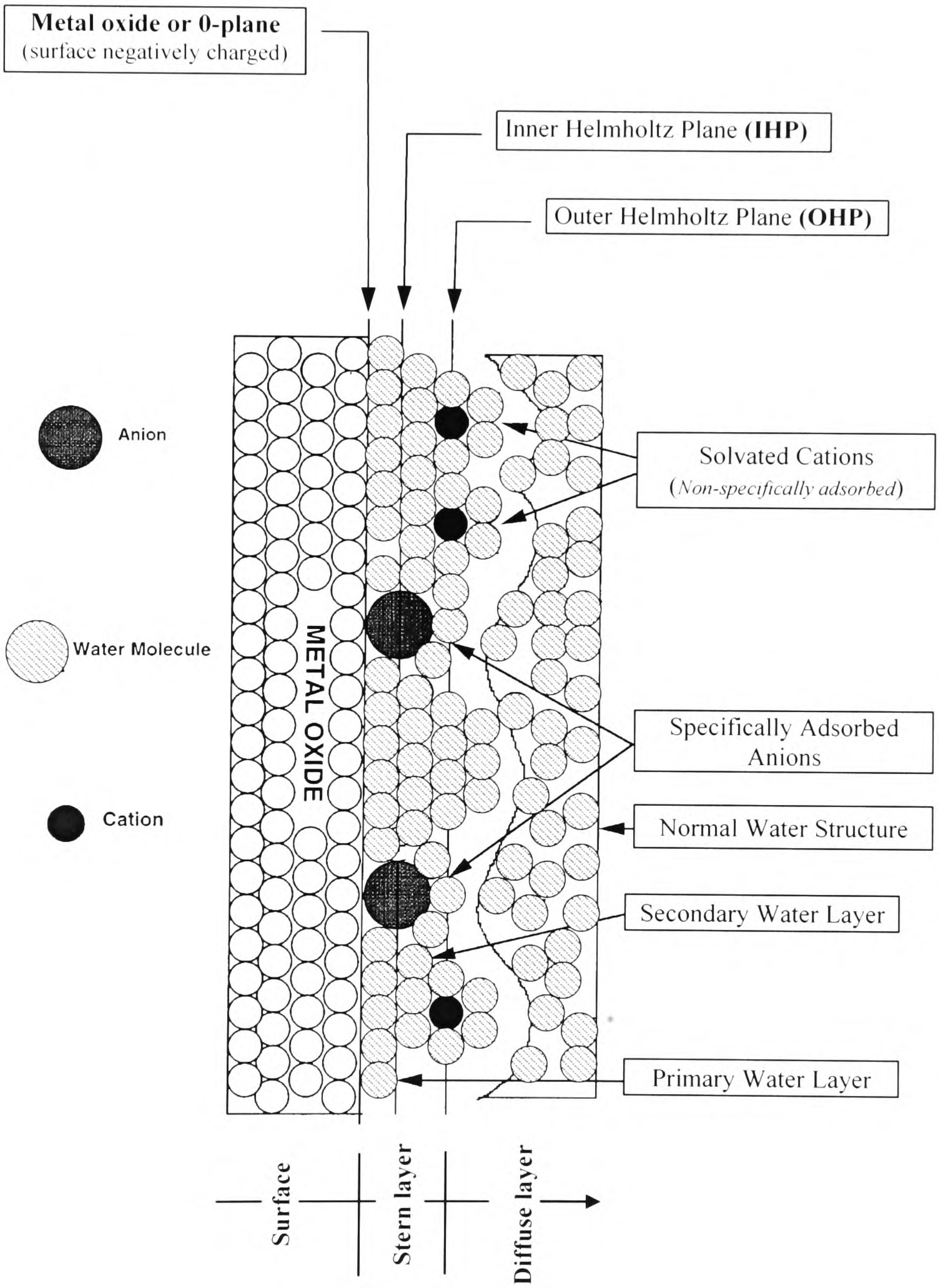

Figure 1-9. Schematic representation of the charges and potentials at a negatively charged interface. The IHP (electric potential ψ^i; charge density σ^i) is the locus of specifically adsorbed ions. The diffuse layer starts at x = d (OHP), with potential ψ^d and charge density σ^d. The slip plane or shear plane is located at x = d^{ek}. The potential at the slip plane is the electrokinetic or zeta-potential, ζ. The electrokinetic charge density is σ^{ek}. Adapted from [37].

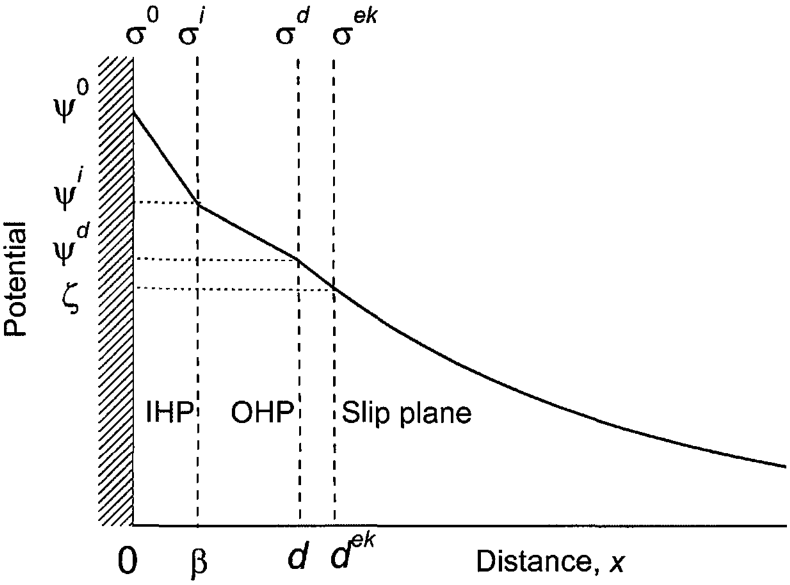

All of the surface charge is compensated by excess counterions in the double layer region. The system as a whole (charged surface and solution) is electrically neutral. The surface-charge density is denoted σ^o, the charge density at the IHP denoted σ^i, and that in the diffuse layer σ^d. As the system is electroneutral [37]:

$$\sigma^o + \sigma^i + \sigma^d = 0 \qquad (1\text{-}4)$$

The potential varies in an approximately exponential manner from the Stern plane into the solution, through the diffuse layer. Tangential liquid flow along a charged solid surface can be caused by an external electric field (*electrophoresis, electro-osmosis*) or by an applied mechanical force (*streaming potential*). In such tangential motion, a very thin layer of fluid adheres to the surface. This thin layer is called the *hydrodynamically stagnant layer*, which extends from the surface to some specified distance, d^{ek}, where a so-called hydrodynamic slip plane is assumed to exist.

The potential at the plane where slip with respect to bulk solution is postulated to occur is identified as the *zeta-potential* (ζ) [37]. The OHP has been interpreted earlier as a sharp boundary between the diffuse and the non-diffuse parts of the EDL, but it is very difficult to locate it exactly. The same applies for the slip plane.

1.4.2. Adsorption isotherms

The investigation of the adsorption behaviour of a surfactant or any solute at a solid-liquid interface begins traditionally with the determination of the adsorption isotherm. An adsorption isotherm shows the relationship between the amount of surfactant adsorbed (Γ) at the solid-liquid interface per unit mass or unit area of the solid adsorbent and the residual or equilibrium surfactant concentration ($C_{eq.}$) at given temperature and pressure. At high surfactant concentrations, the amount of surfactant adsorbed reaches a limiting value, which does not increase with further increase of surfactant concentration. This value is usually referred to as the maximum amount of adsorbed surfactant (Γ_{max}). The degree of surface coverage (θ), given by equation (1-5), may replace the amount of adsorbed surfactant in the adsorption isotherm.

$$\theta = \frac{\Gamma}{\Gamma_{max}} \qquad (1\text{-}5)$$

Experimental adsorption isotherms are usually plotted on three major scales: double linear (lin-lin), linear-logarithmic (lin-log) and double logarithmic (log-log) [38]. The different presentations allow a more detailed analysis of the adsorption behaviour to be made. On a log-log scale, different regions can be clearly distinguished in the isotherm. These regions are believed to reflect distinct modes of interactions among surfactant molecules and between the latter and the solid surface. Moreover, the effects of surface heterogeneity and cooperative adsorption, which occur at very low surface coverages, show up most clearly in log-log plots. The plateau adsorption region markedly manifests itself only on a linear scale [38].

1.4.3. Classification of the adsorption isotherm shapes

Giles *et al.* [39] proposed a general classification for the commonly observed adsorption isotherms. According to this classification, isotherms for the adsorption of organic solutes onto solids are divided into four main classes, according to the slope of the initial part of the curve. Figure 1-10 shows shapes of the different adsorption isotherm classes reported by Giles. The four main classes are:

I. C Curves (constant partition) are linear curves, given by solutes which partition between the solid and the liquid by a constant ratio at any solute concentration. This ratio is usually named ''*the distribution coefficient*'' or ''*the partition coefficient*''.

II. L Curves, (Langmuir isotherms) are usually the ratio between the residual organic solute in solution and that adsorbed onto the solid, which decreases when the solute concentration increases, providing a concave curve. It suggests a progressive saturation of the solid. One usually makes two sub-groups in which the curve reaches a plateau or does not reach a plateau.

III. H Curves (high affinity) is a particular case of the ''L'' isotherm, where the initial slope is very high.

Figure 1-10. The four main types of adsorption isotherms.

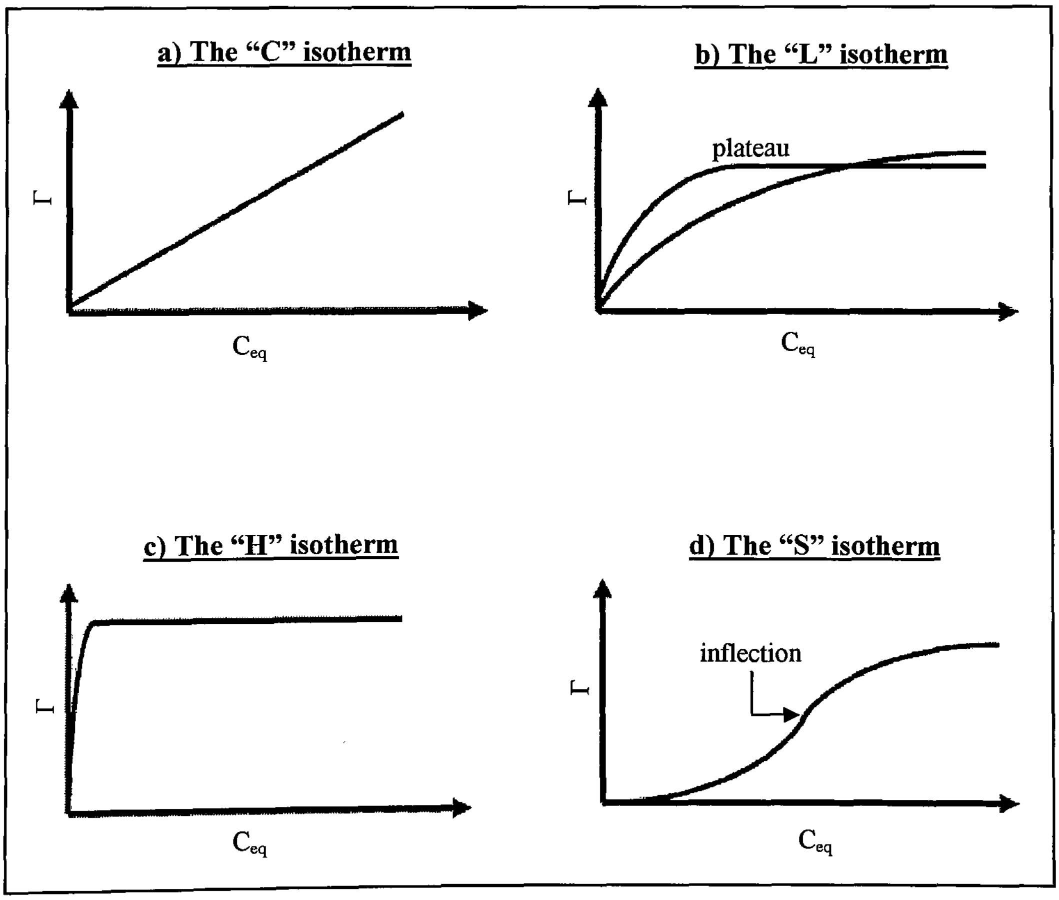

a) The "C" isotherm

b) The "L" isotherm

c) The "H" isotherm

d) The "S" isotherm

IV. In S Curves, the curve is sigmoidal and thus has a point of inflection. The shape of the isotherm is believed to reflect two or more distinct modes of adsorption. The adsorption isotherm for an ionic surfactant onto an oppositely charged solid surface, for example, sodium alkanesulfonates on positively charged alumina particles, is typically S-shaped [40].

1.4.4. Mechanisms of surfactant adsorption

The adsorption of surfactants at the solid-liquid interface is controlled by several factors, which could be summarized by the following three factors:

I. the chemical nature of the species being adsorbed, including the nature of the headgroup (anionic, cationic, non-ionic, etc.) and that of the hydrophobic tailgroup (length and nature of the chain, degree of branching, etc.).

II. the nature of the solid surface onto which the surfactant is being adsorbed (highly charged, nonpolar, etc.).

III. the properties of the solution (polarity, pH, electrolyte content, temperature, additives, etc.).

A slight change in one of these factors could result in a significant change in the adsorption characteristics of the system. The mechanisms of surfactant adsorption are generally parallel to those operative in all intermolecular interactions. Those interactions include electrostatic attraction, covalent bonding, hydrogen bonding or non-polar interactions between the adsorbent and the adsorbate species, and lateral interaction between the adsorbed species as well. However, they often act together successively or even simultaneously in the course of the adsorption process. Accordingly, the net driving force for adsorption ΔG^{o}_{ads} can be considered to be the sum of a number of contributing forces [41]:

$$\Delta G^{o}_{ads} = \Delta G^{o}_{elec} + \Delta G^{o}_{chem} + \Delta G^{o}_{c-c} + \Delta G^{o}_{c-s} + \Delta G^{o}_{H} + \cdots \qquad (1\text{-}6)$$

where ΔG^{o}_{elec} is the electrostatic interaction term, ΔG^{o}_{chem} is the chemical term due to covalent bonding, ΔG^{o}_{c-c} is the lateral interaction term due to chain-chain interactions among adsorbed long-chain surfactant species, ΔG^{o}_{c-s} is due to interaction between hydrocarbon chains and hydrophobic sites on the solid and ΔG_H° is the hydrogen bonding term.

For each surfactant-solid-solvent system, several of the above terms can be significant depending on the solid and the surfactant type, surfactant concentration, electrolyte, solvent and temperature.

1.4.5. Classical analysis of the adsorption isotherms

As no-generally-valid adsorption isotherm for the adsorption from liquids onto solid surfaces exists, most of the commonly used isotherms were derived for gas adsorption, but often they apply well for the adsorption from the liquid phase .

The Henry isotherm is the simplest adsorption model in which the degree of surface coverage is proportional to the equilibrium concentration:

$$\theta = K_H C_{eq.} \tag{1-7}$$

where K_H is the adsorption or partition coefficient. This is commonly termed as Henry's constant. The Henry isotherm is valid for low surface coverage (e.g., at $\theta \leq 0.1$). Another type of adsorption isotherm that is commonly observed in the adsorption of surfactants from solutions is the Langmuir-type isotherm [42], given by the following equation:

$$\theta = \frac{K_L C_{eq}}{1 + K_L C_{eq}} \tag{1-8}$$

where K_L is the equilibrium adsorption constant in M^{-1} when C_{eq} is M. The Langmuir adsorption model is valid in systems where (a) the adsorbent is homogeneous, (b) the adsorption occurs onto localized sites and involves no interactions between adsorbed molecules and (c) the maximum amount of surfactant adsorbed is limited to a monolayer. However, several isotherms involving surfactants have been shown to fit the Langmuir model even when the aforementioned boundary conditions are not met.

An adsorption model empirically found by Freundlich [43] for the adsorption from the liquid phase can be represented as follows:

$$\Gamma = K_f (C_{eq})^n \tag{1-9}$$

where K_f is the equilibrium adsorption constant and n is a dimensionless constant. When n = 1 the Henry equation applies again.

In the Freundlich model, the adsorption is no longer monolayer and several layers of adsorbate can be attached to the adsorbent. Moreover, the energy required for adsorption is not constant, but varies and is exponentially distributed. In order to model adsorption onto heterogeneous surfaces, the Langmuir–Freundlich adsorption model [44] was derived from the empirical Freundlich isotherm [19] by postulating that at infinite concentrations the adsorption coverage has to attain unity, which is not the case for the Freundlich isotherm. The model describes multisite adsorption onto heterogeneous surfaces neglecting interactions between adsorbed species. It is given by the following equation:

$$\theta = \frac{(K\,C_{eq})^h}{1+(K\,C_{eq})^h}. \tag{1-10}$$

where K is the adsorption constant and h $(0 \leq h \leq 1)$ is the heterogeneity parameter.

Taking the lateral interactions between the adsorbed molecules into aount produces the Frumkin isotherm [45].

$$K\,C_{eq} = \left[\frac{\theta}{1-\theta}\right]\exp(-2a\theta) \tag{1-11}$$

where the parameter a is a measure of the lateral interactions between adjacent adsorbed molecules. A positive value of the parameter a indicates a co-operative adsorption.

1.4.6. Recent models for the surfactant adsorption

1.4.6.1. The hemi-micelle or the four-region model

The hemi-micelle model was initially postulated by Gaudin and Fuerstenau [46] and developed by Fuerstenau and Somasundaran [40]. According to this model, the adsorption mechanism of ionic surfactants onto a hydrophilic solid surface is divided into three regions. In the first region (low surfactant concentrations), the surfactant adsorption takes place through ion exchange with ions in the electric double layer. During this exchange, the ζ-potential remains almost unchanged. In region II, upon increasing the surfactant concentration, the effect of hydrophobic interactions of hydrocarbon chains becomes more important and two-dimensional aggregates, called the hemi-micelles, are formed. According to Fuerstenau *et al.*

[47], this phenomenon is analogous to micellization in the bulk phase and at the solid-water interface is called hemi-micellization. After reaching the concentration at which the sign of the ζ-potential reverses, the electrostatic interaction and specific adsorption are opposed to each other and the slope of the adsorption isotherm gets reduced (region III).

A typical isotherm is the adsorption of negatively charged sodium dodecyl sulfate (SDS) onto positively charged alumina, which is shown in Figure 1-11 [40, 48]. It can be seen that the electrophoretic mobility changes sign and then increases with surfactant concentration.

Later on, Somasundaran and Fuerstenau extended the hemi-micelle model into the *four-region* or the *reverse-orientation* model [40, 49] for ionic surfactants adsorbed onto oppositely charged solid surfaces. In region I, surfactant monomers are electrostatically adsorbed to the solid surface with head-groups in contact with the surface. The hydrophobic tail-groups may interact with any hydrophobic regions on the solid surface. Region II involves strong lateral interactions between the adsorbed monomers, resulting in the formation of hemi-micellear aggregates. In the hemi-micelle, the surfactants are oriented with their charged headgroups toward the solid surface, while the hydrocarbon chains project into the aqueous phase, thus forming hydrophobic patches on the surface. Further adsorption results in an increasing number of surfactant aggregates, with molecules adsorbing in an opposite orientation once the surface is neutralized by the oppositely charged surfactant. Other researchers believe that the second layer of adsorbed aggregates is not present until region III, which accounts for the change in slope [30, 31].

Adsorption in region III occurs through the growth of aggregates already formed in region II without an increase in the number of aggregates. The transition between region II and region III is thought to be due to neutralisation of the surface charge. Finally, in region IV, the surface morphology is assumed to be a fully-formed bilayer. Further increases in the solution surfactant concentration do not lead to any further increases in the surface excess.

1.4.6.2. The admicelle model of Harwell

The admicelle or bilayer model for the adsorption of surfactants onto heterogeneous solid surfaces was presented by Harwell *et. al.* [50, 51].

Figure 1-11. Characteristic regions of ionic surfactant adsorption onto hydrophilic solids according to the hemimicelle model. Adapted from [40, 48].

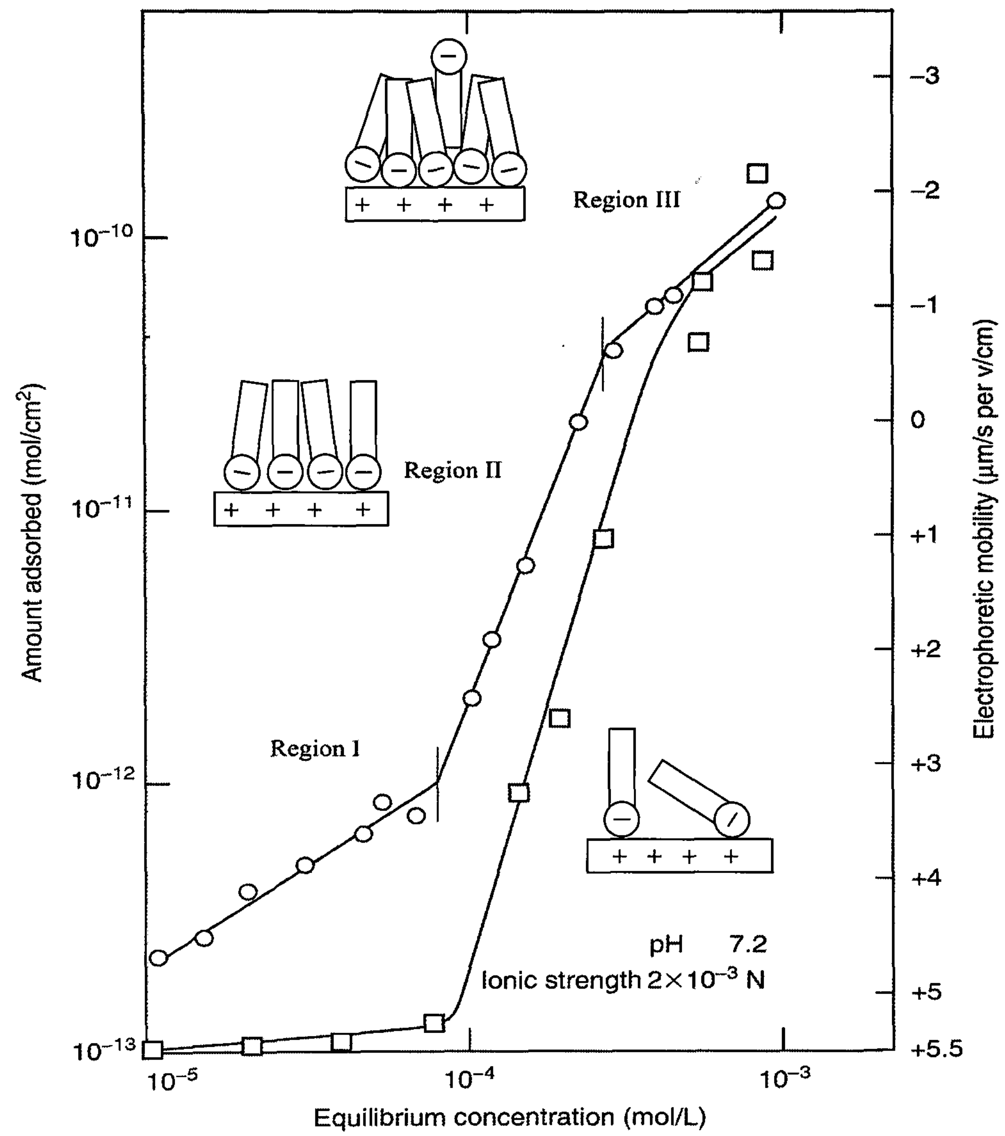

The model (Figure 1-12) divides the course of an adsorption isotherm into the following four regions:

I. *Region I* corresponds to a low surface coverage without signs of aggregate formation.

II. *Region II* is characterized by a large slope increase in the adsorption isotherm due to the beginning of aggregate formation. The aggregates are bilayer structures and form on patches on the solid surface without hemi-micelles. These patches of surfactant bilayers were called "*admicelles*". The concentration at which the region I/region II transition occurs is referred to as the critical admicelle concentration (cac).

III. *Region III* is characterized by a decrease in the adsorption isotherm slope. This is caused either by electrostatic repulsion of surfactant ions on the surface or due to the presence of adsorption sites with different energies. In region II, the high-energy sites will be occupied and the slope in region III is due to the beginning of adsorption to the low-energy sites.

Figure 1-12. Schematic of a typical ionic surfactant adsorption isotherm from aqueous solution onto a hydrophilic solid surface according to the admicelle model. Adapted from [52].

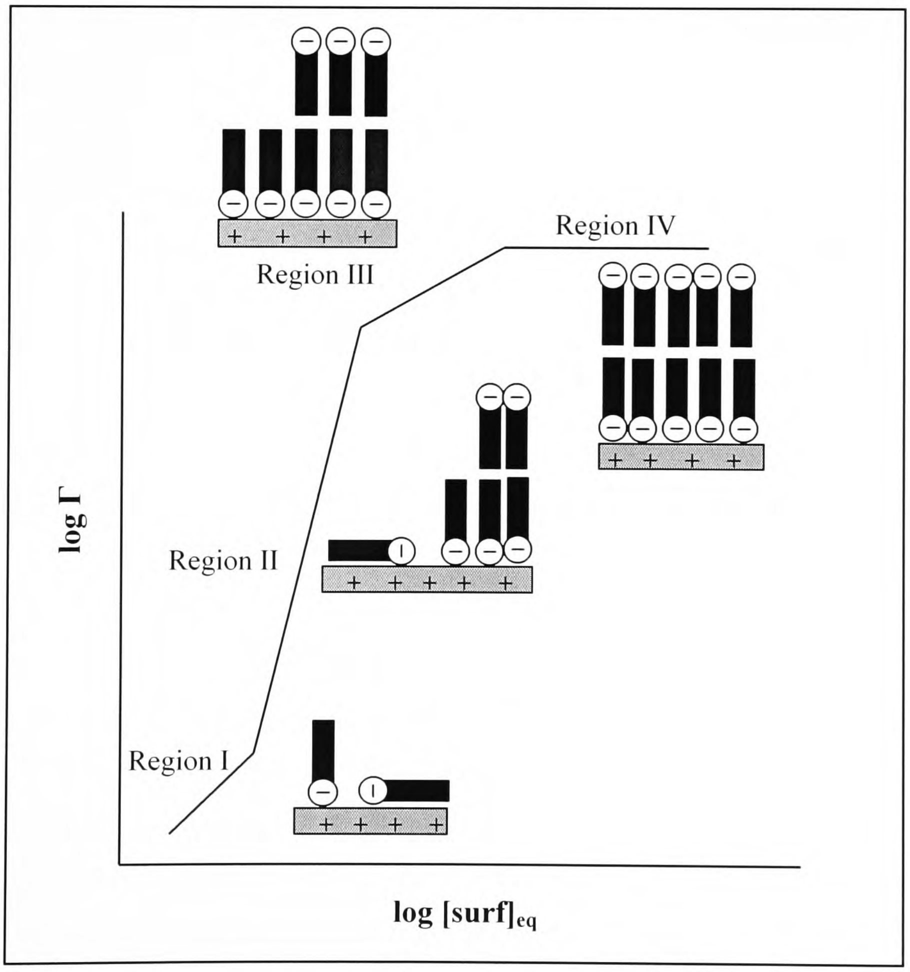

IV. *Region IV* is characterized by either an adsorption plateau or an adsorption maximum. The transition regions III and IV occur either at the cmc or upon completion of a bilayer coverage of the surface. In addition, it is assumed that the incorporation of counterions between the surface and surfactant head groups occurs in the second stage as soon as more surfactant is adsorbed in the first layer.

1.4.6.3. The two-step model by Gu

The two-step model model was proposed by Gu and Zhu [53, 54]. According to this model, the adsorption of the surfactant shows two-steps, which is obvious on a linear scale adsorption isotherm. In the first step, the surface-active species are adsorbed through interactions with the solid surface due to electrostatic interactions and/or van der Waals interactions at low surfactant concentrations below the cmc. In the second step, surfactant molecules are adsorbed through hydrophobic interactions between the adsorbed surfactants and then they form surface aggregates or small "surface micelles".

Based on the two-step adsorption model, a general adsorption isotherm equation was derived:

$$\Gamma = \frac{\Gamma_{max} k_1 C \left(\frac{1}{n} + k_2 C^{n-1}\right)}{1 + k_1 C \left(1 + k_2 C^{n-1}\right)} \qquad (1\text{-}12)$$

where k_1 and k_2 are the equilibrium adsorption constants involved in the first and second step in M^{-1} and n is the aggregation number of surface aggregates.

The above equation has been applied to various types of adsorption isotherms for a relatively large number of systems, with the majority of studies being concerned with silica surfaces [55].

Later on, Gu and Rupprecht [56] divided the adsorption isotherm for ionic surfactants onto polar surfaces into four main regions (Figure 1-13). In region a (very low equilibrium concentrations), the adsorption is chiefly due to electrostatic interactions and therefore is controlled by the surface charge of the solid. The individually adsorbed surfactant ions serve as an anchor for the adsorption of further surfactant monomers from the solution.

In region b (the first adsorption plateau, Γ_{1st}), the adsorption results from both electrostatic attraction and specific interactions between the surfactant and the solid surface accompanied by a change in the ζ-potential (point of zero charge reached at the end of this region). In region c (medium concentrations), surface aggregates occur and the formation of a second adsorption layer permanently affects the adsorption mechanism. The adsorption in this region is mainly due to the hydrophobic interactions between the hydrophobic tail groups of surfactant and it is closely related to the micellization process in the bulk phase. These aggregates are also called hemimicelles. The second adsorption plateau, Γ_{2nd} (region d) is reached at equilibrium concentrations higher than the cmc. In this region, the amount of surfactant adsorbed remain almost constant as the monomer concentration is expected to be constant.

Figure 1-13. Characteristic regions of ionic surfactants adsorption onto hydrophilic solids after Rupprecht [56] with the corresponding state of adsorbed layer at different concentration regions. Adsorption of cationic surfactant onto a negatively charged solid surface [56].

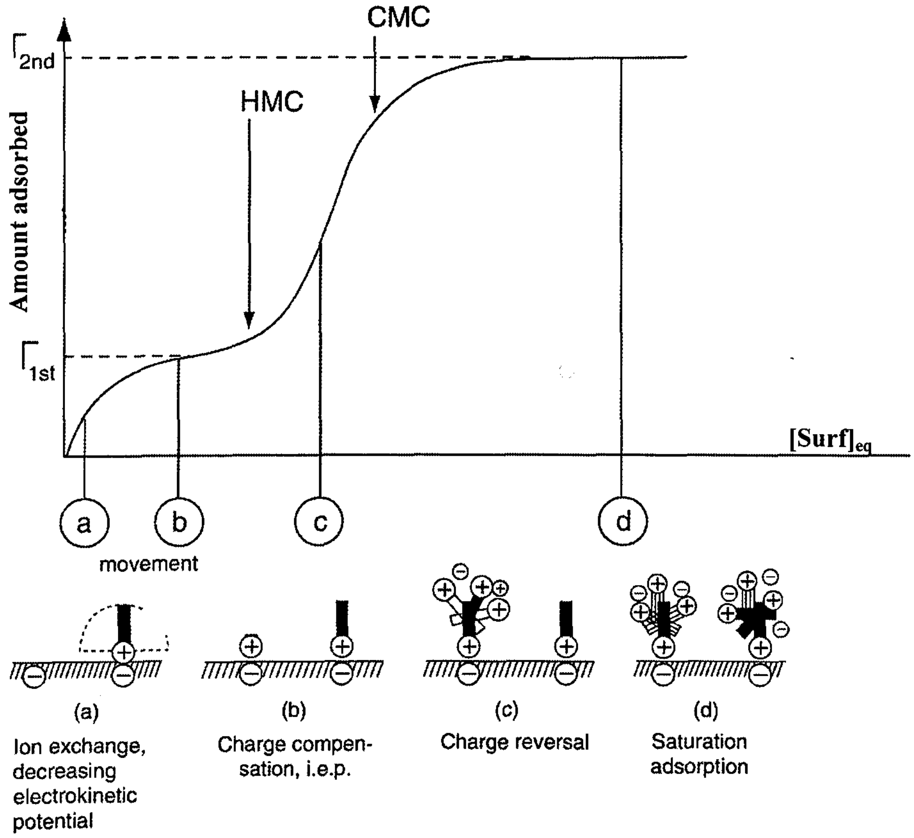

Figure 1-14 shows a schematic diagram showing the structures of adsorbed surfactant molecules according to the bilayer, reverse orientation and the two-step model at equilibrium concentrations higher than the cmc.

Figure 1-14. Adsorption models of ionic surfactants onto hydrophilic surfaces: (a) admicelle, (b) hemimicelle and (c) small surface aggregates incorporating counterions [56].

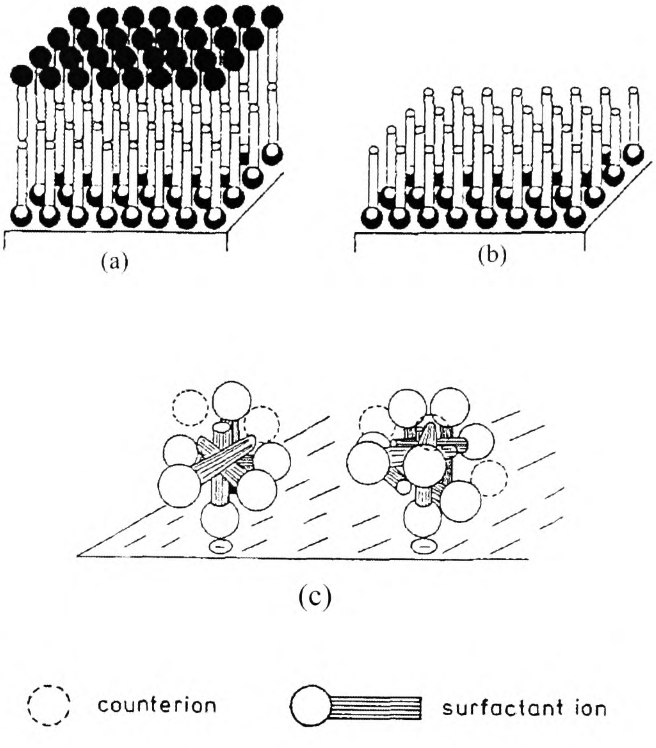

1.5. THE QUARTZ CRYSTAL MICROBALANCE (QCM) TECHNIQUE

The Quartz Crystal Microbalance (QCM) technique is currently experiencing rapid growth in the real-time monitoring of surfactants and macromolecules adsorption at the solid-liquid interface. This is achieved by allowing the simultaneous measurement of changes in the resonance frequency and the dissipation energy of the crystal employed. The change in frequency is proportional to the amount of adsorbed surfactant. The high sensitivity, the low detection limit and the real-time monitoring of mass changes on the sensor crystal make the QCM a very attractive technique for studying the adsorption characteristics of surfactant molecules at the steel-water interface. Moreover, the measured dissipation changes provide additional information about the viscoelastic properties of the adsorbed surfactant layer.

This section addresses the fundamental principles of the Quartz Crystal Microbalance technique. This includes the working principle, instrumentation, use of the QCM in a liquid medium and factors affecting the accuracy of measurements such as density, viscosity, temperature of aqueous solution.

1.5.1. General background and instrumentation

The QCM is an ultra-sensitive mass sensor or balance with the ability to measure mass changes on the nanogram scale. The device consists of a thin quartz disc sandwiched between a pair of electrodes. Applying an AC voltage across its electrodes makes the crystal oscillate laterally owing to the piezoelectric properties of quartz. The resonant frequency of the crystal depends on the crystal mass. The working principle of a typical QCM is illustrated in Figure 1-15 [57]. When a substance is adsorbed onto the crystal, the frequency decreases. If the adsorbed mass is small compared to the mass of the crystal, evenly distributed and rigidly attached, with no slip or deformation due to the oscillatory motion, the resonant frequency decreases proportionally with the mass of the film according to the Sauerbrey equation [58]:

$$\Delta m = -\frac{A\sqrt{\mu_q \rho_q}\Delta f}{2nf_o^2} = -\frac{C\Delta f}{n} \qquad (1\text{-}13)$$

where C is a constant equal to 17.7 ng cm^{-2} Hz^{-1} for a quartz crystal with surface area equal to 1 cm^2 and a fundamental frequency, f_o, of 5 MHz, μ_q is the elastic shear modulus of quartz (2.947×10^{11} g cm^{-1} s^{-2}), ρ_q is the quartz density (2.65 g cm^{-3}), Δf is the measured shift in frequency and n is the overtone number (1, 3, 5,..).

The resonant frequency of 5 MHz quartz crystal can be measured with a precision of about 0.01 Hz (in vacuum) and 0.1 Hz in liquids according to the manufacturer's manual (Q-Sense, QCM-D [59]. Accordingly, very small masses on the nano-gram scale could be measured by the QCM.

Figure 1-15. The heart of the QCM is the AT-cut quartz crystal disc sandwiched between two gold electrodes. (a) The crystal is given a mechanical lateral oscillation by an oscillating potential difference. The circuit can be disconnected to follow the dissipation of a freely oscillating crystal. (b) The larger steel electrode is facing the solution investigated and the area where the adsorption is measured is slightly larger than (c), the smaller counter electrode [57].

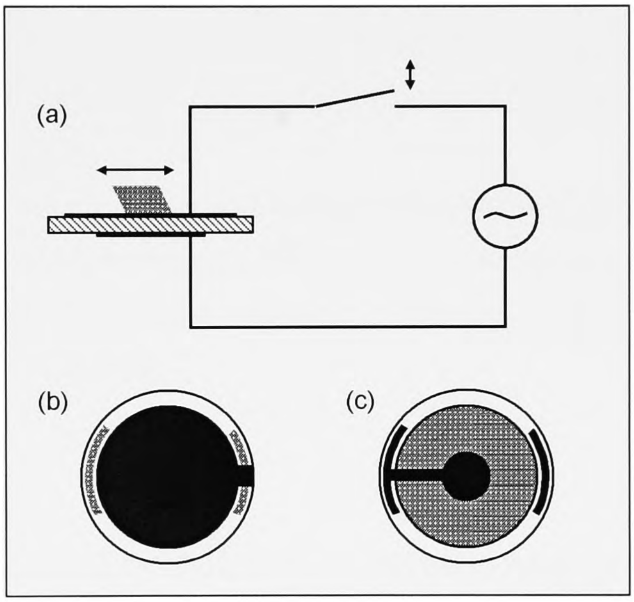

The sensitivity factor of the QCM increased by a factor of *n* by operating at any of its *n* overtones and it increases with the square of the fundamental frequency, f_o [60, 61].

The QCM technique provides a useful tool to characterize the dissipative energy or viscoelastic behaviour of the adsorbed surfactant layer.

In a QCM, the variation in dissipation energy, ΔD, is measured simultaneously with the frequency change and reflects the viscoelastic properties of the adsorbed layer. The energy dissipation factor is defined as the ratio between the energy dissipated per oscillation cycle, $E_{dissipated}$ and the net stored energy in the oscillating system, E_{stored}. The more viscous the adsorbed layer is the more energy is lost from the oscillation. The dissipation energy is a dimensionless quantity and it is given by the following equation [61]:

$$D = E_{dissipated} / 2 \pi E_{stored} \tag{1-14}$$

The dissipation or the damping of the crystal is obtained by measuring the width of the resonance peak; the larger the damping the broader is the resonance peak. An alternative way, which is the commonly employed method, is to measure the decay of the oscillation amplitude for the freely oscillating sensor crystal. In this case, the decay time is inversely proportional to the resonance width and thus the damping of the crystal. The principle of the measurement is to periodically switch on and off the driving power to the sensor and to record the output voltage from the freely decaying oscillator.

For a rigid adsorbed layer, the change in energy dissipation is negligible. In systems where the adsorbed layer is soft, significant dissipative losses occur, which limits the validity of the Sauerbrey equation. These two situations are represented graphically in Figure 1-16 [59].

Figure 1-16. After cutting the driving circuit, the freely decaying oscillation of the crystal is monitored. Attachment of a rigid mass (A) to the crystal surface will only lead to negligible decrease in *D*, while a soft (viscoelastic) mass (B) will affect *D* significantly [59].

(A) Attachment of a rigid mass. (B) Attachment of a soft mass.

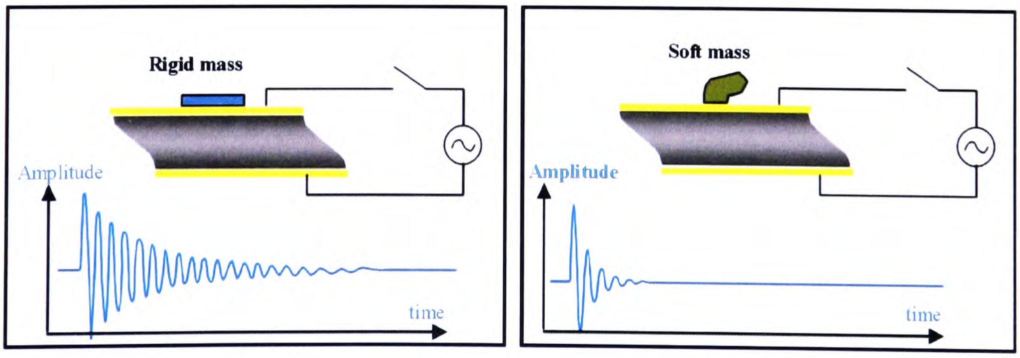

1.5.2. Quartz Crystal Microbalance in Liquid Media

The QCM has been used for many years as mass sensors in vacuum and gas phase experiments and it was initially thought that liquid media would completely dampen the mechanical resonance. However, in the beginning of the 1980's Nomura and Okuhara [62] showed that the quartz crystal does resonate in organic liquids with a frequency change that is dependent on their density and viscosity. Kanazawa and Gordon [63] measured the frequency change in water with increasing concentration of glucose. Glucose does not adsorb at the surface, implying that the measured frequency change in this system is due to changes in bulk viscosity and density of the solution.

The frequency changes from the measurements were in good agreement with the values calculated from the following equation [63]:

$$\Delta f = -\sqrt{n}\, f_0^{3/2} \left(\frac{\rho_l \eta_l}{\pi \mu_q \rho_q} \right)^{1/2} \tag{1-15}$$

where ρ_l and η_l are the density and viscosity of the liquid.

The dissipation factor will change, compared to their values in air, according to the following equation [64]:

$$\Delta D = -\sqrt{n}\, f_0^{1/2} \left(\frac{\rho_l \eta_l}{\pi \mu_q \rho_q} \right)^{1/2} \tag{1-16}$$

1.5.3. Deviations from the Sauerbrey model

Most reported QCM investigations have assumed ideal, rigid-layer behaviour using the Sauerbrey model, when interpreting frequency changes. It is important to remember, however, that the QCM measures frequency changes and not mass changes. Additionally, in the liquid medium, the QCM frequency is highly dependent on the environment of the quartz electrode. Accordingly, the mass sensed by the QCM and the adsorbed amount detected by other techniques were found to be different. Significant differences between the mass sensed by the QCM and the adsorbed mass determined by other techniques have been reported in many studies, for instance, in studies concerned with the adsorption of surfactants [65], vesicles [66], proteins and DNA molecules onto supported lipid bilayers [67].

Several studies have been shown that direct application of the Sauerbrey equation to surfactants [68], polymers [69] and protein [70] adsorption from liquids results in an overestimation of the adsorbed mass. Different interpretations have been introduced in the literature to explain this behaviour. Water sensed by the QCM either in the form of "bound water" in the adsorbed film, as in hydration layers, or mechanically trapped in cavities on a rough surface, is one of the main reasons for such deviations. The hydrated or trapped water is sensed as an additional mass and cannot be differentiated from the actual adsorbed mass. The typical amount of coupled water has been shown to vary significantly in different systems, depending on the nature of the film, between a factor of 1.5 and 4 times larger than the actual adsorbed mass [71, 72].

Stalgren *et al.* [65] studied the adsorption of hexaethylene glycol mono-*n*-tetradecyl ether ($C_{14}EO_6$) onto silica by the QCM and ellipsometry techniques. They reported that the frequency shift obtained from the QCM experiment results in an overestimation of the adsorbed mass. This was attributed to water molecules that are coupled to the adsorbed layer due to hydration of the polar region of the surfactant and second water molecules that for other reasons are trapped within the adsorbed layer.

Caruso *et al.* [68] investigated the adsorption of octaethylene glycol monododecyl ether ($C_{12}E_8$) onto hydrophobic gold and hydrophilic chromium oxide surfaces from aqueous solution using the QCM and the Surface Plasmon Resonance (SPR) method. They found that the amount of $C_{12}E_8$ adsorbed, estimated using the QCM, at saturation coverage is 80% greater than that determined by the SPR technique.

The overestimation of the adsorbed mass calculated by the Sauerbrey equation may be a direct consequence of the change in the density and viscosity of solutions, which is commonly known in the literature as the ''bulk effect''. In the liquid phase, the shear motion of the crystal generates a shear wave, which penetrates into the contacting liquid. This wave is dampened by energy dissipations, due to the viscosity and density of the liquid, resulting in a further decrease in the resonant frequency of the crystal. Therefore, when a QCM crystal contacts a liquid, the frequency shift has contributions from both the mass adsorbed and liquid bulk properties [62, 63, 73].

Corrections based on Kanazawa's equation have been used in several studies [74-76] to eliminate the contribution of the bulk effect to the measured shifts in frequency. In this approach, the expected shift in frequency due to changes in bulk properties is calculated using Kanazawa's equation and is then subtracted from the measured shift in frequency to give the corrected shift in frequency. Then, the corrected shift in frequency is applied in Sauerbrey's equation to calculate the mass of adsorbed molecules.

Schlenoff and Xu [76], have employed this correction method for correcting the shift in frequency measured by the QCM during the adsorption of polystyrene from cyclohexane. They reported that the effect of changing solution bulk properties on frequency measurements was negligible at low polymer concentrations and increases with increasing the polymer concentration.

Recently, Bordes *et al.* [77] have developed an alternative correction method taking into account the effect of bulk properties of solutions on the measured frequency shifts. They investigated the adsorption of a series of dicarboxylic amino acid-based surfactants onto hydrophobized gold surfaces by the SPR and QCM techniques. The amounts of adsorption determined by the QCM were much higher than those determined by the SPR and the magnitude of dissipation change was also significant. This behaviour has been attributed to the change in solution bulk properties. To quantify the bulk effect, experiments with surfactant solutions were carried out using a silica surface onto which the surfactants do not adsorb under the experimental conditions used. Hence, the measured shift in frequency during the adsorption of surfactant onto silica surfaces caused entirely by the bulk effect (as no adsorption is taking place). These values have been used to deduce the bulk effect from the measured Δf values obtained on surfaces (gold) onto which the surfactants adsorb.

Many studies have pointed out that surface roughness affects the resonant frequency and results in an overestimation in the adsorbed mass calculated by the Sauerbrey equation [78, 79]. Ha *et al.* [78] found that the mass calculated from the Sauerbrey equation is about 3 to 6 times larger than the actual value, obtained from fluorescence measurements, due to surface roughness. Rechendorff *et al.* [64] have studied how the frequency and dissipation responses of a QCM depend on the roughness of the surface when it is exposed to liquids with different density-viscosity products. Their main conclusions were that a surface roughness below about 3 nm does not result in frequency and dissipation responses different from a flat surface; surface roughness larger than about 6 nm influences the frequency shift significantly and finally, the shift in dissipation factor remains low for all values of roughness, even as high as about 33 nm.

On the other hand, the application of the Sauerbrey equation may also result in an underestimation of the adsorbed mass as reported by several studies [80-82]. Stengel *et al.* [80] reported an underestimation of the mass calculated by the Sauerbrey equation by up to 25%. The failure of the Sauerbrey model in these situations has been attributed mainly to the formation of a strongly damped viscoelastic film [61, 83]. Strongly damped films include, for example, viscoelastic layers composed of highly hydrated polymer or bimolecular structures e.g., gels or gel-like structures, which do not follow the shear motion rigidly, but are deformed because of the shear motion [84]. The modelling of the measured shift in frequency of a viscoelastic layer can be achieved by employing theoretical models using data collected at multiple overtones.

Several viscoelastic models, which makes use of both frequency and dissipation information, have been developed to overcome limitations of the Sauerbrey model. The Voigt-based model [85, 86] and the Johannsmann model [83, 87] have been used widely in modelling the measured shifts in frequency and dissipation of viscoelastic adsorbed films [71, 72]. These theoretical models describe viscoelastic films by four parameters; thickness, density, and two shear modulus components. The model parameters are "effective" parameters, that is, they represent the entire layer, including the associated/coupled water. Usually, either the effective density, ρ_{eff}, or the effective thickness, d_{eff}, is required as input in the models. Consequently, the mass determined by using either the Voigt or the Johannsmann models corresponds to the total mass of the film, including both adsorbed molecules and coupled water. Hence, to determine the actual effective film mass of the adsorbed species of interest, the mass of water has to be measured independently using another technique [88, 89].

1.5.4. Other Factors Affecting QCM Measurements

In addition to the viscous entrainment, which is always present when a QCM oscillates in a liquid, the surface roughness of the quartz crystal will induce an additional shift in the resonance frequency and in the dissipation factor due to several physical effects, such as trapping of liquid, pressure gradients, and non-laminar flow. Additionally, the interfacial slippage [90] and non-uniform mass distribution [91] of the film, pressure and temperature [75, 90] of the surrounding environment can lead to undesirable frequency shifts. Interfacial slippage affects the accuracy of the measurements, as commonly used models rely on the ''no-slip'' condition, i.e., it is assumed that the first layer of the adsorbate at the QCM metal electrode surface is tightly bound and does not slip during the shear motion of the crystal. However, the literature suggests that interfacial slippage causes relatively slight frequency decreases compared to those attributed to other factors like surface roughness and temperature [71, 90]. Temperature, while it does not significantly affect the properties of the crystal, can have a dramatic effect on the properties of the surrounding medium, such as the density and viscosity of a fluid.

Ryu and Free [75] reported that, the shift in frequency decreased by 64.2 Hz as the temperature of pure water increased from 23.9 to 31.2 °C, which is equivalent to 8.79 Hz per Celsius degree. Some of the observed change is due to the natural shift in oscillation frequency and the remainder is due to the change in viscosity associated with the change in temperature. Using Kanazawa's equation, the predicted change in frequency due to viscosity changes was found to be 6.93 Hz $°C^{-1}$. Consequently, the temperature must be held constant during the course of an experiment.

Pressure can also affect the accuracy of a measurement. For example, often, one side of the crystal faces a liquid while the other is exposed to air; this places a stress on the crystal because of the hydrostatic pressure [90]. However, in most experiments, the pressure effect is likely negligible because the pressure is typically constant over the course of an experiment.

1.6. EFFECT OF THE PARASITIC ADSORPTION OF CORROSION INHIBITORS ON THEIR INHIBITION EFFICIENCY IN OIL FIELD SYSTEMS

The use of organic corrosion inhibitors is the most effective method against internal corrosion of carbon steel pipelines for oil product transportation. Oil in pipelines carries solids, such as sand, clay and corrosion products such as iron carbonate, iron sulfide and wax. Although some may be protective against corrosion in nature (wax/asphaltenes), others can have detrimental effects by either accelerating the corrosion rate or preventing the applied inhibitor from achieving maximum effect [92]. The presence of solids can interfere with the performance of the inhibitor in several ways. When present on the pipe wall, solids constitute an extra physical layer that the inhibitor has to permeate in order to reach to the surface and therefore mass transfer limitations can occur [93].

When an inhibitor is added into a production stream, ideally the molecules diffuse to the pipe surface and form a barrier, which retards the corrosion at the metal surface. This is driven by the tendency of the inhibitor to adsorb at the metal surface. The intended surface for adsorption is obviously the metal-fluid interface so that the adsorbed chemical can prevent corrosion. However, most corrosion inhibitors cannot differentiate between surfaces and will adsorb, to varying degrees, at other available surfaces encountered in the system. Fine solid particles, such as clays and sand particles, can consume a significant amount of the corrosion inhibitor by adsorption. This consumption may cause the inhibitor concentration to drop below the minimum effective concentration and may lead to corrosion failure [94]. This phenomenon has been termed the *parasitic consumption* of corrosion inhibitors [15, 95]. Examples of unintended surfaces, which the inhibitor may adsorb to, are not limited to clays and sand, but also include corrosion products and inorganic scales. The presence of such surfaces in a production system can dramatically reduce the concentration of inhibitor that is available to provide inhibition at the pipe surface [15].

Horsup *et al.* [15] used the depletion method to investigate the adsorption of the commonly used corrosion inhibitor dodecylbenzyldimethylammonium chloride C12BDMAC onto sand, iron carbonate, iron sulphide, barium sulphate and calcium carbonate from a brine solution. These solid surfaces are typical surfaces encountered in the production system. They reported that the inhibitor had the greatest affinity for sand and iron sulphide with uptake percentages of about 95 and 93 %, respectively, whereas barium sulphate, iron carbonate and calcium carbonate were found to only adsorb a small quantity (6-10%) of this particular corrosion inhibitor. In addition, they studied the adsorption of C12BDMAC onto a sample of field debris (containing an appreciable quantity of sand and iron sulfide) obtained following a maintenance pigging operation. They found that the inhibitor has a strong affinity for the field solids with about 78 % of the inhibitor being adsorbed.

Recently, the interaction of corrosion inhibitors with corrosion product deposits in a solution containing carbon dioxide received a great deal of attention by various researchers [96-98]. In these works, the inhibitor performance was investigated and a comparison of the inhibition efficiency of the various corrosion inhibitors used was determined. The main conclusion was that the presence of corrosion products reduces the inhibitor efficiency effectively. Horsup *et al.* [15] reported that the presence of increasing amounts of silica decreases the inhibition efficiency of the corrosion inhibitor C12BDMAC significantly in a CO_2-saturated brine solution.

In addition to the loss of inhibitor onto solids in a production system, losses can also occur through adsorption at the oil-water interface. In general, these losses will be minimal unless there is a significant amount of mixing in the pipe resulting in the formation of a stable emulsion. The generation of an emulsion creates a significant amount of new interface to which an inhibitor can readily adsorb. The inhibitor will compete with natural surfactants present in the crude oil for a position at the interface [15, 99]. Adsorption at this interface stabilizes the emulsion and can lead to separation problems during the production. Additionally, inhibitor involved in stabilizing an emulsion is not as readily available for inhibition as that residing in the aqueous phase. Parasitic consumption of the inhibitor caused by these processes may reduce the activity of the monomeric form of the inhibitor, which is needed to provide corrosion inhibition [15, 100, 101].

Gulbrandsen and Kvarekval have shown that the performance of three corrosion inhibitors containing different surfactants - an amine, a quaternary ammonium chloride and a phosphate ester - is dramatically reduced in the presence of dispersed oil drops [93].

An experiment was performed by Horsup *et al.* [15] to demonstrate the loss of inhibitor through emulsion stabilization. In this experiment, an emulsion was formed by vigorously mixing 50 g of water containing 100 ppm of C12BDMAC and 50 g of a LVT-200 oil in a separatory funnel. Under these conditions, the inhibitor is expected to partition exclusively into the water phase. The emulsion broke slowly and, with the emulsion still present in the vessel, a small quantity of separated water was removed. The inhibitor concentration in the water was then determined. They found that there is a 12 % decrease in the amount of inhibitor present in the water phase that was attributed to the parasitic adsorption of the molecules at the oil-water emulsion droplet interface.

Corrosion inhibitors are amphiphilic and therefore they can often be soluble in both the oil and water phases of the produced fluids. On the other hand, the beneficial effect of a corrosion inhibitor is achieved in the corrosive phase only, which is the water phase. Therefore, the partitioning of a corrosion inhibitor between the oil and water phases has a significant impact on inhibitor efficiency [102].

The amounts of surfactant in each phase depend upon the partition coefficient, which is directly related to the molecular structure of the surfactant, electrolyte concentration and temperature. The partition coefficient of a corrosion inhibitor, P, is defined as follows:

$$P = \frac{[X]_{\text{oil}}}{[X]_{\text{water}}} \tag{1-17}$$

where:

$[X]_{\text{oil}}$ = concentration of corrosion inhibitor in the oil phase and

$[X]_{\text{water}}$ = concentration of corrosion inhibitor in the water phase.

When the corrosion inhibitor is distributed between the oil and water phases, the total concentration of inhibitor will be given by:

$$[X]_{\text{total}} = [X]_{\text{water}}\phi_{\text{water}} + [X]_{\text{oil}}\phi_{\text{oil}} \tag{1-18}$$

where ϕ_{oil} and ϕ_{water} are the volume fractions of oil and water, respectively. Hence, the fraction of corrosion inhibitor present in the water phase can be written as a function of the oil volume fraction as follows:

$$\frac{[X]_{water}}{[X]_{total}} = \frac{1}{(1-\phi_{oil}) + P\phi_{oil}} \tag{1-19}$$

According to equation (1-19), the inhibitor fraction in aqueous solution in contact with an oil phase, may be diminished, if it has high partition coefficient and a high volume fractions of oil. Figure 1-17 shows the fraction of inhibitor present in the water phase as a function of the oil volume-fraction for various inhibitors having different partition coefficients [19]. As shown, even 0.1 vol. % of the oil is sufficient to significantly decrease the fraction of an inhibitor with a partition coefficient of 1000 in the aqueous phase to about zero, which may reduce the performance of the inhibitor in the aqueous phase.

Figure 1-17. Fraction of total inhibitor present in the water phase vs. volume fraction of oil for P values of 10 (black), 100 (red) and 1000 (blue) [19].

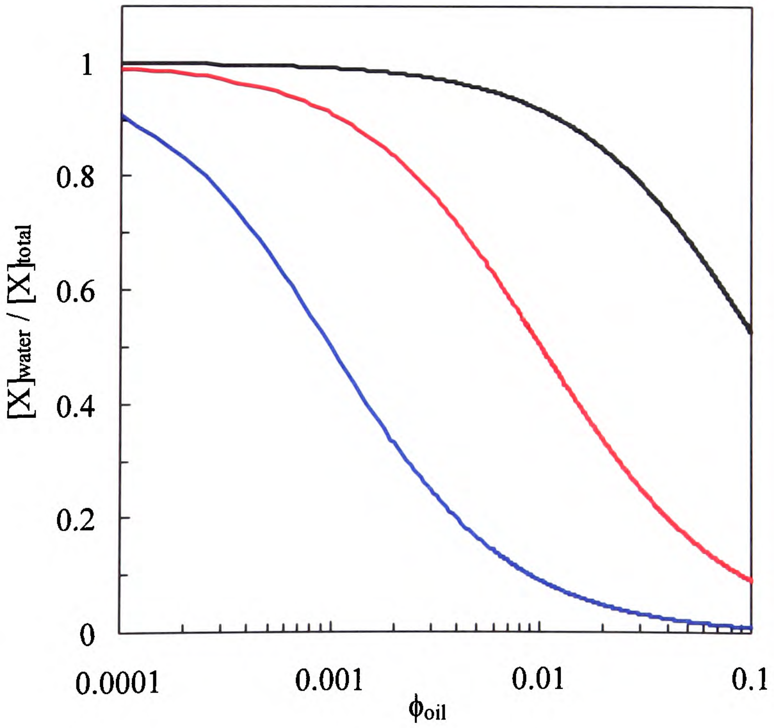

1.7. AIMS OF THE WORK AND STRUCTURE OF THE THESIS

Surfactant addition is one of many ways of inhibiting the corrosion of metals especially on hard-to-reach surfaces, such as the inside of a pipe through which fluid is flowing. Despite the popularity of surfactants as corrosion inhibitors, the mechanisms by which they prevent corrosion are not well understood. Moreover, there is a lack of direct information showing how the extent of inhibitor adsorption is related to corrosion rate under corresponding conditions and how this will affect the inhibitor performance. Indeed, as pointed out by Free [103], many corrosion researchers do not measure the inhibitor adsorption directly, but assume that the extent of inhibition is proportional to the fractional surface coverage of the corroding surface by the inhibitor.

The aim of this study is to investigate the surfactant aspects of corrosion inhibitors, which are often over-looked during electrochemical studies, including much-needed research into the behaviour of corrosion inhibitors added to mixtures of oil and water. The work aims at studying the following:

I. the partitioning behaviour of corrosion inhibitors between an aqueous brine phase and an oil phase and how this is affected by changes in the inhibitor structure, temperature, brine salinity and oil type.

II. the ability of corrosion inhibitors to stabilize both oil-in water and water-in-oil emulsions and the phase inversion of the emulsion as production variables change.

III. the effect of surfactant properties and solution environment on surfactant adsorption at the steel-water interface and the relationship between the surfactant adsorption and the corrosion inhibition efficiency.

IV. how sand and other solids affect the surface concentration of the inhibitor on the steel surface and to combine this with information on how the corrosion rate depends on the inhibitor surface concentration in order to quantitatively predict the inhibitor performance under different production conditions.

In other words, the focus of this research work is to determine the extent to which the competing (and corrosion-efficiency-lowering) processes affect the adsorption of corrosion inhibitors at the metal surface for a range of different inhibitor species. The overall project objective is to gain a greater understanding of how different corrosion inhibitors are affected by changes in system conditions, which would be representative of those faced in the oil and gas production industry.

The thesis is divided into nine chapters. *Chapter 1* covers the theoretical background relevant to oilfield corrosion inhibition and the surfactant aspects of corrosion inhibitors.

Chapter 2 introduces the methods and materials used in the project as well as describing the main techniques employed. The corrosion inhibitor to be investigated in this work is the homologous series of alkylbenzyldimethylammonium chlorides C10, C12, C14 and C16BDMAC, which represents one of the most common corrosion inhibitors used in the oil industry.

In *Chapter 3*, we investigate the adsorption behaviour of alkylbenzyldimethylammonium chlorides (CnBDMAC) at the air-water interface. The investigation addresses the role of the alkyl chain length in the adsorption of these homologues, the effect of temperature and the dependence of the adsorption on the concentration of added electrolyte.

Chapter 4 discusses the experiments concerned with the phase behaviour of model corrosion inhibitors in mixtures of oil and water. We have conducted equilibrium partitioning and emulsion phase inversion experiments to assess the partitioning of the inhibitors under different conditions. We will present the results of electrochemical measurements used to monitor the corrosion rate of steel immersed in an aqueous solution in the presence of the model corrosion inhibitor before and after the addition of an oil phase under conditions, which cause virtually all of the corrosion inhibitor to favour the oil phase.

Chapter 5 investigates the applicability and optimization of the Quartz Crystal Microbalance (QCM) for the measurement of *in-situ* adsorption of CnBDMAC surfactant from aqueous solutions onto stainless steel-coated crystals. The optimization process aims at finding the appropriate experimental setup and procedures for carrying out the adsorption measurements. Additionally, the treatment and analysis of the experimental data will be discussed in this chapter. Moreover, the effects of surfactant chain length, temperature and salinity on the adsorption behaviour of CnBDMAC surfactants onto stainless steel-coated crystals will be investigated using the QCM.

In *Chapter 6*, the adsorption behaviour of CnBDMAC corrosion inhibitors onto mild steel (C1018) and stainless steel (316L) powders will be discussed in detail as a function of the surfactant chain length, temperature and electrolyte concentration. Furthermore, the change in surface charge of the steel particles in alkylbenzyldimethylammonium chlorides solutions will be investigated.

In *Chapter 7*, we are going to investigate the influence of chain length, temperature and brine addition on the adsorption characteristics of CnBDMAC corrosion inhibitors from aqueous solution onto sand as one of the parasitic surfaces encountered in the oilfield systems. In addition, the relative affinity and amounts of adsorption of these surfactants onto steel versus sand particles will be evaluated and discussed.

Chapter 8 investigates the performance of the corrosion inhibitor hexadecylbenzyldimethylammonium chloride (C16BDMAC) in CO_2–saturated brine solution by the means of the linear polarisation resistance technique and how this is affected by sand addition. The aim of this chapter is to quantitatively predict the performance of the corrosion inhibitor in the presence of different amounts of sand.

Finally, *Chapter 9* summarises the main conclusions of all the results of the experiments performed in this study together with a discussion of possibilities for future work.

1.8. REFERENCES

1. V. S. Bagotsky, *Fundamentals of Electrochemistry*, Wiley-Interscience, Hoboken (2006).
2. G. H. Koch, M. P. H. Brongers, N. G. Thompson, Y. P. Virmani and J. H. Payer, *Corrosion Costs and Preventive Strategies in the United States*, Publication No. FWHA-RD-01-156, U.S. Department of Transportation, Federal Highway Administration, Ohio (2002).
3. D. Brondel, R. Edwards, A. Hayman, F. Clamart, D. Hill, S. Mehta and T. Semerad, *Oilfield Review*, **6**, 4 (1994).
4. V. V. Zavyalov, *Prot. Met*, **39**, 274 (2003).
5. W. Villamizar, M. Casales, J. Gonzalez-Rodriguez and L. Martinez, *J. Solid State Electrochem.*, **11**, 619 (2007).
6. W. Villamizar, M. Casales, L. Martinez, J. Chacon-Naca and J. Gonzalez-Rodriguez, *J. Solid State Electrochem.*, **12**, 193 (2008).
7. W. Villamizar, M. Casales, J. G. Gonzales-Rodriguez and L. Martinez, *Mater. Corros.*, **57**, 696 (2006).
8. G. Bereket and A. Yurt, *Anti-Corros. Method. M.*, **49**, 210 (2002).
9. G. Z. Olivares, M. J. H. Gayosso and J. L. M. Mendoza, *Mater. Corros.*, **58**, 427 (2007).
10. J. W. Palmer, W. Hedges and J. L. Dawson, *A Working Party Report on the Use of Corrosion Inhibitors in Oil and Gas Production*, European Federation of Corrosion, London (2004).
11. B.P. Binks, P.D.I. Fletcher, J.T. Hicks, D.I. Horsup and W.H. Durnie, *Proceedings of NACE Corrosion/2005*, Paper No. 05307, NACE International, Houston (2005).
12. A. J. McMahon, *Colloids Surf., A*, **59**, 187 (1991).
13. S. Ramachandran, B. L. Tsai, M. Blanco, H. Chen, Y. C. Tang and W. A. Goddard, *Langmuir*, **12**, 6419 (1996).
14. V. Jovancicevic, S. Ramachandran and P. Prince, *Corrosion*, **55**, 449 (1999).
15. D. I. Horsup, J. C. Clark, B. P. Binks, P. D. I. Fletcher and J. T. Hicks, *Corrosion*, **66**, 036001 (2010).
16. M. L. Free, *Corros. Sci.*, **44**, 2865 (2002).

17. J. Gibbs, *Scientific Papers of J. Willard Gibbs*, Longmans, Green and Co., Yale (1906). [Available online], http://www.archive.org/stream/.scientificpaper00gibbgoog#page/n9/mode/2up, Last accessed 10 January 2011.

18. T. F. Tadros, Applied Surfactants: Principles and Applications, Wiley-VCH, Weinheim (2005).

19. J. T. Hicks, *Surfactants Aspects of Corrosion Inhibitors*, Ph.D. Thesis, Hull University (2007).

20. J. H. Clint, *Surfactant Aggregation*, Chapman and Hall, Glasgow (1992).

21. IUPAC, *Compendium of Chemical Terminology*, 2nd ed. Blackwell Scientific Publications, Oxford (1997).

22. J. N. Israelachvili, Intermolecular and Surface Forces: with Applications to Colloidal and Biological Systems, Academic Press, London (1985).

23. R. Aveyard, B.P. Binks and P.D.I. Fletcher, in *The Structure, Dynamics and Equilibrium Properties of Colloidal Systems*, eds. D.M. Bloor and E. Wyn-Jones, NATO Series C, Kluwer Academic, Amsterdam (1990).

24. R. Aveyard, B. P. Binks and J. Mead, *J. Chem. Soc., Faraday Trans.*, **81**, 2169 (1985).

25. R. Aveyard, B. P. Binks, S. Clark and J. Mead, *J. Chem. Soc., Faraday Trans.*, **82**, 125 (1986).

26. R. Aveyard, B. P. Binks and J. Mead, *J. Chem. Soc., Faraday Trans.*, **82**, 1755 (1986).

27. B.P. Binks, in *Modern Aspects of Emulsion Science*, ed. B.P. Binks, Royal Society of Chemistry, Cambridge (1998).

28. R.G. Lopetinsky, J. H. Masliyah and Z. Xu, in *Colloidal Particles at Liquid Interfaces*, eds. B. P. Binks and T. S. Horozov, Cambridge University Press, Cambridge (2006).

29. H. J. Butt and M. Kappl, *Surface and Interfacial Forces*, Wiley-VCH, Weinheim (2010).

30. H. Helmholtz, *Pogg. Ann.* , **LXXXIX**, 211 (1853).

31. G. Goy, *Compt. Rend.*, **149**, 654 (1909).

32. D. L. Chapman, *Philos. Mag.*, **25**, 475 (1913).

33. O. Stern, *Z. Elektrochem.*, **30** 508 (1924).

34. D. C. Grahame, *Chem. Rev.*, **41**, 441 (1947).

35. J. O. M. Bockris, M. A. V. Devanathan and K. Muller, *Proc. Roal. Soc.*, **A 274**, 55 (1963).

36. A. Delgado, F. González-Caballero, R. Hunter, L. Koopal and J. Lyklema, *Pure Appl. Chem.*, 77, 1753 (2005).

37. G. E. Brown, V. E. Henrich, W. H. Casey, D. L. Clark, C. Eggleston, A. Felmy, D. W. Goodman, M. Gratzel, G. Maciel, M. I. McCarthy, K. H. Nealson, D. A. Sverjensky, M. F. Toney and J. M. Zachara, *Chem. Rev.*, **99**, 77 (1998).

38. J. Zajac and S. Partyka, in *Adsorption on New and Modified Inorganic Sorbents*, A. D. Browski and V. Tertykh, eds., Elsevier Science, Amsterdam (1996).

39. C. Giles, T. MacEwan, S. Nakhwa and D. Smith, *J. Chem. Soc.*, **3**, 3973 (1960).

40. P. Somasundaran and D. W. Fuerstenau, *J. Phys. Chem.*, **70**, 90 (1966).

41. R. Zhang and P. Somasundaran, *Adv. Colloid Interface Sci.*, **123-126**, 213 (2006).

42. I. Langmuir, *J. Am. Chem. Soc.*, **40**, 1361 (1918).

43. H. Freundlich, *Colloid and Capillary Chemistry*, Methuen, London (1926).

44. R. A. Koble and T. E. Corrigan, *Ind. Eng. Chem.*, **44**, 387 (1952).

45. A. N. Frumkin, *Z. Phys. Chem.*, **116**, 66 (1925).

46. A. M. Gaudin and D. W. Fuerstenau, *Trans. AIME*, **202**, 66 (1955).

47. D. W. Fuerstenau and R. Herrera-Urbina, in *Cationic Surfactants: Adsorption of Cationic Surfactant and the Flotation of Minerals*, eds. D. N. Rubingh and P. M. Holland, Marcel Dekker, New York (1991).

48. K. S. Birdi, *Handbook of Surface and Colloid Chemistry*, Taylor & Francis, Boca Raton (2008).

49. J. T. Kunjappu and P. Somasundaran, *J. Phys. Chem.*, **93**, 7744 (1989).

50. J. H. Harwell, J. C. Hoskins, R. S. Schechter and W. H. Wade, *Langmuir*, **1**, 251 (1985).

51. M. A. Yeskie and J. H. Harwell, *J. Phys. Chem.*, **92**, 2346 (1988).

52. D. Bitting and J. H. Harwell, *Langmuir*, **3**, 500 (1987).

53. B. Y. Zhu and T. Gu, *J. Chem. Soc., Faraday Trans.*, **85**, 3813 (1989).

54. B.Y. Zhu and T. Gu, *Adv. Colloid Interface Sci.*, **37**, 1 (1991).

55. B. Y. Zhu, T. R. Gu and X. L. Zhao, *J. Chem. Soc., Faraday Trans.*, **85**, 3819 (1989).

56. H. Rupprecht and T. Gu, *Colloid. Polym. Sci.*, **269**, 506 (1991).

57. J. Sjöblom, G. Øye, W.R. Glomm, A. Hannisdal, M. Knag, Ø. Brandal, M.H. Ese and P.V. Hemmingsen, in *Emulsions and Emulsion Stability*, ed. J. Sjöblom CRC, Boca Raton (2006).

58. G. Sauerbrey, *Z. Phys*, **155**, 206 (1959).

59. Q-Sense, *Spercifications of Q-Sense E4* [Online], Available: http://www.q-sense.com/spercifications-q-sense-e4, [Accessed 03 November 2010].

60. F. Höök, *Development of a Novel QCM Technique for Protein Adsorption Studies,* Ph.D. Thesis, Chalmers University of Technology, Sweden (1997).

61. F. Höök and B. Kasemo, in *Piezoelectric Sensors*, C. Steinem and A. Janshoff, eds., Springer, Heidelberg (2007).

62. T. Nomura and M. Okuhara, *Anal. Chim. Acta*, **142**, 281 (1982).

63. K. Kanazawa and J. Gordon, *Anal. Chem.*, **57**, 1770 (1985).

64. K. Rechendorff, M. B. Hovgaard, M. Foss and F. Besenbacher, *J. Appl. Phys.*, **101** (2007).

65. J. J. R. Stalgren, J. Eriksson and K. Boschkova, *J. Colloid Interface Sci.*, **253**, 190 (2002).

66. E. Reimhult, M. Zäch, F. Höök and B. Kasemo, *Langmuir*, **22**, 3313 (2006).

67. C. Larsson, M. Rodahl and F. Höök, *Anal. Chem.*, **75**, 5080 (2003).

68. F. Caruso, T. Serizawa, D. N. Furlong and Y. Okahata, *Langmuir*, **11**, 1546 (1995).

69. M. T. Müller, X. Yan, S. Lee, S. S. Perry and N. D. Spencer, *Macromolecules*, **38**, 5706 (2005).

70. M. Muratsugu, F. Ohta, Y. Miya, T. Hosokawa, S. Kurosawa, N. Kamo and H. Ikeda, *Anal. Chem.*, **65**, 2933 (1993).

71. F. Hook, B. Kasemo, T. Nylander, C. Fant, K. Sott and H. Elwing, *Anal. Chem.*, **73**, 5796 (2001).

72. F. Caruso, D. N. Furlong and P. Kingshott, *J. Colloid Interface Sci.*, **186**, 129 (1997).

73. D. X. Wang, P. Mousavi, P. J. Hauser, W. Oxenham and C. S. Grant, *Colloids Surf., A*, **268**, 30 (2005).

74. S. M. Lundgren, K. Persson, B. Kronberg and P. M. Claesson, *Tribol. Lett.*, **22**, 15 (2006).

75. D. Y. Ryu and M. L. Free, *J. Colloid Interface Sci.*, **264**, 402 (2003).

76. H. Xu and J. B. Schlenoff, *Langmuir*, **10**, 241 (1994).

77. R. Bordes, J. r. Tropsch and K. Holmberg, *Langmuir*, **26**, 10935 (2010).

78. T. H. Ha, S. Kim, G. Lim and K. Kim, *Biosens. Bioelectron.*, **20**, 378 (2004).

79. A. Bund and M. Schneider, *J. Electrochem. Soc.*, **149**, E331 (2002).

80. G. Stengel, F. Höök and W. Knoll, *Anal. Chem.*, **77**, 3709 (2005).

81. J. C. Munro and C. W. Frank, *Macromolecules*, **37**, 925 (2004).

82. P. Bingen, G. Wang, N. F. Steinmetz, M. Rodahl and R. P. Richter, *Anal. Chem.*, **80**, 8880 (2008).

83. M. Rodahl, F. Hook, C. Fredriksson, C. A. Keller, A. Krozer, P. Brzezinski, M. Voinova and B. Kasemo, *Faraday Discuss.*, **107**, 229 (1997).

84. M. Edvardsson, S. Svedhem, G. Wang, R. Richter, M. Rodahl and B. Kasemo, *Anal. Chem.*, **81**, 349 (2008).

85. M. V. Voinova, M. Rodahl, M. Jonson and B. Kasemo, *Phys. Scr.*, 391 (1999).

86. M. V. Voinova, M. Jonson and B. Kasemo, *Biosens. Bioelectron.*, **17**, 835 (2002).

87. D. Johannsmann, K. Mathauer, G. Wegner and W. Knoll, *Phys. Rev. B*, **46**, 7808 (1992).

88. E. Reimhult, C. Larsson, B. Kasemo and F. Höök, *Anal. Chem.*, **76**, 7211 (2004).

89. X. Liu, D. Wu, S. Turgman-Cohen, J. Genzer, T. W. Theyson and O. J. Rojas, *Langmuir*, **26**, 9565 (2010).

90. D. A. Buttry and M. D. Ward, *Chem. Rev.*, **92**, 1355 (1992).

91. M. D. Ward and E. J. Delawski, *Anal. Chem.*, **63**, 886 (1991).

92. W. Durnie, M. Gough and H. Reus, *Proceedings of NACE Corrosion 2008*, Paper No. 05290, NACE International, Houston (2005).

93. E. Gulbrandsen and J. Kvarekval, *Proceedings of NACE Corrosion 2004*, Paper No. 04365, NACE International, Houston (2004).

94. A. Pedersen, K. Bilkova, E. Gulbrandsen and J. Kvarekvål, *Proceedings of NACE Corrosion 2008*, Paper No. 08632, NACE International, New Orleans (2008).

95. E. Gulbrandsen and A. Pedersen, *SPE International Symposium on Oilfield Corrosion,* Paper No. 106492, *Houston* (2007).

96. M. Foss, E. Gulbrandsen and J. Sjoblom, *Corrosion*, **66**, 025005 (2010).

97. J. Wong and N. Park, *Proceedings of NACE CORROSION/2008,* Paper No. 08345, NACE International, New Orleans (2008).

98. J. Wong and N. Park, *Proceedings of NACE Corrosion 2009*, Paper No. 09569, NACE International, Atlanta (2009).

99. S. Kokal, *SPE Production & Facilities*, **20**, 5 (2005).

100. T. Moon and D.I. Horsup, *Proceedings of NACE Corrosion 2002*, Paper No. 02298, NACE International, Houston (2002).

101. M. Kermani and A. Morshed, *Corrosion*, **59** (2003).

102. M. Joosten, M. Gough, I. Hannah, P. Humble and J. Kolts, *Proceedings of NACE Corrosion 2009*, Paper No. 00018, NACE International, Orlando (2009).

103. M. L. Free, *Corros. Sci.*, **46**, 3101 (2004).

CHAPTER 2

Chapter 2

EXPERIMENTAL

This chapter contains a detailed description of the materials used along with a brief review of all experimental methods used in this work.

2.1. MATERIALS

2.1.1. Water

Water was purified by an Elga Prima reverse osmosis unit and then treated with a Milli-Q reagent water system. The surface tension of this water was periodically checked and found to be 71.9 ± 0.2 mN m^{-1} at 25 °C, which is in excellent agreement with the literature value [1] indicating that the water was free from surface-active impurities. The produced water had a resistivity of 18 MΩ cm or greater.

2.1.2. Oils

Table 2-1 lists the oils used in this work. Prudhoe Bay crude oil was used as received and all other oils were purified by column chromatography using activated alumina (Fluka, UK) to remove polar and surface-active impurities. Heptol was made by mixing 70 vol. % heptane and 30 vol. % toluene.

Table 2-1. Suppliers and purities of oils.

Name	Purity / %	Supplier
Heptane	> 99	Fisher, UK
Toluene	> 99	Fisher, UK
Prudhoe Bay crude oil (inhibitor free)	n/a	Nalco, USA

2.1.3. Surfactants

Table 2-2 lists the purities and suppliers of the alkylbenzyldimethylammonium chlorides (CnBDMAC) surfactants used in this work. All surfactants were used as received unless otherwise stated.

Table 2-2. Suppliers and purities of surfactants.

Name and chemical structure	Purity / %	Supplier
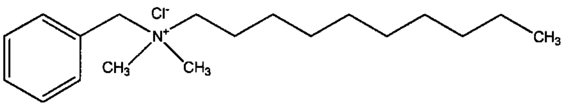 *Decylbenzyldimethylammonium chloride* **(C10BDMAC)**	> 97	Fluka, UK
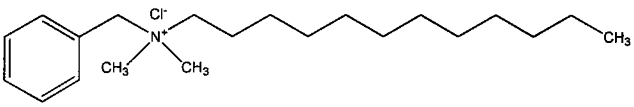 *Dodecylbenzyldimethylammonium chloride* **(C12BDMAC)**	> 99	Fluka , UK
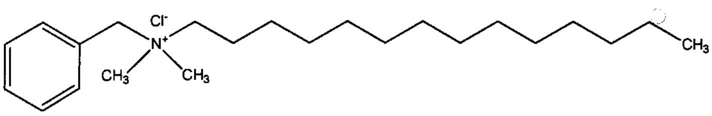 *Tetradecylbenzyldimethylammonium chloride* **(C14BDMAC)**	> 99	Fluka , UK
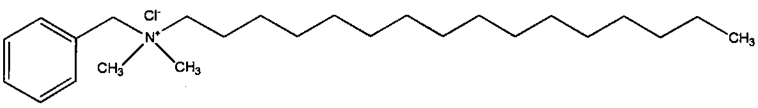 *Hexadecylbenzyldimethylammonium chloride* **(C16BDMAC)**	> 99	Fluka , UK

Figure 2-1 shows a three-dimensional arrangement of C16BDMAC by the space filling model using the Molecular Modeling Pro software package, ChemSW, Inc., USA. The area occupied by a surfactant molecule represents a crucial factor in determining its orientation. The molecular area of a C16BDMAC surfactant laying flat can be calculated from its dimensions according to the following:

If we assume that the density of C16BDMAC is the same as that of bulk water, $d = 0.997\ \text{g cm}^{-3}$ and the molecular weight $M_{wt.}$ is $396\ \text{g mol}^{-1}$, so the molecular volume V, in mL, of C16BDMAC is given by:

$$V = M_{wt.}/d \qquad (2\text{-}1)$$

$$= 6.58 \times 10^{-22}\ \text{cm}^3\ \text{molecule}^{-1}$$

$$= 0.658\ \text{nm}^3\ \text{molecule}^{-1}$$

The volume of one molecule laying flat is given by the product of its thickness, t, which is about 0.54 nm and its cross sectional area, A:

$$V = tA \qquad (2\text{-}2)$$

Equating the two expressions for the volume and solving for A gives:

$$A = V/t = 1.22\ \text{nm}^2\ \text{molecule}^{-1}$$

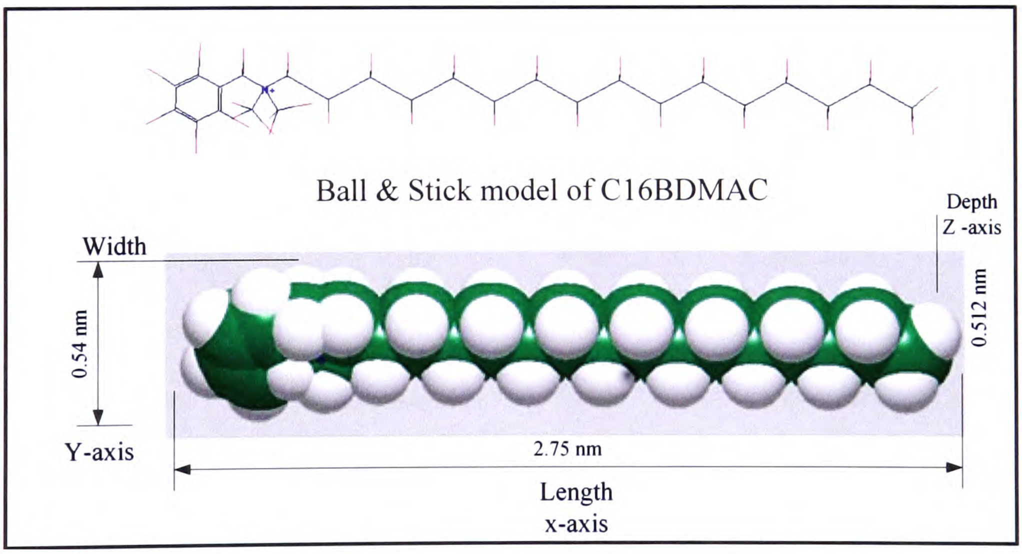

Figure 2-1. Space filling molecular model of C16BDMAC with its molecular dimensions.

Accordingly, in a close-packed monolayer of C16BDMAC molecules lying flat, a C16BDMAC surfactant molecule will have a surface area of about $1.22\ \text{nm}^2$

(122 Å^2). The surface areas occupied by C10, C12 and C14BDMAC lying flat in a closed-packed monolayer will be 0.96, 1.05 and 1.13 nm^2, respectively. On the other hand, the surface area of nay of the CnBDMAC lying perpendicular in a closed-packed monolayer will be governed by the area of the head group, which is 0.32 nm^2 (32 Å^2)

2.1.4. Inorganic solids

Table 2-3 lists the suppliers and purities of inorganic solids used in this research work. All inorganic solids were used as received.

Table 2-3. Suppliers and purities of the inorganic solids.

Name	**Formula**	**Purity / %**	**Supplier**
Boric acid	H_3BO_3	> 99	Fisher, UK
Calcium chloride	$CaCl_2$	> 99	Fisher, UK
Magnesium chloride	$MgCl_2$	> 99	Fisher, UK
Potassium bromide	KBr	> 99	Fisher, UK
Potassium chloride	KCl	> 99	Fisher, UK
Potassium hydroxide	KOH	≥ 85	BDH, UK
Sodium chloride	NaCl	≥ 99.5	BDH, UK
Sodium fluoride	NaF	> 99	Fisher, UK
Sodium hydrogen carbonate	$NaHCO_3$	≥ 99.5	BDH, UK
Sodium sulphate	Na_2SO_4	> 99	Fisher, UK
Sodium sulphide	Na_2S	≥ 60	Fluka, UK
Strontium chloride	$SrCl_2$	≥ 98	BDH, UK

2.1.5. Glassware

All glassware was cleaned in a solution of 10 wt. % KOH in ethanol to remove any surfactant residues. The clean glassware was rinsed with copious amounts of Milli-Q water and then dried in an oven at 45 °C.

2.1.6. Synthetic brine mixture

The synthetic brine mixture was prepared according to the ASTM standard D1141-98(2003) [2]. The composition of this salt mixture in wt. % and molar concentration units is given in Table 2-4.

Table 2-4. Composition of the ASTM D1141-98(2003) [2] synthetic brine standard.

Name	Formula	Composition	
		/ wt.%	/ M
Sodium chloride	NaCl	68.08	11.65
Magnesium chloride	$MgCl_2$	14.43	1.50
Sodium sulphate	Na_2SO_4	11.35	0.80
Calcium chloride	$CaCl_2$	3.22	0.30
Potassium chloride	KCl	1.93	0.26
Sodium hydrogen carbonate	$NaHCO_3$	0.55	0.065
Potassium bromide	KBr	0.28	0.024
Boric acid	H_3BO_3	0.07	0.01
Strontium chloride	$SrCl_2$	0.07	0.0045
Sodium fluoride	NaF	0.008	0.002

The total ionic strength, *I*, of the synthetic brine solution was found to be 17.26 M, which was calculated according to equation (2-3):

$$I = \frac{1}{2}\sum\left(C_i Z_i^2\right) = \frac{1}{2}\left(C_1 Z_1^2 + C_2 Z_2^2 + \cdots\right) \qquad (2\text{-}3)$$

where C_i is the ionic molar concentration, Z_i is the valency of the ion and the summation is continued over all the different species in solution.

The thickness of the electrical double layer, $1/\kappa$ is given by equation (2-4):

$$1/\kappa = \left(\frac{\varepsilon\varepsilon_o RT}{F^2\sum C_i Z_i^2}\right)^{1/2} \qquad (2\text{-}4)$$

where ε_o is the permittivity of the vacuum, ε is the dielectric constant of the solvent, R is the gas constant, T is temperature, F is the Faraday constant, and C_i and Z_i are the concentration and the charge number of the ions of type *i* in the solvent.

When we substitute constants into equation (2-5), we get:

$$\kappa^{-1} = 3.05 \times 10^{-5}\sqrt{I} \qquad (2\text{-}5)$$

Accordingly, the thickness of the electrical double layer, generated when a solid surface is placed into contact with the prepared synthetic brine solution, having the composition given in table 2-4, is going to be 1.3×10^{-9} m.

2.1.7. Sand particles

The sand particles used have a grain size between about 0.1 and 0.3 mm. the sand was purchased from Sigma, UK (purified by acid) and used without any further treatment. The most common constituent of sand is silica (SiO_2), usually in the form of quartz. The composition of sand is highly variable, depending on the local rock sources and conditions. Several sand types contain magnetite, chlorite, alumina or gypsum. The sand particles were sieved in Endecott sieves positioned on a shaker (Vibrax, IKA, Germany). About 64 % by weight of sand particles have a particle size in the range of 212-150 μm and 28 % in the range of 425-212 μm while the rest has a particle size between 150 and 93 μm. Figure 2-2 shows a scanning electron micrograph of the sand particles used. The BET surface area of sand particles was found to be 0.22 ± 0.020 m^2 g^{-1}. Addition of this sand did not change the pH of aqueous solutions to which it was added.

Figure 2-2. Scanning electron micrograph of sand particles.

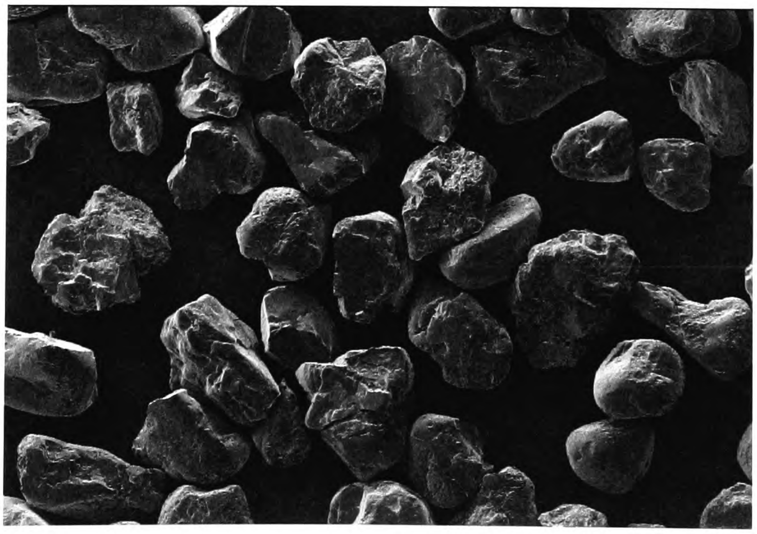

2.1.8. Steel powder

Stainless steel (316L) and mild steel (C1018) powders, having an average particle size of 32 μm, were purchased from Sandvik Osprey Ltd. (UK). The BET surface areas of 316L and C1018 steel powders were determined experimentally to be 0.13 ± 0.0003 and 0.14 ± 0.0009 $m^2 g^{-1}$, respectively. Figures 2.2 and 2.3 show scanning electron micrographs for the 316L and C1018 steel powders. The chemical compositions provided by the manufacturer for both steel powders are given in Table 2-5

2.1.9. Iron carbonate particles

Iron carbonate ($FeCO_3$) powder was supplied by Nalco, USA. The BET surface area was found to be 0.20 ± 0.002 $m^2 g^{-1}$. Figure 2-5 shows a scanning electron micrograph for the used iron carbonate particles.

2.2. METHODS

2.2.1. Emulsion preparation

Five mL of the relevant aqueous surfactant solution and five mL of the relevant oil were added to a sample tube (length 75 mm, internal diameter 25 mm). The mixture was homogenized using an Ultra-Turrax T25 homogeniser (IKA-Werke, Germany) equipped with an 18 mm diameter dispersion head rotating at 13,000 rpm for 2 min.

Table 2-5. Chemical compositions of 316L and C1018 steel powders.

(a) 316L stainless steel

Element	Cr	Ni	Mo	Mn	Si	C	P	S	Fe
% composition	16.5	10.9	2.3	1.31	0.69	0.0019	0.018	0.017	balance

(b) C1018 mild steel

Element	Mn	Si	C	P`	S	Fe
% composition	0.47	0.13	0.43	0.015	0.01	balance

Figure 2-3. Scanning electron micrograph of 316L stainless steel powder.

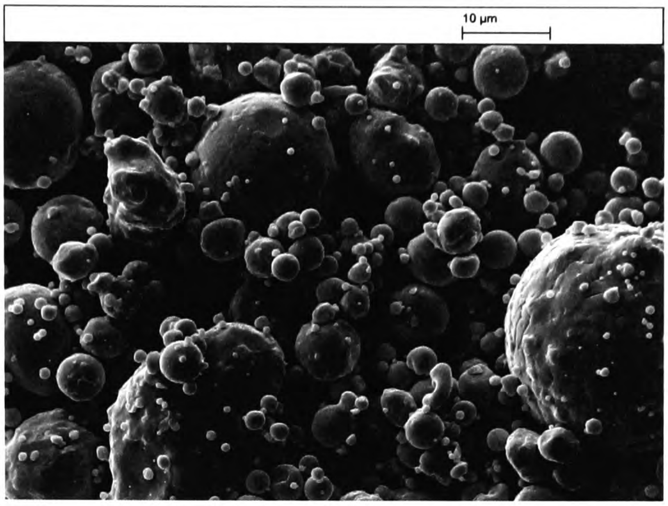

Figure 2-4. Scanning electron micrograph of C1018 mild steel powder.

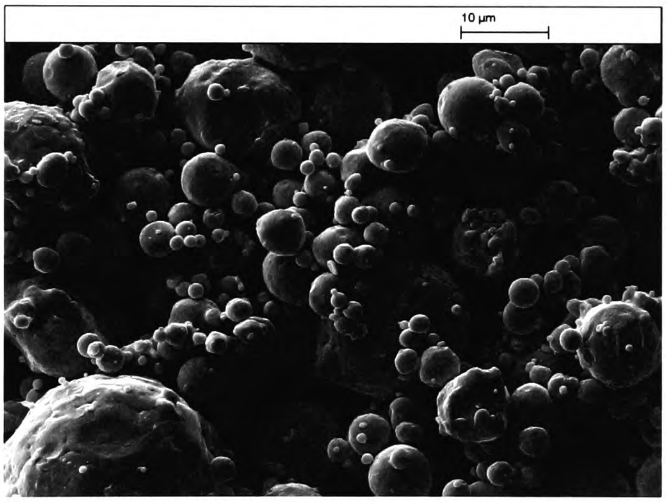

Figure 2-5. Scanning electron micrograph of iron carbonate particles.

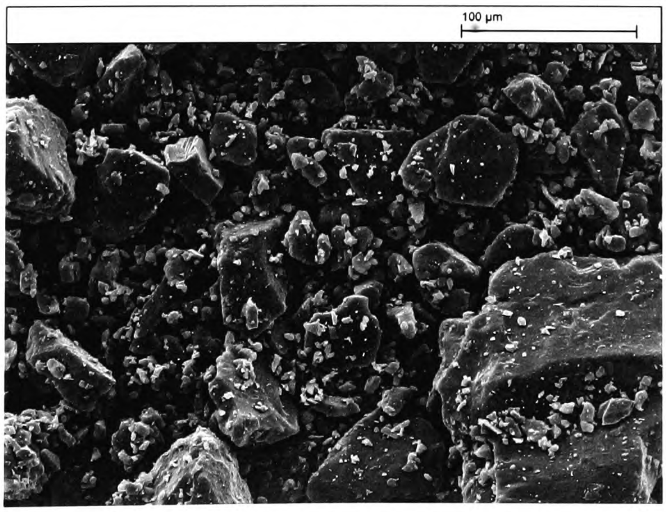

2.2.2. Emulsion characterisation

After homogenization, the emulsion conductivity was measured using a Jenway 4510 conductivity meter (Jenway, UK). The drop test was then performed to determine the emulsion type in combination with the conductivity measurement. The drop test is a simple method for distinguishing between water-continuous and oil-continuous emulsions. A droplet of the emulsion is added into a small sample tube containing either the relevant oil or water phase. If the droplet immediately disperses in the liquid that the droplet is added to, then it is very likely that the liquid is the continuous phase of the emulsion. If the droplet remains intact in the liquid then it is likely that the liquid is the dispersed phase of the emulsion.

Emulsions containing the alkylbenzyldimethylammonium chlorides were emulsified and stored at 40 ± 0.5 °C. The stability of o/w emulsions to creaming and coalescence was assessed by monitoring the change in height of the water-emulsion and oil-emulsion interfaces, respectively. The stability of w/o emulsions to sedimentation and coalescence was assessed by monitoring the change in height of the oil-emulsion and water-interfaces, respectively. The percentages of resolved aqueous and oil phase were calculated using equations (2-6) and (2-7), where h_w is the height of the water-emulsion interface 24 hr after emulsification, h_o is the height of the oil resolved 24 hr after emulsification and h_t is the total height of the emulsion plus the height of oil and/or water resolved (Figure 2-6).

$$\% \text{ water} = \frac{h_w}{h_t} \times 100 \qquad (2\text{-}6)$$

$$\% \text{ oil} = \frac{h_o}{h_t} \times 100 \qquad (2\text{-}7)$$

Photographs of the vessels were taken with a Kodak CX7530 digital camera (Kodak, USA). Optical micrographs of samples of emulsions were obtained using a Nikon Labophot microscope (Nikon, Japan) fitted with a QICam Fast CCD camera (Q-Imaging, UK) linked to a PC equipped with Image-Pro Plus software (Media Cybernetics, UK), which was used to add scale bars to the images. A small sample of the emulsion was placed onto a glass slide (Menzel-Gläser, Germany) with a Pasteur pipette and covered with a glass cover slip (Scientific Laboratory Supplies, UK), which was raised at one edge by a second cover slip.

Figure 2-6. Schematic of types of emulsion breakdown. It is assumed here that the oil phase is less dense than the water phase [3].

(a) Oil-in-water emulsion

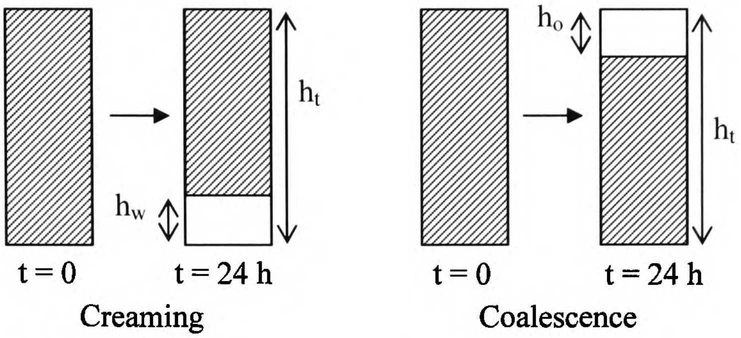

(b) Water-in-oil emulsion

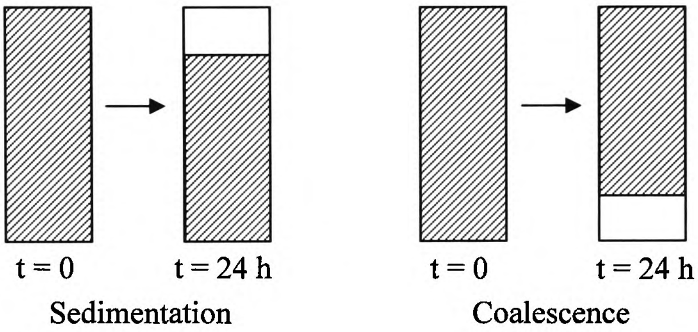

2.2.3. Corrosion inhibitor partitioning between oil and water

Partitioning of the alkylbenzyldimethylammonium chlorides between aqueous and oil phases was investigated at equal volume-ratios of oil and water. A volume of 50 mL of aqueous surfactant solution (with different brine concentration) was placed in a specially designed cell containing a magnetic stirrer bar (Figure 2-7). Then 50 mL of the relevant oil was added very gently down the side of the cell so as not to cause any mixing of the two phases. The cells or test tubes were placed in a double-walled vessel thermostatted by an LTD6G water bath (Grant, UK) positioned above a Multipoint magnetic stirrer (Variomag, Germany) and left to equilibrate for 7 days. The stirring speed was 150 rpm. However, in some cases this was reduced to 100 rpm to prevent mixing of the two phases. In order to determine the concentration of surfactant in each phase a two-phase titration [4] was used, which is based on the method of Epton [5, 6].

Figure 2-7. Schematic representation of the cell used in the determination of the partition coefficient of a solute for equal volume ratios of oil and

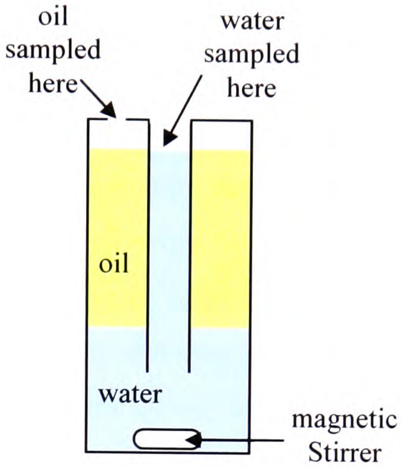

The two phases are chloroform (CH_3Cl) (Fisher, UK, purity > 99 %) and water plus the indicator solution, which is a mixture of two ionic dyes in an acidic aqueous solution: anionic disulphine blue (Sigma, UK, purity 95 %) and cationic dimidium bromide (Sigma, UK, purity 70 %). A colour change is observed in the chloroform layer, which is pink with excess anionic surfactant, and blue with excess cationic surfactant:

start of titration | end of titration

$$\mathbf{AD/CS} + \mathbf{CD} + \mathbf{AT} \longrightarrow \mathbf{CD/AT} + \mathbf{AD} + \mathbf{CS/AT}$$

AD/CS	CD	AT	CD/AT	AD	CS/AT
blue salt soluble in $CHCl_3$	*yellow* present in aqueous phase		*pink salt* soluble in $CHCl_3$	*green/yellow* present in aqueous phase	*colourless salt* soluble in $CHCl_3$

where AD = anionic dye, CD = cationic dye, AT = anionic titrant, CS = cationic sample.

The amount of cationic surfactant in a sample of water or oil can be determined by titrating against an anionic surfactant. A mixture of 10 mL of $CHCl_3$, 5 mL of Milli-Q water and 5 mL of mixed indicator solution were placed in a large test tube. An accurately measured volume of the equilibrium phase was withdrawn from the sample and added to the titration mixture. The mixture was shaken thoroughly by hand and titrated against sodium dodecylsulphate of known concentration until a pink colour was observed in the $CHCl_3$ layer. The titre values were used to calculate the concentration of cationic surfactant in each phase of the equilibrium system.

2.2.4. Adsorption of corrosion inhibitors at the solid-water interface using the depletion method & HPLC analysis

The adsorption isotherms of CnBDMAC corrosion inhibitors from aqueous solution into the powder surfaces were determined by measuring the extent of depletion of surfactant in solution following the adsorption. Surfactant solutions having different initial concentration ranging from 0.01 to 5 times the critical micelle concentration (cmc) were prepared by diluting concentrated stock solutions. A known amount of the solid powder was added to a fixed volume of a surfactant solution in a plastic bottle (wide neck polystyrene). The bottles were placed in a double-walled vessel thermostatted by an LTD6G water bath (Grant, UK), positioned above a Multipoint magnetic stirrer (Variomag, Germany), stirred for two hours and then left to equilibrate for two hours. The stirring speed was about 300 rpm. Following equilibration, the samples were decanted and centrifuged using a B&T Auto Bench Centrifuge at 4000 rpm for 30 min. to obtain a clear supernatant solution. About two mL of the clear supernatant were centrifuged using the Eppendorf MiniSpin plus centrifuge at 14000 rpm for 10 min. to remove all solid particles prior to analysis using the high performance liquid chromatography (HPLC). The amount of corrosion inhibitor adsorbed, Γ, in μmol g^{-1} was determined according to the following equation:

$$\Gamma = (C_o - C_{eq.})V/m \qquad (2\text{-}8)$$

where V is the volume of solution used (in mL), m is the mass of sand in g, and C_o and $C_{eq.}$ are the initial and equilibrium surfactant concentrations (in mM), respectively.

High performance liquid chromatography was used to determine the initial and equilibrium inhibitor concentrations [7, 8]. A Shimadazu liquid chromatograph equipped with LC-6A pump, 759A absorbance detector (Applied Biosystems, UK) operating at 262 nm and connected to a PC was used for the measurements. A SPHERISORB 5 μm CN (25 x 0.46 cm) column was used at a flow rate of 2 mL min^{-1}, and the injection volume was 20 μL. The mobile phase composed of a mixture of acetonitrile and 0.2 M sodium acetate adjusted to pH 5.0 with acetic acid. All the measurements were done at room temperature. The calibration curves demonstrated good linearity in the range of 1×10^{-5} to 25 mM with r^2 values of approximately 0.99.

2.2.5. Surface area determination of the solid particles

The determination of the surface area of particles is a very difficult task due to the ambiguous meaning of the term particle surface – inner or outer surface. An estimation of the surface area by measuring particle size by microscopy may ignore the surface roughness and underestimate the real surface area. The measurement of surface area by adsorption of a dye from solution can give useful information but the area and orientation of the adsorbed species and the accessibility of the surface in cracks and crevices may limit adsorption. Adsorption of gases (the BET method) provides an estimate of the surface area of dry particles but the similarity between dry and dispersed particles may be remote. In addition, the BET method comprises the outer surface area as well as the surface area of the pores.

In order to have true value for the specific surface areas of the used solid particles in this work, three different experimental techniques were used. These techniques are the BET method, the methylene blue method and from the size-distribution curve obtained by analysing the SEM images. The current section describes the theoretical bases and the experimental procedures for those methods.

2.2.5.1. The BET method

The specific surface areas of sand, 316L steel, C1018 steel and iron carbonate powders were determined using nitrogen gas adsorption isotherms analysed according to the Brunauer, Emmett and Teller (BET) method [9, 10]. The total surface area can be estimated by measuring the amount of gas needed to form an adsorbed monolayer by physical adsorption, in which case the number of molecules adsorbed divided by the area per molecule yields the surface area. The nitrogen adsorption isotherms were measured at 77 K using a TriStar 3000 Analyzer, manufactured by Micromeritics, UK.

Brunauer, Emmett & Teller [9, 11] based their theory on the following main assumptions:

I. The surface of the material consists of a great number of discrete equivalent adsorption sites (a homogeneous surface).

II. At a certain vapour pressure a varying number of molecules are adsorbed on any one site. They are stacked on top of each other to form a number of layers.

III. The heat of adsorption and the condensation constant (the fraction of arriving molecules per second actually condensing on empty sites) in all layers above the first are the same and equal to those of bulk liquid.

IV. At saturation, the number of layers becomes infinite. Therefore, the model is from a theoretical point of view only valid for a nonporous material.

V. A molecule covered by another molecule cannot evaporate.

VI. There is no interaction "horizontally" between molecules in different sites.

VII. At dynamic equilibrium the number of molecules evaporating from a layer is equal to the number condensing on the layer below (condensation constant = evaporation constant).

The BET equation in the linear from is given by equation (2-9):

$$\frac{P}{V_a(P^\circ - P)} = \frac{1}{V_m C} + \frac{(C-1)}{V_m V}\left(\frac{P}{P^\circ}\right) \tag{2-9}$$

where:

P is the partial vapour pressure of adsorbate gas in equilibrium with the surface at 77.4 K (b.p. of liquid nitrogen), in pascals

P° is the saturated pressure of adsorbate gas, in pascals

V_a is the volume of gas adsorbed at standard temperature and pressure (STP) [273.15 K and atmospheric pressure (1.013×10^5 Pa)], in millilitres

V_m is the volume of gas adsorbed at STP to produce an apparent monolayer on the sample surface, in millilitres

C is a dimensionless constant, related to the enthalpy of adsorption of the adsorbate gas on the powder sample

In the BET technique, solid samples were pre-treated by applying a combination of heat (90 °C) and a flowing inert gas stream (Helium) to remove adsorbed gases acquired from atmospheric exposure. The solid is then cooled and nitrogen is admitted to the solid in controlled increments. After each dose of the admitted nitrogen, the pressure is allowed to equilibrate and the quantity of gas adsorbed is determined. The gas volume adsorbed at each equilibrium pressure (at constant temperature) defines an adsorption isotherm from which the quantity of gas required to form a monolayer on the external surface of the solid and its pores is determined. With the area covered by each adsorbed gas molecule known, the surface area can also be calculated.

The measured adsorption isotherms for all the investigated solid particles showed no significant hysteresis. Figure 2-9 shows the adsorption and desorption isotherms of N_2 at 77 K onto the iron carbonate particles. As seen in the figure, the shape of the adsorption isotherm is a typical type II one, which indicates that the particles are nonporous or it have pores larger than micropores (mesopores). The inflection point is near the completion of the monolayer.

A plot of $[P/V_a(P^{\circ}-P)]$ against the reduced gas pressure (P/P°) will give a straight line of a slope equal to $(C - 1/V_m\ V)$ and an intercept equal to $(1/V_m C)$. This will allow the determination of the C and V_m constants from the same isotherm. From these values, V_m is calculated as 1/(slope + intercept), while C is calculated as (slope/intercept) + 1. From the value of V_m, the specific surface area, S, in $m^2\,g^{-1}$, is calculated according to the following equation:

$$S = \frac{V_m N_{Av} a}{m \times 22400} \qquad (2\text{-}10)$$

where:

N_{Av} is Avogadro's constant

a is the effective cross-sectional area of one adsorbate molecule, in square metres ($0.162\ nm^2$ for nitrogen)

m is the mass of powder, in grams

22400 is the volume occupied by 1 mole of the adsorbate gas at STP, in millilitres

Figure (2-8) shows an example of the linearized-BET plot for the adsorption of N_2 onto solid particles, in this case the plot is for the iron carbonate particles.

Figure 2-9. Adsorption/desorption isotherms of N_2 at 77 K for iron carbonate particles.

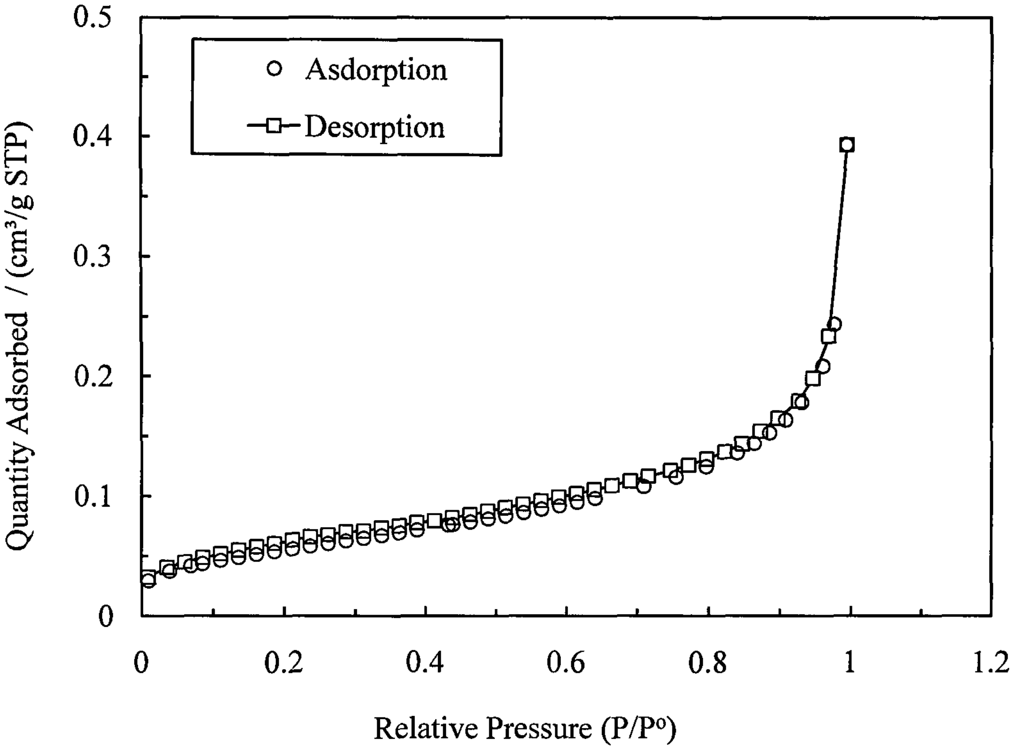

Figure 2-10. Plot of the linearized-BET equation versus the reduced pressure.

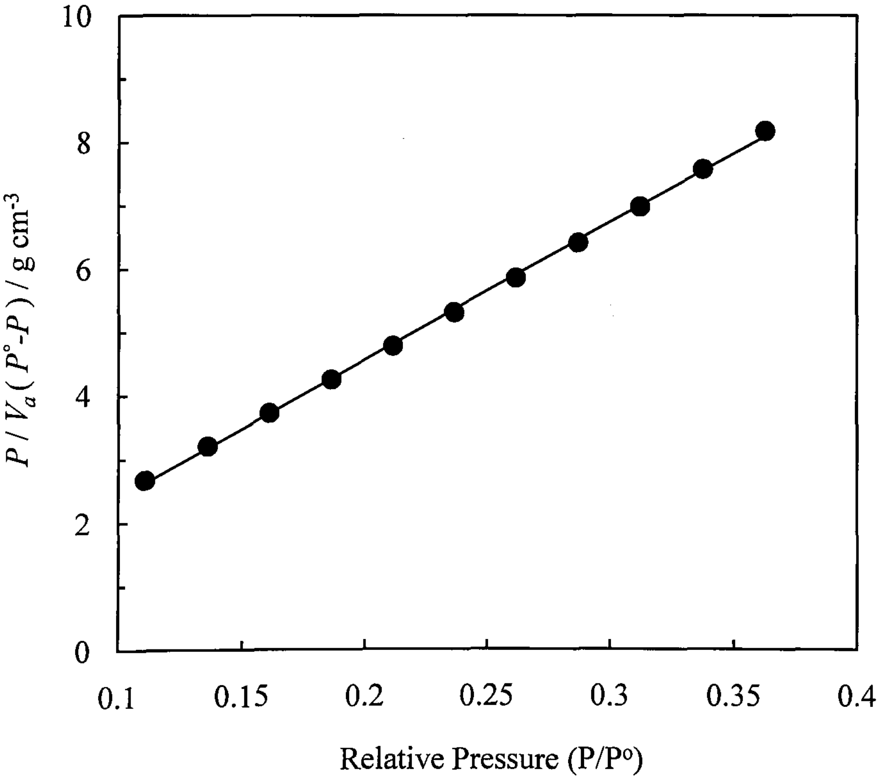

2.2.5.2. The methylene blue adsorption method

Methylene blue (BDH Chemicals Ltd, UK) was dried at 110 °C for 2 hours before use. All of the methylene blue solutions were prepared with Milli-Q water. The concentration of methylene blue was analysed by measuring their absorbance at 662 nm on a Unicom spectrophotometer. This wavelength corresponds to the maximum absorption peak of the methylene blue monomer. A calibration curve (Figure 2-11) of absorbance against the aqueous methylene blue concentrations was obtained by using standard methylene blue solutions of known concentrations at pH values between 6.5 and 7. The experimental data were fitted by a straight line with a high determination coefficient ($R^2 = 0.99$).

The adsorbed amount of methylene blue was determined using the depletion method described in section 2.2.4. The concentrations of methylene blue before and after mixing with the solid particles were determined by measuring the UV absorbance, which was then converted into the corresponding concentration using the pre-determined calibration graph (Figure 2-11). The adsorbed amounts of methylene blue on the solid particles were calculated using equation (2-3) and the adsorption isotherms were then constructed. Two replications were carried out for each of the solid particles investigated. Figure 2-12 shows a typical isotherm for the adsorption of the methylene blue onto the C1018 mild-steel particles. The experimentally determined adsorption isotherms were fitted to the Langmuir model given by the following equation:

$$\Gamma = \Gamma_{\max} \frac{KC}{1+KC} \tag{2-11}$$

where Γ represents the number of moles of methylene blue adsorbed per gram of the solid particle, C is the equilibrium concentration, $\Gamma_{\max}$ is the number of moles of methylene blue per gram of sand required to form a monolayer and K is the equilibrium constant.

The calculation of the specific surface area by the methylene blue method is based on the assumptions that (I) the adsorbate forms a monolayer, (II) the area a_{MB} occupied by each adsorbate molecule is known, (III) the particles are dispersed as individual species and (IV) the access of the adsorbate to the particle surface is not affected by porosity.

Figure 2-11. Calibration graph of the absorbance versus the aqueous concentration of methylene blue at pH = 6.5-7 and λ_{max} = 662 nm.

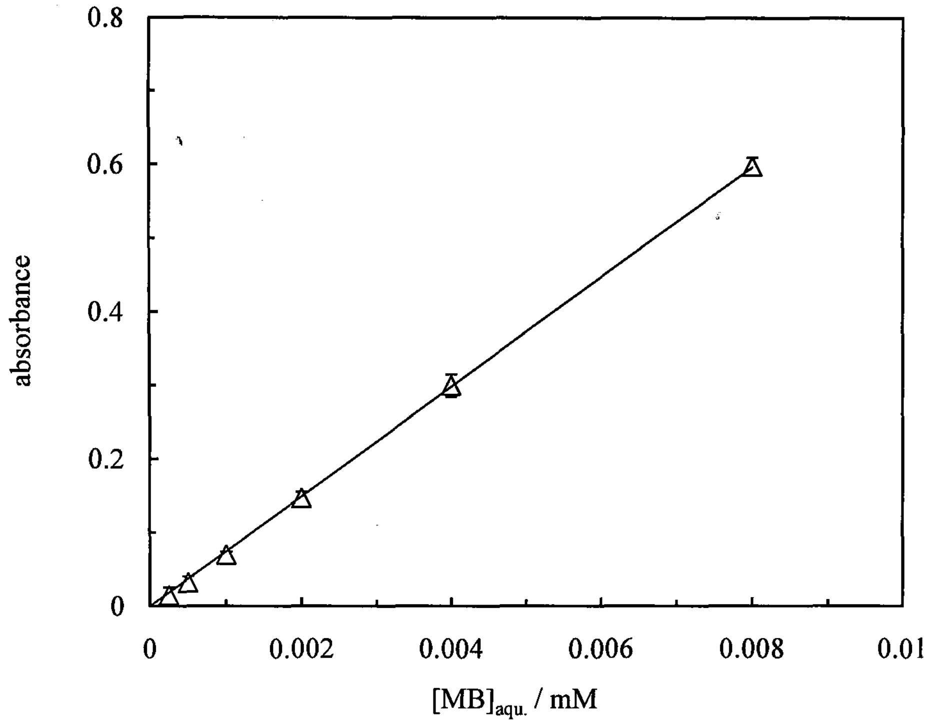

Figure 2-12. Adsorption isotherm of Methylene blue from water onto C1018 mild steel powder at 25 °C, using depletion method, pH =6.5-7. Fitted to the Langmuir model, Γ_{max} = 0. 08 μmol g^{-1} and k = 838 mM^{-1}.

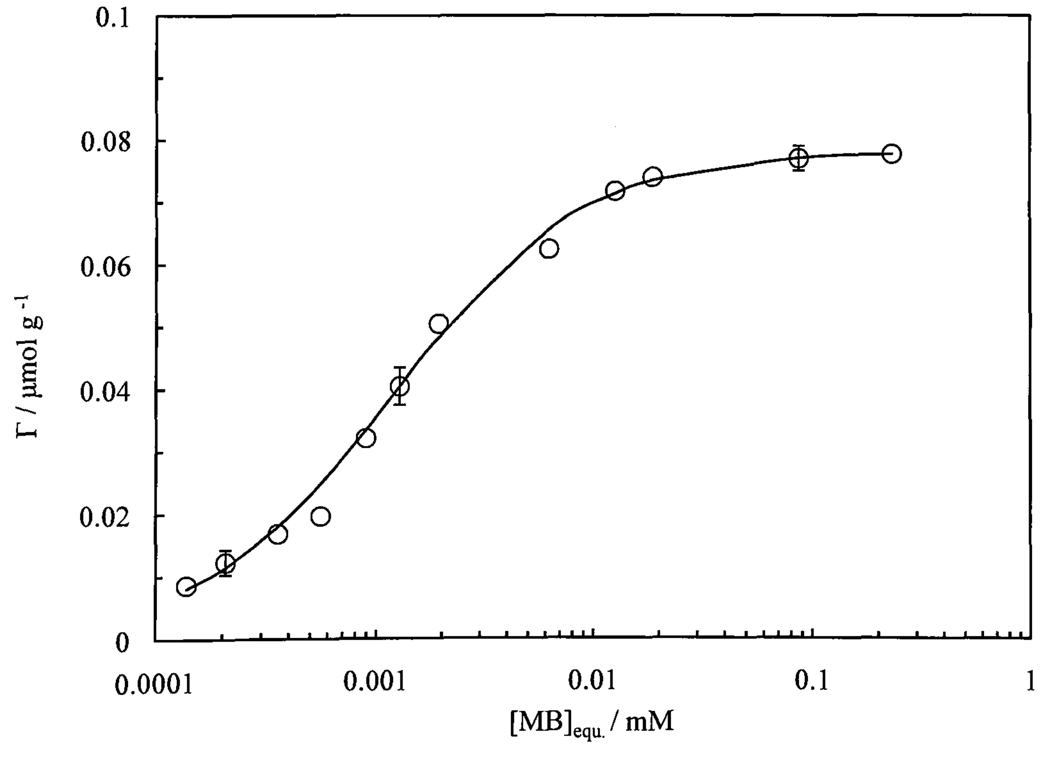

The specific surface area was calculated by using the following equation:

$$S = \Gamma_{\max} \times N_A \times a_{MB} \times 10^{-20} \qquad (2\text{-}12)$$

where S is the specific surface area in $m^2\ g^{-1}$, Γ_{max} in mole g^{-1}, a_{MB} is the surface area occupied by one molecule of methylene blue (197.2 Å^2) and N_A is the Avogadro's number (6.02 x 10^{23} mol^{-1}).

2.2.5.3. Analysis of the SEM Images

The diameters of the individual solid particles were determined by analysing the SEM image with Image-Pro Plus software (Media Cybernetics, Inc., USA). The method of image analysis consisted of measuring the diameter of at least 400 particles. Figures (2-9) to (2-11) show the particle-size distribution by number (%) for 316L, C1018 and sand powder, respectively. The particle-size distributions were expressed in different classes between 3 and 30 microns for stainless and mild steel particles and between 100-450 microns for sand powder. The presented particle diameter is the mean projected diameter, which takes into account both dimensions of the particle in the measurement plane, being the diameter of a circle having the same projected area as the particle [12]. In all calculations, a spherical shape has been assumed for all the investigated solid particles.

The average diameters for C1018 mild-steel and 316L stainless-steel particles, measured from the SEM images, were found to be 5.6 and 6.8 micron, respectively. The average diameter of sand particles was 210 microns.

When a sample powder has a particle size distribution, relationship between specific surface area and the size distribution can be addressed as follows. Supposing that the spherical particles with a true density, ρ and a diameter, d_i exist n_i per unit mass, the specific surface area, S can be given by the following equation [13, 14]:

$$S = \frac{6}{\rho} \frac{\sum n_i d_i^2}{\sum n_i d_i^3} \qquad (2\text{-}13)$$

For taking account of correspondence to particle size distribution, n_i is expressed here with a ratio ν_i to the total number of particles N.

$$n_i = \nu_i N \qquad (2\text{-}14)$$

Figure 2-13. Particle-size distributions by number (%) of the 316L stainless-steel powder.

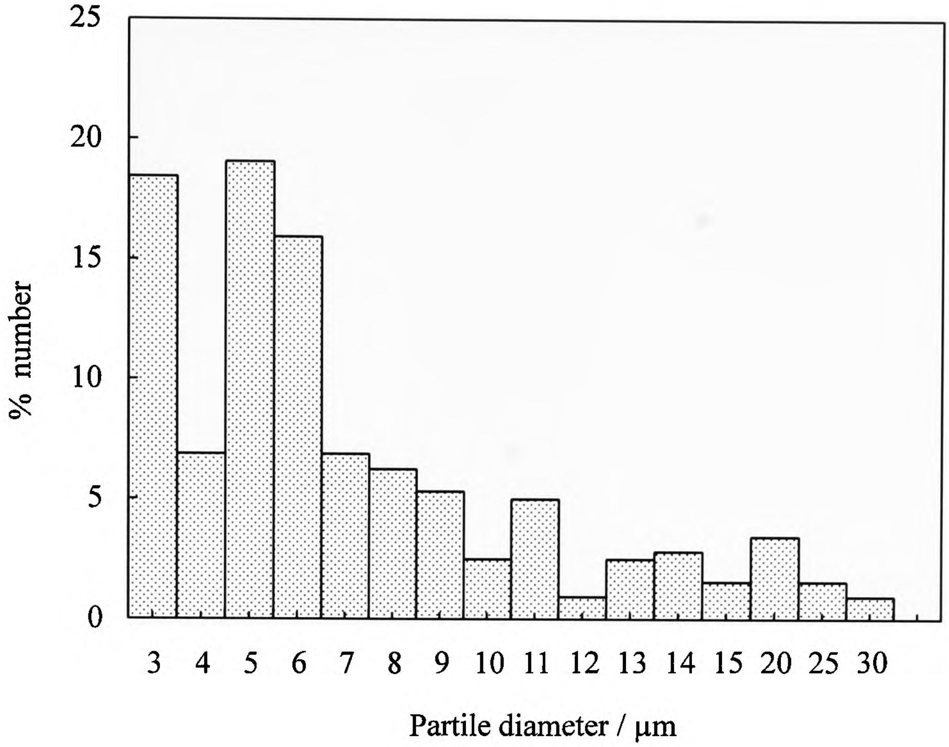

Figure 2-14. Particle-size distributions by number (%) of the C1018 mild-steel powder.

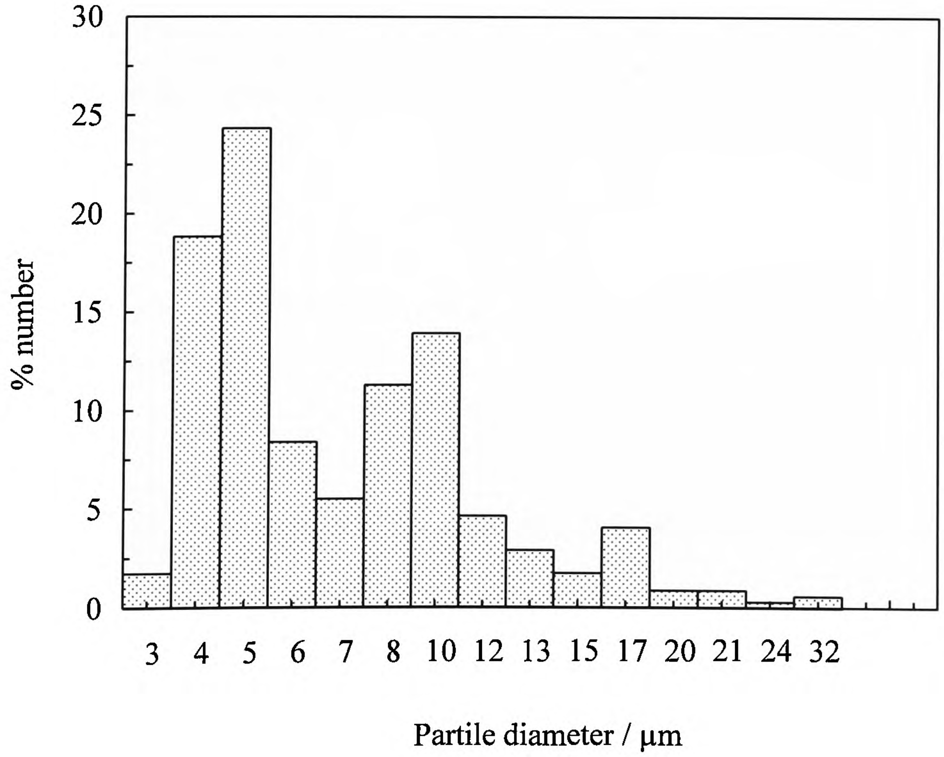

Figure 2-15. Particle-size distributions by number (%) of sand particles.

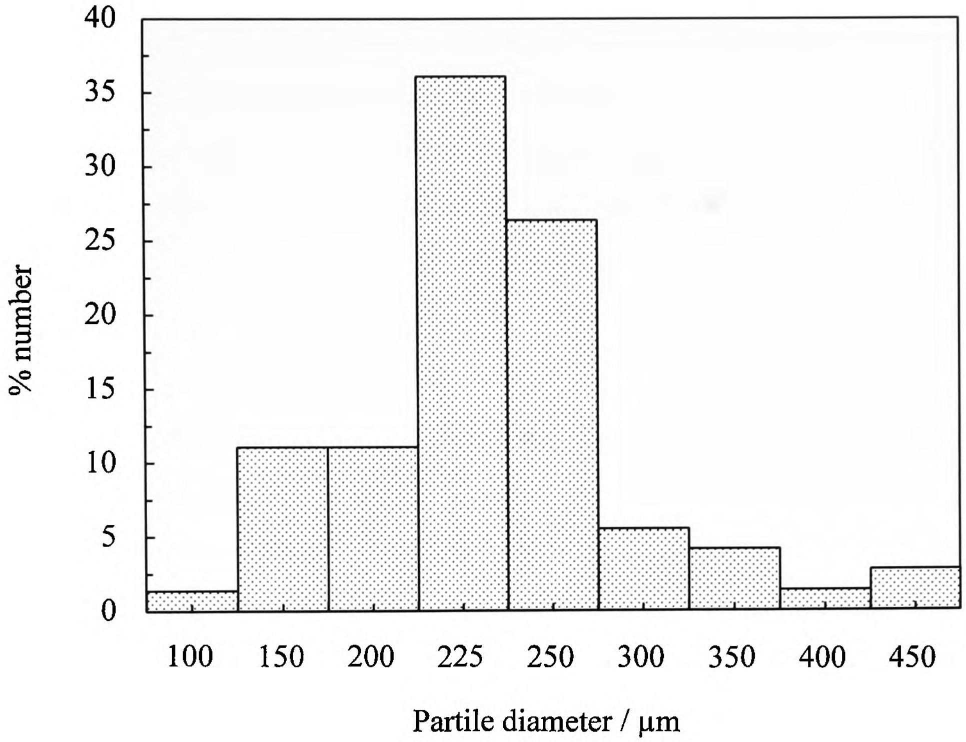

The particle diameter, d_i is also expressed with a ratio λ_i to the mode particle size D.

$$d_i = \lambda_i D \tag{2-15}$$

Substituting equations (2-14) and (2-15) into equation (2-13) gives the following:

$$S = \frac{6f}{\rho D} \tag{2-16}$$

where f is a coefficient depending on shape of the size distribution and is given by the following equation:

$$f = \frac{\sum v_i \lambda_i^2}{\sum v_i \lambda_i^3} \tag{2-17}$$

v_i and λ_i can be obtained from data of particle size distribution using equations (2-14) and (2-15), respectively.

The values of the surfaces areas of the solid particles calculated from the particle-size distribution are shown in Table 2-6 compared to those determined by the BET and methylene blue methods. As shown, the values of the surface areas measured by the three techniques are very close to each other. The values of specific surface areas determined from the SEM images refer only to the outer (geometrical) surface of particles. These values are expected to be less than those determined by the BET method if the measured particles are porous.

The solid particles used in this work are nonporous as indicted from the values of the surface area determined by the BET and SEM methods.

Table 2-6. Surface areas of the solid particles determined by the BET, Methylene blue and analysis of SEM images methods.

Solid particles	Surface area / m^2 g^{-1}		
	Methylene	BET	Image Analysis
CB Reference*	30.40	30.79	—
Sand	0.20	0.22	0.18
C1018 Powder	0.12	0.14	0.16
316L powder	0.14	0.13	0.15

*** Carbon black powder reference-material (surface area = 30.6 ± 0.75 m^2 g^{-1})**

2.2.6. Quartz Crystal Microbalance technique

A Quartz Crystal Microbalance (QCM) with dissipation monitoring instrument, Q-Sense E4 system, from Q-Sense, Sweden (Figure 2-16), was used for the measurement of the *in-situ* adsorption of CnBDMAC surfactants from aqueous solution onto stainless steel coated crystals. Four stainless steel-coated crystals (SS2343 type stainless steel) were purchased from Q-Sense. The crystals have the specification shown in Table 2-7. The QCM device consists of a thin quartz disc sandwiched between a pair of electrodes. Due to the piezoelectric properties of quartz, it is possible to make the crystal oscillate laterally by applying an AC voltage across its electrodes.

Figure 2-16. The complete Q-Sense E4 system. (a) An electronics unit where the signals are generated and data is collected before being sent to the computer, (b) a chamber platform with four flow modules (each flow module holds one sensor crystal), (c) an external 4-channel digital peristaltic pump for sample feeding and (d) a personal computer has the QSoft and QTools software for acquisition and data analysis.

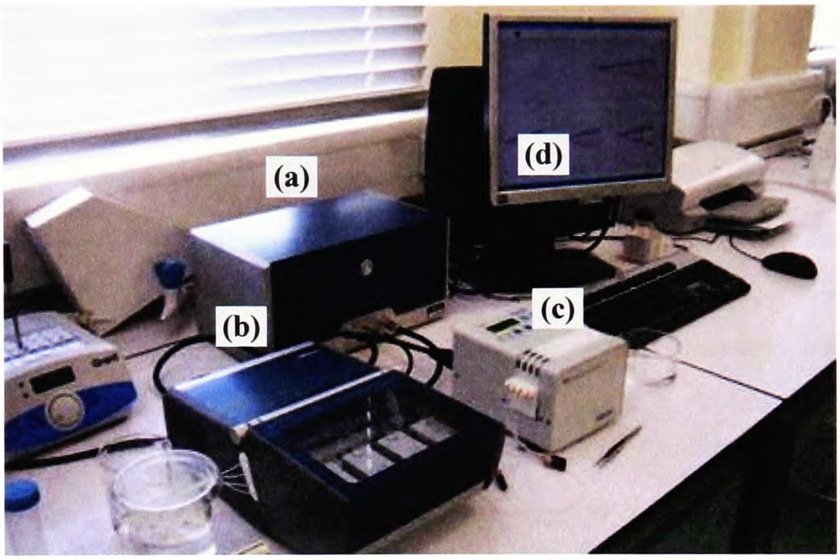

The resonant frequency of the crystal depends on the mass of the crystal. When a substance is adsorbed on to the crystal, the frequency decreases. The decrease in frequency is proportional to the adsorbed mass on the crystal. The QCM operates as a very sensitive balance.

Table 2-7. Specifications of the Q-sense stainless steel-coated crystals.

Frequency	4.95 MHz ± 50 kHz
Diameter	14 mm
Thickness	0.3 mm
Finish	optically polished
Sensor surface coating	stainless steel (SS2343)
Electrode layer	Au, 100 nm
Top layer	SS2343, 50 nm (stainless steel)

The change in adsorbed mass (*Δm*) is calculated using the Sauerbrey equation [15]:

$$\Delta m = -\frac{C \times \Delta f}{n} \tag{2-18}$$

where C is a constant equal to 17.7 ng cm^{-2} Hz^{-1} for a 5 MHz quartz crystal, Δf is the shift in frequency and n is the overtone number.

All the QCM parts in contact with the surfactant solution were rinsed with ethanol solution (96%) and dried with nitrogen gas. The stainless steel-covered crystals were cleaned by a hot basic piranha solution having a 5:1:1 mixture of water, ammonium hydroxide and hydrogen peroxide for 5 min. The crystals were then cleaned in an ethanol solution using an ultrasonic cleaner for 5 min. Finally, the crystals were rinsed with Milli-Q water, flushed with nitrogen and dried in an oven at 45 °C for 15 min. This extensive cleaning was done to remove any organic contaminants that may be present on the crystal surface prior to the introduction of the surfactant solutions. After drying, the crystals were inserted into the measurement chamber and the chamber was filled with gas-free deionised Milli-Q water.

The following experimental procedures were carried out for the preparation of surfactant solutions prior to the adsorption measurement:

I. The aqueous surfactant solution was heated up to 50 °C for about 15 minutes.

II. The heated solution was then placed in a vacuum desiccator and the pressure was lowered gradually to the water vapour pressure for about 5 min. in order to get rid of the dissolved gases. The degassing time was kept to a minimum to decrease the possibility of foam formation.

III. The surfactant solutions were kept thermostatted at 50 °C until the start of the measurement. This in turn reduces the possibility of re-dissolving air gases in the aqueous surfactant solution.

IV. The aqueous surfactant solution was maintained continuously at a temperature above the desired working temperature by about 5 °C during the measurements. This reduces the possibility of forming air bubbles, since the temperature inside the device is much lower than the outside.

V. The flow rate of the aqueous surfactant solution was 100 μ per minute.

The QCM working principle, instrumentation, working in the liquid medium and factors affecting the accuracy of measurements such as density, viscosity, temperature of aqueous solution are discussed in more detail in Chapter 5. Additionally, different experimental setups and procedures for carrying out the adsorption measurements have been evaluated and discussed.

2.2.7. Measurement of the zeta potential and surface charge density

The zeta potential of aqueous dispersions was measured using a Malvern ZetaSizer 3000 instrument. This instrument uses the electrophoresis technique to measure the zeta potential using laser Doppler velocimetry. In this technique, a voltage is applied across a pair of electrodes at either end of a cell containing the particle dispersion. Charged particles are attracted to the oppositely charged electrode and their velocity is measured and expressed in unit field strength as their mobility. Zeta potential (ζ) is related to the electrophoretic mobility (U_E) by the Henry equation [16]:

$$U_E = \frac{2\varepsilon\xi f(\kappa a)}{3\eta} \qquad \text{(2-19)}$$

where ε is the dielectric constant of the solvent, η is the viscosity of the medium, $f(\kappa a)$ is the Henry's function, a is the radius of the particle and κ is the Debye length.

Two values are generally used as approximations for the $f(\kappa a)$ determination, i.e., either 1.0 or 1.5. The electrophoretic determination of the zeta potential is most commonly carried out in an aqueous medium and a moderate electrolyte concentration. The magnitude of $f(\kappa a)$ in this case is 1.5 and is referred to as the Smoluchowski approximation. For small particles in low-dielectric constant-media, $f(\kappa a)$ becomes 1.0. This is referred to as the Hückel approximation and is generally used for non-aqueous systems [17].

The ZetaSizer 3000 instrument (Figure 2-17) is a combination of a laser light scattering spectrometer with an electrophoresis instrument [18]. The electrophoretic cell is constructed to allow the application of an electric field perpendicular to the incident light and the observation of low-angle light scattering. A laser beam split from the incident beam is used as the reference signal, which travels the same optical path as the scattered light to the detector. The magnitude of the Doppler shift is too small to be measured directly with reasonable accuracy.

Figure 2-17. Instrumentation for the Marlven Zetasiszer 3000 [18].

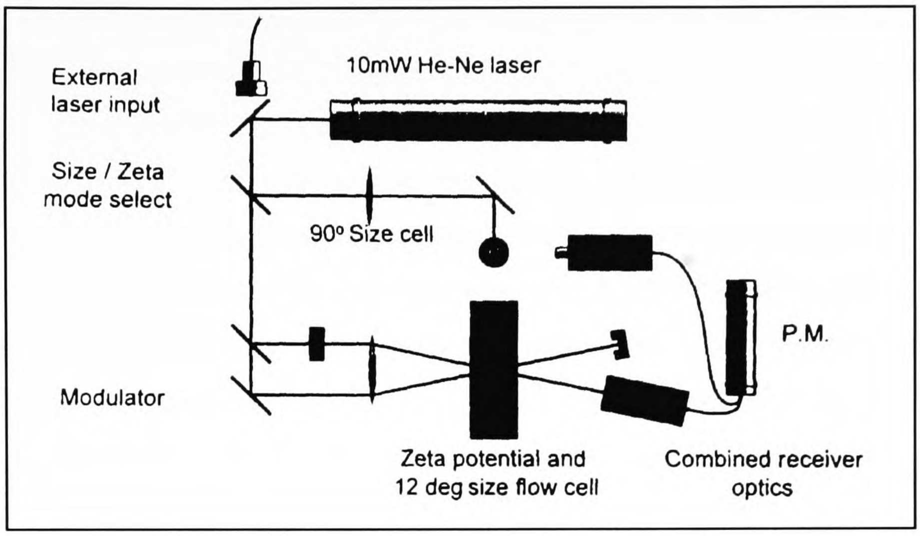

The shift is magnified therefore by heterodyning, which mixes the scattered light with the reference beam at the detector. This produces a fluctuating intensity signal where the rate of fluctuation is proportional to the speed of the particles. A digital signal processor is used to extract the characteristic frequencies in the scattered light [18].

In highly conductive samples, the voltage applied across the cell may create heat. The instrument senses conductivity and, if the conductivity is too high, automatically switches the current between pulses to prevent heating of the sample.

The aqueous solutions have been filtered through a Whatman Grade 5 filter paper (pore size = 2.5 μm) to eliminate the particles having large sizes. This in turn helps in preventing the sedimentation of the solid particles during the measurement of the zeta potential. All the measurements have been carried out at 25 °C.

The surface charge density, σ, of the solid particle was determined according to the Grahame equation [19, 20]:

$$\sigma = \sqrt{8\varepsilon\varepsilon_o kTc_i}\,\sinh(\frac{z_i e\varphi}{2kT}) \qquad (2\text{-}20)$$

where ε_o is the permittivity of the vacuum, ε is the dielectric constant of the solvent, k is the Boltzmann constant, T is temperature, e the electron-charge, φ is the surface potential (≈ ζ, the zeta potential), C_i and Z_i are the concentration and the charge number of the ions of type *i* in the solvent.

2.2.8. Measurement of surface tension

In this study, surface tension measurements were used to determine the critical micelle concentration of surfactants in aqueous solution, in the presence and absence of electrolyte. The measurements were performed using the du Noüy ring method on a K12 processor tensiometer (Krüss, Germany) thermostatted by an LTD6G water bath (Grant, UK). The platinum/iridium du Noüy ring (R = 9.545 mm, r = 0.185 mm) was placed in the apparatus, then the liquid was added to a glass vessel within a thermostatted cell and left to equilibrate. Using the fully automatic measurement method, the tensiometer dips the ring into the liquid and then pulls it out automatically by raising and lowering the height of the thermostatted cell. As the ring is pulled from the liquid surface, a meniscus forms. The force required to raise the meniscus reaches a maximum when the tangent at the point of wetting is perpendicular to the liquid surface. The measurement was repeated until it reaches a plateau. The reproducibility was within ± 0.1 mN m^{-1}. Prior to each measurement, the ring was cleaned in a solution of 10 wt. % KOH in ethanol then rinsed with Milli-Q water and finally heated in a blue Bunsen burner until the ring glowed white.

The du Noüy ring method is one of the detachment methods used for measuring the surface tension and is named after the French physicist who developed it in the late1800s [17]. The method involves slowly raising a platinum ring through a liquid until it detaches from the surface (Figure 2-18). The surface tension, γ, is related to the maximum force, F_{max}, needed to detach the ring from the liquid surface, by the following equation:

$$F_{max} = mg = 2\ (2\pi R_{ring})\ \gamma \qquad for\ \theta = 0 \qquad (2\text{-}21)$$

where m is the mass of the solution raised by the ring g is the acceleration due to gravity, θ is the contact angle and R_{ring} is the radius of the ring. The circumference is $2\pi R_{ring}$, and factor 2 is because of the two sides of contact. The term $4\pi R$ corresponds to the wetted length of the ring.

However, a correction needs to be applied in this method, due to the volume of the liquid hanging from the ring as it is pulled above the surface [21]. Harkins and Jordan [22] pointed out that a factor relating to the shape of the meniscus should be taken into account and a modified equation was given:

$$\gamma = mgF / 4\pi R_{ring} = \Delta\rho VgF / 4\pi R_{ring} \qquad (2\text{-}22)$$

where F is a correction factor to allow for the complex shape of the liquid just before break-away and for the non-vertical surface tension forces [17]. The correction factor is a function of R_{ring}^3/V and R_{ring}/r, where V is the volume of liquid pulled from the surface by the ring and r is the radius of the wire from which the ring is made. The correction factors are applied by measuring the radii of the ring, the wire and the density difference between the fluids $\Delta\rho$. A value of R_{ring}^3/V is calculated for each determination and the correction factor is obtained from tables according to the value of R_{ring}/r. Zuidema and Waters [23] needed correction values for small interfacial tensions. For this reason, they carried out interpolation calculation on the data from Harkins and Jordan in order to cover the range of small interfacial tensions more accurately. The correction factor they introduced is given by the following equation:

$$F = 0.725 + \sqrt{\frac{0.01452\gamma}{(2\pi R_{ring})^2 \times \Delta\rho} + 0.04534 - \frac{1.679}{R_{ring}/r}} \qquad (2\text{-}23)$$

In this study, the tensiometer automatically applies the equation of Zuidema and Waters, which corrects the measured values for the weight of the liquid meniscus.

Figure 2-18. Schematic representation of the du Noüy ring used for the determination of surface tension of liquids.

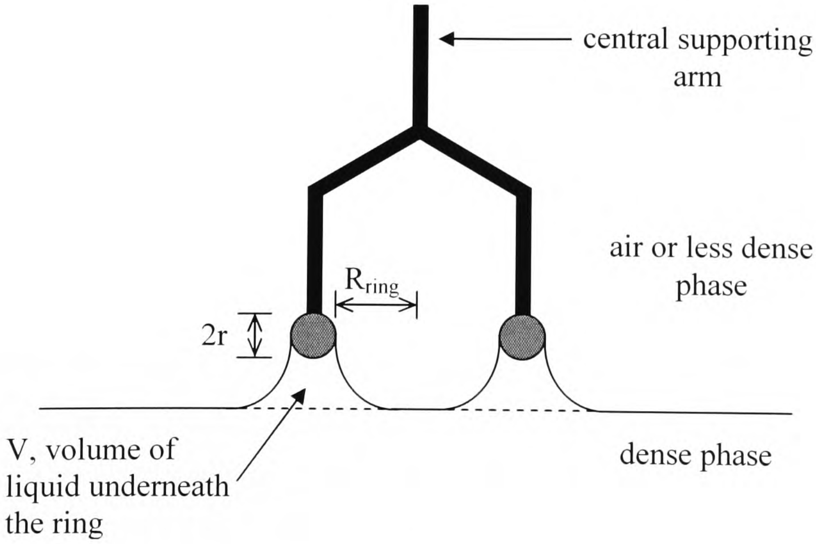

2.2.9. Scanning Electron Microscopy

A scanning electron microscope (SEM) is a type of electron microscope capable of producing high resolution images of a sample surface. In a typical SEM, electrons are emitted from a cathode (typically tungsten or lanthanum hexaboride) and are accelerated towards an anode. The electron beam is focused by one or two condenser lenses into a beam with a very fine focal spot (approximately 1 - 5 nm in diameter). The beam passes through pairs of scanning coils in the objective lens, which deflect the beam in a raster fashion over a rectangular area of the sample surface. Images are produced by monitoring low energy secondary electrons. The brightness of the signal depends on the number of secondary electrons reaching the detector. The resulting signal is rendered into a two-dimensional intensity distribution that can be viewed as a digital image. The SEM is also fitted with a backscattered electron detector, which is used to detect contrast between areas with different chemical compositions.

In this study, an EVO 60 SEM (Carl Zeiss SMT AG, Germany) equipped with an INCAEnergy 350 EDX detector (Oxford Instruments, UK) was used to capture images for the solid powders investigated.

2.2.10. Corrosion rate measurements

The corrosion rates of C1018 mild steel in 4.7 wt. % brine solution in the presences of different gases were determined using the linear polarization resistance method. Mild steel electrodes of the C1018 type (with the following elemental composition: Fe 98.898%, Mn 0.72%, Si 0.19%, C 0.18%, P 0.009% and N 0.003%) of 4 mm diameter and 30 mm length were supplied by European Corrosion Supplies, UK. The electrodes were received in vapour corrosion inhibitor (VCI) impregnated envelopes. They were washed in acetone to remove the VCI and then dried in an oven at 60 °C prior to use.

The Linear Polarization Resistance (LPR) method, which is also known as the 'bubble test', is a widely used electrochemical technique for monitoring the corrosion rates of metals in a variety of applications. Some examples include the evaluation of corrosion inhibitors [24], the oil industry [25] and pipelines [26]. The LPR technique involves applying a potential to a freely corroding steel specimen and measuring the resultant current response. The plot of voltage versus the current intensity is frequently linear. The polarization resistance, R_P is defined as the ratio of the applied potential to the current response near the corrosion potential [27].

$$R_P = \frac{\Delta E}{\Delta I} \tag{2-24}$$

where ΔE is the change in potential and ΔI is the change in current.

The polarization resistance is then converted to a corrosion current using the Stern-Geary equation [28]:

$$I_{corr} = \frac{\beta}{R_P} \tag{2-25}$$

where β is the Stern-Geary constant and I_{corr} is the corrosion current.

The Stern-Geary constant is measured directly in separate experiments from Tafel constants for the anodic and cathodic half-cell reactions [27]. Using Faraday's law of electrolysis, the corrosion current is converted into the mass reacted in the electrochemical reaction and hence the corrosion rate r, in units of millimetres per year, could be calculated according to equation (2-26):

$$r = \frac{I_{corr} M}{nF\rho} \tag{2-26}$$

where F is the Faraday constant (96487 C mol^{-1}), M is the metal atomic weight, n is the number of electrons exchanged and ρ is the density of the metal in g cm^{-3}.

For the corrosion rate measurements, 800 mL of aqueous phase was added to the thermostatted measurement cell fitted with temperature and electrochemical probes, gas dispersion tubes and sealed against ingress of air (Figure 2-19). The electrochemical probe consisted of a stainless steel rod fitted with three C1018 steel electrodes; the working, counter and reference electrodes. The system was thermostatted at 25 ± 0.2 °C using a hotplate and stirred at a speed of 200 rpm with a magnetic stirrer. The aqueous phase in the cell was purged with the desired gas for 2 hr prior to the start of the experiment to ensure gas saturation. In a typical experimental run, corrosion rates in the absence of added inhibitor were monitored for 1-2 hours to determine the baseline corrosion rate. The required concentration of the inhibitor was then added and the corrosion rate was continuously monitored for 15-20 hours, long enough to ensure the rate had reached a steady value.

Figure 2-19. The ‘bubble test’ setup [3].

(a) Schematic representation

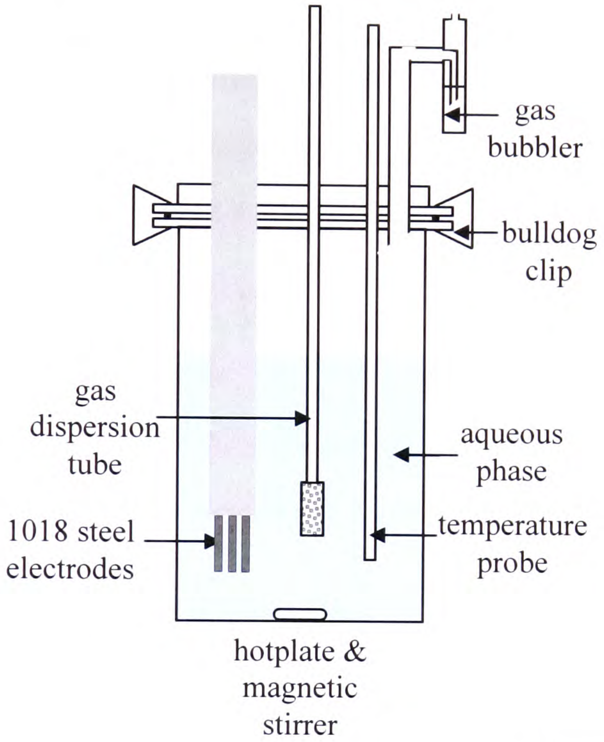

(b) Photograph of the ‘bubble test’ setup.

2.3. REFERENCES

1. D. Lide, *CRC Handbook of Chemistry and Physics*, CRC Press, Boca Raton (2007).
2. ASTM Standard 1141-98, *Standard Practice for the Preparation of Substitute Ocean Water*, ASTM International, West Conshohocken, PA (2003).
3. J. T. Hicks, *Surfactants Aspects of Corrosion Inhibitors*, Ph.D. Thesis, Hull University (2007).
4. V.W. Reid, G.F. Longman and E. Heinerth, *Tenside,* **4**, 292 (1967).
5. S. R. Epton, *Nature (London),* **160**, 795 (1947).
6. S. R. Epton, *Trans. Faraday Soc.,* **44**, 226 (1948).
7. J. Dudkiewicz-Wilczynska, J. Tautt and I. Roman, *J. Pharm. Biomed. Anal.,* **34**, 909 (2004).
8. S. J. Prince, H. J. McLaury, L. V. Allen and P. McLaury, *J. Pharm. Biomed. Anal.,* **19**, 877 (1999).
9. S. Brunauer, P. H. Emmett and E. Teller, *J. Am. Chem. Soc.,* **60**, 309 (1938).
10. S. Lowell, *Introduction to Powder Surface Area*, Wiley-Interscience, New York (1979).
11. G. Fagerlund, *Mater. Struct.,* **6**, 239(1973).
12. T. Allen, *Powder Sampling and Particle Size Determination*, Elsevier, Amsterdam (2003).
13. M. Hosokawa, *Nanoparticle Technology Handbook*, Elsevier, Amsterdam (2007).
14. S. J. Gregg and K. S. Sing, *Adsorption, Surface Area and Porosity,* Academic Press, London (1982).
15. G. Sauerbrey, *Z. Phys.,* **155**, 206 (1959).
16. D. C. Henry, *Trans. Faraday Soc.,* **44**, 1021 (1948).
17. R. J. Hunter, *Foundations of Colloid Science*, Oxford University Press, New York (2001).
18. E. Kissa, *Dispersions: Characterization, Testing and Measurement*, Marcel Dekker, New York (1999).
19. D.C. Grahame, *Chem. Rev.,* **41**, 441 (1947).
20. J. N. Israelachvili, *Intermolecular and Surface Forces*, Academic Press, London (1991).

21. K. S. Birdi, *Surface and Colloid Chemistry: Principles and Applications*, CRC Press, Boca Raton (2010).

22. W. D. Harkins and H. F. Jordan, *J. Am. Chem. Soc.*, **52**, 1751 (1930).

23. H. Zuidema and G. Waters, *Ind. Eng. Chem. Anal. Ed.*, **13**, 312 (1941).

24. D. I. Horsup, J. C. Clark, B. P. Binks, P. D. I. Fletcher and J. T. Hicks, *Corrosion,* **66**, 036001 (2010).

25. R. J. Jasinski and K. D. Efird, *Corrosion,* **41**, 658 (1998).

26. D. I. Horsup, T. S. Dunstan and J. H. Clint, *Corrosion,* **65**, 527 (2009).

27. R. Heidersbach, *Metallurgy and Corrosion Control in Oil and Gas Production,* Wiley-Interscience, Hoboken (2010).

28. M. Stern and A. L. Geary, *J. Electrochem. Soc.*, **104**, 56 (1957).

CHAPTER 3

Chapter 3

ADSORPTION OF ALKYLBENZYLDIMETHYLAMMONIUM CHLORIDES AT THE AIR-WATER INTERFACE

3.1. INTRODUCTION

The adsorption behaviour of corrosion inhibitors at the air-water interface is directly related to their performance at the solid-liquid interface. Corrosion inhibition by surfactant depends on the ability of these compounds to adsorb onto surfaces, which is related to their aggregation tendency to form micelles. The critical micelle concentration (cmc) is a key factor in determining the effectiveness of surfactants as corrosion inhibitors. Below the cmc, as the surfactant concentration increases, the corrosion rate decreases until it reaches a plateau near the cmc. The generally accepted physical picture of surfactant adsorption is that the adsorbed surfactant molecules form an oriented monolayer at the interface. The major driving force for surfactant adsorption is the hydrophobic effect, which is attributed to the removal of the hydrocarbon chains from the aqueous environment. In this chapter, we are going to investigate the adsorption behaviour of alkylbenzyldimethylammonium chlorides, CnBDMAC, at the air-water interface. The investigation addresses the role of the alkyl chain length in the adsorption of these homologues, the effect of temperature and the dependence of the adsorption on the concentration of added electrolyte.

Additionally, we have determined some of the thermodynamic parameters of the micellization process. The knowledge of thermodynamic parameters of the micellization such as $\Delta G^{\circ}_{\mathrm{mic}}$ may help in developing an understanding of the performance of these surfactants as corrosion inhibitors before their application in the actual oil field.

3.2. EFFECT OF SURFACTANT CHAIN LENGTH

Surfactant chain length has a great influence on the adsorption behaviour at the air-water interface and, hence on the cmc value. Generally, in aqueous medium, the cmc decreases as the number of carbon atoms in the hydrophobic group increases at constant temperature. The effect of increasing the chain length of alkylbenzyldimethylammonium chlorides on the surface tension isotherms for C10, C12, C14 and C16BDMAC in aqueous solutions at 25 °C is shown in Figure 3-1. In this figure, the surface tension (γ) in mN m^{-1}, is plotted as a function of the natural logarithm of initial aqueous surfactant concentration $[\mathrm{CnBDMAC}]_{\mathrm{aqu.}}$ in mM units. The solid lines represent the polynomial fits to these data sets. The polynomial equations used to fit the experimental surface tension isotherms and the determined cmc values for the homologous alkylbenzyldimethylammonium chlorides series are given in Table 3-1. The experimentally determined surface tension isotherms were found to fit a 2nd order function successfully with R^2 values of about 0.97 for most of the alkylbenzyldimethylammonium chlorides inhibitors studied.

As seen, the surface tension decreases with an increase in surfactant concentration until it reaches a virtually constant value, which corresponds to the cmc value. These values are shown on Figure 3-1 by the vertical dashed lines. Clearly, the cmc values decrease significantly with increasing alkyl chain length because of growing hydrophobicity of CnBDMAC surfactants. The earliest papers on the interfacial properties of alkylbenzyldimethylammonium halides are due to Walton *et al.* [1] and Cushman *et al.* [2]. Cella *et al.* [3] were the first to report a cmc value of 8.1 mM for C12BDMAC as determined conductometrically. Recently, Rodriguez and co-workers [4-14] have done extensive work on the micellar properties of long chain alkylbenzyldimethylammonium surfactants using different techniques.

Figure 3-1. Plot of surface tension as a function of the natural logarithm of CnBDMAC concentration at 25 °C. The solid lines represent the polynomial fitting. The vertical dashed lines represent the cmc values and the horizontal dotted line represents surface tension value of pure water.

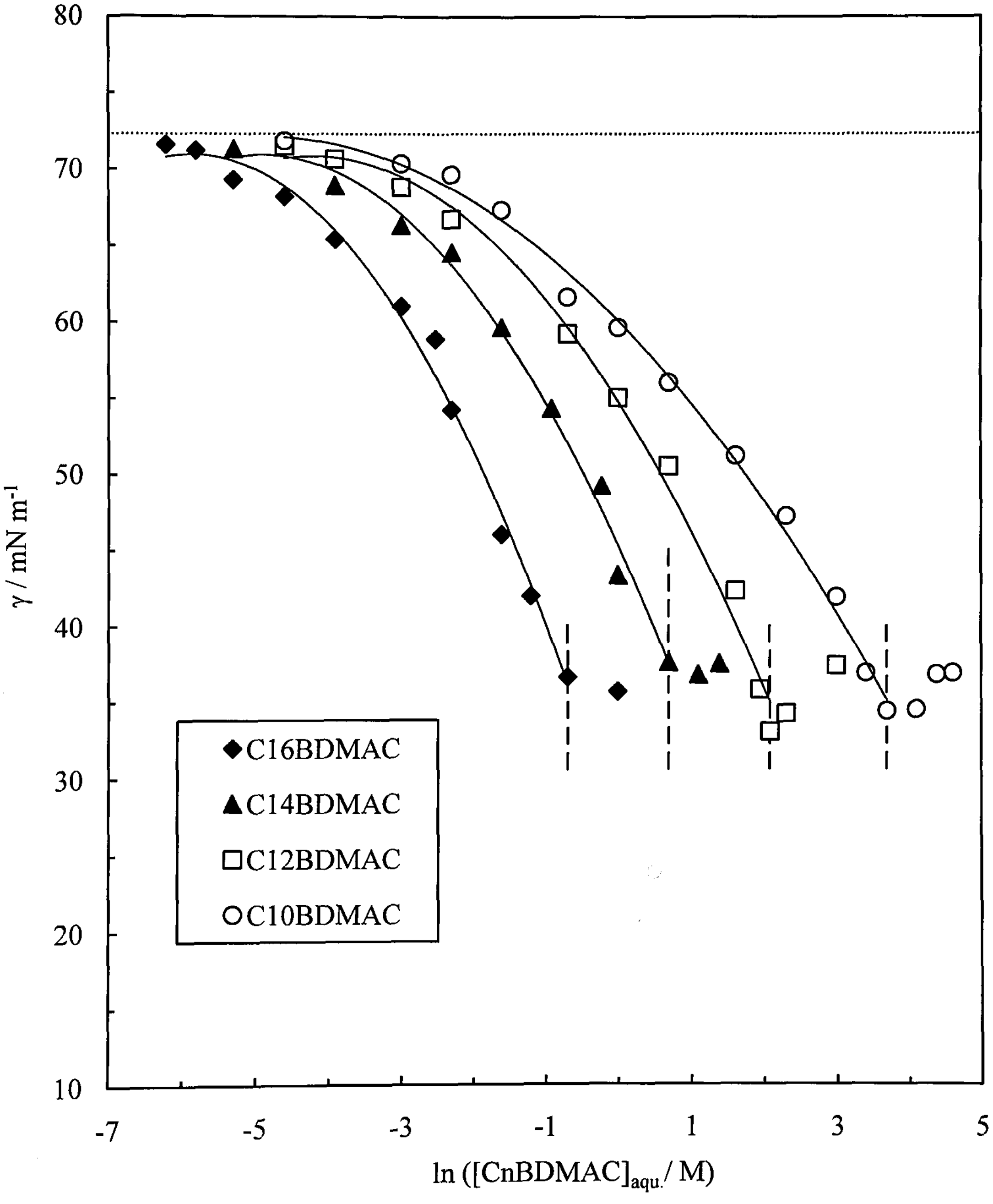

In this work, the cmc value determined for C10BDMAC was 40 mM at 25 °C. The latter value is in a good agreement with that of 39 mM estimated from conductivity measurements [4]. However it is slightly higher compared to earlier reports of 37.0 [15] and 37.8 mM [13], respectively. The value obtained for the cmc for C12DBAC at 25 °C is 7 mM. This is less than the previously reported results of 8.8 [15], 8.1 [3] and 8.8 [13].

Table 3-1. Polynomial equations used to fit the experimental surface tension isotherms and the determined cmc values for the homologous CnBDMAC series in aqueous solution at 25 °C.

Surfactant	cmc / mM	polynomial fitting equation	R^2
C10BDMAC	40.0	$y = -0.5004x^2 - 4.9142x + 60.059$	0.98
C12BDMAC	7.0	$y = -0.904x^2 - 7.6242x + 54.758$	0.99
C14BDMAC	2.0	$y = -1.0639x^2 - 10.442x + 45.289$	0.97
C16BDMAC	0.5	$y = -1.2996x^2 - 15.252x + 26.191$	0.98

The cmc value for C14BDMAC in aqueous solution was found to be 2 mM at 25 °C. This value is in good agreement with those reported in the literature of 2.0 mM [16], 2.0 mM [13] and 1.99 mM [6]. Although the corresponding value for C16BBDMAC (0.5 mM) is slightly higher compared to those reported by other researchers (0.30 [17] and 0.41 mM [16]), it is in excellent agreement with a recent value of 0.49 mM reported by Avranas *et al.* [18] and that of 0.493 mM reported by Gonzalez-Perez *et al.* [6].

A significant minimum in the surface tension isotherm is observed for C10, C12BDMAC and to a lesser extent for C14 and C16BDMAC. This implies that the aqueous solutions of our surfactant samples contain some surface-active impurities. This is a common behaviour of surfactants containing an impurity, which adsorb strongly at the air-liquid interface compared to the surfactant molecules at concentrations close to the cmc. For all the studied alkylbenzyldimethylammonium chlorides the minimum in surface tension appears at a surfactant concentration close to the cmc. Recently, Garcia *et al.* [19] reported the same behaviour during the surface tension measurements of some alkylbenzyldimethylammonium chlorides. Consequently, the accurate determination of the cmc is difficult. An experiment has been carried out to purify C12BDMAC by re-crystallization three times from hot ethyl acetate solution. The product was dried over calcium chloride under vacuum for 24 hours before the measurement. The surface tension isotherm for the purified C12BDMAC is given in Figure 3-2. It is clear from this figure that the purification process was successful in removing the impurities responsible for the minimum, which in turn proves that the presence of impurities in the surfactant is the reason for such a reduction in the surface tension.

3.3. EFFECT OF TEMPERATURE

The surfaces tension isotherms for C16 and C10BDMAC in aqueous solution at 40 °C compared to those at 25 °C are shown in Figure 3-3 and Figure 3-4, respectively. These figures show that an increase in temperature from 25 to 40 °C results in a gradual decrease in the surface tension. The surface tension isotherms for C10 and C12BDMAC have been studied as well at 40 °C. A similar decrease in the surface tension with the increase in temperature has been noticed. The determined cmc values for the homologous CnBDMAC in aqueous solution at 40 °C and the polynomial fitting parameters used to fit the experimental surface tension isotherms are given in Table 3-2. As shown in Figure 3-3, an increase in the temperature of C16BDMAC aqueous solutions results in a lowering of the surface tension over the entire concentration range.

Table 3-2. Polynomial equations used to fit the experimental surface tension isotherms and the determined cmc values for the homologous CnBDMAC series in aqueous solution at 40 °C.

Surfactant	cmc / mM	polynomial fitting equation
C10BDMAC	30	$y = -0.473x^2 - 5.4816x + 53.752$
C12BDMAC	6	$y = -0.64x^2 - 3.912x + 70.21$
C14BDMAC	2	$y = -0.84x^2 - 6.122x + 34.28$
C16BDMAC	0.5	$y = -1.0116x^2 - 14.086x + 20.893$

Figure 3-2. Plot of surface tension versus surfactant concentration for C12BDMAC at 25 °C. The solid line represents the polynomial fitting. The vertical dashed line represents the cmc values and the horizontal dotted line represents the surface tension value of pure water.

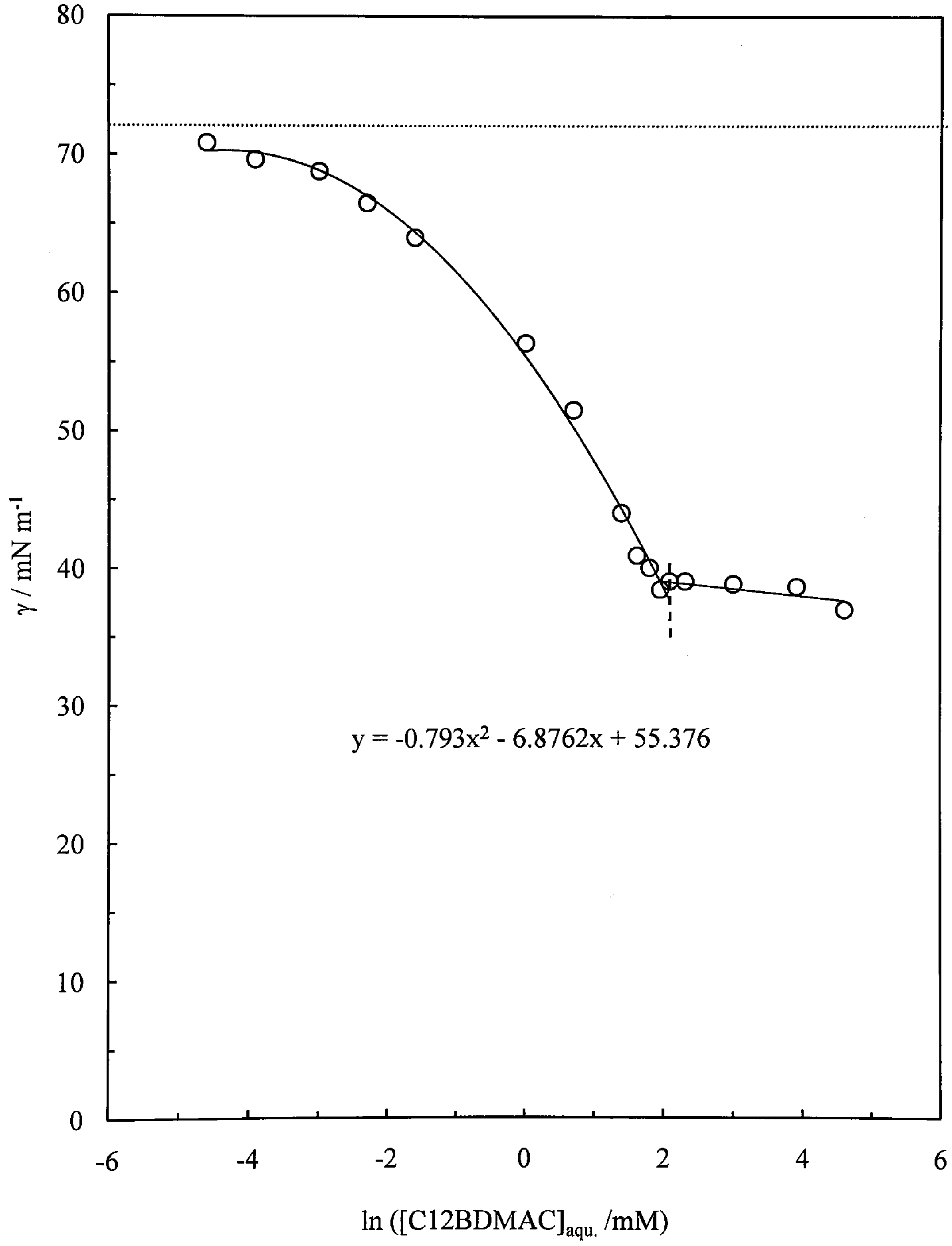

Figure 3-3. Plot of surface tension versus the natural logarithm of aqueous C16BDMAC concentration at 25 and 40 °C. The solid lines represent the polynomial fitting. The vertical dashed lines represent the cmc values.

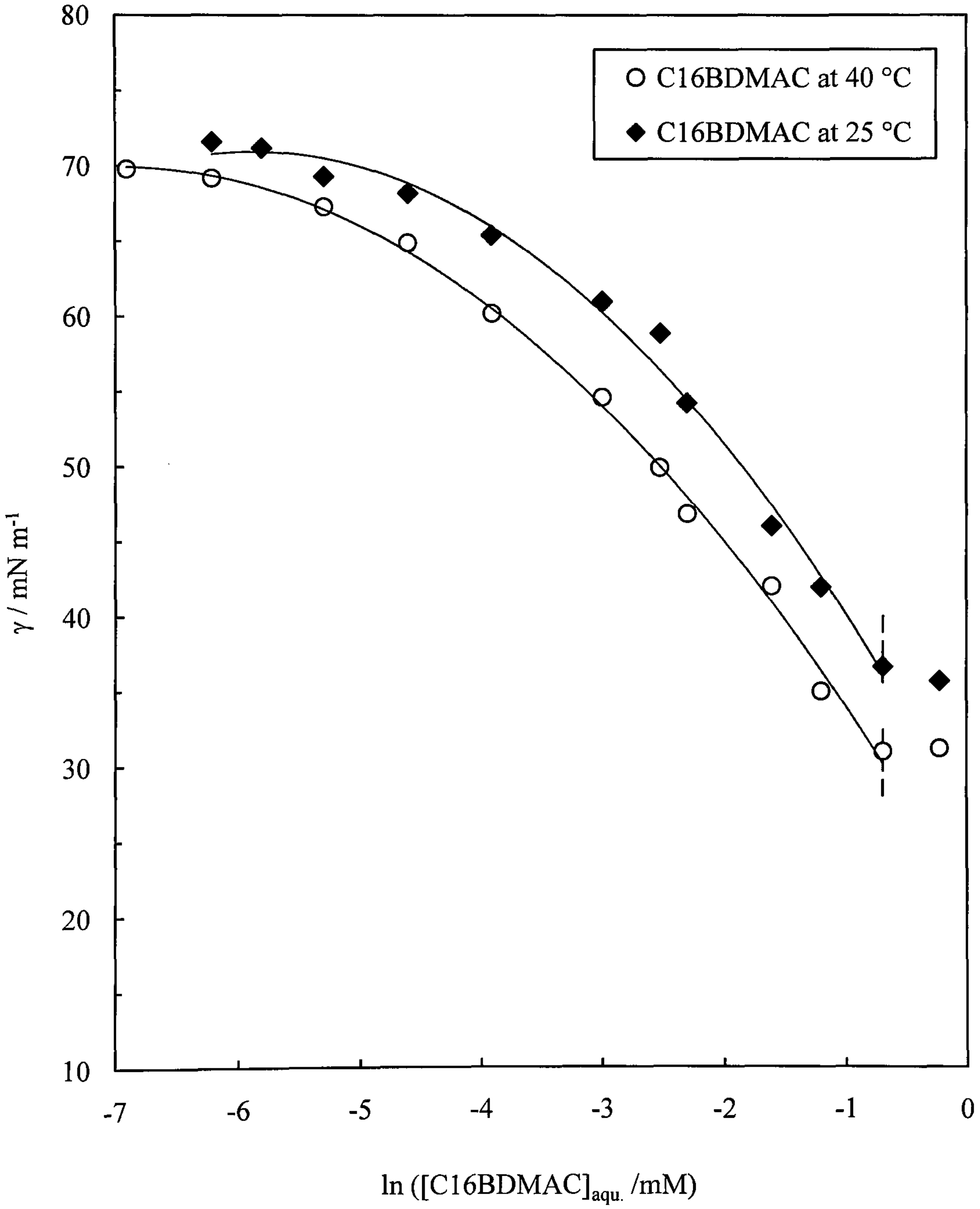

Figure 3-4. Plot of surface tension versus natural logarithm of aqueous C10BDMAC concentration at 25 and 40 °C. The solid lines represent the polynomial fitting. The vertical dashed lines represent the cmc values.

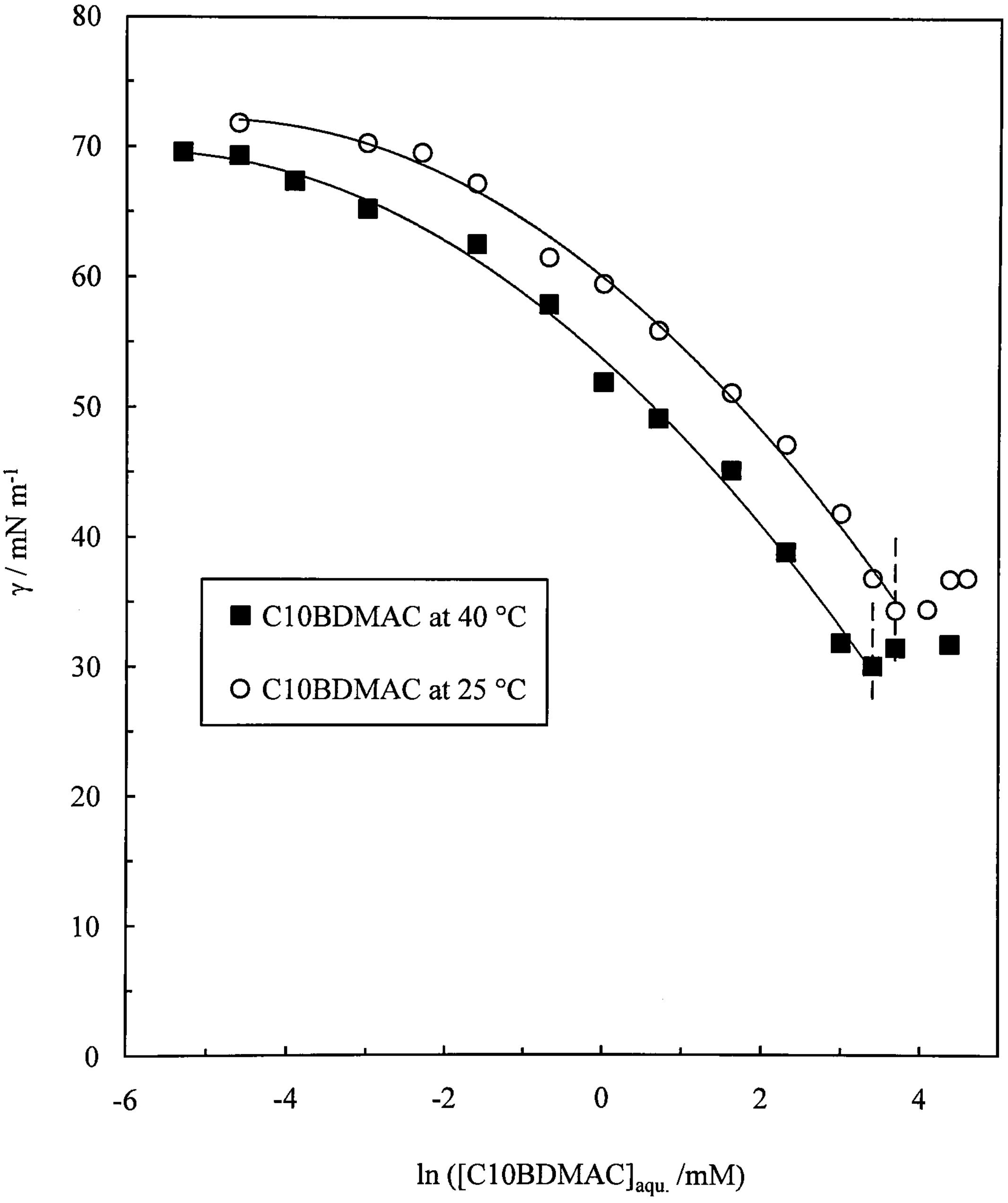

However, the concentration at which the surface tension isotherm breaks does not change upon the rise in temperature to 40 °C. This break point corresponds to the cmc value for C16BDMAC, which amounts to 0.5 mM. The same observation applies for C14BDMAC, in which the cmc value shows no change (2 mM) upon raising the temperature to 40 °C. On the other hand, the rise in temperature results in a slight decrease in the cmc value of C12BDMAC from 7 mM at 25 °C to about 6 mM at 40 °C. The cmc value of C10BDMAC is more temperature dependent. The magnitude of the cmc is reduced to 30 mM upon increasing the temperature to 40 °C compared to 40 mM at 25 °C.

The effects of temperature on the cmc of surfactants have been found to be quite difficult to interpret. Generally, the cmc of most ionic surfactants passes through a minimum with respect to temperature [20]. The cmc decreases to a minimum value and then increases, displaying a U-shaped behaviour [21]. The net effect of increasing or decreasing the cmc will depend on the relative magnitudes of the temperature influence on the hydrophilic and hydrophobic moieties in a surfactant molecule. An expected change in the degree of hydration of the hydrophilic head group will result from the change in temperature. As the temperature of solutions containing surfactant molecules is increased, the degree of surfactant headgroup hydration will decrease, as will the cohesive interactions among water molecules. This leads to a decrease in the tendency of surfactant monomers to remain in the solution and favours micelle formation [20, 21]. On the other hand, the temperature influence on the hydrophobic tail group is not that simple. Generally, ionic surfactant micelle formation is believed to be entropically controlled (driven). At low temperature, the release of structured water molecules around the hydrophobic chain results in an increase in the entropy of the system. As the temperature increases, the hydrogen bonds diminish and the bulk-water molecules will lose its structure [20, 21]. Consequently, the entropy contribution to the system will diminish as well. The result from that situation will be a reduction of the magnitude of the free energy component attributable to the hydrophobic or entropic effect. Such an effect will decrease the ''insolubility'' of the tail in water, a result that is in opposition to micelle formation. At higher temperatures, more precisely, beyond a definite temperature, less energy will be required to break up the three-dimensional water structures. Hence, the change in enthalpy turns out to be exothermic in nature and larger in magnitude. Accordingly, the micellization process becomes much more enthalpy-dependent and the entropic contribution becomes very small [21, 22].

Gonzalez-Perez *et al.* [6, 10] investigated the temperature dependence of the cmc for CnBDMAC in aqueous solution from conductivity data collected in the temperature range 10-35 °C at 5 °C intervals. The U-shaped temperature dependence of cmc has been observed in these studies. They observed a minimum in the cmc for C10BDMAC at a temperature around 35 °C [4]. On the other hand they noticed no change in the cmc values for C14 and C16BDMAC upon increasing the temperature up to 35 °C [6]. Beyond this temperature, the rise in temperature results in a gradual increase in the cmc value in aqueous solutions. For C10BDMAC, the rise in temperature beyond 45 °C was shown to increase the cmc value in aqueous solution as reported by Gonzalez-Perez *et al.* [4]. They concluded that, for a series of homologous CnBDMAC, the cmc-temperature minima is shifted to lower temperatures upon increasing the length of the alkyl chain.

3.4. EFFECT OF BRINE ADDITION

The effect of brine addition on the surface tension behaviour of C16 and C12BDMAC at 25 °C is displayed in Figure 3-5 and Figure 3-6, respectively. These isotherms have been fitted to a second order polynomial equation, shown by the solid lines. The fitting equations and the cmc values for the homologous CnBDMAC series in brine solution at 25 °C are given in Table 3-3.

Table 3-3. Polynomial equations used to fit the experimental surface tension isotherms and the determined cmc values for the homologous CnBDMAC series in 4.7 wt. % brine solutions at 25 °C.

Surfactant	cmc / mM	polynomial fitting equation
C10BDMAC	3.0	$y = -0.262\,x^2 - 56.210\,x + 26.695$
C12BDMAC	0.2	$y = -0.5781\,x^2 - 11.403\,x + 12.595$
C14BDMAC	2×10^{-2}	$y = -0.78\,x^2 - 16.59\,x + 16.289$
C16BDMAC	1×10^{-3}	$y = -1.047\,x^2 - 26.859\,x - 99.671$

Figure 3-5. Plot of surface tension versus natural logarithm of C16BDMAC concentration in water and 4.7 wt.% brine solution. The solid lines represent the polynomial fitting. The vertical dashed lines represent the cmc values.

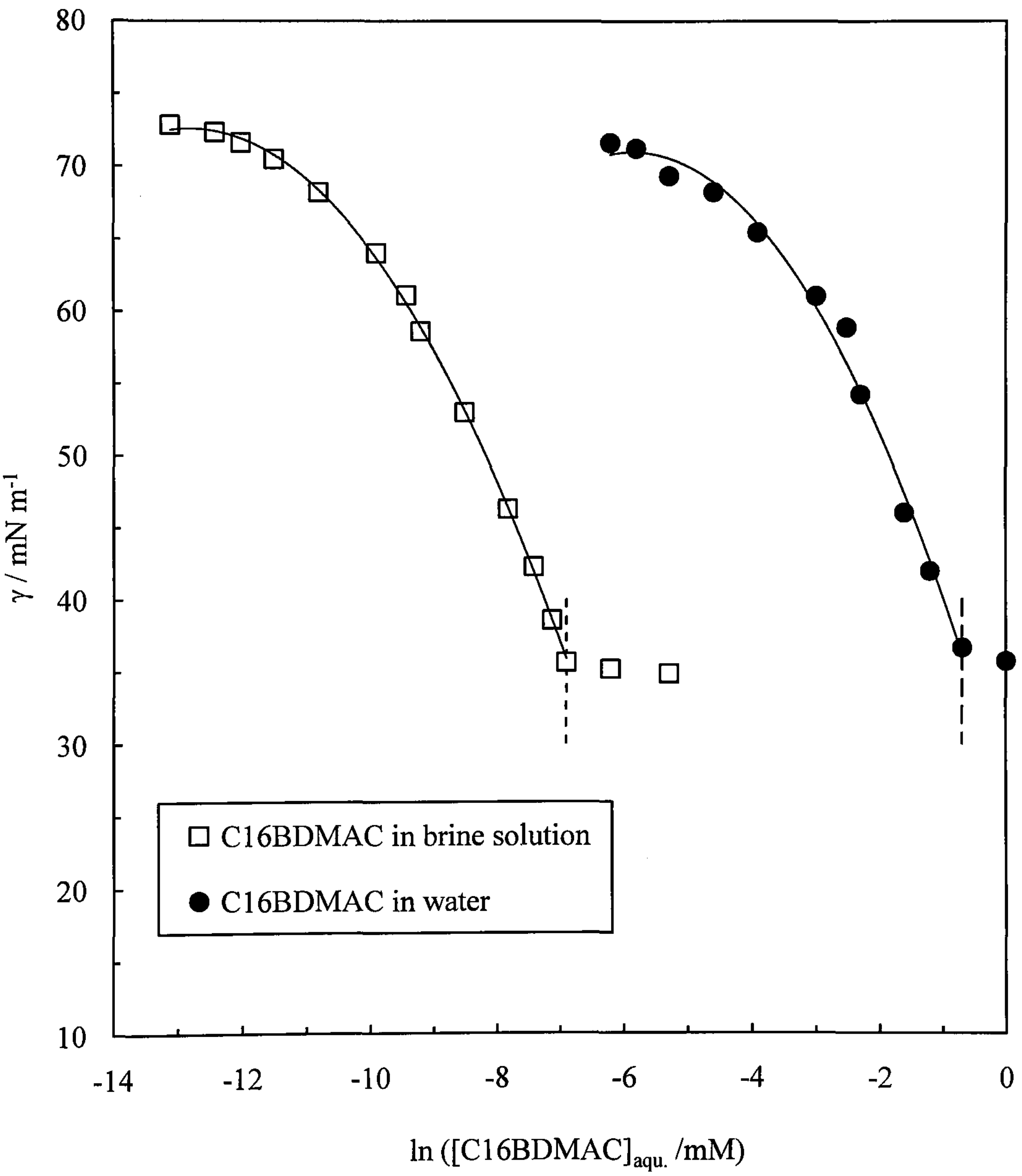

Figure 3-6. Plot of surface tension versus natural logarithm of C12BDMAC concentration in water and 4.7 wt. % brine solution. The solid lines represent the polynomial fitting. The vertical dashed lines represent the cmc values.

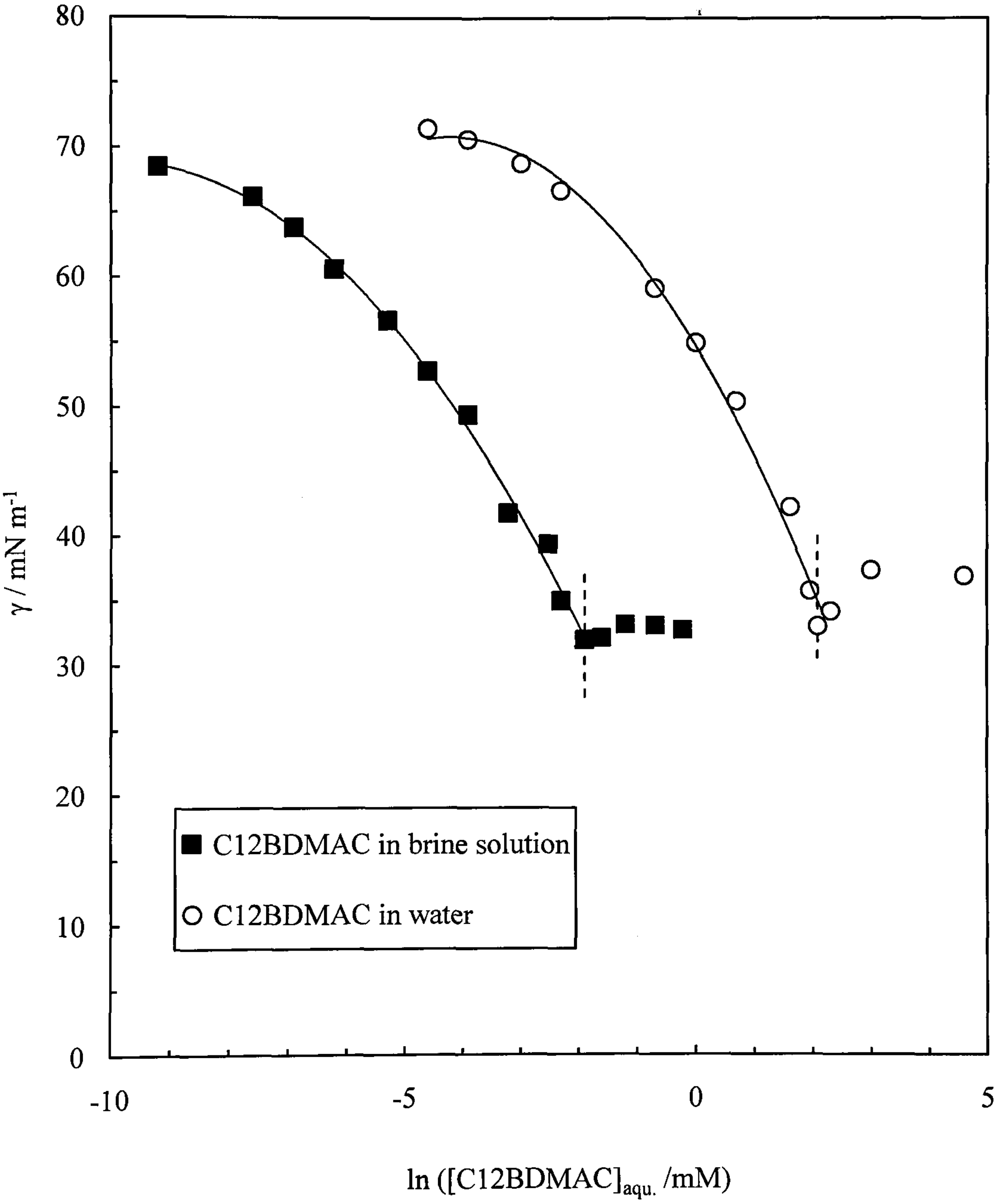

Clearly, the addition of 4.7 wt. % brine to surfactant solutions results in shifting the isotherms to lower concentrations. Moreover, the brine addition leads to a sharp decrease in the cmc values of CnBDMAC compared to those in water. For example, the cmc value for C12BDMAC decrease from 7 mM in aqueous solution to 0.2 mM in brine solution. Brine addition decreases the cmc value for C16BDMAC from 0.5 mM to a value of about 1×10^{-3} mM. Recently, Dar *et al.* [23] reported a cmc value of 0.053 mM for C16BDMAC in aqueous solution containing 30 mM NaCl at 25 °C using tensiometric and fluorimetric techniques. The cmc value for C10BDMAC has been shifted from 30 to 3 mM upon brine addition and that for C14BDMAC has been shifted from 2 to 2×10^{-2} mM.

Generally, the cmcs of ionic surfactants are depressed by the addition of electrolytes by a factor of about 10 for two methylene groups added to the hydrophobic chain [20, 24]. This depression in the cmc values caused by brine addition is mainly due to the decrease in the thickness of the ionic atmosphere surrounding the head groups in the presence of brine and the consequent decreased electrostatic repulsion among them in the micelle [20].

3.5. SURFACE EXCESS CONCENTRATIONS AND MOLECULAR AREA AT AIR-WATER INTERFACE

The adsorption of surfactant molecules at the air-water interface is the reason for the observed decrease in the surface tension of surfactant-containing solutions. For surfactant concentrations below the cmc, the surface excess concentration, Γ, at the interface could be estimated from the slope of the surface tension vs. ln[surfactant] isotherm at constant temperature using the Gibbs' adsorption equation [25] :

$$\Gamma = -(\frac{1}{RT}\cdot\frac{d\gamma}{d\ln a}) \tag{3-1}$$

where γ is the surface tension, R is the gas constant, T is absolute temperature and a is the activity of surfactant. For concentrations below those corresponding to either aggregate formation or phase separation, we assume that the solutions behave ideally, i.e. that activity and concentration of the surfactant can be equated. The slopes could be determined by differentiating the second order polynomial fitting equations which have been used to fit the surface tension isotherms.

The Gibbs' adsorption equation shows that Γ is positive when surface tension is lowered with the addition of surfactant. The positive Γ at the surface means the concentration of surfactant at the surface is higher than that in the bulk liquid. The above equation is applicable to non-ionic surfactants and ionic surfactants in the presence of excess electrolyte. For 1:1 ionic surfactants with zero added electrolyte, both the anions and cations adsorb at the surface to maintain local electrical neutrality, therefore a factor of two is needed for this in the Gibbs' equation. The modified equation for ionic surfactants is given by the following equation:

$$\Gamma = -\left(\frac{1}{2RT} \cdot \frac{d\gamma}{d\ln a}\right) \tag{3-2}$$

If a non-adsorbed electrolyte is present in large excess, then the Gibbs adsorption equation for 1:1 ionic surfactants reduces to equation (3.1), i.e. it becomes identical to that for a non-ionic surfactant.

Moreover, using the surface excess concentrations, Γ, in molecules nm^{-2}, we could calculate the molecular area occupied by surfactant, A, (in Å^2) using the following equation:

$$A = \frac{100}{\Gamma} \tag{3-3}$$

Generally, the area per molecule at the interface provides useful information on the degree of packing and the orientation of the adsorbed surfactant molecules when compared with the dimensions of the molecule. Additionally, the surface excess concentrations at surface saturation Γ_m, and the area per molecule at the interface at surface saturation A_m, are useful measures of the effectiveness of adsorption of the surfactant at the air-water interface as they indicate the maximum value that the adsorption can reach.

The polynomial equations used to fit the experimental surface tension isotherms of the homologous CnBDMAC series in aqueous solutions at 25 °C were differentiated to obtain the corresponding surface excess concentrations. Figure 3-7 shows the Gibbs' adsorption isotherm as a function of the bulk CnBDMAC surfactant concentration in aqueous solution at 25 °C.

Figure 3-7. Gibbs' adsorption isotherms as a function of the bulk CnBDMAC surfactant concentration in aqueous solution at 25 °C. The arrows refer to the maximum surface excess concentration at the cmc.

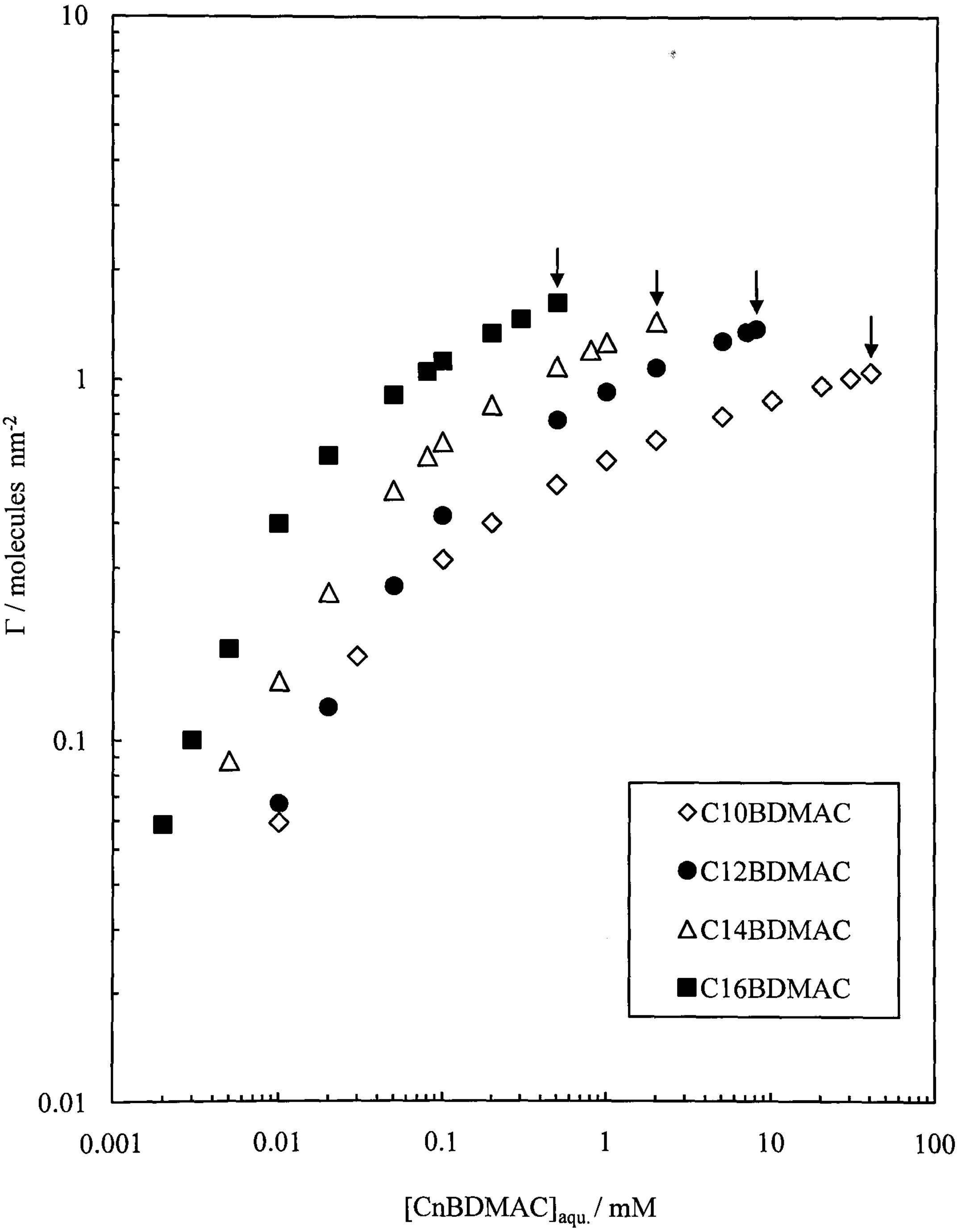

This figure shows that the adsorption isotherms are typically Langmuir in type. Across the series, the maximum surface concentration increases with increasing chain length. On the other hand, the concentration required to reach saturation decreases with increasing chain length. This indicates that the hydrophobicity of the alkyl chain is the main driving force for surfactant adsorption at the air-water interface.

The short chains C10 and C12BDMAC give rise to a maximum surface excess concentration of about 1.05 and 1.35 molecules nm^{-2}. On the other hand, the long chains C14 and C16BDMAC give rise to a maximum surface excess concentration of about 1.45 and 1.63 molecules nm^{-2}.

Figure 3-8 shows the variation of the molecular area occupied by CnBDMAC at the air-water interface as a function of the bulk surfactant concentration in aqueous solutions at 25 °C. The areas per molecule at the interface at surface saturation A_m for C10, C12, C14 and C16BDMAC were found to be 95.64, 73.85, 68.96, and 61.8 Å^2. The area per molecule at the interface at surface saturation for the purified C12BDMAC at the air-water interface was found to be 71.42 Å^2. Trompette *et al.* [26] studied the adsorption of C12BDMAC from water using surface tension measurements and they reported a molecular area of about 70 Å^2 at 25 °C.

Figure 3-9 shows the Gibbs' adsorption isotherm for C16BDMAC at 40 °C compared to that at 25 °C. The corresponding molecular areas occupied by C16BDMAC are given in Figure 3-10. The values of Γ_m and A_m obtained for alkylbenzyldimethylammonium chlorides homologues at 25 and 40 °C without added brine are summarized in Table 3-4. Obviously, the area per molecule decreases as the chain length increases. On the contrary, the rise in temperature increases the area per molecule.

Lu *et al.* [27] investigated the adsorption of the cationic surfactant alkyltrimethylammonium bromide homologous series at the air-water interface by the neutron reflection technique. At the cmc, the area per surfactant molecule (A_m) was found to be 55 Å^2 for decyltrimethylammonium bromide (C10TAB), 48 Å^2 for tetradecyltrimethylammonium bromide (C14TAB) and 43 Å^2 for octadecyltrimethylammonium bromide (C18TAB). They suggested that there must be a significant proportion of alkyl chain immersed in water and the immersion of the alkyl chain decreases as the chain length increases.

Figure 3-8. Variation of the molecular area occupied by CnBDMAC at the air-water interface as a function of the bulk surfactant concentration in aqueous solution at 25 °C. The arrows refer to the cmc values.

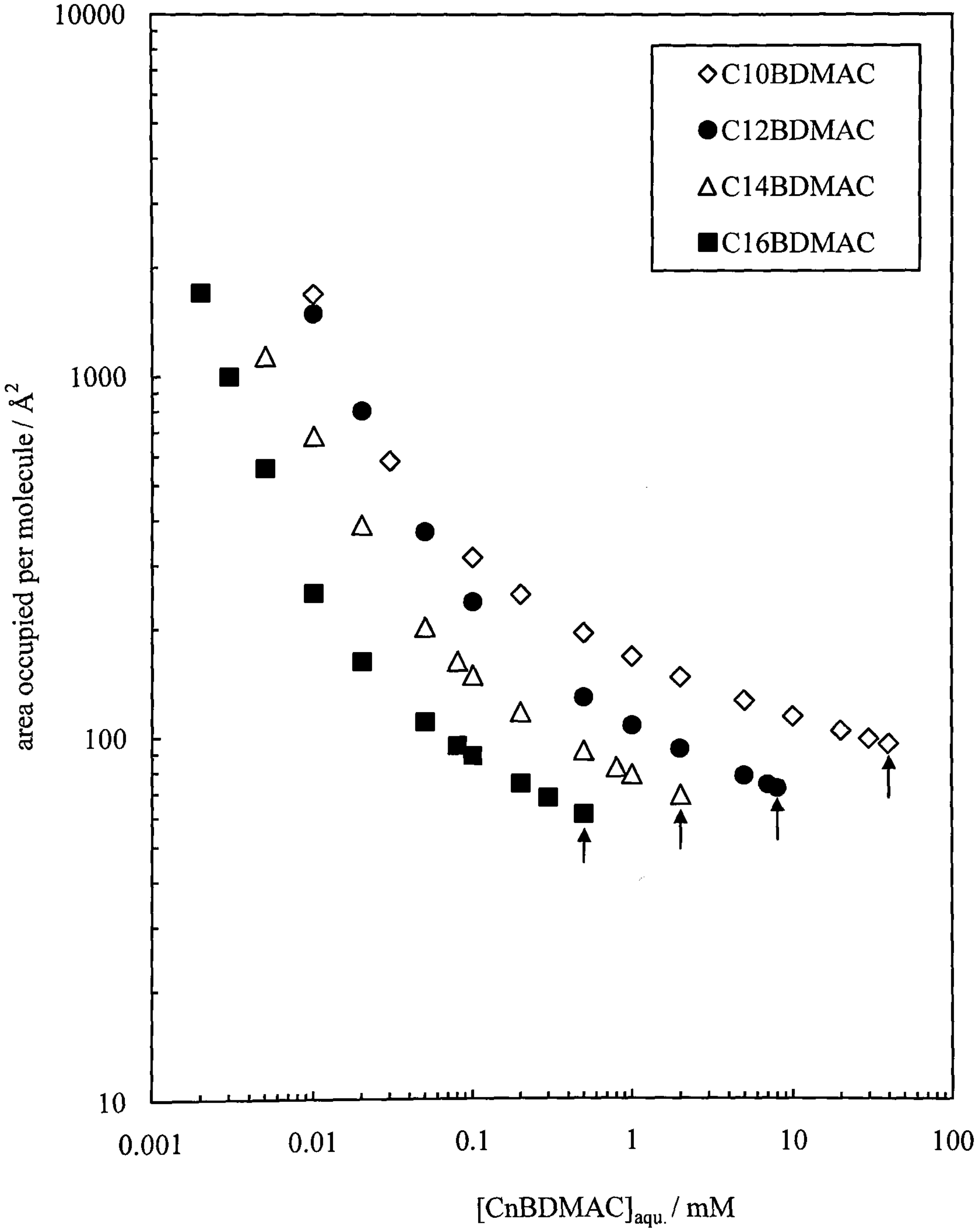

Figure 3-9. Gibbs' adsorption isotherms as a function of the bulk C16BDMAC surfactant concentration in aqueous solution at 25 and 40 °C. The arrow refers to the maximum surface excess concentration at the cmc.

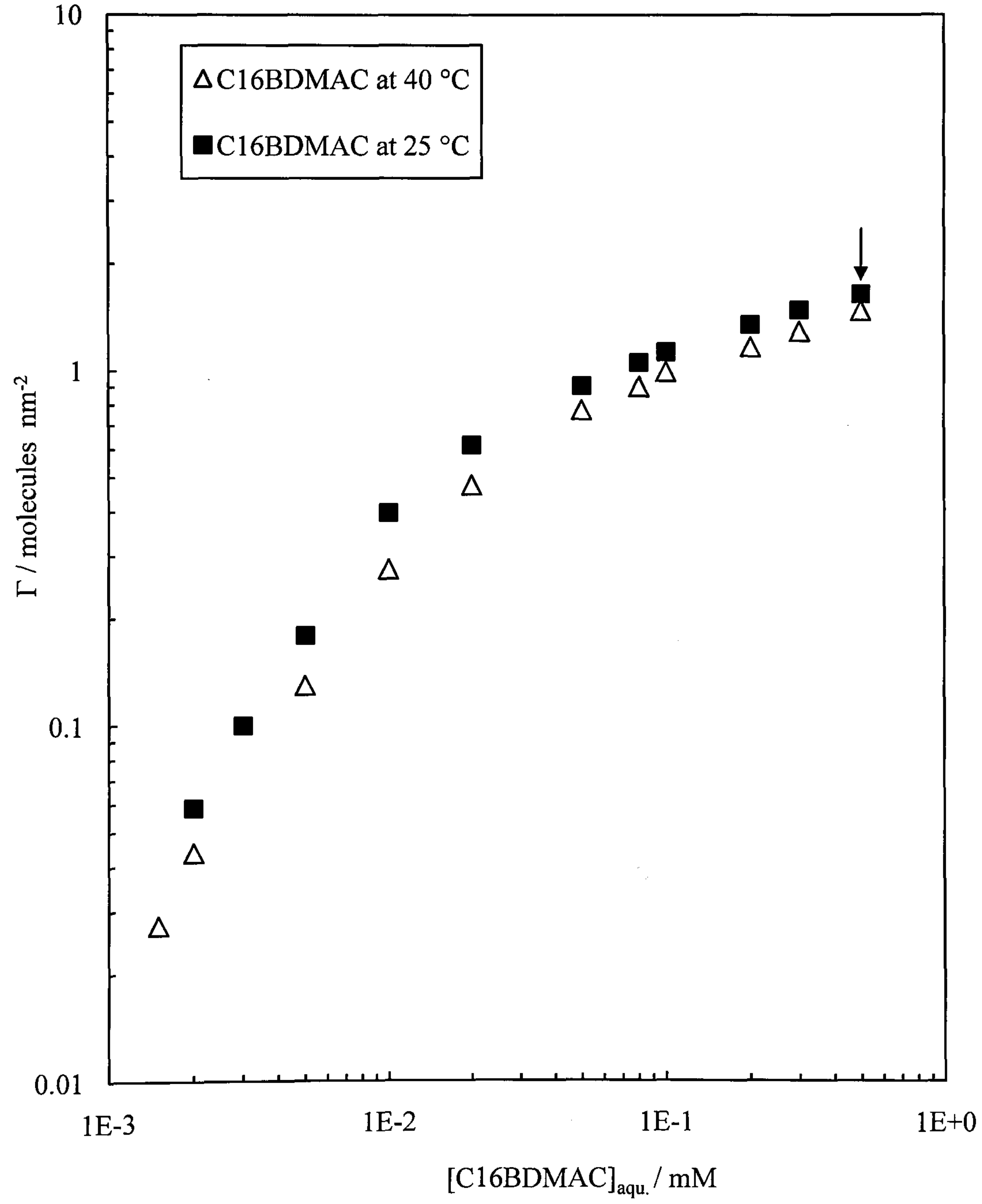

Figure 3-10. Variation of the molecular area occupied by C16BDMAC at the air-water interface as a function of the bulk surfactant concentration in aqueous solution at 25 and 40 °C. The arrows refer to the cmc values.

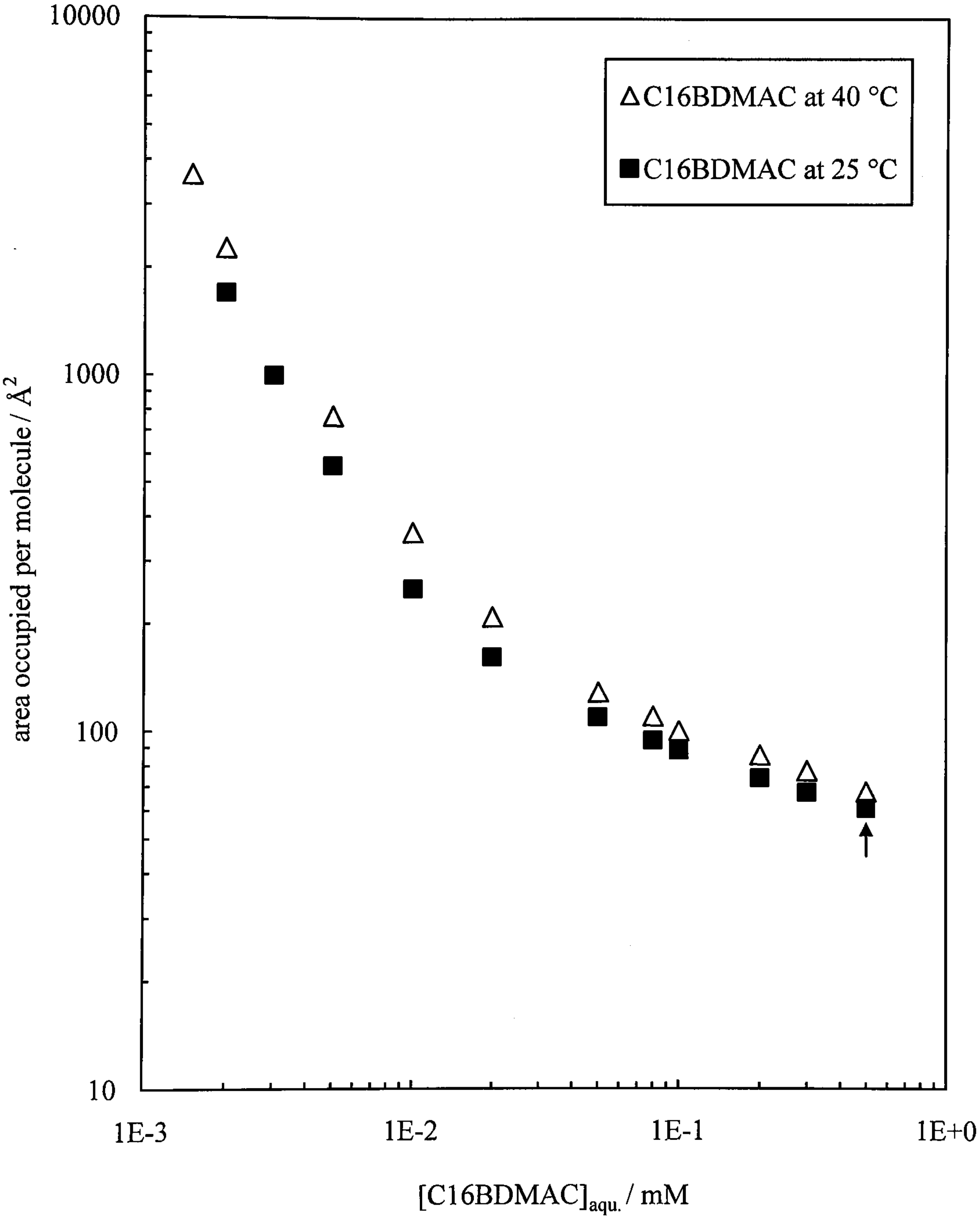

Table 3-4. Area per molecule and maximum surface concentration for alkylbenzyldimethylammonium chlorides in pure water at 25 and 40°C.

Surfactant	25 °C		40 °C	
	Γ_m / molecules nm^{-2}	A_m / Å^2	Γ_m / molecules nm^{-2}	A_m / Å^2
C10BDMAC	1.05	95.64	1.01	99.35
C12BDMAC	1.38	73.85	1.28	78.12
C12 BDMAC (*purified*)	1.40	71.42	—	—
C14BDMAC	1.45	68.96	1.30	76.92
C16BDMAC	1.63	61.8	1.47	68.14

The effect of brine addition on the amount of C12BDMAC adsorbed at the air-water interface and the corresponding molecular area are shown in Figure 3-11 and Figure 3-12, respectively. Clearly, brine addition results in a sharp increase in the adsorbed amount over the entire concentration range. For example, the maximum surface excess concentration shown by C12BDMAC in the presence of brine increased to about 2.32 molecules nm^{-2} with a molecular area of about 33.19 Å^2 in comparison to about 1.40 molecules nm^{-2} in the absence of brine. The addition of brine reduces the repulsive forces between headgroups, which leads to a closer packing of them.

The values of Γ_m and A_m obtained for alkylbenzyldimethylammonium chlorides homologues at 25 °C in the presence of brine are given in Table 3-5. Since the cross-sectional area of an aliphatic chain oriented perpendicular to the interface is about 20 Å^2 and that of a benzene ring oriented in the same fashion is about 25 Å^2 [20], apparently the hydrophobic chains of CnBDMAC surfactants adsorbed at the air-water interface are not in the close-packed arrangement normal to the interface at saturation adsorption. On the other hand, since the cross-sectional area of CnBDMAC lying flat in the interface is about 100-122 Å^2, the molecules are not lying flat in the interface, but are somewhat tilted with respect to the interface.

Figure 3-11. Gibbs' adsorption isotherm as a function of the bulk C12BDMAC surfactant concentration in aqueous and brine solutions at 25 °C. The arrow refers to the maximum surface excess concentration at the cmc.

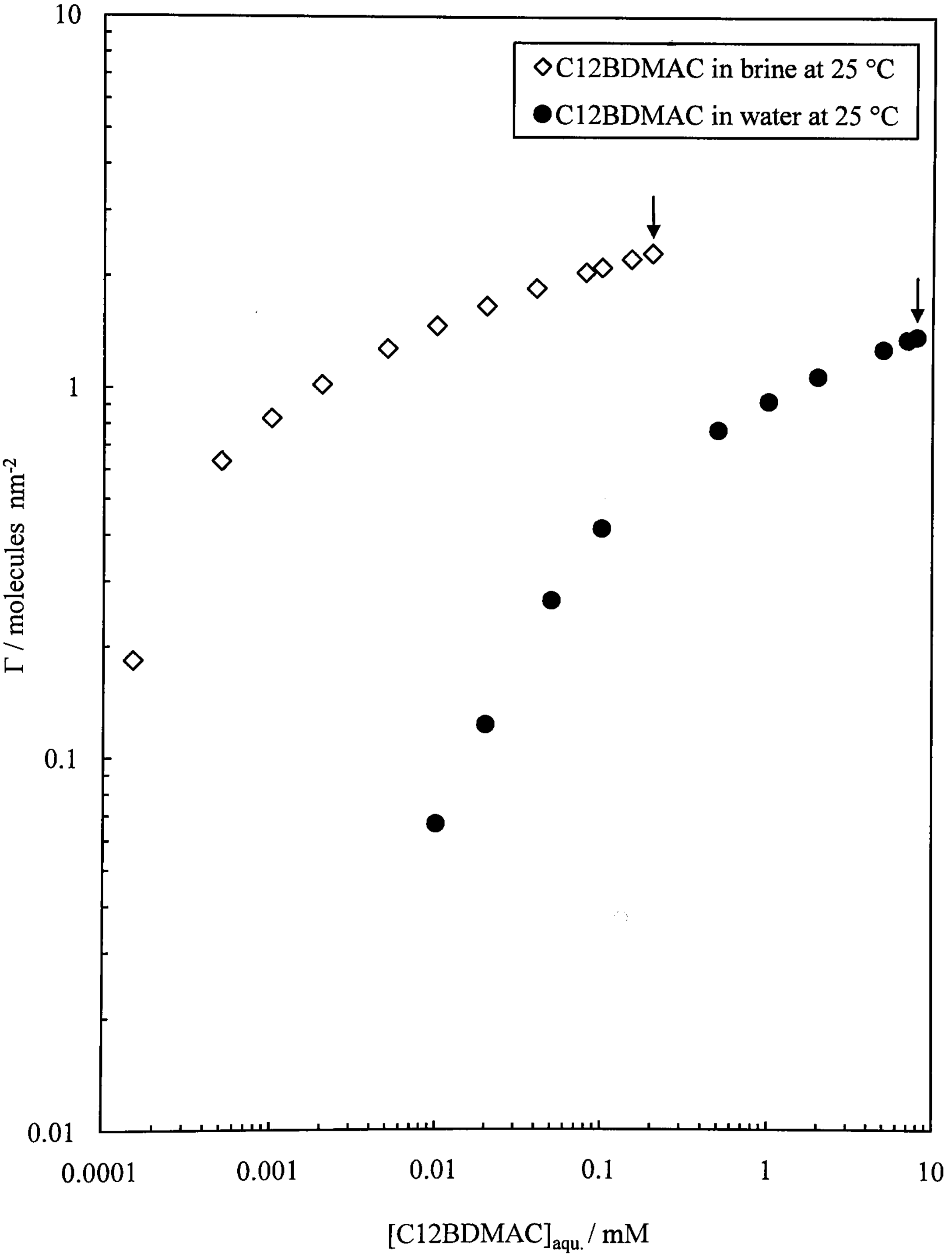

Figure 3-12. Variation of the molecular area occupied by C12BDMAC at the air-water interface as a function of the bulk surfactant concentration in aqueous and brine solutions at 25 °C. The arrows refer to the cmc values.

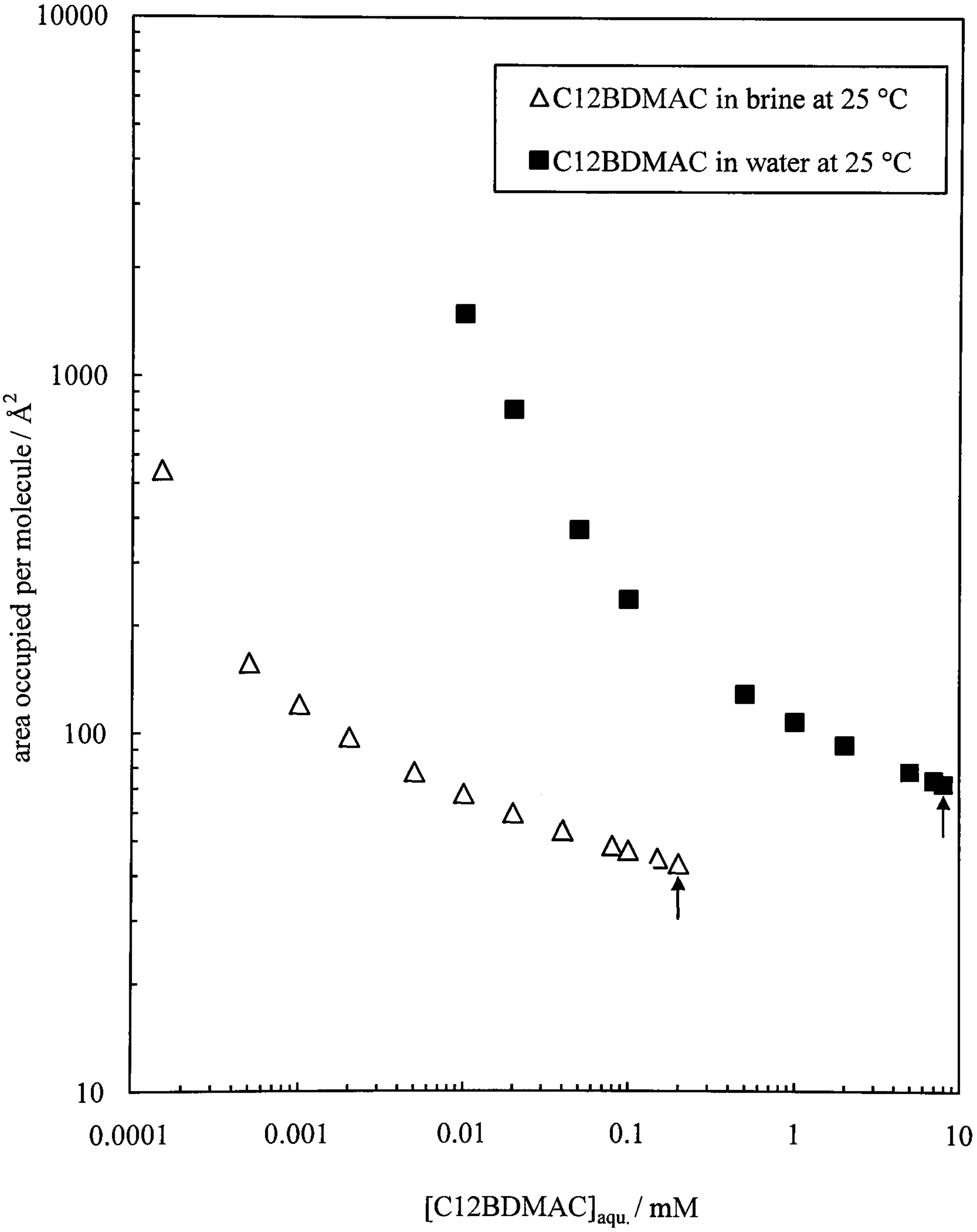

Table 3-5. Area per molecule and maximum surface concentration of alkylbenzyldimethylammonium chlorides in brine solutions at 25 °C.

Surfactant	Γ_m /molecules nm^{-2}	A_m / Å^2
C10BDMAC	2.01	48.78
C12BDMAC	2.32	43.11
C14BDMAC	2.78	35.79
C16BDMAC	3.01	33.19

3.6. DISCUSSION

3.6.1. The cmc dependence of the surfactant chain length

The surfactant chain length has been shown to be a major factor in determining the surfactant's cmc. Commonly, the cmc decreases logarithmically as the number of carbon atoms in the hydrocarbon alkyl chain of homologous series increases [21]. The cmc magnitude of ionic surfactants in aqueous solutions is usually reduced by about one half with the addition of a methylene group to straight-chain surfactants [20, 21]. Several empirical equations have been developed to correlate the surfactant's cmc to the number of carbon atoms present in the hydrophobic chain. Thus, for a homologous straight-chain ionic surfactant series, Klevens [28] proposed a relation between the cmc and the number of carbon atoms N_c in the hydrophobic chain. It is given by the following relation:

$$\log \text{cmc} = A - BN_c \qquad (3\text{-}4)$$

where A and B are constants specific to the homologous series of a particular ionic headgroup under constant conditions of temperature and pressure. In this equation, the magnitude of A depends on the nature of the surfactant headgroup, temperature and the electrolyte concentration. On the other hand, B represents the contribution of each methylene group in the lowering the cmc. It has generally been found that the value of A is approximately constant for a particular ionic head group, while B is constant and approximately equal to log (2) $\approx$ 0.3, for all paraffin chain salts having a single ionic head group in aqueous solutions with no added electrolyte [21]. The basis for the rule mentioned earlier regarding the cmc being halved for each methylene group addition to the hydrophobic chain is obvious from this relation. Figure 3-13 shows the cmc dependence of the homologous CnBDMAC surfactants with the hydrophobic chain length at 25 °C. As shown, the experimentally determined cmc values of CnBDMAC in aqueous solution gives rise to a straight line as a function of the surfactant chain length in accordance with equation (3-4).

The *A* and *B* values were found to be 1.72 and 0.315, respectively. The magnitudes of *A* and *B* are in good agreement with those reported in the literature and as predicted by equation (3-4). Ross *et al.* [29] reported values of 1.61 and 0.36 for *A* and *B* for the homologous alkylbenzyldimethylammonium chlorides series. The quaternary ammonium surfactant molecules were measured in aqueous solution at 25 °C where the alkyl group varied from a 6-carbon-atom straight chain to an 18 carbon-atom straight chain. Table lists several values for the constants *A* and *B* determined from experimental data for several quaternary ammonium surfactants compared to those for CnBDMAC determined in this work.

Table 3-6. Klevens constants for common quaternary ammonium surfactants compared to those for CnBDMAC determined in this work.

Surfactant	Temperature (°C)	A	B	Ref.
Alkylammonium chlorides	25	1.25	0.27	[21]
Alkyltrimethylammonium bromides	25	1.72	0.30	[21]
Alkyltrimethylammonium bromides	60	1.7	0.29	[28]
Alkyltrimethylammonium chlorides (0.1 M NaCl)	25	1.2	0.33	[30]
Alkylpyridinium bromides	30	1.72	0.31	[31]
Alkylbenzyldimethylammonium chlorides	25	1.61	0.36	[29]
Alkylbenzyldimethylammonium chlorides	25	1.72	0.315	This work
Alkylbenzyldimethylammonium chlorides	40	1.4	0.29	
Alkylbenzyldimethylammonium chlorides (4.7 wt. % brine)	25	2.68	0.5	

Figure 3-13. Logarithm of the cmc (molar concentration) versus the number of carbon atoms (N_c) in the alkyl chain of CnBDMAC in aqueous solution at 25 °C.

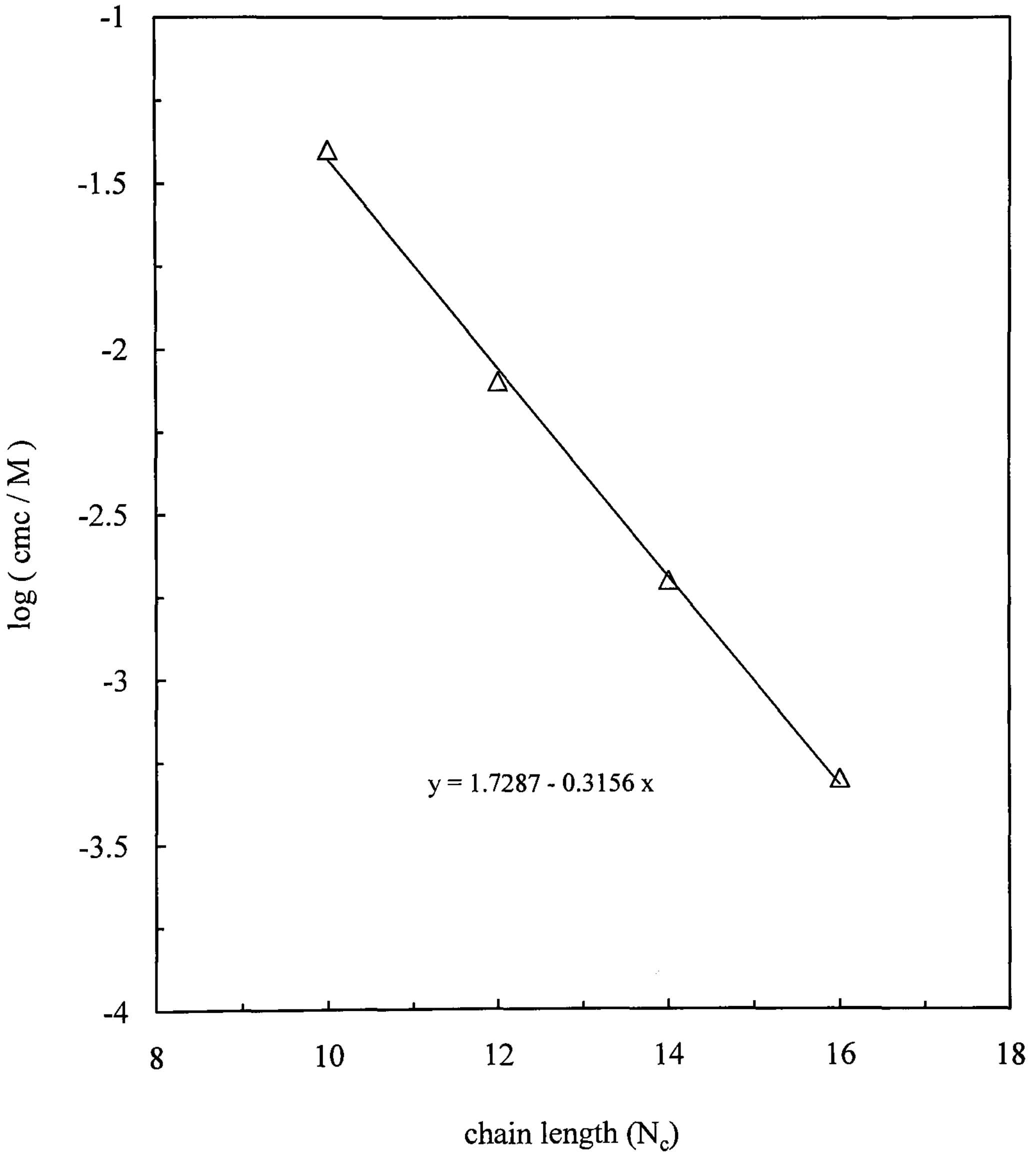

The A and B values for CnBDMAC in aqueous solution at 40 °C were found to be 1.4 and 0.29, respectively as shown by Figure 3-14. The rise in temperature has almost no effect on B while it results in a relatively small decrease in the magnitude of A (from 1.7 to 1.4). The cmc dependence of surfactant chain length in the presence of brine is shown in Figure 3-15. The cmc values were measured at 25 °C in the presence of 4.7 wt.% brine.

Brine addition results in a marked increase in B from 0.3 to 0.5. The obtained value of 0.5 indicates a decrease in the cmc by a factor of about 10 for each two methylene groups added to the hydrophobic chain. Generally, the cmc of ionic surfactants are depressed by the addition of electrolytes. The added electrolytes result in screening the electrostatic repulsion between the headgroups. This screening effectively makes surfactants more hydrophobic, which in turn results in large values for B. A larger value of B indicates a large contribution of the hydrophobic tail groups, which induces micellization at lower concentrations.

3.6.2. Thermodynamics of CnBDMAC micellization

The value of the critical micellization concentration (cmc) of a surfactant in aqueous solution has been commonly used to determine the change in the standard free energy of micellization of the surfactant, $\Delta G^{\circ}_{\mathrm{mic}}$, using the following relationships [24, 32, 33]:

$$\Delta G^{\circ}_{\mathrm{mic}} = RT \ln \mathrm{cmc} \qquad (3\text{-}5)$$

$$\Delta G^{\circ}_{\mathrm{mic}} = (1 + \beta)\, RT \ln \mathrm{cmc} \qquad (3\text{-}6)$$

for nonionic and monovalent ionic surfactants, respectively. R and T are the general gas constant and the absolute temperature, respectively and β is the degree of counterion association. In equations (3-5) and (3-6), the cmc is expressed in molar or mole fraction units. In the presence of excess added electrolyte, equation (3-6) for ionic surfactants is reduced to equation (3-5).

An attempt has been made to estimate $\Delta G^{\circ}_{\mathrm{mic}}$ for the homologous CnBDMAC surfactants using the abovementioned equations. Table 3-7 gives the values obtained at 25 and 40 °C using equation (3-6). For aqueous solutions, the β values reported by Rodrıguez *et al.* [14] have been used. Rodrıguez *et al.* used conductivity techniques to measure the β values.

Figure 3-14. Logarithm of the cmc (molar concentration) versus the number of carbon atoms (N_c) in the alkyl chain of CnBDMAC in aqueous solutions at 40 °C.

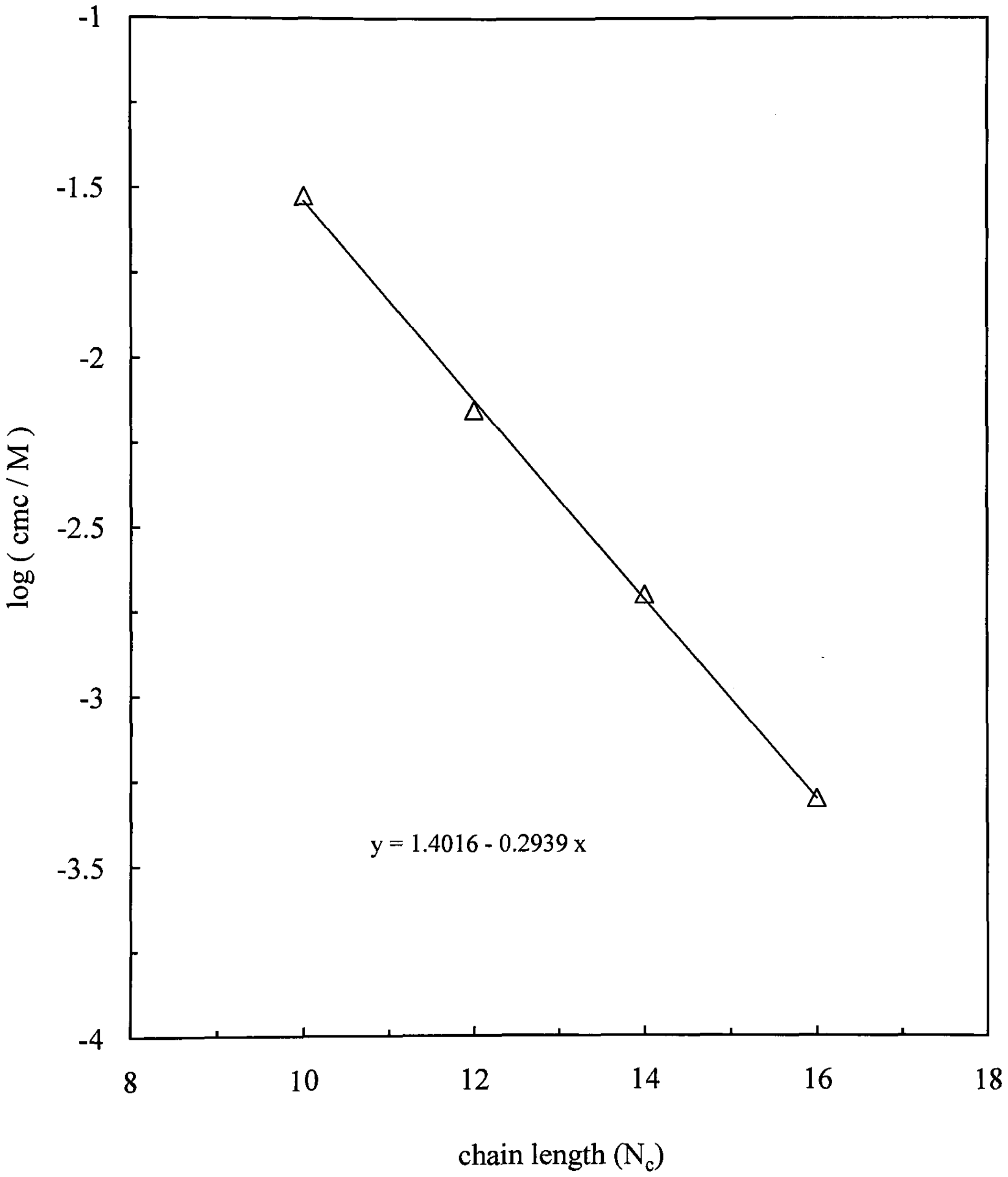

Figure 3-15. Logarithm of the cmc (molar concentration) vs. the number of carbon atoms (N_c) in the alkyl chain of CnBDMAC in brine solutions at 25 °C.

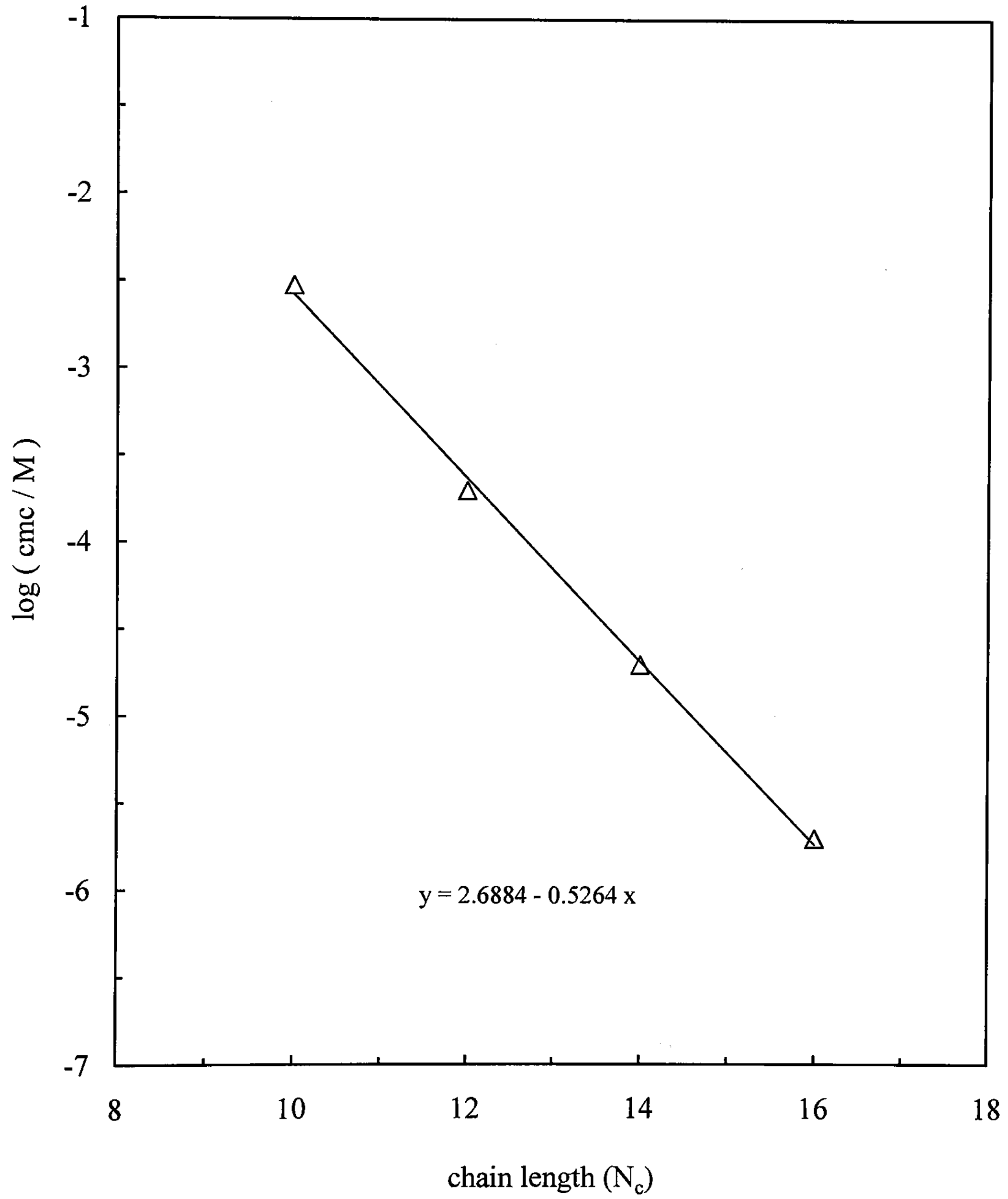

Table 3-7. Thermodynamic quantities for micellization of different alkylbenzyldimethylammonium chlorides in aqueous solution.

Surfactants	Temperature (°C)	β [14]	$\Delta G^{\circ}_{\mathrm{mic}}$ / kJ mol^{-1}
C10BDMAC	25	0.4329	-12.50
C12BDMAC	25	0.4417	-18.64
C14BDMAC	25	0.4594	-23.72
C16BDMAC	25	0.4843	-28.54
C10BDMAC	40	0.47813	-13.89
C12BDMAC	40	0.49332	-19.45
C14BDMAC	40	0.51588	-24.00
C16BDMAC	40	0.53892	-28.90

The reported β values of CnBDMAC are higher than those of alkyltrimethylammonium bromides ($\beta = 0.20 - 0.30$) [24].

As indicated by Table 3-7, the values of $\Delta G^{\circ}_{\mathrm{mic}}$ become more negative with an increase in the surfactant chain length and with a rise in temperature. This results in favoruing the micellization process, which is supported by the previously reported shift in the cmc values.

Table 3-8 reports the calculated values of $\Delta G^{\circ}_{\mathrm{mic}}$ for CnBDMAC in brine solutions at 25 °C using equation (3-5). Again, brine addition causes notable decrease in $\Delta G^{\circ}_{\mathrm{mic}}$ values. This indicates a facilitation of the micellization of each surfactant in the presence of brine, which can obviously be understood on the basis of the reduction in the polar head group repulsions. Czapkiewicz *et al.* [4, 15] reported values of about -23 and -28 kJ mol^{-1} for $\Delta G^{\circ}_{\mathrm{mic}}$ for C14 and C16BDMAC in aqueous solution at 25 °C, respectively.

The free energy of micellization, $\Delta G^{\circ}_{\mathrm{mic}}$, could be considered as the sum of the free energy of transferring the hydrocarbon chain out of water into the oil-like interior of the micelle $\Delta G^{\circ}(CH_2)$, and the free energy associated with the head group interactions, ΔG°(head) [20, 21]. The contribution of the hydrophobic interaction to the total free energy of micellization per mole of methylene group, $\Delta G^{\circ}(CH_2)$ could be determined from the plot of log ($\Delta G^{\circ}_{\mathrm{mic}}$) versus the number of carbon atoms in surfactant molecule. The slope of the obtained straight line equals $\Delta G^\circ(CH_2)$ and the intercept is equal to the headgroup contribution, ΔG° (head), to the free energy of micellization.

Table 3-8. Thermodynamic quantities for micellization of different alkylbenzyldimethylammonium chlorides in brine solution.

Surfactants	Temperature (°C)	ΔG°_{mic} / kJ mol^{-1}
C10BDMAC	25	-14.40
C12BDMAC	25	-21.10
C14BDMAC	25	-26.81
C16BDMAC	25	-32.511

Figure 3-16 shows how ΔG°_{mic} for the homologous CnBDMAC in aqueous and brine solutions varies with the number of carbon atoms at 25 °C. The total free energy of micellization was found to become more negative with an increase in the number of carbon atoms. The value of $\Delta G^\circ(CH_2)$ was found to be -3.00 and -2.66 kJ/mol in brine and aqueous solutions at 25 °C, respectively. These values are in good agreement with values reported in the literature [34]. The value of -3 kJ/mol obtained for ΔG° per methylene group is similar to values observed in processes, which may be considered analogous to micellization, as for example, the transfer of an alkyl chain from an aqueous to a hydrocarbon environment [20, 21, 34]. On the other hand, the value of ΔG° (head) was found to be 15.34 and 13.74 kJ/mol in brine and aqueous solutions at 25 °C, respectively. The large positive contribution of the headgroup to the total free energy of micellization is one of the observations which proves that micellization is mainly due to the hydrophobic effect. This is supported additionally by the magnitude of -3 kJ/mol obtained for ΔG° per methylene group, which as stated earlier is similar to values observed for the transfer of an alkyl chain from an aqueous to a hydrocarbon environment.

Figure 3-16. Free energy of micellization of CnBDMAC versus alkyl chain length in aqueous and brine solutions at 25 °C.

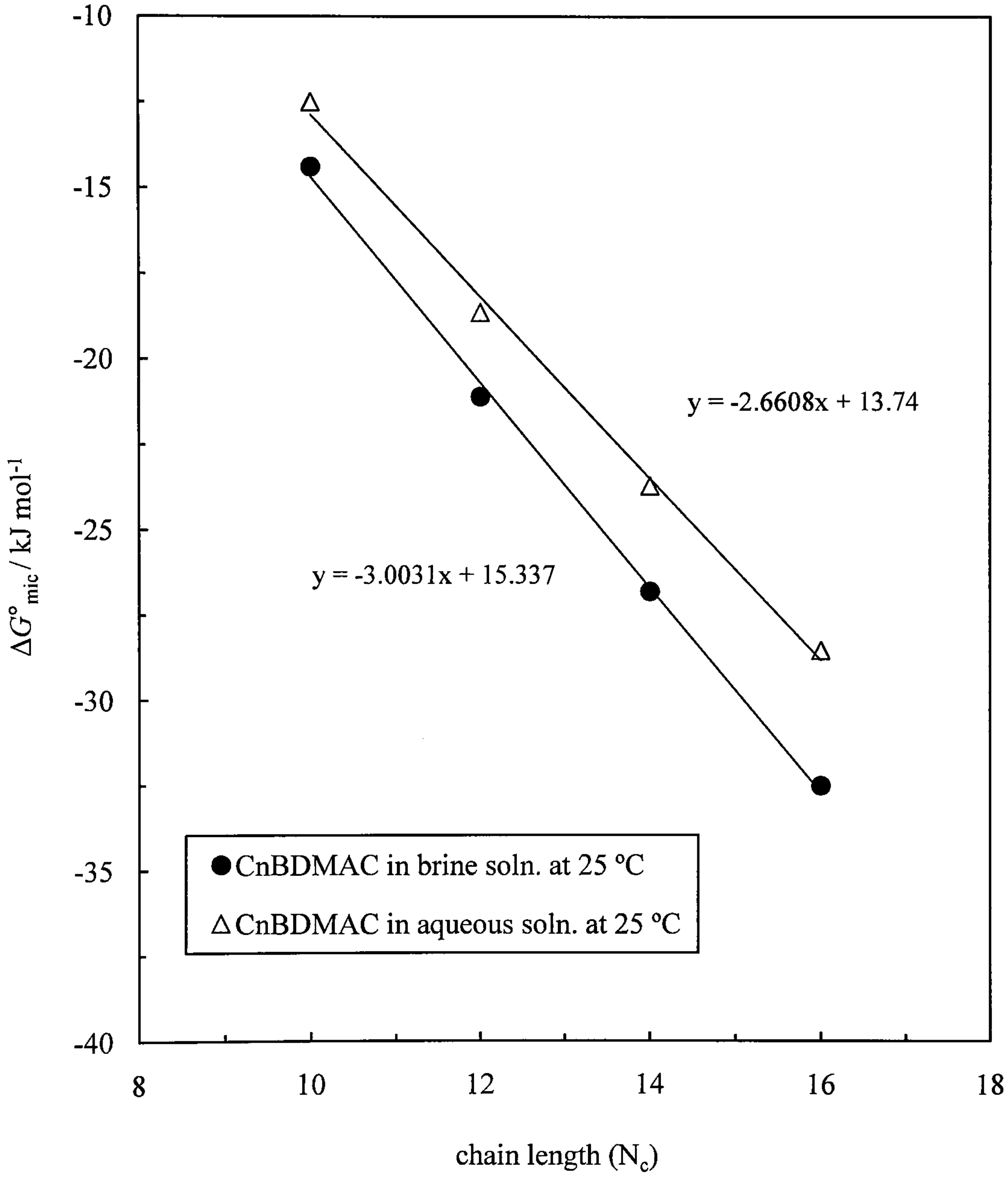

3.7. SUMMARY AND CONCLUSIONS

The adsorption behaviour of the cationic alkylbenzyldimethylammonium chloride surfactants at the air-water interface has been investigated as a function of alkyl chain length, temperature and electrolyte addition using surface tension measurements. For the best of our knowledge, no systematic study concerning the adsorption of this homogeneous series at the air-water interface by measuring the surface tension has been reported in the literature. The key and new findings within this study are summarized below.

I. The surfactant chain length has a great influence on the adsorption behaviour and hence on the cmc value. The cmc values were found to decrease as the number of carbon atoms increases. A significant minimum in the surface tension isotherm was observed for C10, C12BDMAC and to a lesser extent for C14 and C16BDMA due to the presence of certain impurities. This minimum in the surface tension disappeared after purification of the surfactant.

II. An increase in temperature of CnBDMAC solutions results in a decrease in the surface tension over the entire concentration range. The cmc values for the short chain C10 and C12BDMAC are much more temperature dependent compared with the long chain C14 and C16BDMAC surfactants.

III. The addition of 4.7 wt.% brine to surfactant solutions results in moving the isotherms to lower concentrations. Moreover, brine addition leads to a sharp decrease in the cmc values compared to those in water. Across the series, the maximum surface concentration increases with chain length and the concentration required to reach saturation decreases.

IV. The area per molecule and maximum surface concentration seem to be independent of temperature. The experimentally determined cmc values of CnBDMAC in aqueous solution decreases logarithmically as the number of carbon atoms in the alkyl chain increases in accordance with Klevens equation.

V. The total free energy of micellization was found to become more negative with an increase in the number of carbon atoms and with brine addition. This results in favouring the micellization process. The contribution of the hydrophobic interaction to the total free energy of micellization per mole of methylene group, $\Delta G^{\circ}(CH_2)$ was found to be -3.00 and -2.66 kJ/mol in brine and aqueous solutions at 25 °C, respectively.

3.8. REFERENCES

1. H. F. Walton, E. N. Hiebert and E. H. Sholtes, *J. Colloid Interface Sci.*, **1**, 385 (1946).
2. A. Cushman, A. P. Brady and J. W. McBain, *J. Colloid Interface Sci.*, **3**, 425 (1948).
3. J. A. Cella, D. N. Eggenberger, D. R. Noel, L. A. Harriman and H. J. Harwood, *J. Am. Chem. Soc.*, **74**, 2061 (1952).
4. J. Czapkiewicz, A. Gonzalez Perez, J. R. Rodriguez and J. L. del Castillo, *Colloids Surf. A*, **166**, 161 (2000).
5. J. J. Galan, A. Gonzalez-Perez and J. R. Rodriguez, *J. Therm. Anal. Calorim.*, **72**, 465 (2003).
6. A. Gonzalez-Perez, J. Czapkiewicz, J. L. Del Castillo and J. R. Rodriguez, *Colloids Surf. A*, **193**, 129 (2001).
7. A. Gonzalez-Perez, J. Czapkiewicz, J. L. Del Castillo and J. R. Rodriguez, *J. Colloid Interface Sci.*, **262**, 525 (2003).
8. A. González-Pérez, J. Czapkiewicz, G. Prieto and J. R. Rodríguez, *Colloid. Polym. Sci.*, **281**, 1191 (2003).
9. A. González-Pérez, J. Czapkiewicz, J. M. Ruso and J. R. Rodríguez, *Colloid. Polym. Sci.*, **282**, 1169 (2004).
10. A. Gonzalez-Perez, J. L. del Castillo, J. Czapkiewicz and J. R. Rodriguez, *J. Phys. Chem. B*, **105**, 1720 (2001).
11. A. Gonzalez-Perez, J. L. Del Castillo, J. Czapkiewicz and J. R. Rodriguez, *J. Chem. Eng. Data*, **46**, 709 (2001).
12. C. A. Gracia, S. Gomez-Barreiro, A. Gonzalez-Perez, J. Nimo and J. R. Rodriguez, *J. Colloid Interface Sci.*, **276**, 408 (2004).
13. J. R. Rodriguez and J. Czapkiewicz, *Colloids Surf. A*, **101**, 107 (1995).
14. J. R. Rodriguez, A. Gonzalez-Perez, J. L. Del Castillo and J. Czapkiewicz, *J. Colloid Interface Sci.*, **250**, 438 (2002).
15. J. Czapkiewicz and B. Sliwa, *Rocz. Chem.*, **44**, 1565 (1970).
16. C. Treiner and A. Makayssi, *Langmuir*, **8**, 794 (1992).
17. S. Shimizu, P. A. R. Pires, W. Loh and O. A. El Seoud, *Colloid. Polym. Sci.*, **282**, 1026 (2004).

18. A. Avranas, E. Malasidou and I. Mandrazidou, *J. Colloid Interface Sci.*, **207**, 363 (1998).

19. M. T. Garcia, E. Campos, J. Sanchez-Leal and F. Comelles, *J. Dispersion Sci. Technol.*, **27**, 739 (2006).

20. M. J. Rosen, *Surfactants and Interfacial Phenomena*, Wiley-Interscience, Hoboken, (2004).

21. D. Myers, *Surfactant Science and Technology*, J. Wiley, Hoboken (2006).

22. K.-H. Kang, H.-U. Kim and K.-H. Lim, *Colloids Surf. A*, **189**, 113 (2001).

23. A. A. Dar, G. M. Rather, S. Ghosh and A. R. Das, *J. Colloid Interface Sci.*, **322**, 572 (2008).

24. T. F. Tadros, Applied Surfactants: Principles and Applications, Wiley-VCH, Weinheim (2005).

25. J. Gibbs, *Scientific Papers of J. Willard Gibbs*, Longmans, Green and Co., Yale (1906).

26. J. L. Trompette, J. Zajac, E. Keh and S. Partyka, *Langmuir*, **10**, 812 (1994).

27. J. Lu, E. Simister, R. Thomas and J. Penfold, *Prog. Coll. Pol. Sci.*, **93,** 92 (1993).

28. H. Klevens, *J. Am. Oil Chem. Soc.*, **30**, 74 (1953).

29. S. Ross, C. E. Kwartler and J. H. Bailey, *J. Colloid Interface Sci.*, **8**, 385 (1953).

30. J. Caskey and W. Barlage Jr, *J. Colloid Interface Sci.*, **35**, 46 (1971).

31. R. Venable and R. Nauman, *J. Phys. Chem.*, **68**, 3498 (1964).

32. K. Shinoda and E. Hutchinson, *J. Phys. Chem.*, **66**, 577 (1962).

33. R. F. Kamrath and E. I. Franses, *Ind. Eng. Chem. Res.*, **22**, 230 (1983).

34. L. R. Fisher and D. G. Oakenfull, *Chem. Soc. Rev.*, **6**, 25 (1977).

CHAPTER 4

Chapter 4

PHASE BEHAVIOUR OF ALKYLBENZYLDIMETHYLAMMONIUM CHLORIDES IN OIL-WATER SYSTEMS

4.1. INTRODUCTION

Alkylbenzyldimethylammonium chlorides are one of the most widely used corrosion inhibitors in the oil industry. Typically, these molecules are obtained commercially as a mixture of homologues. These corrosion inhibitors are formulated with other types of inhibitors and synergists to form a product, which is then used commercially to inhibit corrosion. Corrosion inhibitor performance tests have shown that emulsion formation results in a significant decrease in the inhibitor performance compared to water free from emulsions [1]. This reduction in the inhibition efficiency could be attributed to the inhibitor loss cither in emulsion formation (surfactant inhibitor is the emulsifier) or by adsorption to the naturally occurring crude oil emulsions. The emulsion droplets constitute a large surface area onto which surfactant inhibitors can adsorb. This "parasitic" consumption of inhibitor molecules constitutes a potential corrosion risk and leads to an increased inhibitor demand.

Recently, a few studies have been conducted to investigate the types of emulsions formed and the partitioning behaviour of these quaternary ammonium inhibitors in different hydrocarbons and crude oil-water mixtures [2, 3].

The present chapter deals with parasitic consumption of corrosion inhibitor molecules due to emulsion formation and partitioning into the oil phase. This chapter will show how common oil-field variables (temperature, brine concentration and oil type) and the inhibitor's molecular structure can affect the equilibrium phase behaviour of corrosion inhibitors in oil-water systems. In addition, an electrochemical technique, namely the *bubble test*, was employed to investigate the effect of corrosion inhibitors partitioning into the oil phase on their inhibition efficiency.

4.2. EMULSION TYPE OF ALKYLBENZYLDIMETHYLAMMONIUM CHLORIDES IN MIXTURES OF OIL AND WATER

The phase behavior of the aggregated surfactant molecules in oil-water systems was investigated by monitoring the transitional phase inversion of the emulsions formed. Aqueous solutions of the alkylbenzyldimethylammonium chlorides C12, C14, and C16BDMAC, containing increasing concentrations of brine, were emulsified with equal volumes of heptane or toluene or heptol (a mixture of heptane and toluene with a volume ratio of 70:30) or Prudhoe Bay crude oil in a batch method. In each case, the concentration of the surfactant was above the cmc and the temperature of the emulsification process was held constant at 40 °C.

Conductivity measurements and drop-tests were performed to characterize the type of emulsions produced. Since water-continuous emulsions are generally of high electrical conductivity and oil-continuous emulsions are of low conductivity, phase inversion of an emulsion system from o/w to w/o is determined by an abrupt decrease in the conductivity. Conductivity of emulsions prepared from equal volumes of aqueous 10 mM alkylbenzyldimethylammonium chlorides and four different oils as a function of the aqueous phase brine concentrations at 40°C were studied. Brine salinities varied from 0.1 to 10 wt.% and a 1:1 phase volume ratio was employed.

4.2.1. Hepatne

The effect of added electrolyte on the conductivity of the emulsions prepared with different CnBDMAC surfactant inhibitors with heptane as the hydrocarbon phase is shown in Figure 4-1.

Figure 4-1. Conductivity versus [brine] for emulsions produced from aqueous phase containing 10 mM CnBDMAC and heptane (1:1 volume ratio) after homogenization for 2 min at 13000 rpm at 40 °C.

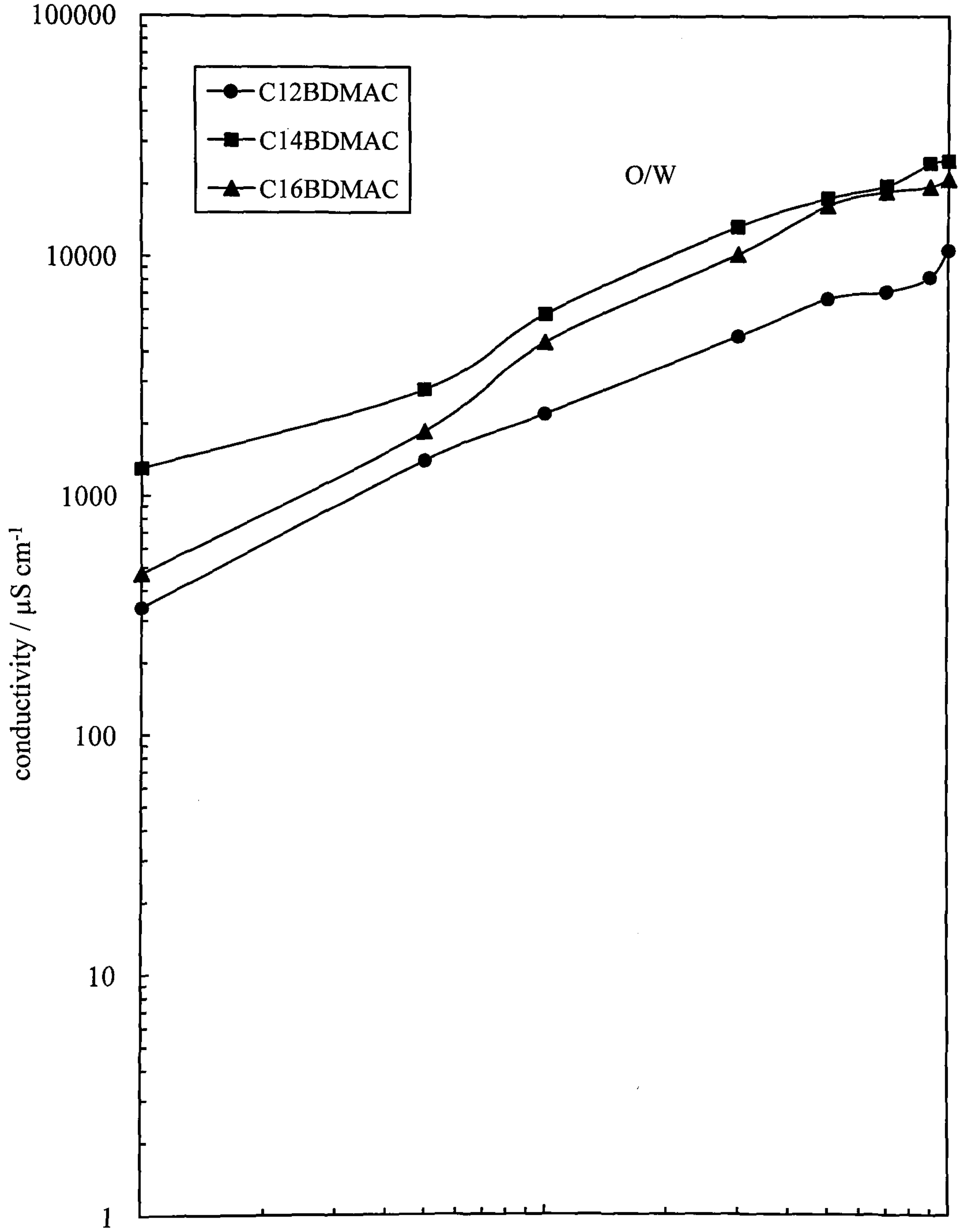

As seen, high conductivity values were obtained over all the tested brine concentrations. The conductivities of the emulsions obtained increase as the salinity of the brine increases for each of the surfactants studied. This indicates the formation of oil-in-water emulsions. Drop tests confirmed that all these emulsions were water continuous. The appearance of the emulsions prepared with different CnBDMAC surfactants after 24 hr is shown in Figure 4-2. At brine concentrations ≥ 3 wt. %, emulsions of C12BDMAC show complete phase separation into clear water and oil phases. Most of the emulsions were unstable to coalescence and creaming as shown in Figure 4-2. Emulsions containing C16BDMAC gave rise to the most stable ones followed by that containing C14BDMAC surfactant. Phase separation has been noticed also for emulsions containing C14BDMAC at brine concentrations between 3 and 7 wt. %. Gelled emulsions formed with systems containing C16BDMAC at brine concentrations greater than 3 wt. %. In addition, systems containing C14BDMAC show the same behaviour at brine concentrations ≥ 9 wt. %.

The formation of gel-emulsions in dilute solutions of surfactants have been reported in the literature [4-6]. Surface-active and amphiphilic molecules, under suitable conditions, strongly stabilize emulsions to form viscous gel-like materials in organic solvents. The formation of the gelled emulsion is, in fact, a result of the high spreading power of the lamellar liquid crystal [7-8]. Figure 4-4 shows a schematic presentation of the mechanism of gel-emulsion formation and the change in shape of the flexible bilayer self-assemblies of surfactant molecules. The water molecules are spontaneously taken up by the layers of surfactant molecules during the formation of lamellar liquid crystal structures. The oil is trapped between two flexible surfactant bilayers, resulting in the formation of micro-oil domains. Since the surfactant bilayers are flexible, the micro-domains are quickly connected to and disconnected from each other.

The emulsions of C14 and C16BDMAC with heptane form gel-like structures because of surfactant aggregates create three-dimensional network structures through self-association. The driving forces for gelation are (I) intermolecular hydrogen-bonding interactions that facilitate the formation of large aggregates and (II) van der Waals interactions that bring the large aggregates close to each other.

The stability of the C12BDMAC emulsions after 24 hr in terms of the percentages of oil and water resolved is shown in Figure 4-3. Clearly, emulsions are highly unstable apart from those having brine concentrations below 1 wt. %.

Figure 4-2. Appearance of emulsions produced from aqueous phase containing 10 mM CnBDMAC, [brine]= 0.1-10 wt.% and heptane (1:1 volume ratio), homogenized for 2 min at 13000 rpm then stored at 40 °C for 24 h. Labels indicate the initial concentration of brine in the aqueous phase.

a) C12BDMAC

b) C14BDMAC

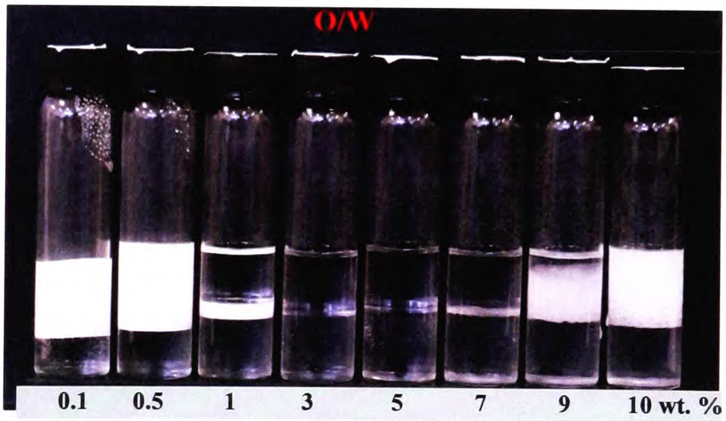

c) C16BDMAC

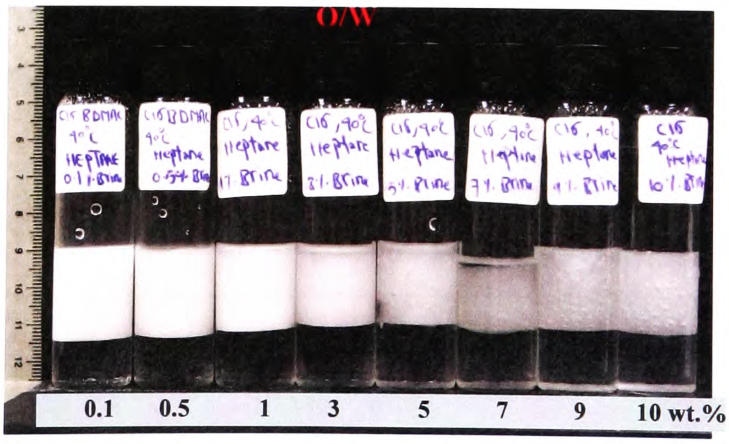

Figure 4-3. Percentages of water and oil phases resolved versus [brine] for emulsions produced from aqueous phase containing 10 mM C12BDMAC and heptane (1:1 oil to water volume ratio), homogenised for 2 min at 13000 rpm and stored at 40 °C for 24 h. 50 % water or oil resolved indicates complete phase separation.

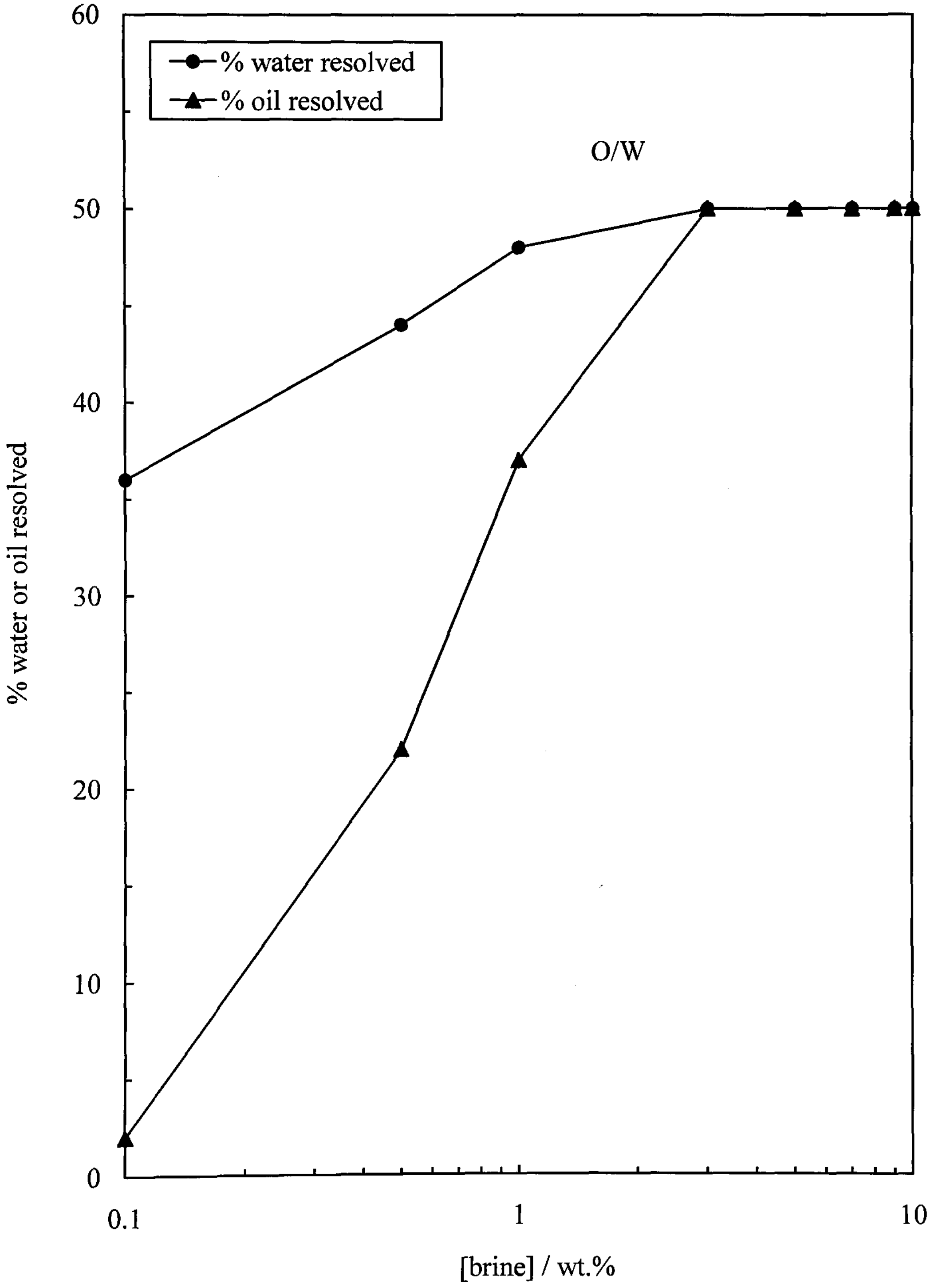

In a similar study carried out in our laboratory under the same experimental conditions [2, 4], it was reported that emulsions containing heptane and 10 mM C12BDMAC were water-continuous over all the same investigated brine concentration range. The measurements were done at 25 and 40 °C. Similarly, emulsions containing the long chain C16BDMAC surfactant and heptane were of the o/w type with no inversion.

Figure 4-4. Schematic presentation of the mechanism of gel-emulsion formation [7].

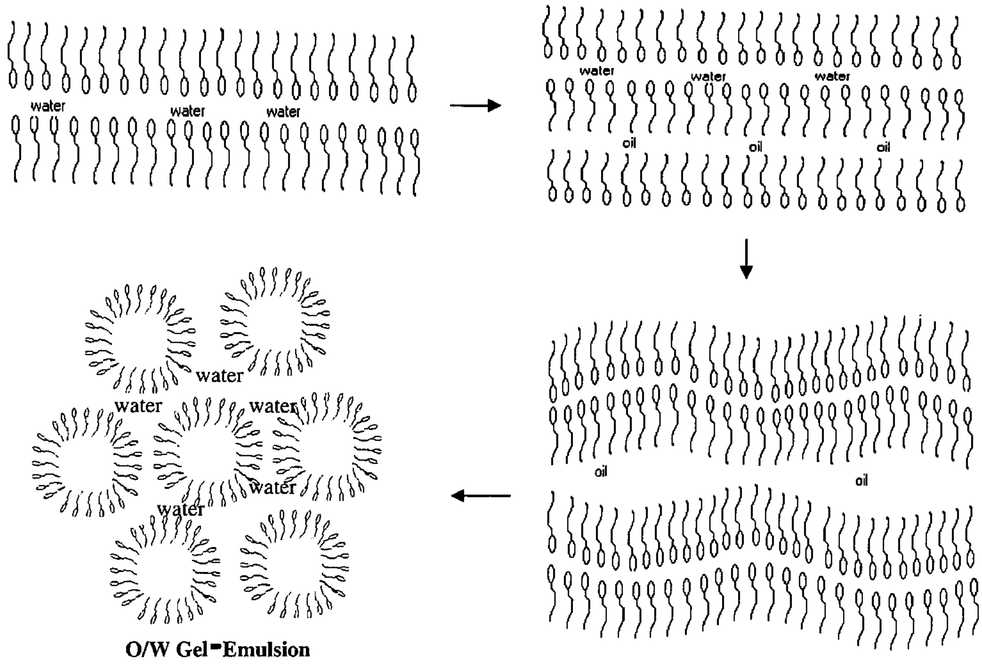

4.2.2. Heptol

Figure 4-5 shows the conductivity of emulsions prepared from equal volumes of 10 mM aqueous CnBDMAC and heptol as a function of aqueous phase electrolyte concentration at 40 °C. The results indicate that the emulsions remain water-continuous as the concentration of the brine increases for all the alkylbenzyldimethylammonium chlorides investigated. Drop tests confirmed that all emulsions were water-continuous. A sharp decrease in the conductivity of the C16BDMAC emulsions at brine concentrations ≥ 3 wt. % was noticed. Despite this relatively low conductivity value, the drop tests showed that all the emulsions were water-continuous.

Figure 4-5. Conductivity versus [brine] for emulsions produced from aqueous phase containing 10 mM CnBDMAC and heptol (1:1 volume ratio) after homogenization for 2 min at 13000 rpm at 40 °C.

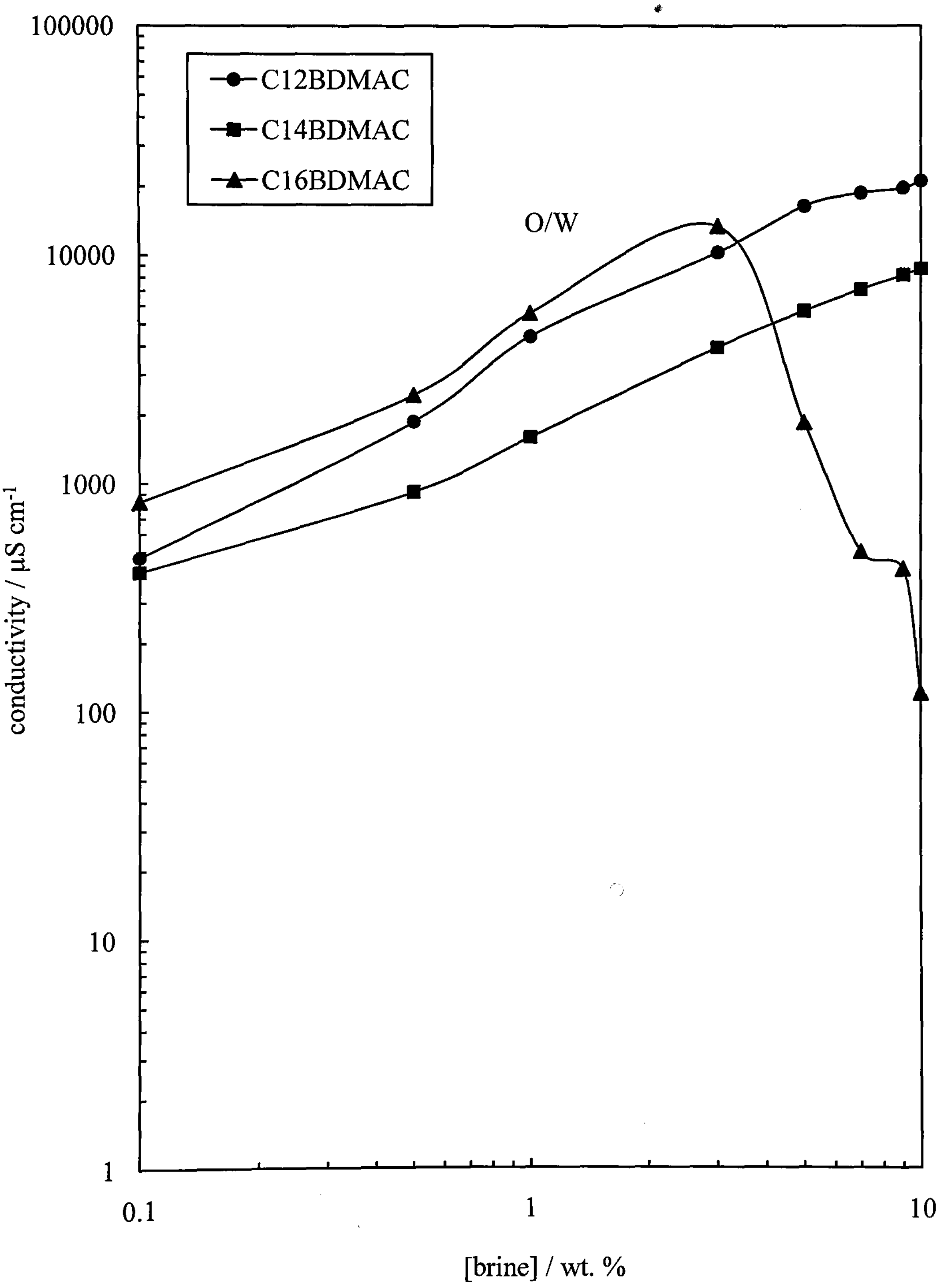

It seems that the brine concentration employed is not enough to invert the emulsion produced into an oil-continuous. Probably, if the brine concentration were increased above 10 wt. %, this may result in the inversion of emulsions into oil-continuous ones. The appearance of CnBDMAC-heptol emulsions after 24 hr is shown in Figure 4-6. Complete phase separation was observed for emulsions containing C12BDMAC and brine concentrations greater than 1 wt. %. Emulsions containing C16BDMAC and brine concentrations between 7 and 10 wt. % phase separate rapidly. The stability of heptol emulsions stabilized by C16BDMAC after 24 h as a function of brine concentration is shown in Figure 4-7 in terms of the percentages of oil and water resolved. Clearly, the stability of these emulsions is lower than those prepared using heptane. On the other hand, no marked differences were noticed in the appearance and stability of emulsions containing C12BDMAC and heptol and those containing heptane after 24 hours. The same observation applies for emulsion containing C14BDMAC and heptol or heptane.

Hicks [9] has reported that in the presence of 10 mM C16BDMAC, all emulsions containing heptol were of the o/w type at 25 °C. Additionally, the same emulsion type was reported for systems containing C12BDMAC and heptol under the same used experimental conditions.

4.2.3. Toluene

The effect of brine concentration on the conductivity of emulsions prepared from different CnBDMAC surfactants with toluene as the hydrocarbon phase is shown in Figure 4-8. Emulsions containing C12BDMAC remain water-continuous as the concentration of the brine increases, while those containing C14BDMAC and C16BDMAC invert into oil-continuous at brine concentrations of 3 and 0.8 wt.% respectively. This was indicated by the sharp decrease in the conductivity of the emulsions at these brine concentrations and was confirmed using the drop test. The last water continuous emulsions tested for C14BDMAC and C16BDMAC were at 2 and 0.7 wt. % under the experimental conditions employed.

The appearance of emulsions prepared from different CnBDMAC and toluene after 24 hr is shown in Figure 4-9. Apparently, for brine concentrations greater than 0.1 wt. %, emulsions containing C12BDMAC and toluene coalesce very quickly with complete phase separation into water and oil.

Figure 4-6. Appearance of emulsions produced from aqueous phase containing 10 mM of different CnBDMAC, [brine]= 0.1-10 wt.% and heptol (1:1 volume ratio), homogenized for 2 min at 13000 rpm then stored at 40 °C for 24 h. Labels indicate the initial concentration of brine in the aqueous phase.

a) C12BDMAC

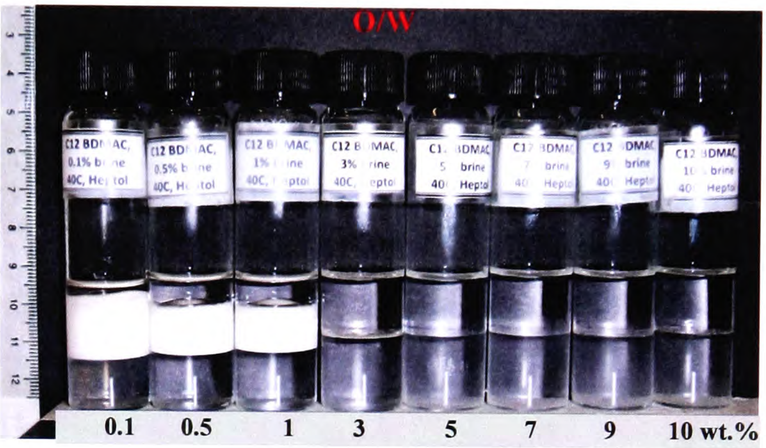

b) C14BDMAC

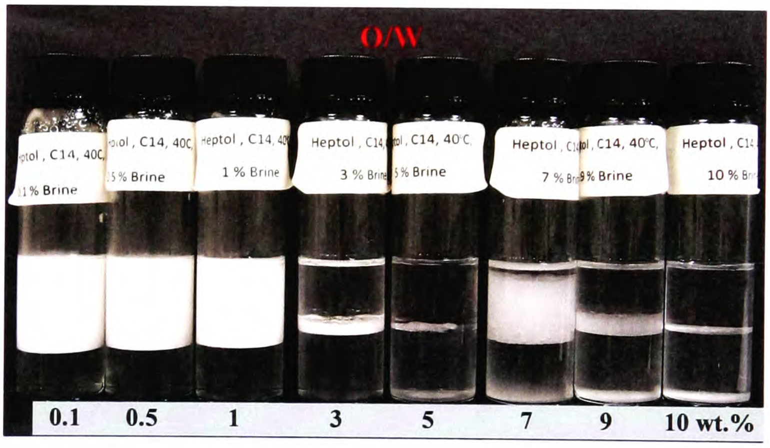

c) C16BDMAC

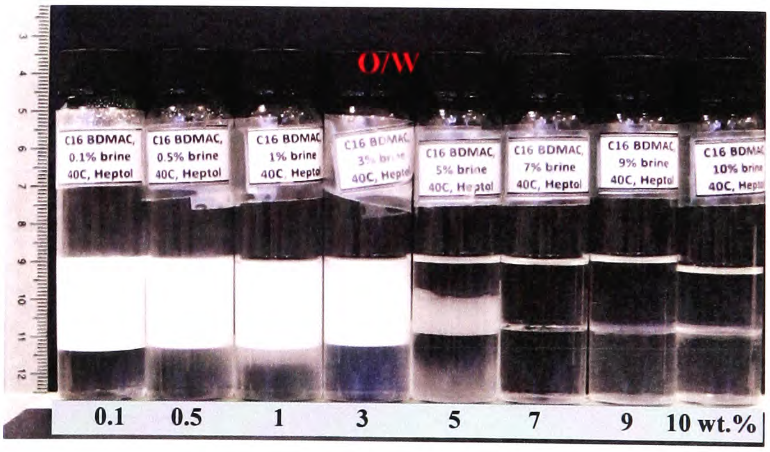

Figure 4-7. Percentages of water and oil phases resolved versus [brine] for emulsions produced from aqueous phase containing 10 mM of C16BDMAC and heptol (1:1 oil to water volume ratio), homogenised for 2 min at 13000 rpm and stored at 40 °C for 24 h. 50% water or oil resolved indicates complete phase separation.

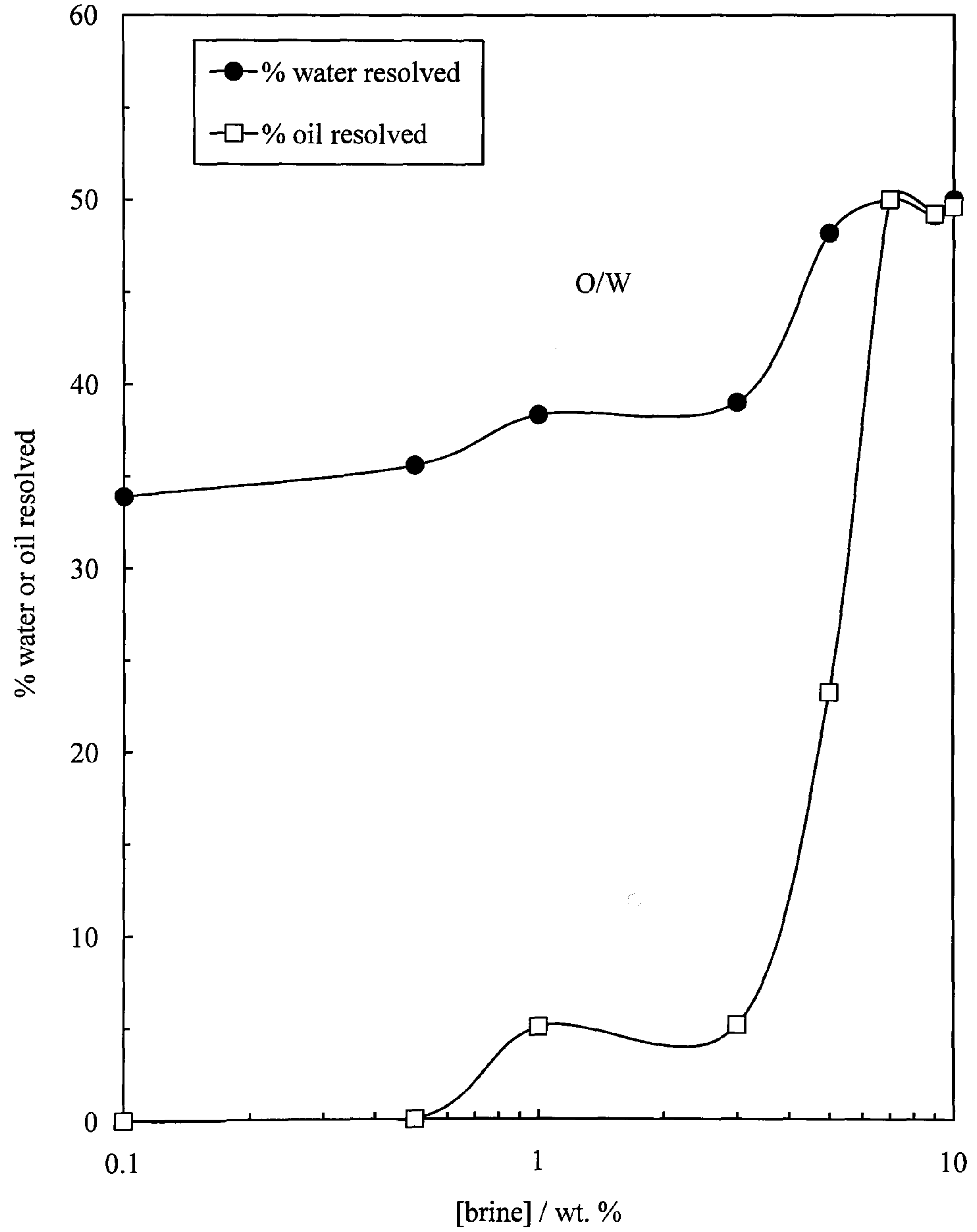

Figure 4-8. Conductivity versus [brine] for emulsions produced from aqueous phase containing 10 mM of different alkylbenzyldimethylammonium chlorides and toluene (1:1 volume ratio) after homogenization for 2 min at 13000 rpm at 40 °C. Vertical lines indicate the transition from water-continuous to oil-continuous emulsions, which was confirmed using the drop test.

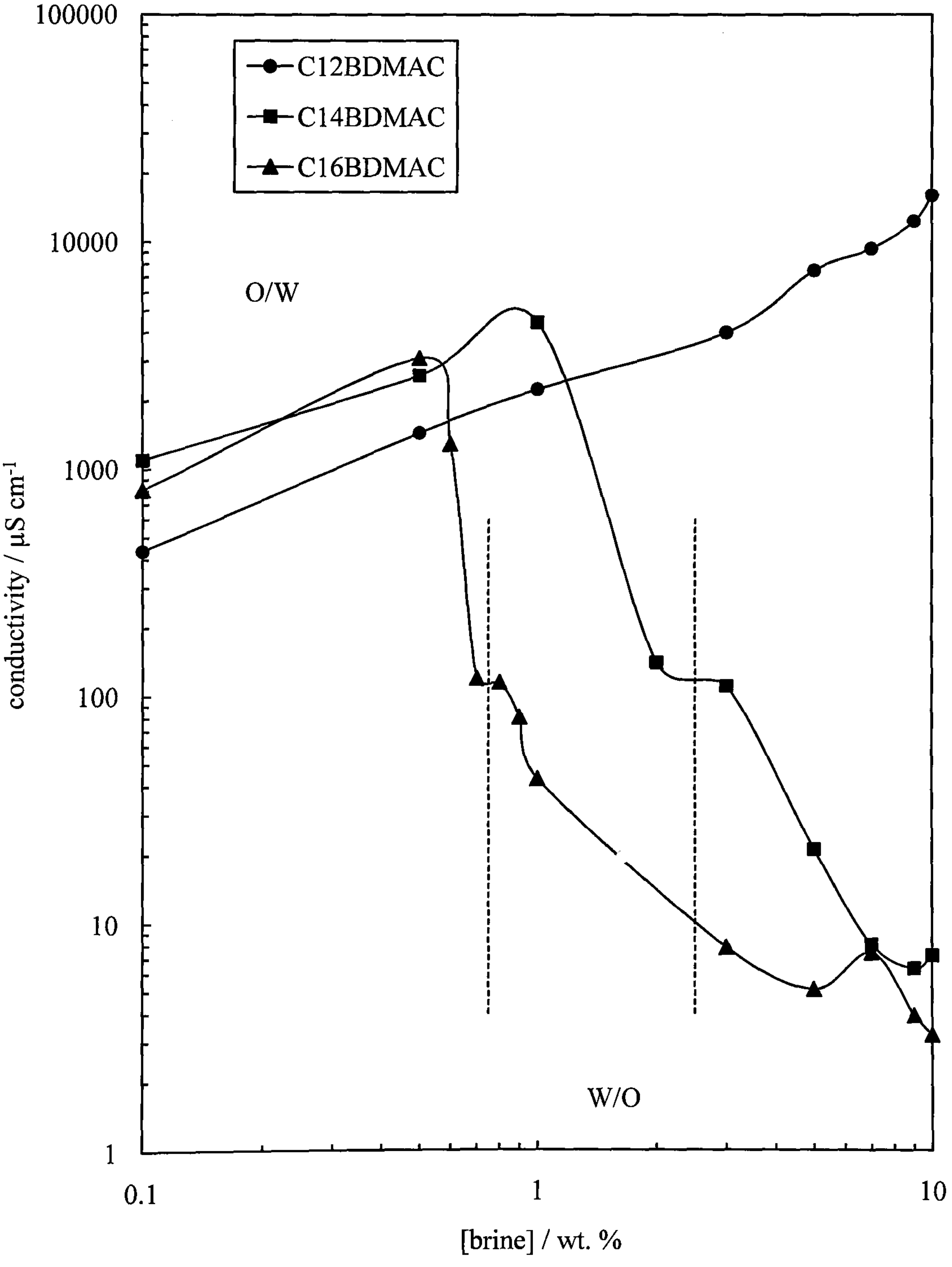

Figure 4-9. Appearance of emulsions produced from aqueous phase containing 10 mM of different CnBDMAC, [brine]= 0.1-10 wt. % and toluene (1:1 volume ratio), homogenized for 2 min at 13000 rpm then stored at 40 °C after 24 h. A red vertical line indicates the transition from o/w to w/o emulsions, which was confirmed using the drop test. Labels indicate the initial aqueous concentration of brine.

a) C12BDMAC

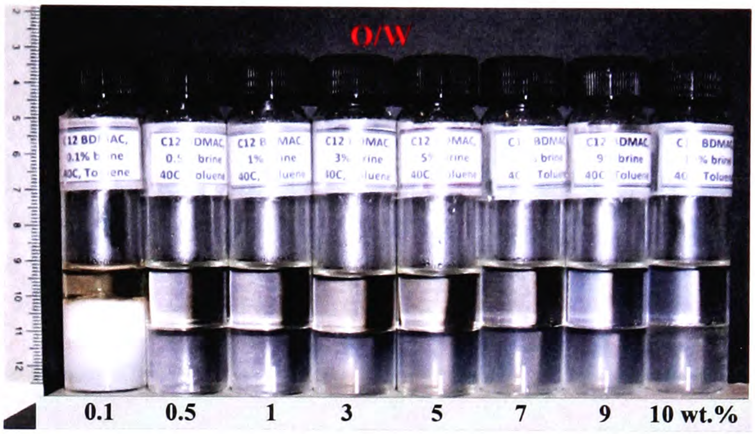

b) C14BDMAC

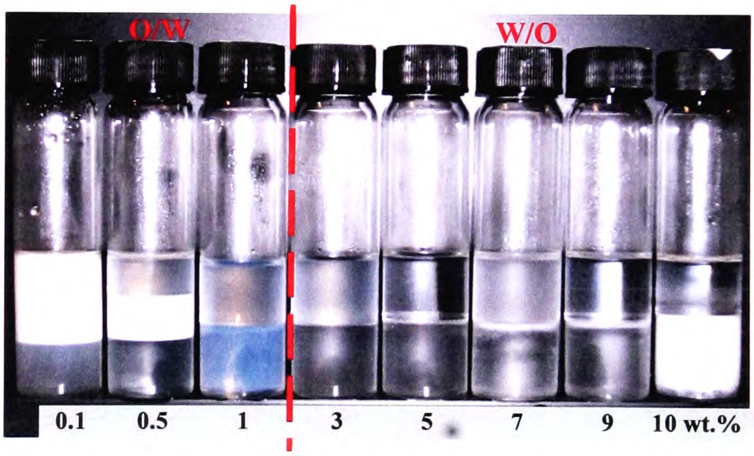

c) C16BDMAC

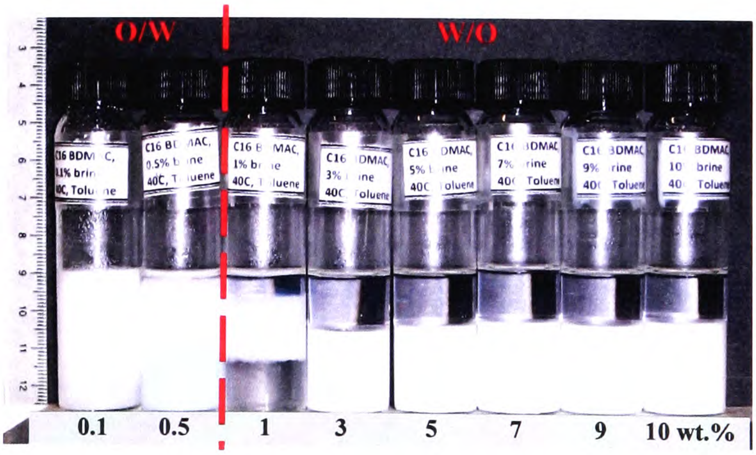

Emulsions containing C14BDMAC and toluene with brine concentrations between 1 and 9 wt. % brine tend to break into clear oil and water phases. Emulsions containing toluene and 1 wt. % brine and stabilized by C14BDMAC coalesce very quickly with the lower phase losing its white intensity and taking on the bluish appearance of the equilibrium o/w microemulsion. The water-in-oil emulsions stabilized by the long chain C16BDMAC are more stable to coalescence compared to those containing C14BDMAC. The lower phase in emulsions containing toluene and 0.5 wt. % brine and stabilized by C16BDMAC takes on the bluish appearance of the equilibrium o/w microemulsion. Upon increasing the brine concentration to 1 wt. %, the blue colour corresponding to the w/o microemulsion move into the upper oil phase.

Hicks [9] reported that at 25 °C, w/o emulsions stabilized by C16BDMAC were produced using toluene as oil when the concentration of electrolyte in the aqueous phase was greater than 2 wt. %. This indicates that the electrolyte concentration at which emulsions containing C16BDMAC and toluene invert into w/o type decreases with a rise in temperature. Additionally, it was reported that emulsions containing C12BDMAC and toluene were water continuous over the entire brine concentrations range (0.1 to 10 wt. %).

The stability of the C12BDMAC-toluene emulsions after 24 hr in terms of percentage of oil and water resolved is shown in Figure 4-10. The high percentage of water and oil resolved reflects the high instability of the produced emulsions. Figure 4-11 shows the stability of C16BDMAC-toluene emulsions in terms of percentage of oil and water resolved after 24 hr. As shown, the o/w emulsions were unstable towards creaming, but stable to coalescence, whereas the w/o emulsions were unstable towards sedimentation, but stable to coalescence. The stability of emulsions decreases around the inversion point.

4.2.4. Crude oil

The effect of brine concentration on the emulsion type formed in systems containing 10 mM of different aqueous CnBDMAC surfactants and Prudhoe Bay crude oil was investigated at 40 °C. The conductivities of the different emulsions formed immediately after homogenization are shown in Figure 4-12. The figure shows that emulsions containing C12BDMAC remain water-continuous while those

Figure 4-10. Percentages of water and oil phases resolved versus [brine] for emulsions produced from aqueous phase containing 10 mM of C12BDMAC and toluene (1:1 oil to water volume ratio), homogenised for 2 min at 13000 rpm and stored at 40 °C for 24 h. 50% water or oil resolved indicates complete phase separation.

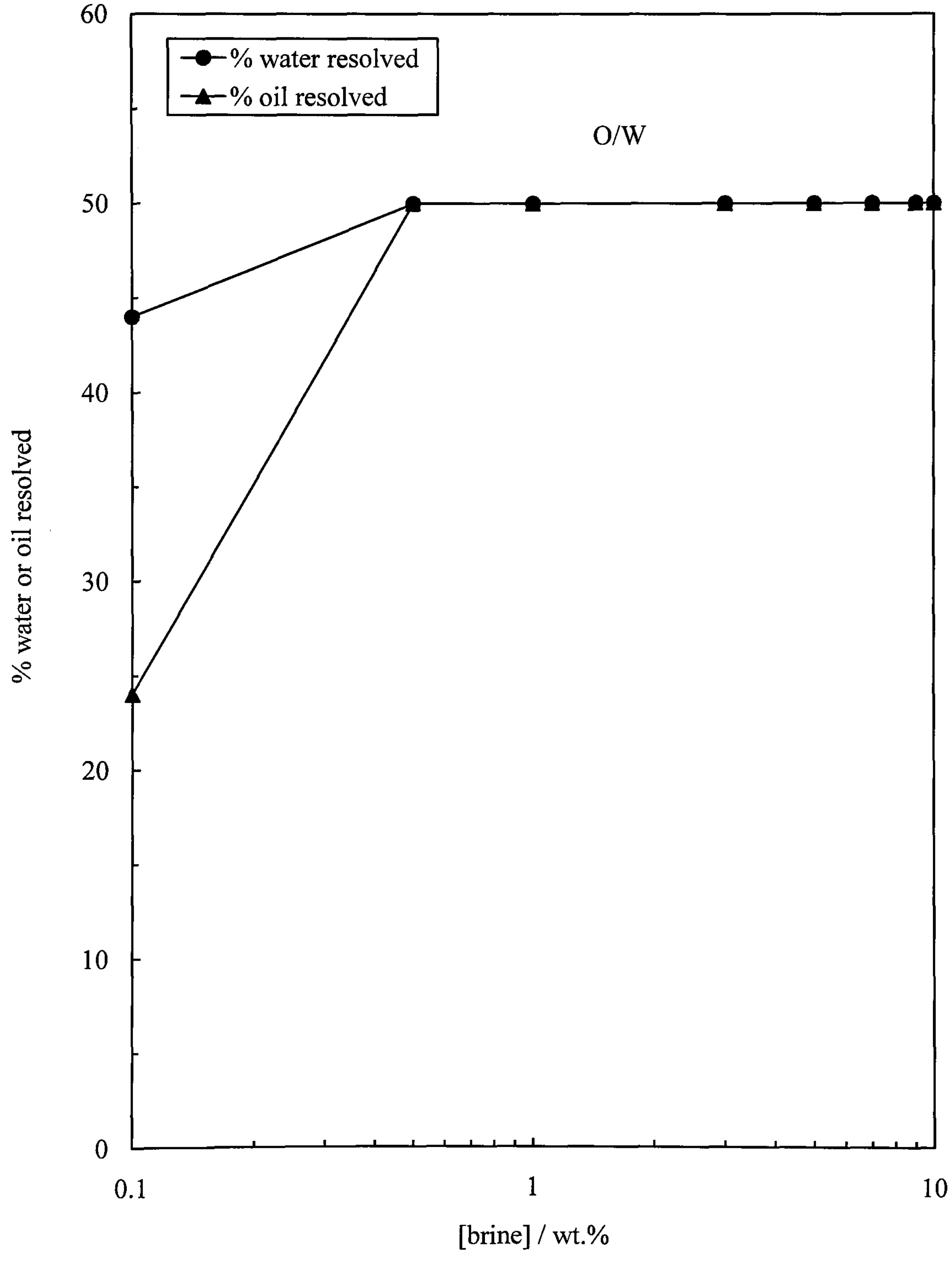

Figure 4-11. Percentages of water and oil phases resolved versus [brine] for emulsions produced from aqueous phase containing 10 mM C16BDMAC and toluene (1:1 oil to water volume ratio), homogenised for 2 min at 13000 rpm and stored at 40 °C for 24 h. Vertical line indicates the transition from o/w to w/o emulsions which was confirmed using the drop test. 50% water or oil resolved indicates complete phase separation.

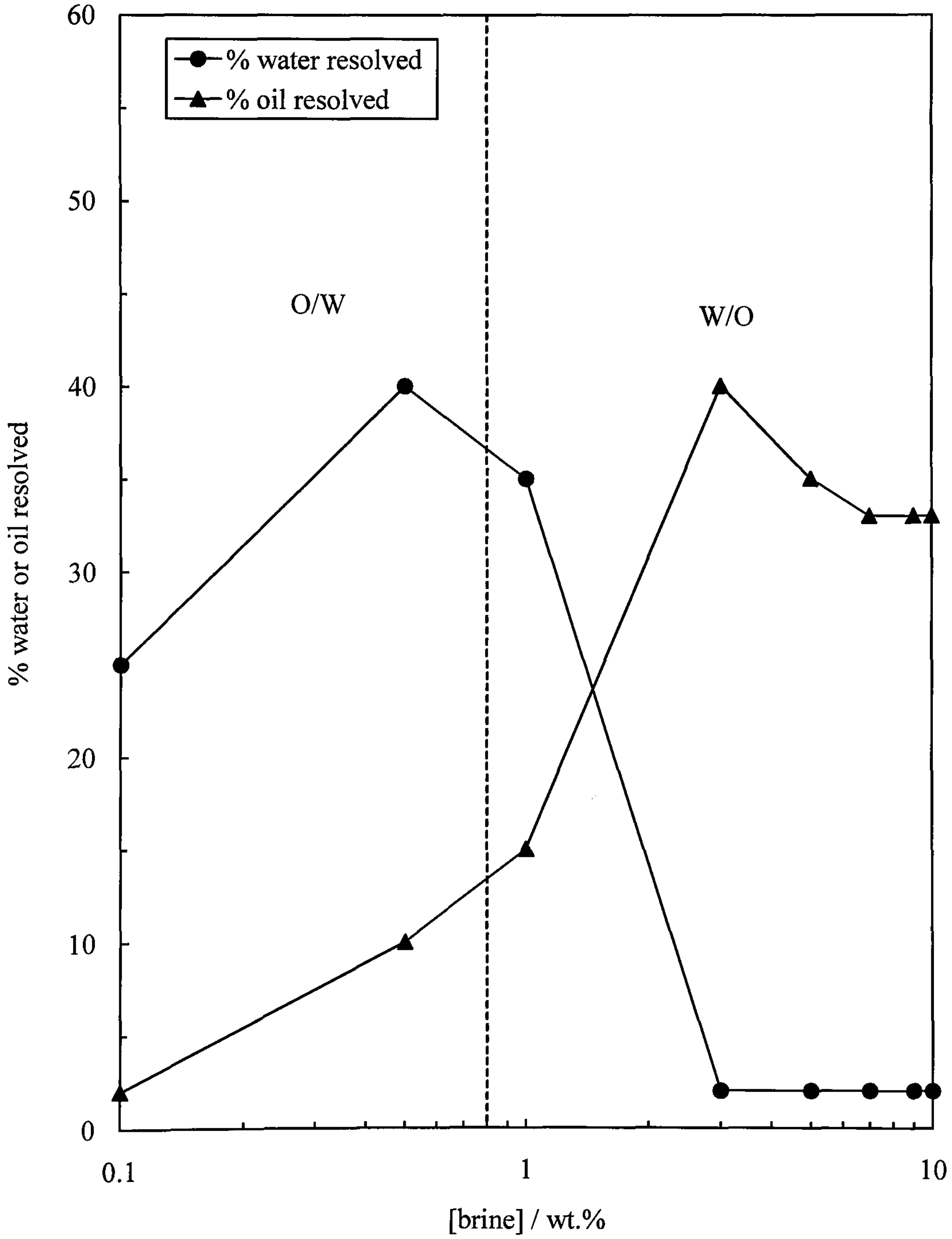

Figure 4-12. Conductivity versus [brine] for emulsions produced from aqueous phase containing 10 mM of different CnBDMAC and crude oil (1:1 volume ratio) homogenized for 2 min at 13000 rpm at 40 °C. Vertical lines indicate the transition from water-continuous to oil-continuous emulsions which was confirmed using the drop test.

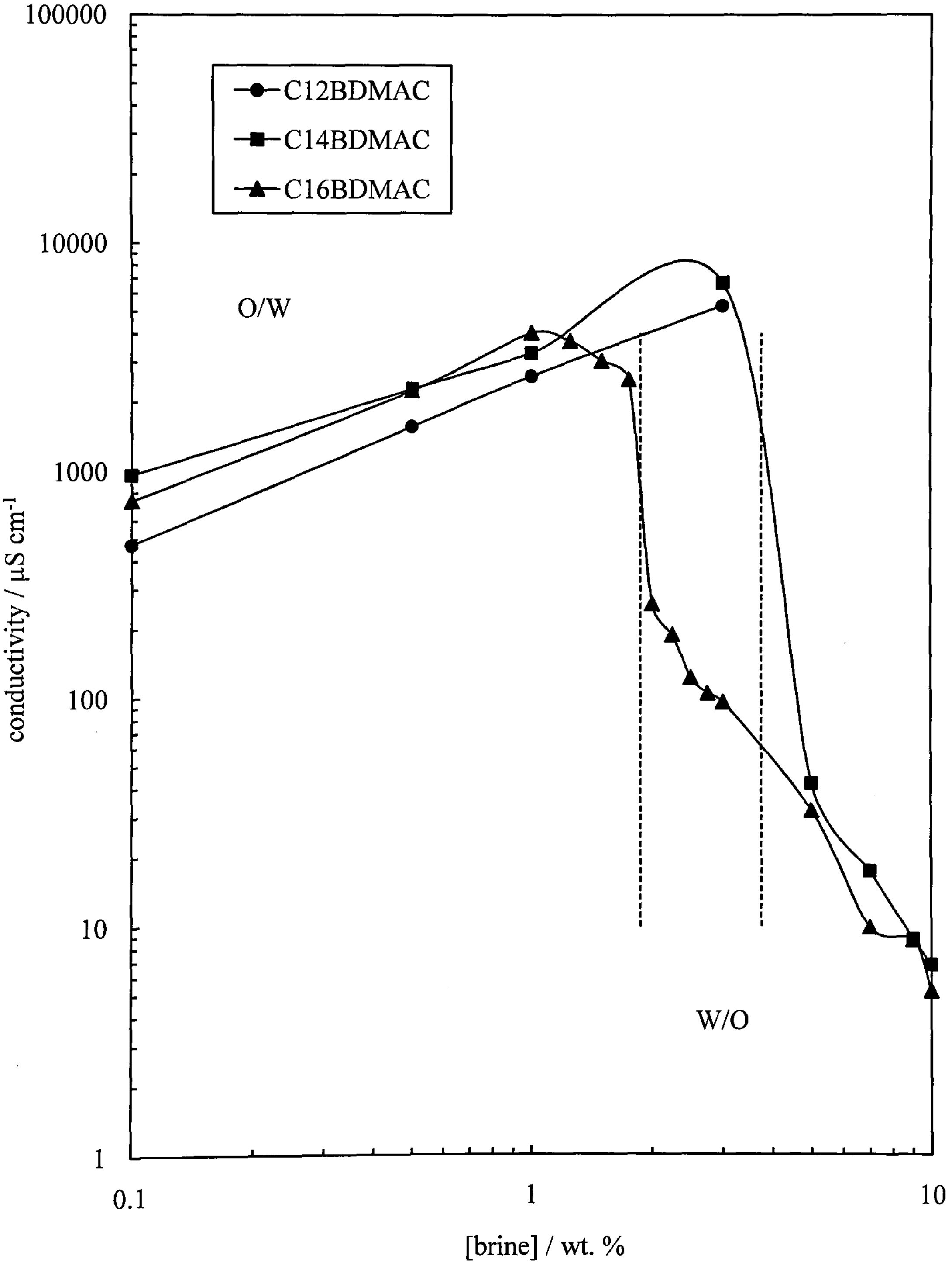

for C14BDMAC and C16BDMAC invert into oil-continuous emulsions at brine salinities of 4 and 2 wt.%, respectively.

This is indicated by the sharp decrease in the conductivity of the emulsions at these brine concentrations and was confirmed by the drop test. The last water continuous emulsions tested for C14BDMAC and C16BDMAC were at brine concentrations of 3.5 and 1 wt. %, respectively under the experimental conditions employed. In a similar study, Hicks [9] reported that at 25 °C, w/o emulsions stabilized by C16BDMAC were produced using Prudhoe Bay crude oil as the oil phase when the concentration of electrolyte in the aqueous phase was greater than 1 wt.%.

The appearance of the emulsions after storage at 40 °C for 24 hr is shown in Figure 4-13. Emulsions containing C12BDMAC and crude oil tend to phase separate at brine concentration $\geq$ 1 wt. % after 24 hr. The aqueous phase is slightly turbid with a light brown colour at brine concentrations between 1 and 5 wt. %. The stability of C12BDMAC-toluene emulsions after 24 hr is shown in Figure 4-14 in terms of the percentage of oil and water resolved. These emulsions were unstable to coalescence and creaming and gave rise to the least stable oil-in-water emulsions compared to those containing C14 or C16BDMAC surfactants under the same experimental conditions.

Emulsions containing C14BDMAC or C16BDMAC and crude oil tend to phase separate completely at brine concentration $\geq$ 5 and 3 wt. %, respectively. The stability of C16BDMAC-toluene emulsions after 24 hr is shown in Figure 4-15.

A summary of emulsions types produced form different CnBDMAC and different oils as a function of the brine concentration at 40 °C compared to those studied by Hicks [9] at 25 °C is given in Table 4.1.

4.3. PARTITIONING OF ALKYLBENZYLDIMETHYLAMMONIUM CHLORIDE CORROSION INHIBITORS IN MIXTURES OF OIL AND WATER

An equilibrium partitioning experiment was carried out to investigate the phase behaviour of C16BDMAC corrosion inhibitor with toluene as the hydrocarbon phase. Equilibrium partitioning studies were carried out using 10 mM C16BDMAC

Figure 4-13. Appearance of emulsions produced from aqueous phase containing 10 mM of different CnBDMAC, [brine] = 0.1-10 wt.% and crude oil (1:1 volume ratio), homogenized for 2 min at 13000 rpm then stored at 40 °C for 24 h. A red vertical line indicates the transition from o/w to w/o emulsions which was confirmed using the drop test. Labels indicate the initial aqueous concentration of brine.

a) C12BDMAC

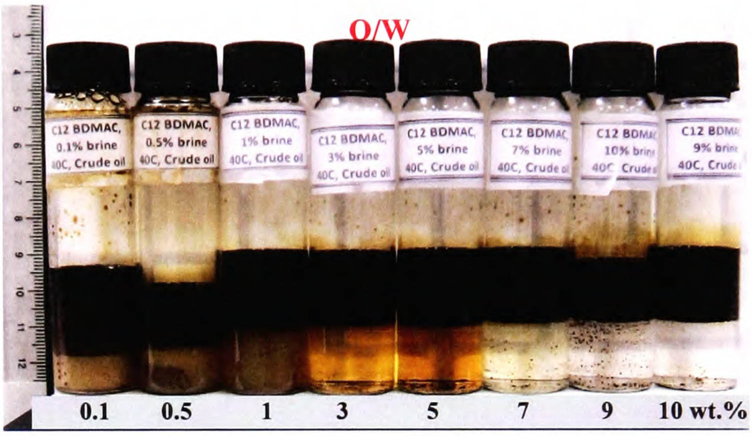

b) C14BDMAC

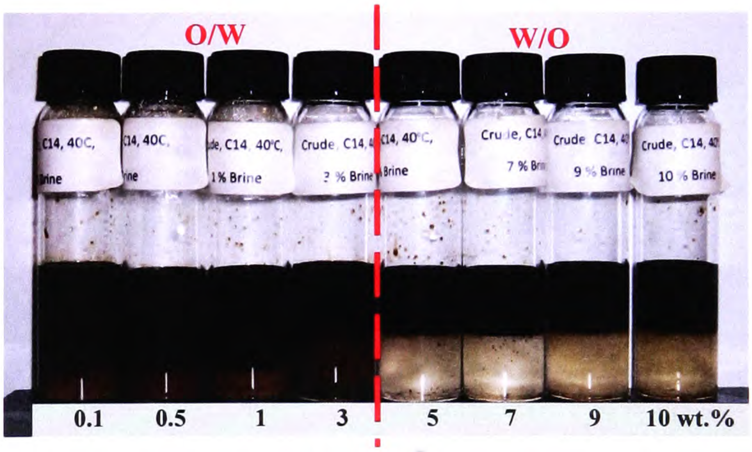

c) C16BDMAC

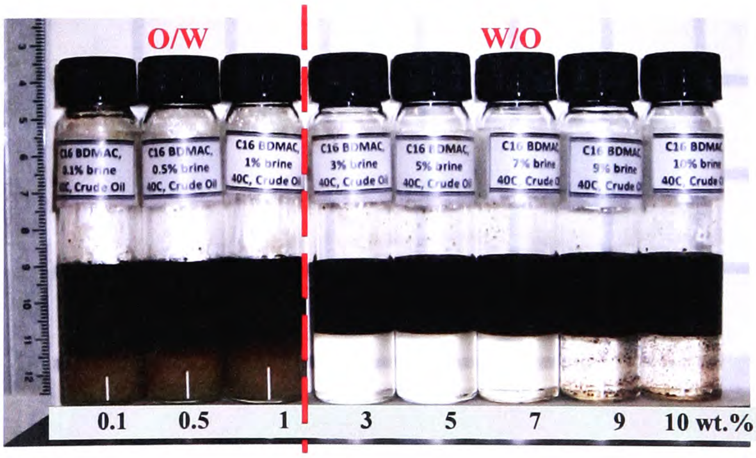

Figure 4-14. Percentage of water and oil phases resolved versus [brine] for emulsions produced from aqueous phase containing 10 mM of C12BDMAC and crude oil (1:1 oil to water volume ratio), homogenised for 2 min at 13000 rpm and stored at 40 °C for 24 h. 50% water or oil resolved indicates complete phase separation.

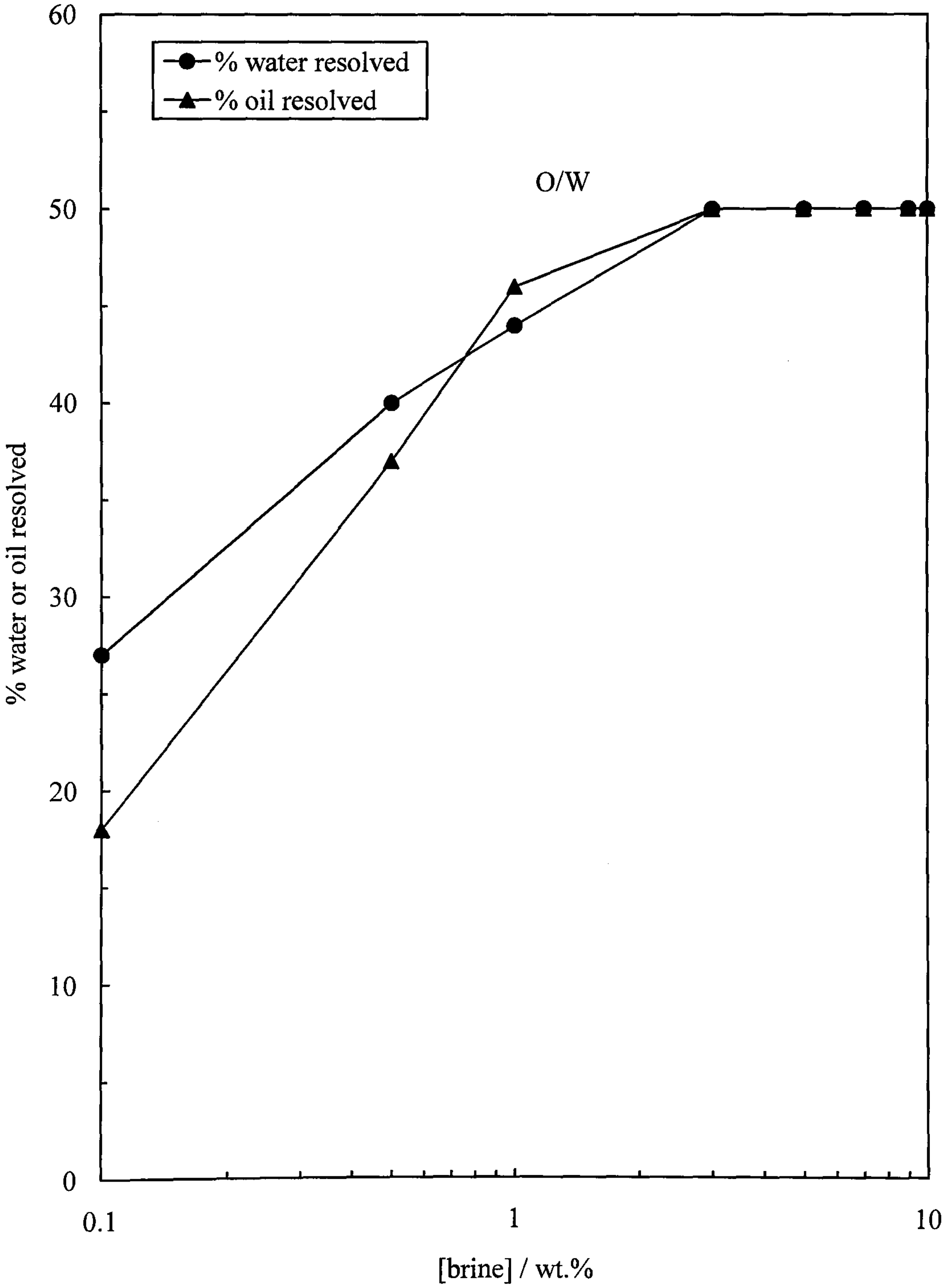

Figure 4-15. Percentage of water and oil phases resolved versus [brine] for emulsions produced from aqueous phase containing 10 mM C16BDMAC and crude oil (1:1 oil to water volume ratio), homogenised for 2 min at 13000 rpm and stored at 40 °C for 24 h. Vertical line indicates the transition from o/w to w/o emulsions which was confirmed using the drop test. 50% water or oil resolved indicates complete phase separation.

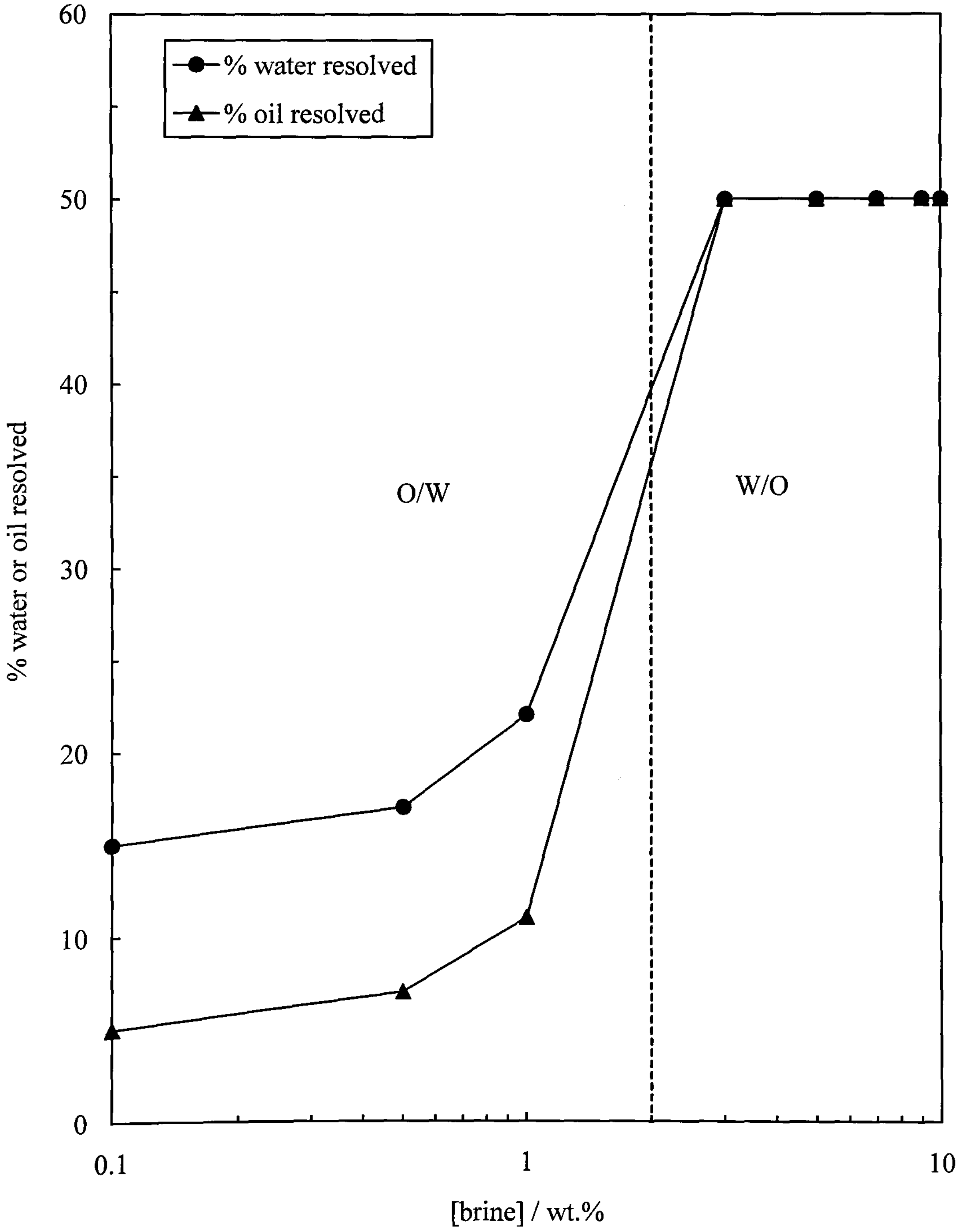

Table 4-1. Type of emulsion produced from aqueous phase containing 10 mM CnBDMAC, [brine] = 0.1-10 wt.% and heptane or toluene or heptol crude oil at 1:1 volume ratio homogenized for 2 min at 13000 rpm and stored for 24 hr at (a) 40 °C and (b) 25 °C.

(a) at 40°C (this work)

System		brine concentration / wt. %							
		0.1	0.5	1	3	5	7	9	10
C12BDMAC	Heptane	o/w	o/w	o/w	o/w	o/w	o/w	o/w	o/w
	Heptol	o/w	o/w	o/w	o/w	o/w	o/w	o/w	o/w
	Toluene	o/w	o/w	o/w	o/w	o/w	o/w	o/w	o/w
	Crude oil	o/w	o/w	o/w	o/w	o/w	o/w	o/w	o/w
C14BDMAC	Heptane	o/w	o/w	o/w	o/w	o/w	o/w	o/w	o/w
	Heptol	o/w	o/w	o/w	o/w	o/w	o/w	o/w	o/w
	Toluene	o/w	o/w	o/w	w/o	w/o	w/o	w/o	w/o
	Crude oil	o/w	o/w	o/w	o/w	w/o	w/o	w/o	w/o
C16BDMAC	Heptane	o/w	o/w	o/w	o/w	o/w	o/w	o/w	o/w
	Heptol	o/w	o/w	o/w	o/w	o/w	o/w	o/w	o/w
	Toluene	o/w	o/w	w/o	w/o	w/o	w/o	w/o	w/o
	Crude oil	o/w	o/w	o/w	w/o	w/o	w/o	w/o	w/o

System		brine concentration / wt. %							
		0.1	0.5	1	3	5	7	9	10
C12BDMAC	Heptane	o/w	o/w	o/w	o/w	o/w	o/w	o/w	o/w
	Heptol	o/w	o/w	o/w	o/w	o/w	o/w	o/w	o/w
	Toluene	o/w	o/w	o/w	o/w	o/w	o/w	o/w	o/w
	Crude oil	o/w	o/w	o/w	o/w	o/w	o/w	o/w	o/w
C14BDMAC	Heptane	o/w	o/w	o/w	o/w	o/w	o/w	o/w	o/w
	Heptol	o/w	o/w	o/w	o/w	o/w	o/w	o/w	o/w
	Toluene	o/w	o/w	o/w	o/w	w/o	w/o	w/o	w/o
	Crude oil	o/w	o/w	o/w	o/w	o/w	w/o	w/o	w/o
C16BDMAC	Heptane	o/w	o/w	o/w	o/w	o/w	o/w	o/w	o/w
	Heptol	o/w	o/w	o/w	o/w	o/w	o/w	o/w	o/w
	Toluene	o/w	o/w	o/w	w/o	w/o	w/o	w/o	w/o
	Crude oil	o/w	o/w	o/w	o/w	w/o	w/o	w/o	w/o

surfactant to determine its partitioning behaviour as a function of brine concentration using 1:1 volume ratio of toluene and water. In all cases, the surfactant was initially present in the aqueous phase. The aim of this partitioning experiment is to investigate the effect of emulsion phase inversion on the availability of C16BDMAC in the aqueous phase.

Table 4-2 shows the concentration and extraction percentage of the C16BDMAC in the aqueous and oil phase after equilibration for 7 days. From the results of these partitioning experiments, we can see that C16BDMAC surfactant molecules were found to partition almost exclusively to the toluene phase at brine concentrations above 1 wt. %. These results are in accordance with those obtained from the emulsification experiments in which emulsions phase inverted into oil-continuous at brine concentrations ≥1 wt. % (Figure 4-7). Beyond this brine concentration, the percentage extracted of C16BDMAC into the oil phase dropped off to about 87 % at brine concentration of 10 wt. %.

At 0.5 wt. % brine concentration, an o/w microemulsion type was formed in the aqueous phase which was confirmed by conductivity measurement. On the other hand, a w/o microemulsion was formed in the oil phase. This situation is shown in Figure 4-16.

Table 4-2. Equilibrium concentrations and extraction percentages of C16BDMAC in aqueous and oil phases for 1:1 toluene/water volume ratio, [brine] = 0-10 wt. % at 40 °C. Initial $[\text{C16BDMAC}]_{\text{aqueous}}$= 10.05 mM.

[brine] / wt.%	$[\text{C16BDMAC}]_{\text{aqueous}}$ / mM	$[\text{C16BDMAC}]_{\text{oil}}$ / mM	% C16BDMAC in water	% C16BDMAC in toluene
No brine	10.03	0.0115	99.85	0.11
0.1	10.02	0.036	99.75	0.36
0.5	Microemulsion (o/w)	0.034	o/w	0.34
1	0.013	Microemulsion (w/o)	0.13	w/o
3	0.011	10.05	0.11	100
5	0.018	10.04	0.18	99.90
7	0.065	9.28	0.64	92.35
9	0.045	8.99	0.44	89.45
10	0.075	8.82	0.74	87.76

Figure 4-16. Appearance of micremulsions produced during the partitioning of C16BDMAC as a function of brine concentration using 1:1 volume ratio of toluene and water at 40 °C. The upper phase is toluene.

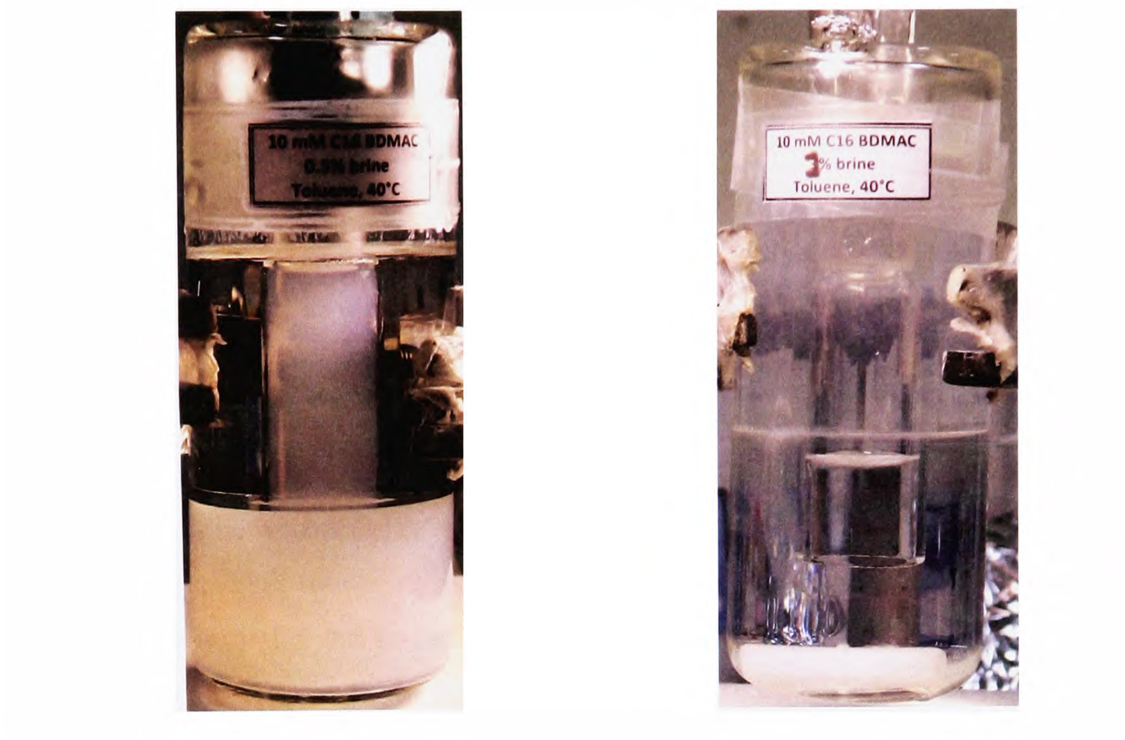

(a) o/w microemulsion in the aqueous phase

(b) w/o microemulsion in toluene

Horsup *et al.* [2], investigated the partitioning behaviour of C12, C14 and C16BDMAC using heptol as the hydrocarbon phase with 10:1 heptol to water volume ratio. The studies were performed in the absence of electrolyte at 25 °C. They reported no change in the aqueous inhibitor concentration after equilibration with heptol for 24 hours. The study was subsequently repeated [9] in the presence of 4.7 wt. % brine. The results showed that at 25 °C in the presence of brine, C12, C14 and C16BDMAC do not partition into the heptol phase.

4.4. DISCUSSION

4.4.1. Relation between emulsion type and equilibrium phase behaviour

Emulsions are defined as thermodynamically-unstable mixtures of two or more immiscible liquids (usually oil and water) where one phase is dispersed in the other as drops [10]. Simple emulsions can be either oil-in-water (o/w) or water-in-oil (w/o). For o/w emulsions, oil drops are dispersed in an aqueous continuous phase and in w/o emulsions water drops are dispersed in an oil-continuous phase. It is frequently observed that in mixtures of equal volumes of water and oil, the type of emulsion formed by the homogenisation of a Winsor I or II system is the same as the equilibrium microemulsion type [11-13]. As mentioned earlier in *Chapter 1*, for a ternary mixture of oil, water and surfactant, which phase separate into a surfactant-rich aqueous phase containing an o/w microemulsion and almost pure oil (Winsor I), the surfactant layer is said to have a positive spontaneous curvature. Under stirring, an o/w emulsion is obtained from a Winsor I system, the continuous phase of which is itself an o/w micromeulsion [13]. For a ternary mixture of oil, water and surfactant which phase separates into an oil phase containing a w/o microemulsion and almost pure water (Winsor II), the surfactant layer is said to have a negative spontaneous curvature. On stirring, a w/o emulsion is obtained, the continuous phase of which is itself a w/o microemulsion [13]. At inversion, the spontaneous curvature is close to zero. A ternary mixture of oil, water and surfactant will separate into three phases: a bicontinuous or liquid crystalline phase (middle phase in Figure 4-17) in equilibrium with oil and water phases (Winsor III). At this stage, both o/w and w/o emulsions are immediately destroyed through coalescence [14].

The results of phase-inversion experiments have shown that emulsions containing a CnBDMAC surfactant and heptane or heptol as the hydrocarbon phase to be water continuous over the entire brine concentration range investigated. The fact that these emulsions do not phase invert indicates that the corresponding microemulsion system will not phase invert under these conditions. In the aqueous phase, the micelles of CnBDMAC have the charged surfactant head groups on the outside with the hydrophobic tail groups in the core of the micelle.

Phase inversion of these emulsions occurs when the curvature of the surfactant monolayer changes from positive to negative as the effective sizes of the head and tail group change (Figure 4-17). As the electrolyte concentration increases, the effective size of the head groups decrease. If the oil phase can penetrate the tail group region, the effective size of the tails will increase. Accordingly, heptol and heptane-containing emulsions stabilized by CnBDMAC surfactants do not phase invert because neither heptane nor heptol penetrate the hydrophobic surfactant tails to a sufficient extent under the temperature and electrolyte concentration employed.

Figure 4-17. Schematic representation of the influence of the relative magnitudes of the cross sectional areas of surfactant head and tail groups on the preferred monolayer curvature [9].

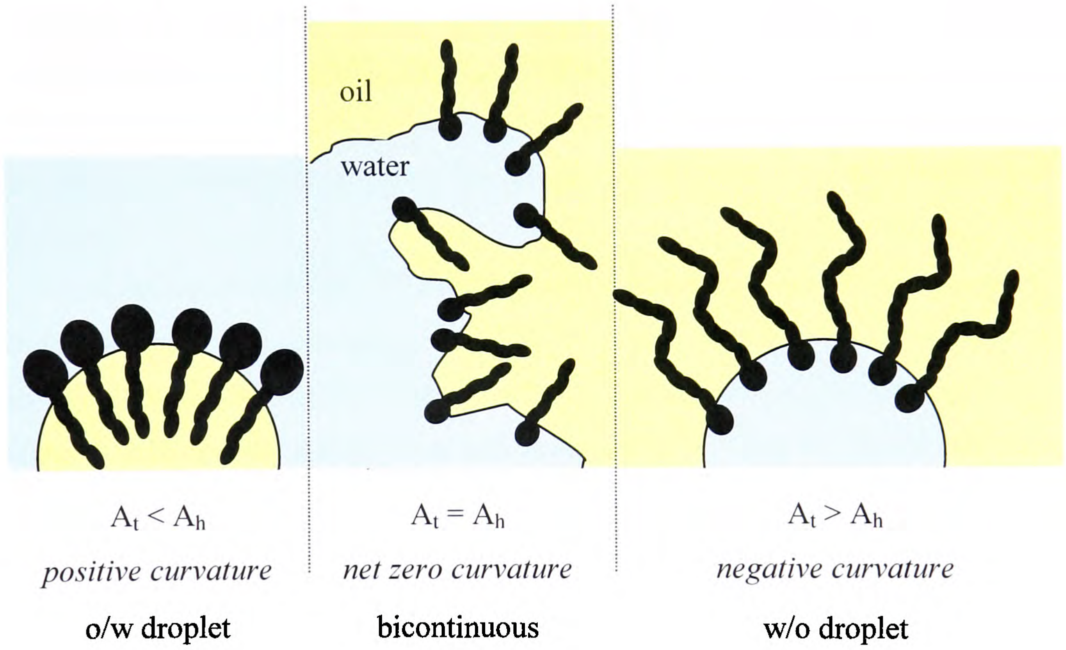

Horsup *et al.* [2] have investigated the partitioning behaviour of the C14BDMAC corrosion inhibitor into heptol with 10:1 volume ratio (heptol to water). The studies were performed in the absence of electrolyte at two different temperatures of 25 and 40 °C. The concentration of the inhibitor in the aqueous phase was found to be almost unchanged after equilibration with heptol. From these results, it is evident, therefore, that neither the monomers nor the micelles of C14BDMAC surfactant partition into the hydrocarbon phase in the absence of electrolyte at 25 and 40 °C. It appears therefore, that under these conditions, a Winsor I system is formed in which the aggregates, oil in water microemulsions, are formed in the aqueous phase at concentrations above the cmc. The study was subsequently repeated [2] in the presence of 4.7 wt. % brine aqueous concentration with 10:1 heptol to water volume ratio at 40 °C. The results showed that C14BDMAC does not partition to the heptol phase. As before, a Winsor I system is produced with microemulsions forming in the brine phase at concentrations above the cmc. This result is in accordance with our result that C14BDMAC-heptol emulsions are of the o/w type at brine concentrations between 0.1 and 10 wt.% at 40 °C.

For a corrosion inhibitor to protect the metal surface effectively, it needs to be present in the aqueous phase in an appropriate amount. The formation of an emulsion and the partitioning of surfactant molecules into the hydrocarbon phase reduce markedly the concentration of surfactant monomers available for adsorption onto steel surfaces. Additionally, the type and stability of the emulsions produced, stabilized by these surfactant molecules, influences the adsorption extent of these molecules onto steel surfaces, which has an adverse effect on it corrosion inhibition performance.

Emulsions containing C12BDMAC and toluene or crude oil remain water continuous. As a result, the corresponding microemulsion systems are expected to be water continuous (Winsor I) systems. At low concentrations of electrolyte, the headgroup area A_h, is greater than tail group area A_t, due to the electrostatic repulsion between the head groups. As the salt concentration increases, A_h decreases. The absence of phase inversion shows that the curvature of the surfactant monolayer remains positive at higher brine concentrations despite the decrease in A_h. This shows that the tail groups of C12BDMAC are not penetrated and swollen sufficiently by these oils.

The phase behaviour of C14BDMAC and C16BDMAC shows a greater dependence upon the oil type. As mentioned earlier, all emulsions prepared with heptane or heptol and C14 or C16BDMAC were of the o/w emulsion type, indicating poor penetration of the tail groups by the aliphatic hydrocarbon. On the contrary, phase inversion of the emulsions stabilized by C14 or C16BDMAC was observed in systems containing either toluene or crude oil as the hydrocarbon phase.

Toluene is an aromatic hydrocarbon and crude oil is a complex mixture of aromatic and aliphatic hydrocarbons. The transition from Winsor I to Winsor II systems is induced by the change in the preferred curvature of the surfactant monolayer as the electrolyte concentration increases. These results show that the tail groups of C14 and C16BDMAC can be penetrated more by the presence of aromatic hydrocarbons than that of C12BDMAC.

The equilibrium-partitioning experiments have shown that C16BDMAC partitions into the toluene phase at brine concentrations ≥ 1 wt.% at 40 °C. At concentrations above the cmc, C16BDMAC forms microemulsion aggregates which partition exclusively into the toluene phase. These aggregates solubilise water upon partitioning to the toluene phase, which leads to the formation of a water-in-oil microemulsion type (Winsor II phase). This indicates that the effective area of the tail group at the oil-water interface exceeds that of the head group. This is thought to be due to the swelling of the tail region by toluene molecules and the reduction of the head group area by salt. This in accordance with the result obtained from the emulsification experiments in which emulsion containing toluene and C16BDMAC surfactant has been phase inverted into a water-in-oil emulsion type at about 1 wt.% brine salt concentration.

Emulsions prepared with heptol, which is a 7:3 volume ratio mixture of heptane and toluene, and C16BDMAC remain water continuous as the concentration of electrolyte increases. Phase inversion was not observed in emulsions containing heptane, but was observed with toluene. This suggests that the higher volume fraction of heptane in heptol mixture prevents the swelling of surfactant tail groups, which results in a positive curvature of the surfactant monolayer at low and high brine concentrations. Binks *et al.* [15] have studied the equilibrium phase behaviour of systems containing the ionic surfactant AOT (sodium diethylhexysulphosuccinate) and various alkanes ranging from heptane to tetradecane as a function of salt concentration at 20 °C. They found that the increase in the chain length of the alkane results in an increase in the salt concentration required for phase inversion to occur and an increase in the magnitude of the minimum tension.

Emulsions containing C14 or C16BDMAC inhibitors and Prudhoe Bay crude oil were found to exhibit a phase inversion at 3.5 and 2 wt.% brine concentrations, respectively. Despite the fact that both heptol and crude oil are mixtures of aliphatic and aromatic oils, the phase inversion was only seen in the crude oil system. This may be attributed to the capacity of crude oil to swell the hydrocarbon chain of C14 and C16BDMAC more effectively than heptane or heptol due to the presence of short chain alkanes in the crude oil. This capacity may be interpreted in terms of the polarity of the employed oil. The oil polarity can affect the formation and the type of emulsion. The oil polarity values depend on the heteroatomic compounds, which are concentrated in the heaviest fractions of the oils [16]. It increases with nitrogen, sulfur, and asphaltene contents as well as the specific gravity and acid number of the oil. High oil polarity always encourages the formation of very stable water-in-oil emulsions [17].

The ability of an oil to penetrate the hydrophobic surfactant tails in a micelle depends several factors including molar volume, polarity, polarisability and chain length of the oil with respect to the surfactant tail [18]. In general, a decrease in the penetration of the oil occurs when the alkyl chain length of a homologues series is increased [10]. Unsaturated compounds penetrate generally more their saturated counterparts. Branching of the hydrocarbon chain of the oil has little effect, but increased penetration is often noted following cyclisation [10-12].

If a hydrocarbon molecule is significantly longer than the surfactant tail, it may not be able to swell the surfactant tail completely and its end may protrude into the aqueous phase. The greater the length of the hydrocarbon molecule, relative to the surfactant tail, the greater the increase in hydrocarbon exposed to a more polar environment and, therefore, the more energetically unfavourable swelling would be [19].

Mukherjee *et. al.* [20] take explicit account of the penetration of alkane molecules into the tail region of surfactant in spherically curved aggregates. It is concluded that as a result of the entropy of mixing, the shorter alkanes penetrate into surfactant layers more effectively than do longer chain homologues. Mixing of oil with the chain region of a surfactant monolayer is favoured on entropic grounds for short alkanes of low molar volume, and this enhanced penetration compared with that for long chain alkanes manifests itself in the emulsion properties [21].

Thus there is a balance between the factors which favour the swelling of surfactant hydrocarbon tails, e.g. entropy of mixing and those which oppose this process, e.g. the protrusion of part of the hydrocarbon molecules into a more hydrophilic region or the loss of configurational entropy associated with the restricted volume available to larger hydrocarbons, which determines the penetration degree [22].

The larger penetration capacity of toluene and crude oil compared with the saturated alkane is interesting and may be a result of the greater polarisability of the benzene ring (10.70 nm^3 [23]) promoting further penetration towards the head group region of the monolayer.

These results show that environmental factors such as salt concentration, temperature and oil composition affect the phase behaviour of corrosion inhibitors in systems containing oil and water phases. These factors can differ greatly between oil fields. Slight differences in these factors can change the preferred phase in which the majority of the corrosion inhibitor will exist. If the corrosion inhibitor prefers the oil phase, it will not be available to act as a corrosion inhibitor in the aqueous phase, where corrosion occurs most rapidly when in contact with the steel surface.

4.4.2. Effect of the presence of oil on the corrosion inhibitor efficiency

Results from the emulsion phase inversion experiments have shown that emulsions 10 mM C16BDMAC and toluene invert into water-in-oil at a brine concentration of about 1 wt.% at 40 °C. Moreover, we have found that the aggregated C16BDMAC molecules partition from water to toluene at nearly the same brine concentration. Partitioning of these water-soluble surfactant molecules involves the migration of surfactant molecules from water (where corrosion occurs most rapidly) to the oil phase. Therefore, the bubble test technique was employed to investigate the effect of corrosion inhibitors partitioning into the oil phase on their inhibition efficiency. All experiments were carried out in a mixture of 4.7 wt.% brine solution and toluene under CO_2 atmosphere at 40 °C. Under these experimental conditions, C16BDMAC molecules are expected to partition into the oil phase and upon emulsification a water-in-oil emulsion type would be obtained.

In total, two bubble test experiments were conducted with 0, 20 and 50 % (v/v) toluene at 40 °C, whilst the two phases were stirred gently without mixing. The mild steel electrode was located in the aqueous phase of the mixture and was left to corrode in the absence of the inhibitor until a steady state was reached. Figure 4-18 shows the corrosion rate versus time for the C1018 mild steel with the addition of 0.5 ppm (1.13×10^{-3} mM) C16BDMAC to the aqueous phase.

The corrosion rate during the pre-corrosion was about 2.5 mm y^{-1} and quickly decreases to approximately 0.23 mm y^{-1} on the addition of 0.5 ppm C16BDMAC after about 17 hr in the absence of added toluene. This corresponds to a protection efficiency of about 91 %.

Figure 4-18. Corrosion rate vs. time for C1018 steel in 4.7 wt.% brine in the presence of CO_2 at 40 °C with 0.5 ppm (1.13×10^{-3} mM) C16BDMAC as a function of toluene (v/v) percent, determined by bubble test. The vertical dashed line refers to the time at which the inhibitor was injected into the system.

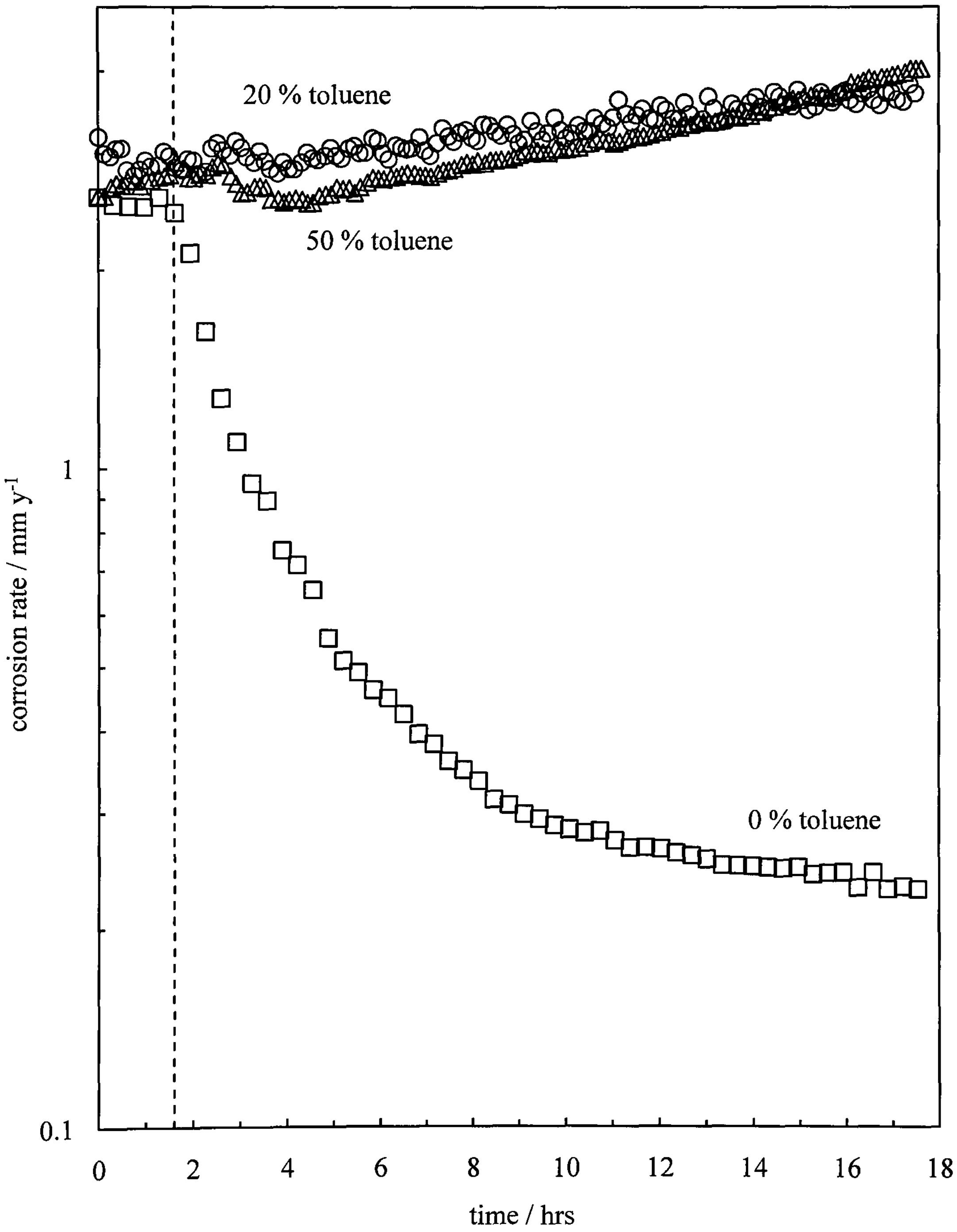

On the other hand, the presence of 20 and 50 % (v/v) toluene increases the corrosion rate progressively to values of about 3.82 and 3.95 mm y^{-1}, respectively after 17 hr. This indicates that the presence of toluene adversely affects the performance and efficiency of the corrosion inhibitor.

Additionally, the effect of toluene presence on the corrosion rate of C1018 mild steel at a higher C16BDMAC surfactant concentration of 2.5 ppm (5.63×10^{-3} mM) under CO_2 at 40 °C has been studied. Figure 4-19 shows that the addition of 2.5 ppm C16BDMAC results in the reduction of the corrosion rate from about 2.6 to 0.18 mm y^{-1} after about 17 hr in the absence of added toluene. This corresponds to a protection efficiency of about 93 %. The corrosion rates of C1018 mild steel in the presence of 20 and 50 % (v/v) were about 1.2 and 1.7 mm y^{-1} after about 17 hr. The latter corrosion rates correspond to protection efficiencies of about 54 and 27 %, respectively. These results indicate that the presence of toluene results in a marked drop in the protection efficiency of the employed C16BDMAC surfactant under the employed experimental conditions. The aforementioned results are in accordance with the observation of the emulsion phase inversion and the partitioning experiments conducted earlier in section 4.2.3 and 4.3. The cmc of C16BDMAC in 4.7 wt.% brine solution was found to be 1×10^{-3} mM at 40 °C. Accordingly, under the employed C16BDMAC surfactant concentrations of 0.5 and 2.5 ppm, the surfactant molecules are in the aggregated form.

Based on the phase inversion and partitioning experiments, the C16BDMAC aggregates will partition extensively into the toluene phase at the employed brine concentrations and temperature. This in turn results in a marked decrease in surfactant concentration in the aqueous phase and drop off the protection efficiency of the employed C16BDMAC inhibitor.

Hicks [9] has used the bubble test technique to investigate whether partitioning of the corrosion inhibitor micelles into the oil phase at high salt concentrations affects the corrosion inhibition efficiency in the aqueous phase. All experiments were carried out in brine solutions containing H_2S in the presence of C12BDMAC and C16BDMAC. The corrosion rate of C1018 steel electrodes was measured in the relevant aqueous solution in the presence of surfactant for 24 hr before adding an equal volume of toluene on top of the aqueous solution. In the first bubble test, the corrosion rate of C1018 steel was measured at 40 °C in 10 wt. % brine solution containing 10 mM C12BDMAC under H_2S conditions with the

Figure 4-19. Corrosion rate vs. time for C1018 steel in 4.7 wt.% brine in the presence of CO_2 conditions at 40 °C with 2.5 ppm (5.63×10^{-3} mM) C16BDMAC as a function of toluene (v/v), determined by bubble test. The vertical dashed line refers to the time at which the inhibitor was injected into the system.

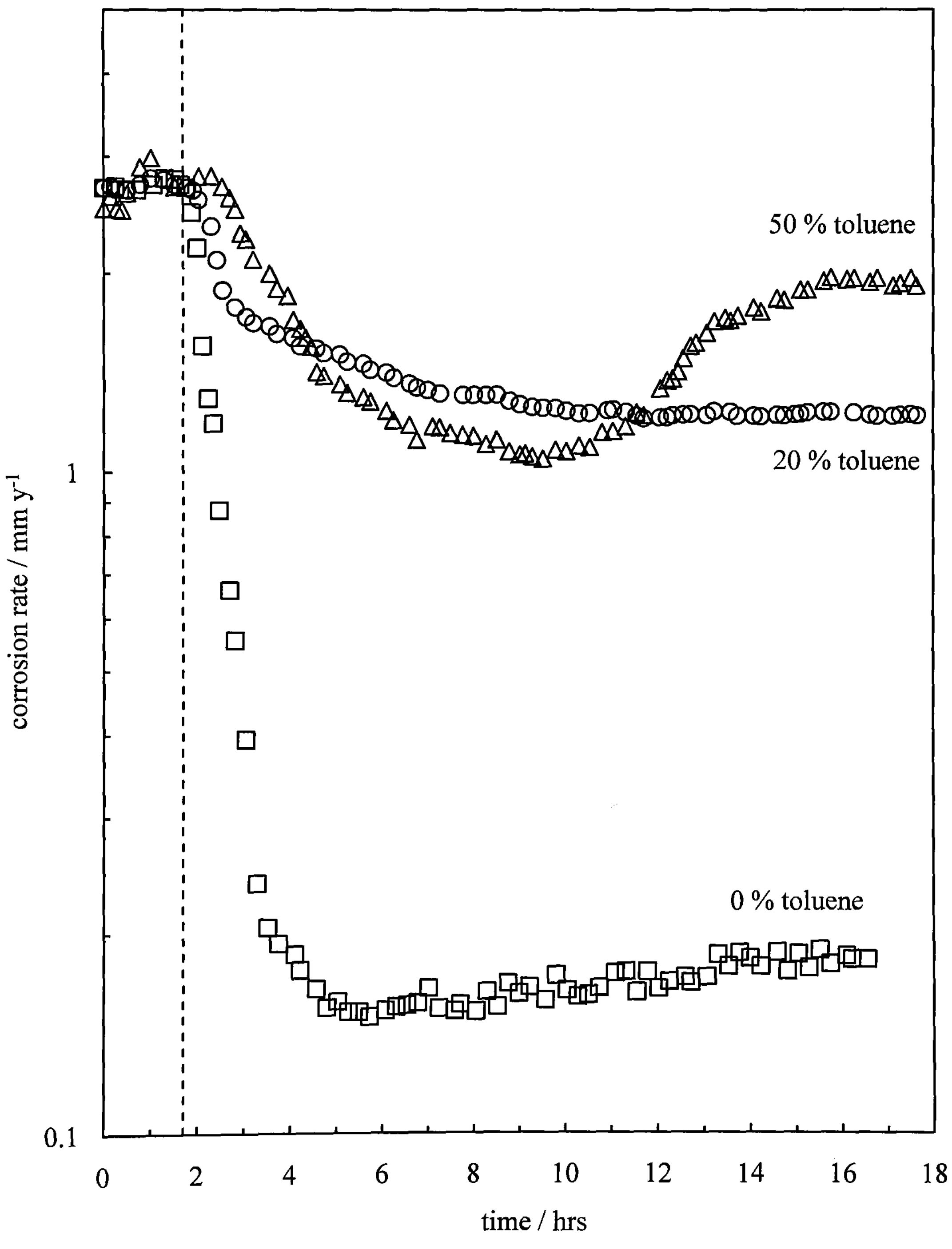

addition of an equal volume layer of toluene after 24 hr. No change in the protection efficiencies of C12BDMAC surfactant was observed in the absence and presence of toluene. The experiment was repeated by replacing the short chain C12BDMAC with the long chain C16BDMAC. The system is expected to phase invert to a water-in-oil microemulsion under these conditions due to the change in the preferred curvature of the surfactant monolayer caused by the high electrolyte concentration and penetration of the hydrocarbon tails by toluene. However, the corrosion rate in the presence of the toluene phase was slightly lower than the corrosion rate in the absence of toluene. The author reported two possible interpretations for this observation. The first is that the protection efficiency is independent of the aggregated surfactant concentration, and therefore, it does not participate in the corrosion inhibition process. The alternative interpretation is that enough monomeric surfactant molecules remain in the aqueous phase after partitioning of aggregates into the oil phase to provide good corrosion inhibition.

In conclusion, it seems that the presence of toluene does not affect the efficiency of C16BDMAC inhibitor at low concentrations under the employed experimental conditions. As mentioned earlier, the inhibition efficiency is dependent on the concentration of surfactant monomer in the aqueous phase. Accordingly, under the conditions where surfactant molecules partition exclusively into the oil phase is expected to happen, the concentration of the remaining surfactant in the aqueous phase will be dependent on the partitioning coefficients and the initial total surfactant concentration. Accordingly, at low initial surfactant concentration, one would expect that the remaining surfactant concentration in the aqueous phase to be extremely low. This in turn would result in an increase in the corrosion rate as there are not enough surfactant monomers in the aqueous phase. On the contrary, at higher initial surfactant concentrations, the remaining aqueous surfactant concentrations will be much higher as the portioning coefficient is independent of the initial surfactant concentration. Therefore, the partitioning of surfactants molecules into the oil phase will not significantly affect the corrosion rate relative to systems with having no oil.

4.5. SUMMARY AND CONCLUSION

The impact of a number of key production variables on the fate of corrosion inhibitors in a multiphase system have been investigated in this chapter. These variables are the ability of corrosion inhibitors to stabilize both oil-in-water and water-in-oil emulsions and the phase inversion of the emulsions as production variables change and the partitioning behaviour of corrosion inhibitors between an aqueous brine phase and an oil phase as a function of brine salinity. The key and new findings within this study are summarized below.

I. For alkylbenzyldimethylammonium chlorides, emulsions containing aqueous surfactant and heptane or heptol do not invert and remain water-continuous while emulsions containing the long chain C14 or C16BDMAC and toluene or crude oil inverted to oil-continuous.

II. The Oilfield corrosion inhibitor molecules will partition between oil and water phases to varying extents given by their partition coefficients. As the concentration of the inhibitor is increased, aggregates (micelles or microemulsions) will form in one of the phases. The partitioning and phase behaviour of a corrosion inhibitor will depend upon the inhibitor's effective geometry in the system.

III. Production variables such as temperature, brine salinity, oil composition and the presence of other production chemicals can all impact an inhibitor's effective head and tail group areas which in turn can have a significant impact on phase behaviour and hence *in-situ inhibitor availability.*

IV. Partitioning experiments indicate that C16BDMAC partitions almost exclusively to the toluene phase at brine concentrations above 1 wt.%. These results are in accordance with those obtained from the emulsification experiments. At low salinity, C16BDMAC was noticed to favour aqueous solubility and the formation of the corresponding Winsor I system where the preferred monolayer curvature was positive. At higher salinities however, the inhibitor partitions almost exclusively into the oil with the formation of the corresponding Winsor II system where the preferred monolayer curvature is negative. Since the preferred curvature of an inhibitor monolayer at an oil-water interface changes with system conditions, the type of emulsion that the inhibitor stabilizes can also change.

V. Corrosion rate measurements conducted in the presence of oil phases show that partitioning of corrosion inhibitor aggregates from water to oil lead to an increase in the corrosion rate of steel in contact with the aqueous phase (relative to systems with having no oil) at the used experimental conditions.

4.6. REFERENCES

1. E. Gulbrandsen and J. Kvarekval, *Proceedings of NACE CORROSION 2004*, Paper No. 04365, NACE International, Houston (2004).
2. D. I. Horsup, J. C. Clark, B.P. Binks, P. D. I. Fletcher and J. T. Hicks, *Corrosion* **66**, 036001 (2010).
3. M. Knag, J. Sjblom and E. Gulbrandsen, *J. Dispersion Sci. Technol.*, **27**, 65 (2006).
4. H. M. Princen, *J. Colloid Interface Sci.*, **71**, 55 (1979).
5. H. Kunieda, C. Solans, N. Shida and J. L. Parra, *Colloid Surface,* **24,** 225 (1987).
6. C., Solans, J. G. Dominguez, J. L. Parra, J. Heuser and S. E. Friberg, *Colloid. Polym. Sci.*, **266**, 570 (1988).
7. D. Khatua and J. Dey, *Langmuir*, **21**, 109 (2005).
8. H. Kunieda, Y. Fukui, H.Uchiyama and C.Solans, *Langmuir*, **12,** 2136 (1996).
9. J. T. Hicks, *Surfactants aspects of corrosion inhibitors*, Ph. D. thesis, Hull University (2007).
10. B.P. Binks, in *Modern Aspects of Emulsion Science*, ed. B.P. Binks, Royal Society of Chemistry, Cambridge (1998).
11. R. Aveyard, B. P. Binks and P. D. I. Fletcher, in *The structure, dynamics and equilibrium properties of colloidal systems*, NATO ASI Series C, D. M. Bloor and E. Wyn-Jones, eds., Kluwer Academic Publishers, Dordrecht (1990).
12. H. Kunieda and K. Shinoda, *J. Colloid Interface Sci.*, **107**, 107 (1985).
13. B. P. Binks, J. Dong and N. Rebolj, *PCCP*, **1**, 2335 (1999).
14. F. Leal-Calderon, J. Bibette and V. Schmitt, in *Emulsion Science*, Springer New York (2007).
15. B. P. Binks H. Kellay and J. Meunier, *Europhys. Lett.*, **16**, 53 (1991).
16. X. Yang, H. Hamza and J. Czarnecki, *Energy Fuels*, **18**, 770 (2004).
17. B. D. Batts and A. Z. Fathoni, *Energy Fuels*, **5**, 2 (1991).
18. A. T. Florence and D. Attwood, *Physicochemical Principles of Pharmacy*, Macmillan, London (2005).
19. R. J. Stokes and D. F. Evans, *Fundamentals of Interfacial Engineering*; Wiely-VCH, Inc., New York (1997).

20. S. Mukherjee, C. A. Miller and T. Fort, *J. Colloid Interface Sci.*, **91**, 223 (1983).

21. R. Aveyard, B. P. Binks, S. Clark and J. Mead, *J. Chem. Soc., Faraday Trans.*, **82**, 125 (1986).

22. J. Weiss, J. N. Coupland, D. Brathwaite and D. McClements, *Colloids Surf. A*, **121**, 53 (1997).

23. D. Lide, *CRC Handbook of Chemistry and Physics*, CRC Press, Boca Raton (2007).

CHAPTER 5

Chapter 5

OPTIMIZATION AND APPLICATION OF THE QUARTZ CRYSTAL MICROBALANCE FOR STUDYING THE ADSORPTION OF ALKYLBENZYLDIMETHYLAMMONIUM CHLORIDES AT THE STEEL-WATER INTERFACE

5.1. INTRODUCTION

Studying the adsorption behaviour of surfactant corrosion inhibitors at solid-liquid interfaces provides important information about their action mechanism, which in turn helps in improving their efficiency. The adsorption of a corrosion inhibitor at a metal-liquid interface can be represented simply as a substitution process between the surfactant molecules in the aqueous solution $CI_{(sol)}$ and the water molecules on the metallic surface $H_2O_{(ads)}$ according to the following equation [1]:

$$CI_{(sol)} + x\,H_2O_{(ads)} \longrightarrow CI_{(ads)} + x\,H_2O_{(sol)} \qquad (5\text{-}1)$$

where $CI_{(sol)}$ and $CI_{(ads)}$ are the corrosion inhibitor in the aqueous solution and those adsorbed on the metallic surface, respectively, $H_2O_{(ads)}$ is the water molecules adsorbed on the metallic surface, x is the size ratio representing the number of water molecules replaced by one mole of surfactant.

The Quartz Crystal Microbalance (QCM) technique is currently experiencing rapid growth in the real-time monitoring of surfactants and macromolecules adsorption at the solid-liquid interface. The research work in the current chapter is divided into two main parts. In the first part, the effects of surfactant chain length, temperature and salinity on the adsorption behaviour of CnBDMAC surfactants onto stainless steel-coated crystals have been investigated using the QCM. Stainless steel was chosen as a model surface instead of the mild steel as the latter is more likely to corrode easily under the employed experimental conditions.

The second part investigates the applicability and optimization of the QCM for the measurement of *in-situ* adsorption of CnBDMAC surfactants from aqueous solution onto stainless steel coated crystals. The optimization process aims at finding the appropriate experimental setup and procedures for carrying out the adsorption measurements. Additionally, the treatment and analysis of the experimental data are discussed in this part.

5.2. ADSORPTION BEHAVIOUR OF CnBDMAC AT THE STEEL-WATER INTERFACE USING THE QCM

In this section, the usage and application of the QCM technique for investigating the adsorption behaviour of CnBDMAC surfactant molecules onto a stainless steel solid surface is discussed. In is worth mentioning here, that these measurements have been carried prior to the optimization experiments presented in section 5.3. The results that emerged from the studies described in this section were the motivation to study the different factor affecting the measured frequency shifts and how it could be optimized. Accordingly, all the results to be presented in this section will be used for qualitative purposes only. All the adsorption measurements have been carried out using the *Stepwise Protocol*. The frequency shift of the third overtone Δf_3, was used for the determination of the amounts of adsorbed surfactant. The *Stepwise Protocol* and the frequency shift of the third overtone were used as several researchers have used them for investigating similar systems [2-5]. The corresponding mass change Δm, has been simply calculated using the Sauerbrey equation without any further treatment or correction. Accordingly, the adsorption isotherms presented in this section provide a *qualitative* measure of the adsorption behaviour of these surfactant molecules onto the stainless steel solid surfaces.

The adsorption behaviour of CnBDMAC surfactant molecules has been studied as a function of the surfactant chain length, temperature and electrolyte concentration.

5.2.1. Effect of surfactant chain length

The adsorption behaviour of alkylbenzyldimethylammonium chloride corrosion inhibitors C10, C12, C14 and C16BDMAC onto a stainless steel-coated crystal from aqueous solution was investigated at 40 °C. Figure 5-1 shows the change in the frequency during the adsorption of C16BDMAC from aqueous solution onto stainless steel-coated crystals as a function of time. The arrows shown in the figure indicate the injection time for each surfactant concentration. The numbers above the arrows refer to the normalized surfactant concentration with respect to the cmc. As can be seen from the figure, the adsorption of surfactant molecules results in a noticeable decrease in the frequency of the oscillating stainless steel-coated crystal. The magnitude of this shift increases with increasing surfactant concentration up to the cmc. Upon reaching the cmc, the shift in the frequency reaches a plateau and becomes apparently independent of the surfactant concentration.

The desorption process of surfactant from stainless steel-coated crystals upon flushing with water was not complete (the recorded frequency shift does not return to the zero baseline before surfactant injection as shown in Figure 5-1). This could be misinterpreted as an irreversible adsorption process, which has not been reported before for such systems. This may be attributed to the deviation caused by the device itself due to working for a long time. The manufacturer reports an expected deviation of about 1.5 Hz per hour.

The corresponding changes in the dissipation energy during the adsorption of C16BDMAC are shown in Figure 5-2. Noticeably, the dissipation change seems to be apparently independent of the surfactant concentration up to a value of about 0.2 times the cmc. The dissipation changes do not exceed a value of about 1×10^{-6} up to this concentration.

Figure 5-1. Change in the frequency as a function of time during the adsorption of C16BDMAC onto stainless steel-coated crystal at 40 °C, pH = 6.5-7, n = 3. The arrows indicate the injection time for each concentration. Numbers shown refer to the concentration normalized with respect to the cmc (0.5 mM).

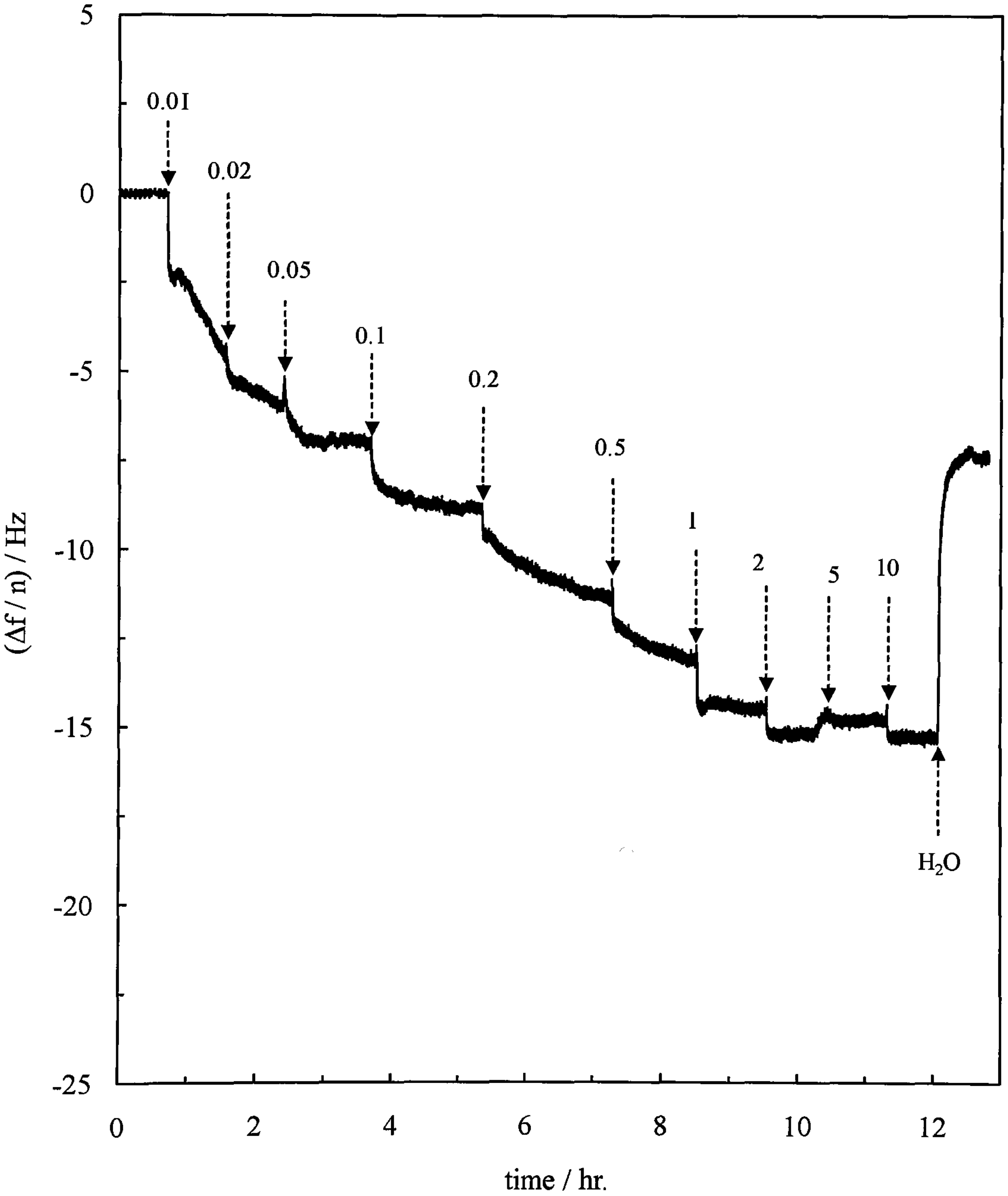

Figure 5-2. Change in the dissipation as a function of time during the adsorption of C16BDMAC onto stainless steel-coated crystal at 40 °C, n = 3. The arrows indicate the injection time for each concentration. Numbers shown refer to the concentration normalized with respect to the cmc (0.5 mM).

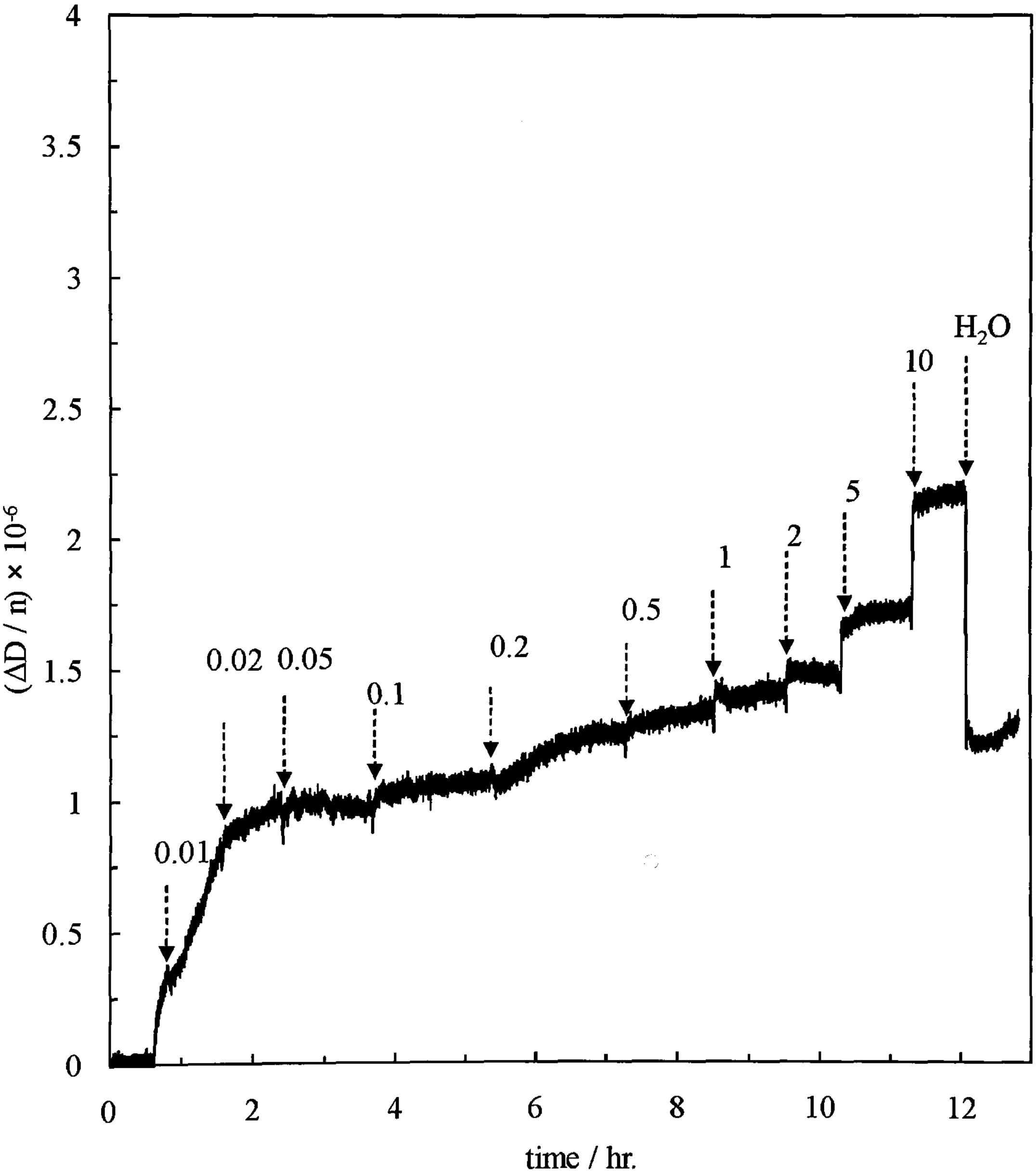

The increase in the surfactant concentration beyond 0.2 times the cmc results in a gradual increase in ΔD. For example, the dissipation change at a surfactant concentration of 5 times the cmc is about 1.5×10^{-6}. The corresponding change in the adsorbed surfactant mass Δm as a function of time is shown in Figure 5-3 for different C16BDMAC concentrations. As mentioned earlier, the change in mass was calculated from the measured Δf in the third overtone by applying the Sauerbrey equation without any corrections. In order to construct the adsorption isotherm, the adsorbed amount per area (in molecules nm^{-2}) was calculated using equation (5-12).

Figure 5-4 shows the adsorption isotherms for C10, C12, C14 and C16BDMAC surfactants onto stainless steel-coated crystals at 40 °C from aqueous solution. Two main observations are noticeable in these isotherms. Firstly, they give rise to a classical Langmuir type isotherm, with a maximum near to the cmc for C10, C12 and C14BDMAC. Isotherms with a maximum have been reported widely in the literature [2-4] but the origin of this behaviour appears to differ from one system to another. In our study, this behaviour has been attributed to the presence of an impurity in the surfactant. This impurity is known to be responsible for the appearance of a minimum in the surface tension isotherm near the cmc [5, 6]. As reported earlier in section 3.2, a significant minimum in the surface tension isotherms was observed for C10, C12BDMAC and to a lesser extent for C14 and C16BDMAC. This implies that the aqueous solution of CnBDMAC surfactant samples contains some surface-active impurities.

For all the alkylbenzyldimethylammonium chlorides studied, the minimum in the surface tension isotherm appeared at a surfactant concentration close to the cmc as shown in Figure 5-4. The minimum in the surface tension isotherm appears at nearly the same concentration at which the maximum appears in the adsorption isotherm. For C12BDMAC, the minimum in surface tension appeared at a surfactant concentration around 7 mM and the corresponding maximum in adsorption emerged around 8 mM.

The adsorption behaviour of the purified C12BDMAC from aqueous solution onto stainless coated-crystals has been investigated using the QCM. The adsorption isotherms for purified and unpurified C12BDMAC are given in Figure 5-5. No maximum was observed in the adsorption isotherm for the purified C12BDMAC. This proves that the appearance of the maximum in the adsorption isotherm is due to the presence of impurities in the surfactant solution.

Figure 5-3. Change in the mass adsorbed as a function of time during the adsorption of C16BDMAC onto stainless steel-coated crystal at 40 °C, n = 3. The arrows indicate the injection time for each concentration. Numbers shown refer to the concentration normalized with respect to the cmc (0.5 mM). Mass changes are calculated using the Sauerbrey equation.

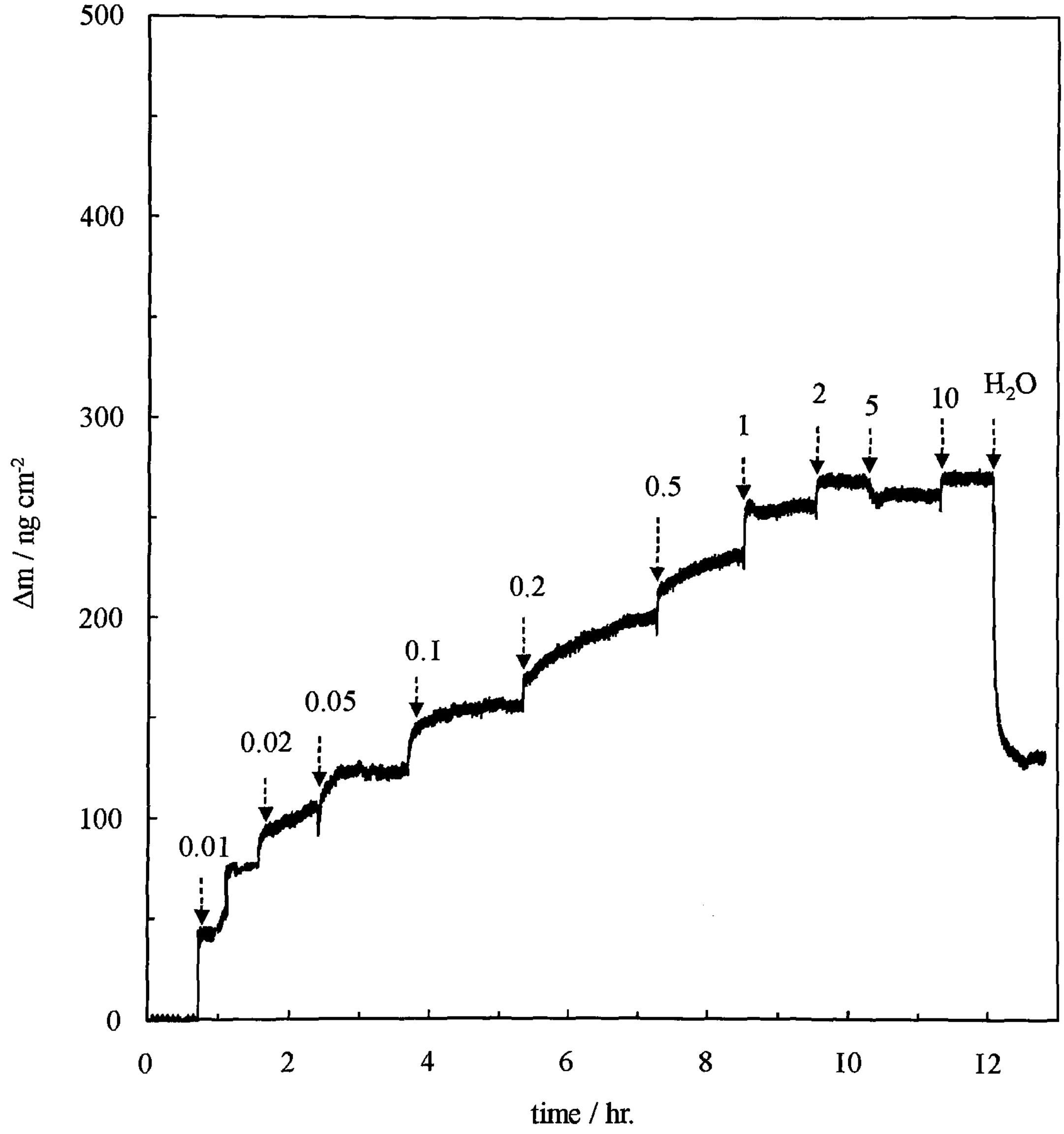

Figure 5-4. Adsorption isotherms of alkylbenzyldimethylammonium chlorides surfactants (CnBDMAC) from water onto stainless steel-coated crystals using the QCM at 40 °C, pH = 6.5-7 and n = 3. The vertical lines refer to the cmc.

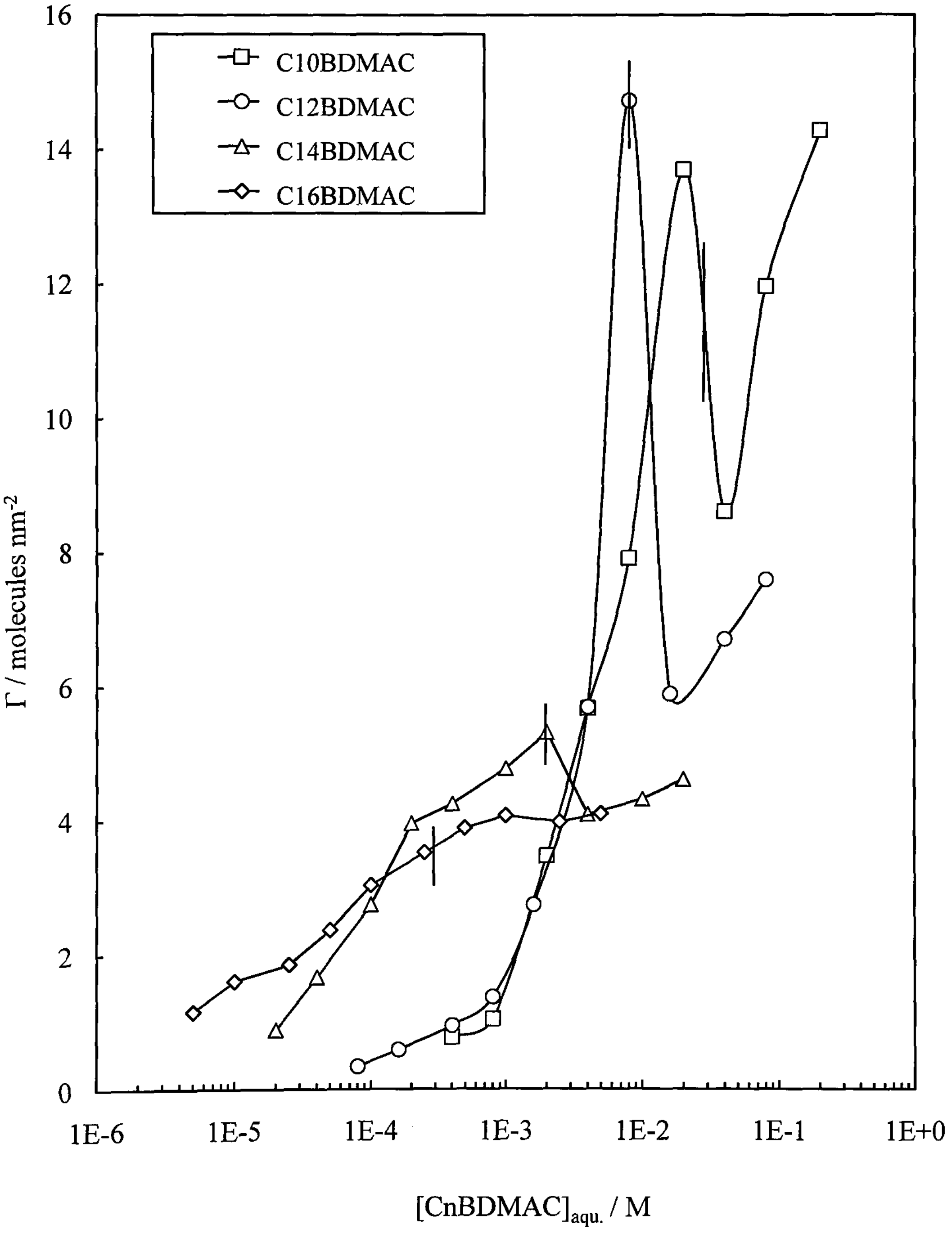

Figure 5-5. Adsorption isotherms for the purified C12BDMAC surfactant from water onto stainless steel-coated crystals using the QCM at 40 °C, compared to the unpurified one, pH = 6.5-7 and n = 3.

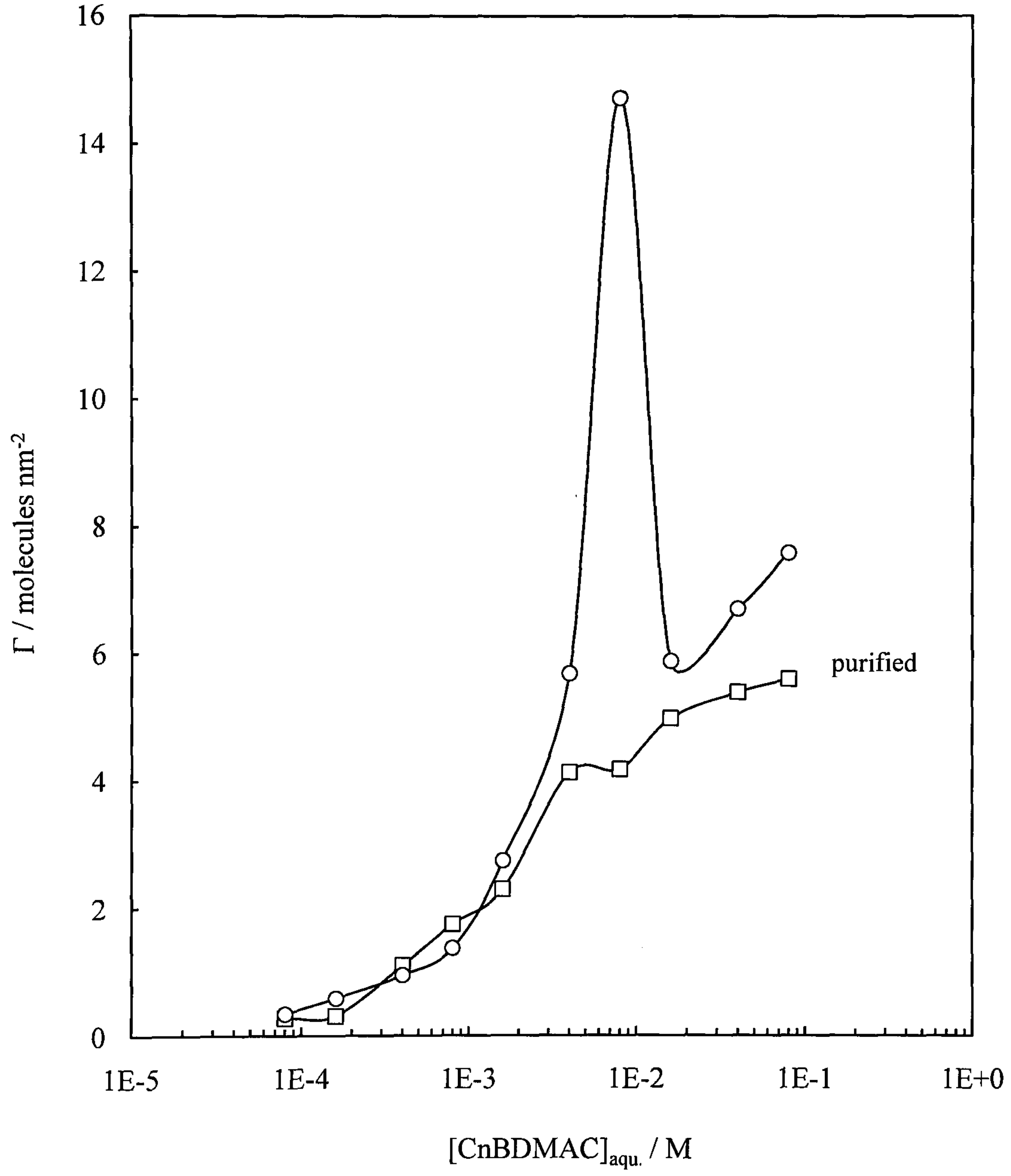

The second observation in the adsorption isotherms shown in Figure 5-4, is that these adsorption isotherms give rise to relatively high adsorption values. The short chains C10 and C12BDMAC give rise to the highest amounts of adsorption compared to the long chains C14 and C16BDMAC. This could be attributed to the deviation from the Sauerbrey equation as a direct consequence of the formation of a soft viscoelastic surfactant film adsorbed on the surface. The formation of such elastic adsorbed films significantly decreases the resonance frequency, which in turn results in an overestimation of the calculated adsorbed mass.

Despite the overestimated adsorption values, we have fitted these adsorption isotherms to the simple Langmuir adsorption model, which helps in providing a general idea about the adsorption parameters including the maximum amount adsorbed and the area per molecule at the solid-water interface.

Figure 5-6 shows the fitted isotherms for the adsorption of C10, C12, C14 and C16BDMAC onto stainless steel-coated crystals at 40 °C. The amounts adsorbed shown in the isotherms are the average of two measurements determined by using two different stainless steel-coated crystals under the same experimental conditions. The error bars represent the standard deviation of the average adsorption amounts from the two measured amounts of adsorption.

Table 5-1 illustrates the parameters used to fit the experimentally determined adsorption isotherm to the Langmuir model.

Table 5-1. Langmuir model Fitting parameters used for the adsorption isotherms of CnBDMAC from aqueous solution onto stainless steel-coated crystals at 40 °C.

Surfactant	K / M^{-1}	Γ_{max} / molecules nm^{-2}	R^2
C10BDMAC	150	13.20	94
C12BDMAC	575	5.53	99
C14BDMAC	11673	5.08	96
C16BDMAC	28257	3.97	98

Figure 5-6. Adsorption isotherms of CnBDMAC surfactants from aqueous solution onto stainless steel-coated crystals at 40 °C, pH = 6.5-7, using the QCM. The solid lines represent Langmuir model fits. The arrows refer to the cmc values of different CnBDMAC surfactants.

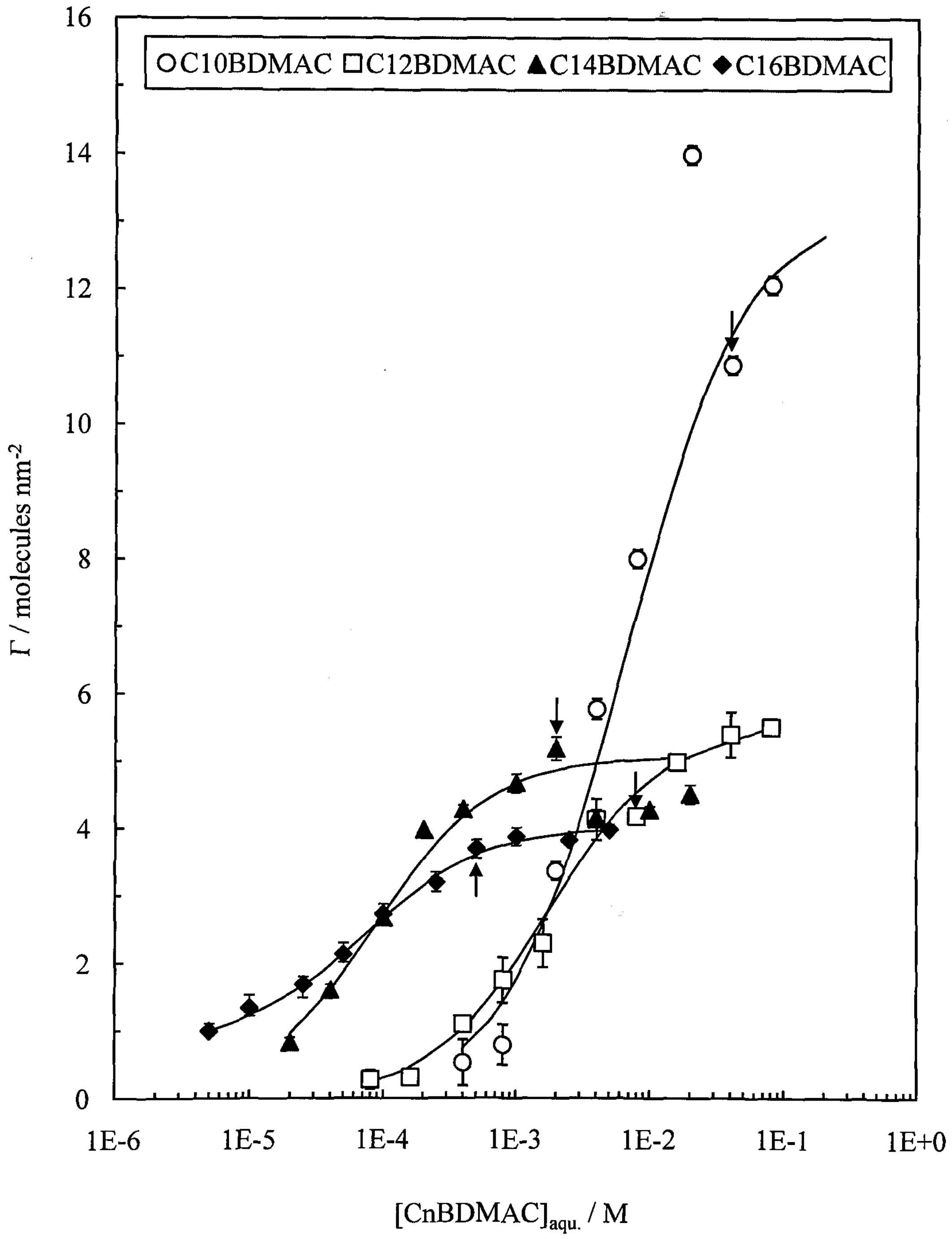

It is obvious from Figure 5-6 that the adsorption behaviour of CnBDMAC surfactants is directly related to the hydrocarbon chain length. The maximum amounts of short chains adsorbed are higher than those for the long chains. The short chains C10 and C12BDMAC give rise to maximum amounts of adsorption of about 13 and 5.5 molecules nm^{-2}, respectively, while the long chains C14 and C16BDMAC results in a lower amount of adsorption corresponding to about 5 and 4 molecules nm^{-2}, respectively. This behaviour is not common for the adsorption of cationic surfactants onto a hydrophilic surface with an opposite charge. In general, with increasing hydrocarbon chain length, the maximum adsorbed amount at saturation is expected to increase mainly because of increasing hydrophobic interactions.

Earlier in *Chapter 3*, we reported that the adsorption of CnBDMAC corrosion inhibitors at air-water interfaces gave rise to a maximum surfaces excess of about 2 molecules nm^{-2} at surfactant concentration corresponding to the cmc. Arguably, we could assume that an adsorption amount of about 2 -3 molecules nm^{2} of CnBDMAC corresponds to a monolayer at the steel-water interfaces. The aforementioned amounts of adsorption indicate that the adsorption of CnBDMAC corrosion inhibitors onto the stainless-steel surfaces is not limited to a monolayer.

The hydrophobic effect has shown to play an important role in the adsorption of CnBDMAC surfactants from aqueous solution onto the stainless steel surface studied using the depletion method (section 6.2). As the alkyl chain length increases the contribution of the hydrophobic interaction increases, overcoming repulsion forces among the cationic surface and surfactant headgroups and promoting the adsorption process. Accordingly, the long chains C14 and C16BDMAC exhibit a higher adsorption affinity than the short chains C10 and C12BDMAC for steel surfaces.

Recently, the adsorption of a homologous series of alkyltrimethylammonium bromides with alkyl groups from C10 to C16 onto solid surfaces (iron and cementite (Fe_3C)) has been investigated [7]. The authors have reported that short chain homologues adsorb better than the long-chain homologues. According to the authors, the shorter compounds obviously suffer from the bulk effect, which explains the contradiction that short-chain compounds apparently adsorb better to these solid surfaces than long chain compounds.

5.2.2. Effect of temperature

The effect of temperature on the adsorption behaviour of C10 and C16BDMAC from aqueous solution onto a stainless steel-coated crystal has been investigated using the QCM at two different temperatures. Figure 5-7 shows the measured shift in the frequency of the third overtone as a function of time during the adsorption of C16BDMAC at 25 °C. The corresponding mass change Δm, is shown in Figure 5-8.

The isotherms for the adsorption of C16BDMAC and C10BDMAC at 25 and 40 °C are shown in Figure 5-9 and Figure 5-10, respectively. Both adsorption isotherms, have been fitted to the Langmuir model and the fitting parameters are given inTable 5-2.

At low surfactant concentrations, the temperature rise has no effect on the amount of C10BDMAC being adsorbed onto the stainless steel, but it increases the amount adsorbed of C16BDMAC. At moderate and high surfactant concentration, the increase in temperature results in a significant increase in the amount of C16BDMAC adsorbed. The rise in temperature from 25 to 40 °C increases the maximum adsorbed amount of C16BDMAC form about 2.6 to 4 molecules nm^{-2}.

This contradicts the adsorption behaviour observed for the short chain C10BDMAC, which exhibits the opposite behaviour as shown by Figure 5-10. In the latter figure, the amount adsorbed decreases with the increase in temperature. The maximum amount adsorbed of C10BDMAC onto stainless steel-coated crystals decreased from about 30 molecules nm^{-2} at 25 °C to about 13 molecules nm^{-2} upon increasing the temperature to 40 °C. The depletion method has been used to study the temperature effect on the adsorption behaviour of C10BDMAC from aqueous solution onto stainless steel particles (316L) in section 6.4. The results of this study revealed that the temperature has no, or only a slight effect on the amount adsorbed at low equilibrium concentration. On the other hand, an increase in the temperature increases the amount of C10BDMAC adsorbed from aqueous solutions onto 316L particles at higher surfactant concentrations. The depletion method measures the actual amounts of surfactant being adsorbed while the QCM technique measures the shift in the frequency measured during the adsorption. In addition, the QCM is very sensitive to changes in the temperature and density and viscosity of solutions. Accordingly, one would rely more on the results of the depletion method.

Figure 5-7. Change in the frequency of the third overtone as a function of time during adsorption of C16BDMAC form aqueous solution onto stainless steel-coated crystals at 25 °C, pH = 6.5-7. The arrows indicate the injection time for each concentration. Numbers shown refer to the concentration normalized with respect to the cmc (0.5 mM).

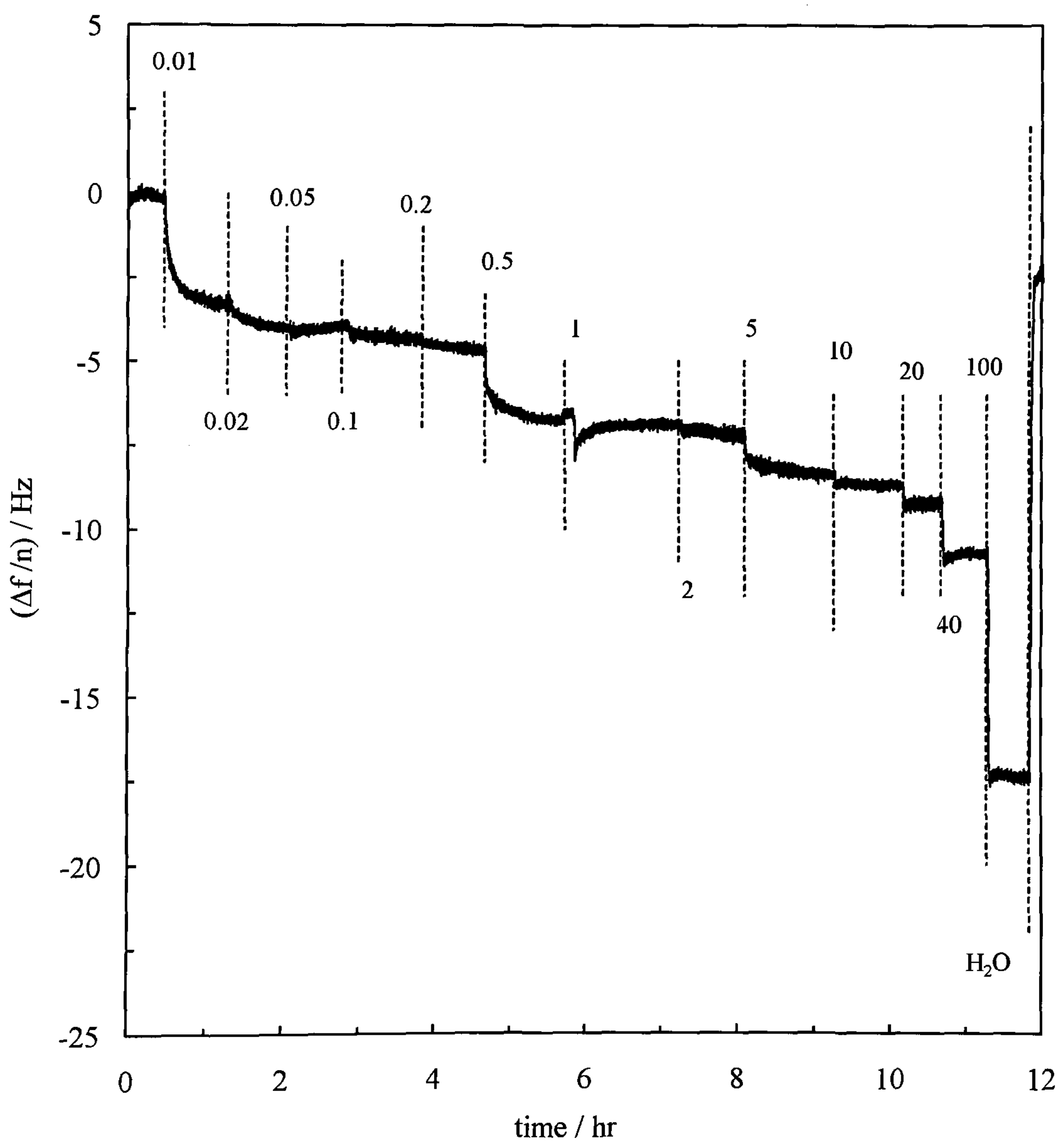

Figure 5-8. Change in the mass adsorbed as a function of time during adsorption of C16BDMAC on stainless steel-coated crystals at 25 °C. The arrows indicate the injection time for each concentration. Numbers shown refer to the concentration normalized with respect to the cmc (0.5 mM).

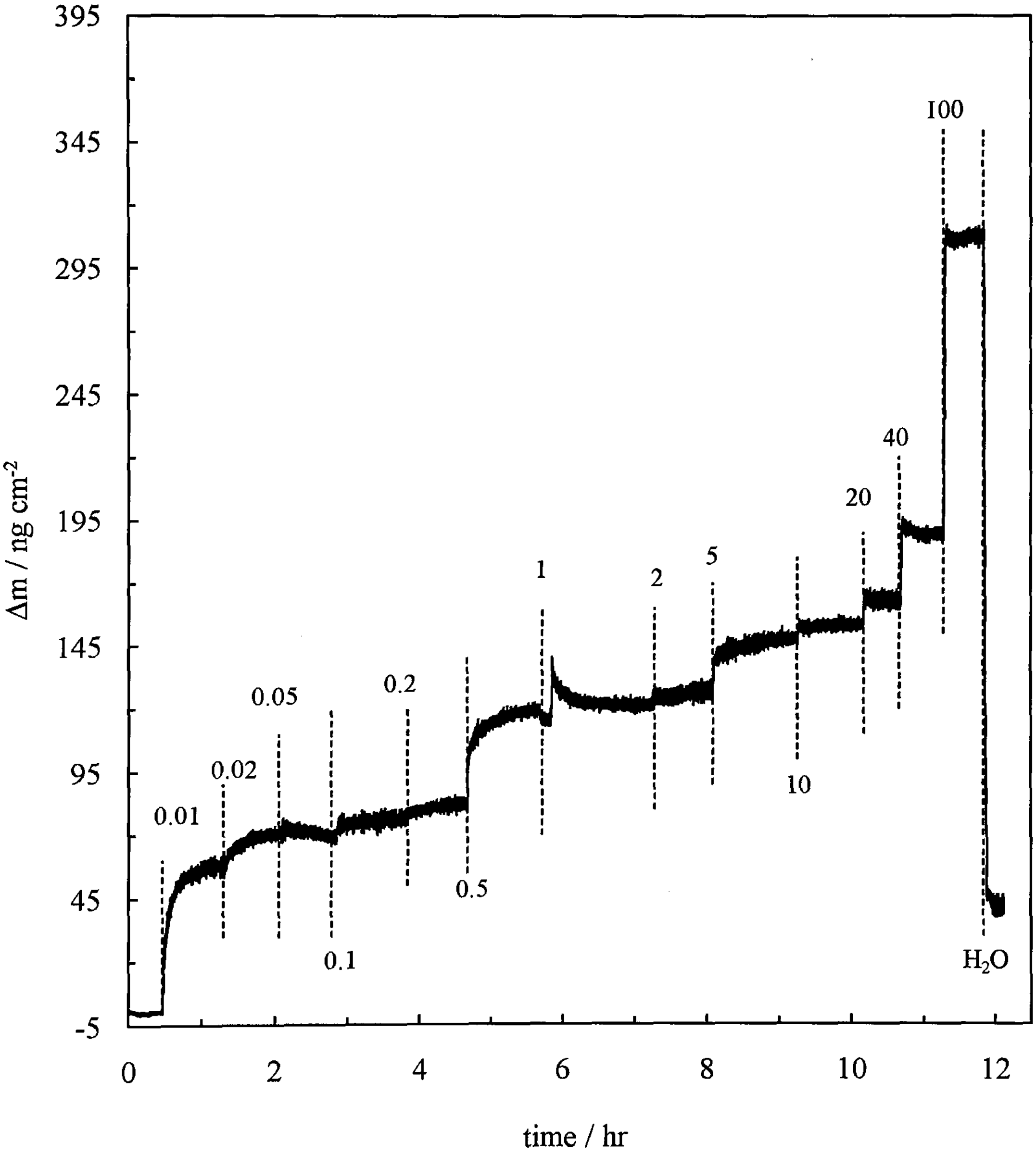

Figure 5-9. Adsorption of C16BDMAC from aqueous solution onto stainless steel coated crystals at 25 and 40 °C, using the QCM, pH = 6.5-7. The solid lines represent Langmuir model fits.

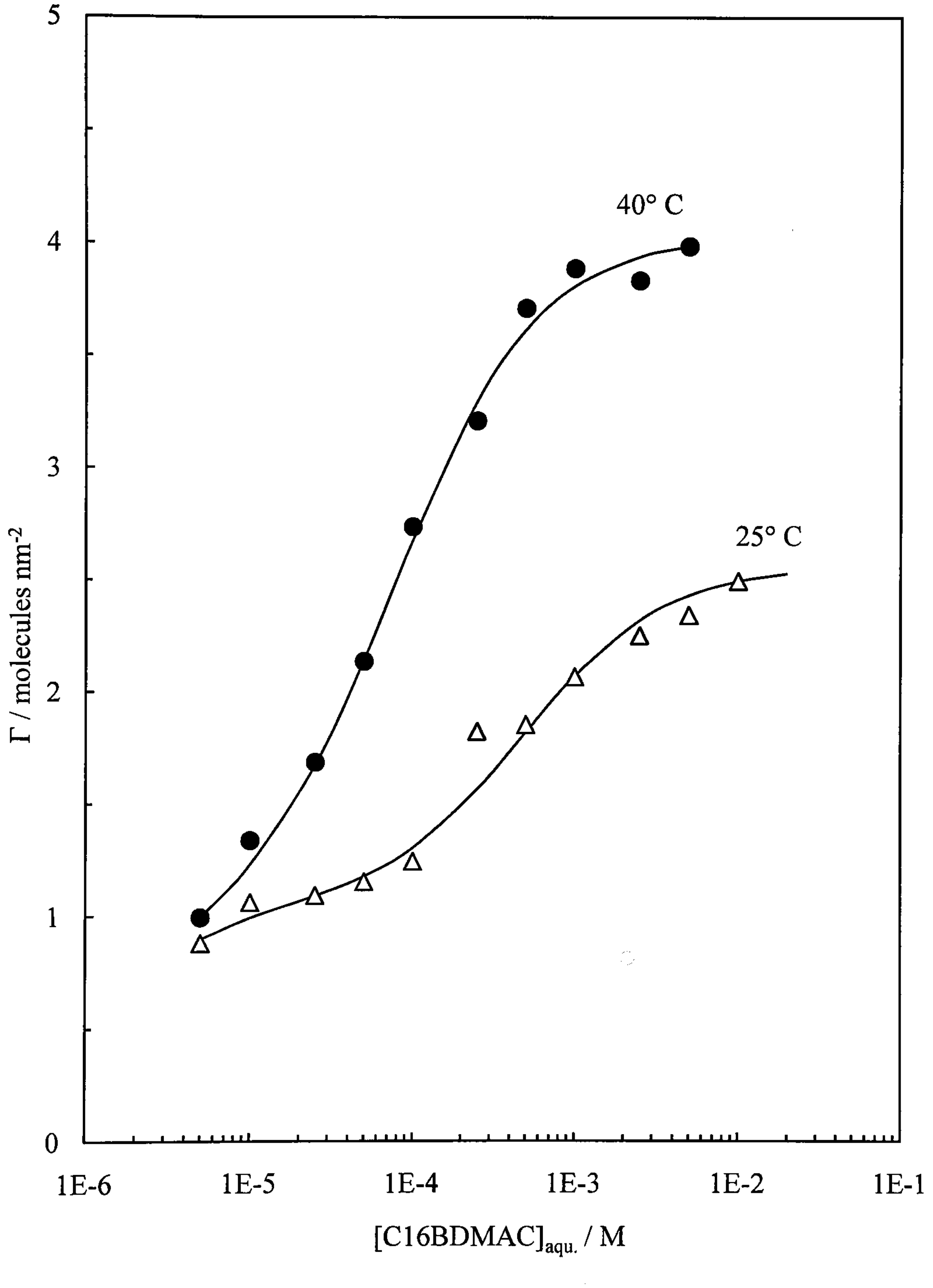

Figure 5-10. Adsorption of C10BDMAC from aqueous solution onto stainless steel coated crystals at 25 and 40 °C, using the QCM, pH = 6.5-7. The solid lines represent Langmuir model fits.

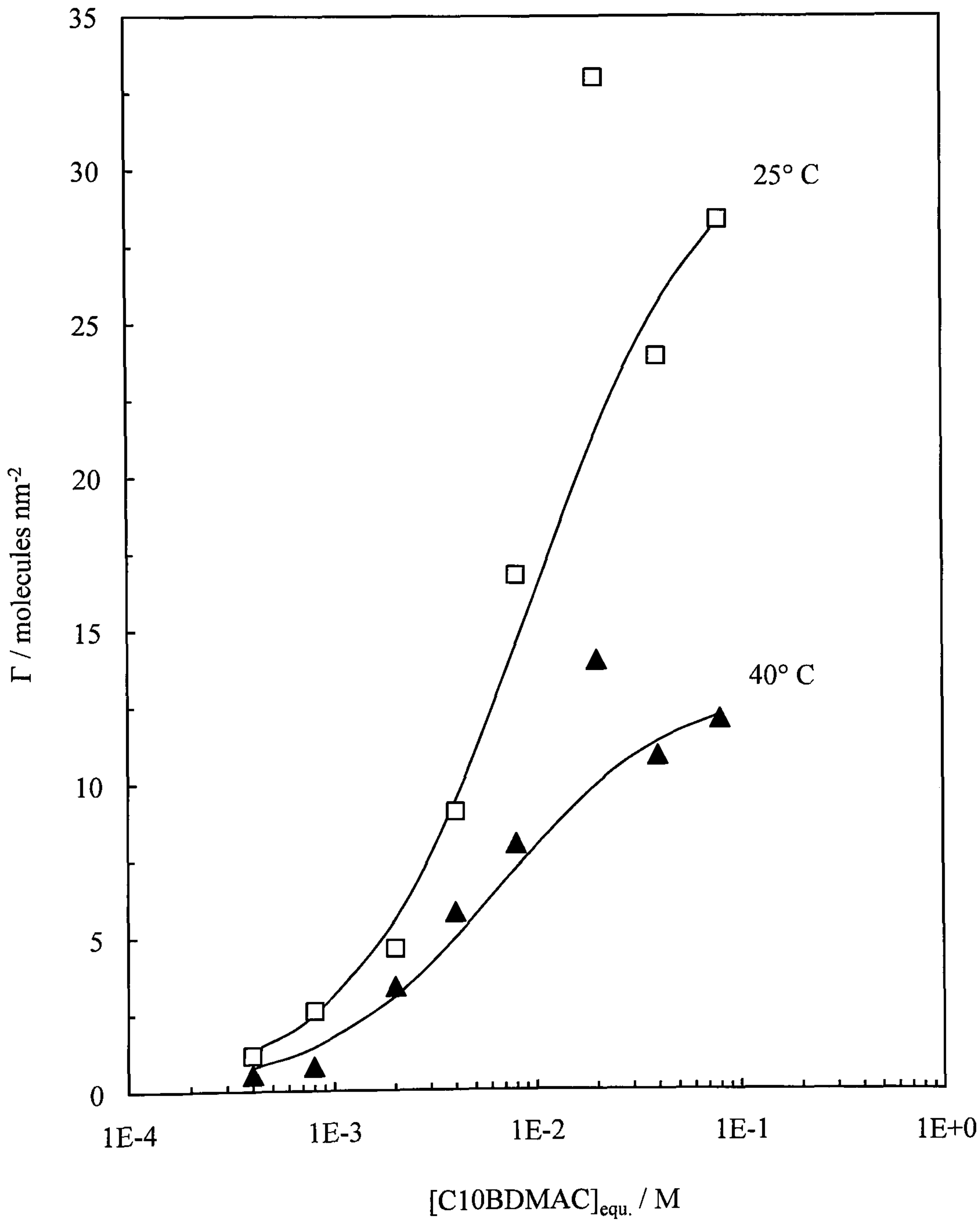

Table 5-2. Langmuir model fitting parameters used for the adsorption isotherm of C10 and C16BDMAC from aqueous solution onto stainless steel-coated crystals at 25 °C.

Surfactant	K / M^{-1}	Γ_{max} / molecules nm^{-2}	R^2
C10BDMAC	170	13.20	94
C16BDMAC	28257	2.56	98

The maximum amount adsorbed of C10BDMAC onto 316L particles increased from about 2 molecules nm^{-2} at 25 °C to about 5 molecules nm^{-2} upon increasing the temperature up to 40 °C. This indicates a disagreement between the results of the temperature effect on the adsorption of C10BDMAC by the QCM and that for the depletion method. The depletion method measures the actual amount of surfactant adsorbed, while the QCM measures the shift in the frequency. Accordingly, adsorption isotherms determined by the depletion method are more accurate than those determined from the QCM.

5.2.3. Effect of brine addition

The effect of electrolyte concentration on the adsorption behaviour of C16BDMAC surfactant at 40 °C has been studied using the QCM. The change in the frequency due to the adsorption of C16BDMAC from 4.7 wt.% brine solution onto stainless steel-coated crystals is shown in Figure 5-11. The frequency shifts measured for each concentration were then converted into mass using the Sauerbrey equation and the adsorption isotherm was then constructed.

Figure 5-12 shows the change in the mass of the adsorbed surfactant as a function of time for the different C16BDMAC surfactant concentrations. Figure 5-13 shows the isotherm for the adsorption of C16BDMAC from 4.7 wt. % brine compared to that with no added brine at 40 °C. The experimentally-determined adsorption isotherm has been fitted to the Langmuir adsorption model shown by the solid lines in the figure. Obviously, the amount of surfactant adsorbed is higher in brine solution compared to water over the entire concentration range of the surfactant investigated. The addition of brine results in increasing the maximum amount of surfactant adsorbed from about 4 to 9 molecules nm^{-2}.

Figure 5-11. Change in the frequency as a function of time during adsorption of C16BDMAC containing 4.7 wt.% brine on stainless steel surface at 40 °C, f_0 = 5 MHz, n = 3, pH = 8. The vertical bars show injection time for each concentration. Numbers shown indicate the concentration normalized with respect to the cmc (1x10^{-3} mM).

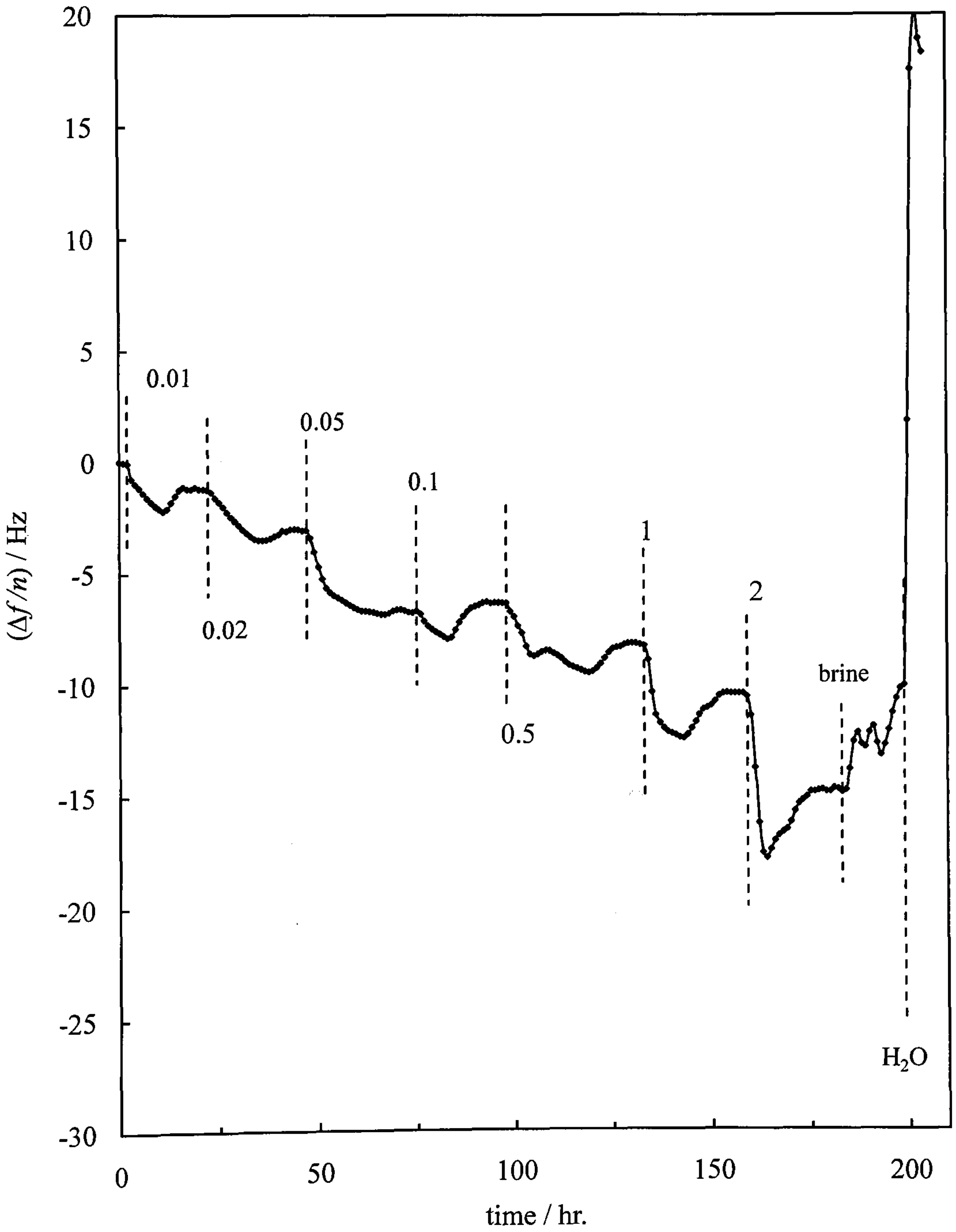

Figure 5-12. Change in the mass adsorbed as a function of time during adsorption of C16BDMAC containing 4.7 wt.% brine on stainless steel surface at 40 °C, f_0 = 5 MHz, n = 3. The vertical bars show injection time for each concentration. Numbers shown indicate the concentration normalized with respect to the cmc ($1\text{x}10^{-3}$ mM).

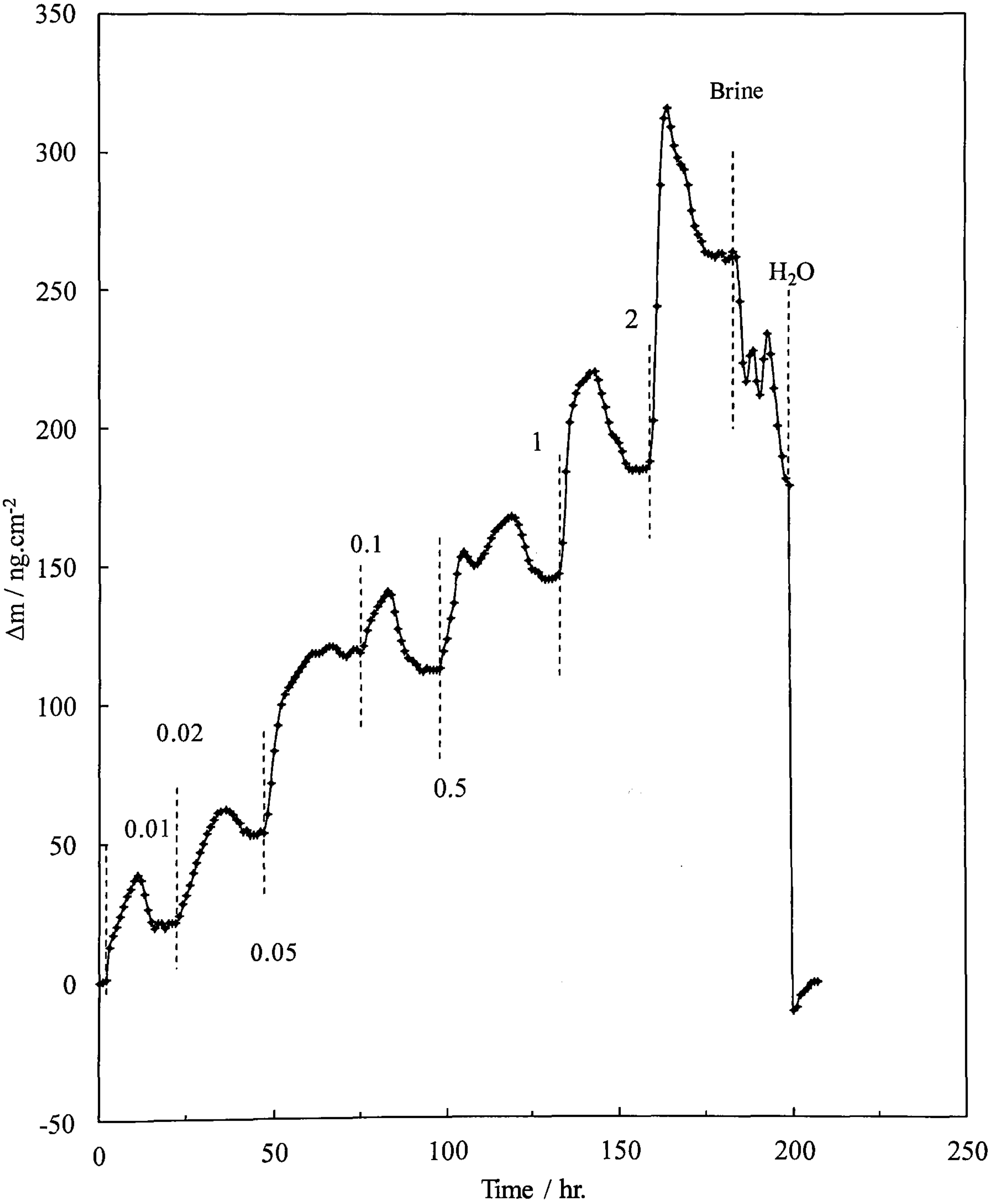

Figure 5-13. Adsorption isotherm of C16BDMAC from aqueous solution containing 4.7 wt. % brine onto stainless steel-coated crystal at 25 °C, compared to that with no added brine. The solid lines represent the Langmuir model fits.

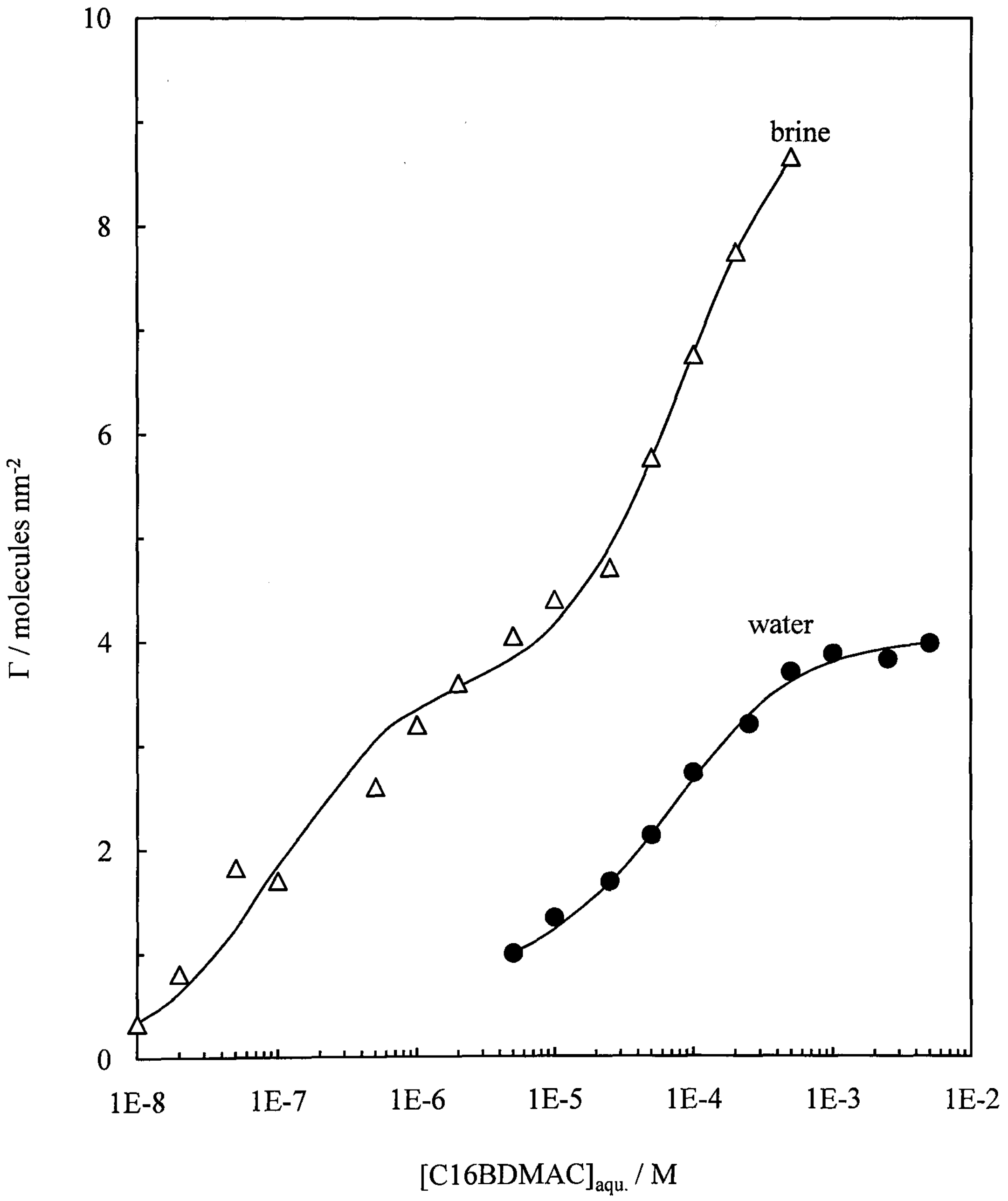

Moreover, the addition of brine results in shifting the adsorption isotherms towards lower equilibrium concentrations. This in turn indicates an increased affinity between the surfactant molecules and the steel surface in the presence of electrolytes. Since the electrostatic interaction is weakened by increasing ionic strength, this allows more molecules to adsorb onto the steel surface. The greater hydrophobic interactions are another reason for the higher amount adsorbed of surfactant with increasing brine concentration. Since steel is a hydrophilic, negatively-charged surface, the adsorption of cationic surfactant initially occurs mainly by cation exchange with water molecules on the surface [41] and this process is supported by the hydrophobic interactions among the tail groups. In the presence of electrolyte, adsorbed surfactant molecules are packing densely due to increased lateral interactions between the tails (hydrophobic bonding), as electrical repulsion between the headgroups is weakened. Knag *et al.* [7] have reported a similar observation. They reported that the adsorption of alkyltrimethylammonium bromide onto Fe_3C-coated crystals in the presence of 2.9 %wt.% NaCl takes place at lower concentrations in comparison to solutions with no added salt. Additionally, they found the amount of adsorbed surfactant is higher in the presence of electrolyte compared to water. This has been attributed to the screening of the head-group charge by the electrolyte, which reduces the surfactant head-group area and allows more tightly-packed surfactant aggregates to form. More recently, Hodges and Biggs [8] investigated the effect of electrolyte concentration on the adsorption of cetyltrimethylammonium chloride onto silica and alumina surfaces using the QCM. Their results indicated that the amount of surfactant adsorbed, on both surfaces, increases with the increase in salt concentration up to 4 M NaCl.

5.2.4. Discussion

Despite the higher degree of adsorption determined for CnBDMAC surfactants onto the stainless steel surfaces using the QCM method, it provides an effective qualitative way to describe the adsorption behaviour of these surfactants at the solid-liquid interface. The isotherms determined gave rise to a typical behaviour of an ionic surfactant molecule being adsorbed onto an oppositely charged surface. A stainless steel surface has a point of zero charge (PZC) in the range of pH 4.4-5.2. Accordingly, under the experimental condition employed, the stainless steel-coated crystal will be negatively charged. Consequently, the adsorption process at low surfactant concentrations will be driven primarily through electrostatic interactions between negative surface charges on steel surfaces and the positive ammonium surfactant head groups. The increase in the surfactant chain length shifts the adsorption isotherms to a lower surfactant concentration indicating that hydrophobic interactions between the adsorbed surfactant molecules appear to influence on the adsorption processes as well. So both the electrostatic and hydrophobic interactions are operative at these low surfactant concentrations with the first being the dominant one. The dominance of the electrostatic interactions over the hydrophobic interactions at low surfactant concentrations is supported by two observations. Firstly, at low surfactant concentration, the adsorption of CnBDMAC has been shown to be temperature independent. Secondly, the amounts of adsorption increase with the increases in electrolyte concentrations.

At moderate surfactant concentrations, a sharp increase of adsorption is observed, indicating an increase in the affinity of surfactant molecules for the solid surface. The surfactant adsorption at these moderate surfactant concentrations seems to be governed by the hydrophobic interactions between the surfactant chains. The sharp increase in the amounts of adsorption could be attributed to surface aggregates or a multilayer formation [9-11].

Beyond the cmc, the shape of the adsorption isotherms of C10 and C12 differ from those for C14 and C16BDMAC as shown by Figure 5-6. The long-chain surfactants C14 and C16BDMAC adsorption isotherms tend to approach saturation. On the other hand, the increase in surfactant concentrations of the short chains C10 and C12BDMAC results in increasing the degree of adsorption. The adsorption measurents of CnBDMAC onto stainless steel particles using the depletion method gave rise to a similar behaviour (see section 6.2).

The electrolyte addition has a considerable influence on the extent of adsorption similar to increasing the hydrocarbon chain length. Electrolyte "salts out" the hydrocarbon chains of the surfactant and therefore, results in adsorption at lower concentrations [12]. The effect of electrolyte on the adsorption of surfactant at the solid–liquid interface have been studied widely in the literature [5, 9]. Koopal *et al.* [12] have studied the effect of ionic strength on the adsorption of cationic (alkyl pyridinium salts) and anionic (alkyl benzene sulphonates) surfactants onto the mineral oxide rutile. They reported an increase in the ionic strength of the bulk medium causes a screening of the electrostatic repulsions between surfactant headgroups, leading to an increase in the maximum amount adsorbed. The adsorption mechanism of CnBDMAC surfactants from aqueous solution onto stainless and mild steel surfaces will be described in more detail in *Chapter 6.*

5.3. OPTIMIZATION OF THE QCM FOR THE *In-Situ* ADSORPTION MEASUREMENTS

5.3.1. Choice of the experimental protocol

The QCM is a powerful technique for monitoring the adsorption of surfactants and many other molecules onto solid surfaces. The instrumentation of a QCM system is quite simple, and no prior chemical modification is needed. However, the choice of an experimental procedure has a marked influence on the measured frequency and dissipation changes detected by the QCM. In this section, we have studied the effect of employing different flow patterns on the measured frequency shifts and dissipation changes during the adsorption of different C12BDMAC concentrations from aqueous solution onto stainless steel-coated crystals at 25 °C. Three different protocols have been investigated under the same experimental conditions of surfactant concentration, sample volume, temperature and the flow rate. A schematic diagram describing the three different experimental protocols or flow patterns are shown in Figure 5-14. These protocols are:

A) Stepwise Protocol: measuring shift in frequency of an increasing aqueous surfactant concentration without cleaning the crystals between each increase in the surfactant concentration.

B) Batch Protocol: the same as the stepwise protocol, but the crystal is removed and cleaned after each concentration.

C) Loop Protocol: the same as the batch protocol, but the surfactant solution is being circulated instead of passing to the waste.

In the *Stepwise Protocol*, deionised water was first passed over the crystals until a zero baseline was reached. Then the lowest surfactant concentration was introduced until equilibrium was attained. The next higher surfactant concentration was then pumped onto the same crystal without stopping the device or cleaning the crystal until equilibrium was reached.

Figure 5-14. A schematic diagram describing the three investigated experimental procedures.

(A) Stepwise Protocol

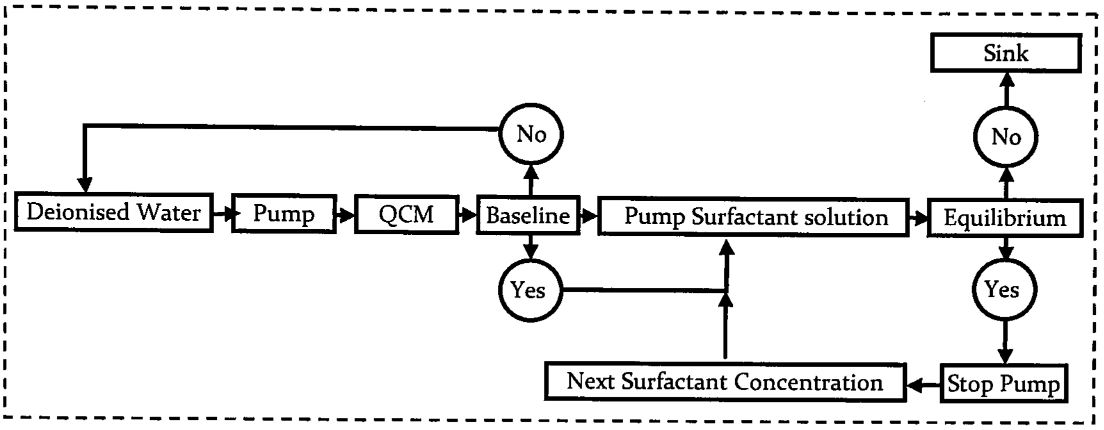

(B) Loop Protocol

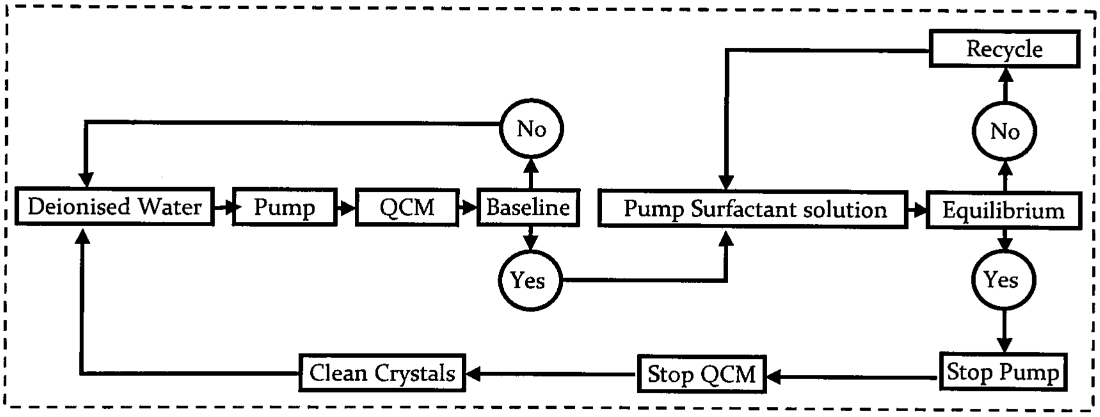

(C) Batch Protocol

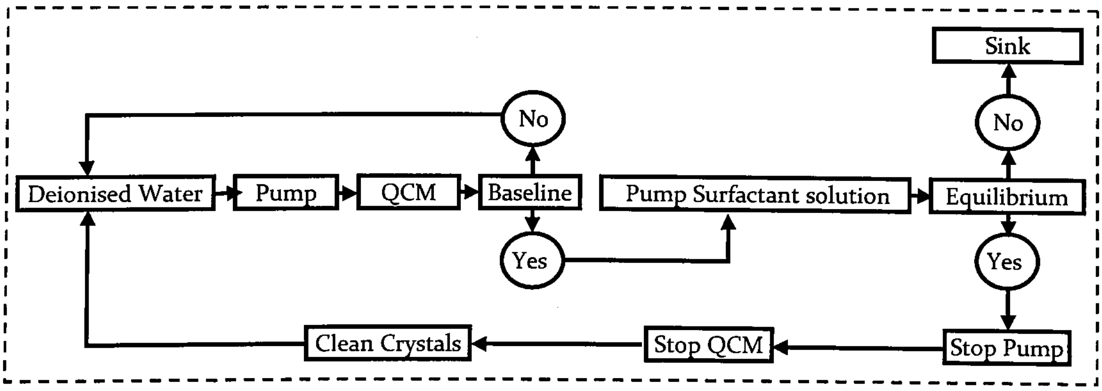

This was repeated until the whole range of surfactant concentrations to be investigated was finished. The crystal was then flushed with deionised water and cleaned for further usage.

The adsorption behaviour of C12BDMAC onto a stainless steel-coated crystal was investigated at 25 °C using the *Stepwise Protocol*. The change in the frequency recorded during the adsorption process of different C12BDMAC concentrations as a function of time is shown in Figure 5-15. In this figure, the recorded shift in frequency is the normalized shift in frequency with respect to the overtone, $\Delta f/n$, not the absolute one. The normalized shift in frequency, $\Delta f/n$, equals the absolute shift in frequency divided by the overtone number at which the frequency was monitored. In all the figures showing recorded changes in the frequency in this work, this change refers to the normalized shift in frequency. The arrows shown in the figure indicate the time at which each concentration was injected into the system. The numbers shown above the arrows refer to the normalized surfactant concentrations with respect to the cmc (7 mM).

Clearly, the introduction of the surfactant solution results in lowering the frequency of the stainless steel-coated crystals due to the adsorption of surfactant molecules (Figure 5-15). The magnitude of the frequency shift Δf, increases with the increase in the surfactant concentration up to values of about 0.8 times the cmc. This maximum in Δf before the cmc has been attributed previously to the presence of impurities in the surfactant composition. Upon increasing the surfactant concentration to a value corresponding to the cmc, the magnitude of Δf decreases.

Beyond the cmc, the increase in surfactant concentration has apparently no large effect on the recorded Δf up to concentration values of about two times the cmc. Noticeably, flushing the crystals with water did not bring the measured frequency back to the baseline (where $\Delta f \approx 0$) before pumping surfactant solutions. This may be attributed to a frequency drift by the QCM device during the measurements. According to the manufacturer, a clean 5 MHz crystal sensor operating in a liquid at 25 °C drifts by up to about 1.5 Hz hour^{-1} in the frequency values and by 2×10^{-7} per hour in the dissipation values when measured at the 15 MHz harmonic.

The second protocol, which has been investigated, was the *Batch Protocol*. In this protocol, the change in frequency was monitored individually for each surfactant concentration.

Figure 5-15. Change in the frequency, $\Delta f/n$, as a function of time during the adsorption of different aqueous C12BDMAC concentrations onto stainless steel coated crystals at 25°C, n = 3, pH = 6.5-7, using the *Stepwise Protocol*. The arrows indicate the time at which each concentration has been introduced. The numbers refer to the normalized surfactant concentrations with respect to the cmc (7 mM).

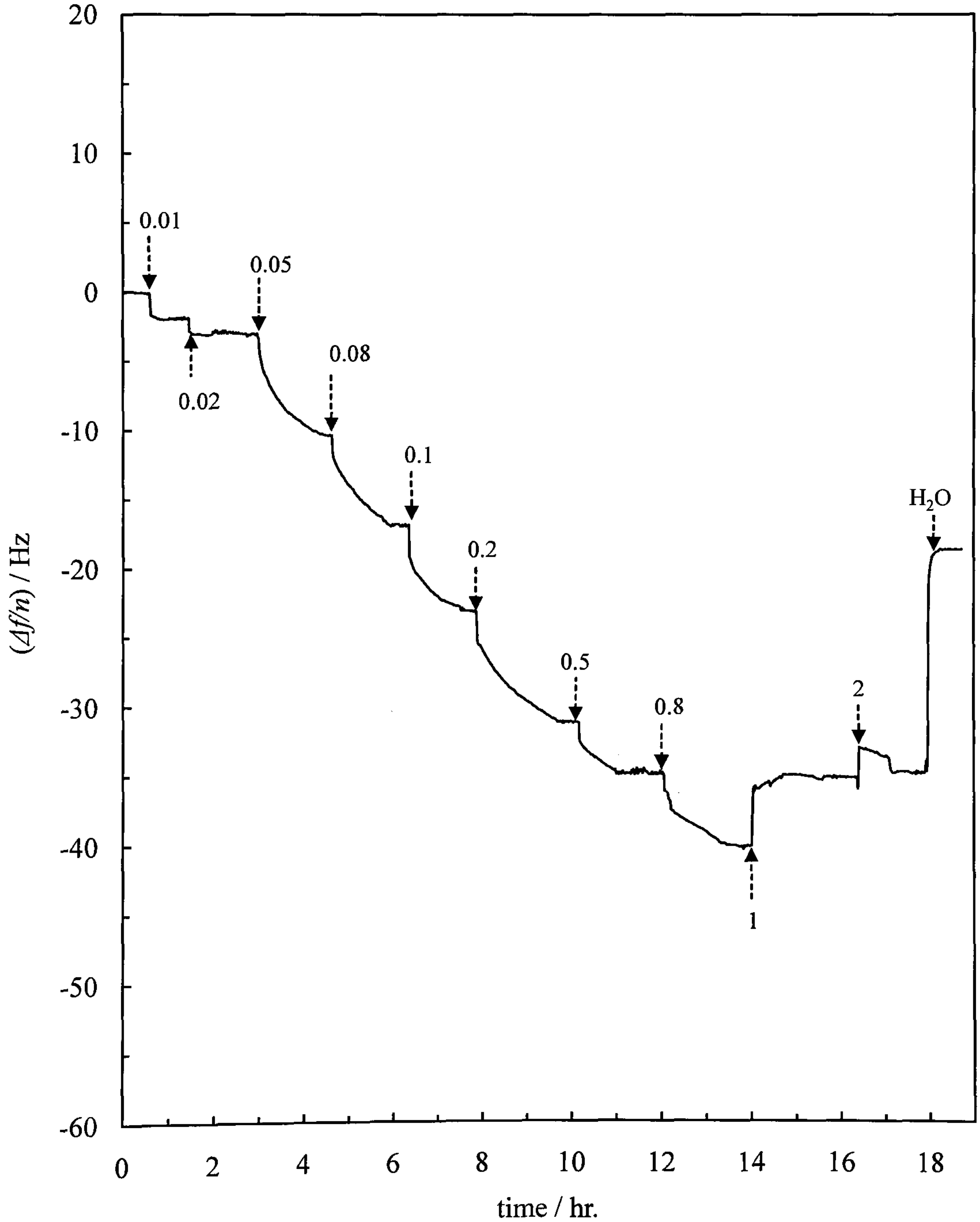

For each C12BDMAC concentration, deionised water was first passed over the crystals until a baseline was reached. Then a definite surfactant concentration solution was introduced until equilibrium was attained. The crystal was then flushed with deionised water and the device was stopped. Then the crystal was removed from the flow cell and cleaned. These steps were repeated for each surfactant concentration until the whole range of surfactant concentration to be investigated was done. The surfactant solutions tested were prepared from the same starting stock solution.

The changes in the frequency as a function of time during the adsorption of two different aqueous C12BDMAC concentrations (0.2 and 1 ×times the cmc) onto stainless steel-coated crystals using the *Batch Protocol* are shown in Figure 5-16 and Figure 5-17, respectively. The recorded shift in the frequency corresponds to the changes in the third overtone.

Similar to the *Stepwise Protocol*, the introduction of surfactant solution lowers the frequency of the oscillation and the magnitude of this shift increases with increasing surfactant concentration. This indicates an increase in the degree of adsorption as a function of the surfactant concentration. The *Stepwise Protocol* gave rise to higher Δf values than those measured by the *Batch Protocol*. For example, the magnitude of Δf measured using the *Batch Protocol* for 7 mM C12BDMAC surfactant solution was about -13 Hz, while this value was about -35 Hz as measured by the *Stepwise Protocol*.

Finally, the effect of using the *Loop Protocol* on the shift in frequency measured during the adsorption of C12BDMAC surfactant onto stainless steel-coated crystal was investigated. This protocol is similar to the *Batch protocol*, where the frequency shift was monitored individually for each surfactant concentration. However, in the *Loop Protocol* the surfactant solution was made to pass over the crystal in a closed circuit (instead of passing a fresh solution) until equilibrium was attained. In the *Loop Protocol*, for each C12BDMAC concentration, deionised water was first pumped over the crystals until a baseline was reached. Then a definite surfactant concentration solution was circulated over the crystal until equilibrium was attained. The crystal was then flushed with deionised water and the device was stopped. Then the crystal was removed from the flow cell and cleaned for further usage. These steps were repeated for each surfactant concentration until the whole range of surfactant concentration to be investigated was done.

Figure 5-16. Change in the frequency as a function of time during the adsorption of aqueous solution of C12BDMAC has a concentration of 0.2 times the cmc onto stainless steel-coated crystals at 25°C, n = 3, pH = 6.5-7, using the *Batch Protocol.*

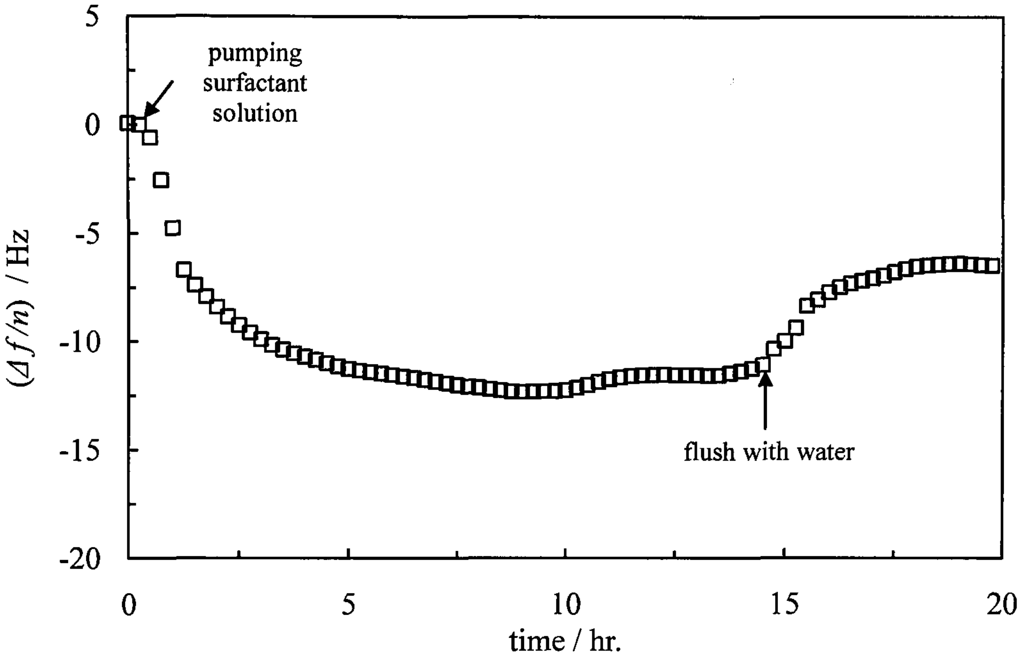

Figure 5-17. Change in the frequency as a function of time during the adsorption of aqueous solution of C12BDMAC has a concentration equals the cmc onto stainless steel coated crystals at 25°C, pH = 6.5-7, n = 3, using the *Batch Protocol.*

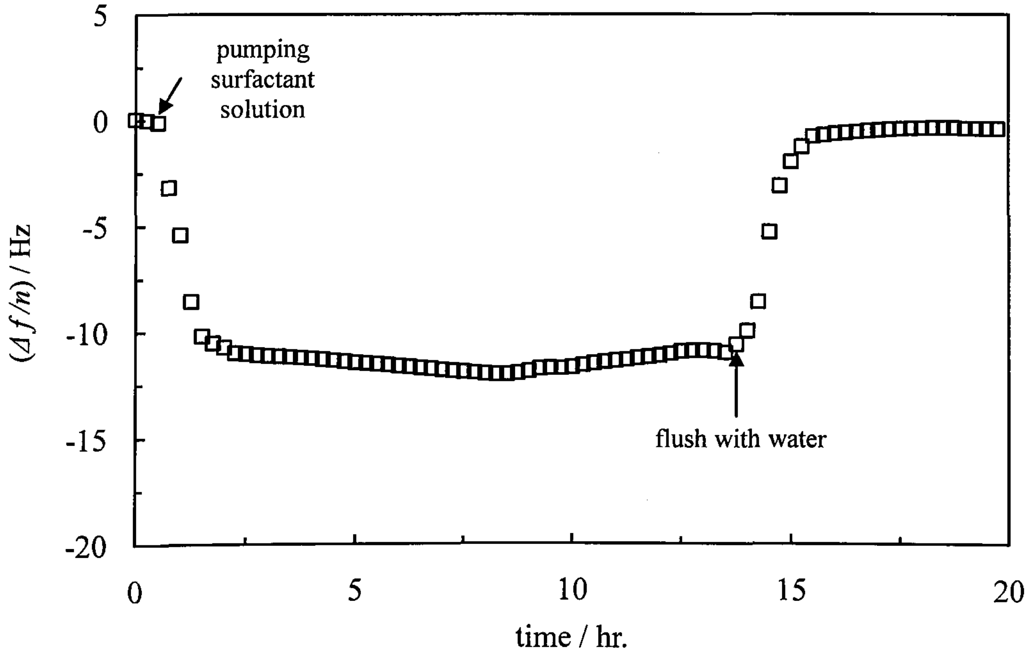

Figure 5-18 and Figure 5-19 showing how the frequency change during the adsorption process of two C12BDMAC solutions with concentrations of 2 and 0.05 times the cmc as a function of time at 25 °C. A comparison of the frequency shift, measured using the three different protocols, as a function of the normalized C12BDMAC concentration is shown in Figure 5-20. The presented frequency shift shown in this figure is the average frequency change, $\Delta f_{average}$, of the 3rd, 5th, 7th, 9th, 11th and 13th overtones for two different stainless steel-coated crystals. The average frequency change, $\Delta f_{average}$, is defined as follows:

$$\Delta f_{average} = \frac{\Delta f_{1st} + \Delta f_{2nd}}{2} \tag{5-2}$$

$$\Delta f_{1st} = \left(\frac{\frac{\Delta f_3}{3} + \frac{\Delta f_5}{5} + \frac{\Delta f_7}{7} + \frac{\Delta f_9}{9} + \frac{\Delta f_{11}}{11} + \frac{\Delta f_{13}}{13}}{6} \right)_{1st} \tag{5-3}$$

$$\Delta f_{2nd} = \left(\frac{\frac{\Delta f_3}{3} + \frac{\Delta f_5}{5} + \frac{\Delta f_7}{7} + \frac{\Delta f_9}{9} + \frac{\Delta f_{11}}{11} + \frac{\Delta f_{13}}{13}}{6} \right)_{2nd} \tag{5-4}$$

where Δf_{1st} refers to the average of the normalized frequency change of the 3rd, 5th, 7th, 9th, 11th and 13th overtone for the first crystal; and Δf_{2nd} refers to the average of the normalized frequency change of the 3rd, 5th, 7th, 9th, 11th and 13th overtone for the second crystal.

The error bars shown in Figure 5-20 represent the standard deviations of $\Delta f_{average}$ from the average shift in frequency detected by the two crystals Δf_{1st} and Δf_{2nd}. The corresponding changes in the dissipation of the QCM stainless steel-coated crystals during the adsorption process, is given in Figure 5-21. The presented change in the dissipation in this figure represents the average dissipation change, $\Delta D_{average}$, in the 3rd, 5th, 7th, 9th, 11th and 13th overtone for two different stainless steel coated crystals. The average dissipation change, $\Delta D_{average}$, is defined as follows:

$$\Delta D_{average} = \frac{\Delta D_{1st} + \Delta D_{2nd}}{2} \tag{5-5}$$

Figure 5-18. Change in the frequency as a function of time during the adsorption of aqueous solution of C12BDMAC has a concentration of 2 times the cmc (14 mM) onto stainless steel-coated crystal at 25°C, pH = 6.5-7, n = 3, using the *Loop Protocol.*

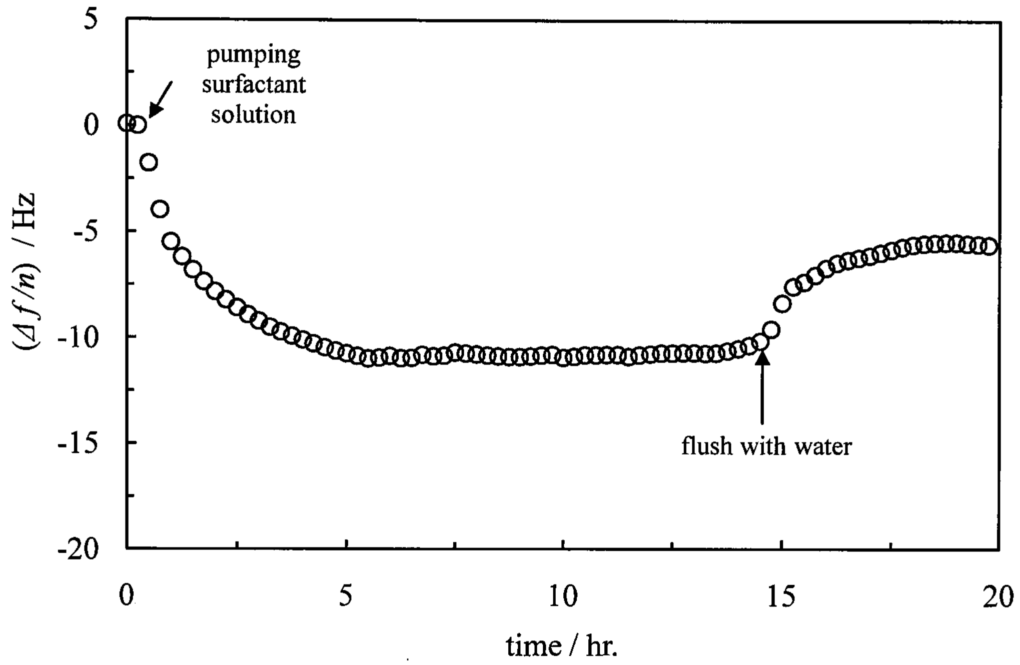

Figure 5-19. Change in the frequency as a function of time during the adsorption of aqueous solution of C12BDMAC has a concentration of 0.05 times the cmc (0.035 mM) onto stainless steel-coated crystal at 25°C, n = 3, pH = 6.5-7, using the *Loop Protocol.*

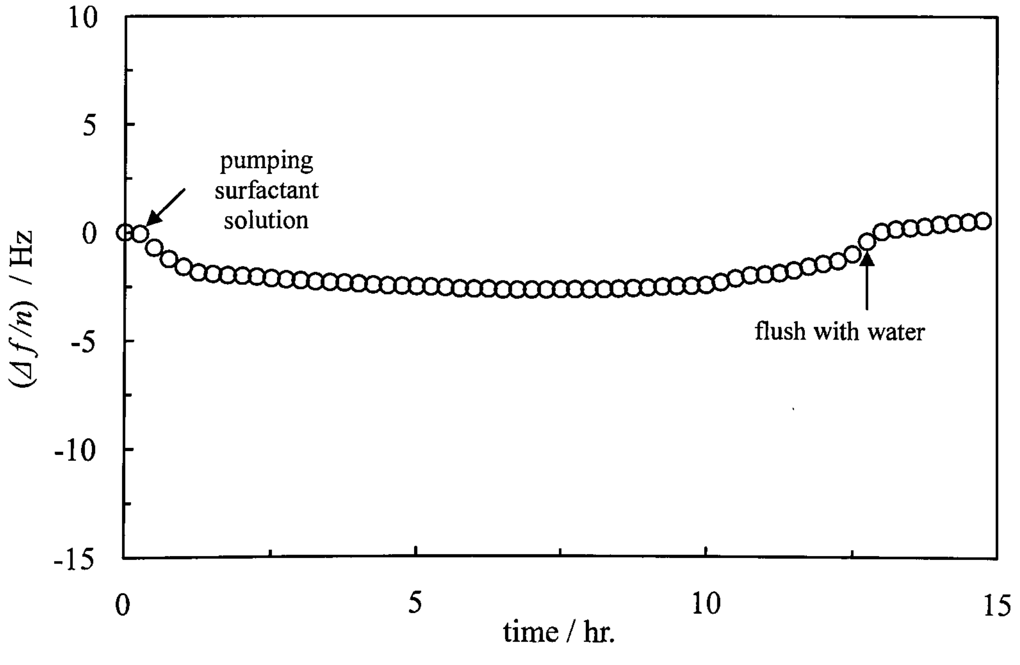

Figure 5-20. Variation of the average frequency change of different overtones (3, 5, 7, 9, 11, 13) as a function of the normalized concentration of C12BDMAC during the adsorption from aqueous solution onto stainless steel-coated crystals at 25 °C, pH = 6.5-7, using different protocols.

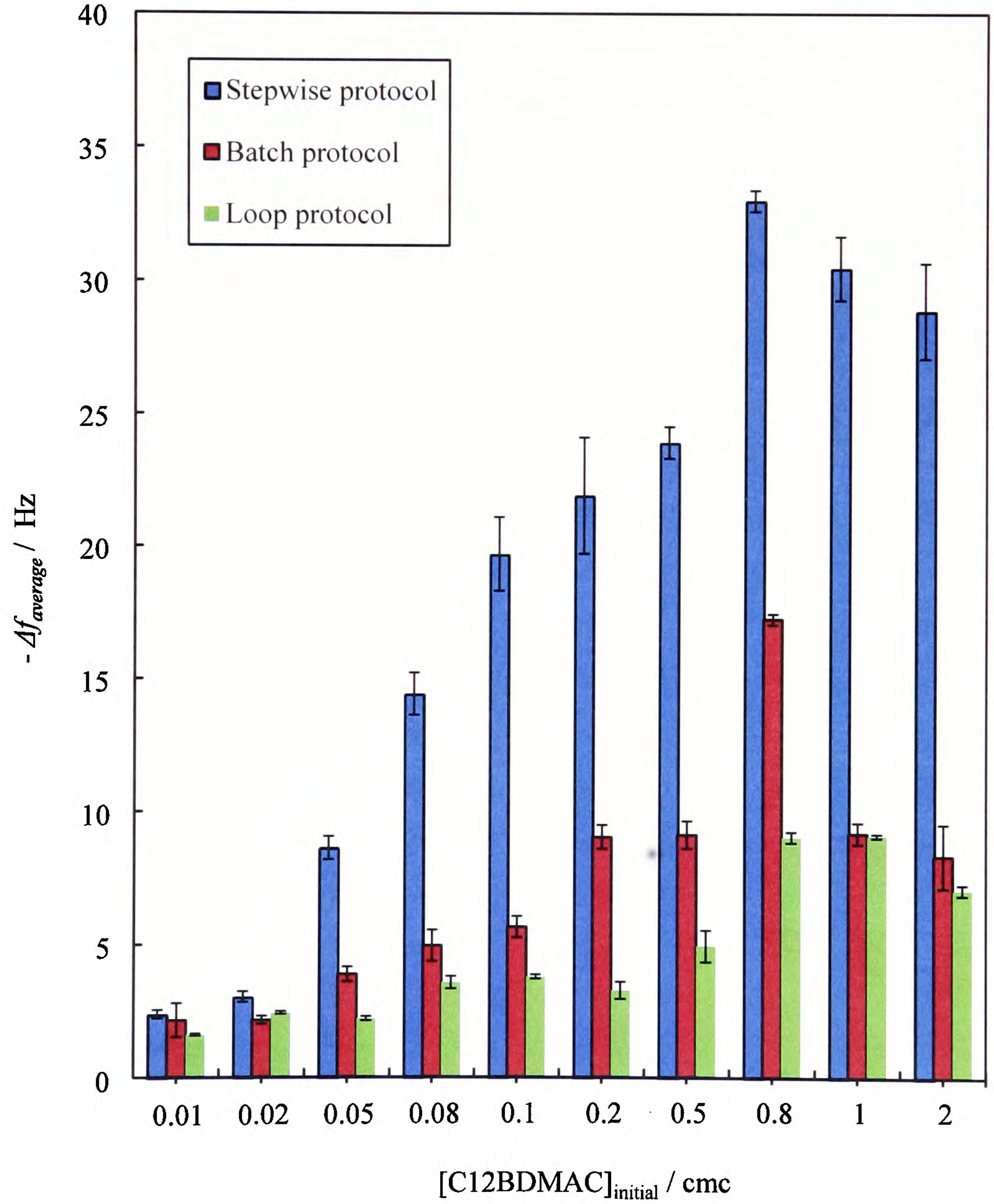

$$\Delta D_{1st} = \left(\frac{\frac{\Delta D_3}{3} + \frac{\Delta D_5}{5} + \frac{\Delta D_7}{7} + \frac{\Delta D_9}{9} + \frac{\Delta D_{11}}{11} + \frac{\Delta D_1}{13}}{6} \right. \tag{5-6}$$

$$\Delta D_{2nd} = \left(\frac{\frac{\Delta D_3}{3} + \frac{\Delta D_5}{5} + \frac{\Delta D_7}{7} + \frac{\Delta D_9}{9} + \frac{\Delta D_{11}}{11} + \frac{\Delta D}{13}}{6} \right. \tag{5-7}$$

where ΔD_{1st} refers to the average dissipation change of the 3rd, 5th, 7th, 9th, 11th and 13th overtone for the first crystal; and ΔD_{2nd} refers to the average dissipation change of the 3rd, 5th, 7th, 9th, 11th and 13th overtone for the second crystal.

The error bars shown in Figure 5-21 represent the standard deviation of $\Delta D_{average}$ from the average dissipation change detected by the two crystals ΔD_{1st} and ΔD_{2nd}. It is clear from Figure 5-21 that the measured $\Delta f_{average}$ for the three tested experimental protocols show an obvious divergence among them. The average frequency shifts detected by the *Stepwise Protocol* give rise to the most higher values followed by those for the *Batch* and *Loop Protocols* over all the studied concentrations range. The magnitudes of these differences are small at low surfactant concentration and increase gradually with increasing surfactant concentrations. For example, the $\Delta f_{average}$ values measured by the *Stepwise Protocol*, at the cmc, is about -48 Hz, and that measured by the *Batch* and *Loop Protocols* are about -17 and -9 Hz, respectively. The aforementioned observations apply also for the measured dissipation changes by the three protocols. The *Stepwise Protocol* gave rise to higher dissipation values compared to the other two protocols. The average dissipation values measured by the *Batch* and *Loop Protocols* are relatively close to each other. For example, the measured $\Delta D_{average}$ by the *Stepwise Protocol,* at the cmc, is about 8×10^{-6}, and those measured by the *Batch* and *Loop Protocols* are about 1.3×10^{-6} and 1.2×10^{-6}, respectively. As mentioned earlier, the change in the measured dissipation values provide information about how rapidly the energy of the oscillating crystal is given up to the surroundings. Firmly attached, smooth and homogeneous layers give rise to a low dissipation, whereas loosely bound, rough and extended layers containing a lot of solvent result in a high dissipation—Sauerbery equation is not applicable for such a system.

Figure 5-21. Variation of the average dissipation change of different overtones (3, 5, 7, 9, 11, 13) as a function of the normalized concentration of C12BDMAC during adsorption from aqueous solution onto stainless steel-coated crystals at 25 °C, pH = 6.5-7, using different protocols.

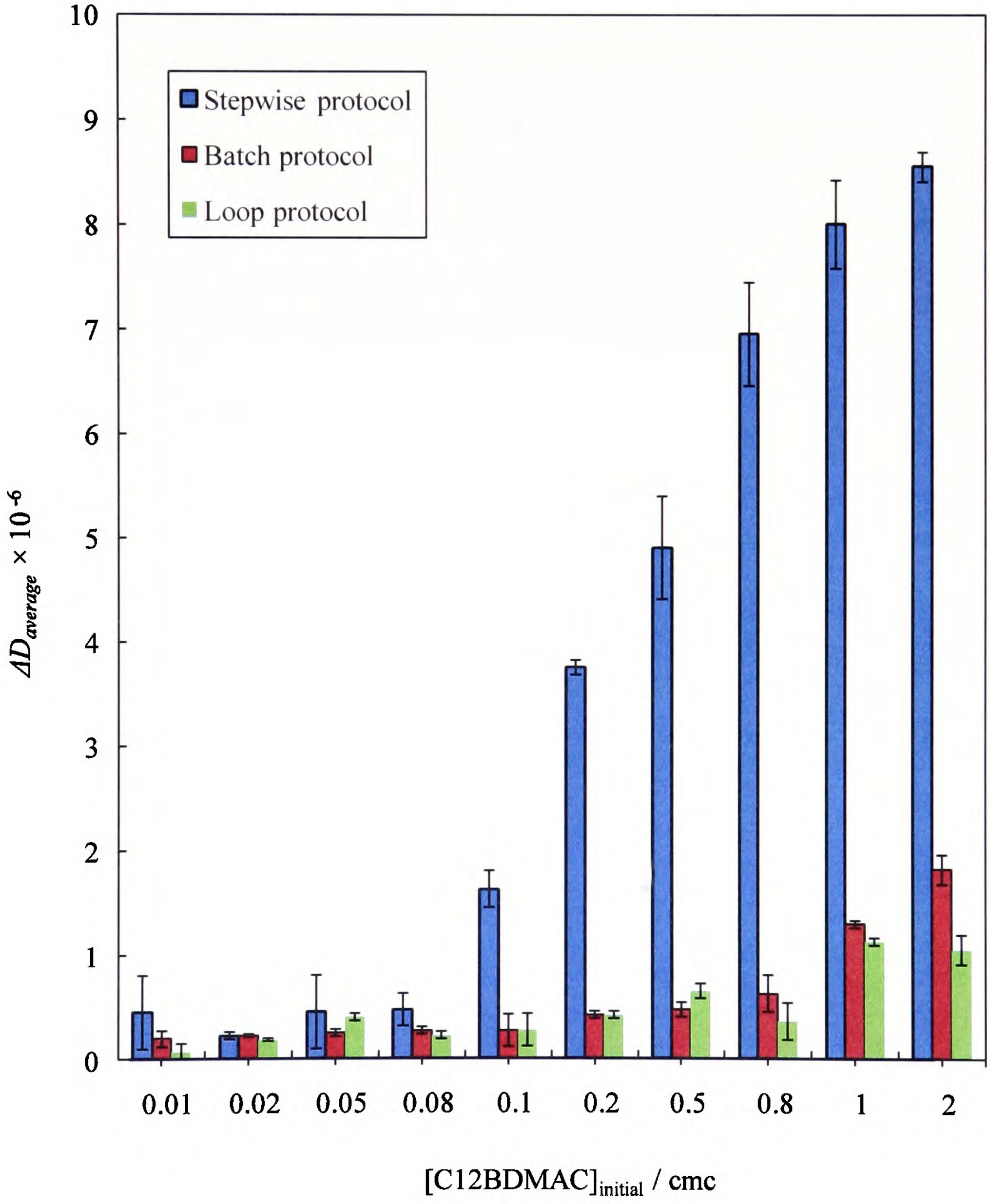

Noticeably, the $\Delta D_{average}$ values measured by the *Batch* and *Loop* protocols are less than 1×10^{-6} up to surfactant concentrations corresponding to a value of about 0.8 times the cmc. This indicates that the QCM senses the mass adsorbed as a rigid mass and not as a viscoelastic layer. However, the measured $\Delta f_{average}$ by the two protocols show noticeable differences between them. In most cases, the values of $\Delta D_{average}$ measured by the *Loop Protocol* are the smallest compared to those measured by the other protocols. Accordingly, one would recommend the *Loop Protocol* to be used as a convenient experimental procedure to monitor the adsorption of CnBDMAC surfactants onto solid surfaces in this work. As concluded from the abovementioned results, the reason for choosing the *Loop Protocol* lies in the low dissipation values measured by this protocol compared to the other.

Recently, Striolo *et al.* [13] studied the influence of employing different flow regimes on the amounts of CTAB surfactant adsorbed onto gold and silica surfaces using the QCM. They investigated the adsorption process using two different flow patterns. The first was the step-by-step adsorption isotherm in which a clean surface is exposed to surfactant solutions in one discrete step. Whereas in the second pattern, a clean surface was exposed to solutions of increasing surfactant concentration in a series of steps. The first pattern resembles the *Stepwise Protocol* and the second resembles the *Patch Protocol*. Their results indicated that, the amounts of surfactant adsorbed using the step-by-step regime was larger than those measured by the patch regime by a factor two in most cases. This behaviour has been attributed to potential rearrangements of adsorbed surfactants and possible templating effects provided by those surfactants adsorbed at low bulk concentrations that are likely to occur freely when the adsorbed amount increases slowly [13].

5.3.2. Analysis of the experimental data

5.3.2.1. Choice of the overtone

The process of selecting an overtone, at which the frequency change of the oscillating crystal will be measured, is very crucial for the accuracy of the whole measurement. In the air, no differences are noticed between the measured $\Delta f/n$ values regardless of which overtone has been used and the same observation applies for the dissipation changes $\Delta D/n$ values as well. On the other hand, in liquids, the measured $\Delta f/n$ and $\Delta D/n$ values vary with the overtone number. Generally, the magnitude of these differences decreases with the increase in the overtone number. Figure 5-22 shows how the normalized-frequency shifts vary with the overtone number during the adsorption of an aqueous solution of C12BDMAC with concentration of 0.8 times the cmc, using the *Loop Protocol*. As shown, the measured $\Delta f/n$ values vary with the overtone number. For example, the $\Delta f/n$ value measured at the third overtone is about -12 Hz and that at the eleventh and thirteenth overtones are -8.5 and -8.2 Hz, respectively. These differences in the measured $\Delta f/n$ values at the different overtones indicate that the adsorbed surfactant layer is not rigid and the QCM senses it as a viscoleastic film. Accordingly, applying these measured $\Delta f/n$ values in the Sauerbrey equation will result in different masses.

In order to minimize these differences and their impact on the calculated Sauerbrey mass, three different representations of the measured frequency shifts have been employed. These three different quantities are:

I. shift in the frequency of the third overtone, Δf_3;

II. average shifts in frequencies of all overtones, $\Delta f_{average}$; and

III. shift in the frequency of the overtone with the lowest dissipation energy, $\Delta f_{lowestD}$.

The plan is to find which one of these quantities gives rise to the closest value to the actual mass adsorbed, when applying in the Sauerbrey equation. The actual mass of adsorbed surfactant will be determined with the aid of the depletion method under the same experimental conditions.

In addition, the changes in the dissipation energy of the abovementioned change in the frequency have been measured.

These dissipation change quantities are as follows:

I. dissipation change of the third overtone, ΔD_3;

II. average dissipation change of the all overtones, $\Delta D_{average}$; and

III. dissipation change of the overtone with the lowest dissipation energy, ΔD_{lowest}.

The variation of Δf_3, $\Delta f_{average}$ and $\Delta f_{lowestD}$ as a function of the C12BDMAC concentrations during the adsorption from aqueous solution onto stainless steel-coated crystals at 25 °C, using the *Loop Protocols* is shown in Figure 5-23.

Figure 5-22. Change in the normalized frequency and dissipation as a function of time during the adsorption of an aqueous solution of C123BDMAC having concentration of 0.8 times the cmc onto stainless steel-coated crystal at 25 °C, pH = 6.5-7. *ΔD_n* refers to the change in the dissipation energy and *Δf_n* corresponds to the change in frequency of the nth overtone.

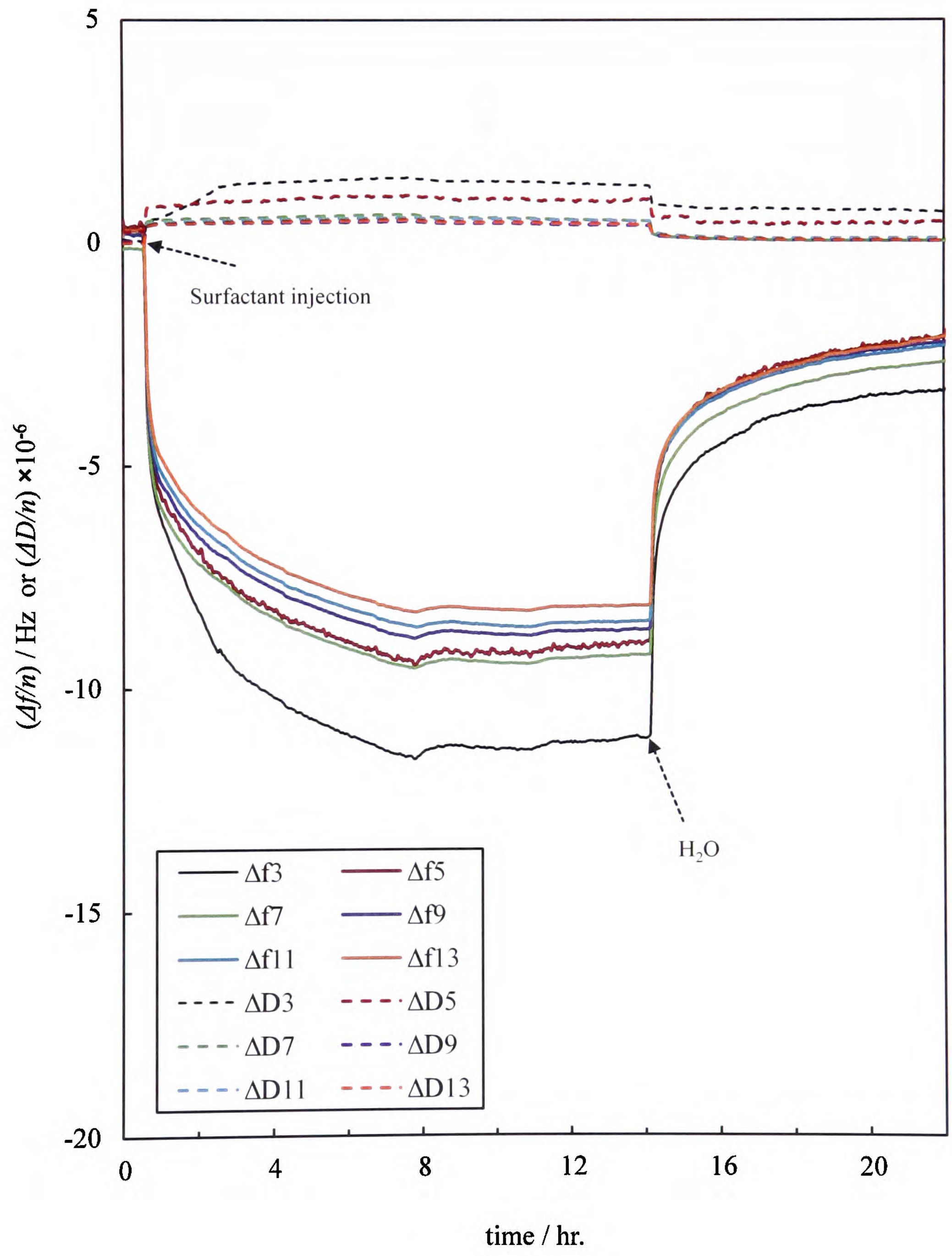

Figure 5-23. Variation of Δf_3, $\Delta f_{average}$ and $\Delta f_{lowestD}$ as a function of the normalized C12BDMAC concentration during the adsorption from aqueous solution onto stainless steel-coated crystals at 25 °C, pH = 6.5-7, using the *Loop Protocol.*

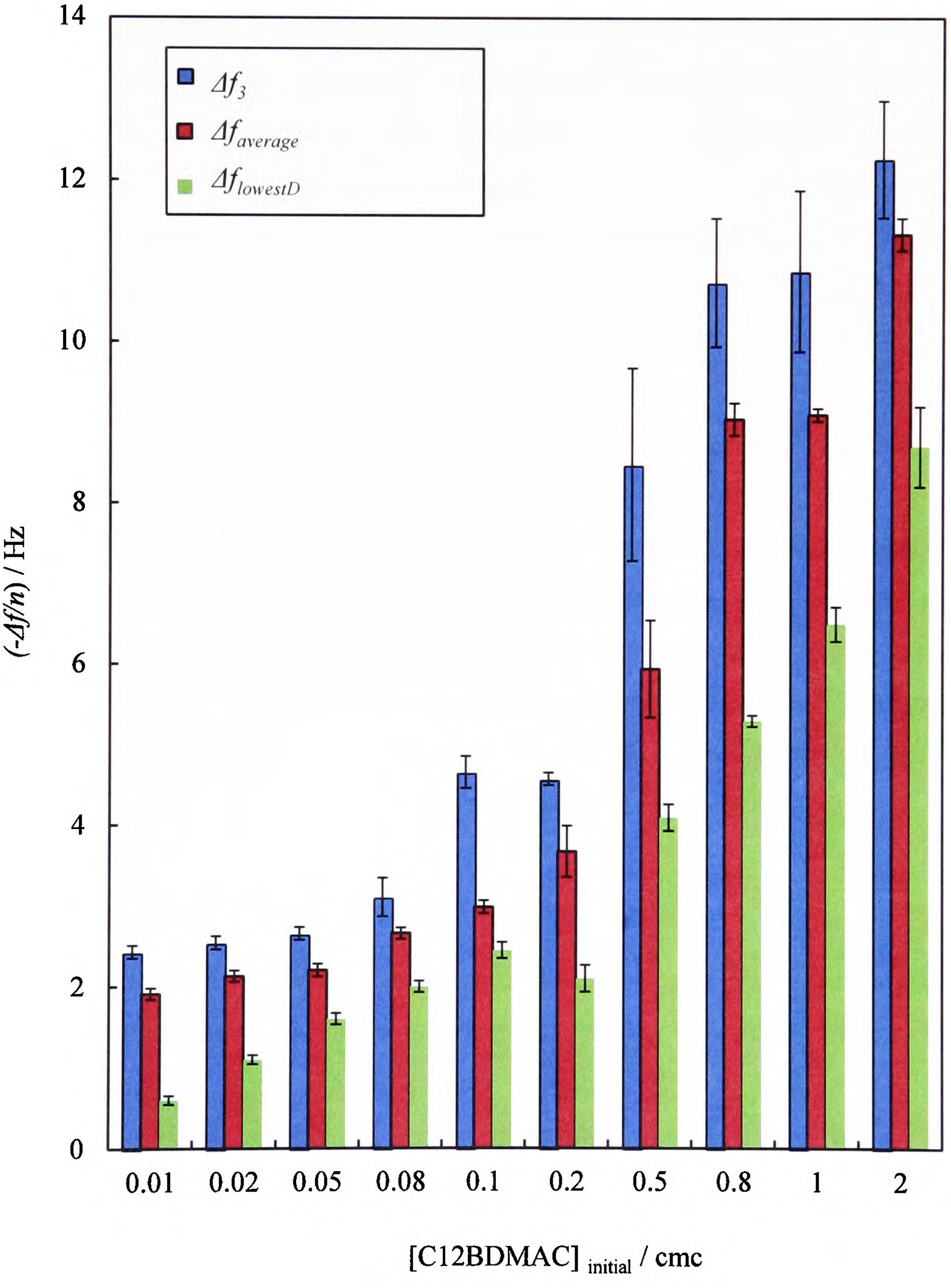

The values represented in this figure are the average of frequency changes of two independent stainless steel-coated crystals. The error bars shown refer to the standard deviation of the average value form the shift in frequency detected by the two crystals. Clearly, the magnitude of the three frequency shifts is different and these differences increase with increasing surfactant concentration. The magnitude of Δf_3 is the highest followed by $\Delta f_{average}$ and $\Delta f_{lowestD}$ over the entire investigated concentration range. For example, the measured Δf_3 at the cmc is about -11 Hz, and that for $\Delta f_{average}$ and $\Delta f_{lowestD}$ are about -9 and -6 Hz, respectively.

The corresponding variations in the dissipation energy during the adsorption of C12BDMAC from aqueous solution onto stainless steel-coated crystals are shown in Figure 5-24. The figure gives the variation of ΔD_3, $\Delta D_{average}$ and $\Delta D_{lowestD}$ as a function of the normalized C12BDMAC surfactant concentration at 25 °C. The three measured dissipation changes do not agree as shown in the figure. The values of ΔD_3 give rise to higher values than those for $\Delta D_{average}$ and $\Delta D_{lowestD}$ over the entire concentration range studied. For example, the ΔD_3 measured at the cmc is about 1.5×10^{-6}, and that for $\Delta D_{average}$ and ΔD_{lowest} are about 1.4×10^{-6} and 1.6×10^{-6}, respectively.

Recently, similar observations have been reported by Bordes *et al.* [14] during the adsorption of dicarboxylic amino acid-based surfactants onto silica surfaces using the QCM. They found that the measured frequency shifts are overtone-dependent with the values decreasing with an increase in the overtone number. Additionally, very strong dissipation changes were also reported. They attributed this behaviour to a strong contribution from the bulk effect.

5.3.2.2. Data analysis using Kanazawa's equation

As mentioned earlier the frequency change of the QCM working in liquid media is dependent on their density and viscosity and it is defined by the Kanazawa equation (Equation 1-15).

In the previous section, we have demonstrated that the measured Δf values are overtone-dependent and their magnitudes are greatly dependent on the experimental protocol employed. We have attributed this behaviour, in part, to the bulk effect caused by the change in viscosity and density of the aqueous solution. The aim of this section is to investigate the applicability of the Kanazawa equation in

Figure 5-24. Variation of ΔD_3, $\Delta D_{average}$ and ΔD_{lowest} as a function of the normalized C12BDMAC concentration during the adsorption from aqueous solution onto stainless steel-coated crystals at 25 °C, pH = 6.5-7, using the *Loop Protocol.*

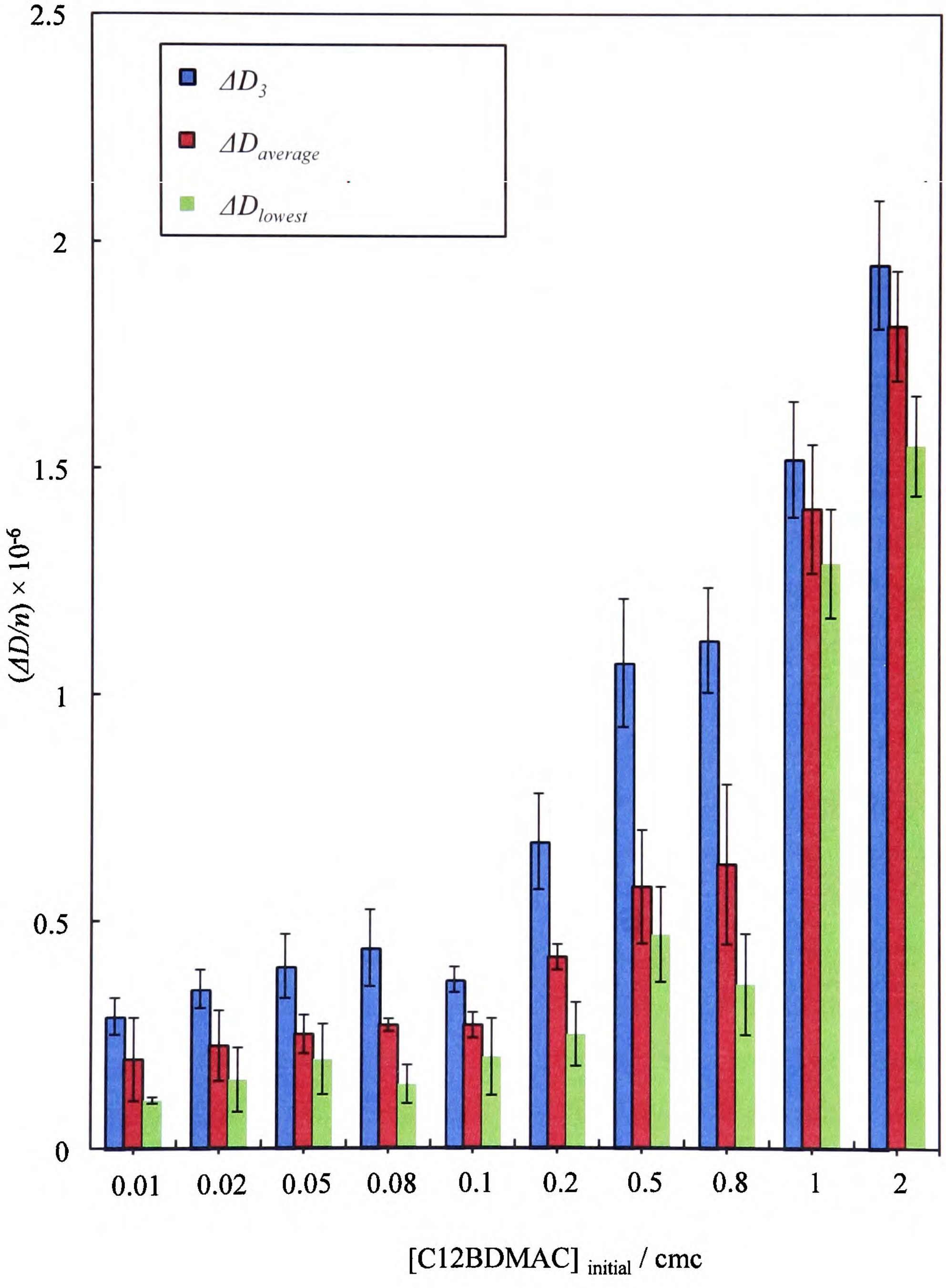

describing the measured shifts in frequency and dissipation changes during the adsorption of C12BDMAC surfactant molecules onto stainless steel-coated crystals.

When a 5 MHz QCM crystal is placed in contact with deionised water at 25 °C, the frequency should shift to a lower value by about 672 Hz according to Kanazawa's equation. This value is based on a measured viscosity of about 0.889 cp and density of 0.997 g cm^{-3} for the deionised water used in this work. In practice, a shift of about 1-2 kHz is expected, depending on the surface roughness. The effect of roughness is also related indirectly to the viscosity and density, since the hydrodynamic flow regime at the surface is altered as a result of roughness [15]. Figure 5-25 shows the change in the frequency and dissipation as a function of time on moving stainless steel-coated crystal from the air to Milli-Q water at 25 °C.

The figure shows the change in the normalized frequency and dissipation in the fundamental frequency, Δf_o, and the overtone number 3, 5 and 13. The arrow refers to the time at which Milli-Q water was introduced into the device. As shown, there is no change in the frequency and dissipation in the presence of the air. On the introduction of water into the system, the frequency and dissipation starts to change rapidly. The measured shift in the fundamental frequency, Δf_o, was about 716 Hz, which represents a good indication of the crystal surface roughness and shows a good agreement with the value calculated from the Kanazawa equation. Noticeably, the measured $\Delta f/n$ and $\Delta D/n$ values are overtone-dependent, in accordance with the Kanazawa equation.

A comparison between the experimentally determined frequencies shifts and those predicted by Kanazawa's equation, on moving the stainless steel-coated crystal from the air to Milli-Q water at 25 °C, is shown in Figure 5-26. The shifts in frequencies correspond to the normalized ones ($\Delta f/n$).

Clearly, the measured frequency changes were in good agreement with the values calculated by the Kanazawa equation. The ability of using the Kanazawa equation to predict or describe the frequency change of a stainless steel-coated crystal in aqueous solutions of different C12BDMAC concentrations has been investigated.

The expected changes in the frequency of different C12BDMAC concentrations, at 25 °C, using Kanazawa's equation have been calculated using the density and viscosity values given in Table 5-3.

Figure 5-25. Change in the normalized frequency and dissipation as a function of time on moving stainless steel-coated crystal from the air to Milli-Q water at 25 °C. ΔD_n refers to the change in the dissipation energy and Δf_n corresponds to the change in frequency of the nth overtone. The arrow refers to the time at which Milli-Q water was introduced.

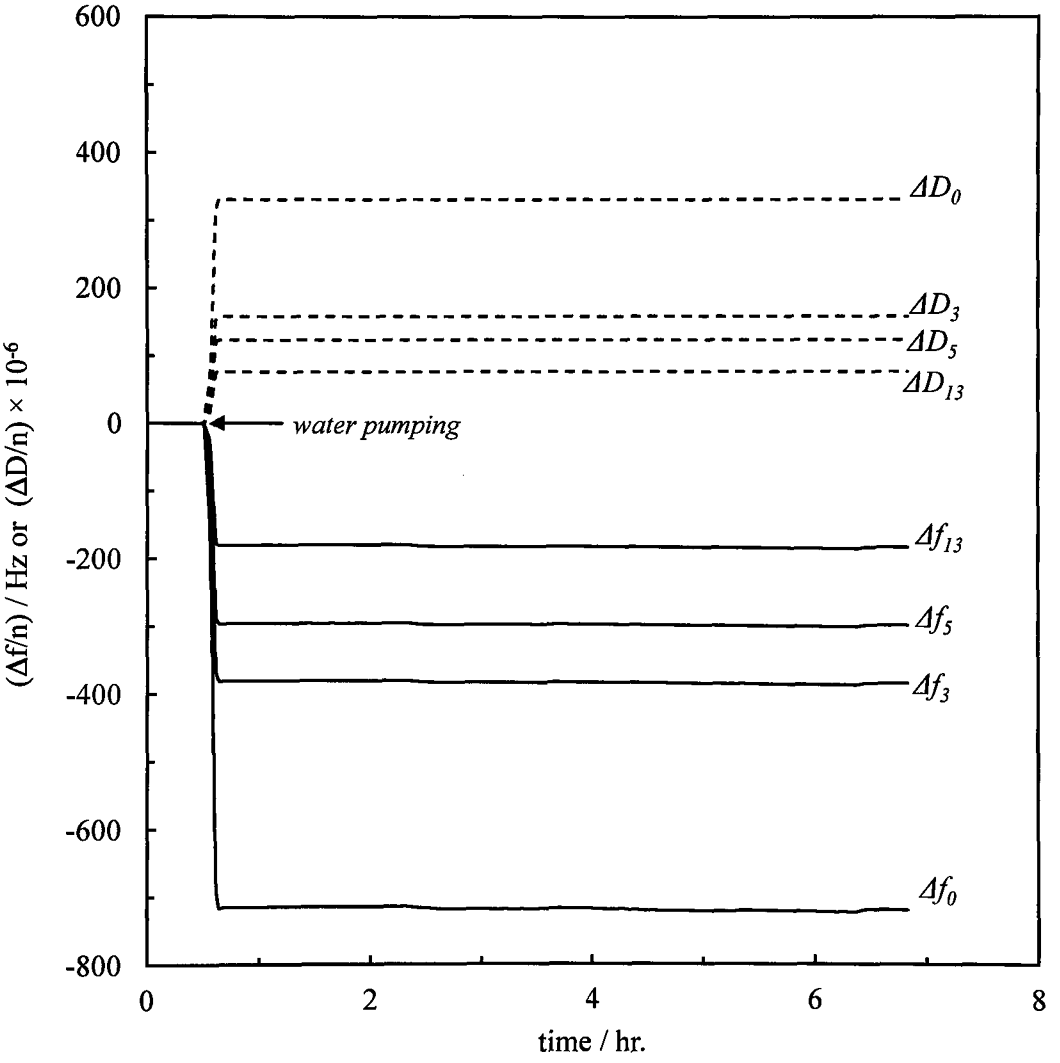

Figure 5-26. A comparison between the experimentally determined frequency shifts, at different overtones, and those predicted by Kanazawa equation on moving stainless steel coated-crystal from the air to Milli-Q water at 25 °C. Δf_n corresponds to the change in the frequency of the nth overtone.

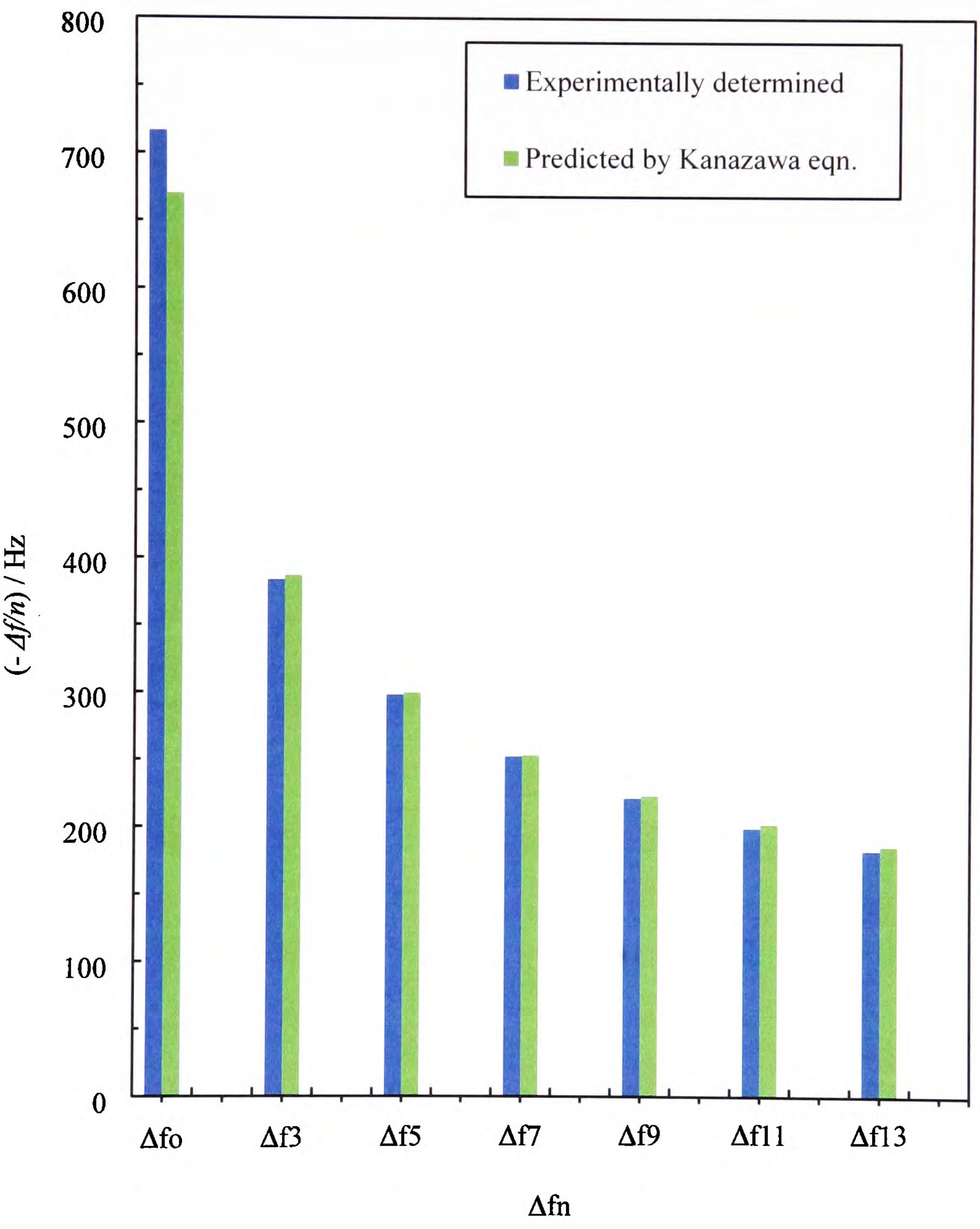

The calculated Kanazawa shifts in frequencies, compared to those determined experimentally using the three different protocols discussed earlier, are shown in Figure 5-27. The frequency change presented is the average frequency change, $\Delta f_{average}$ calculated according to equation (5-2).

Obviously, the calculated $\Delta f_{average}$ values using the Kanazawa equation show marked deviations from those values determined experimentally by the QCM. The magnitudes of the calculated $\Delta f_{average}$ are smaller than those values determined by any of the tested protocols. The magnitudes of these differences are large especially in comparison with the $\Delta f_{average}$ detected by the *Stepwise Protocol*. For example, the measured $\Delta f_{average}$ by the Kanazawa equation at the cmc is about -3.4 Hz, and that measured through the *Stepwise Protocol* is about -48 Hz while those measured by the *Batch* and *Loop Protocols* are -17 and -9 Hz, respectively. The differences between the predicted $\Delta f_{average}$ by the Kanazawa equation and those measured by the *Loop Protocol* are the smallest in magnitude.

Table 5-3. Density and viscosity values for the investigated C12BDMAC surfactant solutions at 25 °C.

[C12BDMAC] / cmc	Density / g cm^{-3}	Viscosity / cP
0.01	0.9970	0.889
0.02	0.9969	0.891
0.05	0.9969	0.893
0.08	0.9968	0.895
0.1	0.9968	0.897
0.2	0.9967	0.898
0.5	0.9966	0.898
0.8	0.9965	0.903
1	0.9964	0.910
2	0.9962	0.915

Figure 5-27. A comparison between the experimentally determined $\Delta f_{average}$ using different protocols and that predicted by Kanazawa eqn. as a function of C12BDMAC concentration at 25 °C. $\Delta f_{average}$ refers to the average frequency change of all the overtones.

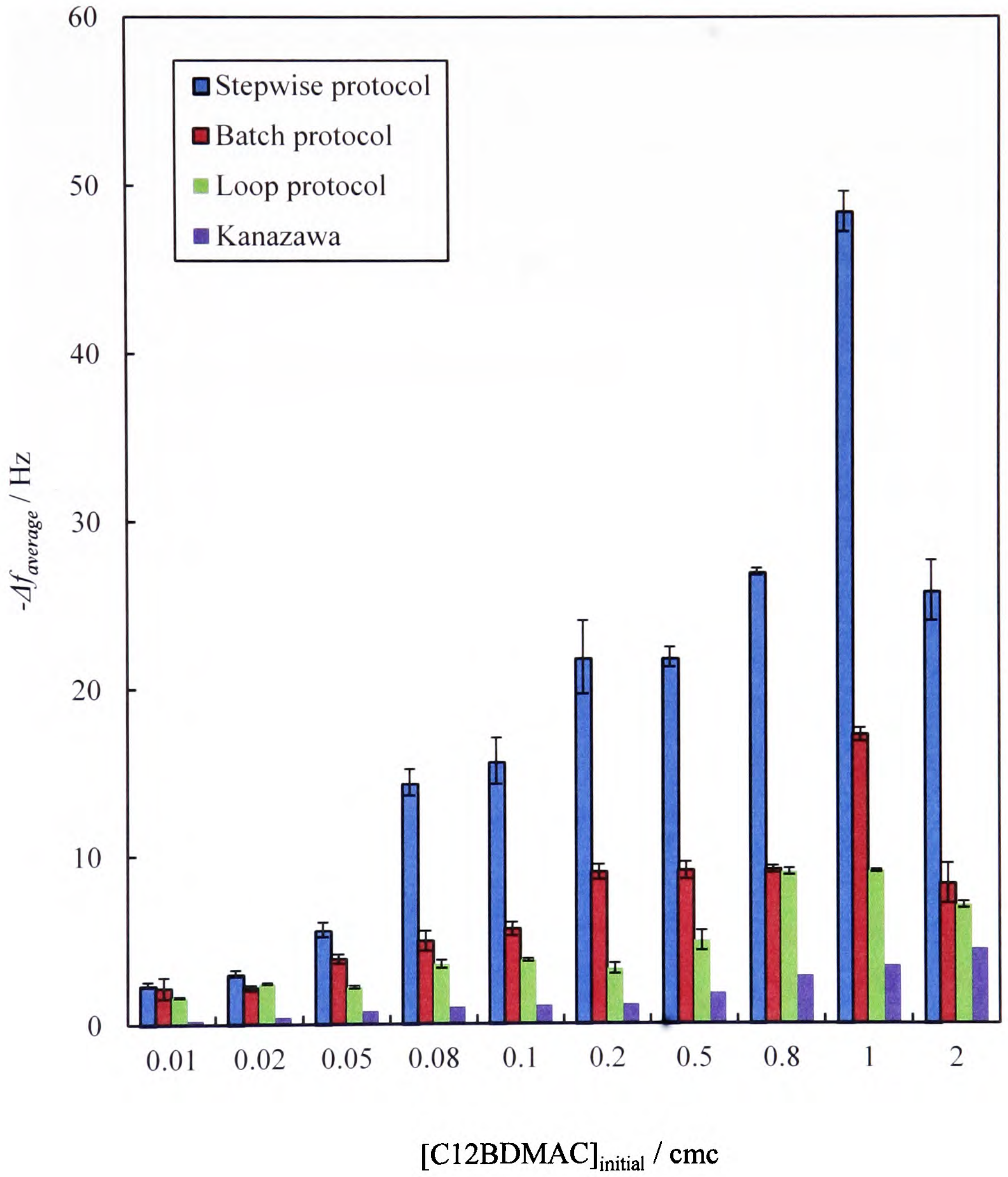

A comparison between the $\Delta f_{lowestD}$ values determined by the *Loop Protocol* with those calculated by the Kanazawa equation is shown in Figure 5-28. Clearly, the $\Delta f_{lowestD}$ values determined by the *Loop Protocol* are higher than those predicted by the Kanazawa equation. The deviation of the experimentally determined Δf from those predicted by the Kanazawa equation are quite reasonable as the latter does not take into account the contribution of the adsorbed mass to the total shift in frequency. The Kanazawa equation accounts only for Δf brought about by the change in density and viscosity of surfactant solution.

Accordingly, the measured shift in the frequency, $\Delta f_{lowestD}$, determined by employing the *Loop Protocol,* will be the one to be employed as it exhibits the smallest deviation from the shift in frequency calculated by the Kanazawa equation.

5.3.2.3. Data analysis using the Sauerbrey model

As a first step in the analysis of the QCM data, in order to convert the measured frequency shift into an adsorbed mass, the adsorbed surfactant layer will be treated as a thin rigid film. Accordingly, the Sauerbrey equation will be used to calculate the mass of surfactant adsorbed, $\Delta m_{\text{Sauerbrey}}$ from the measured Δf values. The measured shift in the frequency, $\Delta f_{lowestD}$, determined by employing the *Loop Protocol,* will be the one to be employed in the Sauerbrey equation. The calculated $\Delta m_{\text{Sauerbrey}}$, in ng cm^{-2}, values were then converted into the corresponding amount of adsorption $\Gamma_{\text{Sauerbrey}}$, in molecules nm^{-2} using the following equation:

$$\Gamma_{\text{Sauerbrey}} = \frac{\Delta m_{\text{Sauerbrey}} \times N_A \times 10^{-14}}{M_{wt}} \qquad (5\text{-}8)$$

Additionally, the adsorption of C12BDMAC surfactant molecules onto 316L stainless steel particles has been studied using the depletion method. The adsorption experiments carried out using the depletion method has been done under the same experimental conditions used for the QCM. The QCM stainless steel-coated crystal has the same composition as the 316L stainless steel particles. More details regarding the adsorption behaviour of CnBDMAC surfactants from aqueous solutions onto 316L particles using the depletion method are discussed in Chapter 6.

Figure 5-28. A comparison between the experimentally determined $\Delta f_{lowestD}$ using the *Loop Protocol* and that predicted by Kanazawa equation as a function of C12BDMAC concentration at 25 °C. $\Delta f_{lowestD}$ refers to the change in the frequency of the overtone with the lowest dissipation change.

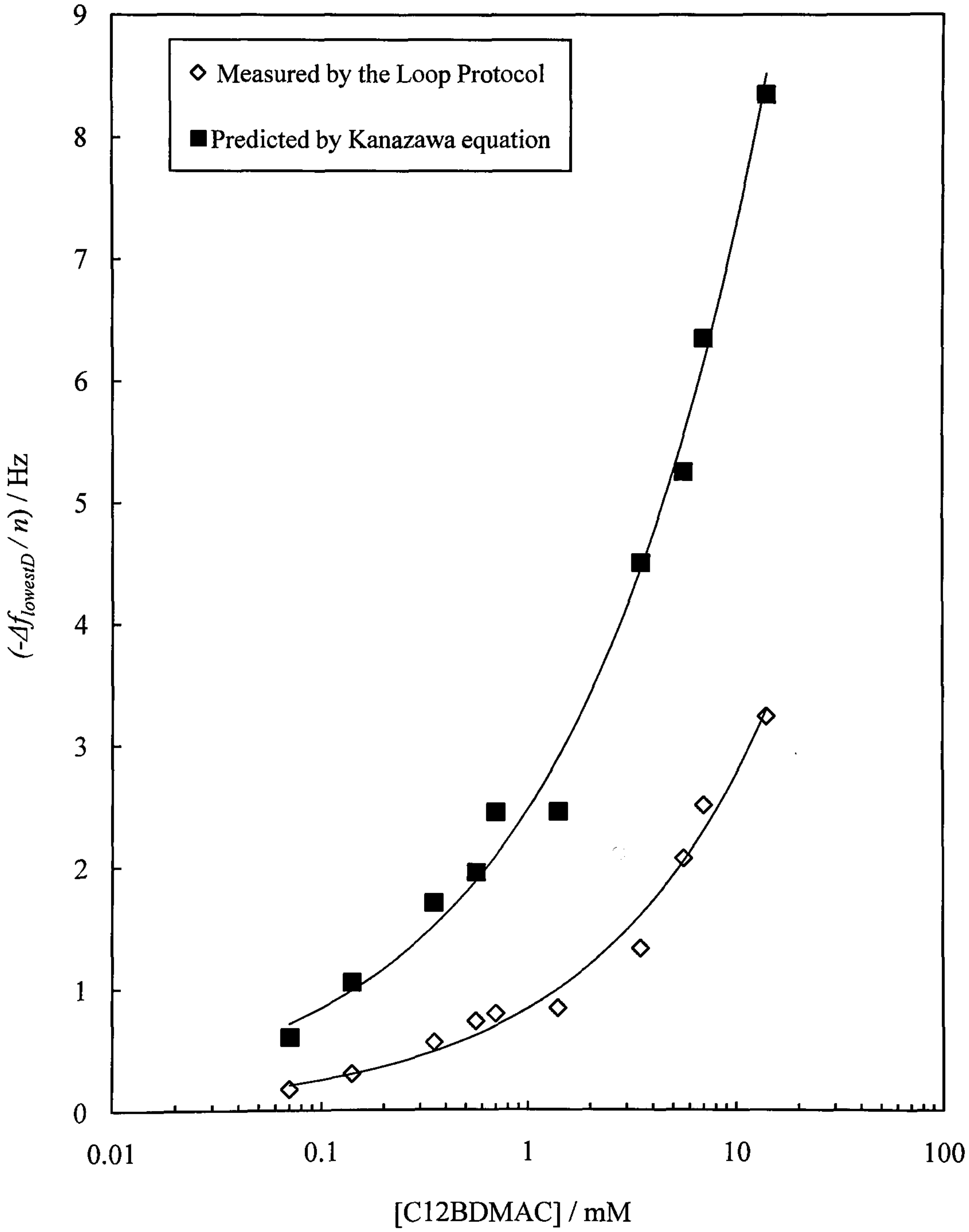

The amounts of C12BDMAC adsorbed onto 316L steel particles using the depletion method, $\Gamma_{\mathrm{Depletion}}$, were compared to those determined by the QCM, $\Gamma_{\mathrm{Sauerbrey}}$ as shown in Figure 5-29. In this figure, the solid lines represent the fitting of the experimentally determined adsorption data to the two-stage Langmuir model. The experimentally determined adsorption isotherms have been fitted to the Langmuir model for the purpose of the quantitative comparison. The assumptions of the Langmuir model are not fulfilled for the adsorption of C12BDMAC onto stainless steel surfaces. Clearly, the amounts of adsorption calculated from the measured QCM shift in the frequency give rise to higher values than those determined by the depletion method. The magnitude of these differences is significant at low concentrations and decreases at high surfactant concentrations. For example, at a surfactant concentration of about 3.5×10^{-4} M, the amount adsorbed using the QCM was determined to be about 0.53 molecules nm^{-2} while the depletion method gave rise to a value of about 0.32 molecules nm^{-2}. This represents a factor of two differences between the two-measured amounts of adsorption. At a higher surfactant concentration, for example at the cmc, the amount of C12BDMAC adsorbed using the QCM is about 2 molecules nm^{-2}, while this amount is about 1.1 molecules nm^{-2} as determined by the depletion method.

Deviations from Sauerbrey's equation have been reported in several occasions for systems involving adsorption of surfactants at solid-liquid interfaces [7, 13, 16]. The deviation from the Sauerbrey equation has been attributed to many factors as discussed earlier in section 1.5.3. In this work, the deviation from the Sauerbrey model could be mainly attributed to the bulk effect due to the change in density and viscosity of surfactant solutions. This means that the measured frequency shift is not entirely due to the adsorption of surfactant molecules and that it has an additional contribution from the solution bulk properties (viscosity and density).

5.3.2.4. Data analysis considering the effects of solution's bulk properties

In order to overcome this overestimation in the mass detected by the QCM, two approaches have been investigated. In the first, a simple approach has been used to achieve this goal by making use of the calculated shift in the frequency of different surfactant solutions using Kanazawa's equation, $\Delta f_{lowestK}$. The calculated $\Delta f_{lowestK}$ corresponds to the change in the frequency with the lowest dissipation

Figure 5-29. A comparison between the amounts of C12BDMAC adsorbed onto stainless steel surfaces determined experimentally by the QCM and the Depletion method. The measured $\Delta f_{lowestD}$ values were applied in the Sauerbrey equation to determine the amounts of surfactant adsorbed.

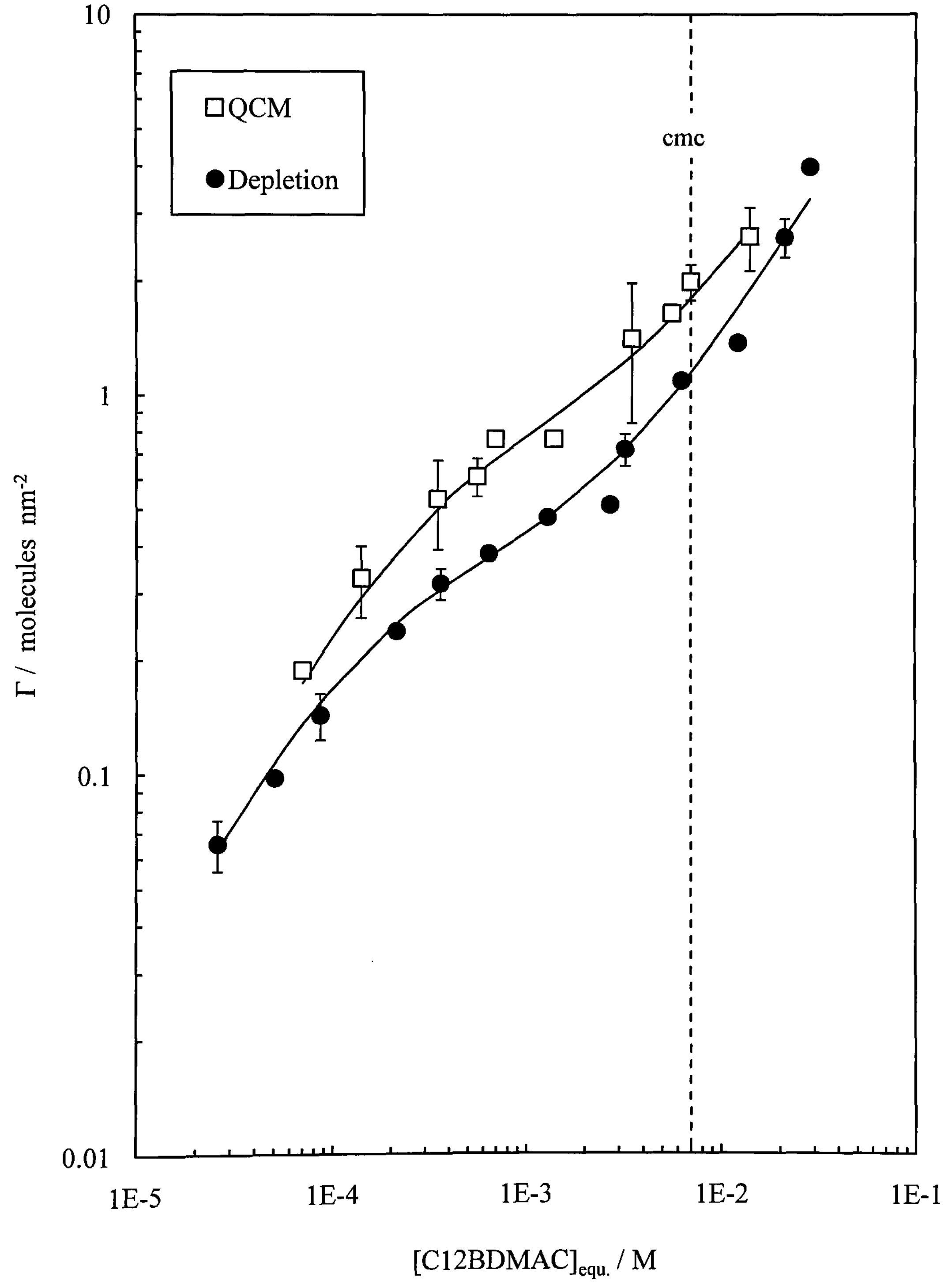

change, which for the Kanazawa equation is the change in the frequency of 13th overtone.

The calculated shift in frequency using Kanazawa's equation for water is subtracted from the calculated shift in frequency using Kanazawa's equation for the aqueous surfactant solution, $\Delta f_{lowestK}$. This frequency shift is then subtracted from the experimental measured frequency shift, $\Delta f_{lowestD}$ and a frequency shift corrected for the changes in bulk properties, *corrected* $\Delta f_{lowestD}$ is obtained. Therefore, the *corrected* $\Delta f_{lowestD}$ is given by the following equation:

$$corrected\ \Delta f_{lowestD} = \text{measured } \Delta f_{lowestD} - (\text{water } \Delta f_{lowestK} - \text{surfactant } \Delta f_{lowestK}) \tag{5-9}$$

where water $\Delta f_{lowestK}$ refers to the calculated changes in the frequency with the lowest dissipation change (13th overtone) for water and surfactant solution concentrations using the Kanazawa equation, respectively.

The corrected value (*corrected* $\Delta f_{lowestD}$) is then applied in the Sauerbrey equation to calculate the corrected mass. Adsorption isotherms for C12BDMAC adsorbed onto a stainless solid surface using this correction procedure compared to those determined using the depletion method are shown in Figure 5-30. Clearly, the figure demonstrates the success of the correction procedures employed in minimizing the differences between the adsorption isotherms for C12BDMAC onto stainless steel surfaces determined using the QCM and the depletion method. A similar correction procedure for the bulk properties have used by several researchers to overcome the overestimated mass detected by the QCM [17, 18].

5.3.2.5. Data analysis using the calibration method

The second approach, used to overcome the excess mass detected by the QCM, was to calibrate the QCM using the amounts of surfactant adsorbed as determined by the depletion method. In the first approach, the amounts of surfactant adsorbed, $\Delta m_{depletion}$ in ng cm^{-2} units, at the same concentration used in the QCM measurements, were calculated using the two-stage Langmuir fitting parameters employed earlier to fit the adsorption isotherms determined by the depletion method.

Figure 5-30. A comparison between the amounts of C12BDMAC adsorbed onto stainless steel surfaces determined by the QCM and the Depletion method. The amounts of adsorptions presented were calculated using *corrected* $\Delta f_{lowestD}$ values in the Sauerbrey equation.

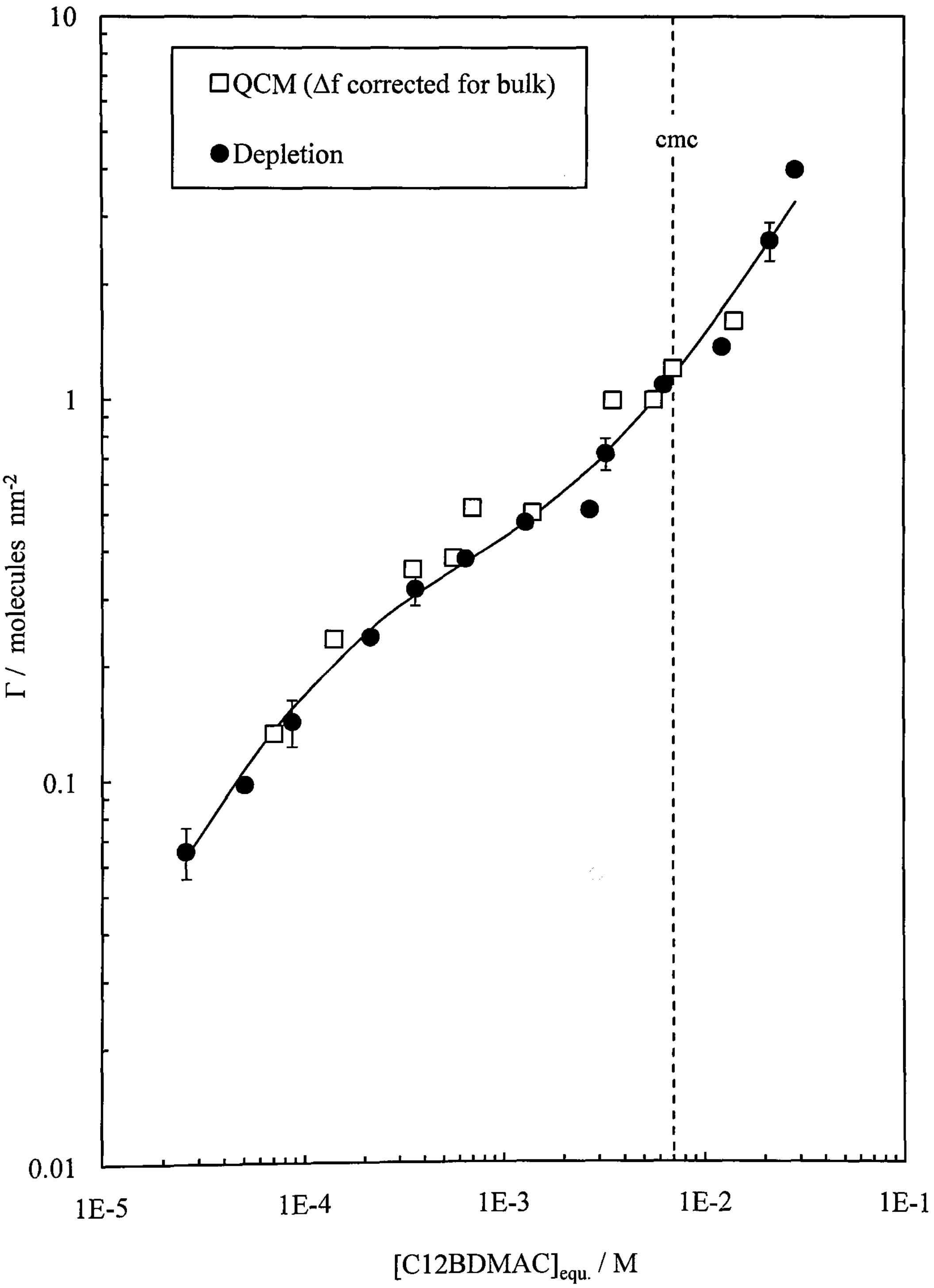

Then, these calculated amounts of surfactant adsorption have been represented graphically as a function of the $\Delta f_{lowestD}$ values measured by the QCM at the corresponding surfactant concentrations as shown in Figure 5-31 in comparison to those calculated by Sauerbrey equation, $\Delta m_{\mathrm{Sauerbrey}}$. As shown in this figure, the calculated amounts of adsorbed surfactant, using the depletion method, seem to vary linearly with the measured $\Delta f_{lowestD}$. Accordingly, the relation between the calculated amounts of adsorbed surfactant, using the depletion, and the measured $\Delta f_{lowestD}$ could be described by the following equation:

$$\Delta m_{depletion}\ (\mathrm{ng\ cm^{-2}}) = 10.7\ (\mathrm{ng\ cm^{-2}\ Hz^{-1}}) \times \Delta f_{lowest}\ (\mathrm{Hz}) \qquad (5\text{-}10)$$

On the other hand, according to Sauerbrey equation (5-2), the relation between the measured Δf_{lowest} and the amounts of surfactant adsorbed is given as follows:

$$\Delta m_{Sauerbrey}\ (\mathrm{ng\ cm^{-2}}) = 17.7\ (\mathrm{ng\ cm^{-2}\ Hz^{-1}}) \times \Delta f_{lowest}\ (\mathrm{Hz}) \qquad (5\text{-}11)$$

The value of 17.7 refers to the constant, C in the Sauerbrey equation for a quartz crystal with a fundamental frequency, f_o, of 5 MHz, oscillating in air. Accordingly, one would expect that the value of this constant would be different, if the crystal is oscillating in liquid. This means that, the Sauerbrey equation constant, C, needs to be experimentally determined (or calibrated) if it is going to be applied for liquids.

Based on equations (5-10) and (5-11), the calibration factor, CF, could be defined as the ratio of the slopes of these two equations (10.7/17.7= 0.6). Therefore, in order to correct the amounts of surfactant adsorbed, calculated from the measured Δf_{lowest} values, using the Sauerbrey equation, these values should be multiplied by the determined calibration factor (0.6).

Alternatively, we could simply multiply the measured $\Delta f_{lowestD}$ values by the value of calibrated Sauerbrey's constant (10.7) in aqueous solutions instead of the value of 17.7.

Figure 5-31. A comparison between the amounts of C12BDMAC adsorbed onto stainless steel surfaces determined by the QCM and the Depletion method as a function of the measured $\Delta f_{lowestD}$ values. The amounts of adsorptions presented were calculated using $\Delta f_{lowestD}$ values in the Sauerbrey equation.

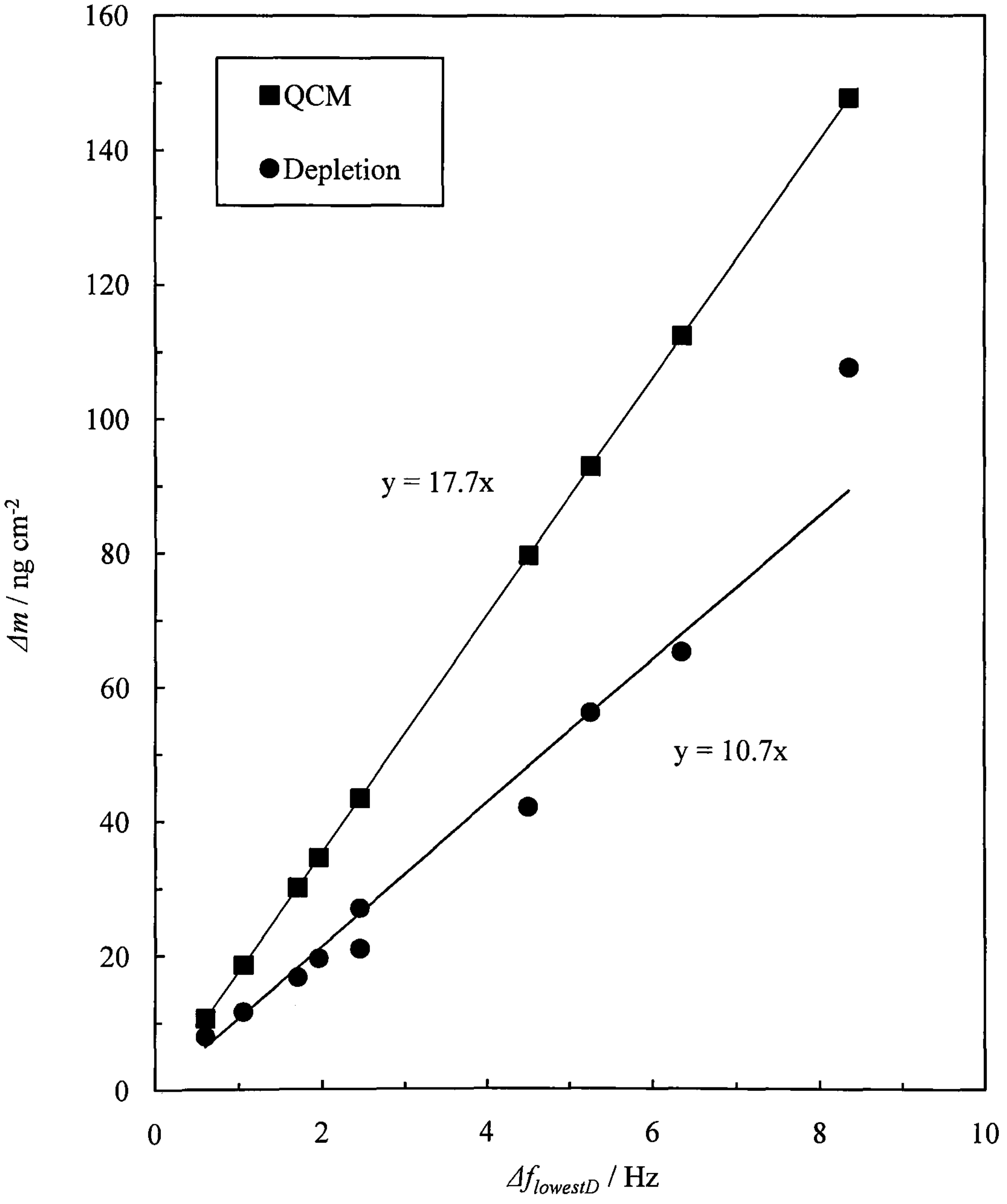

Accordingly, equation (5-10) will change into equation (5-11), the latter equation enables us to calculate the corrected $\Delta m_{Sauerbrey}$ values.

$$corrected\,\Delta m_{Sauerbrey}\ (\text{ng cm}^{-2}) = 10.7\ (\text{ng cm}^{-2}\ \text{Hz}^{-1}) \times \Delta f_{lowestD}\ (\text{Hz}) \qquad (5\text{-}12)$$

Figure 5-32 shows the corrected adsorption isotherms for C12BDMAC, determined using the calibrated Sauerbrey equation constant (10.7), compared to that determined using the depletion method. Clearly, the two-adsorption isotherms converge over the entire surfactant concentration range. This in turn demonstrates the success of the proposed correction procedures in overcoming the overestimation of the adsorbed amount, calculated using the Sauerbrey equation.

5.3.3. Discussion

The experimental procedures used for studying the adsorption behaviour of CnBDMAC surfactant molecules using the QCM have been proved to have a marked influence on both of the measured frequency shifts and dissipation energy changes. It has been shown that the average frequency shift measured using the stepwise protocol gives rise to the highest values followed by those measured using the *Batch* and *Loop* protocols. The average frequency and dissipation values measured by the *Batch* and *Loop* protocols are relatively close to each other. The magnitude of the dissipation change measured using the *Loop* protocols was found to be the smallest compared to the other protocols. The higher frequency shifts measured by the *Stepwise* protocol could be attributed to a frequency drift by the QCM device during the measurements. According to the manufacturer, a clean 5 MHz crystal sensor operating in a liquid at 25 °C drifts by about 1.5 Hz hour^{-1} in the frequency values and by 2×10^{-7} per hour in the dissipation values when measured at 15 MHz harmonic (3rd overtone) [4].

A similar results result has been reported by Lundgren *et al.* [18] during the adsorption of the unsaturated fatty acid linolenic acid from non-aqueous solution onto stainless steel-coated crystals using the QCM. They found that the measured frequency changes obtained by increasing the concentration stepwisely to differ from those obtained by injecting one given concentration per experiment by about 8%.

Figure 5-32. Adsorption isotherm for C12BDMAC onto stainless steel surfaces form aqueous solutions at 25 °C, determined using the calibrated Sauerbrey equation constant (10.7 ng cm^{-2} Hz^{-1}), compared to that determined using the depletion method. The vertical dashed line refers to the cmc of surfactant in water (7 mM).

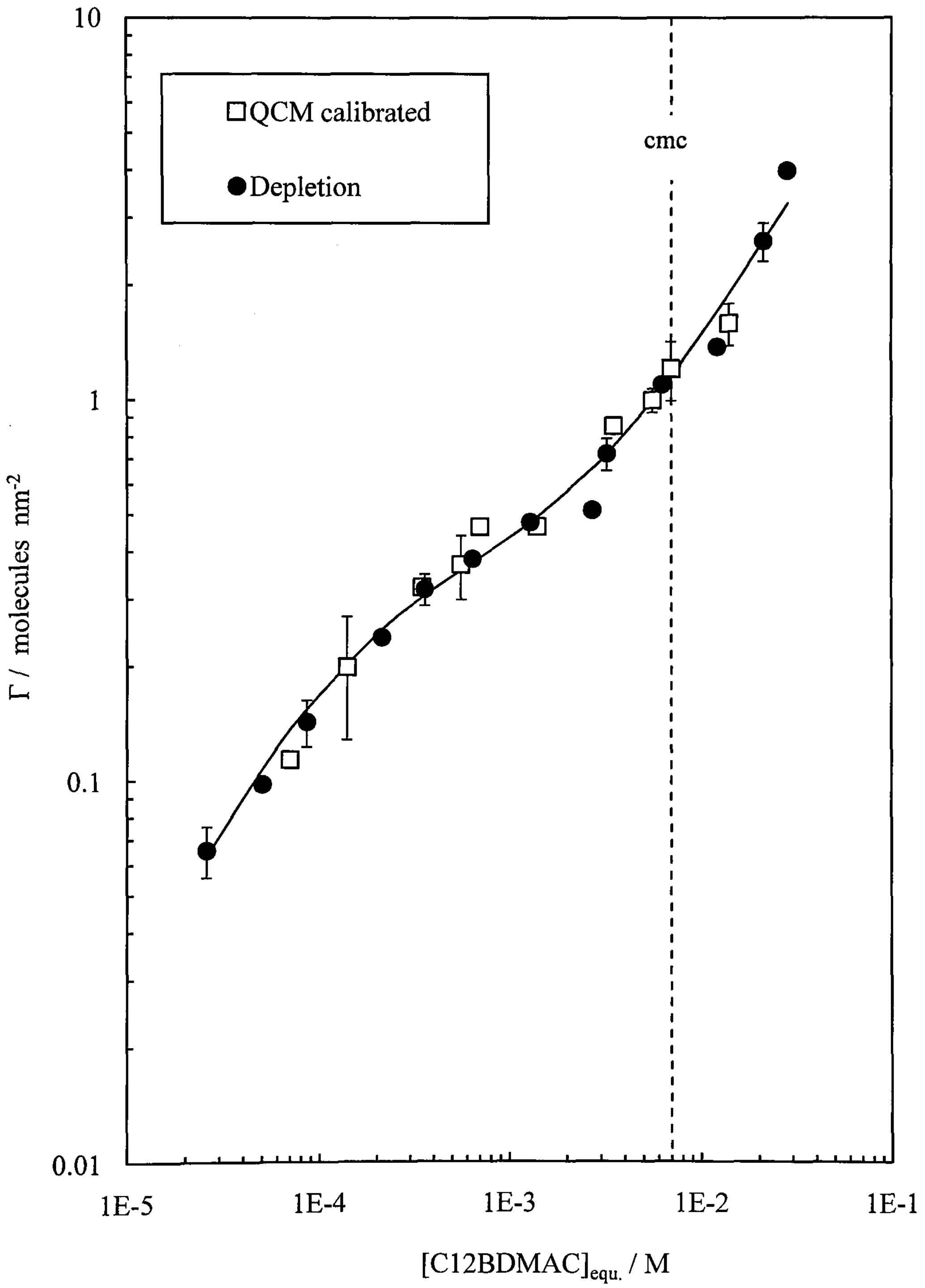

The measured $\Delta D_{average}$ by the *Loop* protocol was found to be less than than1×10^{-6} up to surfactant concentrations of about 0.8 times the cmc. This indicates that QCM senses the adsorbed surfactant as a rigid mass rather than a viscoelastic film. Accordingly, it is recommended to use the *Loop* protocol to carry out the adsorption measurements as it enables us to apply the Sauerbrey equation to calculate the change in mass of surfactant adsorbed from the corresponding frequency changes. However, the normalized frequency shift of different overtones measured using the Loop protocol show noticeable variations in magnitude. The magnitude of Δf_3 was the highest followed by $\Delta f_{average}$ and $\Delta f_{lowestD}$ over the entire concentration range investigated. The same observation applies for the measured dissipation changes.

The fact that the measured normalized Δf vary with the overtone numbers indicates that solution bulk properties and other factors influence the oscillation of the crystal. The ability of Kanazawa equation to describe the frequency change of a stainless steel coated crystal in aqueous solutions of CnBDMAC surfactant molecules has been investigated. The calculated $\Delta f_{average}$ values using the Kanazawa equation showed marked deviations from those values determined experimentally by the QCM. The Kanazawa equation assumes that the fluid is completely coupled to the oscillatory motion of the crystal and the surface of the crystal is smooth. Experimentally, we found that the measured Δf values agree with those calculated using the Kanazawa equation (1.15), when the QCM crystal was moved from air to water. This indicates that the liquid couples to the oscillating surface without slip and that the crystal is sufficiently smooth so that no significant amount of liquid is trapped in cavities. However, the interaction with the surfactant solutions would be different due to the contribution of the mass of surfactant adsorbed on the oscillation of the crystal.

The analysis of the measured frequency changes using the simple Sauerbrey model results in an overestimation in the mass detected by the QCM as shown by the adsorption measurements carried out using the depletion method. Accordingly, a correction procedure or another model relating the frequency change to the mass adsorbed is needed to work out the actual mass adsorbed on the crystal.

QCM is very sensitive not only to mass changes at the crystal solution interface, or density and viscosity changes, but also to temperature changes and surface roughness as well. Accordingly, the overall frequency change may be expressed as follows [15]:

$$\Delta f = \Delta f_m + \Delta f_p + \Delta f_{\eta\rho} + \Delta f_r + \Delta f_T \tag{5-13}$$

where Δf_m is the mass effect caused by the added mass which is attached to the surface, Δf_p is the compression effect caused by changes of pressure of the fluid in contact with the quartz, $\Delta f_{\eta\rho}$ is the density and viscosity effect (which is referred to as the bulk effect), Δf_T is the temperature effect and Δf_r is the roughness effect.

Additionally, in the QCM measurements, water (or any other liquid or solvent) may couple as an additional mass via direct hydration, viscous drag or entrapment in cavities in the adsorbed film. This means that the layer is essentially detected as a viscoelastic film composed of surfactant molecules and the coupled water. The typical amount of coupled water has been shown to vary significantly depending on the nature of the film, with mass-uptake estimations between a factor of 1.5 and 4 times larger than the molar mass [19, 20].

In the current experiments the effects of pressure, temperature and roughness seem to be negligible as the experiments are carried out in a thermostatted flow cell at fixed temperature using a constant flow rate on the same crystal. This leaves us with the shift in frequency that may result due to the changes in density and viscosity (bulk effects) of tested solutions. A simple approach has been adapted, using Kanazawa's equation, to calculate the effect of changes in density and viscosity. The correction procedures employed have been shown to be effective in minimizing the differences between the adsorption isotherms for C12BDMAC onto stainless steel surfaces determined using the QCM and that determined by the depletion method.

The correction procedures used for the bulk properties have been used by several researchers to overcome the overestimated mass detected by the QCM [17, 18]. Lundgren *et al.* [18] have employed the same procedures to correct the measured shift in the frequency during the adsorption of the unsaturated fatty acid linolenic acid from non-aqueous solution onto stainless steel-coated crystals for the changes in bulk properties. They reported that above a concentration of 0.1 wt.% of the fatty acid, it is vital to make corrections for changes in bulk viscosity and density for these systems. It is not clear which overtone has been used by Lundgren for applying correction procedures.

Another approach has been investigated to overcome the excess mass detected by the QCM, namely the calibration method. This method gives rise to better results than the correction method for the bulk changes. As mentioned earlier, the measured frequency change Δf, does not depend only on the mass of surfactant adsorbed and the bulk properties of the solution, also it depends on the crystal roughness and the viscoelastic properties of the adsorbed surfactant molecules. The calibration method provides a reasonable approach to all the other interfering factors that affect the measured shift in the frequency.

Several authors [21-23] have reported that the calibration method as an effective technique for correcting the adsorbed mass calculated by the Suerabary equation. Caruso *et al.* [21] investigated the adsorption of a series of polyethylene glycol monododecyl ethers ($C_{12}E_n$, n = 3, 5, and 8) from benzene onto silica surfaces using the QCM and depletion methods. Corrected frequency shifts for $C_{12}E_3$ and $C_{12}E_5$, adsorbed onto silica crystals yielded calibration factors of 1.06 and 1.05 for the QCM. This indicated that the resonance frequency shifts in benzene are as predicted by the Sauerbrey equation for $C_{12}E_3$ and $C_{12}E_5$ surfactant molecules. For $C_{12}E_8$ adsorbed onto silica, however, a calibration factor of 4.8 was obtained which indicates the failure of the Sauerbrey equation for these surfactant molecules.

Despite the success of the calibration method in correcting the overestimated mass resulted from applying the Sauerbrey equation, it suffers from a serious drawback as the determined calibration factor (CF) is specific and limited for the system to which the correction has been made. So if for example, we used different values for the measured Δf instead of using Δf_{lowest} values or if, we employ a different experimental protocol instead of the *Loop Protocol* used in this system, one should expect that the CF value would be different.

5.4. SUMMARY AND CONCLUSION

The adsorption behaviour of CnBDMAC surfactant molecules has been studied as a function of the surfactant chain length, temperature and electrolyte concentration using the QCM. For the best of our knowledge, no studies concerning the adsorption of these surfactant molecules have been reported in the literature. The key and new findings within this study are summarized below.

I. The adsorption isotherms for C10, C12, C14 and C16BDMAC surfactants onto stainless steel-coated crystals give rise to a classical Langmuir-type isotherm, with a maximum near to the cmc for C10, C12 and C14BDMAC.The short chains C10 and C12BDMAC give rise to the highest degree of adsorption compared to that for the long chain C14 and C16BDMAC surfactants.

II. At low surfactant concentration, the temperature rise has no effect on the amount of surfactant being adsorbed on the stainless steel surfaces for C10BDMAC. At moderate and high surfactant concentration, an increase in temperature results in a significant increase in the amount of C16BDMAC adsorbed. On the other hand, the increase in the temperature has an adverse effect on the amount of C10BDAC adsorbed onto the steel.

III. The amount of surfactant adsorbed is higher in a brine solution compared to that in water over the entire concentration range investigated. The electrolyte addition has a considerable influence on the extent of adsorption similar to increasing the hydrocarbon chain length.

IV. The QCM techniques provides an effective, easy-to-setup and a quick in-situ monitoring method for studying qualitatively the adsorption behaviour of surfactants at the solid-liquid interface.

V. The optimization of the QCM for studying the adsorption behaviour of the cationic surfactant alkylbenzyldimethylammonium chlorides at the solid-liquid interface is one of the main insights in the current chapte, which has been investigated. The experimental procedures used for studying the adsorption behaviour of CnBDMAC surfactant molecules using the QCM have been proved to have a marked influence on both of the measured frequency shift and dissipation energy changes. The average frequency shift detected by the *Stepwise* protocol gave rise to the highest values followed by those for the *Batch* and *Loop* protocols over all the studied concentration range. The magnitudes of these differences are small at low surfactant concentrations and increases gradually with increasing surfactant concentrations. The same conclusions apply also for the measured dissipation changes by the three protocols.

VI. The measured normalized frequency shifts were found to vary with the overtone number. This indicates that the adsorbed surfactant layer is not rigid. The Kanazawa equation failed in describing the measured frequency shifts during the adsorption of C12BDMAC surfactant molecules onto stainless steel-coated crystals. This is because that Δf values predicted by the Kanazawa equation do not take in account the contribution of the adsorbed mass to the total shift in frequency. The Kanazawa equation accounts only for Δf brought about only by the change in density and viscosity of surfactant solution. The degree of adsorption calculated from the vales of the measured QCM shift in the frequency, using the Sauerbrey equation, were higher than those determined by the depletion method. The deviation from the Sauerbrey model could be mainly attributed to the bulk effect, which occurs due to the changes in density and viscosity of surfactant solutions.

5.5. REFERENCES

1. A. A. Atia and M. M. Saleh, *J. Appl. Electrochem.*, **V33**, 171 (2003).
2. A. V. Sineva, A. M. Parfenova and A. A. Fedorova, *Colloids Surf. A*, **306**, 68 (2007).
3. D. G. Hall, *J. Chem. Soc. Farad. T 1*, **76**, 386 (1980).
4. J. E. Gebhardt and D. W. Fuerstenau, *J. Colloid Interface Sci.*, **101**, 278 (1984).
5. S. Paria and K. C. Khilar, *Adv. Colloid Interface Sci.*, **110**, 75 (2004).
6. S. C. Biswas and D. K. Chattoraj, *J. Colloid Interface Sci.*, **205**, 12 (1998).
7. M. Knag, J. Sjoblom, G. Oye and E. Gulbrandsen, *Colloids Surf. A*, **250**, 269 (2004).
8. C. Hodges and S. Biggs, *Adv. Powder Technol.*, **18**, 615 (2007).
9. R. Atkin, V. S. J. Craig, E. J. Wanless and S. Biggs, *Adv. Colloid Interface Sci.*, **103**, 219 (2003).
10. P. Somasundaran, T. W. Healy and D. W. Fuerstenau, *J. Phys. Chem.*, **68**, 3562 (1964).
11. A. M. Gaudin and D. W. Fuerstenau, *Transactions AIME*, **202**, 958 (1955).
12. L. K. Koopal, E. M. Lee and M. R. Bohmer, *J. Colloid Interface Sci.*, **170**, 85 (1995).
13. C. Gutig, B. P. Grady and A. Striolo, *Langmuir*, **24**, 4806 (2008).
14. R. Bordes, J. r. Tropsch and K. Holmberg, *Langmuir*, **26**, 10935 (2010).
15. V. Tsionsky, L. Daikhin, M. Urbakh and E. Gileadi, in *Electroanalytical Chemistry*, A. J. Bard, ed., Marcel Dekker Inc, New York (2004).
16. L. Goual, G. Horvath-Szabo, J. H. Masliyah and Z. Xu, *Langmuir*, **21**, 8278 (2005).
17. D. Y. Ryu and M. L. Free, *J. Colloid Interface Sci.*, **264**, 402 (2003).
18. S. M. Lundgren, K. Persson, B. Kronberg and P. M. Claesson, *Tribol. Lett.*, **22**, 15 (2006).

19. F. Hook, B. Kasemo, T. Nylander, C. Fant, K. Sott and H. Elwing, *Anal. Chem.*, **73**, 5796 (2001).

20. F. Caruso, D. N. Furlong and P. Kingshott, *J. Colloid Interface Sci.*, **186**, 129 (1997).

21. F. Caruso, H. A. Rinia and D. N. Furlong, *Langmuir*, **12**, 2145 (1996).

22. D. Shen, F. Wang, Q. Kang and D. Yang, *Sen Trans J.*, **40**, 152 (2004).

23. M. Laatikainen and M. Lindström, *J. Colloid Interface Sci.*, **125**, 610 (1988).

CHAPTER 6

Chapter 6

ADSORPTION OF ALKYLBENZYLDIMETHYLAMMONIUM CHLORIDES AT THE STEEL-WATER INTERFACE USING THE DEPLETION METHOD

6.1. INTRODUCTION

The efficiency of a corrosion inhibitor to prevent mild steel corrosion is directly related to the amount and structure of the adsorbed corrosion inhibitor. Therefore, it is crucial to understand the adsorption behaviour of these compounds onto the mild steel surface to optimize their use and efficiency. Based on adsorption isotherms, the amount of surfactant adsorbed per unit mass or unit area of the solid adsorbent at a given temperature and consequently, the effectiveness with which the surfactant is adsorbed could be determined. In this chapter, the adsorption characteristics of alkylbenzyldimethylammonium chlorides corrosion inhibitors onto mild steel (C1018) and stainless steel (316L) particles, from aqueous solution under aerated conditions, will be determined and evaluated using the depletion method. Furthermore, the change in surface charge of steel particles in the presence of alkylbenzyldimethylammonium chlorides solutions will be investigated. The depletion method, has been used to study the adsorption of CnBDMAC from aqueous solution onto a stainless steel powder as the determined adsorption isotherms using the QCM were found to overestimate the adsorbed amount calculated using Sauerbrey's equation as shown previously in *Chapter 5.* A 316L stainless-steel-type powder has been used for these experiments as it has a comparable composition to that of the crystals used in the QCM experiments.

In this chapter, we are going to investigate the influence of chain length, temperature and brine addition on the adsorption characteristics of alkylbenzyldimethylammonium chloride from aqueous solution onto mild steel.

6.2. EFFECT OF SURFACTANT CHAIN LENGTH

The hydrocarbon chain length is of critical importance in determining the adsorption behaviour of a surfactant molecule. Goloub and Koopal [1] reported that, for the adsorption of an homologous alkylpyridinium chloride series of surfactants from aqueous solutions onto amorphous silica, increasing the chain length of the monomer by four methylene units, from C12 to C16, lowers the concentration at which the characteristic features of the isotherm occur by approximately an order of magnitude. Adsorption isotherms determined for the homologous alkyldimethylbenzylammonium chlorides onto C1018 mild steel and 316L stainless steel powder, from aqueous solutions at 25 °C, are given in Figure 6-1 and Figure 6-2, respectively. In these figures, the amount of surfactant adsorbed (Γ), in molecules/nm^2, is plotted as a function of the equilibrium *non-adsorbed* surfactant concentration $[\mathrm{CnBDMAC}]_{eq}$, in M units, on a logarithmic scale. In addition, variation of zeta-potential (ζ) of C1018 mild steel particles as a function of C12, C14 and C16BDMAC equilibrium concentration at 25 °C is shown in Figure 6-3. The adsorption isotherms were fitted to a two-stage Langmuir model, shown in the figures as solid lines.

The Langmuir model is one of the most commonly used adsorption models. However, its strict application is only valid, if the adsorbent surface is homogeneous, if all adsorbed species interact only with a site and not with each other, and if adsorption is thus limited to a monolayer [2]. These restrictions limit the applicability of this model to a few systems, whose surface is energetically homogeneous and consequently flat, and the adsorbates are retained without interactions among them. Despite these limitations, the Langmuir model has proved to be a useful tool to study a great variety of systems [2, 3].

Figure 6-1. Adsorption isotherms of C10, C12, C14 and C16BDMAC from aqueous solutions onto C1018 mild steel at 25 °C using the depletion method at pH = 8-9. The vertical dashed lines represent the cmc. The solid lines represent the two-stage Langmuir model fits.

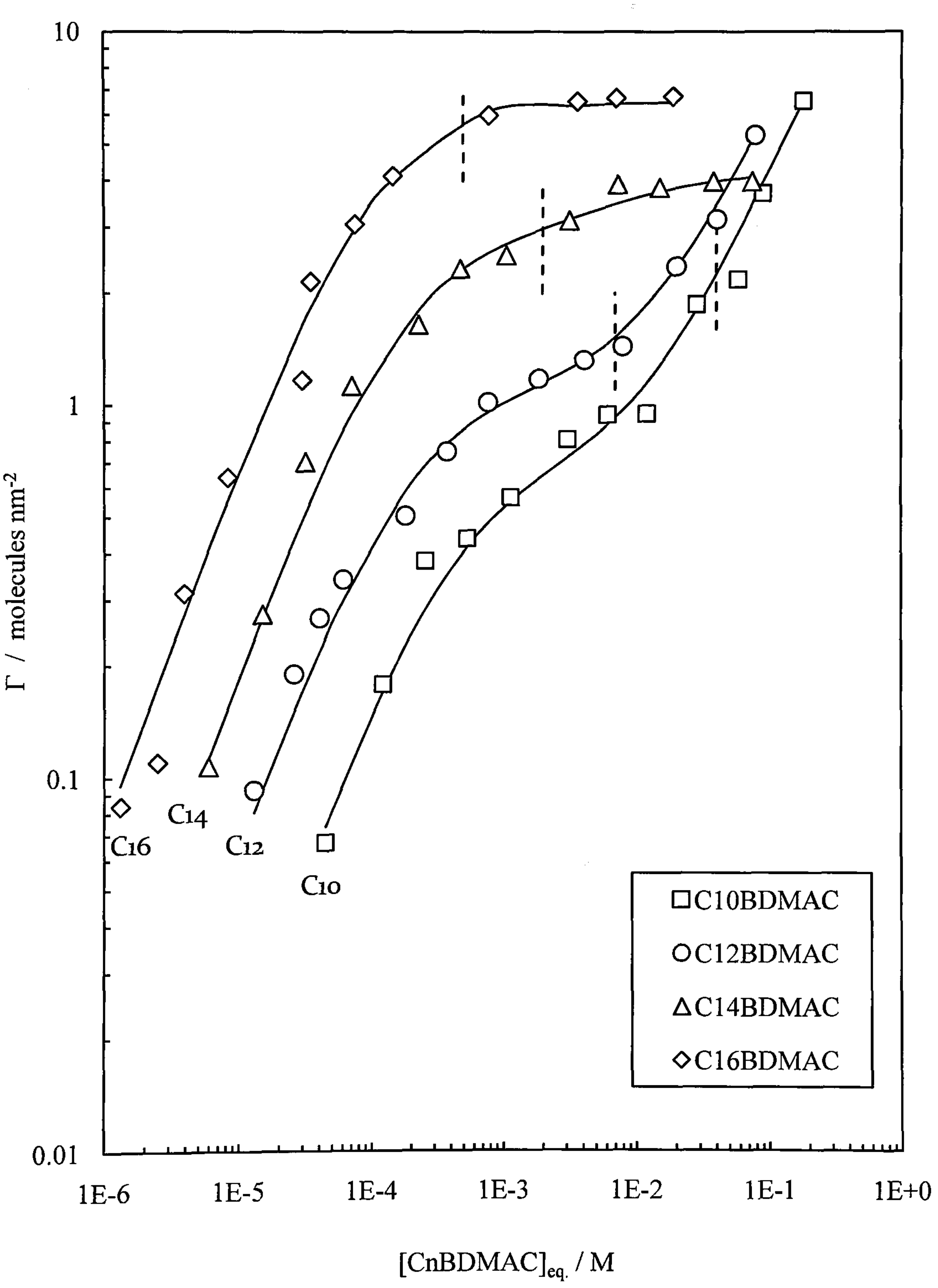

Figure 6-2. Adsorption isotherms of C10, C12, C14 and C16BDMAC from aqueous solutions onto 316L stainless steel particles at 25 °C using the depletion method at pH = 6.5-7. The vertical dashed lines represent the cmc. The solid lines represent the two-stage Langmuir model fits.

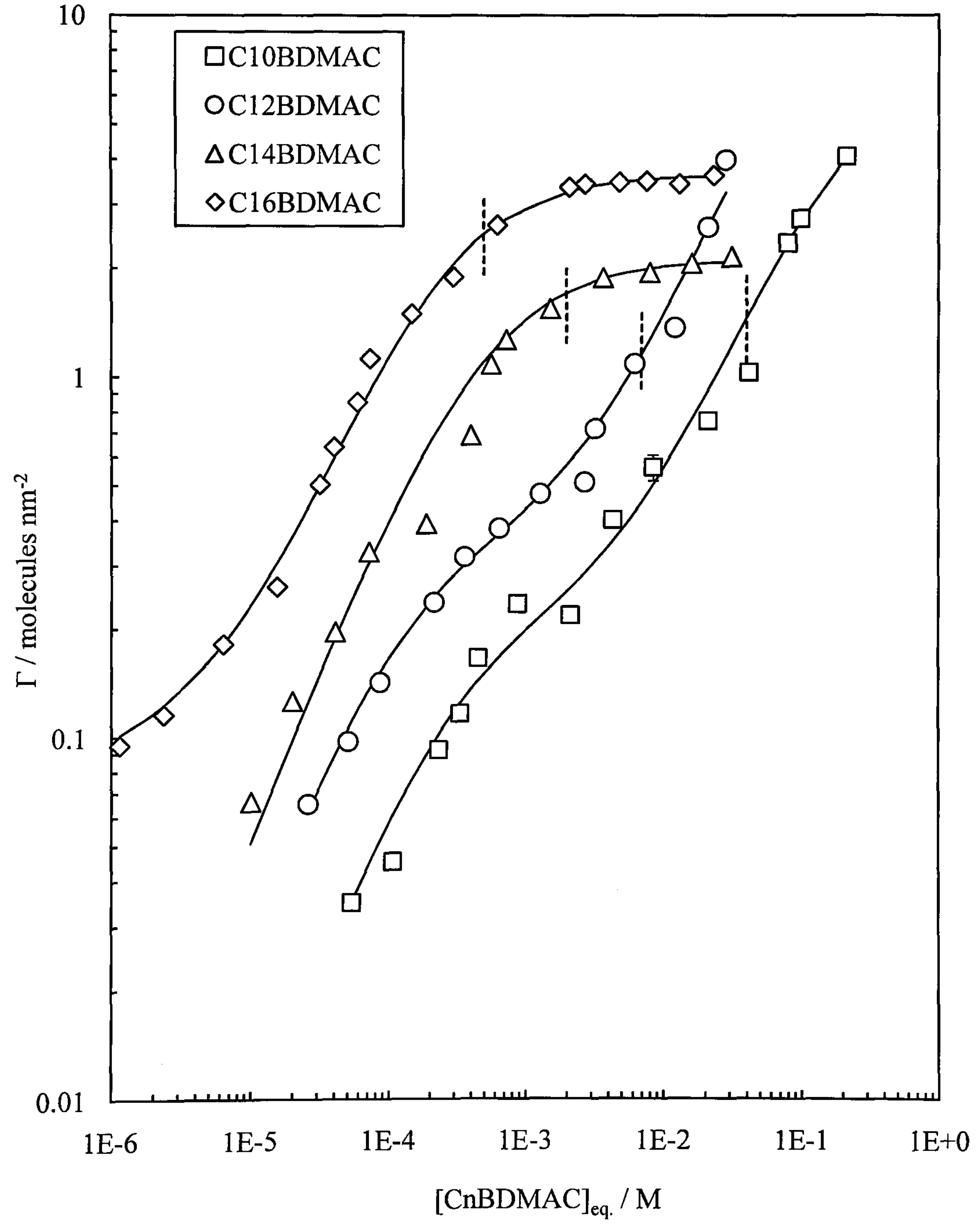

Figure 6-3. Variation of zeta-potential of C1018 mild steel particles as a function of CnBDMAC equilibrium concentration at 25 °C and pH of 8-9.

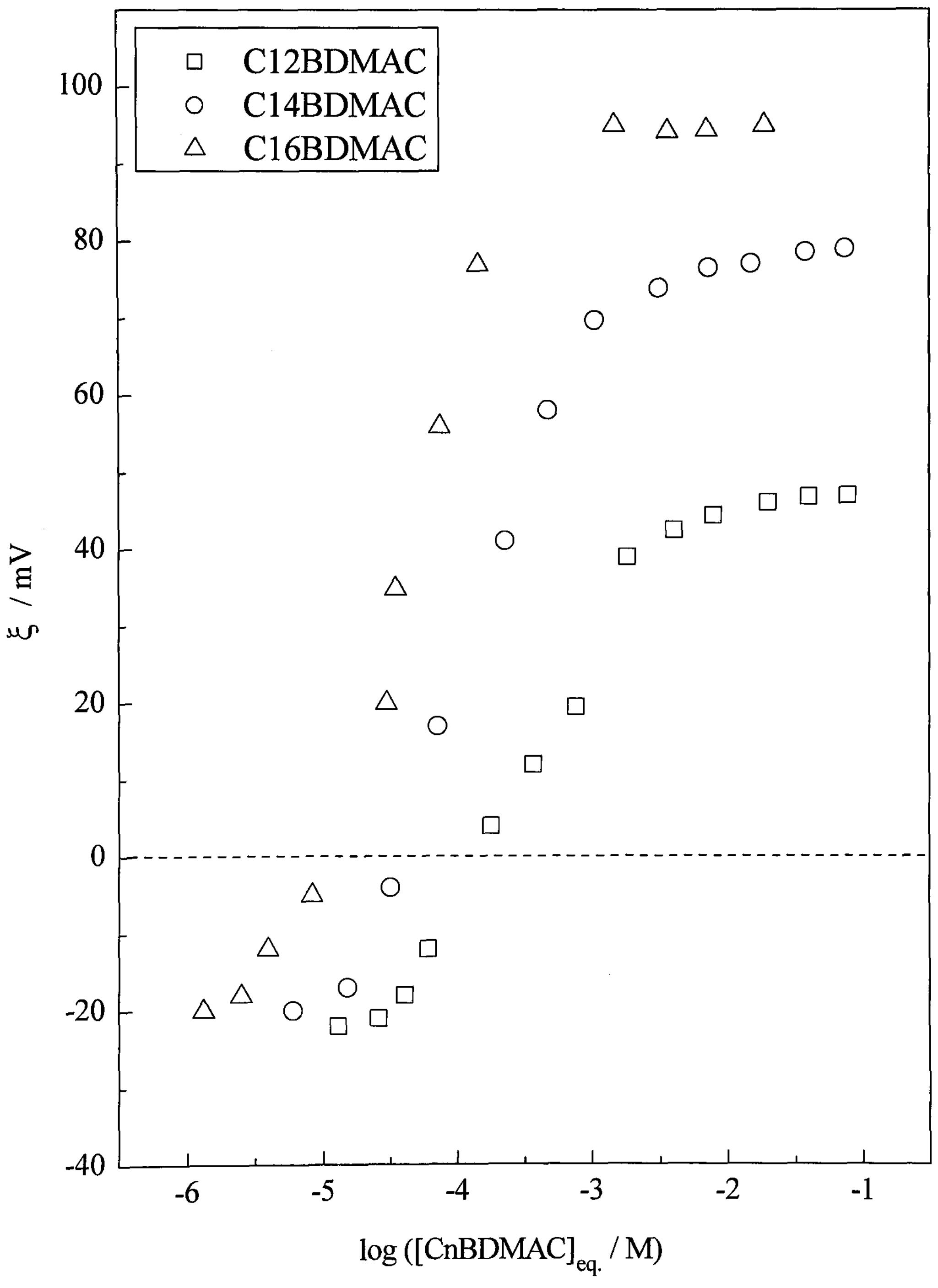

Recently, an analysis of the adsorption behaviour of sodium dodecyl sulphate from aqueous solutions onto carbon black has been reported using a two-stage Langmuir adsorption model [4]. We have fitted our experimental results to the two-stage Langmuir model, assuming that the adsorption process goes through a two-step process, each of which described by a Langmuir equation. In the first stage, it is assumed that surfactant molecules are adsorbed until they form a monolayer, followed by the formation of a second layer without any lateral interactions between the adsorbed surfactant molecules.

$$\Gamma = \Gamma_{1\,(\max)} \frac{k_1 C_{eq}}{1+k_1 C_{eq}} + \Gamma_{2\,(\max)} \frac{k_2 C_{eq}}{1+k_2 C_{eq}} \tag{6-1}$$

where k_1 and k_2 are the equilibrium adsorption constants in the first and second stages in M^{-1} units, $C_{eq.}$ is the surfactant equilibrium concentration in M units and $\Gamma_{1\,(\max)}$ and $\Gamma_{2\,(\max)}$ are the maximum amount adsorbed corresponding to the first and the second layers, respectively. Table 6-1 and Table 6-2 illustrate the fitting parameters used to fit the experimentally determined adsorption isotherms to the two-stage Langmuir model.

The adsorption isotherms were fitted to the two-step model proposed by Gu *et al.* [5]. In this model, given by Equation (6-2), the adsorption of surfactant ions onto oppositely charged polar surfaces can be described by a two-step mechanism as follows:

$$\Gamma = \frac{\Gamma_{\max} k_1 C_{eq} (\frac{1}{n} + k_2 C_{eq}^{n-1})}{1+k_1 C_{eq} (1+k_2 C_{eq}^{n-1})} \tag{6-2}$$

where k_1 and k_2 are the equilibrium adsorption constants involved in the first and second step in M^{-1} units, $C_{eq.}$ is the surfactant equilibrium concentration in M units and n is the aggregation number of surface aggregates or hemi-micelles.

In the first step, the surfactant ions are individually adsorbed at low concentrations ($c < cmc$) mainly through electrostatic interactions with the oppositely charged surface. During the second step ($c \geq cmc$), the surfactant ions aggregate, rather associate, around the primarily adsorbed species through hydrophobic interactions and form surface-aggregates or hemi-micelles. The average aggregation number, n, of these aggregates is limited.

Table 6-1. Fitting parameters for the two-stage Langmuir adsorption isotherm of CnBDMAC from aqueous solutions onto C1018 mild steel powder.

Parameters	C10	C12	C14	C16
k_1 / M^{-1}	2690	11584	16211	16849
k_2 / M^{-1}	1.64	4.35	5.50	7.22
$\Gamma_{1\,(max)}$ / molecules nm^{-2}	0.67	0.87	1.07	1.08
$\Gamma_{2\,(max)}$ / molecules nm^{-2}	25.7	22.9	2.93	4.40
R^2	0.99	0.98	0.98	0.99

The experimentally determined adsorption isotherms were found to fit the two-step model by Gu *et al.* successfully with R^2 values of about 0.97 for most of the alkylbenzyldimethylammonium chlorides inhibitors studied. However, the fit to the two-stage Langmuir model gave rise to higher R^2 values ≥ 0.98. Moreover, the two-stage Langmuir model has more fitting parameters than the two-step model. Accordingly, in this work, the fitting to the two-stage Langmuir model is the one to be presented here. The two-stage Langmuir model has been selected over the classical Langmuir model, i.e., one-stage Langmuir model, as the latter is limited only to a monolayer formation. Accordingly, it can be used to describe the higher amount of adsorption exhibited by the alkylbenzyldimethylammonium chloride investigated in this work.

Table 6-2. Fitting parameters for the two-stage Langmuir adsorption isotherm of CnBDMAC from aqueous solutions onto 316L stainless steel powder.

Parameters	C10	C12	C14	C16
k_1 / M^{-1}	3578	7990	8203	9.3×10^6
k_2 / M^{-1}	5.0	7.1	1944	4163
$\Gamma_{1\,(max)}$ / molecules nm^{-2}	0.20	0.35	0.2	0.1
$\Gamma_{2\,(max)}$ / molecules nm^{-2}	7.50	17.24	1.93	3.5
R^2	0.99	0.98	0.98	0.99

Obviously, as shown in Figure 6-1 and Figure 6-2, the increase in length of the alkyl group leads to an increase in the amount of the alkylbenzyldimethylammonium chlorides (from C10 to C16) adsorbed on both types of the steel powders. This effect has been reported previously in the literature [1, 6] and it is mainly attributed to the increasing affinity of the long-chain surfactants towards the interfacial region as a direct consequence of the increased hydrophobic interactions.

The hydrophobic interactions are not limited only to those laterally between the tails of adsorbed molecules at the solid surface, but also include those interactions between the tails of adsorbed molecules and those present in solution and also those between the surfactant tail and surface, i.e., when adsorption occurs on hydrophobic sites. In addition, the long-chain alkylbenzyldimethylammonium chlorides (C16 and C14) adsorb more at low surfactant concentrations in comparison to the short-chain (C12 and C10) homologues as inferred from Figures (6-1) and (6-2). Moreover, the long-chain C14 and C16BDMAC tends to reach a plateau near to the cmc in contradiction to the short-chain C10 and C12BDMAC in which the amount adsorbed of the long-chain inhibitors increases with the increase in surfactant equilibrium concentration above the cmc.

The increase in the amount adsorbed of the alkylbenzyldimethylammonium chlorides on mild steel as the alkyl chain length of the cationic surfactant increases is a behaviour typical of an ionic surfactant being adsorbed onto an oppositely charged surface. These results are consistent with several studies reported in the literature which describe the adsorption of an homologues series of the alkylbenzyldimethylammonium (C12-C16BDMAC) on activated sludge [7], (C4-C12BDMAC) on sodium montmorillonite [8] and adsorption of alkyltrimethylammonium surfactants (C12-C16) at the silica-water interface using optical reflectometry [6].

Recently, the adsorption of a homologous series of alkyltrimethylammonium bromides with alkyl groups from C10 to C16 onto solid surfaces, i.e., iron and cementite (Fe_3C) has been investigated using the QCM technique [9]. The authors have reported that short chain homologues adsorb better than the long-chain homologues. A survey of the literature on the adsorption of quaternary ammonium salts on steel surfaces using the depletion method shows that such studies are very limited.

McMahon [10] studied the adsorption of 2-imidazoline from oil onto oil-wet iron powder, and he reported that the adsorption process was fast and followed a Langmuir isotherm to give a monolayer coverage of about 1.54 molecules nm^{-2} at a solution concentration of about 1.4×10^{-3} M. X-ray photoelectron spectroscopy (XPS) of the iron powder used showed a typical spectrum for a Fe_2O_3 surface oxide.

Partyka *et al.* [11] investigated the adsorption behaviour of benzyldimethyldodecylammonium bromide (C12BDMAB) and benzyltrimethylammonium bromide (BTMAB) on hydrophilic silica using the depletion technique. They found that the adsorption of C12BDMAC is much higher than that of BTMAB over the whole concentration range. This finding highlights the key role of the hydrocarbon tail of a surfactant in promoting the adsorption process. The presence of the alkyl chain increases the affinity of surfactant ions with respect to the interfacial region. This effect results from pushing out the hydrophobic moiety of surfactant molecules from the bulk aqueous phase and from chain-chain interactions between the hydrophobic moieties of the adsorbed ions [3, 12, 13].

More recently, the adsorption of the commonly used corrosion inhibitor, C12BDMAC, has been investigated for a series of typical surfaces encountered in the oilfield production [14]. The depletion method was employed to study the adsorption of the inhibitor onto sand, iron carbonate, iron sulphide, barium sulphate and calcium carbonate. The initial inhibitor aqueous stock solution for these studies contained 3×10^{-4} M of C12BDMAC. These studies show that the inhibitor has the greatest affinity for sand and iron sulphide with uptake percentages of 95 % and 93 %, respectively.

6.3. EFFECT OF BRINE ADDITION

Brine is one of the main constituents of the water present in crude oil that being transferred in pipelines. The effect of brine addition on the adsorption behaviour of C10 and C12BDMAC from brine onto the C1018 mild-steel powder at 25 °C was studied using the depletion method. Figure 6-4 and Figure 6-5 show the isotherms for the adsorption of C10 and C12BDMAC from 4.7 wt.% brine in comparison to those with no added brine at 25 °C, respectively. The addition of brine results in an increasing degree of adsorption over the entire concentration range. Additionally, the brine addition results in shifting the adsorption isotherms towards

Figure 6-4. Adsorption isotherms of C10BDMAC corrosion inhibitor from aqueous solution containing 4.7 wt.% brine onto C1018 mild steel at 25 °C, compared to that with no added brine. The vertical dashed lines represent the cmc. The solid lines represent the two-stage Langmuir model.

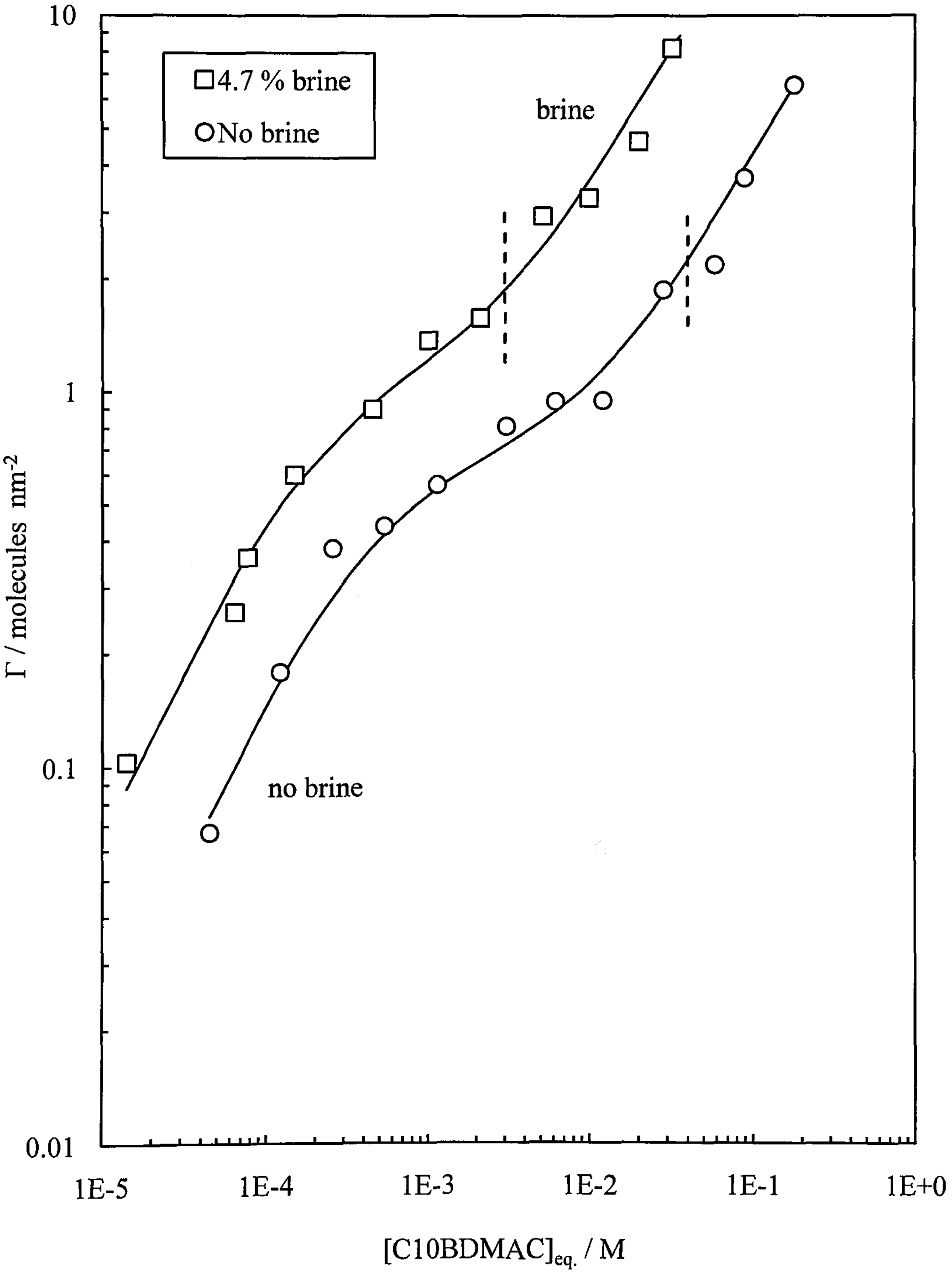

Figure 6-5. Adsorption isotherms of C12BDMAC corrosion inhibitor from aqueous solution containing 4.7 wt.% brine onto C1018 mild steel at 25 °C, compared to that with no added brine. The vertical dashed lines represent the cmc. The solid lines represent the two-stage Langmuir model.

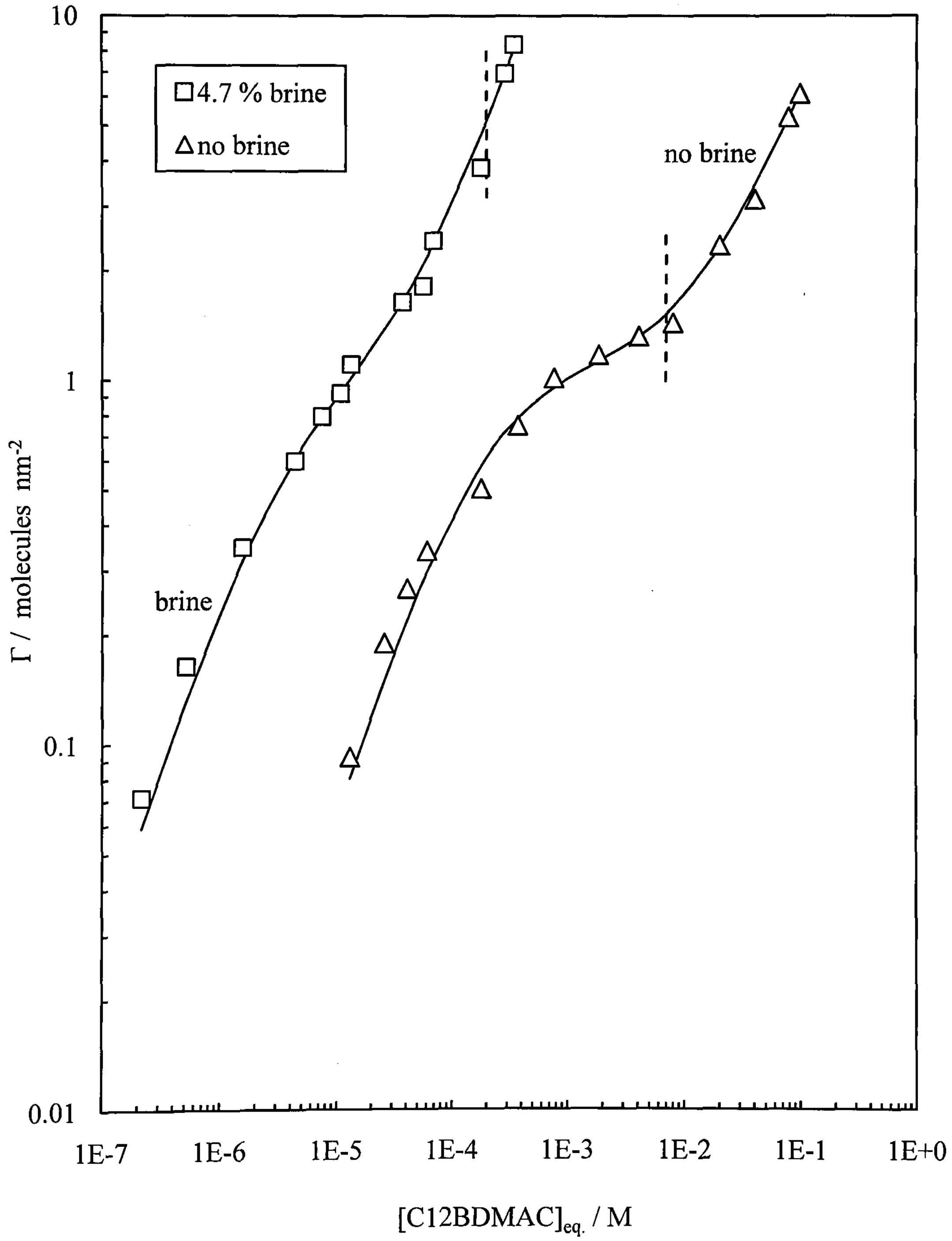

lower equilibrium concentrations. This in turn indicates an increased infinity between the surfactants molecules and the steel surface in the presence of electrolytes. A similar observation has been reported by Atkin *et al.* [6, 15]. They reported that the adsorption of CTAB onto silica particles in the presence of 0.01 M KBr takes place at lower concentrations in comparison to solutions with no added salt. Moreover, they found the amount of adsorption to be higher in the presence of electrolyte. This has been attributed to the screening of the headgroup charge by electrolyte, which reduces the surfactant headgroup area and allows more tightly packed surfactant aggregates to form.

The combined effect of the electrolyte addition and change in the hydrocarbon chain length on the adsorption characteristics of CnBDMAC from brine solution onto C1018 mild steel powder at 25 °C is given in Figure 6-6. The adsorption isotherms were fitted to a two-stage Langmuir model, shown in the figures as solid lines. Table 6-3 illustrates the fitting parameters used to fit the experimentally determined adsorption isotherms to the two-stage Langmuir model. Noticeably, the long chain C16BDMAC adsorption isotherm tends to reach plateau value of about 5 molecules nm^{-2} at surfactant equilibrium concentration of about 7×10^{-5} M in comparison with 3.6 molecules nm^{-2} at the same concentration in the absence of brine (Figure 6-6). On the other hand, the short chains C10 and C12BDMAC do not tend to level off under the studied concentration range. The maximum amount adsorbed by C10 and C12BDMAC are about 9 molecules nm^{-2} at surfactant equilibrium concentration of 3.2×10^{-2} and 3.5×10^{-4} M, respectively.

Table 6-3. Fitting parameters for the two-stage Langmuir adsorption isotherm of CnBDMAC from 4.7 wt.% brine solutions onto C1018 mild steel powder at 25 °C.

Parameters	C10	C12	C16
k_1 / M^{-1}	5924	3.34×10^5	1.16×10^6
k_2 / M^{-1}	7.92	348	5.72×10^4
$\Gamma_{1\,(max)}$ / molecules nm^{-2}	1.09	1.00	1.57
$\Gamma_{2\,(max)}$ / molecules nm^{-2}	35.11	56.9	3.38

Figure 6-6. Adsorption isotherms of C10, C12 and C16BDMAC from aqueous solution containing 4.7 wt.% brine on C1018 mild steel at 25 °C, using the depletion method, pH = 8. The vertical dashed lines represent the cmc. The solid lines represent the two-stage Langmuir model.

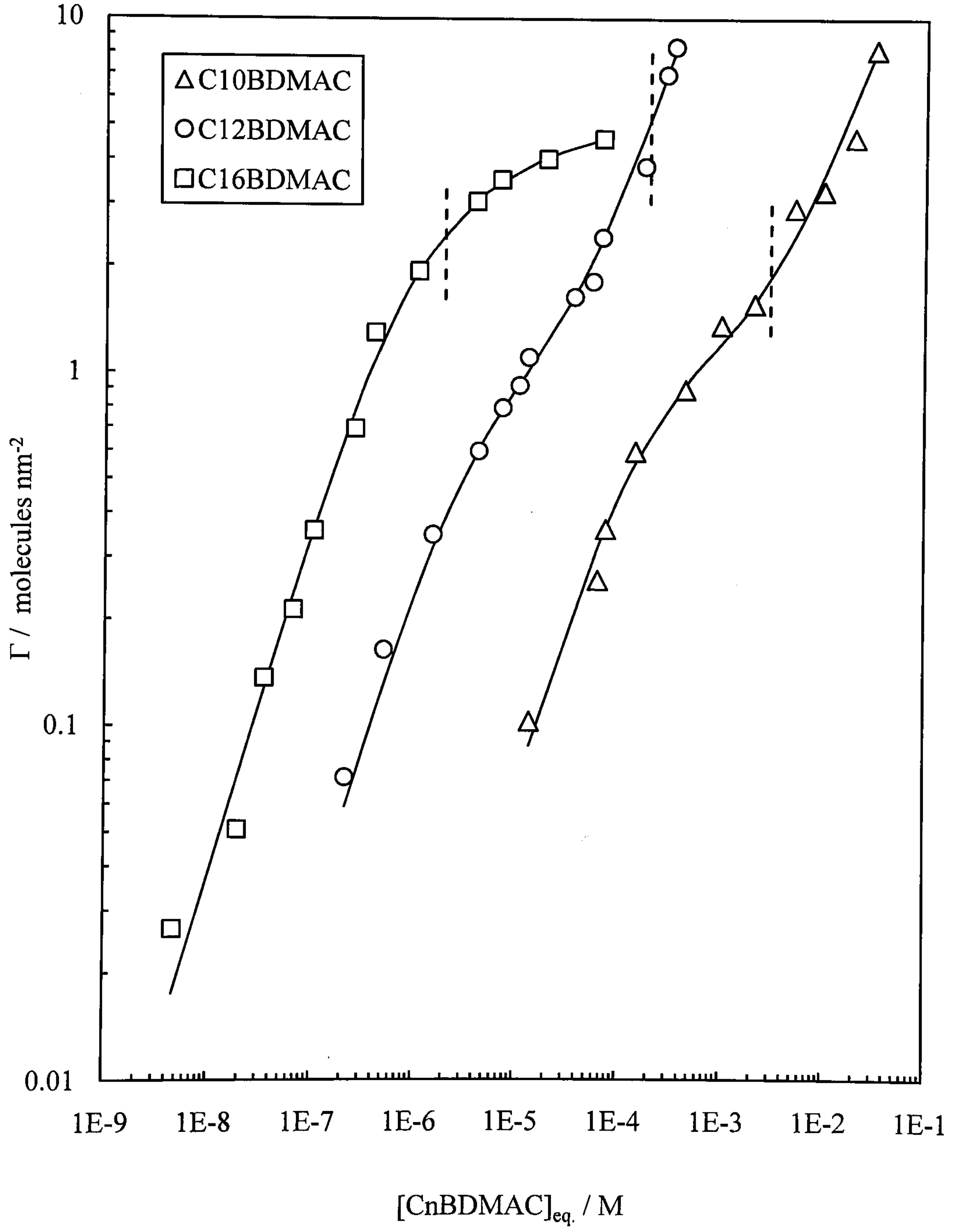

6.4. EFFECT OF TEMPERATURE

The adsorption experiments to investigate the effect of temperature were carried out at two temperatures, i.e., 25 and 40 °C in the presence and absence of electrolyte. Figure 6-7 and Figure 6-8 show the influence of temperature on the adsorption behaviour of C10 and C16BDMAC from aqueous solution onto C1018 mild steel in the absence of brine at 25 and 40 °C, respectively. Additionally, the effect of temperature on the adsorption behaviour of C10BDMAC from aqueous solution onto 316L steel, in the absence of brine, is represented in Figure 6-9. The experimentally determined adsorption isotherms have been fitted to the two-stage Langmuir model. Table 6-4 illustrates these fitting parameters. Noticeably, the temperature has no or just a slight effect on the amount adsorbed at low equilibrium concentration in the absence of electrolyte. All of the isotherms converge and no significant difference is observed among them. However, on increasing the equilibrium surfactant concentration, near to the cmc, the rise in temperature results in a marked decrease in the amount of surfactant adsorbed onto mild steel particles. Figure 6-7 shows that the rise in temperature results in a reduction of the maximum amount of C10BDMAC adsorbed onto the mild steel from about 7 molecules nm^{-2} at 25 °C to about 1 molecules nm^{-2} at 40 °C. In addition, the amount of C16BDMAC adsorbed on to the mild steel drops from 6.7 molecules nm^{-2} at 25 °C to about 4 molecules nm^{-2} at 40 °C as shown in Figure 6-8.

On the other hand, a higher the temperature increases the amount of C10BDMAC adsorbed onto C1018 mild steel particles in the presence of brine at higher equilibrium surfactant concentrations as shown in Figure 6-10. The rise in temperature results in increasing the maximum amount of C10BDMAC adsorbed onto the mild steel from about 2 molecules nm^{-2} at 25 °C to about 5 molecules nm^{-2} at 40 °C. Similarly, the increase in the temperature increases the amount of C10BDMAC adsorbed from aqueous solutions on 316L particles at higher equilibrium surfactant concentrations as shown in Figure 6-9. Accordingly, the maximum amount adsorbed of C10BDMAC increases onto 316L particles from about 4 molecules nm^{-2} at 25 °C to about 6 molecules nm^{-2} upon increasing the temperature to 40 °C. This observation contradicts the QCM adsorption result, which showed that the adsorption of C10BDMAC onto stainless steel-coated crystals decreases with the increases in temperature (*Chapter 5*).

Figure 6-7. Adsorption of C10BDMAC from aqueous solution on C1018 mild steel at 25 and 40 °C, and pH = 8-9 using the depletion method. The solid lines represent the two- stage Langmuir model.

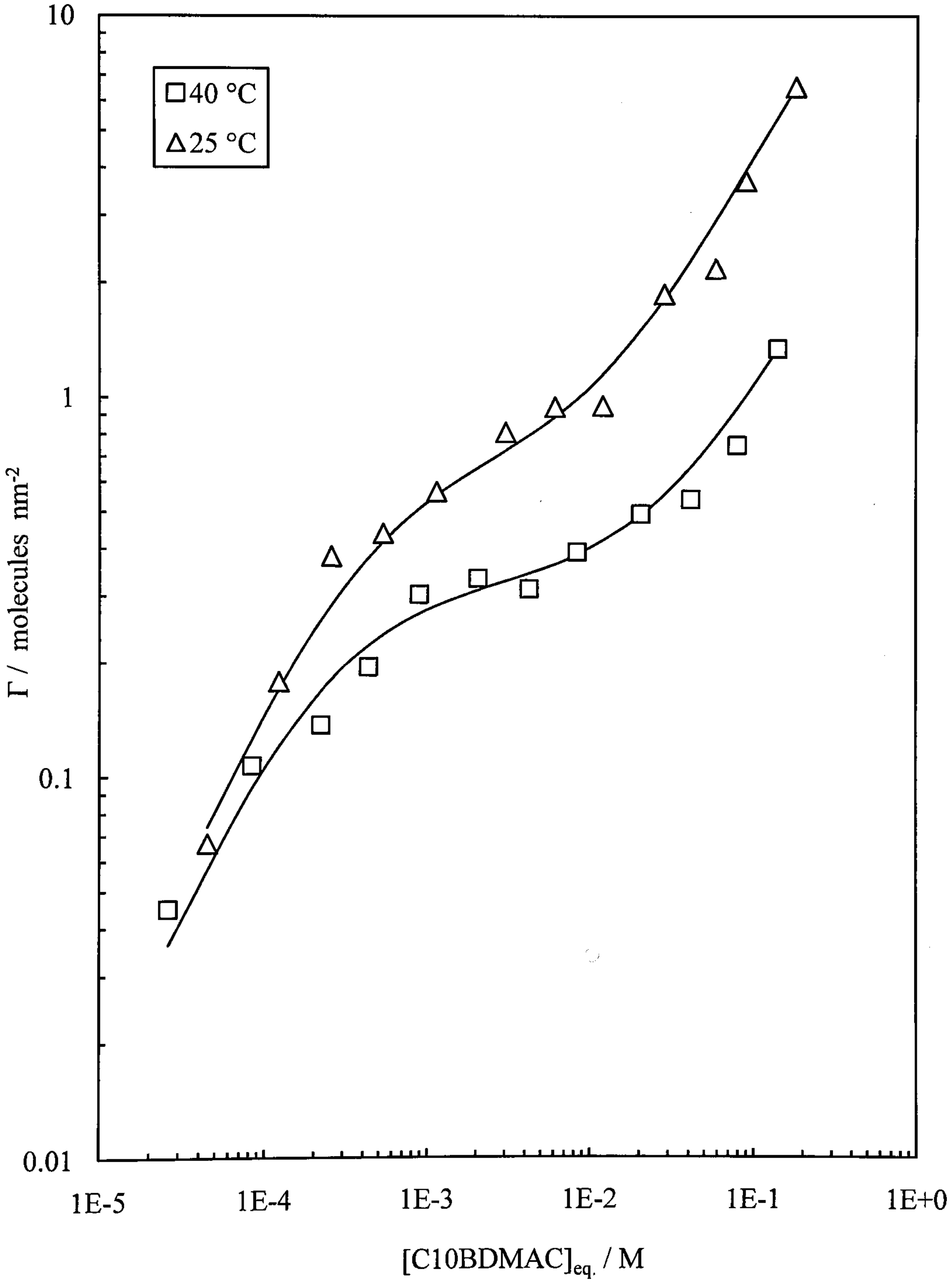

Figure 6-8. Adsorption of C16BDMAC from aqueous solution on C1018 mild steel at 25 and 40 °C, and pH = 8-9 using the depletion method. The solid lines represent the two- stage Langmuir model.

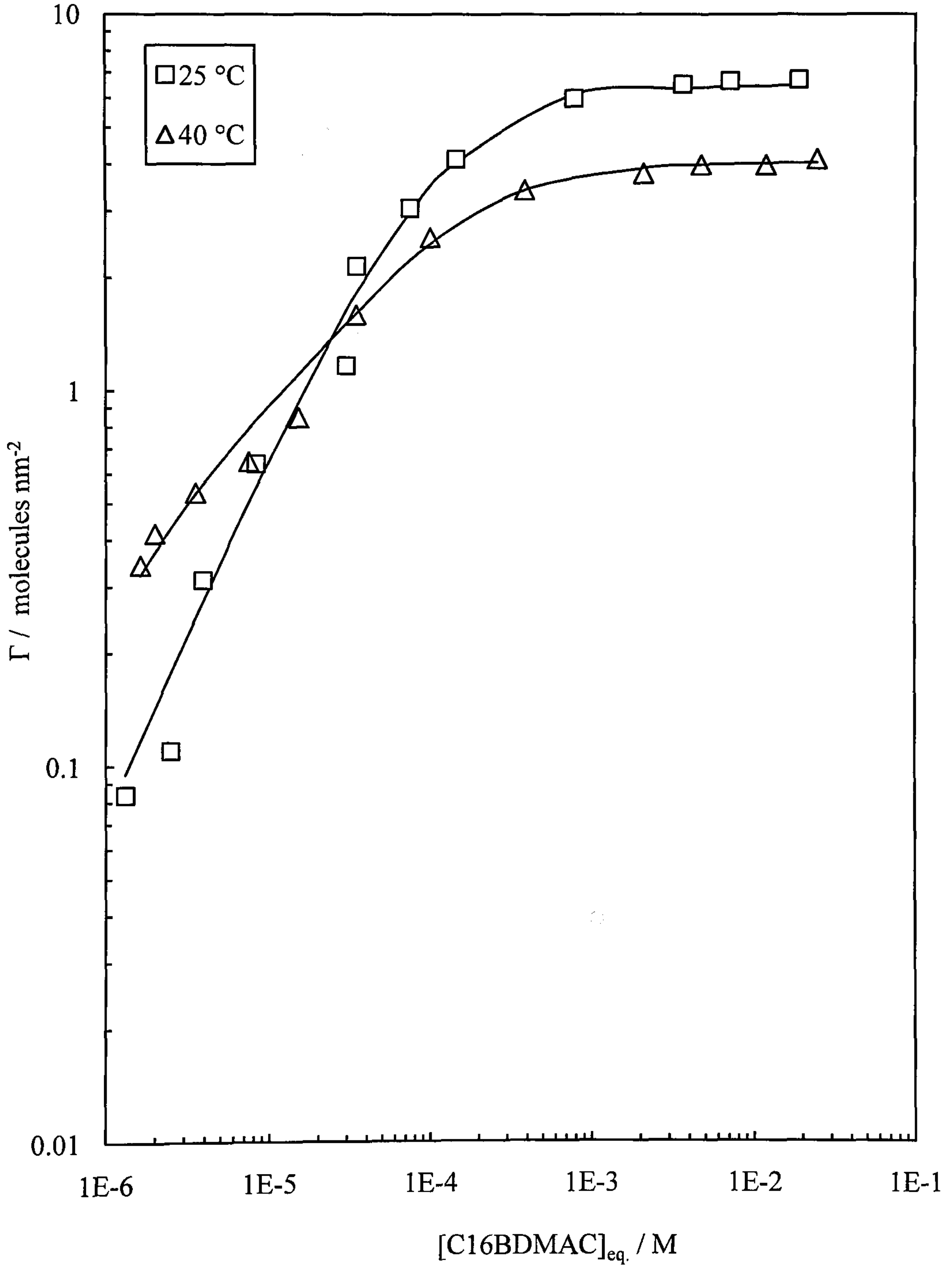

Figure 6-9. Adsorption of C10BDMAC from aqueous solution on 316L stainless steel at 25 and 40 °C, and pH = 6.5-7 using the depletion method. The solid lines represent the two-stage Langmuir model.

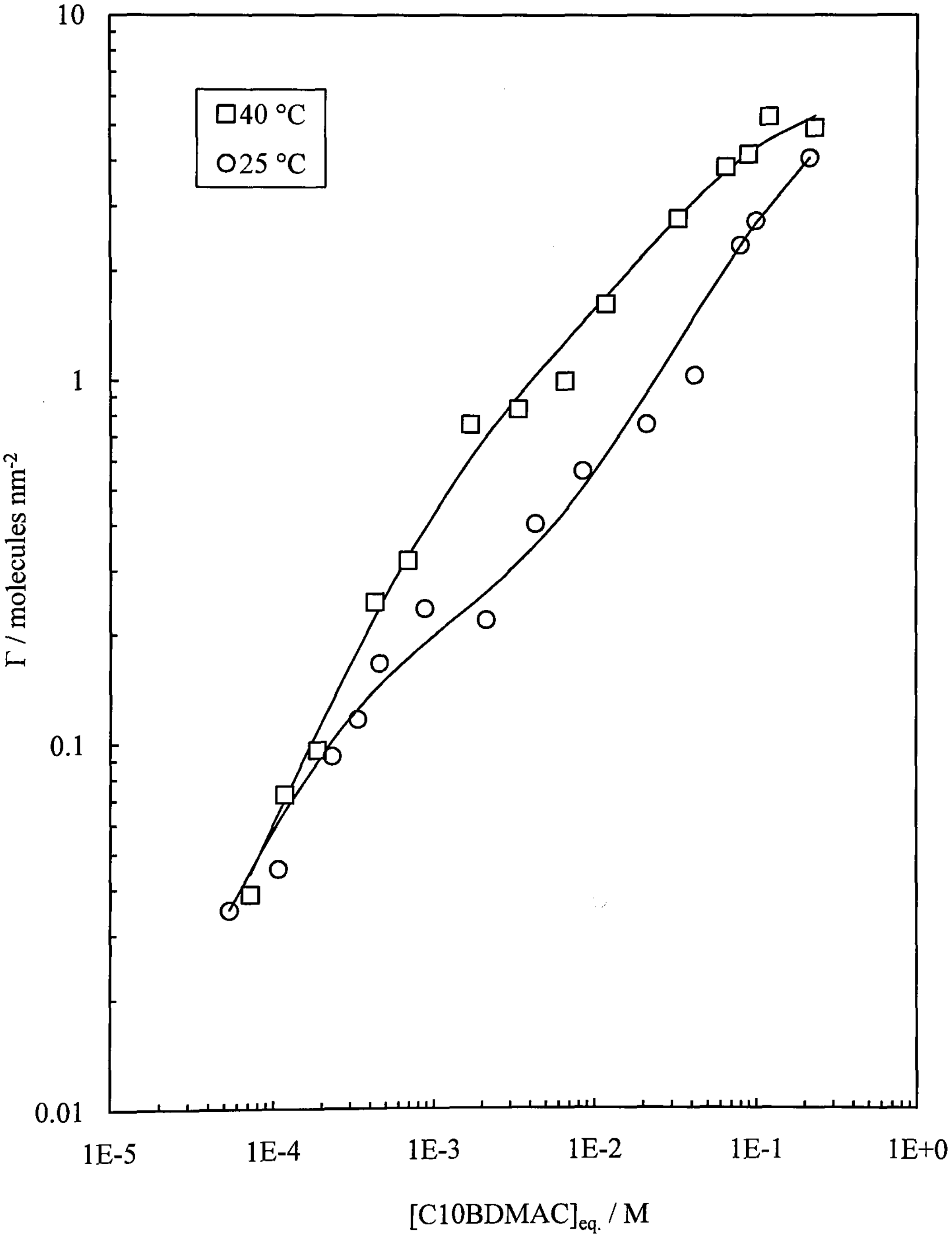

Figure 6-10. Adsorption of C10BDMAC from aqueous solution containing 4.7 wt.% brine onto C1018 mild steel at 25 and 40 °C and pH = 8 using the depletion method. The vertical dashed lines represent the cmc. The solid lines represent the two-stage Langmuir model.

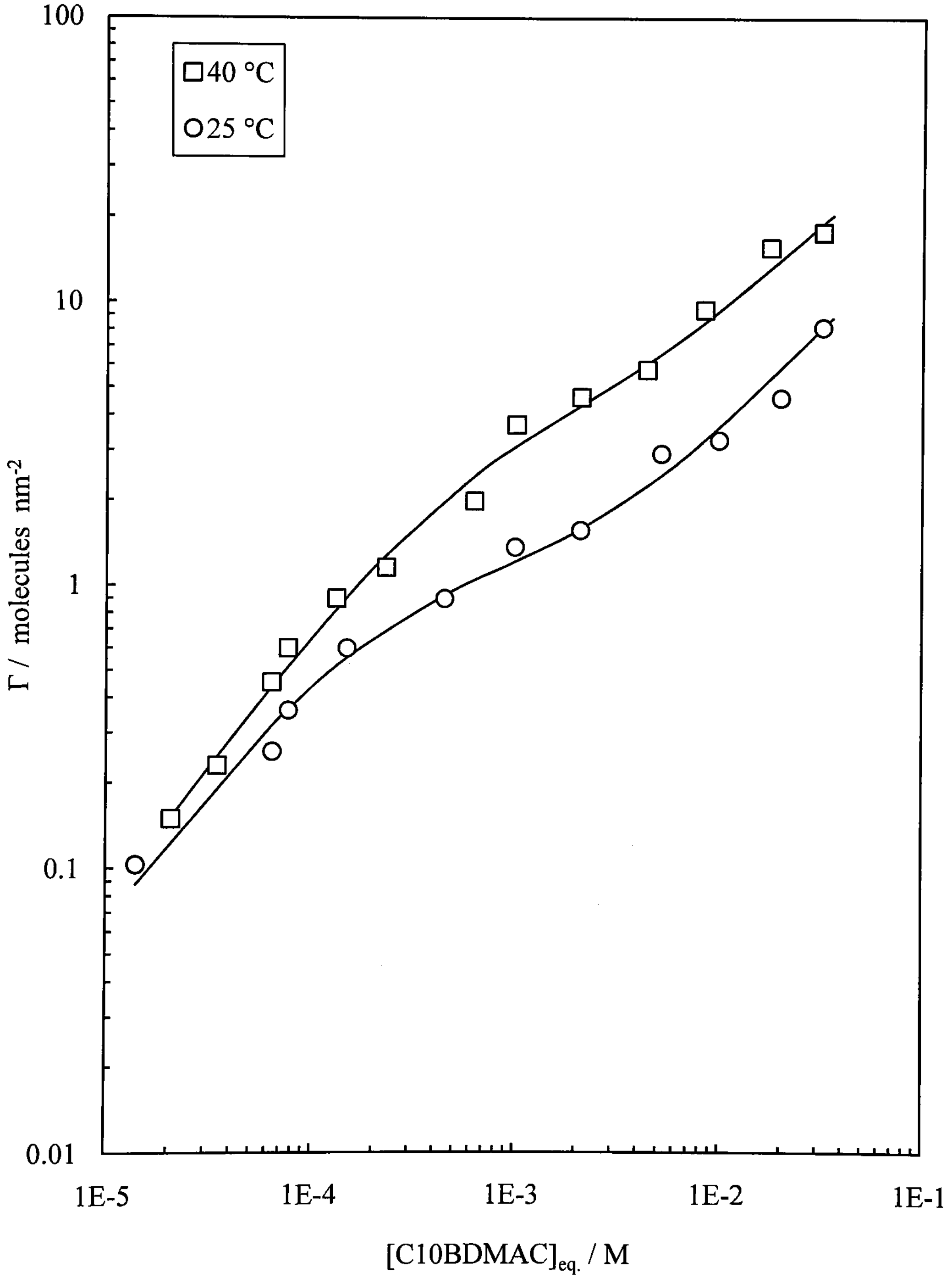

Partyka *et al.* [16] reported that the amount of benzyldimethyloctylammonium bromide (C8BDMAB) adsorbed onto silica particles increases with increasing the temperature. Similarly, we have found that the adsorption of C10BDMAC from aqueous solutions onto sand particles was found to be greater at higher temperatures at pH 5-6 (Section 7.1).

Table 6-4. Fitting parameters for the two-stage Langmuir adsorption isotherm of CnBDMAC from aqueous and 4.7 wt.% brine solutions onto C1018 mild steel powder at 40 °C.

Parameters	C10		C16
	aqueous	brine	aqueous
K_1 / M^{-1}	4828	1826	3.23×10^5
K_2 / M^{-1}	1.21	10	1.09×10^4
Γ^1_{max} / molecules nm^{-2}	0.32	3.7	0.77
Γ^2_{max} / molecules nm^{-2}	7.03	25	3.28
R^2	0.99	0.99	0.99

6.5. DISCUSSION

6.5.1. Mechanism of CnBDMAC adsorption at the steel-water interface

The adsorption isotherms obtained for alkylbenzyldimethylammonium chlorides at the water-steel interface can be classified as a Langmuir type, following the Giles *et. al.* [17] classifications of the adsorption isotherms. The adsorption of the ionic surfactants CnBDMAC onto the oppositely charged steel surfaces can be interpreted as being a three-stage adsorption process. Noticeably, the log-log adsorption isotherms of all the investigated CnBDMAC inhibitors onto both steel types exhibit three different stages or regions. Each of these stages has a different slope, which reflects different modes of surfactant-surface and surfactant-surfactant interactions. An analysis of the zeta-potential behaviour for the adsorption of CnBDMAC gives some insight into the possible mechanism of the process. The variation in the zeta-potential of steel particles displays three different stages as well.

The isotherms are divided into the following stages or regions: an ion exchange stage, a charge reversal stage and a plateau or increased adsorption stage. These three stages of the adsorption process are shown more clearly in Figure 6-11, Figure 6-12 and Figure 6-13 for the adsorption of C10 and C14BDMAC from water onto C1018 mild steel and the adsorption of C12 and C16BDMAC onto 316L stainless steel, respectively. These three stages are discussed in more details below.

Stage I (A→B): The Ion Exchange Stage

($[\mathrm{CnBDMAC}]_{\mathrm{eq.}} \leq 0.1$ cmc) & ($\Gamma_{\mathrm{I}\rightarrow\mathrm{II}} = 0.2\text{-}0.3$ molecule nm^{-2} onto 316L

= 0.5-1 molecules nm^{-2} onto C1018)

In this stage, the individual surfactant ions are expected to adsorb tilted or lying flat to the solid steel surface, in which the head group is in contact with the polar (ionic) sites. Both of the steel types are expected to be negatively charged under the employed experimental condition as their surface charges are pH dependent. The stainless steel 316L particles have a point of zero charge (PZC) in the range of pH 4.4-5.2 [18]. The point of zero charge for iron hydrous oxide, which is the main constituent of mild steel, is in the range of about pH 7-8 [19].The organic surfactant cation can be considered as the counter ions for the negative sites on the steel surface, which are adsorbed in the Stern layer. Consequently, the adsorption process in this stage is believed to occur principally through electrostatic interactions between the negative surface charges on steel particles and the positive ammonium surfactant head groups and partially by the hydrophobic interactions. The evidences that adsorption process in this stage is driven electrostatically came from the following observations:

(I) As shown clearly in Figure 6-12, Figure 6-14 and Figure 6-15, the zeta-potential of steel particles is nearly independent of the equilibrium surfactant concentration and the amount surfactant adsorbed in this stage. The possible explanation for this observation is that adsorption takes the form of an ion exchange between the organic cation, alkylbenzyldimethylammonium ion and some other ions, which are present at the steel water interface as pre-adsorbed counter ions (water molecules and electrolytes). This in turn represents an indication of the electrostatic interaction between surfactants molecules and the steel surface.

Figure 6-11. Adsorption isotherms of C10 and C14BDMAC from aqueous solutions onto C1018 mild steel particles at 25 °C, using the depletion method, pH = 8-9. The vertical dashed lines represent the cmc.

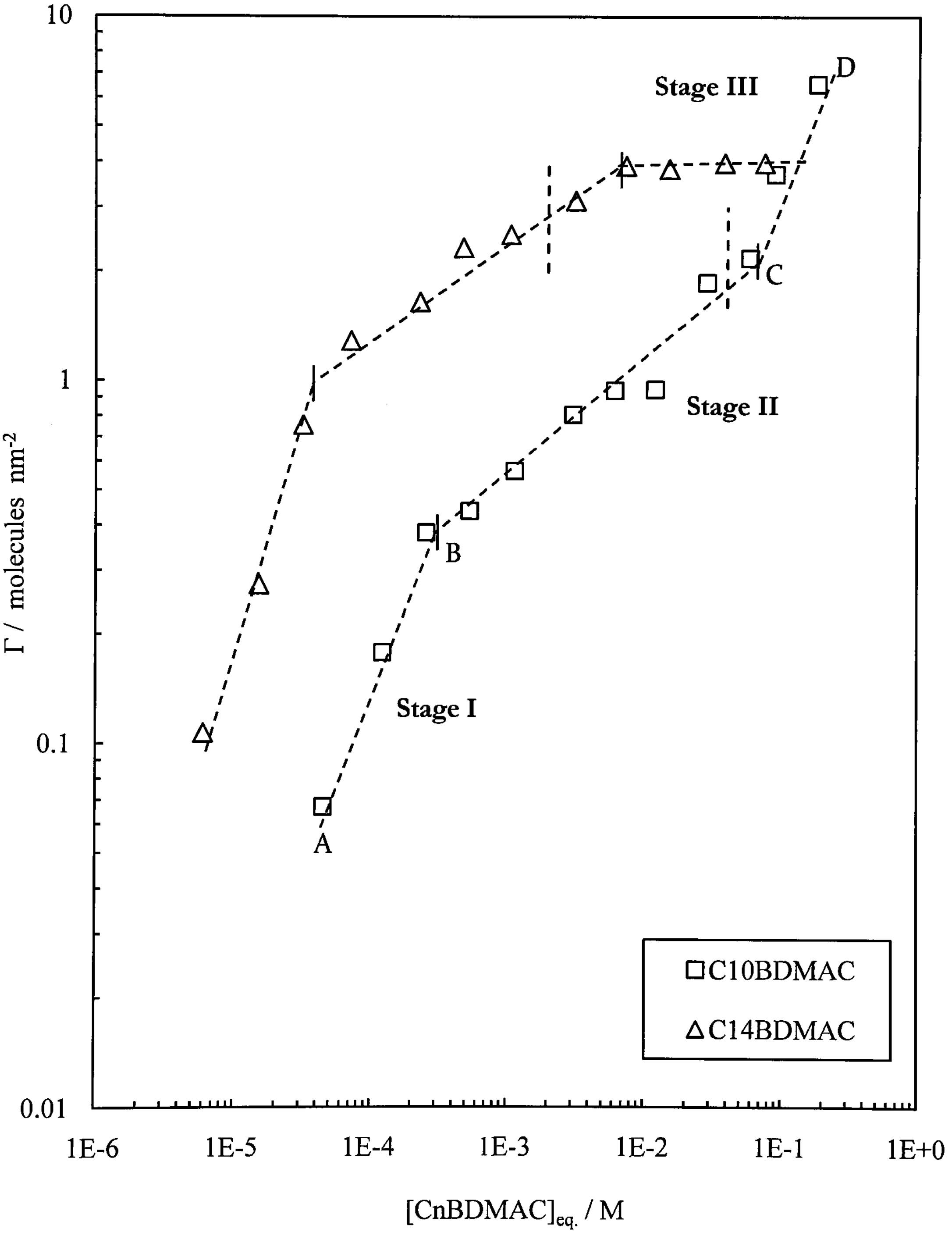

Figure 6-12. Variation of zeta-potential of C1018 mild steel particles as a function of the amount of C12BDMAC adsorbed at 25 °C and pH of 8-9.

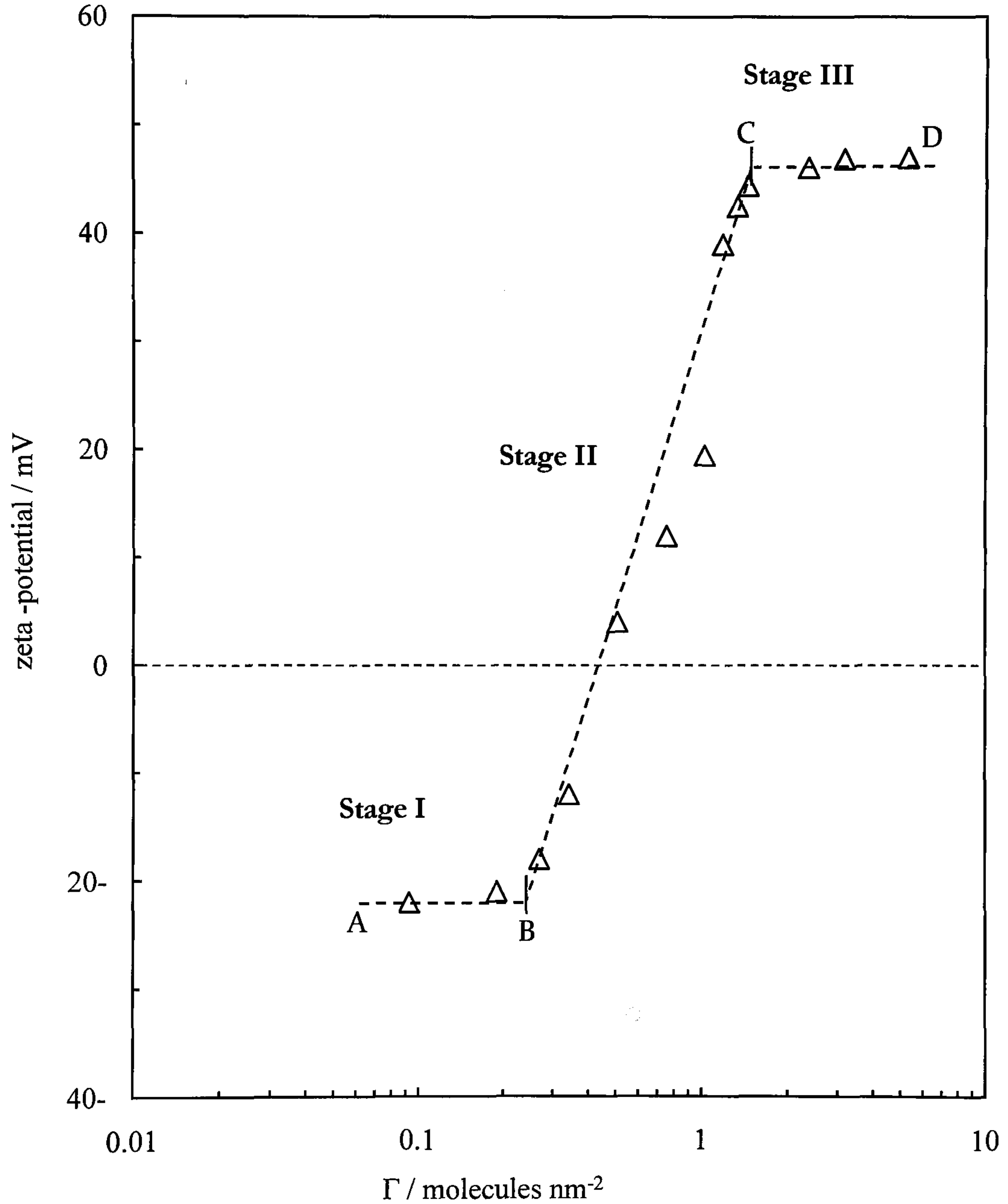

Figure 6-13. Adsorption isotherms of C12 and C16BDMAC from aqueous solutions onto 316L satinles steel particles at 25 °C, using the depletion method, pH = 6.5-7. The vertical dashed lines represent the cmc.

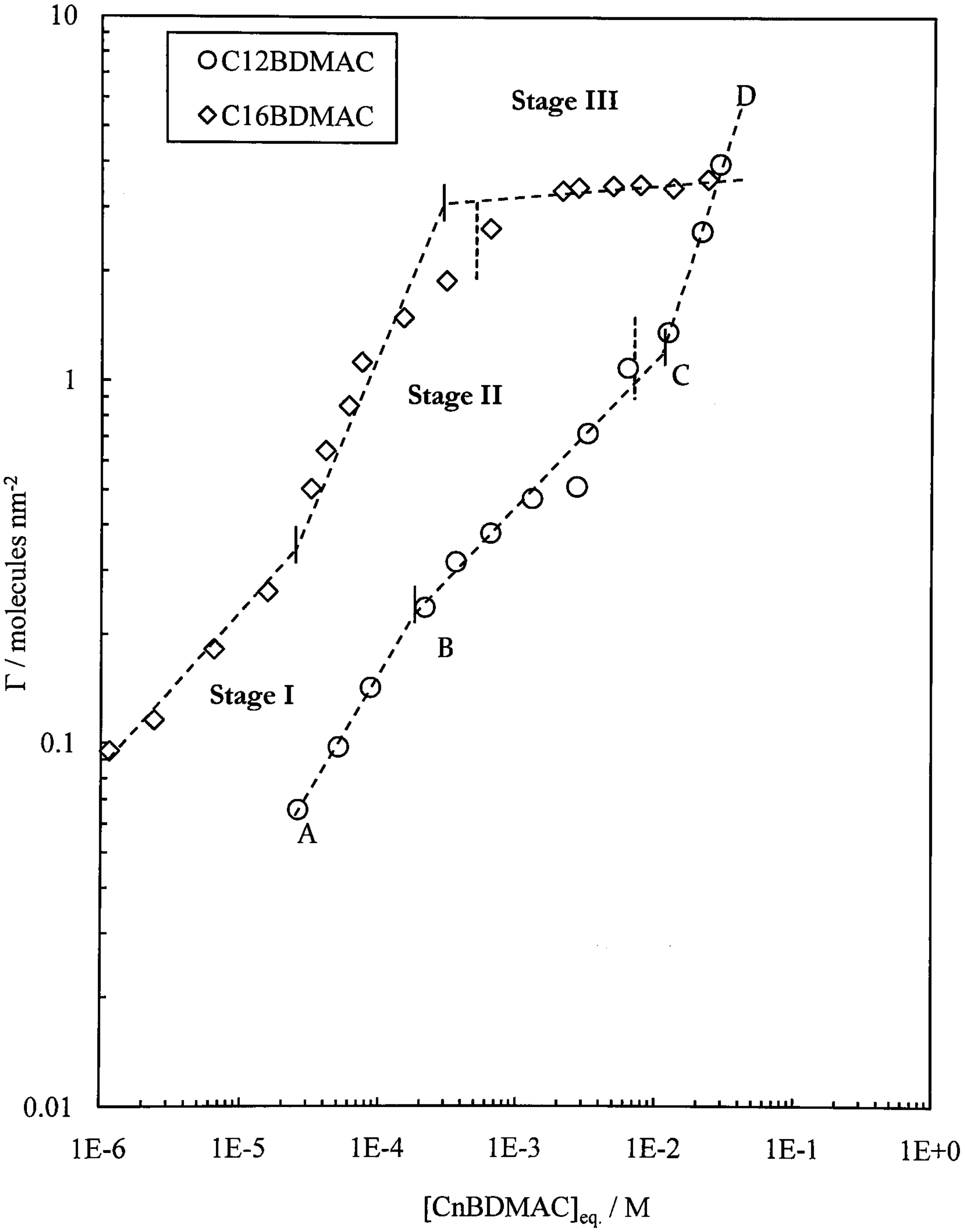

Figure 6-14. Variation of zeta potentials of 316L steel particles as a function of C12BDMAC equilibrium concentration and the amount of adsorption at 25 °C, using the depletion method, pH = 6.5-7. The vertical dashed lines represent the cmc.

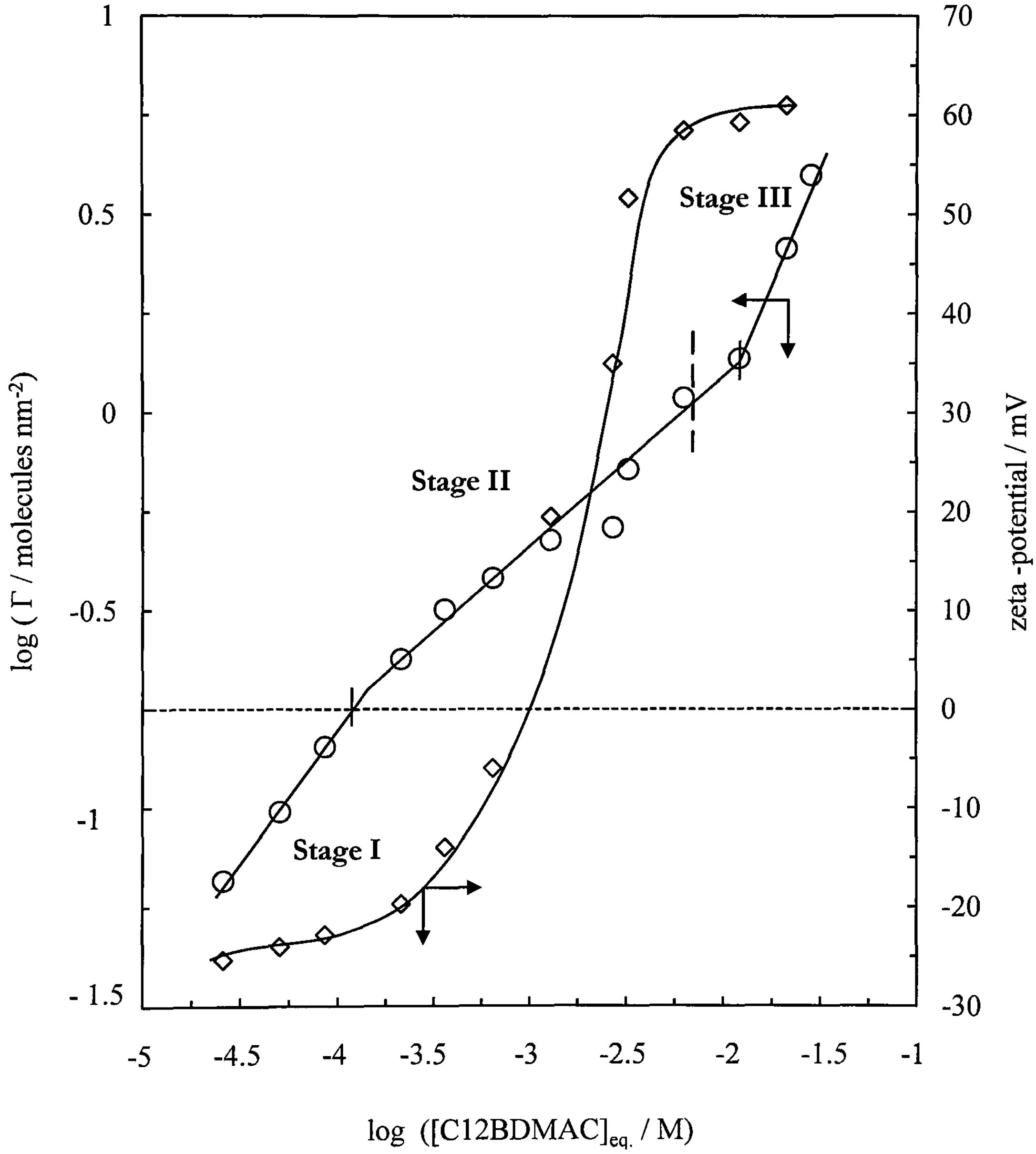

Figure 6-15. Variation of zeta potentials of C1018 steel particles as a function of C12BDMAC equilibrium concentration and the amount of adsorption at 25 °C, using the depletion method, pH = 8-9. The vertical dashed lines represent the cmc.

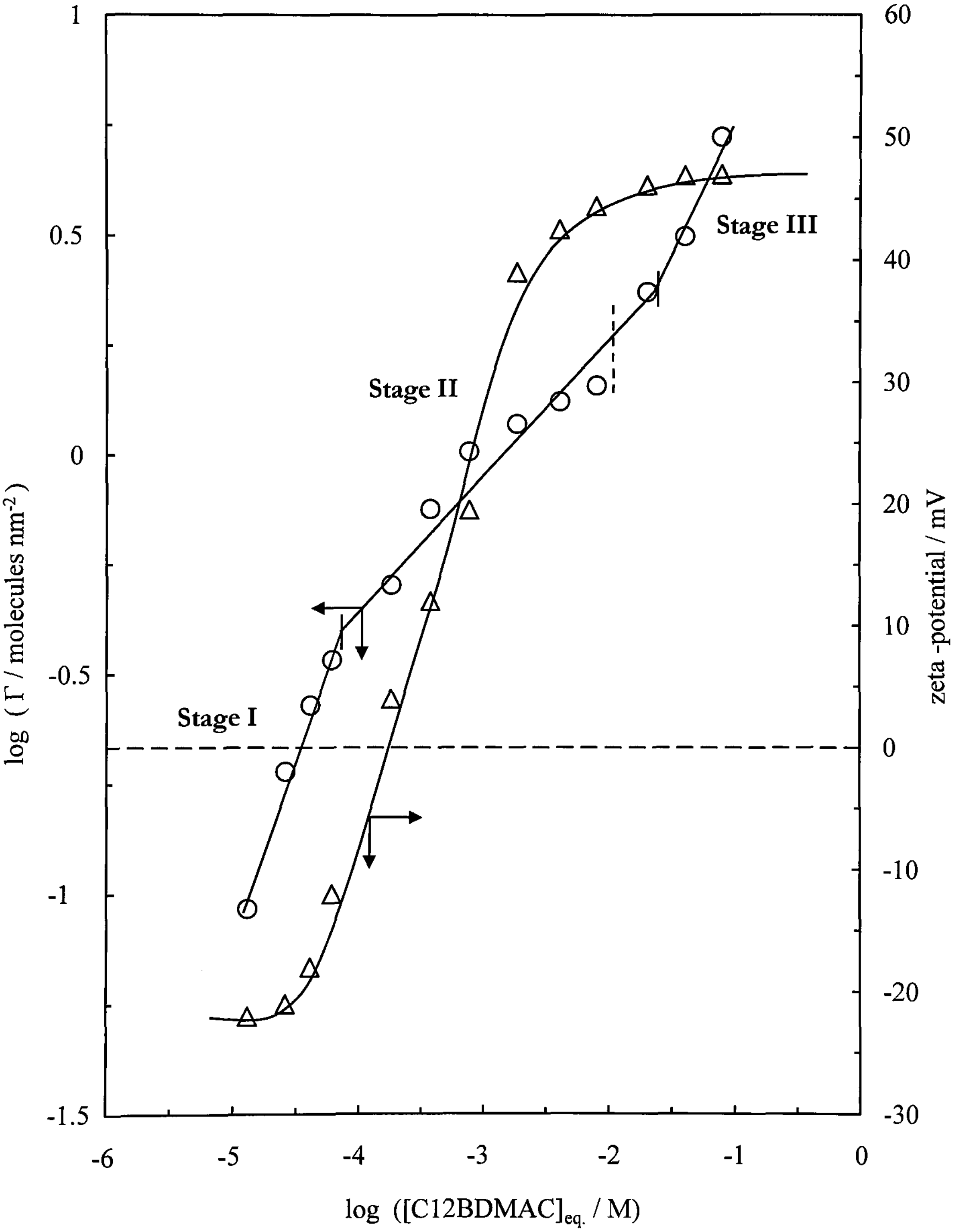

(II) The amount of surfactant adsorbed is higher in the presence of brine in comparison with water. Typically, electrolytes screen Coulombic repulsion and hence, the variation of the amount of surfactant adsorbed with electrolyte concentration is an indication for the presence of the electrostatic interactions. The higher brine concentrations results in screening the head-group charge by increasing the ionic strength, which reduces the surfactant head-group area and allows more molecules to adsorb on the steel surface (Figure 6-4 and Figure 6-5).

(III) From the temperature dependence, an insight into the driving force is obtainable. Noticeably, the temperature has no or slight effect on the amount adsorbed at this stage. As shown in Figures 6-7 to 6-10, all isotherms converge and no significant difference is observed among them. This is in agreement with an ion being adsorbed electrostatically onto an oppositely charged surface.

Stage or region I is generally referred to in the literature as the "Henry's region" and its trend line has a slope of unity in the ideal case [27]. The slopes of experimentally determined log Γ vs. log $[\text{CnBDMAC}]_{eq.}$ plots are invariably less than unity. This in turn means that the adsorption process takes place on sites of progressively decreasing affinity [28]. This is in accordance with the gradual increase in the surface charge of steel particles (being more positive) with the increase in the adsorption amount at the late stage in this region.

Although we claim that, the adsorption process in this stage is dominated by the ion exchange mechanism only, the equilibrium concentration at which the transition from stage I to II take place, over the homologous series, decreases with the increase in the surfactant chain length. This observation highlights the impact of the hydrophobic interactions on the adsorption process. The increase in the alkyl chain length increases the affinity of surfactant ions to the interfacial region by pushing out the hydrophobic moiety of surfactant molecules from the bulk aqueous phase. Other authors have pointed out similar results based on a thermodynamic analysis of the adsorption isotherms corresponding to the adsorption of cationic surfactants being adsorbed on negatively charged surfaces [20, 21]. The magnitude of the surface excess at the transition from stage I to II, is approximately equal for all the surfactants especially for those being adsorbed onto stainless steel surfaces. In the absence of brine, the amount adsorbed onto 316 L particles at the end of this stage tends to be about 0.2-0.3 molecules nm^{-2} at 25 °C. Hence, the average surface area occupied by one adsorbed surfactant ion is equal to about 5 nm^2. For C1018 mild steel, the short chains give rise to adsorption values of about 0.5 molecules nm^{-2} while those for the long chain are 1 molecules nm^{-2}. These are corresponding to an average surface area of about 2 and 1 nm^2 per one adsorbed surfactant molecule, respectively. These high surface areas occupied by the adsorbed surfactant indicate a flat orientation with negligible lateral interactions between them in this stage of the adsorption process.

Additionally, the concentrations at which the transitions from stage I to II occur are comparable regardless of the solid surface nature. For example, the adsorption of C12 and C14BDMAC on C1018 mild steel occurs at 0.1 and 0.04 mM, respectively. While for the adsorption on 316L steel these values are 0.1 and 0.05 mM, respectively.

To sum up, in the first stage of the adsorption process, surfactants adsorb as individual ions with the ionic group directly attached to charged sites on the steel surface. They displace interfacial water molecules and may exchange with some other ions, which are present at the solid-water interface as pre-adsorbed counter ions.

Stage II (B→C): The Charge Reversal and Association Stage

([CnBDMAC]eq. = 0.1 - 1 cmc) & ($\Gamma_{II\rightarrow III}$ = 1 - 2 molecule nm^{-2} onto 316L
= 1-3 molecule nm^{-2} onto C1018)

The second stage of adsorption isotherms starts at surfactant concentrations about an order of magnitude below the surfactant cmc and it extends to a higher surfactant concentration below or close to the cmc. In this stage, the amount of adsorption continuous to increase, indicating an increase in the affinity of the surfactant for the solid surface. Generally, an increase in the number of CH_2 in the alkyl chain, in this region, results in a parallel increase in the amount of surfactant adsorbed. The surfactant adsorption in this stage is believed to be governed by the hydrophobic interactions between the surfactant chains. This conclusion has been derived based on the following observations:

(I) The adsorption process in this stage is accompanied by a sharp change in the zeta-potential and charge reversal as well (Figure 6-14 and Figure 6-15). Under these conditions, the zeta-potential became positive because there are more cations in the Stern layer than negative charges at the steel surface. This results in a decrease in the slope of the adsorption isotherm at this stage because of the increased repulsion between the surfactant head-groups. Consequently, further adsorption of surfactant ions in stage II is no longer electrostatically favoured because of the overcompensation of the surface charge by the surfactant.

(II) The length of hydrocarbon tail group has a pronounced influence on the mount of surfactant adsorbed as shown in Figure 6-11 and Figure 6-13. Noticeably, in this stage the adsorption isotherms are characterised by shifting to lower equilibrium concentrations resulted from the increased hydrophobicity imparted by longer tail groups. Additionally, the maximum amount of adsorption and the affinity towards steel surfaces increases with the increase in the chain length. The long chain surfactant molecules adsorb more than the short chain ones.

(III) As shown in Figure 6-8 and Figure 6-9, on increasing the equilibrium surfactant concentration, the rise in temperature results in marked decrease in the amount of the surfactant adsorbed for both types of steel in Stage II. This in accordance with the exothermic nature of the hydrophobic interactions between alkyl chains.

(IV) The increase in the adsorbed surfactant amount with increasing brine concentrations may be attributed to the increased hydrophobic interactions as a direct consequence of the recued repulsion between the surfactant head-groups adsorbed in the first stage (see Figure 6-4 and Figure 6-5). Consequently, in the presence of electrolyte, adsorbed surfactant molecules are placed densely due to increased lateral interactions between tails.

Many authors attributed the increase in the amount of adsorption in this stage to the beginning of surface aggregate formation, which start to form because of the hydrophobic effect. The monomers electrostatically adsorbed in stage II are thought to act as anchors (or nucleation sites) for the formation of such aggregates [29]. These aggregates are either described as hemi-micelles, i.e., half micelles [30-31], admicelles, i.e., patches of bilayers [32] or hemicylinders [33-34] in which the head groups of the first surfactant layer oriented toward the solid surface and the head groups of the second layer being oriented toward the aqueous media. Gaudin and Fuerstenau [30-31] introduced the term hemimicelles to describe the two dimensional hydrophobic aggregates of closely packed surfactants at the solid liquid interface. Harwell *et. al.* [32] suggested the name admicelles for the bilayer aggregates. It should be mentioned here that, the exact mechanisms and the structure of the formed aggregates are the subject of some controversy [29]. Even direct spectroscopic studies reported on a given adsorption system are not able to dispel doubts since the proposed interpretations of the spectroscopic data are often contradictory. Moreover, the adequacy of such an experimental method is sometimes questioned because of a number of uncertainties concerning the location of the probe molecules in the host microstructures and their specific mutual interactions [29].

As shown in Figure 6-1 and Figure 6-2, the magnitude of the surface excess at the transition from stage II to III, is comparable for all the surfactants adsorbed from aqueous solutions. In the absence of brine, this value tends to be about 1-2 molecules nm^{-2} at 25 °C for all of the adsorbed surfactants onto 316L stainless steel particles. These amounts of adsorption are corresponding to an average surface area of about 100 and 50 Å^2 per adsorbed surfactant molecule, respectively. In the case of C1018 mild steel, the short chains give rise to adsorption values of 1 molecules nm^{-2} while those for the long chain are 3 molecules nm^{-2}. Accordingly, the corresponding average surface areas per adsorbed molecule are 100 and 33 Å^2, respectively. This in turn indicates a titled or a perpendicular orientation of the adsorbed molecules. This conclusion is based on an average area per molecules adsorbed at air-water interface of about 33-48 Å^2, which has been determined experimentally from air-water surface tension isotherms earlier in *Chapter 3*. Such an orientation minimizes the contact area between surfactant molecules and water molecules and results in increasing the hydrophobic interaction between the tails groups.

Recently, the *in-situ* Surface-Enhanced Raman spectroscopy (SERS) has been used by De Marco *et. al.* [35] to investigate the adsorption of benzyldimethylhexadecylammonium chloride (C16BDMAC) onto mild steel electrodes. The SERS spectrum for C16BDMAC indicated a tilted orientation of the benzyl ring at the surface with three benzene carbons intimately in contact with the steel surface at a concentration of about 1.1 × 10^{-4} M.

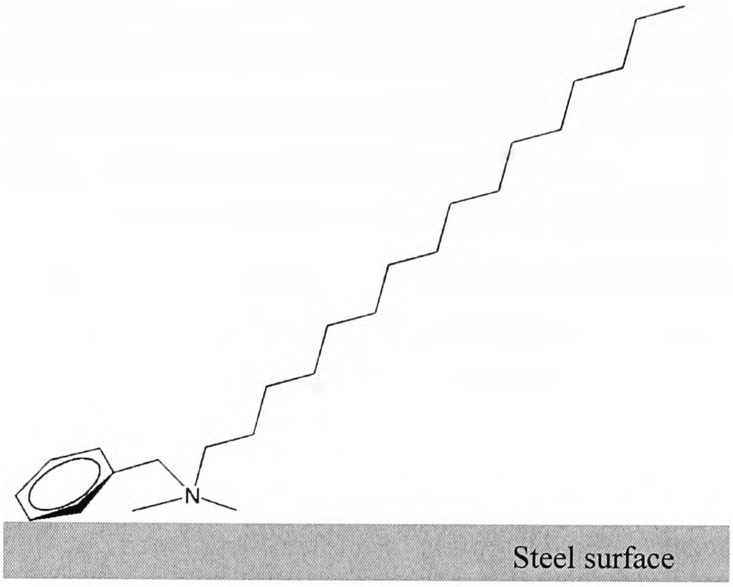

Figure 6-16. The orientation of benzyldimethylhexadecylammonium chloride (1.1 × 10^{-4} M) onto a mild-steel surface [35].

Additionally, it can be noticed from Figure 6-1 and Figure 6-2 that the concentrations at which the transitions take place are very comparable regardless of the solid particles nature. The II/III transitions occur at 1 × 10^{-2} M for C14BDMAC on both the 316L and C1018 mild steel surfaces. For C16BDMAC, this transition appears at 5 × 10^{-4} and 4 × 10^{-4} M on C1018 and 316L steel powder, respectively.

Stage III (C→D): The Plateau or Increased Adsorption Stage

([CnBDMAC]$_{eq.}$ ≥ 1 cmc) & (Γ_{max} ≥ 2-4 molecule nm^{-2} onto 316L
= 4-7 molecule nm^{-2} onto C1018)

The third stage starts at surfactant concentrations close to the cmc and it is characterised by the formation of fully formed aggregates or multilayers and saturation levels of surface coverage. The adsorption process in this stage shows little if no effect on the zeta-potential of the steel particles. In this stage, the increase in the alkyl chain length led to a shift of the adsorption isotherms toward lower equilibrium surfactant concentrations. Noticeably, the shape of the adsorption isotherm at this stage third stage corresponding to C10 and C12 is different from that for C14 and C16BDMAC. Obviously, beyond the II→III transition, the long chain surfactants (C14 and C16) adsorption isotherms tend to approach a saturation value and therefore a major increase in the surfactant concentration does not lead to a corresponding change in the amount of adsorption (Figures 6-1 and 6-2). On the other hand, the increase in the surfactant concentration of the short chains C10 and C12BDMAC results in an adsorption maximum above the cmc.

The amount of C14 and C16BDMAC adsorbed on C1018 particles gives rise to a plateau value of about 4 and 7 molecules nm^{-2} and those corresponding to 316L are 3 and 4 molecules nm^{-2}, respectively. The aforementioned maximum quantities of adsorption corresponding to an area of about 25 and 14.3 $Å^2$ per one adsorbed molecule of C14 and C16BDMAC on C1018 particles while this tend to be 50 and 25 $Å^2$ for 316L particles, respectively. The short chains C10 and C12BDMAC have a maximum adsorption of about 7 molecules nm^{-2} at C1018-water interface and 4 molecules nm^{-2} at 316L-water interface. This corresponds to a molecular area of about 14.3 $Å^2$ for C10 and C12BDMAC adsorbed onto C1018 particles while this tend to be 25 $Å^2$ for 316L particles, respectively.

By taking the minimum spatial requirements of 0.32 $Å^2$ for the alkylbenzyldimethylammonium head group, oriented perpendicular to the interface [36-38] a theortical occupation densitie of 3 molecule nm^{-2} is obtained. Earlier in *Chapter 3*, we reported that the adsorption of CnBDMAC corrosion inhibitors at air-water interfaces gave rise to a maximum surfaces excess of about 2 molecules nm^{-2} at surfactant concentration corresponding to the cmc. Arguably, we could assume that an adsorption amount of about 2 -3 molecules nm^2 of CnBDMAC corresponds to a monolayer at the steel-water interfaces. The aforementioned amounts of adsorption, indicate that the adsorption of CnBDMAC corrosion inhibitors onto the 316L and C1018 steel surfaces is not limited to a monolayer.

In a previous work conducted in our research group [22], the variation of C1018 mild steel discs contact angle as a function of the adsorbed C12BDMAC corrosion inhibitor under air and CO_2 conditions has been investigated with and without brine. In all cases, it has been reported that the exposure to high C12BDMAC concentrations causes the contact angle to decrease. This reflects an increased affinity of the mild steel surface for water. This observation was attributed to the formation of a bilayer arrangement of the adsorbed surfactant on the mild steel, which render the surface hydrophilic.

As discussed earlier in *Chapter 1*, one of the important features in the sequential adsorption of cationic surfactant is the interaction of the cationic headgroup with anionic charged sites the steel surface. This leads to changes in the effective surface charge density and concomitant changes in the overall structure of the electrical double layer. In a simple manner, this can be discussed qualitatively in terms of the electrical double layer model presented earlier in *Chapter 1*.

A schematic diagram summarizing the proposed adsorption mechanism of CnBDMAC surfactants molecules onto steel particles, the possible orientation and effect on the Stern potential in each stage is shown in Figure 6-17.

6.5.2. Effect of brine addition

The brine addition has been shown to increase the amount of adsorption in all stages of the adsorption process as has been shown in Figure 6-4 and Figure 6-5. There are two types of electrostatic interactions govern the adsorption of cationic surfactants on negatively charged surfaces, namely: (a) that between the surfactant and the solid surface; attractive and (b) that among the surfactants headgroups, which is repulsive.

The addition of brine results in screening the electrostatic repulsive interactions among the surfactants head-groups. Hence, one would expect that more molecules would be adsorbed onto steel surface in the presence of brine. Consequently, in the presence of electrolyte, adsorbed surfactant molecules are placed densely due to increased lateral interactions between the tails as electrical repulsions between the head-groups are weakened. The added electrolyte and the length of the hydrocarbon chain have a considerable influence on the extent of adsorption.

The effect of electrolyte on the adsorption of surfactant at the solid-liquid interface have been studied widely in literature [24]. Koopal *et al.* [25] have studied the effect of electrolyte concentration on the adsorption of anionic and cationic surfactant onto a oppositely charged solid surfaces. They observed that, at the initial part of the isotherm, stages I and II, adsorption occurs at lower concentrations when the electrolyte concentration is low.

Figure 6-17. A schematic diagram describes three-stage adsorption mechanism with the possible orientation and effect on the Stern potential in each stage [23].

Stage I: The Ion Exchange Stage

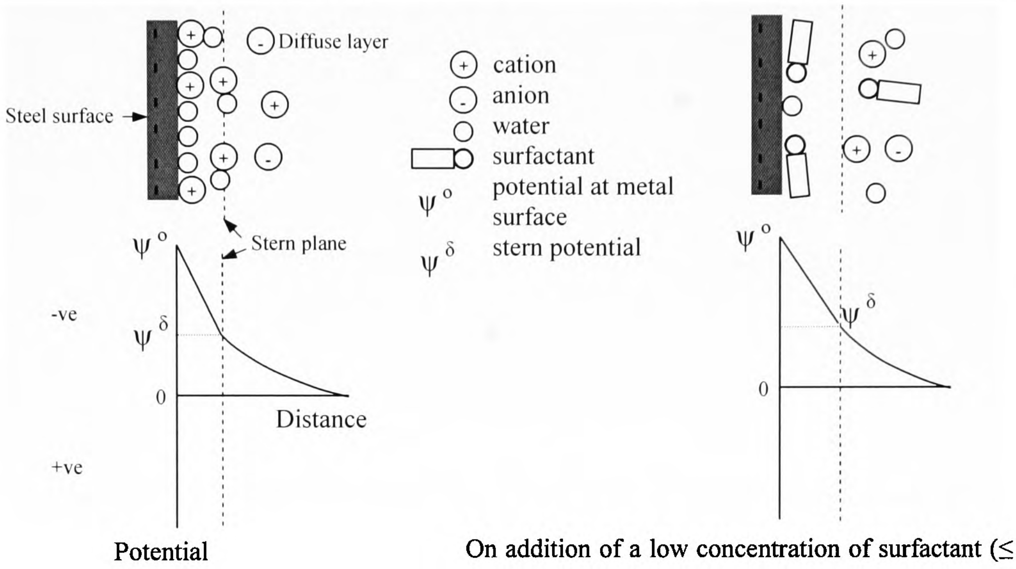

In a simple electrolyte solution, some counterions are adsorbed in the Stern layer, and some in the diffuse layer

On addition of a low concentration of surfactant (≤ 0.1 cmc), ion exchange occurs both in the Stern layer and in the diffuse layer. The Stern potential decreases slightly (less negative). Surfactants are expected to adsorb tilted or perpendicular to the solid steel surface.

Stage II: The Charge Reversal Stage

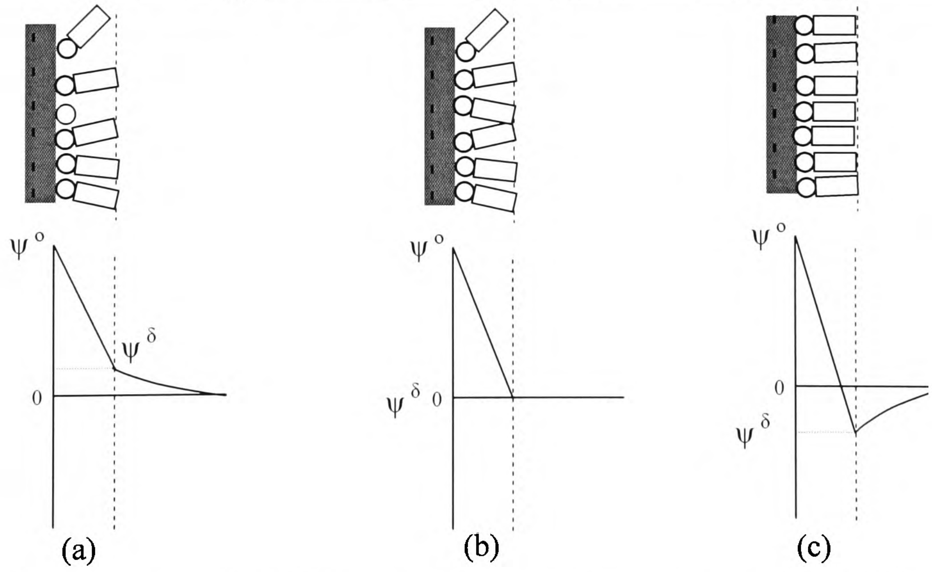

(a) (b) (c)

On increasing surfactant concentration (0.1 - 1 cmc), more surfactants molecules adsorbed on metal surface, which results in; (a) a sharp change in the Stern potential, followed by (b) a neutralization of the surface charge and finally (c) a charge reversal. The hydrophobic effect dominate this stage and promote the self-assembly of adsorbed monomers and results in the formation of a monolayer.

Stage III: The Plateau or Increasing Adsorption Stage

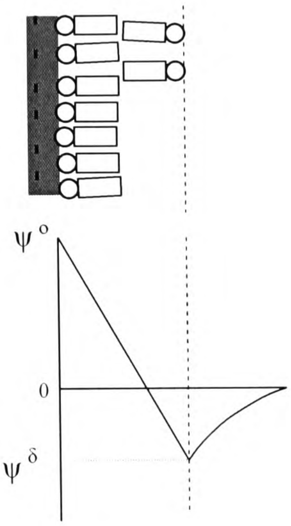

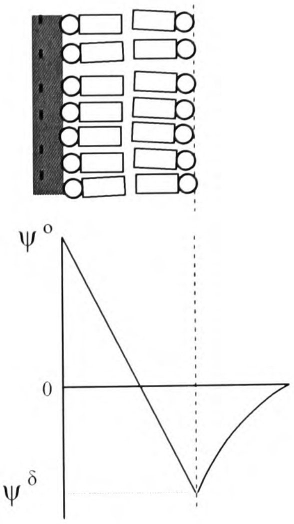

At surfactant concentration ≥ the cmc, the amount of surfactant adsorbed onto the steel surface increases slightly and then may approach a saturation value or continue to increase. Accordingly, the Stern potential now becomes more positive. The adsorbed surfactant molecules associate because of the increased hydrophobic interactions. There are three possible structures of the associated adsorbed molecules; a bilayer or a hemimicelle or a surface micelle. The formation of spherical associates around a single anchor molecule, i.e., surface micelle, must, however, be regarded as doubtful. Better arrangement would be the formation of monolayer structures in region II followed by a. bilayer formation in region III under the influence of hydrophobic interactions only after compensation of the surface charge at the PZC. The formation of a hemi-micelle is expected to take place at high surface coverage, probably in the presence of electrolytes.

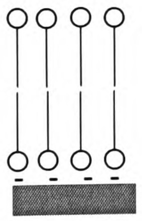
Admicell or bilayer

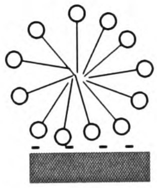
Hemi-micelle

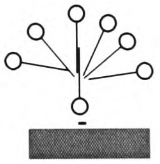
Surface micelle

Additionally, an increase in the ionic strength of the bulk medium causes a screening of the Coulombic repulsion among surfactants head-groups, leading to an increase in the maximum amount of adsorption.

Recently, Atkin, *et al.* [6, 15] studied the equilibrium and kinetic aspects of the adsorption of alkyltrimethylammonium surfactants at the silica-water interface using optical reflectometry. Their results indicated that, the adsorption of CTAB in the presence of 0.01 M KBr takes place at lower concentrations in comparison to solutions with no added salt. Additionally, they found the level of adsorption to be higher in the presence of electrolyte. This has been attributed to the screening of the head-group charge by electrolyte, which reduces the surfactant headgroup area and allows more tightly packed surfactant aggregates to form. They reported that above the critical micelle concentration, micelles are adsorbed directly to the surface and that as the chain length and electrolyte concentration increased, the hydrophobicity of the surfactant has a greater influence on the adsorption kinetics. It is also has been reported that upon addition of electrolyte, the steps in the isotherm are no longer observed. This was not the same in our case in which as shown clearly in Figure 6-6 that, three different region can still be distinguishable in the adsorption isotherms.

More recently, Gurses *et al.* [26] studied the effect of electrolyte addition on the adsorption of cetyltrimethylammonium bromide (CTAB) onto a clayey soil. They found that the amount of surfactant adsorbed increases with the increase in the electrolyte concentration. They interpreted this behaviour to the increase in the ionic strength, which increases the tendency of the long hydrophobic tail to escape from the bulk solution to the solid surface.

6.5.3. Effect of temperature

The increase in temperature usually decreases the amount of ionic surfactant adsorbed onto hydrophilic solid surfaces [6]. The increase in temperature (25 to 40 °C) had no influence on the adsorption extent of CnBDMAC onto steel surfaces in stage I in the absence and presence of brine. This in agreement with surfactant molecules being adsorbed electrostatically on the oppositely charged steel surfaces. On the other hand, the temperature has a pronounced influence on the adsorption extent in the second and third stages of the adsorption process. In the absence of brine, the rise in temperature decreases the amount of adsorption. This may be attributed to the increases in the solubility of ionic surfactants with the rise in temperature [27]. Additionally, in stages II and III, an aggregation process occurs both in the liquid phase and arguably on the surface and hence the adsorption process became dominated by the hydrophobic interaction between alkyl chains, which have an exothermic nature [11, 28]. This explains the decreasing in the surfactant amount adsorbed in stages II and III with the rise in temperature.

Partyka *et al.* [13] have investigated the temperature influence on the adsorption behaviour of benzyldimethyldodcylammonium bromide C12BDMAB from aqueous onto silica at free pH using depletion, calorimetric and electrophoretic methods. They reported the adsorption process was exothermic in the second and third stages. This in accordance with the decrease in the amount of surfactant adsorbed with the rise in temperature. Recently, a similar effect has been reported by Sabah and Celik [31] during the adsorption of dodecyltrimethylammonium bromide (DTAB) and hexadecyltrimethylammonium bromide (CTAB) from water by a clay mineral, sepiolite.

On the contrary, in the presence of brine, the rise in temperature increases the amount of adsorption in stages II and III of the adsorption process. Several authors have divided the adsorption of ionic surfactants from solution onto solid surfaces into two main processes depending on surfactant concentration, more precisely on the point of zero charge (PZC) [29, 30]. Lyklema *et al.* [29] studied the temperature effect on the adsorption of dodecylpyridinium chloride (C12PC) and dodecyltrimethylammonium bromide (C12TAB) on sodium kaolinite. They reported that adsorption on sodium kaolinite is not much dependent on temperature before the PZC; whereas beyond the PZC adsorption passes through a maximum as a function of temperature (T_{max} is 15 °C for C12TAB and 20-23 °C for C12PC). The position of this maximum depends on the nature of the interacting organic molecules and on their degrees of freedom in which T_{max} may be different for adsorbed and free molecules. They interpreted the adsorption below the PZC as caused by exchange of $C12P^+$ or $C12TA^+$ cations against Na^+ and H^+ accompanied by a small change in the enthalpy. They claimed that the hydrophobic bonding drives the second part and the temperature effect on enthalpy shows the same trend as that for micellization of these surfactants.

Biswas *et al.* [31] reported a similar conclusion during their adsorption studies of CTAB from electrolyte solution onto cellulose. They reported that the adsorption of CTAB from sodium chloride containing solution, at regions II and III, at 20 °C was found to be higher than that at 30 °C but less at 36°C. This observation confirms that adsorption of CTAB from electrolyte solution onto cellulose passes through a maximum as a function of temperature as well (T_{max} is 30 °C). Recently Mishra and Panda [32] reported that that adsorption of cetyltrimethylammonium bromide CTAB onto coal sample also increases with temperature up to 70 °C.

Another possible justification for the increased amount of adsorption caused by the rise in temperature in stages II and III may be attributed to change of the structure of surface aggregate from flat layer into a cylinder or a sphere [33, 34]. The latter two structures allow more surfactant monomer to be adsorbed in comparison with the flat structure. Using atomic force microscopy (AFM), Liu and Ducker [34] studied the structure of adsorbed surface aggregates of alkyltrimethylammonium bromide (CnTAB) surfactants to mica surface from aqueous solution. They observed that for a given salt concentration, a transition from a flat structure to cylinders as the temperature raise. They claimed that addition of alkali-halide salts leads to a transition from a flat layer to cylinders for C16TAB, C18TAB and C20TAB or spheres for C16TACl [33, 34]. The concentration of electrolyte required to break up the flat layer structure was a function of temperature and the length of the alkyl chain.

6.5.4. Thermodynamical analysis of the adsorption data

Using the experimentally determined adsorption isotherms, we could retrieve important information on the thermodynamic aspects of the adsorption of alkylbenzyldimethylammonium chlorides onto steel particles. Two approaches have been used to investigate some of the thermodynamic aspects of the adsorption process. The first approach is based on the adsorption equilibrium constants determined from the fitting of the adsorption isotherms to the two-stage Langmuir model. The standard free energy of adsorption ΔG°_{ads}, corresponding to each of the two assumed Langmuir stages, could be evaluated from the equilibrium constant K_1 and K_2, (determined from the fitting process), according to the following equation:

$$\Delta G^{\circ}_{ads} = -RT \ln K \qquad (6\text{-}3)$$

Equation (6-3) is widely used to calculate the standard free energy of surfactant adsorption at air-water and water-solid interfaces [39]. Table 6-5 and Table 6-6 show the standard free energy of adsorption ΔG^{o}_{ads}, corresponding to the adsorption of CnBDMAC from water onto C1018 and 316L steel powder 25 °C respectively.

Generally, values of ΔG^{o}_{ads} up to -40 kJ mol^{-1} are consistent with the electrostatic interaction between the charged molecules and the charged metal (physical adsorption) while those more negative than -40 kJ mol^{-1} involve sharing or transfer of electrons from the inhibitor molecules to the metal surface to form a co-ordinate type of bond (Chemisorption) [40].

Table 6-5. The standard free energy corresponding to the adsorption of different alkylbenzyldimethylammonium onto C1018 steel from water at 25 °C.

Parameters	C10	C12	C14	C16
ΔG^{o}_{ads1} / kJ mol^{-1}	- 19.1	- 22.7	- 23.5	- 23.5
ΔG^{o}_{ads2} / kJ mol^{-1}	- 1.20	- 3.60	- 4.13	- 4.80

The standard free energy of adsorption ΔG^{o}_{ads} corresponding to the adsorption of C10, C12 and C16DMAC from brine solution onto C1018 steel particles at 25 °C is given in Table 6-7. Clearly, the values of ΔG^{o}_{ads} in the presence of electrolyte tend to be more negative than those corresponding to adsorption from water. However, the standard free energy of adsorption ΔG^{o}_{ads1} values for CnBDMAC corrosion inhibitors from brine solution still more positive than -40 kJ mol^{-1}.

Table 6-6. The standard free energy corresponding to the adsorption of different alkylbenzyldimethylammonium onto 316L steel from water at 25 °C.

Parameters	C10	C12	C14	C16
ΔG^{o}_{ads1} / kJ mol^{-1}	- 20.0	- 21.7	- 22.0	- 22.9
ΔG^{o}_{ads2} / kJ mol^{-1}	- 3.90	- 4.13	-	-

Dawson and Zvauya [41] reported a standard free energy ΔG°_{ads}, of about -46 kJ mol^{-1} for the adsorption C16BDMAC onto pure iron rods from 3% sodium chloride solutions at 25 °C. This value has been calculated from the equilibrium constant estimated by fitting the degree of surface coverage, θ, determined electrochemically, to the Frumkin adsorption isotherm. Accordingly, they claim that CnBDMAC was adsorbed both via the positively charged nitrogen atom and the π- electrons of the benzene ring. Therefore, they conclude that adsorption of CnBDMAC on iron is not limited to a Physisorption, but it may involve Chemisorption, which involves charge transfer, or charge sharing.

Recently, the *in-situ* Surface-Enhanced Raman Spectroscopy (SERS) has been used by De Marco *et. al.* [35] to investigate the adsorption of benzyldimethylhexadecylammonium (C16BDMAC) onto mild steel electrodes. They found no significant shift in peak positions upon adsorption, inferring that the inhibitor is probably physisorbed to the steel surface with the possibility of some π-electrons donation by the aromatic ring.

Table 6-7. The standard free energy corresponding to the adsorption of different alkylbenzyldimethylammonium onto C1018 steel from 4.7 wt.% brine at 25 °C.

Parameters	C10	C12	C16
ΔG°_{ads1} / kJ mol^{-1}	- 21.0	- 31.8	- 33.8
ΔG°_{ads2} / kJ mol^{-1}	- 5.00	- 14.2	-26.5

The second approach that we have used in the thermodynamical analysis of the adsorption data is based on the Stern-Grahame equation for adsorption in the Stern layer [42]. By means of the Stern-Grahame model of the double layer, the change in the free energy required to remove one mole of CH_2 groups from the aqueous pahse can be evaluated. The amount adsorbed of a surfactant ion in the Stern layer, Γ_{δ}, is controlled by the standard free energy of adsorption ΔG°_{ads}, and it is related to the surfactant concentration, C, in the bulk as follows [42]:

$$\Gamma_\delta = 2rC\exp\left[\frac{-\Delta G^\circ_{ads}}{RT}\right] = 2rC\exp\left[\frac{-ze\psi_\delta - n\phi}{RT}\right] \qquad (6\text{-}4)$$

where r is the effective radius of the organic ion, T is the absolute tempewrature , Γ_δ is expressed in molecules/nm^2, C in mol/cm^3, z is the valence of adsorbed surfactant ions, e is the electronic charge, ψ_δ is the potential at the Stern plane in volts, n is the number of carbon atoms for an alkyl chain, ϕ is the free energy change involved in removing one CH_2 group from the aqueous phase.

Under conditions where ζ is zero, the hydrophobic interactions will take place and all other adsorption effects become negligible. Hence, the Stern-Grahame expression for the specific adsorption of surfactant ions could be writing as follows:

$$\ln C_\circ = -n(\phi / RT) + \ln \Gamma_\circ / 2r \qquad (6\text{-}5)$$

where $C = C_0$ at $\psi = 0$ (approximately ζ=o). Assuming $\ln \Gamma_\circ / 2r$ to be constant, $\ln C_0$ should be a linear function of alkyl chain length (n) with a slope of ϕ/RT. The concentration C_o, at which the ζ potential is reduced to zero is plotted as a function of the number of carbon atoms (n) surfactant alkyl chain and represented in Figure 6-18. The linear relation between $\ln C_0$ and n as predicted by equation (6-5) is verified. The slope of this line is about -0.5, which indicates that, the free energy involved in removing one CH_2 group from the aqueous phase is -1.20 kJ mol^{-1}. This value is not in the same order of magnitude as that for the micellization of CnBDMAC, which has been determined previously in section 3.6.2 to be about - 3 kJ mol^{-1}.

Following this approach for analyzing ζ potential data for the quartz - alkylammonium acetates with hydrocarbon chains ranging from 10 to 18 carbon atoms, Somasundaran *et al.* [12] calculated ϕ (the free energy change per methylene group upon transfer of a monomer in aqueous solution to the hemimicelle) to be -1.0 RT (about -2.5 kJ mol^{-1}). They reported that, this value is in the same order of magnitude as for the micellization of alkylammonium acetate surfactants in aqueous solutions. They claim that there is analogy between the micellization and the hemimicellization process. Additionally, Fuerstenau [43] and Rosen [39] reached the same conclusion, that the van der Waals cohesive energy of hemi-micelle formation is similar to that of micellization.

Figure 6-18. Variation of natural logarithm of BDMAC equilibrium surfactant concentration, at which the ζ-potential of C1018 mild steel particles is reduced to zero, as a function of the number of carbon atoms (n). Adsorption experiments conducted at 25 °C and pH of 8-9.

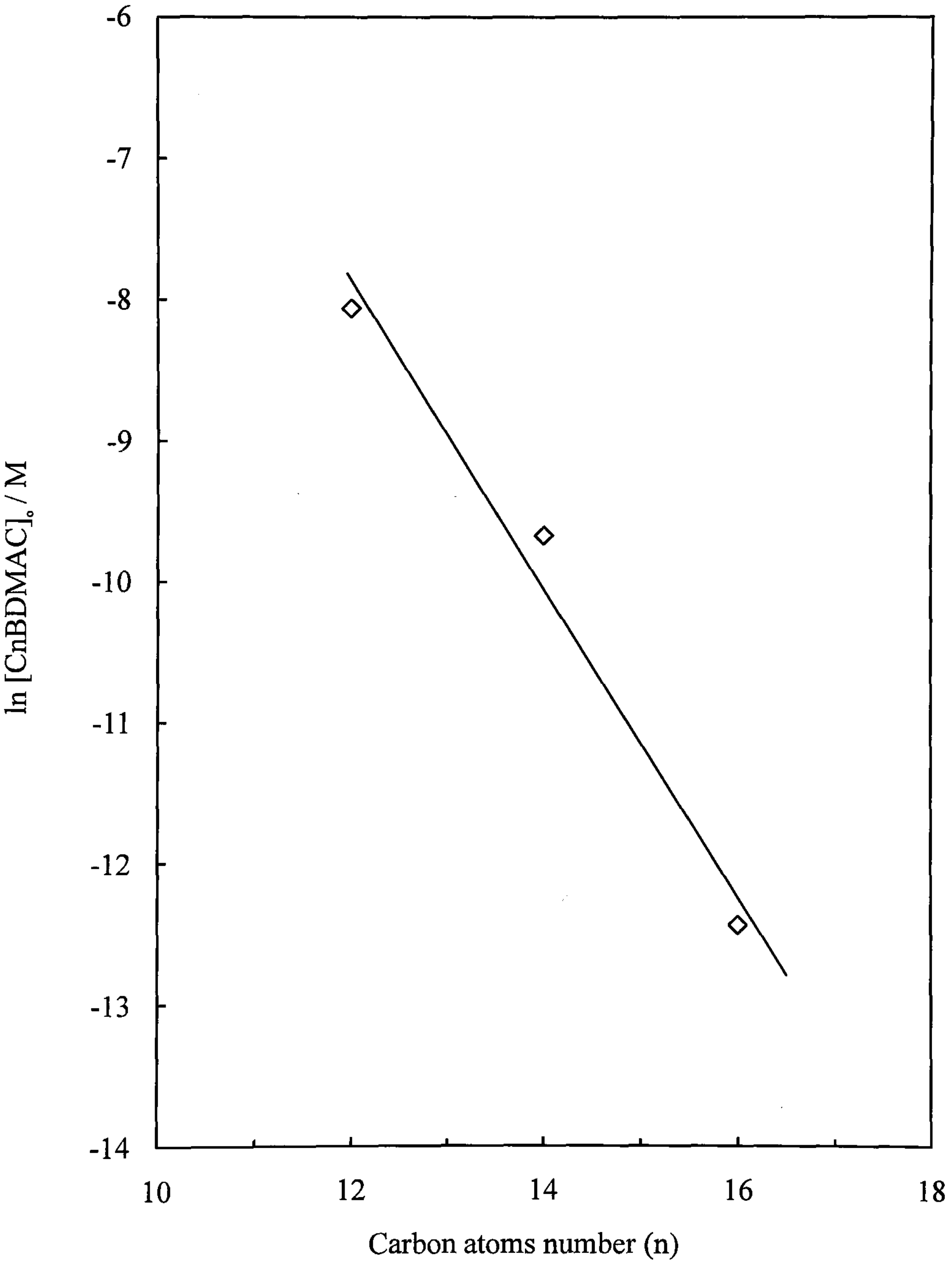

6.5.5. Adsorption of CnBDMAC onto C1018 mild steel vs. 316L stainless steel

The alkylbenzyldimethylammonium chlorides corrosion inhibitors have been shown to exhibit a higher affinity for C1018 mild-steel compared to 316L stainless steel particles as shown earlier by the adsorption isotherms. This conclusion is true for all the adsorption isotherms determined under the experimental studied conditions. Obviously, as shown in Figure 6-19 the amount adsorbed of C10 and C16BDMAC onto C1018 mild-steel from aqueous water at 25 °C is higher than that for 316L stainless steel for the concentration range studied. For C10BDMAC system, the maximum amount adsorbed by C1018 mild-steel is about 7 molecules nm^{-2} compared to about 4 molecules nm^{-2} adsorbed on 316L stainless-steel at nearly the same surfactant equilibrium concentration.

Similarly, the adsorption of C16BDMAC gives rise to the same maximum amount of adsorption on C1018 of about 7 and less than 4 molecule nm^{-2} onto 316L particles, but at much lower surfactant equilibrium concentrations. The difference in the adsorption affinity and extent of these quaternary ammonium surfactants could be attributed possibly to three main reasons.

Firstly, the continuous change in pH of the surfactant solution during C1018 steel adsorption experiments caused by the corrosion process. This process results in raising the pH of the surfactant solutions up to pH 9 compared to a pH value of about 7 for the 316L. Therefore, the rise in pH values results in an increase in the degree of adsorption due to the expected increase in the negatively charged sites on C1018 mild-steel. The rise in pH of surfactant aqueous solutions containing the mild steel particles is attributed to the formation of $Fe(OH)_2$. The pH of saturated $Fe(OH)_2$ solutions is about 9.5 [44], so that the surface of iron corroding in aerated pure water is always alkaline.

Secondly, as the two steel have a different chemical and surface composition. Consequently, one should expect a parallel different adsorption characteristic as well. The 316L stainless steel alloy contains a maximum of 0.03 % Carbon, a minimum of 16% Chromium, 10 % Nickel, a maximum of 2 % Manganese and the rest is iron. On the other hand, the C1018 mild steel alloy is composed of iron mainly, about 99-98 % iron. Recently, a surface analysis study using conversion electron and X-ray Mössbauer spectra (CEMS and XMS), has been applied to characterize stainless steel thin films.

Figure 6-19. Adsorption of C10 and C16BDMAC from water onto 316L and C1018 steel powder at 25 °C using depletion method. The solid lines represent the two-stage Langmuir model fits. The vertical dashed lines represent the cmc.

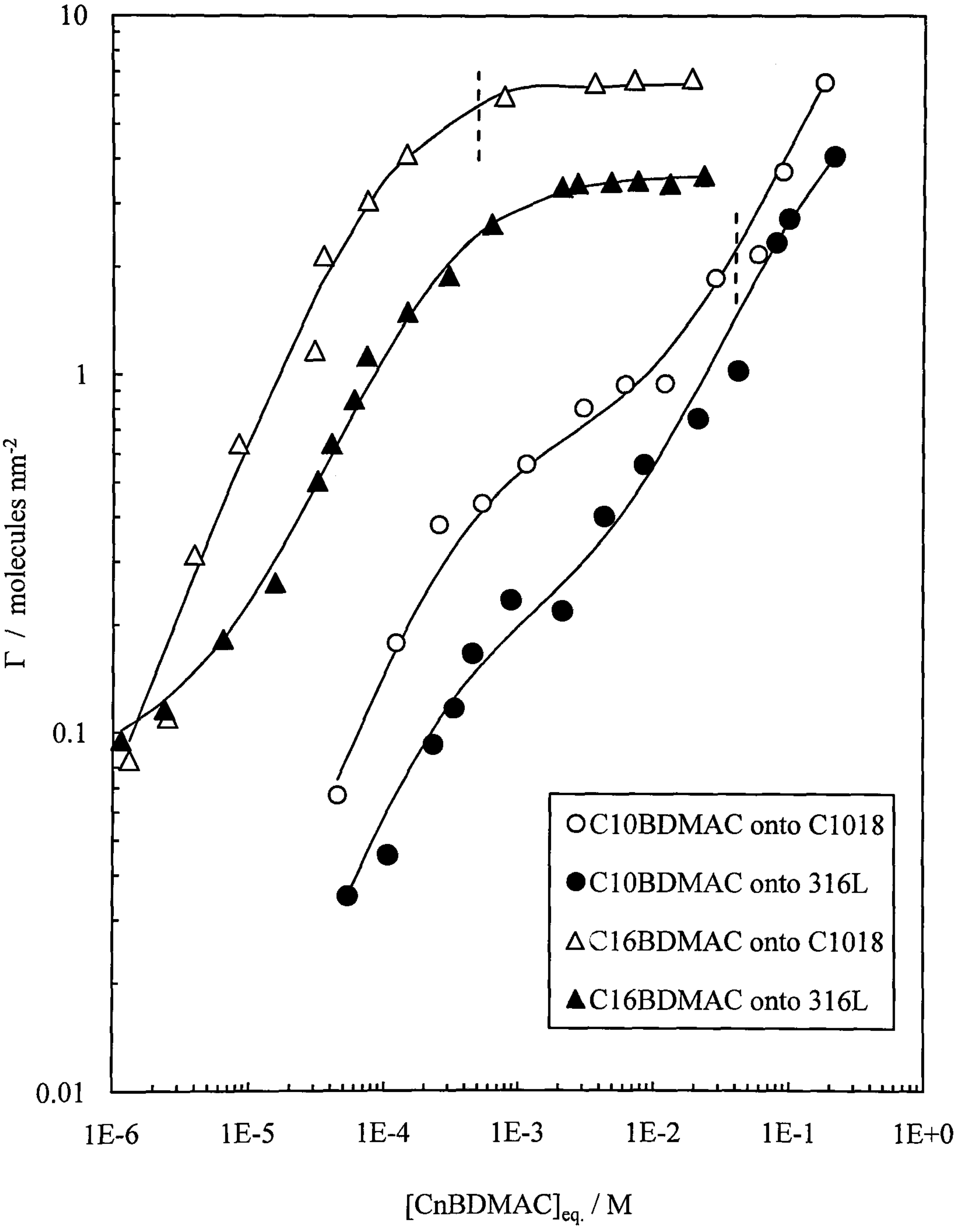

This study showed that stainless steel surface oxide layers in the air are composed mainly of Cr_2O and Fe_2O_3 [45]. This conclusion proves that, the surface of 316L steel alloy is not purely iron in comparison to the C1018 mild steel, which contains up to 98 % iron. This in turn could explain the difference in the adsorption behaviour of CnBDMAC onto the two steel types.

Finally, the surface charge density of the two-steel particles plays a crucial role in the adsorption behaviour of CnBDMAC. Figure 6-20 shows the change in the surface charge density of C1018 and 316L steel particles during the adsorption of C12BDMAC from aqueous solution at 25 °C. As seen in the figure, at low surfactant concentrations, the negative surface charge in C1018 solution is slightly higher than that in 316L solution. This in turn explains the higher affinity of C12BDMAC surfactant molecules for the C1018 particles compared to the 316L. Similarly, with increasing the surfactant concentration, the C1018 steel particles exhibit a higher positive surface charge density than that for the 316L steel particles. This could be attributed to the increased hydrophobic interactions between the surfactant tails – initially adsorbed at lower surfactant concentrations.

6.6. SUMMARY AND CONCLUSION

In this chapter, the adsorption behaviour of the cationic surfactant alkylbenzyldimethylammonium chlorides (C10-C16) onto two different steel particles, namely C1018 mild-steel and 316L stainless-steel has been studied for the first time in detail. This study investigated the effects of the alkyl chain length of the surfactants, temperature and the electrolyte concentration on the amount of surfactant adsorbed. The key and new findings within this study are summarized below.

I. The adsorption isotherms shape gave rise to classical profiles of a typical cationic surfactant being adsorbed onto a negatively charged surface.

II. The log-log representation of the adsorption isotherms and the ζ-potential curves give rise to three distinct regions of different slopes indicating distinctive mechanisms. Stage I is characterized by the adsorption of surfactant monomers, which is mainly driven by electrostatic interactions. In stage II the hydrophobic effect intervened essentially to promote the self-assembly of adsorbed monomers, namely, the transition from a flat to a

Figure 6-20. Variations in the surface charge densities of C1018 and 316L steel particles as a function of C12BDMAC equilibrium concentration at 25 °C.

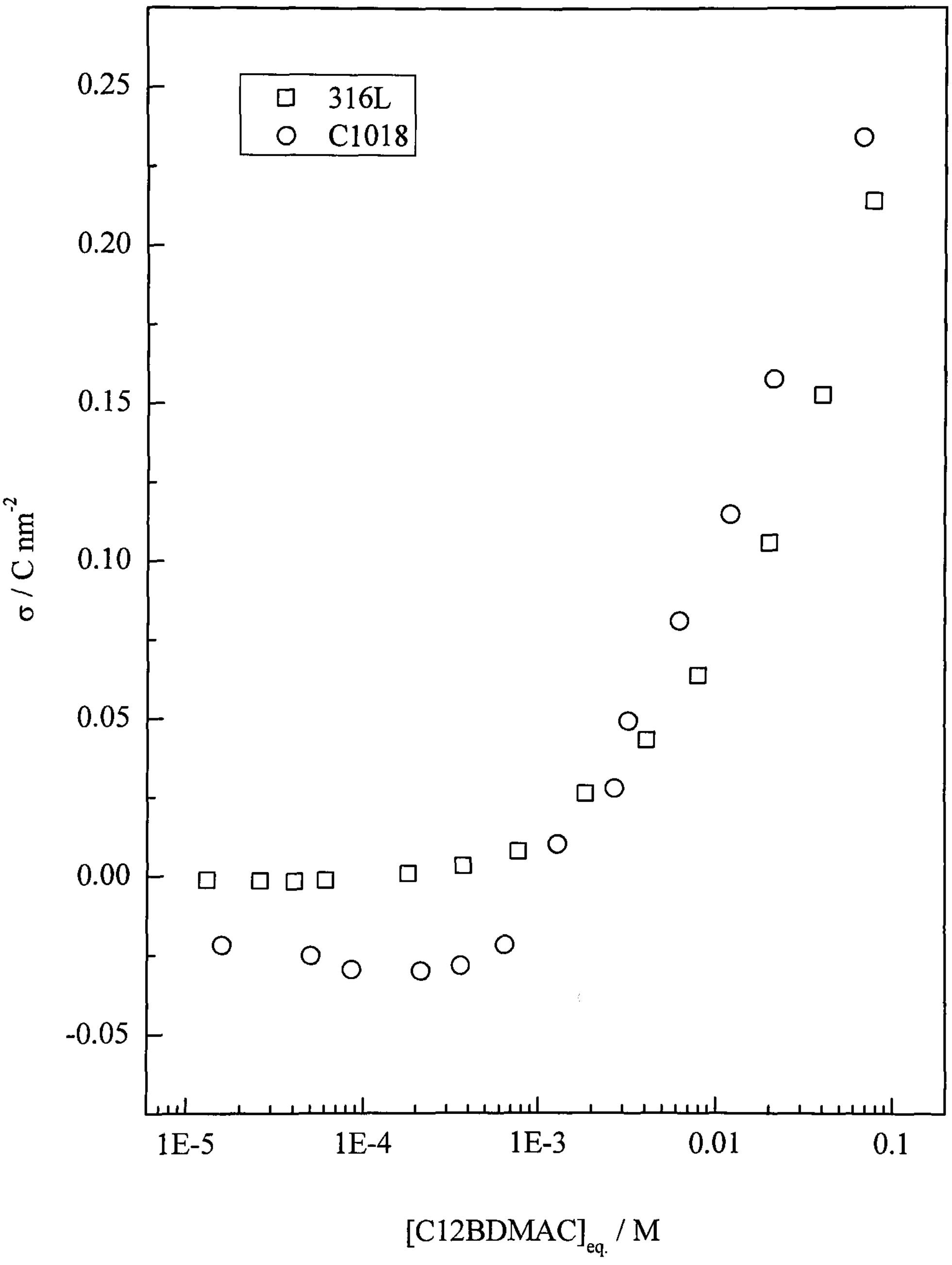

perpendicular conformation followed by association of the surfactant monomers (surface aggregation). In Stage III, the surface aggregates continue to grow.

III. The hydrophobic effect has shown to play an important role in the adsorption of surfactants from aqueous solution onto the steel surface. As the alkyl chain length increases the contribution of the hydrophobic interaction increases, overcoming repulsion forces among the cationic surface and surfactant headgroups and promoting the growth of a second layer. Accordingly, the short chain C16 and C14BDMAC have higher adsorption affinity for steel surfaces. Generally, the extent of adsorption has been shown to increase with the increase in the surfactant equilibrium concentration.

IV. The addition of brine increases the surfaces excess over the range of surfactant concentrations studied and results in the maximum amount adsorbed being reached at lower surfactant equilibrium concentrations.

V. The temperature effect on the adsorption behaviour is quite controversial. Whereas the rise in temperature results in a decrease in the amount adsorbed in the absence of electrolyte, it has the opposite effect in the presence of electrolyte.

VI. At higher equilibrium concentrations, the alkylbenzyldimethylammonium chlorides appear to adsorb on C1018 mild steel as multilayers (bilayer) or as surface micelles. On the other hand, it is limited to a monolayer at 316L stainless steel.

VII. The Alkylbenzyldimethylammonium chlorides have a higher affinity for C1018 mild steel compared 316L stainless steel under the investigated experimental conditions.

6.7. REFERENCES

1. T. P. Goloub and L. K. Koopal, *Langmuir*, **13**, 673 (1997).
2. A. W. Adamson, *Physical Chemistry of Surfaces*, Wiley, New York (1990).
3. D. B. Hough and M. G. Rendall, in *Adsorption from Solution at the Solid/Liquid Interface*, G. Parfitt and C. Rochester, eds., Academic press, London (1983).
4. C. M. González-García, M. L. González-Martín, A. M. Gallardo-Moreno, V. Gómez-Serrano, L. Labajos-Broncano and J. M. Bruque, *Sep. Sci. Technol.*, **37**, 2823 (2002).
5. B. Y. Zhu and T. Gu, *J. Chem. Soc., Faraday Trans.*, **85**, 3813 (1989).
6. R. Atkin, V. S. J. Craig, E. J. Wanless and S. Biggs, *J. Colloid Interface Sci.*, **266,** 236 (2003).
7. M. T. Garcia, E. Campos, J. Sanchez-Leal and F. Comelles, *J. Dispersion Sci. Technol.*, **27**, 739 (2006).
8. T. Kwolek, M. Hodorowicz, K. Stadnicka and J. Czapkiewicz, *J. Colloid Interface Sci.*, **264**, 14 (2003).
9. M. Knag, J. Sjoblom, G. Oye and E. Gulbrandsen, *Colloids Surf., A*, **250**, 269 (2004).
10. A. J. Mcmahon, *Colloid. Surface.*, **59**, 187 (1991).
11. S. Partyka, M. Lindheimer and B. Faucompre, *Colloids Surf., A*, **76**, 267 (1993).
12. D. W. Fuerstenau and R. Herrera-Urbina, in *Cationic Surfactants: Physical Chemistry*, D. N. Rubingh and P. M. Holland, eds., Marcel Dekker Inc., New York (1991).
13. J. L. Trompette, J. Zajac, E. Keh and S. Partyka, *Langmuir*, **10**, 812 (1994).
14. D. I. Horsup, J. C. Clark, B. P. Binks, P. D. I. Fletcher and J. T. Hicks, *Corrosion*, **66**, 036001 (2010).
15. R. Atkin, V. S. J. Craig and S. Biggs, *Langmuir*, **16**, 9374 (2000).
16. J. Zajac, J. L. Trompette and S. Partyka, *Langmuir*, **12**, 1357 (1996).
17. C. Giles, T. MacEwan, S. Nakhwa and D. Smith, *J. Chem. Soc.*, **3**, 3973 (1960).
18. E. McCafferty, *Electrochim. Acta*, **55**, 1630 (2010).

19. M. Kosmulski, *Surface Charging and Points of Zero Charge*, CRC Press, Boca Raton (2009).

20. E. J. Sullivan, J. W. Carey and R. S. Bowman, *J. Colloid Interface Sci.*, **206**, 369 (1998).

21. B. Ersoy and M. S. Celik, *Clays Clay Min.*, **51**, 172 (2003).

22. B. P. Binks, P. D. I. Fletcher, J. T. Hicks, D. I. Horsup and W. H. Durnie, *Proceedings of NACE Corrosion/2005*, Paper No. 05307, NACE International, Houston (2005).

23. B. T. Ingram and R. H. Ottewill, in *Cationic Surfactants: Physical Chemistry*, D. N. Rubingh and P. M. Holland, eds., Marcel Dekker Inc. , New York (1991).

24. S. Paria and K. C. Khilar, *Adv. Colloid Interface Sci.*, **110**, 75 (2004).

25. L. K. Koopal, E. M. Lee and M. R. Bohmer, *J. Colloid Interface Sci.*, **170**, 85 (1995).

26. A. Gurses, S. Karaca, M. Acikyildiz and M. Ejder, *Chem. Eng. J.*, **147**, 194 (2009).

27. R. Farn, *Chemistry and Technology of Surfactants*, Blackwell Publishing Ltd., New Delhi, India (2006).

28. J. Zajac, J. Trompette and S. Partyka, *J. Therm. Anal. Calorim.*, **41**, 1277 (1994).

29. T. Mehrian, A. De Keizer and J. Lyklema, *Langmuir*, **7**, 3094 (1991).

30. S. Partyka, M. Lindheimer and B. Faucompre, *Colloids Surf., A*, **76**, 267 (1993).

31. D. Chattoraj, P. Mahapatra and S. Biswas, in *Surfactants in Solution*, A. K. Chattopadhyay and K. L. Mittal, eds., CRC Press, New York (1996).

32. M. J. dos Reis, F. Silverio, J. Tronto and J. B. Valim, *J. Phys. Chem. Solids*, **65**, 487 (2004).

33. R. E. Lamont and W. A. Ducker, *J. Am. Chem. Soc.*, **120**, 7602 (1998).

34. J. F. Liu and W. A. Ducker, *J. Phys. Chem. B*, **103**, 8558 (1999).

35. W. H. Durnie, R. De Marco, A. Jefferson and B. J. Kinsella, *Surf. Interface Anal.*, **35**, 536 (2003).

36. J. Zajac and S. Partyka, in *Adsorption on New and Modified Inorganic Sorbents*, A. D browski and V. Tertykh, eds., Elsevier Science, Amsterdam (1996).

37. B. Dobias, X., Qiu and W., Rybinski, *Solid-Liquid Dispersions,* Marcel Dekker, New York (1999).

38. Z. Z. Ismail, U. Tezel and S. G. Pavlostathis, *Water Res.*, **44**, 2303 (2010).

39. M. J. Rosen, *Surfactants and Interfacial Phenomena*, Wiley-Interscience, Hoboken, N.J. (2004).

40. B. Trapnell and D. Hayward, *Chemisorption*, Butterworths, London (1964).

41. R. Zvauya and J. L. Dawson, *J. Appl. Electrochem.*, **24**, 943 (1994).

42. D. C. Grahame, *Chem. Rev.*, **41**, 441 (1947).

43. D. Fuerstenau, *Pure Appl. Chem.*, **24**, 135 (1970).

44. R. W. Revie and H. H. Uhlig, *Corrosion and Corrosion Control : an Introduction to Corrosion Science and Engineering*, Wiley-Interscience, Hoboken, N.J. (2008).

45. K. Nomura, T. Okubo and M. Nakazawa, *Spectrochim. Acta, Part B*, **59**, 1259 (2004).

CHAPTER 7

Chapter 7

ADSORPTION OF ALKYLBENZYLDIMETHYLAMMONIUM CHLORIDES AT THE SAND-WATER INTERFACE USING THE DEPLETION METHOD

7.1. INTRODUCTION

Sand is one of the main corrosion inhibitor consuming-solids encountered naturally in the oilfield along with clays, iron carbonate, iron sulphide, calcium carbonate and barium sulphate. Despite this fact, studies on the adsorption behaviour of the corrosion inhibitors on such parasitic surfaces and how these affect the ultimate fate of the inhibitor in a production system are limited. This chapter focuses on the determination of CnBDMAC adsorption characteristics from aqueous solution onto sand. Furthermore, the change in surface charge of the sand in alkylbenzyldimethylammonium chlorides solutions will be investigated. In this chapter, we describe the influence of chain length, temperature and brine addition on the adsorption characteristics of alkylbenzyldimethylammonium chlorides from aqueous solution onto sand under aerated conditions. In addition, the relative affinity and amount of adsorption of these surfactants onto steel versus sand particles will be evaluated and discussed.

7.2. EFFECT OF SURFACTANT CHAIN LENGTH

Adsorption isotherms determined for the homologous CnBDMAC onto sand particles, from aqueous solutions at 25 °C, are given in Figure 7-1. The adsorption isotherms were constructed by graphing the adsorbed amount of surfactant, Γ in molecules nm^{-2} units, versus the surfactant equilibrium concentration, $[CnBDMAC]_{eq.}$ in M units, in a logarithmic scale. The isotherms were fitted to the two-stage Langmuir model. The solid lines represent the two-stage Langmuir model fits. Table 7-1 illustrates the fitting parameters used to fit the experimentally determined adsorption isotherms to the two-stage Langmuir model.

As shown in Figure 7-1, the increase in length of the alkyl group is accompanied by an increase in the adsorption of the homologues series (from C10 to C16) onto sand particles. This result from the increasing affinity of the long chain surfactants toward the interfacial region because of growing hydrophobic interactions. The hydrophobic interactions include those laterally between the tails of adsorbed molecules at the solid surface and those between the tails of adsorbed molecules and that present in solution.

Table 7-1. Fitting parameters for the two-stage Langmuir adsorption isotherm of CnBDMAC from aqueous solutions onto sand particles at 25 °C.

Parameters	C10	C12	C14	C16
k_1 / M^{-1}	1.24×10^5	2.75×10^5	3.59×10^5	2.39×10^4
k_2 / M^{-1}	525	1.88×10^3	1.91×10^3	2.09×10^4
$\Gamma_{1\,(max)}$ / molecules nm^{-2}	1.60	1.05	1.42	1.09
$\Gamma_{2\,(max)}$ / molecules nm^{-2}	2.00	1.3	1.35	2.52
R^2	0.99	0.99	0.99	0.99

Figure 7-1. Adsorption isotherms of C10, C12, C14 and C16BDMAC from aqueous solutions onto sand particles at 25 °C using the depletion method at pH = 6.5-7. The vertical dashed lines represent the cmc. The solid lines represent the two-stage Langmuir model fits.

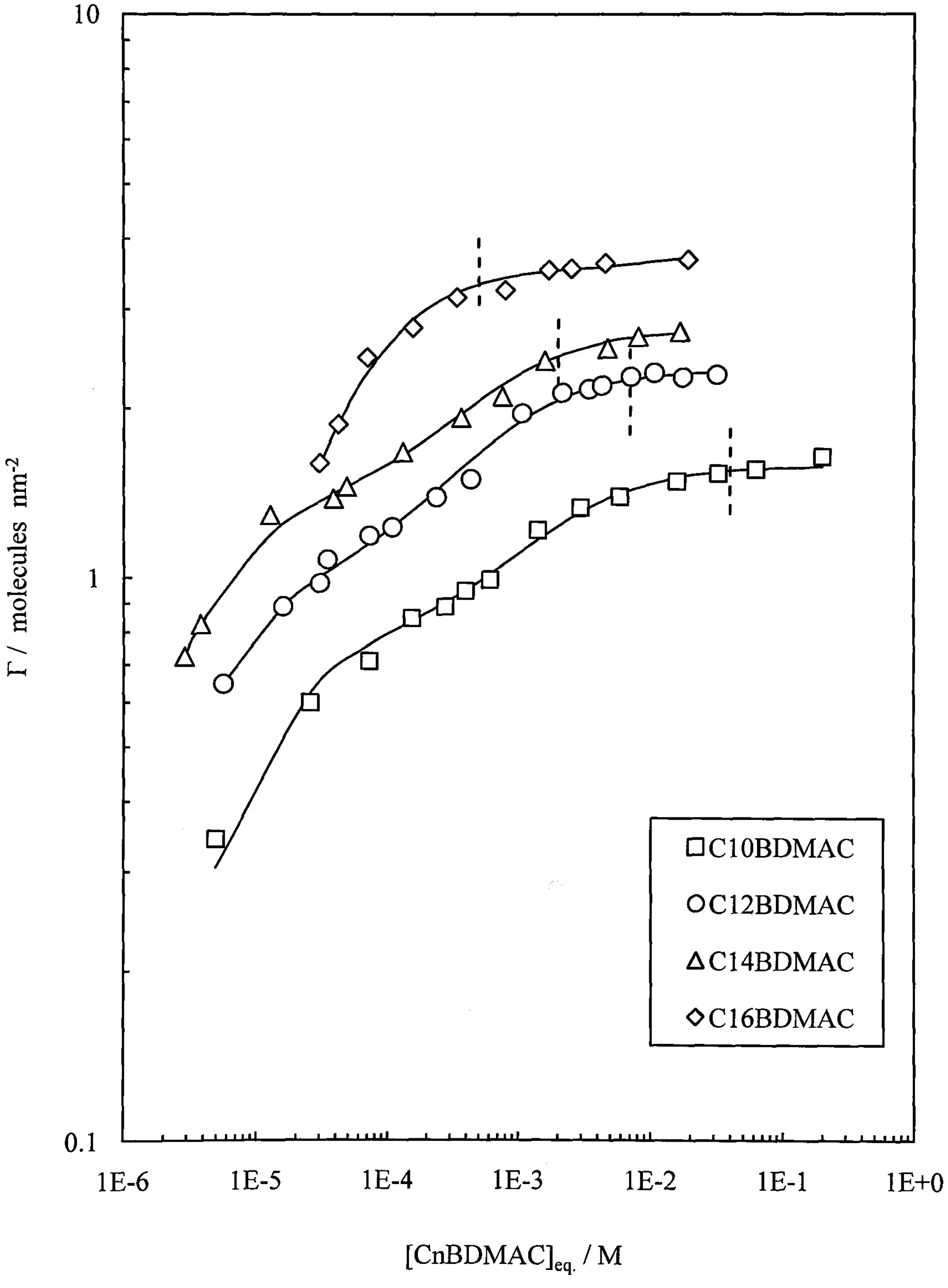

With increasing surfactant equilibrium concentrations, the amounts adsorbed of these surfactants onto sand approach plateau values. Clearly, the alkyl chain length appears to have a substantial influence on the plateau value of the isotherms. Noticeably, the adsorption isotherms exhibit a three-stage adsorption mechanism very similar to that reported in *Chapter 6* corresponding to the adsorption of CnBDMAC onto steel particles.

Figure 7-2 shows the variation of the ζ-potential of sand particles as a function of C14BDMAC equilibrium concentrations and the amount of adsorption at 25 °C from aqueous solutions. Similar to the adsorption isotherms, the ζ-potential graph of sand particles exhibits three distinguishable stages, which reflect different modes of surfactant-solid and surfactant-surfactant interactions.

The increase in the amount adsorbed of alkylbenzyldimethylammonium chlorides onto sand particles as the alkyl chain length of the cationic surfactant increases is a typical behaviour of an ionic surfactant being adsorbed onto an oppositely charged surface. As reported earlier in *Chapter 6,* the amounts of adsorption of these quaternary surfactants onto steel particles were found to increase similarly with increasing the surfactant chain length.

Recently, Paria and Yeut [1], studied the adsorption of four cationic surfactants homologues series(n-Alkylpyridinium bromides) with different chain lengths (C10-C16) from aqueous solution onto sand at 25 °C. They showed that, with increasing tail length, the maximum amount adsorbed at saturation increases, mainly because of increasing hydrophobic interactions. The maximum amounts adsorbed at saturation were 0.30, 0.60, 0.90 and 1.40 molecules nm^{-2} for C10, C12, C14, and C16 surfactants, respectively. Higher adsorbed amounts have been shown for our system correspond to about 1.60, 2.30, 2.70 and 3.60 molecules nm^{-2} for C10, C12, C14, and C16BDMAC.

7.3. EFFECT OF TEMPERATURE

The effect of temperature on the adsorption of C10BDMAC from aqueous solutions onto sand particles is shown in Figure 7-3, as a function of surfactant equilibrium concentrations. The experimentally determined adsorption isotherms were fitted to the two-stage Langmuir adsorption model using the fitting parameter shown in Table 7-2.

Figure 7-2. Variation of zeta potentials of sand particles as a function of C14BDMAC equilibrium concentration and the amount of adsorption at 25 °C from aqueous solution, using the depletion method at pH = 6.5-7.

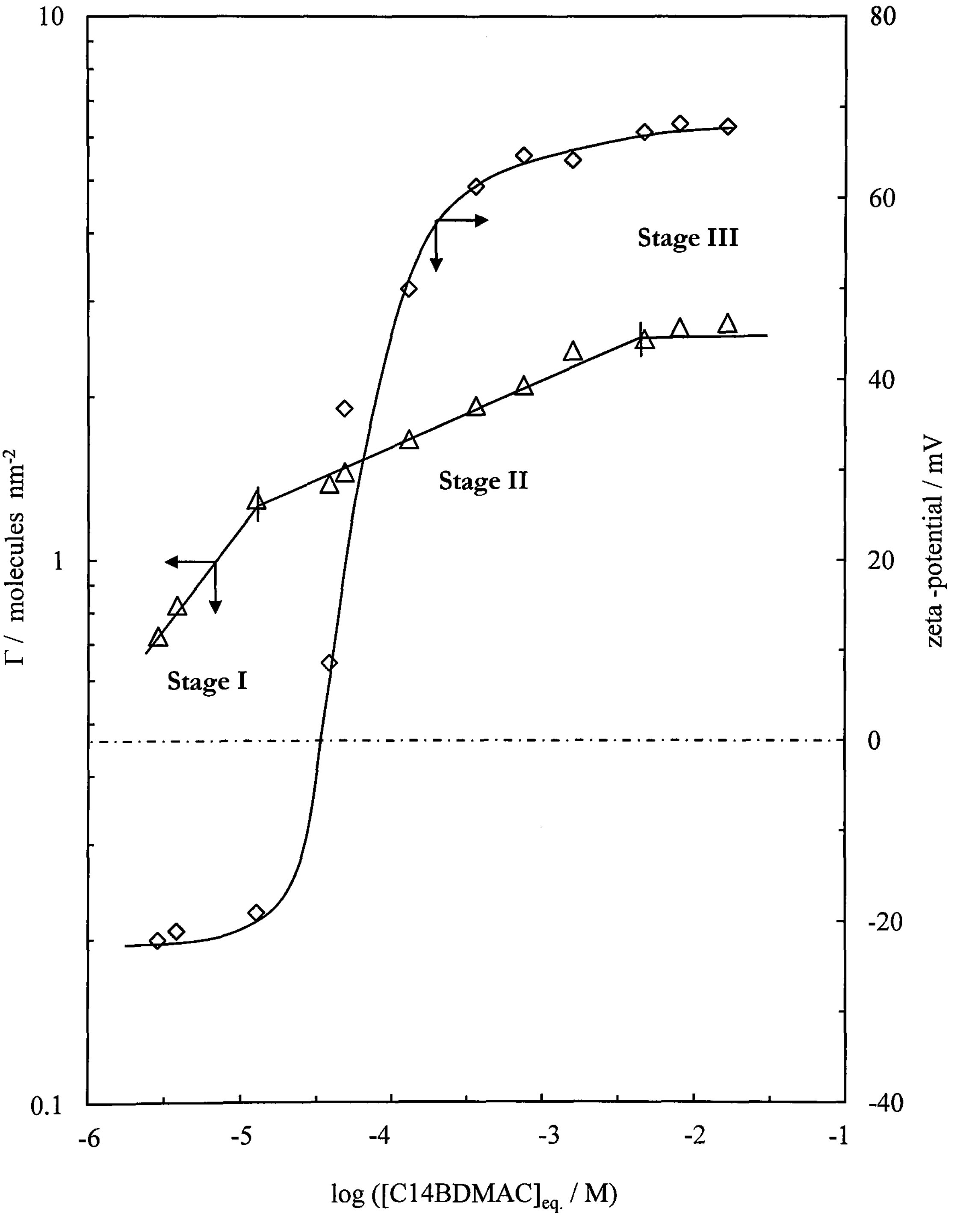

Figure 7-3. Adsorption of C10BDMAC from aqueous solution onto sand at 25 and 40 °C, and pH = 6.5-7 using the depletion method. The solid lines represent the two-stage Langmuir model. The vertical dashed line represents the cmc.

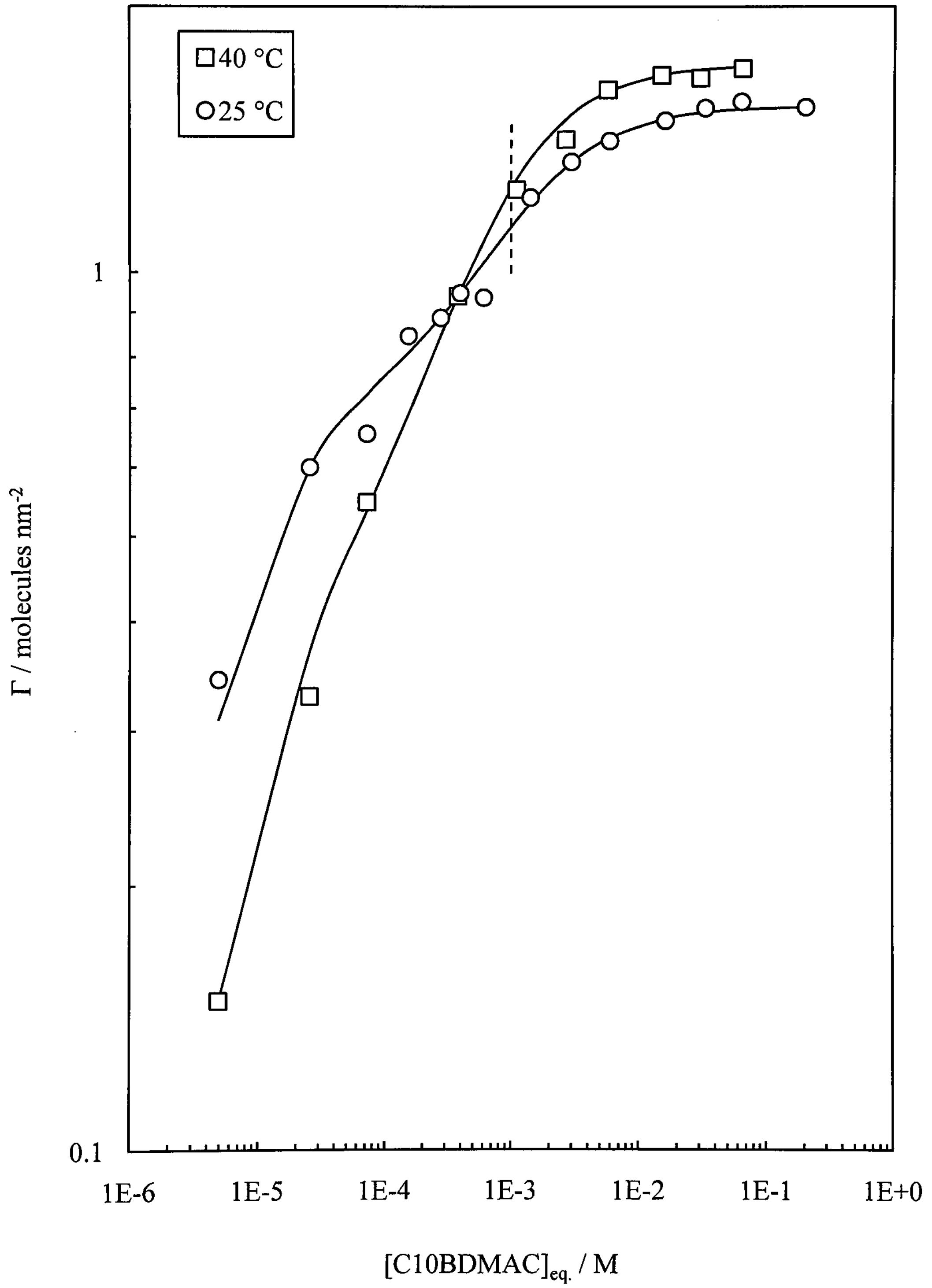

As shown in Figure 7-3, the rise in temperature slightly decreases the amount of surfactant adsorbed up to a surfactant concentration of about 3 × 10^{-4} M. At higher surfactant concentrations, the rise in temperature increases the amount of surfactant adsorbed. The maximum amount of C10BDMAC adsorbed onto sand particles is about 1.55 molecules nm^{-2} at 25 °C while at 40 °C, this amount tends to be 1.7 molecules nm^{-2}.

Table 7-2. Fitting parameters for the two-stage Langmuir adsorption isotherm of CnBDMAC from aqueous solutions onto sand particles at 40 °C.

Parameters	C10	C16
k_1 / M^{-1}	8.55×10^{4}	1.54×10^{5}
k_2 / M^{-1}	1.69×10^{3}	6.75×10^{3}
$\Gamma_{1\,(max)}$ / molecules nm^{-2}	0.5	0.58
$\Gamma_{2\,(max)}$ / molecules nm^{-2}	1.3	2.5
R^2	0.99	0.99

On the contrary, the rise in temperature has a reverse influence on the adsorption of C16BDMAC onto sand at low surfactant concentrations as inferred from Figure 7-4. Accordingly, the rise in temperature increases the amount of surfactant adsorbed up to an amount of adsorption of about 2.5 molecules nm^{-2} ($[C16BDMAC]_{eq.}$= 7×10^{-5} M). Then upon increasing surfactant equilibrium concentrations, the rise in temperature brings about a small decrease in the amount of surfactant adsorbed. The maximum amount of C16BDMAC adsorbed onto sand particles is about 3.6 molecules nm^{-2} at 25 °C while at 40 °C this amount tends to be 3.0 molecules nm^{-2}. It seems that above amount of adsorption of about 2.5 molecules nm^{-2}, the rise in temperature has no major influence on the amount of adsorption upon increasing surfactant concentrations. It is worth mention here, that the rise in temperature was found to have no effect on the amount of CnBDMAC surfactant molecules adsorbed onto steel particles in the first stage of the adsorption process. In the further stages of the adsorption process, the higher temperature was found to decrease the amount of adsorption as reported in *Chapter 6*.

Figure 7-4. Adsorption of C16BDMAC from aqueous solution onto sand at 25 and 40 °C, and pH = 6.5-7 using the depletion method. The solid lines represent the two-stage Langmuir model. The vertical dashed line represents the cmc.

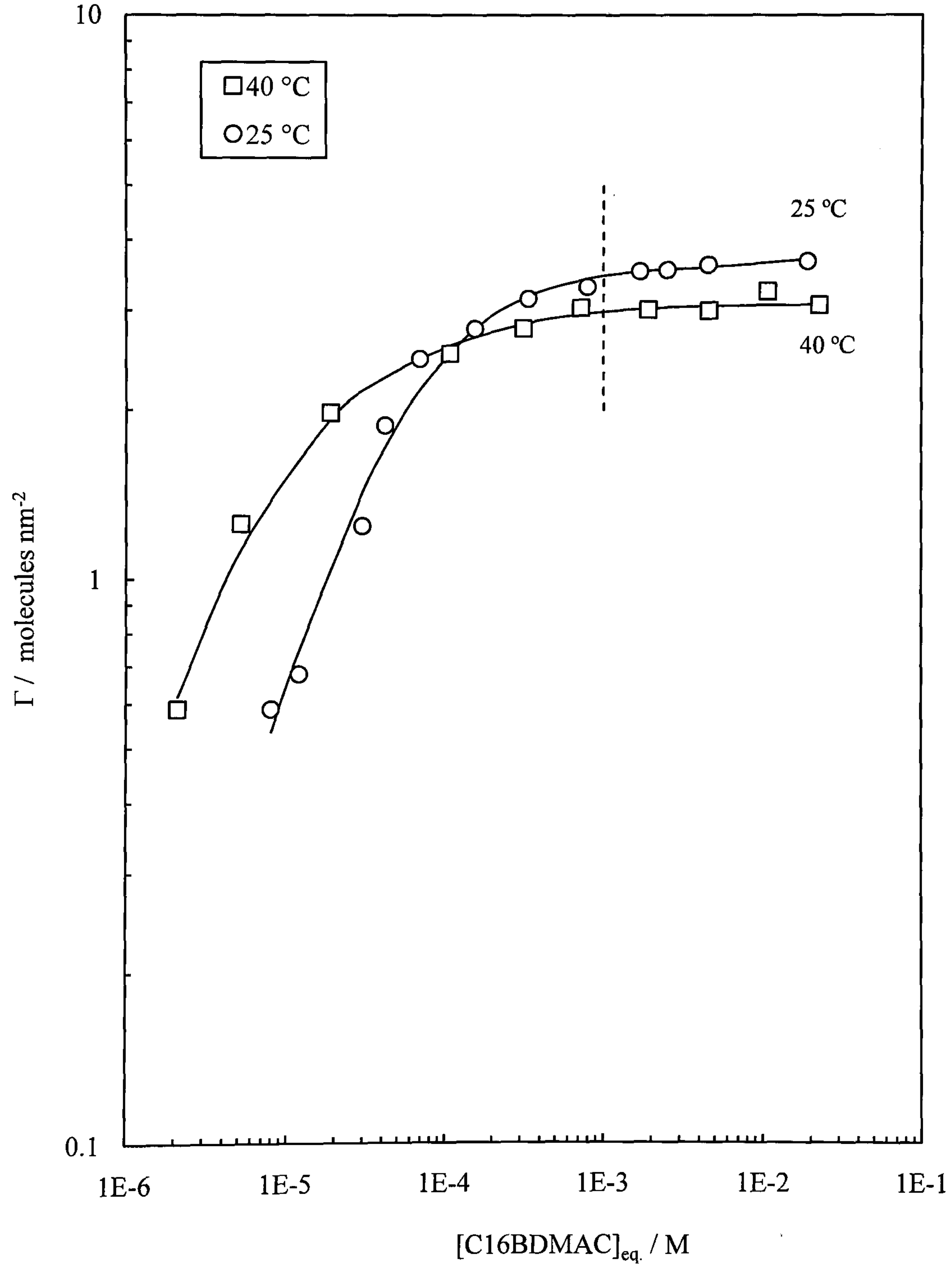

7.4. EFFECT OF BRINE ADDITION

This section investigates the effect of brine addition on the adsorption behaviour of alkylbenzyldimethylammonium chlorides onto sand particles. The effect of brine addition on the adsorption behaviour of C10, C12 and C16BDMAC from brine water onto sand particles at 25 °C was studied using the depletion method. The adsorption isotherms were fitted to the two-stage Langmuir model, shown in the figures as solid lines. Table 7-3 illustrates the fitting parameters used to fit the experimentally determined adsorption isotherms to the two-stage Langmuir model. Figure 7-5 and Figure 7-6 show the isotherms for the adsorption of C10 and C12BDMAC from 4.7 wt.% brine onto sand, in comparison to those with no added brine at 25 °C, respectively. The addition of brine results in increasing of the amount of adsorption over the entire concentration range except in the first stage of C10BDMAC adsorption isotherm. Additionally, the brine additions results in shifting the adsorption isotherms towards lower equilibrium concentrations. The brine additions results in increasing the ionic strength, which screens the electrostatic repulsions between adsorbed surfactant headgroups and increases the level of counter ion binding. Both effects lead to a closer packing of surfactant monomers and an increase in the surface excess.

Noticeably, the short chain C10BDMAC adsorption isotherm tends to reach plateau value of about 11 molecules nm^{-2} in comparison to about 2 molecules nm^{-2} at in the absence of brine.

Table 7-3. Fitting parameters for the two-stage Langmuir adsorption isotherms of CnBDMAC from 4.7 wt.% brine solutions onto sand particles at 25 °C.

Parameters	C10	C12
k_1 / M^{-1}	1.03×10^4	1.29×10^6
k_2 / M^{-1}	95.20	1.06×10^3
$\Gamma_{1\,(max)}$ / molecules nm^{-2}	3.94	0.85
$\Gamma_{2\,(max)}$ / molecules nm^{-2}	9.22	3.56
R^2	0.99	0.99

Figure 7-5. Adsorption isotherms of C10BDMAC corrosion inhibitor from aqueous solution containing 4.7 wt.% brine onto sand at 25 °C compared to that with no added brine. The vertical dashed lines represent the cmc. The solid lines represent the two-stage Langmuir model.

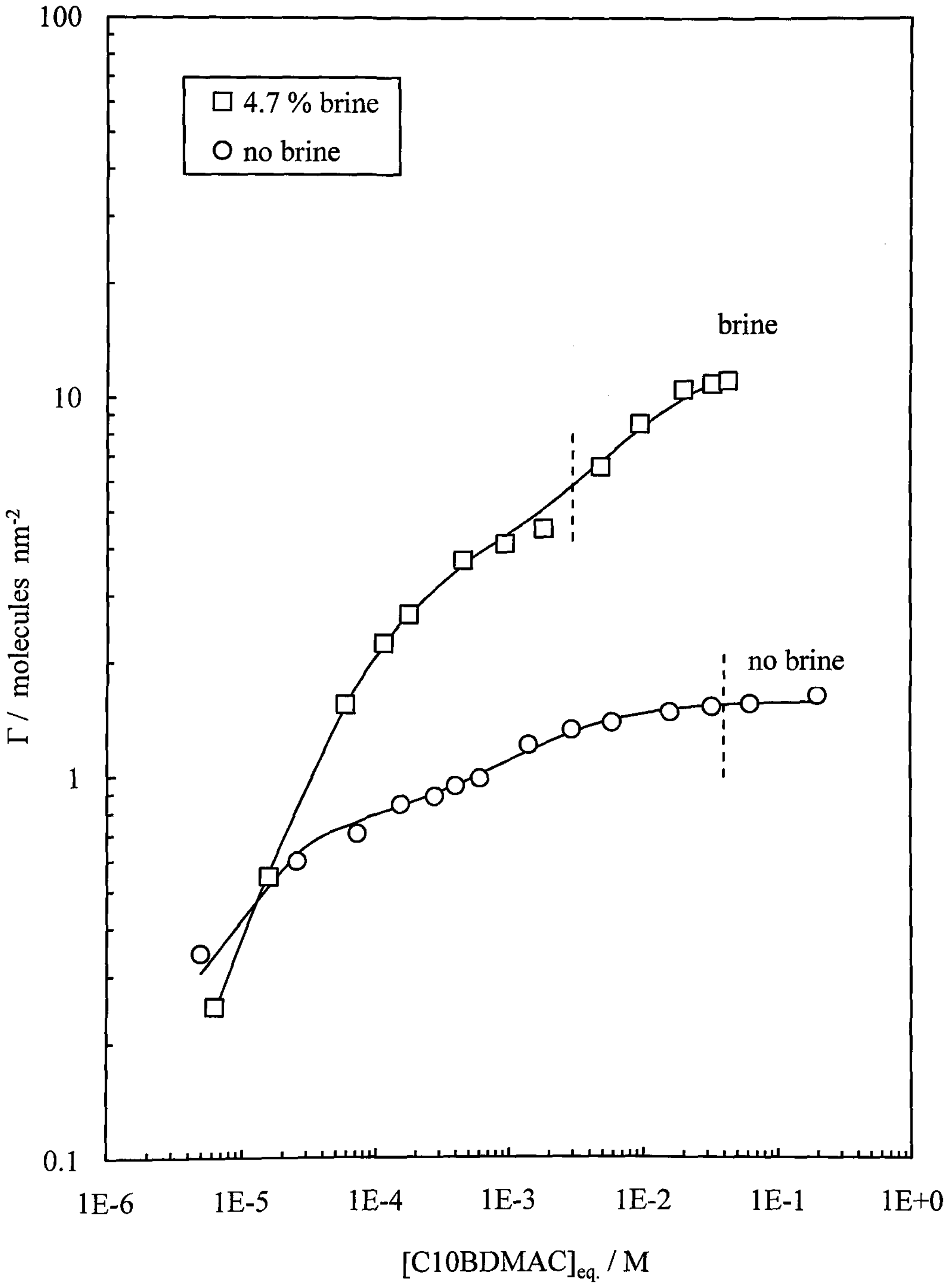

Figure 7-6. Adsorption isotherms of C12BDMAC corrosion inhibitor from aqueous solution containing 4.7 wt.% brine onto sand at 25 °C compared to that with no added brine. The vertical dashed lines represent the cmc. The solid lines represent the two-stage Langmuir model.

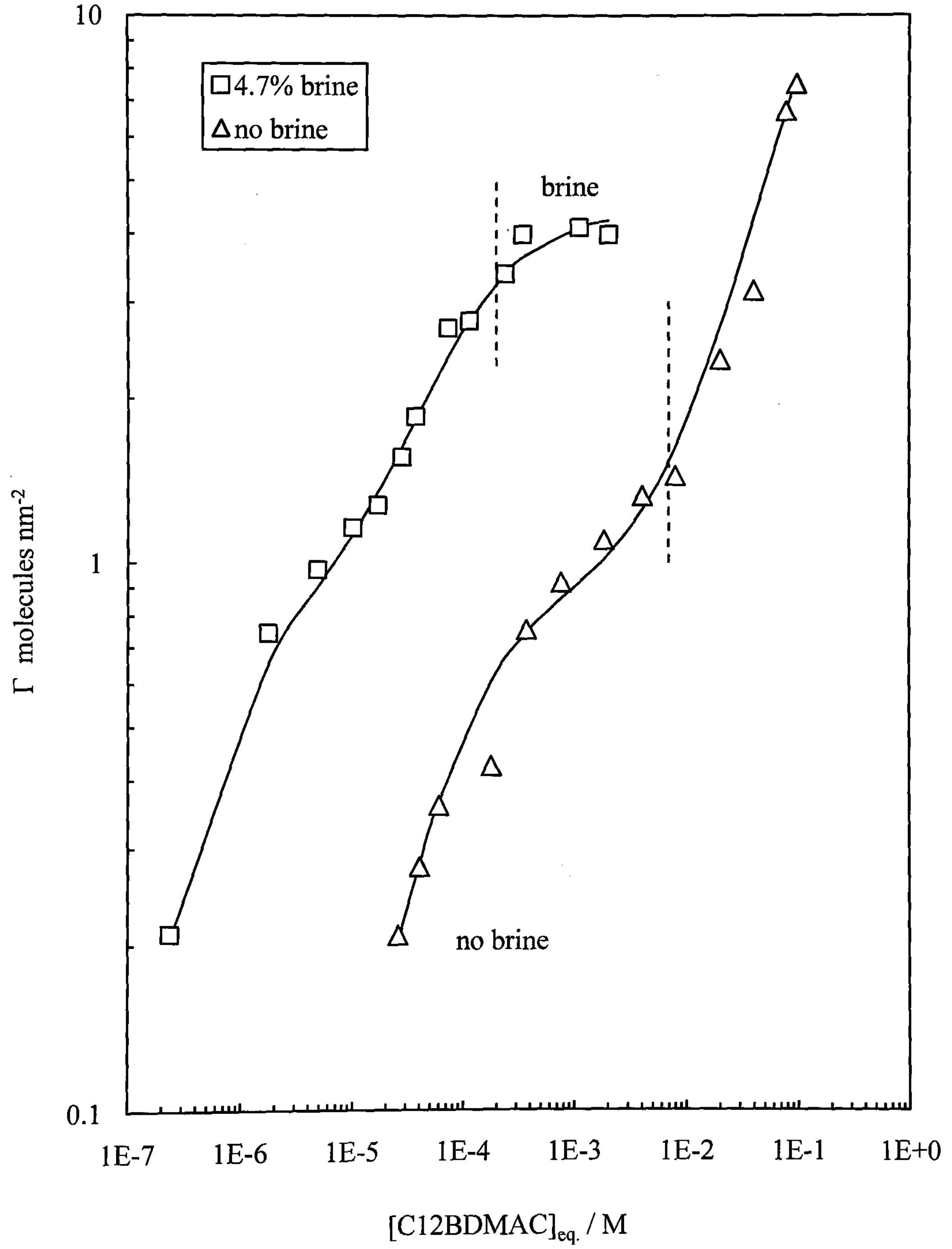

The maximum amount adsorbed by C12BDMAC in the presence of brine is about 8 molecules nm^{-2} at surfactant equilibrium concentration of 2×10^{-3} M. Similarly, the brine addition has been shown in Chapter 6 to increase the amount of surfactants adsorbed onto steel particles as well.

A similar observation has been reported by Atkin *et al.* [2, 3]. They reported that the adsorption of CTAB in the presence of 0.01 M KBr takes place at lower concentrations in comparison to solutions with no added salt. Additionally, they found the level of adsorption to be higher in the presence of electrolyte. This has been attributed to the screening of the head-group charge by electrolyte, which reduces the surfactant head-group area and allows more tightly packed surfactant aggregates to form.

7.5. DISCUSSION

7.5.1. Mechanism of the adsorption of CnBDMAC onto sand particles

The adsorption isotherms of alkylbenzyldimethylammonium chlorides surfactants give rise to a three-stage adsorption process. The shapes of these adsorption isotherms are very similar to those corresponding to the adsorption of CnBDMAC onto steel particles, which have been discussed in Chapter 6. Those three stages are shown more clearly in Figure 7-7. Stage I occur at low equilibrium surfactant concentration, below cmc, and it is characterized by a lower amount of adsorption in comparison with the other two regions. Sand surface is expected to be negatively charged under the employed experimental condition because their surface charges are pH dependent. Sand mineral is composed mainly of silica (SiO_2), usually in the form of quartz, with a PZC (point of zero charge) equals to pH 2 [4]. Consequently, surfactant cations will be adsorbed physically as individual ions on the negatively charged surface sites. In this first stage of the adsorption process, surfactant molecules displace water molecules and exchange with protons and other counter ions present at the solid-water interface. In aqueous solution, CnBDMAC dissociates to positively charged alkylbenzyldimethylammonium cation ($CnBDMA^+$) and negative charged Cl^- anion and $CnBDMA^+$ will be adsorbed on the negatively charged SiO_2 surface. Hence, the adsorption process in this stage is believed to occur principally through electrostatic interactions between negative surface charges onto sand particles and the positive charged ammonium surfactant headgroups.

Figure 7-7. Adsorption isotherms of CnBDMAC from aqueous solutions onto sand particles at 25 °C, using the depletion method, pH = 6.5-7. The vertical dashed lines represent the cmc.

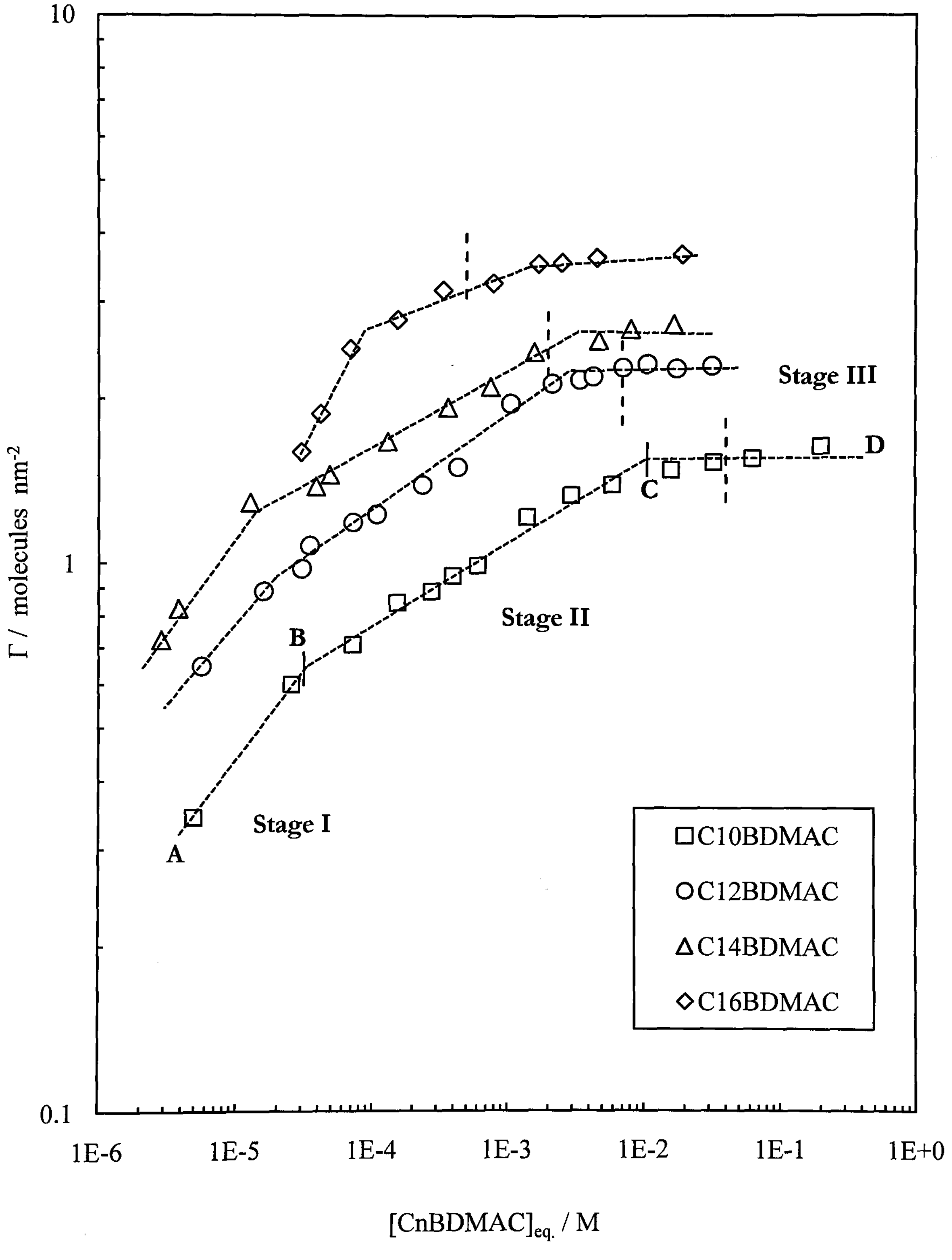

This conclusion is based on the fact that zeta-potential plots exhibits an almost negligible dependence on surfactant concentration and remains almost unchanged during the adsorption process in this stage as shown in Figure 7-2.

Stage I is known as Henry's region as the amount adsorbed is directly proportional to the surfactant equilibrium concentration. The slopes of experimentally determined log Γ vs. log $[\text{CnBDMAC}]_{\text{eq.}}$ plots in Stage I for C10, C12 and C14 chain length are invariably less than unity. Deviations from the theoretically expected unit slope can be explained on the assumption that adsorption takes place on sites of progressively decreasing affinity and indicating anti-cooperative adsorption. On the other hand, the slope of experimentally determined log Γ vs. log $[\text{C16BDMAC}]_{\text{eq.}}$ plot is more than unity. The amount adsorbed of CnBDMAC corrosion inhibitor increases with the increase in the chain length, which proves the influence on the hydrophobic interaction in this stage as inferred from Table 7-4. On the contrary, the magnitude of the surface excess at the transition from stage I to II, has been shown to be independent from chain length for all CnBDMAC surfactants being adsorbed onto steel surfaces as reported earlier in Chapter 6.

Table 7-4. Equilibrium concentration, amount of adsorption and surface area occupied per one molecule of surfactant onto sand particles from aqueous solutions at the transition from stage I to stage II at 25 °C.

Surfactant	$[\text{CnBDMAC}]_{\text{eq.}}$ / M	Γ / molecules nm^{-2}	occupied area per molecule / Å^2
C10BDMAC	3×10^{-5}	0.61	163
C12BDMAC	2×10^{-5}	0.90	111
C14BDMAC	1×10^{-5}	1.10	90
C16BDMAC	8×10^{-5}	2.30	43

The average molecular areas occupied by alkylbenzyldimethylammonium chlorides surfactants molecules in the absence of brine are shown in Table 7-4. Based on these molecular areas, one would expect that the short chains C10 and C12 will lie flat or tilted, while the long chain C14 and C16 will be vertically oriented at the end of this stage. The equilibrium concentrations and the amount adsorbed of alkylbenzyldimethylammonium chloride surfactant onto sand surface at which the transitions from stages I to II take place are given in Table 7-4.

Obviously, the concentrations at which the transitions from region I to II occur are comparable despite the difference in the chemical structure of these surfactants. The equilibrium concentration at which the transition occurs for C10, C12 and C14BDMAC is in the range of 1-3 × 10^{-5} M. On the other hand, the equilibrium C16BDMAC concentration corresponds to the transition I to II is about 8 × 10^{-5} M.

Stage II starts at surfactant concentrations of about an order of magnitude below the surfactant cmc and it extends to a higher surfactant concentration below or close to the cmc. In this stage, the amount of adsorption continues to increase with the increase in surfactant equilibrium concentration. The degree of adsorption increases as well with the increases in surfactant chain length, indicating an increase in the affinity of the surfactant for the solid surface. The adsorption process in this stage is characterized by a positive increase in the ζ-potential and charge reversal of sand particles as well (Figure 7-2). The ζ-potential of sand particles became positive because there are more cations in the Stern layer than negative charges on the sand surface. This decreases the slope of the adsorption isotherm at this stage due to the increased repulsion between the surfactant headgroups. Consequently, the further adsorption of surfactant ions in stage II is no longer electrostatically favoured because of the overcompensation of the surface charge by the surfactant. Hence, the surfactant adsorption in this region is governed mainly by the hydrophobic interactions between the surfactant chains.

The equilibrium concentrations corresponding to the stage II → III transitions, the related amount of surfactant adsorbed and the average molecular areas occupied by one surfactant molecule at the sand-water interface are given in Table 7-5. Clearly, the adsorption saturation values increase with the increase in the length of surfactant's tail groups. C10BDMAC and C12BDMAC surfactant molecules gave rise to a maximum amount of adsorption of about 1.5 and 2.3 molecules nm^{-2}, respectively. The corresponding maximum of adsorption for C14BDMAC and C16BDMAC are 2.7 and 3.7 molecules nm^{-2}, respectively. Noticeably, the concentrations at which the transitions take place are very comparable. The II/III transitions occur at an equilibrium surfactant concentration between 1 × 10^{-2} and 3 × 10^{-2} M for all the studied CnBDMAC molecules.

Based on the molecular areas shown in Table 7-5, one would expect a change in the conformation of adsorbed surfactant molecules from a flat or tilted to a perpendicular orientation, which minimizing their contact area with water molecules. This conclusion is based on an average area per molecules adsorbed at the air-water interface of about 33-48 Å^2, which has been determined experimentally from air-water surface tension isotherms earlier in *Chapter 3.*

Table 7-5. Equilibrium concentrations, amounts of adsorption and surface area occupied per one molecule of surfactant on sand particles from aqueous solutions at the transition from stage II to stage III at 25 °C.

Surfactant	$[CnBDMAC]_{eq.}$ / M	Γ / molecules nm^{-2}	occupied area per molecule / Å^2
C10BDMAC	1×10^{-2}	1.50	66.7
C12BDMAC	3×10^{-2}	2.30	43.5
C14BDMAC	3×10^{-2}	2.70	37.0
C16BDMAC	2×10^{-2}	3.50	28.5

Moreover, the low surface areas exhibited by the short chains C14 and C16BDMAC may be attributed to the beginning of the formation of a bilayer or surface aggregates, which starts to form because of the hydrophobic effect. The adsorbed surfactant cations with alkyl chains oriented toward the solution act as nucleation centres for such structures through chain-chain association in the later stage of adsorption. The mechanism and structure of these surface aggregates have been discussed in detail in *Chapter 6.*

Stage III starts at surfactant concentrations close to the cmc and the adsorption attains saturation and a major increase in the surfactant concentration does not lead to a corresponding change in the amount of adsorption as pointed out in Figure 6-1. The adsorption process in this stage shows little or if no effect on the zeta-potential (ζ) of the sand particles. The amounts of C10, C12, C14 and C16BDMAC adsorbed onto sand particles give rise to a plateau value of about 1.6, 2.3, 2.7 and 3.7 molecules nm^{-2}, respectively. Given the specific surface area of sand particles is 0.22 m^2 g^{-1}, the aforementioned maximum quantities of adsorption corresponding to an area of about 62, 43, 37 and 27 Å^2 per one adsorbed molecule of

C10, C12, C14 and C16BDMAC at the sand-water interface, respectively. Arguably, we could assume that an amount of adsorption of 2 molecules CnBDMAC nm^{-2} corresponds to a monolayer at the sand-water interfaces as well. The aforementioned amount of adsorption, at the sand-water interface, indicates that adsorption of the C10 and C12BDMAC corrosion inhibitors onto sand surfaces is limited to a monolayer (tailgroups pointed out towards water). On the other hand, one would expect that C14 and C16BDMAC would be adsorbed as a multilayer onto sand surfaces.

The increase in the amount adsorbed of alkylbenzyldimethylammonium chlorides on sand particles as the alkyl chain length increases is a typical behaviour of an ionic surfactant being adsorbed onto an oppositely charged surface. Adsorption of cationic surfactant at the silica-water interface has been studied extensively for a number of years by different experimental techniques [5]. Dixit *et al.* [6] have studied the adsorption characteristics of tetradeceyltrimethylammonium bromide (TTAB) from aqueous solution onto a quartz sample of 4.85 m^2 g^{-1} surface area. The determined adsorption isotherms, using the depletion method at 30 and neutral pH = 7, exhibit a typical three region with a charge reversal of the zeta potential of quartz particles. TTAB gave rise to a relatively low maximum amount of adsorption of about 0.02 μmol m^{-2} in comparison to 0.22 μmol m^{-2} for C14BDMAC adsorbed onto sand surface. In a similar study, Summ *et al.* [7] reported a higher amount of adsorption of TTAB onto quartz corresponding to 24 μmol m^{-2}. The tested quartz sample has a surface area of about 0.5 m^2 g^{-1} and the adsorption batch experiments were counted at pH = 7.5 and at 20 °C.

Bi *et al.* [8] studied the adsorption of cetyltrimethylammonium bromide (CTAB) at a smooth surface of SiO_2 film by ellipsometry. The results show an agreement with a two-step model of the adsorption with monolayer (2.6 nm thickness) and bilayer (4.6 nm thickness) adsorption occurring at different concentrations of CTAB. The Adsorption isotherms have been fitted to the two-step model.

7.5.2. Temperature Effect

The temperature influence on the adsorption behaviour of the long chain C16BDMAC was found to be different from that for the short chain C10BDMAC.

This different temperature dependent of the short chain CnBDMAC from the long chain has been reported by Partyka *et al.* [9-12]. They have investigated the adsorption behaviour of benzyldimethyloctylammonium bromide C8BDMAB [12] and benzyldimethyldoodcylammonium bromide C12BDMAB [9] onto silica using the depletion, calorimetric and electrophoretic methods. The calorimetric investigation indicated that, at low surfactant concentrations, the enthalpy of the short chain C8BDMAB is exothermic and decreases continuously with increasing quantity of adsorption [12]. Upon increasing the surfactant concentrations, the enthalpy effect of displacement becomes endothermic and reaches a plateau value. This behaviour could be linked to the reported the decrease in the amount adsorbed of C10BDMAC at higher temperatures (exothermic reaction) at the lower surfactant concentrations. Then at higher surfactant concentrations, the temperature rise will be accompanied by an increase in the amount adsorbed as the adsorption process has been of an endothermic nature. On the contrary, C12BDMAC shows the opposite behaviour wherein the adsorption process at low surfactant equilibrium concentration is of an endothermic nature as reported by Partyka *et al.* [11, 12]. Then it turns gradually into an exothermic process with the increase in surfactant equilibrium concentration. This in turn explains the increased amount of adsorption showed by the long chain C16BDMAC at the low surfactant concentrations (endothermic reaction). At higher surfactant concentrations, the adsorption process became exothermic and the increase in temperature results in decreasing the amount adsorbed.

Additionally, the adsorption of alkyltrimethylammonium bromides surfactants (DTAB: n = 12; TTAB: n = 14; CTAB: n = 16) from aqueous solutions onto silica at neutral pH has been studied using two methods: the determination of adsorption isotherms and the corresponding differential enthalpies by Partyka *et al* [13]. They reported that, at very low coverage, the molecules are adsorbed individually at the solid surface and enthalpies of adsorption are exothermic. Whereas, at higher coverage of the solid surface, the enthalpies of adsorption became endothermic in nature.

Recently, Stodghill *et al.* [14] studied the enthalpy change of adsorption of the cationic alkyltrimethylammonium bromide surfactants (DTAB, TTAB and CTAB) onto HiSil 233 precipitated silica type. The adsorption experiments were conducted using the isothermal titration calorimetry (ITC) technique at 28, 30, and

35 °C and pH = 8. The change in enthalpy due to surfactant adsorption onto a hydrophilic silica surface was determined from the plots of the heat of displacement, ΔH_{disp} versus concentration. In the graphs of ΔH_{disp}, the transitions between regions I and II and regions II and III were marked by noticeable exothermic and endothermic peaks, respectively. This in agreement with the observations reported by Partyka [13]. These peaks have been attributed to a change in how the surfactant adsorbs in each of the three regions. Additionally, they concluded that there is no visible correspondence of the enthalpy of the displacement curve with changing temperature was observed.

The two studies by Stodghill and Partyka reported that both of the exothermic and endothermic contributions decrease with the increase in the chain length and temperature rise. In other words, at low surfactant concentration, with increasing surfactant chain length, the value of the exothermic enthalpy starts to decrease gradually and may be even become endothermic. On the other hand, at higher surfactant concentrations, the endothermic enthalpy magnitude will decrease as a function of chain length and may be turned into an exothermic one. Both situations have been reported in our case for the short chain C10BDMAC in comparison with the long chain C16BDMAC. This in turn could reflect the impact of the hydrophobicity of the surfactant aqueous system on the adsorption characteristics at the solid-liquid interface. Additionally, this brought us back to the conclusion reported by Lyklema *et al.* [15]. They reported that adsorption passes through a maximum as a function of temperature. The position of this maximum depends on the nature of the solid surface, the interacting organic molecules and on their degrees of freedom in which T_{max} may be different for adsorbed and free molecules.

Recently, the adsorption of dodecyltrimethylammonium bromide (DTAB) and hexadecyltrimethylammonium bromide (CTAB) from water onto a clay mineral, Sepiolite was reported to be temperature independent [16]. The mineral Sepiolite is composed mainly of silica and magnesia. The adsorption experiments were conducted using the depletion method at pH= 8.5 at three different temperatures 25, 40 and 60 °C. The adsorption isotherms were marked by three distinct regions of different slopes with no apparent temperature dependence.

More recently, the amount of cetyltrimethylammonium bromide (CTAB) adsorbed from aqueous solution onto clayey soil (with 85% silica content) at pH 7 was found to increase with increasing temperature [17]. The authors claim that the rise in the temperature facilitates the adsorption of CTA^+ ion onto the clay surface. Accordingly, the higher temperatures lead to more dehydration of the CTA^+ ions. Thus, these ions could easily reach active sites on the clay matrix.

The aforementioned examples highlight the role of solid nature on the dependence of the adsorption of ionic surfactants at solid liquid interfaces on temperature.

7.5.3. Adsorption of CnBDMAC onto sand vs. steel surfaces

The alkylbenzyldimethylammonium chloride corrosion inhibitors give rise to higher amounts of adsorption onto sand particles compared to steel particles up to surfactant concentration close to the cmc as shown in Figure 7-8 and Figure 7-9. This conclusion is true for all the experimentally determined adsorption isotherms under the experimental conditions studied. Obviously, as shown in these figures the amounts adsorbed of C10 and C12BDMAC onto sand are higher than those for steel particles up to the cmc. Beyond the cmc, the amounts adsorbed onto the steel particles, from aqueous solutions, exceed those for sand particles. In the presence of brine, the amount of C12BDMAC adsorbed on sand is slightly higher than that for C1018 mild-steel, up to an amount of about 1 molecules nm^{-2}, as shown in Figure 7-10. Then the amount adsorbed onto C1018 mild-steel exceeds that for sand particles. Generally, in the presence of brine, these differences in amounts of adsorption onto sand and steel surfaces are not significant as those reported from the aqueous solutions.

The difference in the adsorption extent of these quaternary ammonium surfactants onto sand and steel could be attributed possibly to the difference in the surface charge densities of these solid particles. Figure 7-11 shows the change in the surface charge densities of sand and C1018 steel particles during the adsorption of C14BDMAC surfactant molecules from water at 25 °C. Clearly, the surface charge of sand particle, at low surfactant concentrations, is more negative than that for steel particles. In addition, the heterogeneity of solid surfaces affects the amount of adsorption.

Figure 7-8. Adsorption of C10BDMAC from aqueous solutions onto sand, 316L and C1018 particles at 25 °C, using the depletion method. The solid lines represent the two-stage Langmuir model fits. The vertical dashed line represents the cmc.

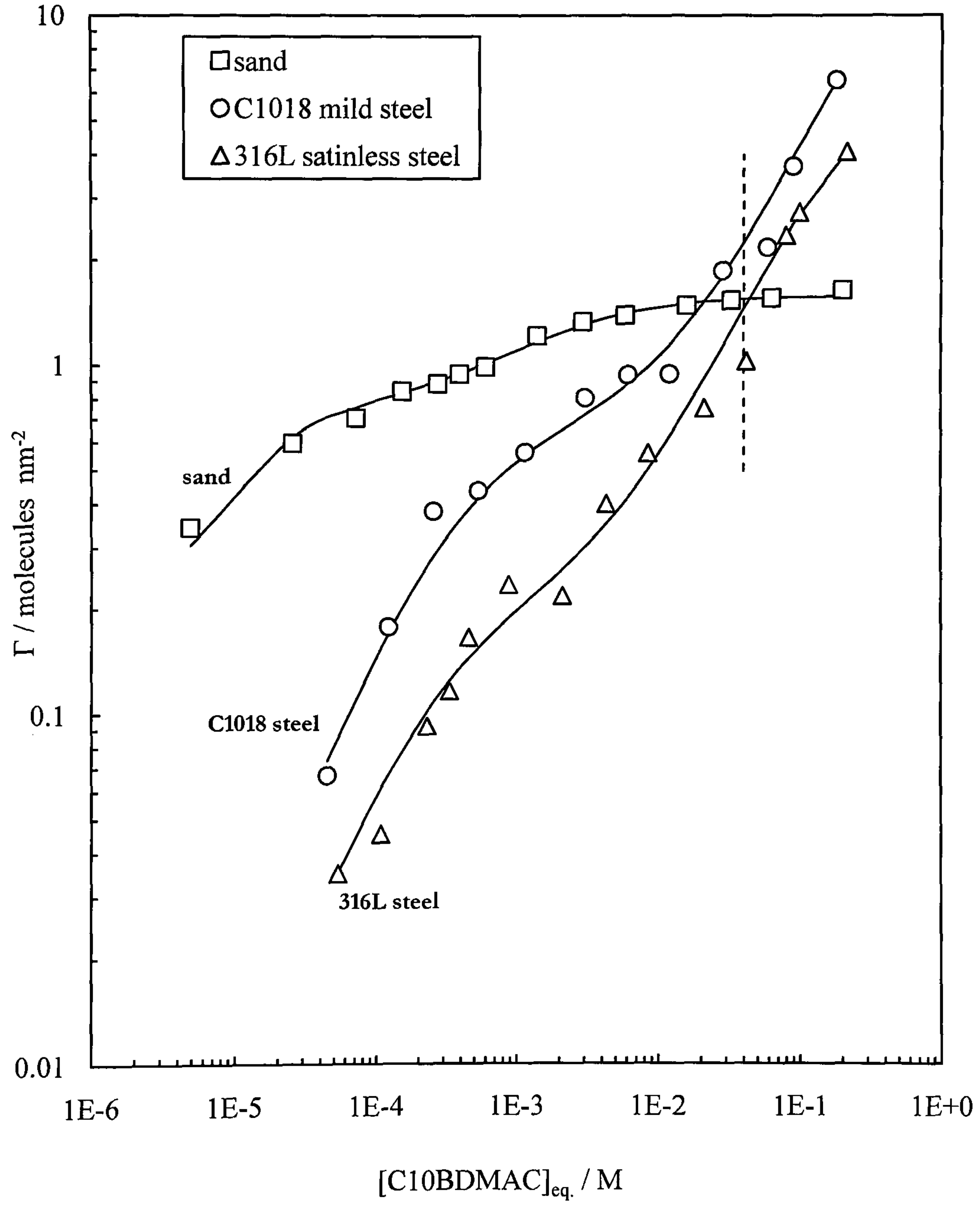

Figure 7-9. Adsorption of C12BDMAC from aqueous solutions onto sand, 316L and C1018 particles at 25 °C using the depletion method. The solid lines represent the two-stage Langmuir model fits. The vertical dashed line represents the cmc.

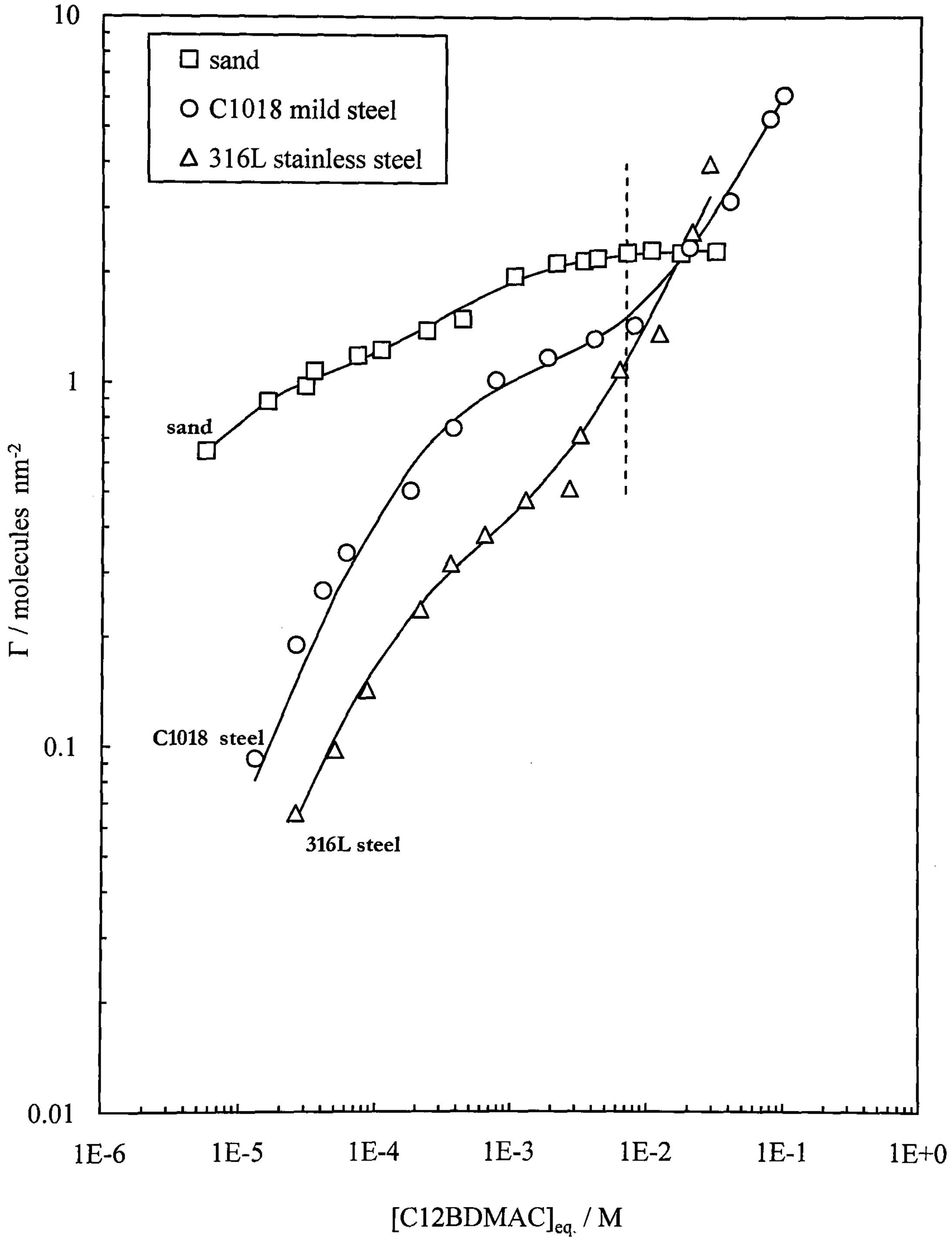

Figure 7-10. Adsorption of C12BDMAC from 4.7 wt.% brine solutions onto sand and C1018 particles at 25 °C, using the depletion method. The solid lines represent the two-stage Langmuir model fits. The vertical dashed line represents the cmc.

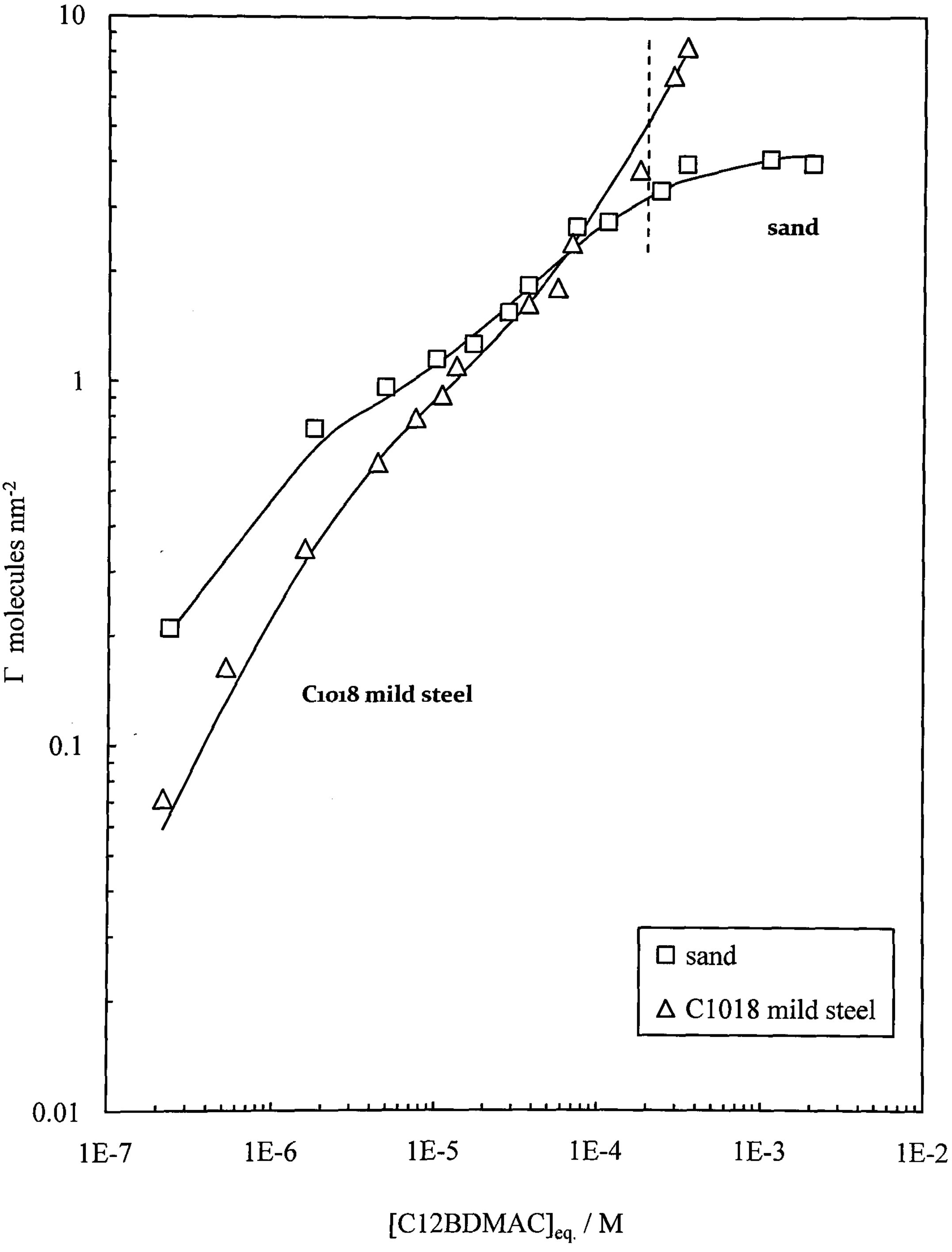

Figure 7-11. Variations in the surface charge densities of C1018 steel and sand particles as a function of C14BDMAC equilibrium concentration at 25 °C.

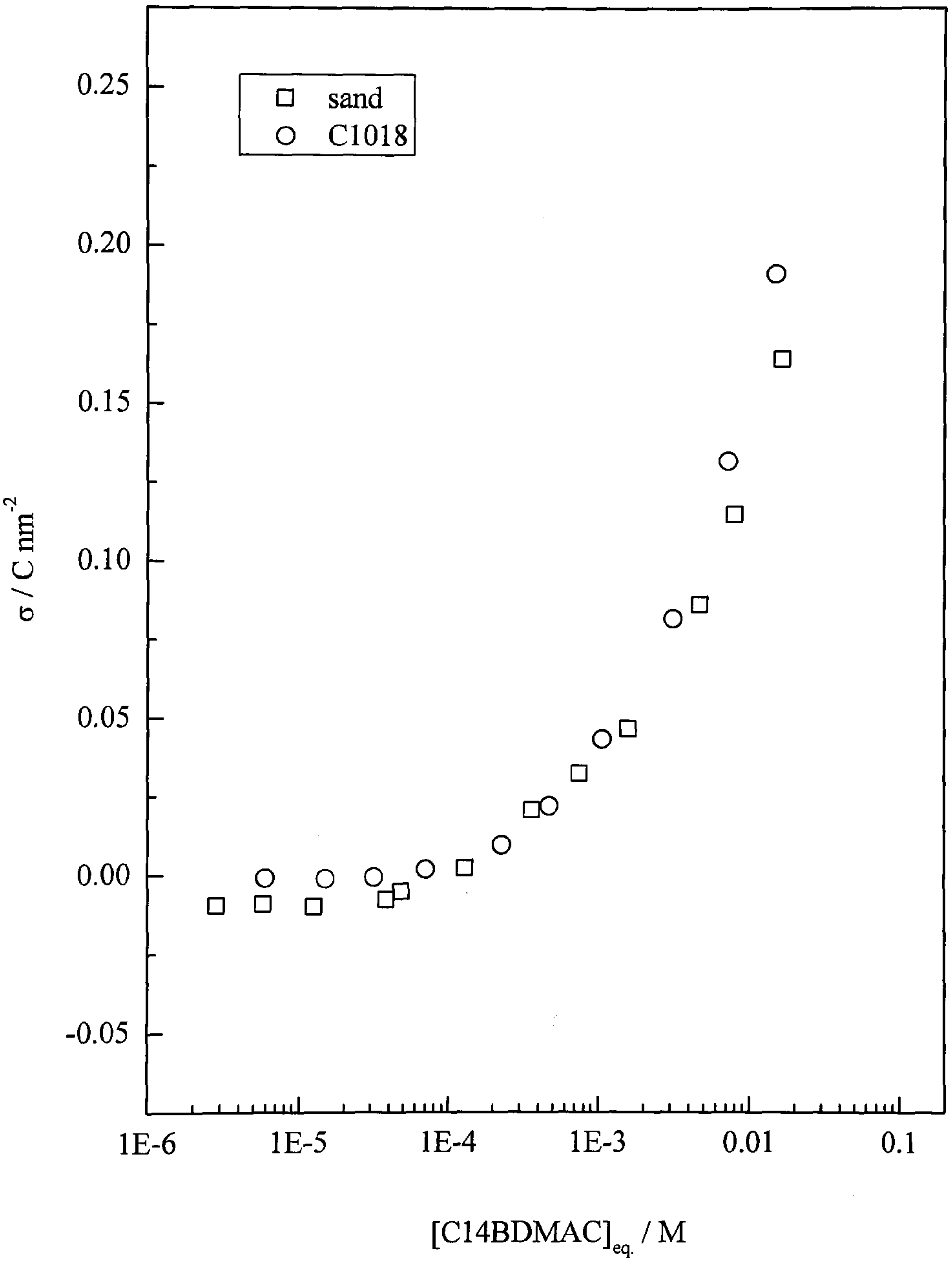

7.6. SUMMARY AND CONCLUSION

In this chapter, the adsorption behaviour of alkylbenzyldimethylammonium chlorides on sand particles has been studied in detail. For the best of our knowledge, no studies concerning the adsorption of this surfactant homogenous on sand particles have been reported in the literature. The key and new findings within this study are summarized below.

I. The adsorption behaviour of these surfactant molecules is dependent upon surfactant structure, temperature, salinity and the surface area available for them.

II. Studies performed in the presence alkylbenzyldimethylammonium chlorides and sand revealed that these inhibitors have a strong affinity for sand particles, particularly at low temperatures and diluted inhibitor concentrations.

II. The shape of adsorption isotherms gave rise to classical profiles of a typical cationic surfactant being adsorbed onto a negatively charged surface and the log-log representation of the adsorption isotherms give rise to three distinct steps or regions of different slopes indicating distinctive mechanisms.

VI. The adsorption of CnBDMAC surfactants has been shown to increase with the increase in the surfactant equilibrium concentration, chain length and brine concentration. Adsorption of C10, C12 and C14BDMAC corrosion inhibitors onto sand surface is limited to a monolayer (tailgroups pointed out towards water). On the other hand, C16BDMAC would be adsorbed as a multilayer (patchy bilayer) or as surface aggregates (headgroups of the second layer pointed out towards water) onto sand surface.

7.8. REFERENCES

1. S. Paria and P. K. Yuet, *Ind. Eng. Chem. Res.*, **45**, 712 (2006).
2. R. Atkin, V. S. J. Craig and S. Biggs, *Langmuir*, **16**, 9374 (2000).
3. R. Atkin, V. S. J. Craig, E. J. Wanless and S. Biggs, *J. Colloid Interface Sci.*, **266**, 236 (2003).
4. M. Kosmulski, *Surface Charging and Points of Zero Charge*, CRC Press, Boca Raton (2009).
5. R. Atkin, V. S. J. Craig, E. J. Wanless and S. Biggs, *Adv. Colloid Interface Sci.*, **103** 219 (2003).
6. S. G. Dixit, A. K. Vanjara, J. Nagarkar, M. Nikoorazm and T. Desai, *Colloids Surf., A*, **205**, 39 (2002).
7. O. A. Soboleva, A. A. Yaroslavtsev, G. A. Badun and B. D. Summ, *Colloid J.*, **66**, 470 (2004).
8. Z. Bi, W. Liao and L. Qi, *Appl. Surf. Sci.*, **221**, 25 (2004).
9. J. L. Trompette, J. Zajac, E. Keh and S. Partyka, *Langmuir*, **10**, 812 (1994).
10. J. Zajac and S. Partyka, in *Adsorption on New and Modified Inorganic Sorbents*, A. D browski and V. Tertykh, eds., Elsevier Science, Amsterdam (1996).
11. J. Zajac, J. Trompette and S. Partyka, *J. Therm. Anal. Calorim.*, **41**, 1277 (1994).
12. J. Zajac, J. L. Trompette and S. Partyka, *Langmuir*, **12**, 1357 (1996).
13. S. Partyka, M. Lindheimer and B. Faucompre, *Colloids Surf., A*, **76**, 267 (1993).
14. S. P. Stodghill, A. E. Smith and J. H. O'Haver, *Langmuir*, **20**, 11387 (2004).
15. T. Mehrian, A. De Keizer and J. Lyklema, *Langmuir*, **7**, 3094 (1991).
16. E. Sabah and M. S. Çelik, *Sep. Sci. Technol.*, **37**, 3081 (2002).
17. A. Gürses, S. Karaca, M. Açikyildiz and M. Ejder, *Chem. Eng. J.*, **147**, 194 (2009).

CHAPTER 8

Chapter 8

CORROSION INHIBITION BY ALKYLBENZYLDIMETHYLAMMONIUM CHLORIDES AND THE EFFECT OF PARASITIC ADSORPTION

8.1. INTRODUCTION

The protection efficiency of a surfactant molecule against corrosion under specific experimental conditions is routinely investigated using rapid electrochemical methods. These methods include potentiodynamic polarization, linear polarization resistance (LRP), electrochemical impedance spectroscopy (EIS) and electrochemical noise [1]. In this chapter, we are going to investigate the performance of hexadecylbenzyldimethylammonium chlorides (C16BDMAC) corrosion inhibitor in brine solutions by the means of the linear polarisation resistance technique, which is commonly known as the "*bubble test*". This corrosion inhibitor has been shown to exhibit higher amount of adsorption and affinity for C1018 mild steel compared to the other CnBDMAC surfactants. So, one would expect that C16BDMAC will exhibit a better protection efficiency against corrosion. The protection efficiency of C16BDMAC will be investigated as a function of sand amounts, presence of oil and type of gas.

In addition, in order to obtain a quantitative assessment of the effects of sand addition on the amount of C16BDMAC being adsorbed onto the steel surface, a model has been proposed. This model enables us to determine the magnitude of changes in the amount adsorbed of C16BDMAC surfactant onto steel, with changes in the amount of sand added. Additionally, we are going to discuss to what extent these predicted or determined changes in the amount of adsorption is related to the corresponding changes in the corrosion protection efficiency of C16BDMAC surfactant molecules.

8.2. EFFECT OF DISSOLVED GASES ON THE CORROSION OF STEEL

The corrosion inhibition performances of C16BDMAC surfactant in 4.7 wt.% brine solution at 25 °C under air, carbon dioxide and hydrogen sulphide are shown in Figure 8-1, Figure 8-2 and Figure 8-3, respectively. In these figures, the corrosion rate, in mm y^{-1} units, is plotted as a function of time, in hour units. The corrosion rate of C1018 steel electrode is usually monitored until it reaches a steady baseline rate before the addition of the corrosion inhibitor. As shown in Figure 6-1, the corrosion rate of mild steel in brine solutions does not reach a baseline under aerated conditions. On the other hand, in the presence of CO_2 and H_2S, the corrosion rates of mild steel from brine solutions reach steady values of about 1.4 and 0.2 mm y^{-1}, respectively. Generally, the time required for the corrosion rate of C1018 mild steel to reach a steady rate is relatively higher than that for carbon dioxide and hydrogen sulphide atmosphere. In a previous study [2], the bubble test corrosion rate of C1018 mild steel in aerated brine solutions was found to reach a plateau value of about 0.3 mm y^{-1} after 10 hours. In the same study, the corrosion rates for C1018 mild steel in the presence of CO_2 and H_2S were found to be 1.70 and 0.15 mm y^{-1}.

The addition of 0.5 ppm (1.13×10^{-6} M) C16BDMAC corrosion inhibitor to the brine solution reduces the corrosion rates of mild steel with different magnitudes depending on the type of gas. Under aerated conditions, the corrosion rate dropped to about 0.3 mm y^{-1}. Whereas this value was about 0.6 mm y^{-1} in saturated CO_2 solutions and 0.01 mm y^{-1} in the presence of H_2S. The protection efficiency of C16BDMAC in H_2S containing solution is about 90 % while those for air and carbon dioxide are 53 and 26 %, respectively.

Figure 8-1. Corrosion rate vs. time for C1018 steel in 4.7 wt.% brine solutions under aerated conditions at 25 °C, in the presence of 0.5 ppm (1.13×10^{-6} M) C16BDMAC, determined by the bubble test. The vertical dashed line indicates the time at which C16BDMAC was added.

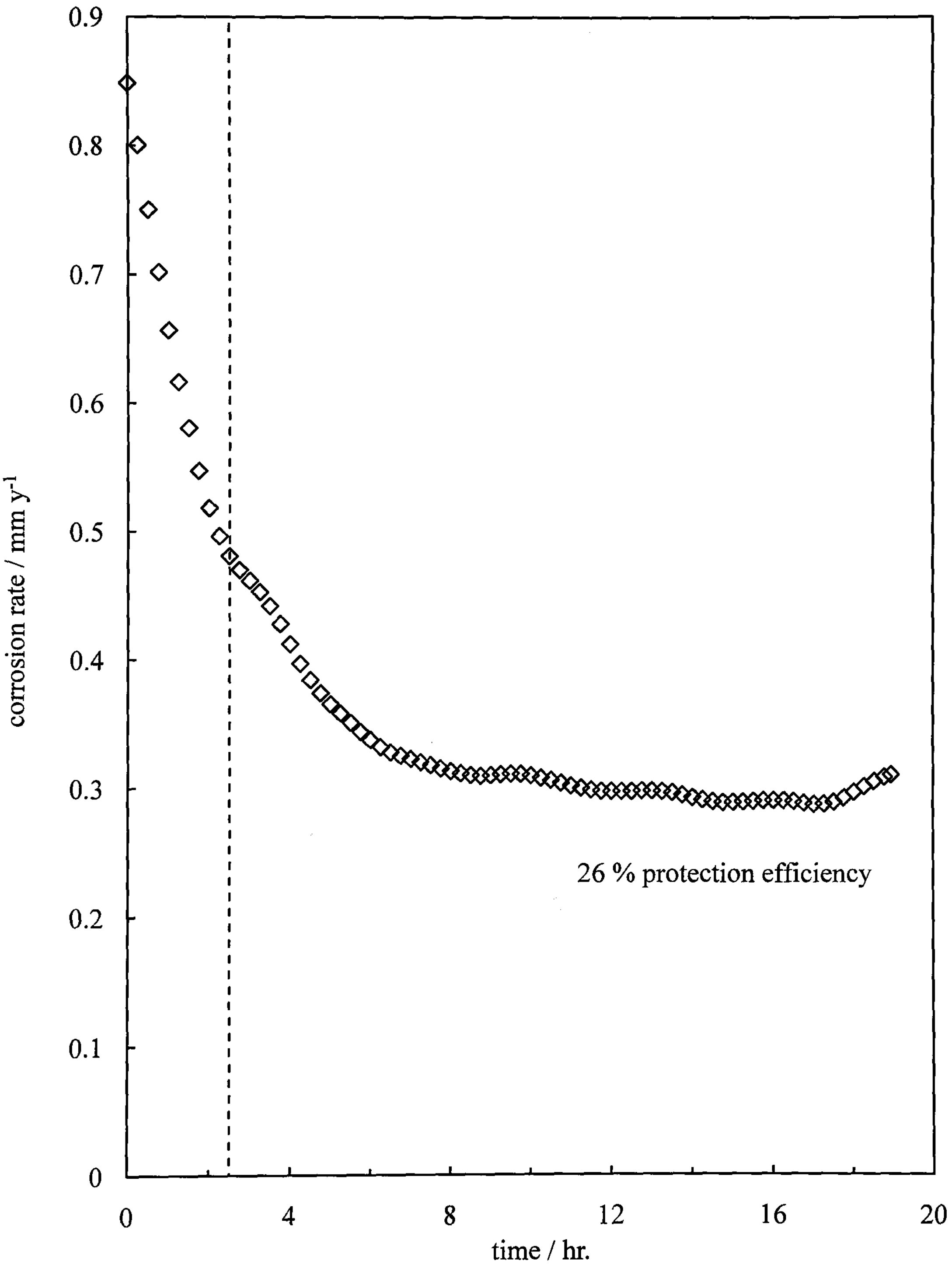

Figure 8-2. Corrosion rate vs. time for C1018 steel in 4.7 wt.% brine - saturated CO_2 solutions at 25 °C, in the presence of 0.5 ppm (1.13×10^{-6} M) C16BDMAC, determined by the bubble test. The vertical dashed line indicates the time at which C16BDMAC was added.

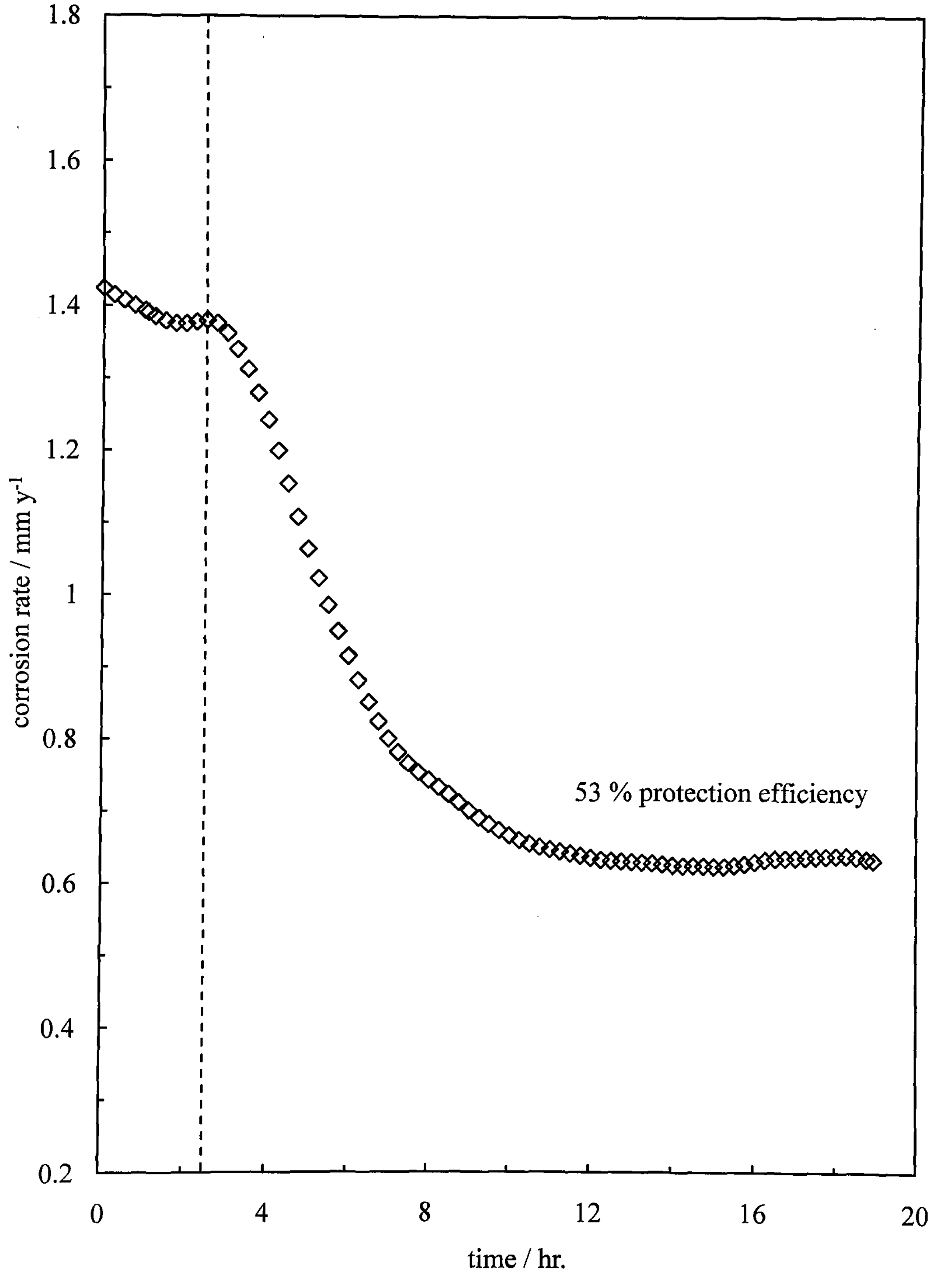

Figure 8-3. Corrosion rate vs. time for C1018 steel in 4.7 wt.% brine-saturated H_2S solutions at 25 °C, in the presence of 0.5 ppm (1.13 × 10^{-6} M) C16BDMAC, determined by the bubble test. The vertical dashed line indicates the time at which C16BDMAC was added.

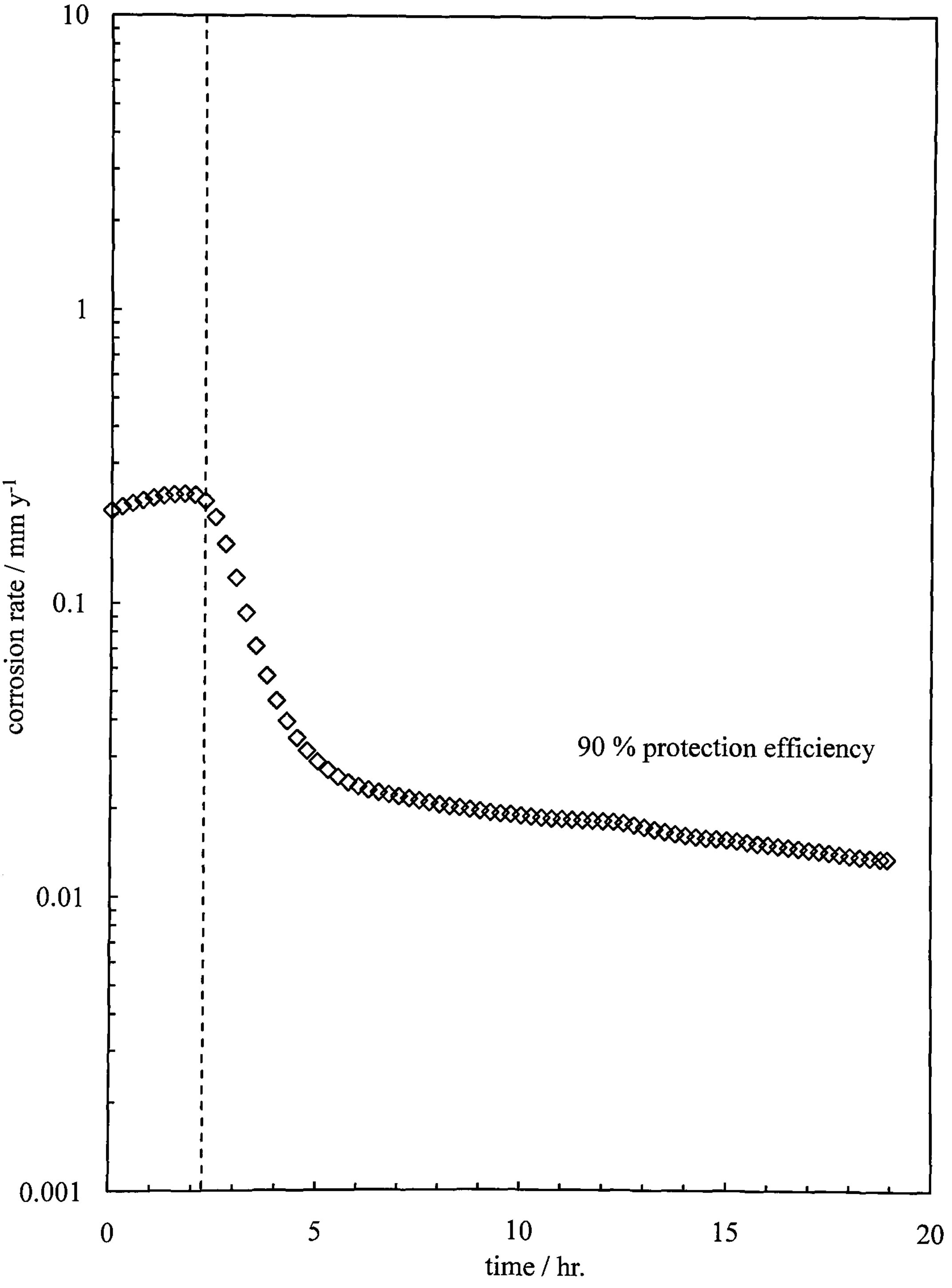

The percentage of the protection efficiency, % P is given by the following equation:

$$\% P = [(R_o - R_{inh.})/(R_o)] \times 100 \qquad (8\text{-}1)$$

where R_o is the corrosion rate in the absence of inhibitor (baseline corrosion rate) and $R_{inh.}$ is the corrosion rate in the presence of inhibitor.

Binks *et al.* [3] have investigated the corrosion rates of C1018 mild steel under aerated, CO_2 and H_2S conditions in brine solutions. They measured the effect of gas type on the corrosion rate of mild steel in brine solutions containing C12BDMAC at 25 °C using the linear polarization method under different surfactant concetrations. The C12BDMAC protection efficiency was found to follow the order $H_2S > CO_2 >$ air under the used experimental conditions.

8.3. EFFECT OF SAND ADDITION ON THE CORROSION RATES OF STEEL IN THE PRESENCE OF C16BDMAC

The low protection efficiency exhibited by C16BDMAC under aerated conditions in addition to the long time required to reach a plateau, makes the investigation of the effect of sand addition on the protection efficiency quite difficult and not practical. In addition, working with solutions containing hydrogen sulphide gas is fairly hazard. Accordingly, we decided to study the effect of sand addition on the protection efficiency of C16BDMAC in brine solutions saturated with carbon dioxide.

Figures 1 to 8 in the Appendix show the effect of addition of different amounts of sand on the corrosion rates of C1018 mild steel in brine solutions containing CO_2 in the presence of various C16BDMAC concentrations. For each C16BDMAC concentration, the corrosion rate was measured as a function of time in the absence and presence of 1 and 2 wt. % sand. All the measurements were conducted in aqueous solutions containing 4.7 w.% brine in the presence of carbon dioxide at 25 °C. The corrosion rate of C1018 mild steel electrodes was left first to reach a steady state corrosion rate (a baseline) before the addition of C16BDMAC in the presence of sand. Upon reaching a baseline, the surfactant was introduced into solution and was left to reach a steady state. In these figures (Figures1 to 8 in the Appendix), the LPR corrosion rates were plotted versus time. Noticeably, an initial corrosion rate around of about 1-1.5 mm y^{-1} was measured. The corrosion rate dropped to about 0.8-1 mm y^{-1} after three hours. The addition of C16BDMAC leads to a very sharp decrease in corrosion rate of C1018 mild steel electrodes in the absence of sand. However, the magnitude of this decrease in corrosion rates is less pronounced in the presence of sand. As shown in these figures, the addition of sand decreases the corrosion inhibitor efficiency. The magnitude of this decrease is related to the added sand amount and the inhibitor concentration. Table 8-1 summarises the protection efficiencies for different C16BDMAC concentrations as a function of sand amount in brine solutions at 25 °C.

Table 8-1. Protection efficiencies for different C16BDMAC concentrations as a function of sand amount in brine solutions at 25 °C.

$[C16BDMAC]_{total}$ *		% protection efficiency		
/ ppm	/ M	0 % sand	1 % sand	2 % sand
0.1	2.28×10^{-7}	21.8	6.6	4.1
0.5	1.13×10^{-6}	73.1	42.2	32.4
1.5	3.36×10^{-6}	96.5	78.2	64.0
2.5	5.63×10^{-6}	87.3	82.0	69.2
4	9.01×10^{-6}	97.5	89.7	83.6
5	1.13×10^{-5}	91.3	88.0	79.4
10	2.25×10^{-5}	97.1	89.3	85.6
20	4.50×10^{-5}	97.8	88.7	79.8

* $[C16BDMAC]_{total}$ refers to the initial surfactant concentration (free + adsorbed).

Various researchers have reported a similar decrease in the protection efficiency of corrosion inhibitors caused by the presence of sand [4-7]. Reus *et al.*[4] reported that there is a rapid drop in the corrosion rate of the mild steel electrode in the presence of an Imidazoline based corrosion inhibitor to about 0.02 mm y^{-1} with no added sand. On the other hand, the addition of thin sand layer on the tested electrode using the same inhibitor concentration increases the corrosion rate to about 5 mm y^{-1}. In all measurements, Reus has used the Linear Polarization Resistance technique to measure the corrosion rate in brine solutions under CO_2.

8.4. MODELLING OF THE COMPETITIVE ADSORPTION OF SURFACTANT IHIBITIOR ONTO DIFFERENT SOLID SURFACES

The competitive adsorption of corrosion inhibitors onto various solid surfaces encountered in the oilfield pipeline and its impact on the inhibitor efficiency constitutes one of the key objectives of the current Ph.D. research project. The presence of increasing concentrations of sand was found to reduce progressively the inhibitory effect of the C16BDMAC, i.e. sand addition increases the corrosion rate, as shown earlier. Hence, we can see qualitatively that effects of sand addition on corrosion rates are observed experimentally. In order to obtain a quantitative assessment of such effects on the amount of CnBDMAC being adsorbed onto steel surfaces, we have constructed a Microsoft Excel spreadsheet. The aim of this spreadsheet is to model the amounts adsorbed of corrosion inhibitors onto solid surfaces (steel and sand particles). This in turn could be used to predict the changes in the adsorption behaviour and the corresponding changes in the protection efficiency of these surfactants with changes in the production parameters. These production parameters include the amounts and nature of solids encountered in oilfield pipelines, chemical structure of surfactant, brine concentration and temperature.

The developed spreadsheet is based on the adsorption parameters that have been used to fit the experimentally determined adsorption isotherms. Generally, this spreadsheet is composed of two main parts or panels. The *first panel* is used by the operator to input the adsorption parameters for the competing surfaces Solid 1 and Solid 2, which have been determined experimentally for each CnBDMAC surfactants. These parameters are determined by fitting the adsorption isotherms to a sutiable theoretical adsorption model. The two-stage Langmuir model has been used to model the experimental data. The choice of the proper adsorption model depends on the fitting accuracy and the number of fitting parameters. In the *second part,* we input the surface areas for the competing solid surfaces per unit volume of the aqueous solution (A_{solid1} and A_{solid2}). Then, for a set value of $[CnBDMAC]_{free}$ (this represents the residual, not adsorbed or the equilibrium concentration), we calculate the surface concentrations on both *Solid 1* (Γ_{solid1}) and *Solid 2* (Γ_{solid2}) using the two-stage Langmuir equation. We then calculate the overall, total concentration of CnBDMAC using:

$$[CnBDMAC]_{total} = [CnBDMAC]_{free} + \Gamma_{solid1} A_{solid1} + \Gamma_{solid2} A_{solid2} \qquad (8\text{-}2)$$

These calculations enable us to determine quantitatively the effects of change in the following parameters on the relative amounts being adsorbed on both solids:

I. changing the overall (i.e. before any adsorption occurs) concentration of the inhibitor $[CnBDMAC]_{total}$.

II. changing the surfactant chemical structure, i.e. effect of surfactant chain length.

III. changing the amount of *solid 1* surface per solution volume and surface area of *solid 1* surface which controls A_{solid1}.

IV. changing the *solid 2* concentration and its surface area which controls A_{solid2}.

Figure 8-4 shows an overview of the proposed Excel spreadsheet. In the next section, we are going to apply this model to evaluate the effect of addition of different sand amounts on the amount of C16BDMAC adsorbed on iron carbonates in brine solutions at 25 °C. Then we are going to correlate these changes in the amount of adsorption with corresponding changes in the protection efficiency upon sand addition.

8.4.1. Modelling the effects of sand addition on the adsorption of C16BDMAC onto iron carbonate particles and its impact on the inhibitor efficiency

The proposed spreadsheet was used to model the effect of the amount of sand added on the relative amounts of C16BDMAC adsorbed onto two surfaces, **surface1** (iron carbonate particles) and **surface2** (sand particles). The adsorption isotherms of C16BDMAC onto sand particles and iron carbonate particles, at constant temperature 25 °C from brine solutions are shown in Figure 8-5. As inferred for these adsorption isotherms, C16BDMAC adsorbs more strongly onto sand particles than to iron carbonate over the entire concentration range.

Figure 8-4. An overview for the proposed Excel spreadsheet.

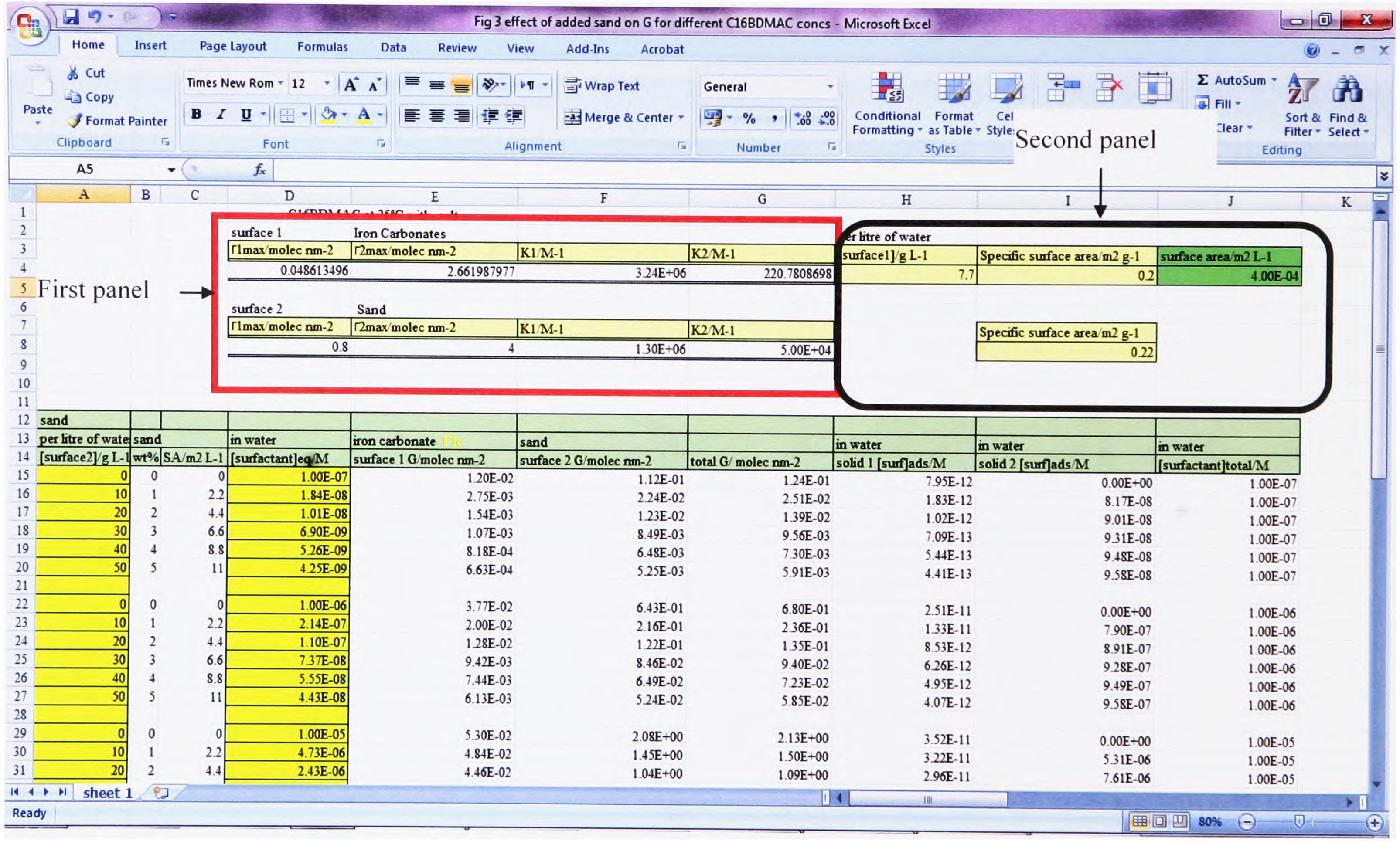

surface 1 Iron Carbonates

Γ1max/molec nm-2	Γ2max/molec nm-2	K1/M-1	K2/M-1
0.048613496	2.661987977	3.24E+06	220.7808698

surface 2 Sand

Γ1max/molec nm-2	Γ2max/molec nm-2	K1/M-1	K2/M-1
0.8	4	1.30E+06	5.00E+04

er litre of water

surface1]/g L-1	Specific surface area/m2 g-1	surface area/m2 L-1
7.7	0.2	4.00E-04

Specific surface area/m2 g-1
0.22

sand									
per litre of wate	sand		in water	iron carbonate	sand		in water	in water	in water
[surface2]/g L-1	wt%	SA/m2 L-1	[surfactant]eq/M	surface 1 G/molec nm-2	surface 2 G/molec nm-2	total G/ molec nm-2	solid 1 [surf]ads/M	solid 2 [surf]ads/M	[surfactant]total/M
0	0	0	1.00E-07	1.20E-02	1.12E-01	1.24E-01	7.95E-12	0.00E+00	1.00E-07
10	1	2.2	1.84E-08	2.75E-03	2.24E-02	2.51E-02	1.83E-12	8.17E-08	1.00E-07
20	2	4.4	1.01E-08	1.54E-03	1.23E-02	1.39E-02	1.02E-12	9.01E-08	1.00E-07
30	3	6.6	6.90E-09	1.07E-03	8.49E-03	9.56E-03	7.09E-13	9.31E-08	1.00E-07
40	4	8.8	5.26E-09	8.18E-04	6.48E-03	7.30E-03	5.44E-13	9.48E-08	1.00E-07
50	5	11	4.25E-09	6.63E-04	5.25E-03	5.91E-03	4.41E-13	9.58E-08	1.00E-07
0	0	0	1.00E-06	3.77E-02	6.43E-01	6.80E-01	2.51E-11	0.00E+00	1.00E-06
10	1	2.2	2.14E-07	2.00E-02	2.16E-01	2.36E-01	1.33E-11	7.90E-07	1.00E-06
20	2	4.4	1.10E-07	1.28E-02	1.22E-01	1.35E-01	8.53E-12	8.91E-07	1.00E-06
30	3	6.6	7.37E-08	9.42E-03	8.46E-02	9.40E-02	6.26E-12	9.28E-07	1.00E-06
40	4	8.8	5.55E-08	7.44E-03	6.49E-02	7.23E-02	4.95E-12	9.49E-07	1.00E-06
50	5	11	4.43E-08	6.13E-03	5.24E-02	5.85E-02	4.07E-12	9.58E-07	1.00E-06
0	0	0	1.00E-05	5.30E-02	2.08E+00	2.13E+00	3.52E-11	0.00E+00	1.00E-05
10	1	2.2	4.73E-06	4.84E-02	1.45E+00	1.50E+00	3.22E-11	5.31E-06	1.00E-05
20	2	4.4	2.43E-06	4.46E-02	1.04E+00	1.09E+00	2.96E-11	7.61E-06	1.00E-05

Figure 8-5. Adsorption C16BDMAC from 4.7 wt.% brine solutions onto sand and iron carbonate particles at 25 °C, using the depletion method. The solid lines represent the two-stage Langmuir model fits. The vertical dashed line represents the cmc.

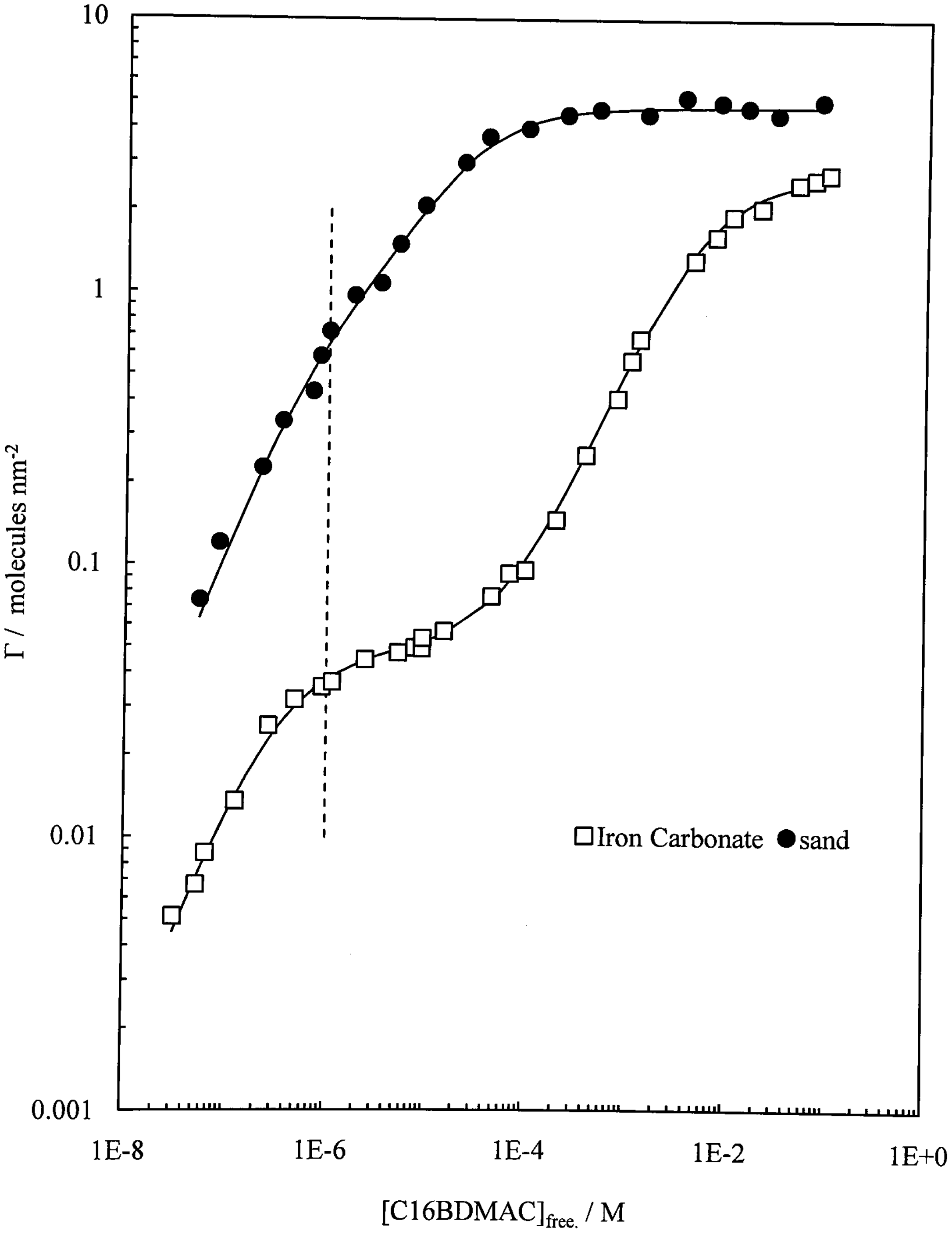

The adsorption parameters, which have been determined previously for the two surfaces separately, have been inserted into the first panel as shown below.

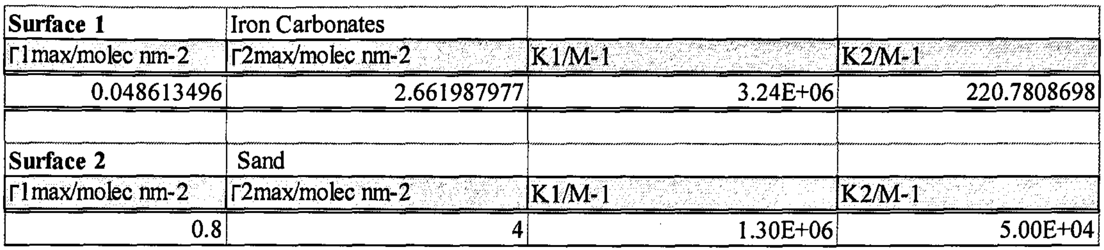

Surface 1	Iron Carbonates		
Γ1max/molec nm-2	Γ2max/molec nm-2	K1/M-1	K2/M-1
0.048613496	2.661987977	3.24E+06	220.7808698
Surface 2	Sand		
Γ1max/molec nm-2	Γ2max/molec nm-2	K1/M-1	K2/M-1
0.8	4	1.30E+06	5.00E+04

The adsorption fitting parameters in addition to the surface areas for sand and iron carbonates are shown in Table 8-2. Using these fitting parameters and specific surface areas, we have calculated the amounts of C16BDMAC adsorbed onto iron carbonate, Γ_{ic}, as a function of sand added for a range of fixed values of $[\mathrm{C16BDMAC}]_{total}$. These calculations have been done using the Excel spreadsheet at different percent weights of sand and are represented graphically in Figure 8-6.

Table 8-2. Powder surface area values and fitting parameters for the two-stage Langmuir adsorption isotherms for C16BDMAC from 4.7 wt. % brine solution onto iron carbonate and sand particles at 25°C.

Parameters	Sand	Fe CO_3
Specific surface area/m^2 g^{-1}	0.22	0.20
k_1 / M^{-1}	1.30×10^6	3.24×10^6
k_2 / M^{-1}	4.99×10^4	2.21×10^2
$\Gamma_{1\,(max)}$ / molecules nm^{-2}	0.80	0.05
$\Gamma_{2\,(max)}$ / molecules nm^{-2}	3.99	2.66
R^2	0.99	0.99

Figure 8-6 shows how Γ_{ic} changes with the addition of sand for various fixed values of $[\mathrm{C16BDMAC}]_{total}$. For the calculations shown in this figure, we have taken A_{ic} to be 4 x 10^{-4} m^2 L^{-1}, which corresponds to the surface area per unit solution volume of corroding steel electrode (under CO_2 atmosphere) in the corrosion cell used for measuring the corrosion rates. In a practical application such as a solution flowing down a pipe, A_{ic} will be typically equal to the internal surface area of the pipe divided by its volume.

Figure 8-6. Variation of the surface concentration of C16BDMAC onto iron carbonate surface as a function of added sand (wt.%) for different, fixed total concentrations of C16BDMAC (indicated in the plot). The calculations refer to a surface area of the iron carbonate per litre of solution is 4 x 10^{-4} m^2.

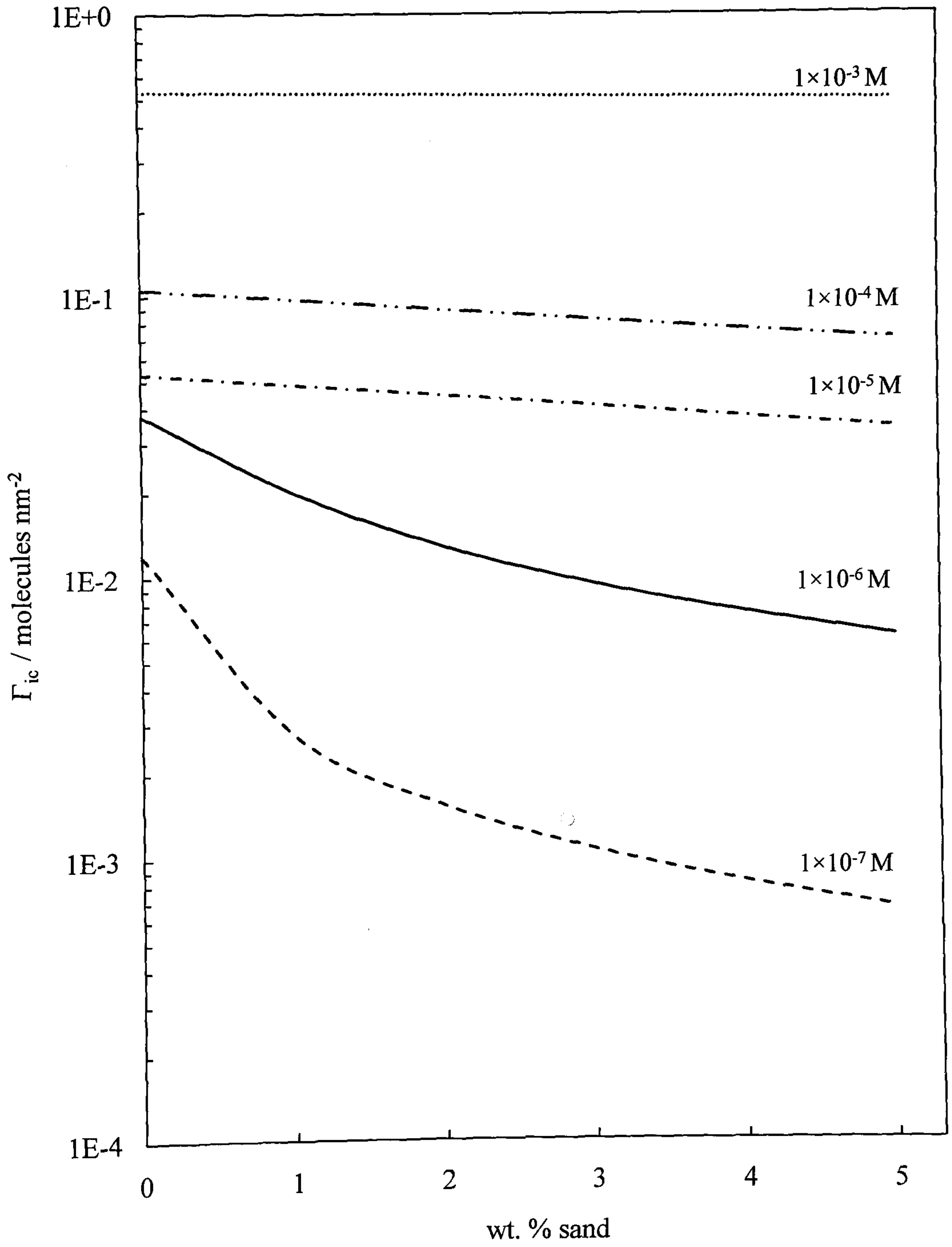

The specific surface area of the sand used here is 0.22 $m^2 g^{-1}$; hence a sand concentration of 1 wt.% corresponds to $A_s = 2.2$ $m^2 L^{-1}$. From Figure 8-6, we can see that, at a fixed value of $[C16BDMAC]_{total}$, Γ_{ic} is reduced by sand addition with the effect being most pronounced at low overall inhibitor concentrations. This range is relevant to field conditions since most of the corrosion inhibitors are added in the actual oilfield pipelines in low concentrations ranging from 1×10^{-6} to 1×10^{-4} M.

Accordingly, the protection efficiency of these surfactants will be markedly affected by the presence of sand under these low surfactant concentrations. In order to model quantitatively the effects of sand addition on the protection efficiency of C16BDMAC, we need to understand how the corrosion rate is linked to the amount of C16BDMAC adsorbed onto steel in the absence of added sand. Therefore, we have plotted the experimentally determined corrosion rates of C1018 electrodes (described in section 8.2) versus the corresponding amounts of adsorption. These amounts were determined using the proposed model employing the above-mentioned procedures.

Figure 8-7 shows how the experimentally determined corrosion rates are related to the amounts of C16BDMAC adsorbed onto the iron carbonate surface, Γ_{ic}. Clearly, the corrosion rate is reduced by about 2 orders of magnitude as Γ_{ic} increases from 0 to a quite low value of only 0.08 molecules nm^{-2}. The data in this figure has been fitted in two different ways. Firstly, for the entire data set, the corrosion rates decrease approximately exponentially with Γ_{ic} but we note that the measured rates do show significant deviation from the fitted line. This observation is supported by the relatively low value of the regression coefficient corresponding to the exponential fitting ($R^2 = 0.93$). Secondly, for values of Γ_{ic} less than about 0.06 molecules nm^{-2}, the corrosion rates decrease linearly with Γ_{ic} and the corresponding fitting quality is improved ($R^2 = 0.99$). It worth mentioning here that these amounts of adsorption correspond to inhibitors concentrations are relevant to the practical oilfield conditions. Consequently, we have decided to adopt the linear fit to model the relation between the corrosion rate and the amount of adsorption. This relation is given by the following equation, for Γ_{ic} less than about 0.06 molecules nm^{-2}:

$$\text{Corrosion rate (mm year}^{-1}\text{)} = -18.015\,\Gamma_{ic}\,\text{(molecules nm}^{-2}\text{)} + 1.0343 \qquad (8\text{-}3)$$

Figure 8-7. Variation of the corrosion rate of mild steel with the surface concentration of adsorbed C16BDMAC under CO_2 in 4.7 wt. % brine at 25 °C. The upper plot (with corrosion rate on a logarithmic scale) shows the fit to an exponential function and the lower plot shows a linear fit to the initial part of the plot

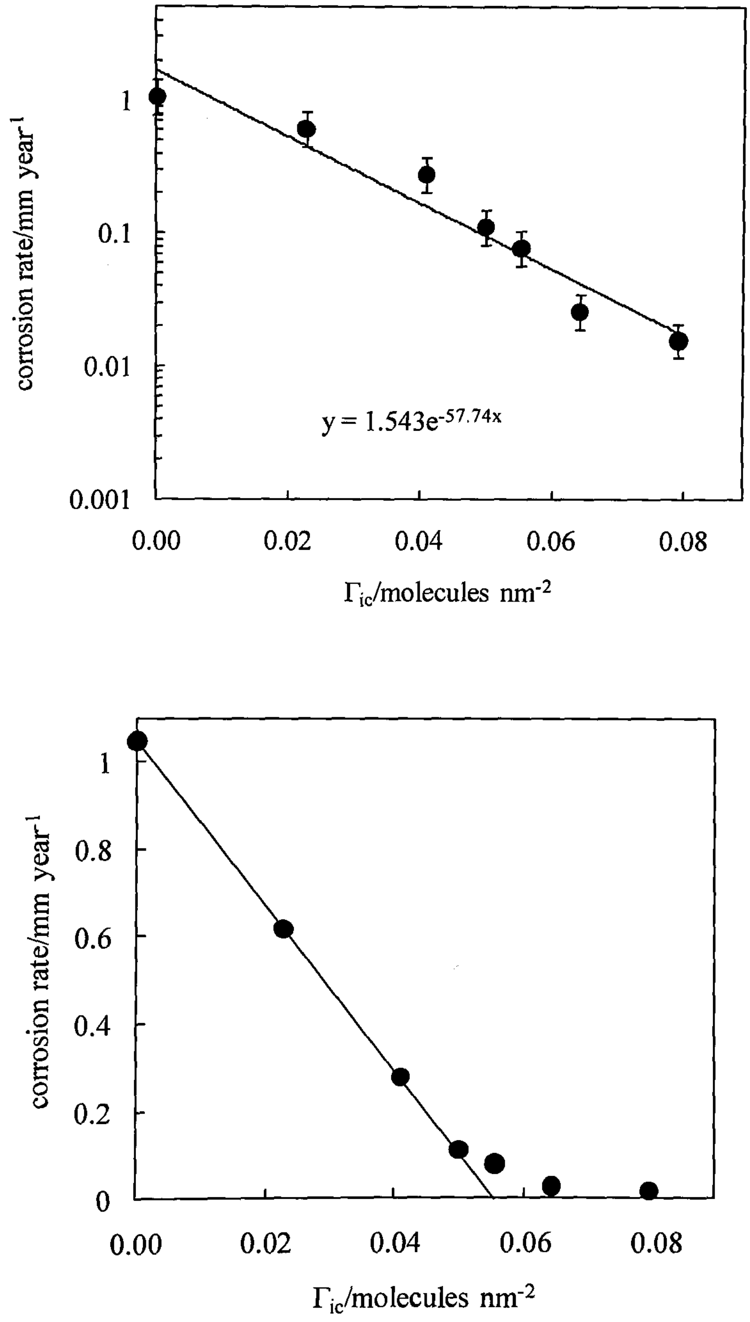

Based on equation (8-2), it is possible to propose a mathematical expression to determine quantitatively the effect of sand addition on the decrease in the protection efficiency. Hence, the calculated percentage decrease in the corrosion protection efficiency, % $\Delta P_{calc.}$, due to the presence of a particular sand concentration, will be given by the following equation:

$$\% \Delta P_{calc.} = [(R_S - R_{NS})/(R_o - R_{NS})] \times 100 \qquad (8\text{-}4)$$

where R_o is the corrosion rate in the absence of inhibitor (baseline corrosion rate), R_{NS} is the corrosion rate in the presence of inhibitor with no sand and R_S is the rate in the presence of inhibitor with either 1 or 2 wt. % of sand. Hence, these corrosion rates will be calculated by the use of equation (8-2) with the aid of the predicted amount of C16BDMAC adsorbed on iron carbonate Γ_{ic}.

Figure 8-8 compares the experimentally determined % decrease in the protection efficiency of C16BDMAC, % $\Delta P_{exp.}$, caused by the addition of sand with those theoretically calculated, % $\Delta P_{calc.}$, using equation (8-3). The experimentally determined percentages decrease in the protection efficiency, % $\Delta P_{exp.}$, are given by:

$$\% \Delta P_{exp.} = [(P_{NS} - P_S)/(P_{NS})] \times 100 \qquad (8\text{-}5)$$

where P_{NS} is the protection efficiency in the presence of inhibitor with no added sand and P_S is the protection efficiency in the presence of inhibitor with either 1 or 2 wt. % added sand. The changes in percentage protection efficiency for different C16BDMAC concentrations as a function of sand amount in brine solutions at 25 °C are reported in Table 8-1.

Figure 8-8 shows that there is an excellent agreement between the experimentally determined and theoretically calculated percentages decrease in the protection efficiency of C16BDMAC upon sand addition. The conditions used for this experiment correspond to those for which the corrosion rate decreases linearly with Γ_{ic}, consistent with the good quality of fit seen in Figure 8-8.

In the above mentioned example, we have demonstrated how the proposed spreadsheet can be used to determine or predict the change in the amount of adsorption on steel and sand surfaces with change in amount of sand. These predicted or determined changes in the amount of adsorption resulted from changes in production variables has been used to predict and measure the corresponding

Figure 8-8. Percentage change in the corrosion protection efficiency of C16BDMAC as a function of the total inhibitor concentration caused by the addition of 1 (filled symbols and dashed line) and 2 (open symbols, and solid line) wt% of sand. The solid and dashed lines show the predicted changes based on the corrosion rate decreasing linearly with the amount of C16BDMAC adsorbed on the iron carbonate surface. Measurements were made under CO_2 in 4.7 wt% brine at 25°C.

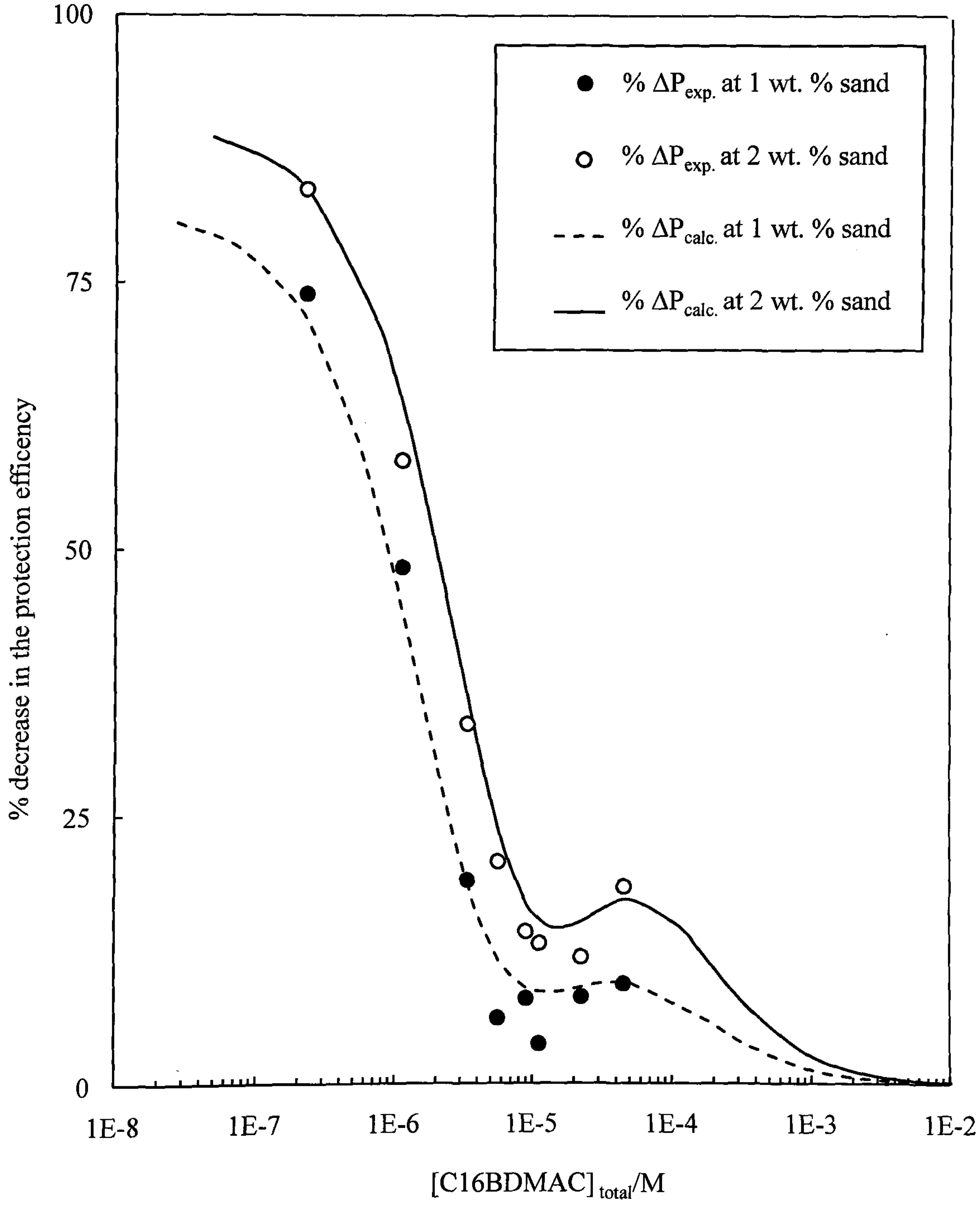

changes in the protection efficiency or effectiveness of these surfactants molecules. By analogy, we could use the spreadsheet to detect the changes in the amount of adsorption of any other CnBDMAC surfactants. Additionally, it is possible to simulate the effect of temperature, brine addition and change in total steel surface area on the amount of adsorption.

8.5. DISCUSSION

8.5.1. Effect of dissolved gases on the corrosion rate of steel

The electrochemical theory of corrosion relates corrosion to a network of short-circuited galvanic cells on the metal surface [5]. Metal ions go into solution at anodic areas in an amount chemically equivalent to the reaction at cathodic areas. At *anodic areas*, the following reaction takes place:

$$Fe_{(S)} \rightarrow Fe^{2+}_{(aq)} + 2e^- \qquad (8\text{-}6)$$

This reaction is rapid in most media and did not affect by the gas type [5]. When iron corrodes, the rate is usually controlled by the cathodic reaction, which, in general, is much slower than the anodic reaction. The type of gas encountered in the corroding environment is one the key factors, among other, including temperature, pH and temperature, influences the cathodic reactions. In deaerated solutions, the cathodic reaction is given by the following reaction:

$$2H^+_{(aq)} + 2e^- \rightarrow H_{2\,(g)} \qquad (8\text{-}7)$$

This reaction proceeds rapidly in acids and proceeds slowly in alkaline or neutral aqueous media [5].

In aerated solutions, dissolved oxygen will accelerate the cathodic reaction in accord with the following reactions:

$$\tfrac{1}{2}O_{2\,(g)} + 2H^+_{(aq)} + 2e^- \rightarrow H_2O_{(l)} \qquad (8\text{-}8)$$

$$\tfrac{1}{2}O_{2\,(g)} + H_2O_{(l)} + 2e^- \rightarrow 2OH^-_{(aq)} \qquad (8\text{-}9)$$

Dissolved oxygen reacts with hydrogen atoms adsorbed at random on the iron surface. The oxidation reaction proceeds as rapidly as oxygen reaches the metal surface. Adding equations (8-6), (8-8) and (8-9), we obtain:

$$Fe_{(S)} + H_2O_{(l)} + \frac{1}{2}O_{2(g)} \rightarrow Fe(OH)_{2\,(S)} \qquad (8\text{-}10)$$

Hydrous ferrous oxide ($FeO{\cdot}nH_2O$) or ferrous hydroxide $Fe(OH)_2$ composes the diffusion-barrier layer next to the iron surface through which O_2 must diffuse. The colour of $Fe(OH)_2$, although white when the substance is pure, is normally green to greenish black because of oxidation by air. At the outer surface of the oxide film, access to dissolved oxygen converts ferrous oxide to hydrous ferric oxide or ferric hydroxide, as shown by equation (8-6).

$$Fe(OH)_{2\,(s)} + \frac{1}{2}H_2O_{(l)} + \frac{1}{4}O_{2\,(g)} \rightarrow Fe(OH)_{3\,(s)} \qquad (8\text{-}11)$$

Hydrous ferric oxide is orange to reddish brown in colour and comprises most of the ordinary rust. It exists as nonmagnetic α Fe_2O_3 (hematite) or as magnetic γ Fe_2O_3, with the α form having the greater negative free energy of formation, that is, greater stability. Saturated $Fe(OH)_3$ is nearly neutral in pH. A magnetic hydrous ferrous ferrite, $Fe_3O_4{\cdot}nH_2O$, often forms a black intermediate layer between hydrous Fe_2O_3 and FeO. Hence, rust films normally consist of three layers of iron oxides in different states of oxidation.

Corrosion in the presence of dissolved carbon dioxide gas is often termed 'sweet' corrosion. Carbon dioxide gas forms carbonic acid when dissolved in water, which decreases the pH of the solution and is slightly corrosive (equation (8-12)).

$$CO_{2\,(g)} + H_2O_{\,(l)} \rightarrow H_2CO_{3\,(aq)} \qquad (8\text{-}12)$$

Several mechanisms have been proposed for iron corrosion in aqueous CO_2 containing solutions. In the presence of carbon dioxide gas, three cathodic reactions could be proposed (equations (8-7), (8-13) and (8-14)) [6, 7] .

$$2H_2CO_{3(aq)} + 2e^- \rightarrow H_{2\,(g)} + 2HCO_3^-{}_{(aq)} \qquad (8\text{-}13)$$

$$2HCO_3^-{}_{(aq)} + 2e^- \rightarrow H_{2\,(g)} + 2CO_3^{2}{}_{(aq)} \qquad (8\text{-}14)$$

Carbonic acid reacts with iron in carbon steel to form an iron carbonate layer next to the steel surface. The properties of this layer and its influence on the corrosion rate are important factors to be taken into account when studying the corrosion of steels in CO_2 aqueous solutions. Iron carbonate, $FeCO_3$, plays an important role in the formation of protective layers and it formation can be explained using equations (8-14) to (8-16) [7]. Because of its low solubility, $FeCO_3$ precipitates out of solution ($pK_{sps} = 10.54$ at 25 °C) [8] and act as a barrier to corrosion.

$$Fe^{2+}_{(aq)} + CO_3^{2-}{}_{(aq)} \rightarrow FeCO_{3(s)} \quad (8\text{-}15)$$

$$Fe^{2+}_{(aq)} + 2HCO_3^{-}{}_{(aq)} \rightarrow Fe(HCO_3)_{2\,(aq)} \quad (8\text{-}16)$$

$$Fe(HCO_3)_{2(aq)} \rightarrow FeCO_{3(s)} + CO_{2(g)} + H_2O_{(l)} \quad (8\text{-}17)$$

Precipitation of iron carbonates on the surface of the metal decreases the corrosion rate by acting as a diffusion barrier for the corrosive species to travel to the metal surface by blocking a small number of areas on the steel surface and preventing electrochemical reactions from happening on the surface [9]. The corrosion rate will depend on the protectiveness of this scale. This in turn explains the higher protection efficiency of C16BDMAC in the presence of carbon dioxide compared with that under aerated conditions.

H_2S corrosion or 'Sour' corrosion is caused by the presence of hydrogen sulphide, which also lowers the pH of the solution to approximately 4 in saturated systems due to its dissociation in water. A 'sour' pipeline will generally contain dissolved CO_2 and H_2S. However, the presence of only 3-5 parts per million of H_2S can significantly affect the corrosion rate of steel and causes the formation of iron sulphide (FeS) corrosion products. The dissociation of H_2S in aqueous solutions is given by the following equations [10, 11]:

$$H_2S_{(g)} \rightarrow HS^{-}_{(aq)} + H^{+}_{(aq)} \quad (8\text{-}18)$$

$$HS^{-}_{(aq)} \rightarrow S^{2-}_{(s)} + H^{+}_{(aq)} \quad (8\text{-}19)$$

The solution chemistry of H_2S depends on the solution pH [12]. Depending on the pH, sulfur can be present in three different forms; H_2S, HS^- and S^{2-}. The pH of brine saturated with H_2S is 4 at room temperature [13]. At this pH value H_2S is the dominating species in solution. These sulphur species combine with ferrous ions to form different iron sulphide species (Table 8-3) which may or may not be protective depending on conditions such as pH, H_2S concentration and temperature [14]. The overall H_2S corrosion reaction for iron in an aqueous medium is shown by equation (8-20) [1].

$$Fe_{(s)} + H_2S_{(g)} \rightarrow FeS_{(s)} + H_{2(g)} \tag{8-20}$$

Generally, at lower pH values (< 2), iron is dissolved and iron sulfide is not precipitated on the surface of the metal due to a very high solubility of iron sulfide in such solutions. At pH values from 3 to 5, an inhibitive effect of H_2S is seen as FeS species may form Mackinawite [13].

The metastable Mackinawite can convert into other forms of sulfides which are more protective such as troilite, and the protective or inhibitive effect of H_2S depends on the stability and compactness of the transformed sulfide [15]. At higher pH values between 6 to 8.8, it was reported that sulfide formed was most unprotective, with Mackinawite being the main corrosion product [16]. In general, a compact sulfide phase provides corrosion protection while a porous phase is unprotective. Highly defective films formed especially at high H_2S concentrations can be unprotective [17]. Especially at the higher temperatures, even a compact sulfide surface phase such as Pyrrhotite is unprotective in view of the fast diffusion of iron ions through it [18].

Figure 8-3 shows that the presence of H_2S causes the corrosion rate of C1018 steel to decrease, suggesting that the corrosion product film is more protective under these conditions than in the presence of CO_2, where the corrosion product is $FeCO_3$. Nesic *et al.* [19] reported that, trace amounts of H_2S were shown to rapidly reduce the corrosion rate of C1018 steel.

Table 8-3: Naturally occurring forms of iron sulphides [14].

Sulphide	**Chemical Formula**	**Stoichiometry**	**Crystal Structure**
Greigite	Fe_3S_4	-	Cubic
Mackinawite	$Fe_{1+x}S$	$x = 0.057 - 0.064$	Tetragonal
Marcasite	FeS_2	-	Orthorhombic
Pyrite	FeS_2	-	Cubic
Pyrrhotite	$Fe_{1-x}S$	$x = 0 - 0.14$	Monoclinic
Smythite	$Fe_{3+x}S_4$	$x = 0 - 0.25$	Hexagonal

8.5.2. The correlation between the adsorption extent of C16BDMAC and its corrosion inhibition efficiency under CO_2 conditions

Iron carbonate $FeCO_3$ constitutes one of the main corrosion products that encountered in typical oilfield pipelines due to sweet corrosion. The obtained adsorption isotherm for C16BDMAC onto iron carbonates from brine solutions (Figure 8-5) give rise to a three-sage adsorption mechanism similar to that reported for C1018 mild steel. Additionally, the adsorbed amounts of C16BDMAC onto iron carbonates are smaller than that adsorbed onto sand particles. Despite this fact, we have found that in the presence of carbon dioxide, C16BDMAC provides a high protection efficiency against corrosion. This indicates that the amount of adsorption is not the only factor that controls the corrosion inhibitor efficiency.

This conclusion is true and many authors claim that, the amount of adsorption extent and the structure of the adsorbed film are the key factors that determine the corrosion inhibitors efficiency.

If we assume that the adsorbed C16BDMAC molecules lie flat on the iron carbonate surface at low values of Γ_{ic} and that the thickness of the molecule is about 0.54 nm, we can estimate that the value of Γ_{ic} corresponding to a close-packed monolayer of C16BDMAC molecules lying flat on the surface is approximately 0.82 molecules nm^{-2}.

From the electrochemical corrosion measurements of steel under carbon dioxide conditions, it is clear that the corrosion protection efficiency reach more than 97 % at about 9.01×10^{-6} M C16BDMAC. This concentration corresponds to an amount of adsorption Γ_{ic}, of about 0.05 molecules nm^{2}. Based on the aforementioned calculation in *Chapter 2* regarding the area of a close-packed monolayer of C16BDMAC molecules lying flat on the surface (0.82 molecules nm^{-2}), it can be concluded that the corrosion rate is reduced approximately 100-fold, which corresponds to only about 6 % of complete coverage by flat C16BDMAC molecules. This suggests that iron carbonate surface is not covered entirely by C16BDMAC molecules and coverage of only a small fraction of the total iron carbonate surface provides almost complete protection.

The higher protection efficiency exhibited by C16BDMAC at these low amounts of adsorption could be attributed to the blocking of the active sites on steel surfaces [20, 21]. These active sites correspond to the cathodic ones where the negative surface charge is likely to cause strong adsorption of this cationic inhibitor [20-25]. The resultant adsorbed inhibitor is then responsible for protection by physically blocking the surface from the corrosion environment and retarding the electrochemical processes.

Veawab *et al.* [20] proposed that *N*-contacting corrosion inhibitors in the presence of CO_2 functions by suppressing the reduction of active agents (such as HCO_3^-, HO^-, HS^- and S^{2-}) at the cathodic sites. As illustrated in Figure 8-9, when the inhibitor is introduced into the system, it is adsorbed onto the metal surface and prevents the oxidizing agents from undergoing reduction (accepting electrons) on the cathodic sites.

Forge *et al.* [21] reported that, inhibition of steel corrosion in acidic solutions by *N*-contacting corrosion inhibitors is mainly due to electrostatic adsorption of nitrogen atom onto the cathodic sites, which act as cathodic inhibitors. The presence of these surfactants reduces the cathodic current and prevents hydrogen adsorption onto steel surfaces by favouring H-H recombination, *i.e.*, the atomic hydrogen concentration at the metal surface will be relatively small.

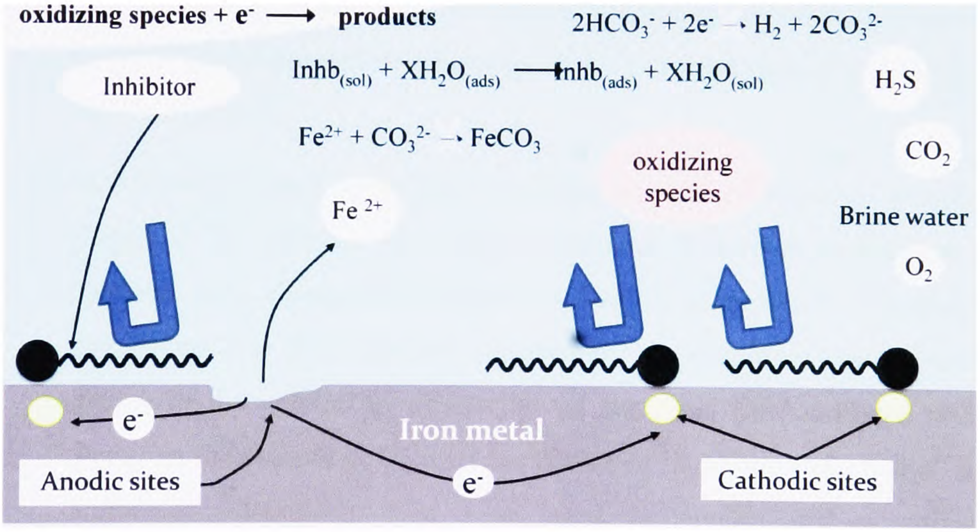

Figure 8-9. Schematic diagram of inhibiting function of C16BDMAC corrosion inhibitor in the presence of CO_2. Reproduced with some modifications from [20].

8.6. SUMMARY AND CONCLUSION

We have shown, for the first time, how adsorption isotherms for the adsorption of the C16BDMAC corrosion inhibitor onto the relevant surfaces can be used to quantitatively predict the conditions under which the inhibitor efficiency will decrease due to loss through adsorption to a competitive surface.

Electrochemical methods were used to determine the corrosion rate of C1018 mild steel in brine solutions under aerated CO_2 and H_2S conditions in the presence and absence of C16BDMAC corrosion inhibitors at 25 °C. In addition, the effect of the presence of different amounts of sand on the corrosion rate of C1018 mild steel in CO2 saturated- brine solutions has been investigated for the first time. The key and new findings within this study are summarized below.

I. The C16BDMAC protection efficiency was found to follow the order $H_2S > CO_2 >$ air. Steel corroded under aerated conditions exhibited a reddish brown iron oxide-hydroxide corrosion product and steel corroded in CO_2-containing environments acquired a grey iron carbonate corrosion film. Under H_2S conditions the steel electrodes were covered with a black corrosion film thought to be an iron sulphide compound.

II. The addition of sand to a brine solution containing C16BDMAC was found to decrease the protection efficiency for C1018 mild steel in the presence of carbon dioxide.

III. A Microsoft Excel spreadsheet has been constructed to model visually the change in the amounts of corrosion inhibitors adsorbed on different solid surfaces with changes in typical production parameters. The proposed spreadsheet has been applied successfully to determine and predict the change in the amount of adsorption on steel and sand surfaces with the change in the amount of sand. These predicted or determined changes in the degree of adsorption have been used to predict and measure the corresponding changes in the protection efficiency.

IV. The corrosion rate of mild steel, in the presence of C16BDMAC, was reduced approximately 100-fold, which corresponds to only about 6 % of the complete coverage by flat C16BDMAC molecules. This suggests that an iron carbonate surface is not covered entirely by C16BDMAC molecules and coverage of only a small fraction of the total steel (iron carbonate) surface provides almost complete protection.

V. The higher protection efficiency exhibited by C16BDMAC at these low amounts of adsorption could be attributed to the blocking of the active sites on steel surfaces. These active sites correspond to the cathodic ones where the negative surface charge is likely to cause strong adsorption of this cationic inhibitor.

VI. Optimisation of the overall performance of a corrosion inhibitor for a particular set of operating conditions needs to take account of the affinity of the inhibitor for competitor surfaces present in addition to that for the primary target surface undergoing corrosion.

VII. The approach described in this work is easily extendable to cover inhibitor loss to multiple competitor surfaces; for example, in addition to inhibitor loss to sand surfaces considered here, we could include additional loss by adsorption to the oil-water interface present for a system containing emulsion oil drops in addition to sand.

8.7. REFERENCES

1. V. S. Sastri, E. Ghali and M. Elboujdaini, *Corrosion Prevention and Protection : Practical Solutions*, Wiley, Hoboken (2007).
2. J. T. Hicks, *Surfactants Aspects of Corrosion Inhibitors*, Ph.D. thesis, Hull University (2007).
3. B. P. Binks, P. D. I. Fletcher, J. T. Hicks, D. I. Horsup and W. H. Durnie, *Proceedings of NACE Corrosion 2005*, Paper No. 05307, NACE International, Houston (2005).
4. H. Reus, M. Gough, W. Durnie, L. A. Hendriksen, Y. Al-Habsi and M. Wilms, *Proceedings of NACE Corrosion 2005*, Paper No. 05288, NACE International, Houston (2005).
5. H. H. Uhlig and R. W. Revie, *Corrosion and Corrosion Control : an Introduction to Corrosion Science and Engineering*, Wiley-Interscience Hoboken (2008).
6. D. A. Lopez, T. Perez and S. N. Simison, *Mater. Des.*, **24**, 561 (2003).
7. G. I. Ogundele and W. E. White, *Corrosion*, **42**, 71 (1986).
8. D. R. Lide, *CRC Handbook of Chemistry and Physics*, CRC Press, Boca Raton (2009).
9. S. Nesic, J. Lee and V. Ruzic, *Proceedings of NACE Corrosion 2002*, Paper No. 02237, NACE International, Denver (2002).
10. G. Schmitt, T. Simon and R. H. Hausler, *Proceedings of NACE Corrosion 90*, Paper No. 22, NACE International, Houston (1990).
11. J. Smith and J. Miller, *Br. Corros. J.*, **10**, 136 (1975).
12. D. Abayarathna, A. Naraghi and N. Obeyesekere, *Proceedings of NACE Corrosion 2003*, Paper No. 03340, NACE International, San Diego (2003).
13. E. Abelev, J. Sellberg, T. Ramanarayanan and S. Bernasek, *J. Mater. Sci.*, **44**, 6167 (2009).
14. A. K. Agarwal, C. Durr and G. H. Koch, *Proceedings of NACE Corrosion 2004*, Paper No. 04388, NACE International, New Orleans (2004).
15. H. Ma, X. Cheng, G. Li, S. Chen, Z. Quan, S. Zhao and L. Niu, *Corros. Sci.*, **42**, 1669 (2000).

16. J. B. Sardisco and R. E. Pitts, *Corrosion (Houston, TX, United States)*, **21**, 350 (1965).

17. D. W. Shoesmith, P. Taylor, M. G. Bailey and D. G. Owen, *J. Electrochem. Soc.*, **127**, 1007 (1980).

18. H. Vedage, T. A. Ramanarayanan, J. D. Mumford and S. N. Smith, *Corrosion*, **49**, 114 (1993).

19. B. Brown, S. Nesic and S. Parakala, *Proceedings of NACE Corrosion 2004*, Paper No. 04736, NACE International, New Orleans (2004).

20. A. Veawab, P. Tontiwachwuthikul and A. Chakma, *Ind. Eng. Chem. Res.*, **40**, 4771 (2001).

21. M.I. Rodríguez, R. Réquiz, H. Ng and G. Jorge, *Anti-Corros. Method M.*, **54**, 93 (2007).

22. L. A. Avaca, E. R. González and A. R. Filho, *J. Appl. Electrochem.*, **12**, 405 (1982).

23. G. Bereket, M. Glec and A. Yurt, *Anti-Corros. Method M.*, **53**, 52 (2006).

24. P. Kern and D. Landolt, *Electrochim. Acta*, **47**, 589 (2001).

25. T. Vasudevan, S. Muralidharan, S. Alwarappan and S. V. K. Iyer, *Corros. Sci.*, **37**, 1235 (1995).

CHAPTER 9

Chapter 9

SUMMARY OF CONCLUSIONS AND FUTURE WORK

9.1. SUMMARY OF CONCLUSIONS

In this study we have aimed to investigate the surface-active properties of corrosion inhibitors. This involves the study of CnBDMAC corrosion inhibitors behaviour at the air-water, oil-water and solid water interfaces with changes in oilfield systems.

The adsorption behaviour of the cationic alkylbenzyldimethylammonium chloride surfactants at the air-water interface has been investigated as a function of alkyl chain length, temperature and electrolyte addition using surface tension measurements. The surfactant chain length has been found to have a great influence on the adsorption behaviour and hence on the cmc values. The cmc values were found to decrease as the number of carbon atoms increases. A significant minimum in the surface tension isotherm was observed for C10, C12BDMAC and to a lesser extent for C14 and C16BDMA due to the presence of certain impurities. This minimum in the surface tension disappeared upon surfactant re-crystallization.

An increase in temperature of CnBDMAC solutions results in a decrease in the surface tension over the entire concentration range. The cmc values for the short chain C10 and C12BDMAC are much more temperature dependent compared with the long chain C14 and C16BDMAC surfactants.

The addition of 4.7 wt. % brine to surfactant solutions results in moving the isotherms to lower concentrations. Moreover, brine addition leads to a sharp decrease in the cmc values compared to those in water. Across the series, the maximum surface concentration increases with chain length and the concentration required to reach saturation decreases.

The total free energy of micellization was found to become more negative with an increase in the number of carbon atoms and with brine addition. This results in favouring the micellization process.

The impact of a number of key production variables on the fate of corrosion inhibitors in a multiphase system has been investigated. These variables are: the ability of corrosion inhibitors to stabilize both oil-in-water and water-in-oil emulsions and the phase inversion of the emulsions as production variables change and the partitioning behaviour of corrosion inhibitors between an aqueous brine phase and an oil phase as a function of brine salinity.

For CnBDMAC, emulsions containing aqueous surfactant and heptane or heptol do not invert and remain water-continuous while emulsions containing the long chain C14 or C16BDMAC and toluene or crude oil inverted to oil-continuous.

Oilfield corrosion inhibitor molecules will partition between oil and water phases to varying extents given by their partition coefficients. As the concentration of the inhibitor is increased, aggregates (micelles or microemulsions) will form in one of the phases. The partitioning and phase behaviour of a corrosion inhibitor will depend upon the inhibitor's effective geometry in the system.

Production variables such as temperature, brine salinity, oil composition and the presence of other production chemicals can all impact an inhibitor's effective head and tail group areas which in turn can have a significant impact on phase behaviour and hence *in-situ inhibitor availability.*

Partitioning experiments indicate that C16BDMAC partitions almost exclusively to the toluene phase at brine concentrations above 1 wt. %. These results are in accordance with those obtained from the emulsification experiments. At low salinity, C16BDMAC was noticed to favour aqueous solubility and the formation of the corresponding Winsor I system where the preferred monolayer curvature was positive. At higher salinities however, the inhibitor partitions almost exclusively into the oil with the formation of the corresponding Winsor II system where the preferred monolayer curvature is negative. Since the preferred curvature of an inhibitor monolayer at an oil-water interface changes with system conditions, the type of emulsion that the inhibitor stabilizes can also change.

Corrosion rate measurements conducted in the presence of oil phases show that partitioning of corrosion inhibitor aggregates from water to oil lead to an increase in the corrosion rate of steel in contact with the aqueous phase (relative to systems with having no oil) at the used experimental conditions.

Studying the adsorption behaviour of surfactant corrosion inhibitors at solid-liquid interfaces provides important information about their action mechanism, which in turn helps in improving their efficiency. The Quartz Crystal Microbalance (QCM) technique is currently experiencing rapid growth in the real-time monitoring of surfactants and macromolecules adsorption at the solid-liquid interface. Adsorption studies carried out using the QCM are in two parts.

The first part investigates the applicability and optimization of the QCM for the measurement of *in-situ* adsorption of CnBDMAC surfactants from aqueous solution onto stainless steel coated crystals. Stainless steel was chosen as a model surface instead of the mild steel as the latter is more likely to corrode easily under the employed experimental conditions. The optimization process aims at finding the appropriate experimental setup and procedures for carrying out the adsorption measurements. Additionally, the treatment and analysis of the experimental data have been discussed in this part.

In the second part, the effects of surfactant chain length, temperature and salinity on the adsorption behaviour of CnBDMAC surfactants onto stainless steel-coated crystals have been investigated.

The results of the optimization process indicated that the employed experimental procedures have a marked influence on both of the measured frequency shift and dissipation energy changes. The average frequency shift detected by the *Stepwise* protocol gave rise to the most higher values followed by those for the *Batch* and *Loop* protocols over all the studied concentration range. The magnitude of these differences is small at low surfactant concentrations and increases gradually with increasing surfactant concentrations. The same conclusions apply for the measured dissipation changes by the three protocols.

The measured normalized frequency shifts were found to vary with the overtone number which indicates that the adsorbed surfactant layer is not rigid and the QCM feels it as a viscoelastic film. The Kanazawa equation failed in describing the measured frequency shifts during the adsorption of C12BDMAC surfactant molecules onto stainless steel-coated crystals. This is because the Δf values predicted by the Kanazawa equation do not take in account the contribution of the adsorbed mass to the total shift in frequency. The Kanazawa equation accounts only for Δf brought about by the change in density and viscosity of surfactant solution only. The amounts of adsorption calculated from the measured QCM shift in the frequency, using the Sauerbrey equation, gave rise to higher values than those determined by the depletion method. The deviation from the Sauerberey model could be mainly attributed to the bulk effect that occurred due to the change in density and viscosity of surfactant solutions.

A simple approach has been used to eliminate the contribution of the bulk effect by making use of the calculated shift in the frequency of different surfactant solutions using Kanazawa's equation. The employed correction procedures succeeded in minimizing the differences between the adsorption isotherms for C12BDMAC onto stainless steel surfaces determined using the QCM and the depletion method. The second approach, used to overcome the excess mass detected by the QCM, was to calibrate the QCM using the amounts of surfactant adsorption determined by the depletion method. It succeeded in overcoming the overestimation of the adsorbed amount, calculated using the Sauerbrey equation. However, it is specific and limited for the system to which the correction has been made.

In conclusion, the usage of the QCM for studying quantitatively the adsorption of surfactants onto solids is not a straightforward process. The measured frequency shift is not only limited to the mass of adsorbed surfactant but it also has a contribution from the bulk solution properties. Accordingly, the measured frequency shift needs to be corrected for the bulk properties. Although, the utilized correction procedures in this work were successful, it requires information about the density and viscosity of the tested surfactant solution. This in turn makes the measurements time consuming and complicated. Therefore, the usage of the QCM for quantitative purposes is not competitive compared to other techniques. The QCM technique demonstrates itself as an excellent qualitative tool rather than a quantitative one.

The adsorption behaviour of CnBDMAC surfactant molecules has been studied as a function of the surfactant chain length, temperature and electrolyte concentration using the QCM. The adsorption isotherms for C10, C12, C14 and C16BDMAC surfactants onto stainless steel-coated crystals give rise to a classical Langmuir type isotherm, with a maximum near to the cmc for C10, C12 and C14BDMAC. The short chains C10 and C12BDMAC give rise to the highest amounts of adsorption compared to the long chains C14 and C16BDMAC.

At low surfactant concentration, the temperature rise has no effect on the amount of surfactant being adsorbed on the stainless steel surfaces for C10BDMAC. At moderate and high surfactant concentration, the increase in temperature results in a significant increase in the adsorbed amount of C16BDMAC. On the other hand, the rise in temperature has an adverse effect on the amount of C10BDAC adsorbed onto the steel.

The amount of adsorbed surfactant is higher in brine solution compared to water over the entire concentration range. The electrolyte addition has a considerable influence on the extent of adsorption similar to increasing the hydrocarbon chain length.

The QCM techniques provides an effective, easy to setup and quick *in-situ* monitoring method for studying qualitatively the adsorption of surfactants at the solid-liquid interface.

As the mild steel is the main constituent of pipies used for the oil transportation, the adsorption characteristics of CnBDMAC inhibitors onto mild steel (C1018) has been investigated. Additionally, since the determined adsorption isotherms of CnBDMAC using the QCM were found to overestimate the adsorbed amount, the depletion method, has been used to study the adsorption onto a stainless steel powder.

The adsorption isotherms determined by the depletion method shape gave rise to classical profiles of a typical cationic surfactant being adsorbed onto a negatively charged surface. The analysis of ζ potential measurements gave us additional information to describe more precisely phenomena associated with the adsorption of a cationic surfactant on the charged steel surface.

The log-log representation of the adsorption isotherms and the ζ-potential curves gives rise to three distinct regions of different slopes indicating distinctive mechanisms. Stage I is characterized by the adsorption of surfactant monomers, which is mainly driven by electrostatic interactions. In stage II the hydrophobic effect intervened essentially to promote the self-assembly of adsorbed monomers, namely, the transition from a flat to a perpendicular conformation followed by association of the surfactant monomers (surface aggregation). In Stage III, the surface aggregates continue to grow.

The hydrophobic effect has been shown to play an important role in the adsorption of surfactants from aqueous solution onto the steel surface. As the alkyl chain length increases the contribution of the hydrophobic interaction increases, overcoming repulsion forces among the cationic surface and surfactant headgroups and promoting the growth of a second layer. Accordingly, the short chain C16 and C14BDMAC have higher adsorption affinity for steel surfaces. Generally, the extent of adsorption has been shown to increase with the increase in the surfactant equilibrium concentration.

The addition of brine increases the surfaces excess over the range of surfactant concentrations studied and results in the maximum amount adsorbed being reached at lower surfactant equilibrium concentrations.

The temperature effect on the adsorption behaviour is quite controversy. Whereas the rise in temperature results in a decrease in the adsorbed amount in the absence of electrolyte, it has the opposite effect in the presence of electrolyte. At higher equilibrium concentrations, the alkylbenzyldimethylammonium chlorides appear to adsorb at C1018 mild steel as multilayers (bilayer) or as surface micelles. On the other hand, it is limited to a monolayer at 316L stainless steel.

Sand is one of the main corrosion inhibitor consuming-solids encountered naturally in the oilfield along with clays, iron carbonate, iron sulphide, calcium carbonate and barium sulphate. Despite this fact, studies on the adsorption behaviour of the corrosion inhibitors on such parasitic surfaces and how these affect the ultimate fate of the inhibitor in a production system are limited. Therefore, the adsorption characteristic of CnBDMAC from aqueous solution onto sand has been studied. The results revealed that these inhibitors have a strong affinity for sand particles, particularly at low temperatures and diluted inhibitor concentrations. The shape of adsorption isotherms gave rise to classical profiles of a typical cationic surfactant being adsorbed onto a negatively charged surface and the log-log representation of the adsorption isotherms give rise to three distinct steps or regions of different slopes indicating distinctive mechanisms.

The adsorption of CnBDMAC surfactants have been shown to increase with the increase in the surfactant equilibrium concentration, chain length and brine concentration.

The corrosion inhibition performance of hexadecylbenzyldimethylammonium chlorides (C16BDMAC) corrosion inhibitor in brine solutions has been investigated by the means of the linear polarisation resistance technique, which is commonly known as the "*bubble test*". The protection efficiency of C16BDMAC was investigated as a function of sand amounts, presence of oil and type of gas.

The protection efficiency was found to follow the order $H_2S > CO_2 >$ air. Steel corroded under aerated conditions exhibits reddish brown iron oxide-hydroxide corrosion product and steel corroded in CO_2-containing environments acquires a grey iron carbonate corrosion product film. Under H_2S conditions, the steel electrodes are covered with a black corrosion product film thought to be an iron sulphide compound.

The addition of sand to brine solution-containing C16BDMAC was found to decrease the protection efficiency of C1018 mild steel in the presence of carbon dioxide. A Microsoft Excel spreadsheet has been constructed to model visually the change in the adsorbed amounts of corrosion inhibitors on different solid surfaces with changes in typical production parameters. The proposed spreadsheet has applied successfully to determine or predict the change in the amount of adsorption on steel and sand surfaces with change in amount of sand. These predicted or determined changes in the amount of adsorption have been used to predict and measure the corresponding changes in the protection efficiency.

The corrosion rate of mild steel, in the presence of C16BDMAC, is reduced approximately 100-fold by an extent of adsorption which corresponds to only about 6 % of complete coverage by flat C16BDMAC molecules. This suggests that iron carbonate surface is not covered entirely by C16BDMAC molecules and coverage of only a small fraction of the total steel (iron carbonate) surface provides almost complete protection.

The higher protection efficiency exhibited by C16BDMAC at these low amounts of adsorption could be attributed to the blocking of the active sites on steel surfaces. These active sites correspond to the cathodic ones where the negative surface charge is likely to cause strong adsorption of this cationic inhibitor.

9.2. SUMMARY OF THE NEW INSIGHTS

- The surfactant chain length, temperature and brine addition were found to have a great influence on the adsorption of CnBDMAC surfactant molecules at the air-water interface.
- The experimentally determined cmc values of CnBDMAC in aqueous solution decreases logarithmically as the number of carbon atoms in the alkyl chain increases in accordance with Klevens equation.
- Emulsions containing alkylbenzyldimethylammonium chlorides and heptane or heptol do not invert and remain water-continuous while emulsions containing the long chain C14 or C16BDMAC and toluene or crude oil inverted to oil-continuous.
- Partitioning experiments indicate that C16BDMAC partitions almost exclusively to the toluene phase at brine concentrations above 1 wt.%. These results are in accordance with those obtained from the emulsification experiments.
- Corrosion rate measurements conducted in the presence of oil phases show that partitioning of corrosion inhibitor aggregates from water to oil lead to an increase in the corrosion rate of steel in contact with the aqueous phase (relative to systems with having no oil) at the used experimental conditions.
- The adsorption behaviour of CnBDMAC molecules has been studied as a function of the surfactant chain length, temperature and electrolyte concentration using the Quartz Crystal Microbalance (QCM) technique. The adsorption isotherms for C10, C12, C14 and C16BDMAC surfactants onto stainless steel-coated crystals give rise to a classical Langmuir-type isotherm, with a maximum near to the cmc for C10, C12 and C14BDMAC.The short chains C10 and C12BDMAC give rise to the

highest degree of adsorption compared to that for the long chain C14 and C16BDMAC surfactants.

- The QCM techniques provides an effective, easy-to-setup and a quick in-situ monitoring method for studying qualitatively the adsorption behaviour of surfactants at the solid-liquid interface.
- The effects of surfactant structure, temperature and electrolyte concentration on the adsorption behaviour of CnBDMAC onto mild steel and sand particles using the depletion method have been investigated.
- Studies performed in the presence alkylbenzyldimethylammonium chlorides and sand revealed that these inhibitors have a strong affinity for sand particles, particularly at low temperatures and diluted inhibitor concentrations.
- Optimisation of the overall performance of a corrosion inhibitor for a particular set of operating conditions needs to take account of the affinity of the inhibitor for competitor surfaces present in addition to that for the primary target surface undergoing corrosion.

9.3. SUGGESTIONS FOR FUTURE WORK

- The parasitic adsorption model could be extended for other parasitic surfaces including emulsion droplets and other solids like clays and corrosion products. In addition, it is highly desirable to develop the parasitic model in order to include the effect of surfactant partitioning into oils on the availability of surfactant monomers.
- The investigation into the phase behaviour of corrosion inhibitors offers possibilities for further study. The equilibrium partitioning and emulsion phase inversion experiments can be extended to study other corrosion inhibitor types, such as alkylamines, alkylpyridinium salts and other imidazoline derivatives. The range of system conditions can also be widened. The effects of high temperatures, brine composition, the oil to water volume ratio and the nature of the oil phase (particularly the relative volumes of aliphatic and aromatic hydrocarbons) can be studied in greater detail. By examining a wide range of inhibitor types and environmental

conditions it will be easier to predict the phase behaviour of an inhibitor when applied to a particular oil field.

- Commercially oilfield corrosion inhibitors usually contain up to six surface active organic compounds dissolved in a carrier solvent. The carrier solvent can be water, alcohol or hydrocarbon. Demulsifier species may also be included in order to reduce any impact on water-oil separation in the field Corrosion inhibitor packages used in the oilfield. Accordingly, the adsorption behaviour of a mixture of two or more different surfactant molecules will be very useful for the actual oilfield applications.
- Development of a new generation of aqueous polyelectrolytes possessing both passive matrix functionality and active response to changes in the local environment.

APPENDIX

Appendix

Due to the large volume of data collected and presented in this work, raw data for *Chapters* 4, 5, 6, 7, and 8 –mainly excel files– are provided electronically on the attached CD with the thesis.

Chapter 3

Figure 3-1.

C10BDMAC

ln([C10BDMAC]/mM)	γ / mNm^{-1}
-4.605170186	71.9
-2.995732274	70.4
-2.302585093	69.6
-1.609437912	67.3
-0.693147181	61.6
0	59.6
0.693147181	56.0
1.609437912	51.2
2.302585093	47.2
2.995732274	41.9
3.401197382	36.9
3.688879454	34.4
4.094344562	34.5

C12BDMAC

ln([C12BDMAC]/mM)	γ / mNm-1
-4.605170186	71.5
-3.912023005	70.7
-2.995732274	68.8
-2.302585093	66.7
-0.693147181	59.2
0	55.0
0.693147181	50.5
1.609437912	42.3
1.945910149	35.8
2.079441542	33.05
2.302585093	34.2
2.995732274	37.4
4.605170186	36.9

C14BDMAC

ln([C14BDMAC]/mM)	γ / mNm-1
-5.298317367	71.3
-3.912023005	68.92
-2.995732274	66.3
-2.302585093	64.5
-1.609437912	59.6
-0.916290732	54.3
-0.223143551	49.2
0	43.3
0.693147181	37.6
1.098612289	36.8
1.386294361	37.5
1.609437912	39.1
2.302585093	38.8

C16BDMAC

ln([C16BDMAC]/mM)	γ / mNm-1
-6.214608098	71.6
-5.80914299	71.2
-5.298317367	69.3
-4.605170186	68.2
-3.912023005	65.4
-2.995732274	61.0
-2.525728644	58.8
-2.302585093	54.2
-1.609437912	46.0
-1.203972804	41.96
-0.693147181	36.64
0	35.7
1.609437912	36.0

Figure 3-2.

ln([C12BDMAC]/mM)	γ / mNm-1
-4.605170186	70.9
-3.912023005	69.7
-2.995732274	68.8
-2.302585093	66.5
-1.609437912	64.0
0	56.4
0.693147181	51.5
1.386294361	44.0
1.609437912	40.9
1.791759469	40
1.945910149	38.4
2.079441542	39.0
2.302585093	39.0
2.995732274	38.8
3.912023005	38.6
4.605170186	36.9

Figure 3-3.

ln([C16BDMAC]/mM)	γ / m Nm-1
-6.907755279	69.8
-6.214608098	69.2
-5.298317367	67.3
-4.605170186	64.9
-3.912023005	60.2
-2.995732274	54.6
-2.525728644	49.9
-2.302585093	46.8
-1.609437912	42.0
-1.203972804	35
-0.693147181	31
-0.223143551	31.2
0.693147181	33.2

Figure 3-4.

ln([C10BDMAC]/mM)	γ / m Nm-1
-5.298317367	69.6
-4.605170186	69.4
-3.912023005	67.4
-2.995732274	65.3
-1.609437912	62.6
-0.693147181	58.0
0	52.0
0.693147181	49.2
1.609437912	45.2
2.302585093	38.9
2.995732274	31.9
3.401197382	30.1
3.688879454	31.5
4.382026635	31.8

Figure 3-5.

ln([C16BDMAC]/mM)	γ / m Nm-1
-13.12236338	72.9
-12.4292162	72.4
-12.02375109	71.6
-11.51292546	70.5
-10.81977828	68.2
-9.903487553	64.0
-9.433483923	61.1
-9.210340372	58.6
-8.517193191	53.0
-7.824046011	46.3
-7.418580903	42.3
-7.13089883	38.6
-6.907755279	35.7
-6.214608098	35.2
-5.298317367	34.9
-4.605170186	35.6
-3.912023005	35.1

Figure 3-6.

ln([C12BDMAC]/mM)	γ / m Nm-1
-9.210340372	68.5
-7.60090246	66.2
-6.907755279	63.9
-6.214608098	60.7
-5.298317367	56.7
-4.605170186	52.8
-3.912023005	49.4
-3.218875825	41.8
-2.525728644	39.4
-2.302585093	35
-1.897119985	32
-1.609437912	32.1
-1.203972804	33.2
-0.693147181	33.1
-0.223143551	32.8
0	32.1
1.609437912	32.9

Figure 3-7.

[C10BDMAC]/mM	Γ / molecules nm-2
1.0E-02	5.91E-02
3.0E-02	1.71E-01
1.0E-01	3.17E-01
2.0E-01	4.02E-01
5.0E-01	5.13E-01
1.0E+00	5.97E-01
2.0E+00	6.82E-01
5.0E+00	7.93E-01
1.0E+01	8.77E-01
2.0E+01	9.61E-01
3.0E+01	1.01E+00
4.0E+01	1.05E+00

[C12BDMAC]/mM	Γ / molecules nm-2
1.0E-02	6.69E-02
2.0E-02	1.24E-01
5.0E-02	2.68E-01
0.1000	4.21E-01
0.5000	7.74E-01
1.0000	9.27E-01
2.0000	1.08E+00
5.0000	1.28E+00
7.0000	1.35E+00
8.0000	1.38E+00

[C14BDMAC]/mM	Γ / molecules nm-2
5.0E-03	8.77E-02
1.0E-02	1.46E-01
2.0E-02	2.57E-01
0.0500	4.94E-01
0.0800	6.16E-01
0.1000	6.74E-01
0.2000	8.53E-01
0.5000	1.09E+00
0.8000	1.21E+00
1.0000	1.27E+00
2.0000	1.45E+00

[C16BDMAC]/mM	Γ / molecules nm-2
2.00E-03	5.86E-02
3.00E-03	1.00E-01
5.00E-03	1.79E-01
1.00E-02	3.98E-01
2.00E-02	6.17E-01
5.00E-02	9.07E-01
8.00E-02	1.06E+00
1.00E-01	1.13E+00
2.00E-01	1.34E+00
3.00E-01	1.47E+00
5.00E-01	1.63E+00

Figure 3-8.

[C10BDMAC]/mM	Am / Å2
1.0E-02	1692.006816
3.0E-02	584.2436536
1.0E-01	314.9857084
2.0E-01	248.9359867
5.0E-01	194.9081115
1.0E+00	167.420826
2.0E+00	146.7282034
5.0E+00	126.1217244
1.0E+01	114.0095128
2.0E+01	104.0198722
3.0E+01	98.94827194
4.0E+01	95.63980579

[C12BDMAC]/mM	Am / Å2
1.0E-02	1495.6
2.0E-02	807.148
5.0E-02	372.692
0.1000	237.747
0.5000	129.159
1.0000	107.929
2.0000	92.693
5.0000	78.1155
7.0000	73.8506
8.0000	72.2844

[C14BDMAC]/mM	Am / Å2
5.0E-03	1140.496591
1.0E-02	685.7278
2.0E-02	388.6583756
0.0500	202.3252583
0.0800	162.3905373
0.1000	148.4768445
0.2000	117.2666015
0.5000	91.76702781
0.8000	82.55853648
1.0000	78.80419077
2.0000	69.05027879

[C16BDMAC]/mM	Am / Å2
2.00E-03	1706.207012
3.00E-03	1000.061789
5.00E-03	557.3607283
1.00E-02	250.9864036
2.00E-02	161.9593465
5.00E-02	110.2589797
8.00E-02	94.74534969
1.00E-01	88.8125853
2.00E-01	74.35068696
3.00E-01	67.88448389
5.00E-01	61.18100639

Figure 3-9.

[C16BDMAC]/mM	Γ / molecules nm-2
1.50E-03	2.74E-02
2.00E-03	4.40E-02
5.00E-03	1.30E-01
1.00E-02	2.76E-01
2.00E-02	4.76E-01
5.00E-02	7.74E-01
8.00E-02	9.03E-01
1.00E-01	9.92E-01
2.00E-01	1.16E+00
3.00E-01	1.28E+00
5.00E-01	1.47E+00

Figure 3-10.

[C16BDMAC]/mM	Am / Å2
2.00E-03	3646.227312
3.00E-03	2274.362278
5.00E-03	768.7611846
1.00E-02	362.0572037
2.00E-02	209.9195174
5.00E-02	129.1816757
8.00E-02	110.6960369
1.00E-01	100.8170775
2.00E-01	86.17624079
3.00E-01	77.88719052
5.00E-01	68.13797396

Figure 3-11.

[C12BDMAC]/mM	Am / Å2
1.50E-04	1.84E-01
5.00E-04	6.36E-01
1.0E-03	8.31E-01
2.0E-03	1.03E+00
0.0050	1.28E+00
0.0100	1.48E+00
0.0200	1.67E+00
0.0400	1.87E+00
0.0800	2.06E+00
0.1000	2.12E+00
0.1500	2.24E+00
0.2000	2.32E+00

Figure 3-12.

[C12BDMAC]/mM	Am / Å2
1.50E-04	544.3389149
5.00E-04	157.2555726
1.0E-03	120.3863761
2.0E-03	97.52196271
0.0050	77.950998
0.0100	67.67692626
0.0200	59.79574694
0.0400	53.55867944
0.0800	48.49984466
0.1000	47.06860986
0.1500	44.67316379
0.2000	43.116282

Figure 3-13.

Chain length	log (cmc/M)
10	-1.397940009
12	-2.096910013
14	-2.698970004
16	-3.301029996

Figure 3-14.

Chain length	log (cmc/M)
10	-1.522878745
12	-2.15490196
14	-2.698970004
16	-3.301029996

Figure 3-15.

Chain length	log (cmc/M)
10	-2.522878745
12	-3.698970004
14	-4.698970004
16	-5.698970004

Figure 3-16.

Water

Chain length	ΔG°mic / kJ mol-1
10	-12.4976
12	-18.6412
14	-23.7208
16	-28.5433

Brine

Chain length	ΔG°mic / kJ mol-1
10	-14.3926
12	-21.102
14	-26.8068
16	-32.5116

Figure 1. Corrosion rate vs. time for C1018 steel in 4.7 wt.% brine solution saturated with CO_2 at 25 °C with 0.1 ppm (2.28×10^{-7} M) C16BDMAC as a function of sand (w/v) percent, determined by the bubble test. The vertical dashed line indicates the time at which C16BDMAC was added.

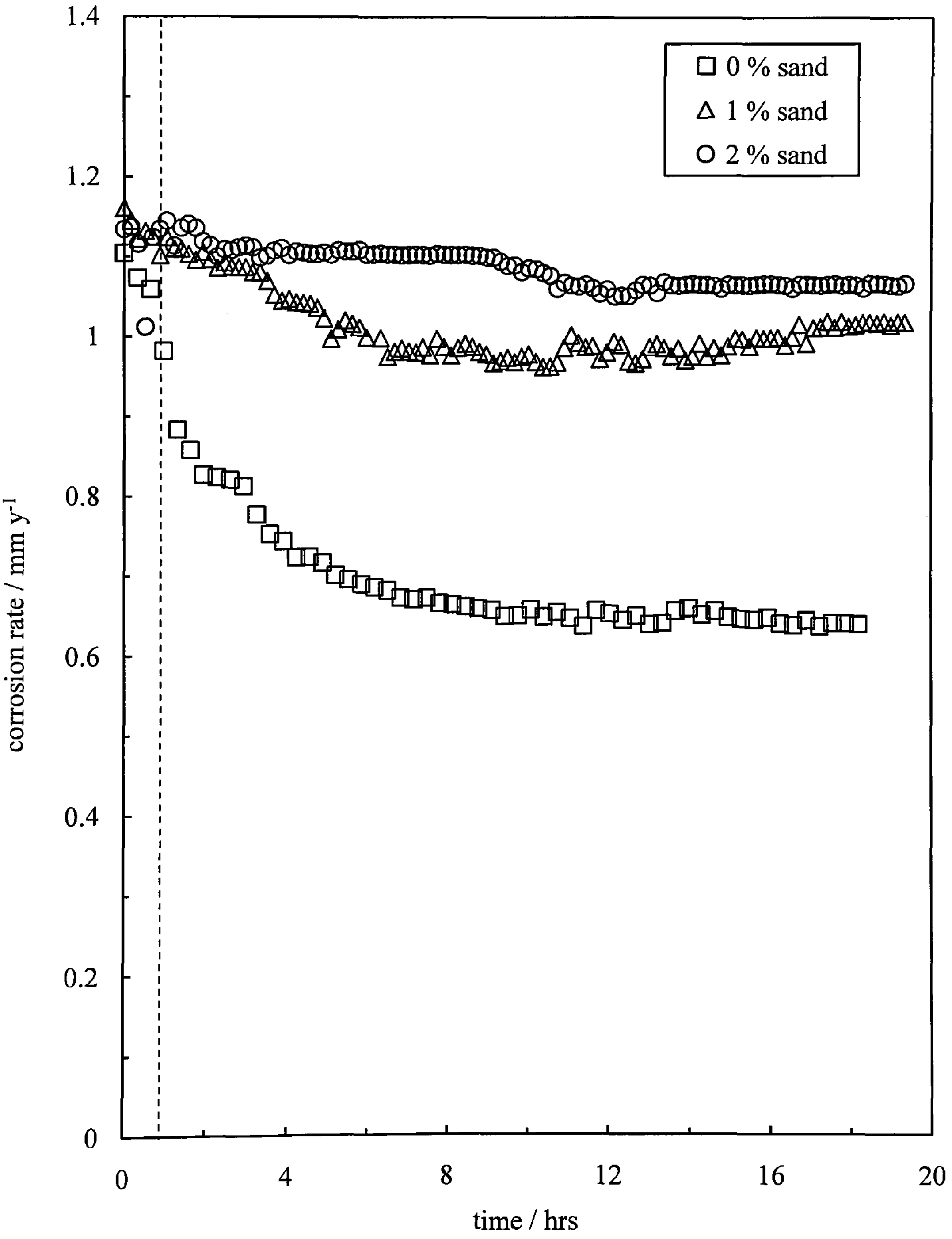

Figure 2. Corrosion rate vs. time for C1018 steel in 4.7 wt.% brine solution saturated with CO_2 at 25 °C with 0.5 ppm (1.13×10^{-6} M) C16BDMAC as a function of sand (w/v) percent, determined by the bubble test. The vertical dashed line indicates the time at which C16BDMAC was added.

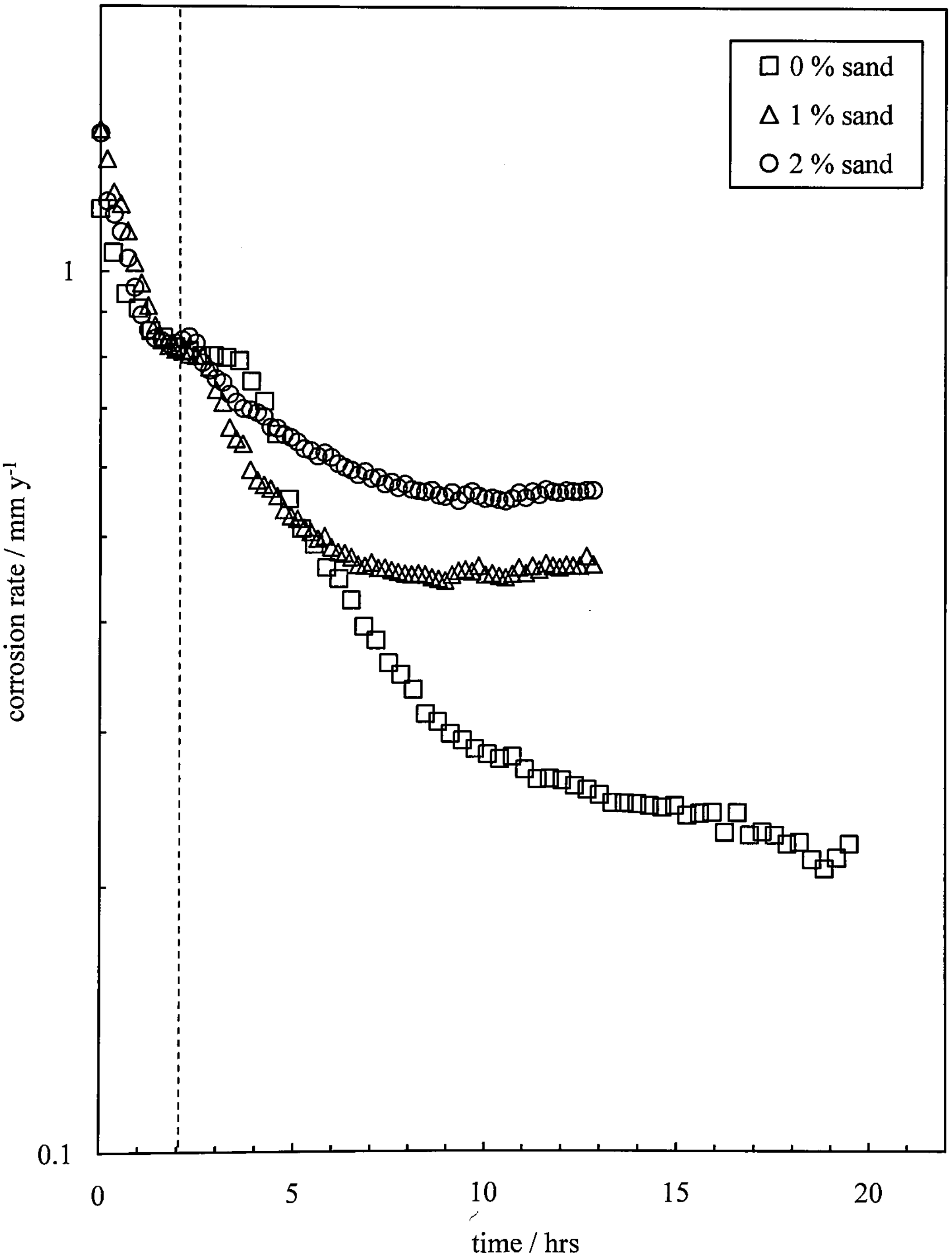

Figure 3. Corrosion rate vs. time for C1018 steel in 4.7 wt.% brine solution saturated with CO_2 at 25 °C with 1.5 ppm (3.36×10^{-6} M) C16BDMAC as a function of sand (w/v) percent, determined by the bubble test. The vertical dashed line indicates the time at which C16BDMAC was added.

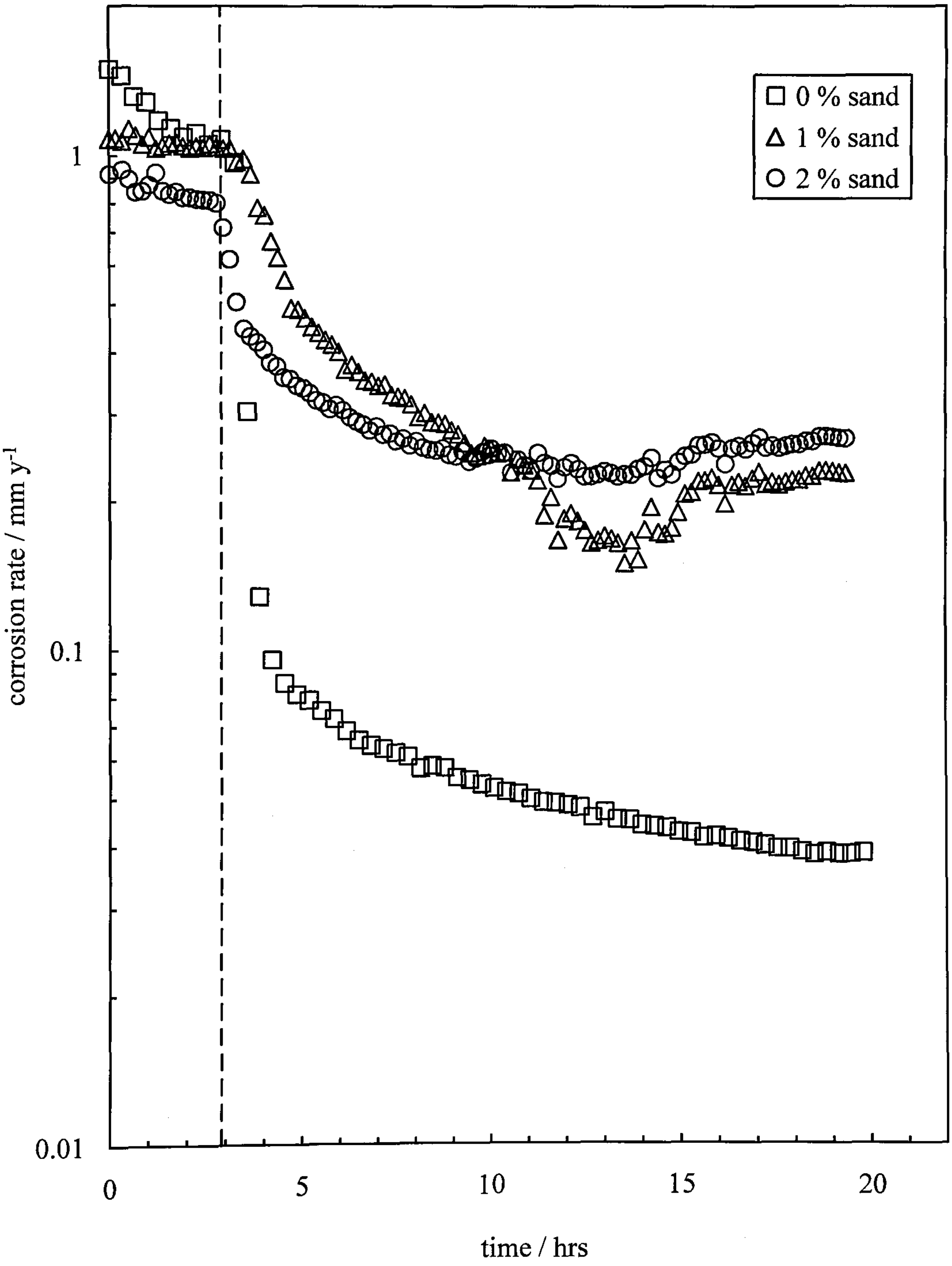

Figure 4. Corrosion rate vs. time for C1018 steel in 4.7 wt.% brine solution saturated with CO_2 at 25 °C with 2.5 ppm (5.63×10^{-6} M) C16BDMAC as a function of sand (w/v) percent, determined by the bubble test. The vertical dashed line indicates the time at which C16BDMAC was added.

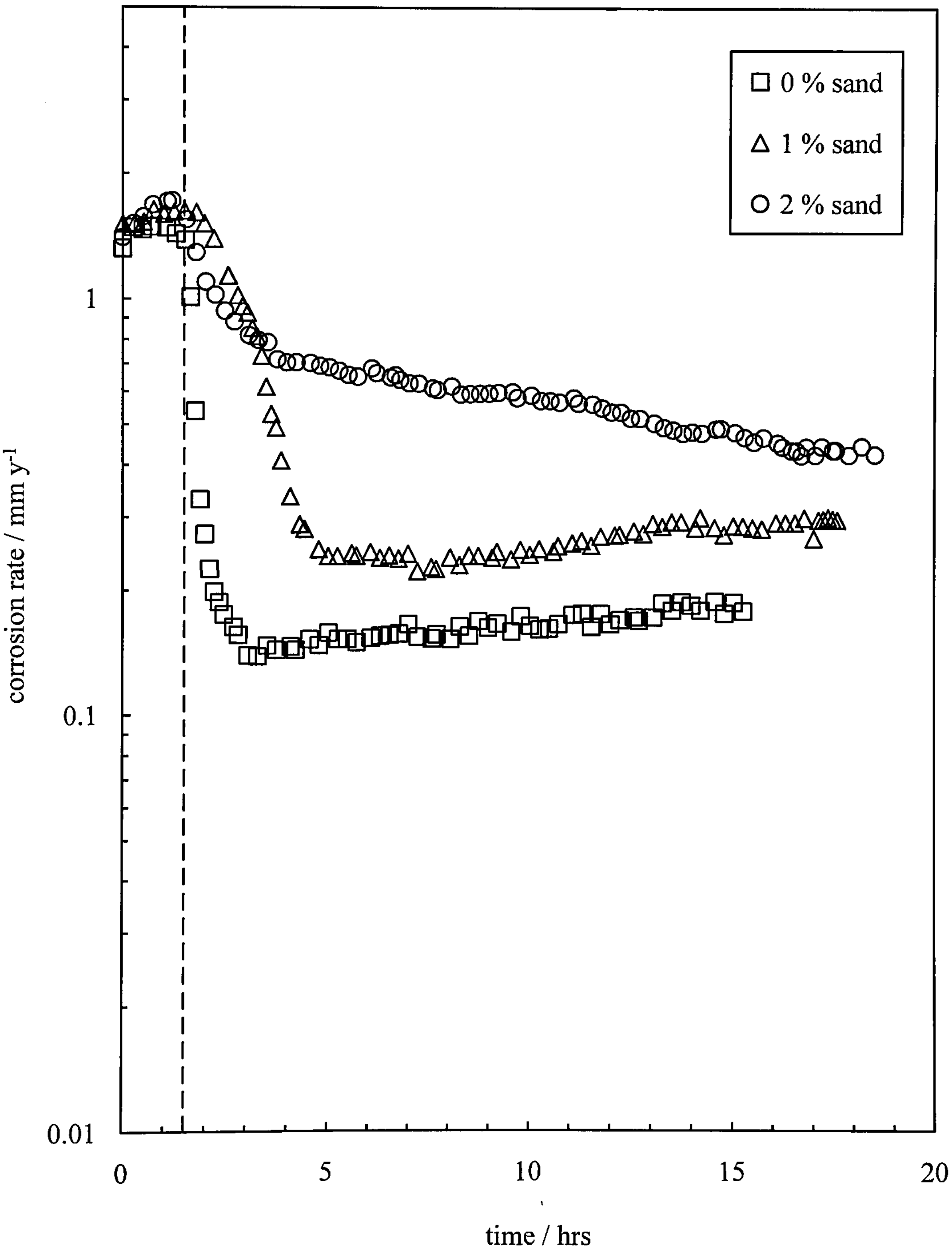

Figure 5. Corrosion rate vs. time for C1018 steel in 4.7 wt.% brine solution saturated with CO_2 at 25 °C with 4 ppm (9.01×10^{-6} M) C16BDMAC as a function of sand (w/v) percent, determined by the bubble test. The vertical dashed lines indicate the time at which C16BDMAC was added.

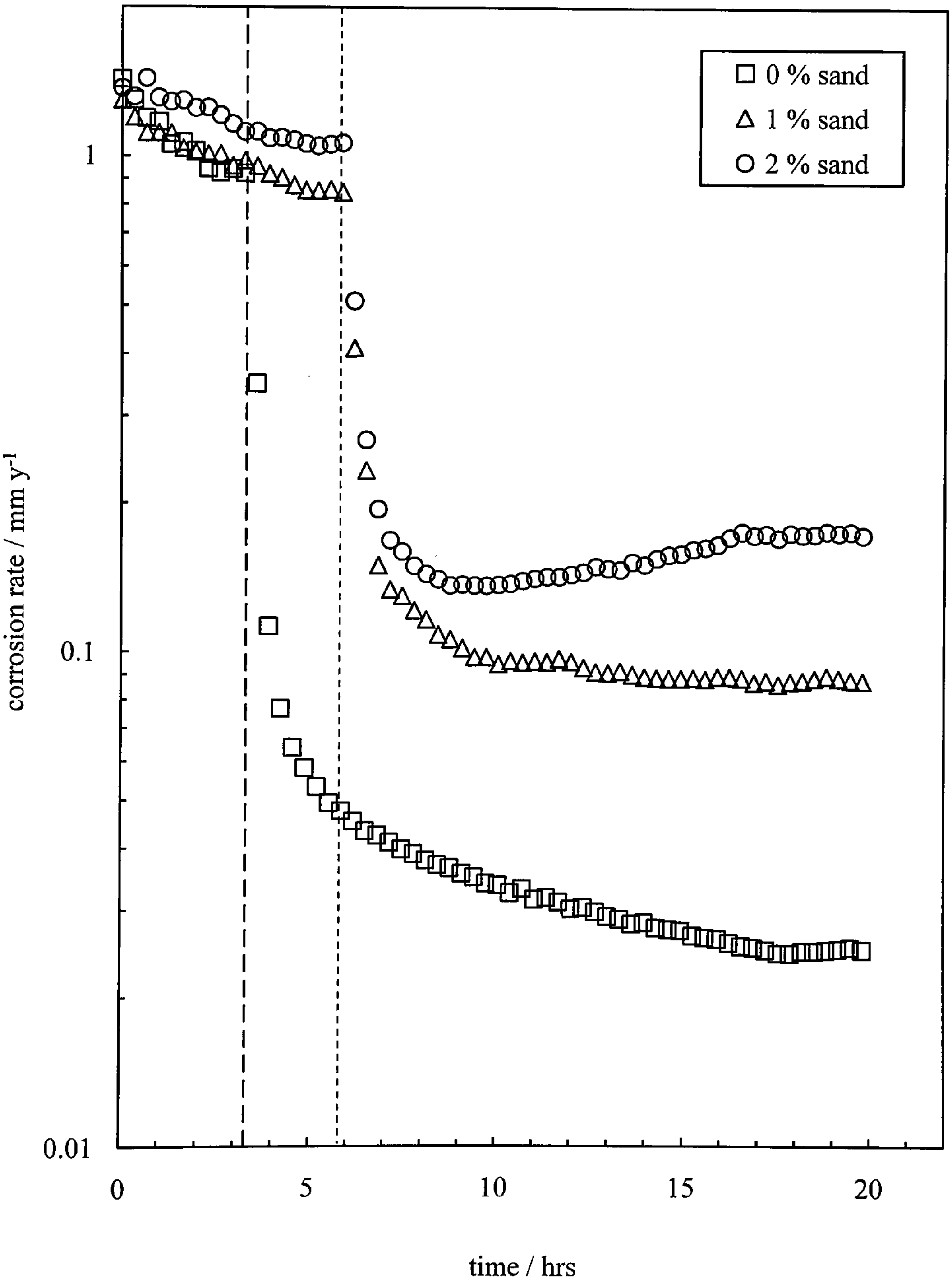

Figure 6. Corrosion rate vs. time for C1018 steel in 4.7 wt.% brine solution saturated with CO_2 at 25 °C with 5 ppm (1.13×10^{-5} M) C16BDMAC as a function of sand (w/v) percent, determined by the bubble test. The vertical dashed line indicates the time at which C16BDMAC was added.

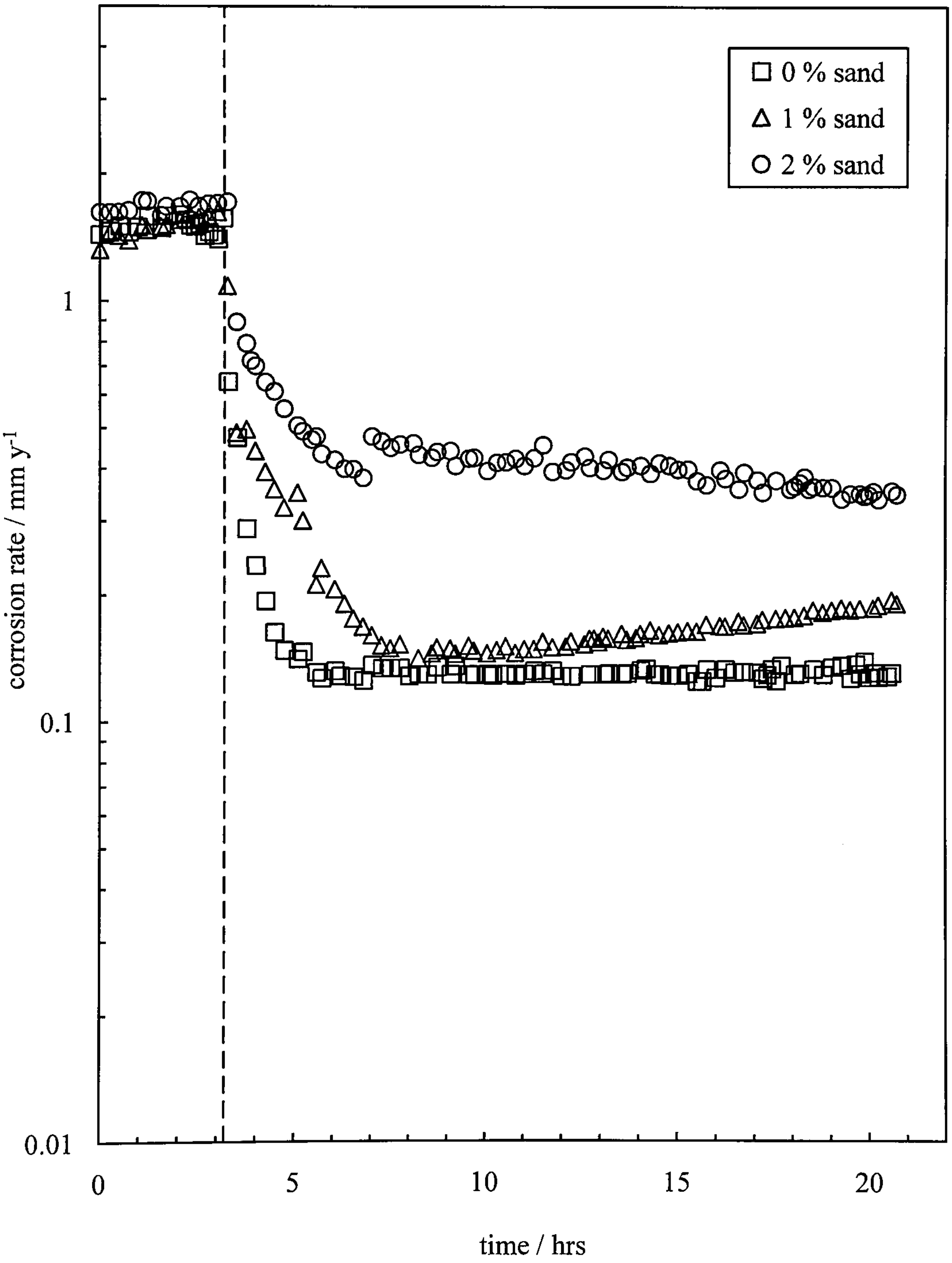

Figure 7. Corrosion rate vs. time for C1018 steel in 4.7 wt.% brine solution saturated with CO_2 at 25 °C with 10 ppm (2.25×10^{-5} M) C16BDMAC as a function of sand (w/v) percent, determined by the bubble test. The vertical dashed lines indicate the time at which C16BDMAC was added.

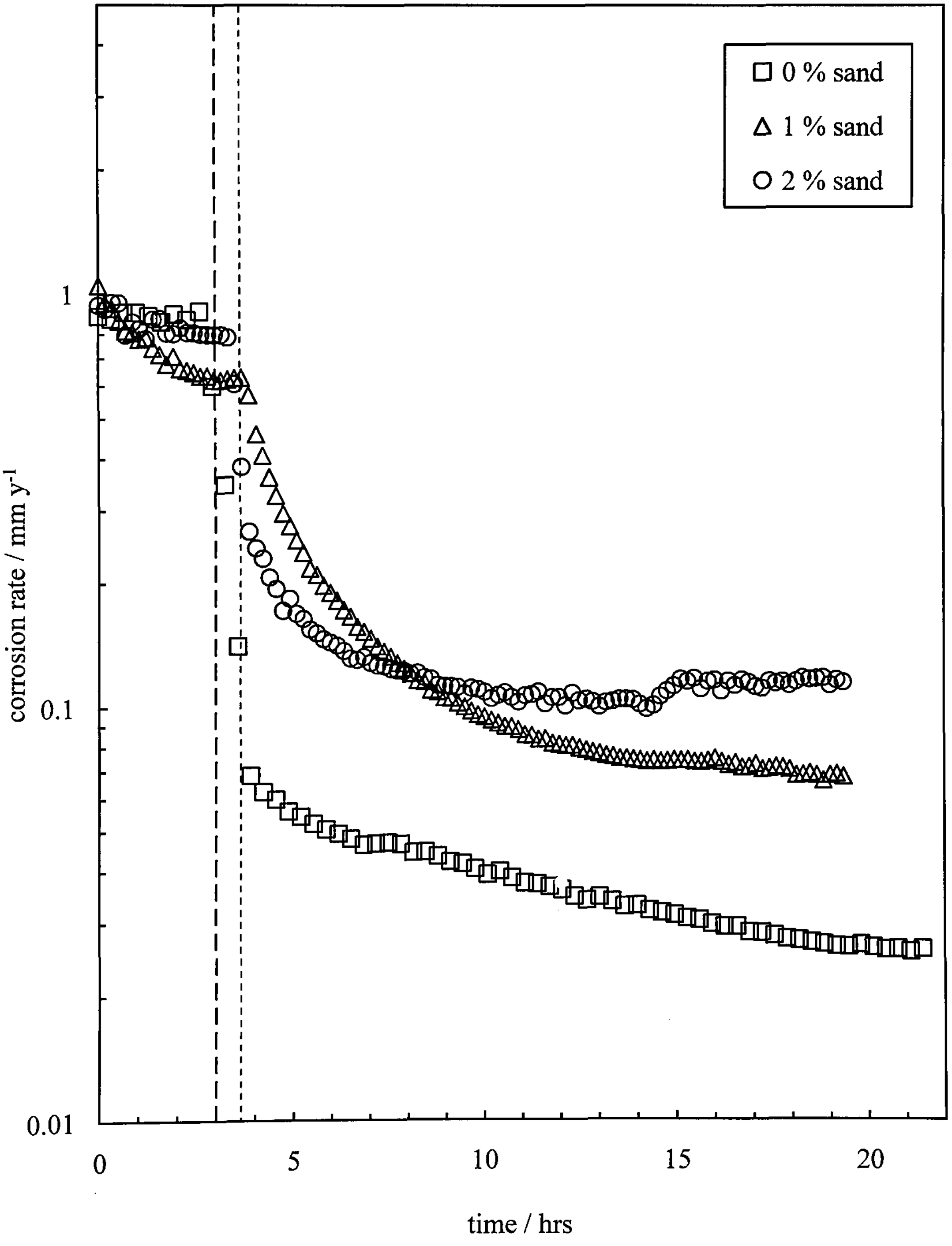

Figure 8. Corrosion rate vs. time for C1018 steel in 4.7 wt.% brine solution saturated with CO_2 at 25 °C with 20 ppm (4.50×10^{-5} M) C16BDMAC as a function of sand (w/v) percent, determined by the bubble test. The vertical dashed line indicates the time at which C16BDMAC was added.